



**HAL**  
open science

# Investigating PRMT5 functions in triple-negative breast cancers

Rayan Dakroub

► **To cite this version:**

Rayan Dakroub. Investigating PRMT5 functions in triple-negative breast cancers. Cancer. Université Paris sciences et lettres; Université Libanaise, 2023. English. NNT : 2023UPSL060 . tel-04521599

**HAL Id: tel-04521599**

**<https://theses.hal.science/tel-04521599>**

Submitted on 26 Mar 2024

**HAL** is a multi-disciplinary open access archive for the deposit and dissemination of scientific research documents, whether they are published or not. The documents may come from teaching and research institutions in France or abroad, or from public or private research centers.

L'archive ouverte pluridisciplinaire **HAL**, est destinée au dépôt et à la diffusion de documents scientifiques de niveau recherche, publiés ou non, émanant des établissements d'enseignement et de recherche français ou étrangers, des laboratoires publics ou privés.



**THÈSE DE DOCTORAT**  
**DE L'UNIVERSITÉ PSL**

Préparée à Institut Curie – Breast Cancer Biology Group  
Dans le cadre d'une cotutelle avec Université Libanaise

**Etude du rôle de PRMT5 dans les cancers du sein triple-négatifs**

Investigating PRMT5 functions in triple negative breast cancer

Soutenue par

**Rayan DAKROUB**

Le 07/12/2023

Ecole doctorale n° 582

**Cancérologie, biologie,  
médecine, santé**

**Composition du jury :**

Rihab, NASR Professeure, American University of Beirut	<i>Rapporteur, Présidente</i>
Marie-Bérengère, TROADEC Professeure, Université de Bretagne Occidentale	<i>Rapporteur</i>
Reini, LUCO Directrice de recherche, Institut Curie	<i>Examinatrice</i>
Ghassan, DBAIBO Professeur, American University of Beirut	<i>Examineur</i>
Max, CHAFFANET Directeur de recherche, Institut Paoli-Calmettes	<i>Examineur</i>
Thierry, DUBOIS Responsable d'équipe, Institut Curie	<i>Directeur de thèse</i>
Hussein, FAYYAD-KAZAN Professeur, Université libanaise	<i>Directeur de thèse</i>



***“Education is the most powerful weapon which you can use to change the world.”***

*Nelson Mandela*

*To my parents, who worked so hard and gave all what they have to our education, this work is dedicated for you.*

إلى من بذل المَهَج في سبيل أن أصلَ إلى هنا ..  
إلى من قدّم لي كلّ ما يملكان ، لتكونَ ثمرةَ جهودهما هذا البحث المتواضع ..

إلى أمّي وأبي ، أهدى عملي هذا ..





## Acknowledgments

My PhD journey at the breast cancer biology group was a delightful experience that nourished my research, professional, and personal life. I am therefore grateful for the opportunity I had in perusing my studies and spending three years working there.

First and foremost, I express my sincere gratitude to my thesis supervisor in France, Dr. Thierry Dubois. Thierry, thank you for accepting me to join your team as a cotutelle PhD student between Lebanon and France, and for being a great teacher and mentor who followed me at every step of the way. You have taught me tremendous experimental and critical thinking skills, and your constructive criticism pushed me to always provide the best of what I have. Most importantly, thank you for the personal support you provided me, especially upon my arrival to France. Picking me up from the airport when I came for the first time is a kind gesture of you which I will not forget, and forever grateful to. Being a kind and humble mentor is a rare blessing, and you aspired me to be so in my future professional life. After the unfortunate circumstances we faced in Lebanon and losing half of my third-year financial grant, you took a step in helping not only me, but all the Lebanese students affected, and I thank you for that on the behalf of all of us. You then helped me to obtain a new funding to compensate what I lost, and further extend my PhD to a fourth year.

I would also like to express my sincere gratitude to my supervisor in Lebanon, Dr. Hussein Fayyad-kazan. Hussein, you were extremely supportive when I first informed you of my plans to seek a PhD and helped me in the application process. Among all of your students in the master's programs you coordinate, you chose me to do my Master internship with you and later encouraged me in doing a PhD, and I thank you for the trust you have put in me and in my academic abilities. Since then, you have been more of a friend for me, and I thank you for all the support you provided. I wish you all the best in your future professional and personal life.

I would like to thank my PhD thesis jury members for dedicating time and agreeing to be part of my thesis defense. I thank my two reporters, Prof. Rihab Nasr and Prof. Marie-Bérengère Troadec for accepting to review my work and to provide their feedback. I am honoured to have your valuable comments regarding my manuscript and project. I would also like to thank Dr. Reini Luco, Prof. Ghassan Dbaibo, and Dr. Max Chaffanet for agreeing to be examiners and for their professional input.

I am also grateful to the members of my thesis follow up committee, Dr. Sylvie Tuffery-Giraud, Dr. Muriel Le Romancer, Dr. Clara Nahmias, and Dr. Virginie Marcel for their insightful feedback and their valuable advice that helped to shape my PhD project. Dr. Sylvie, thank you for the tools you provided me with and the meetings we did, besides the committee ones, that helped me in executing some critical experiments.

This work would not have been carried out without the SAFAR grant I received from the french embassy in Lebanon and the EDST at the Lebanese University, in addition to Institut Curie that provided me with a 5-month contract at the end of my thesis.

I would like to acknowledge the professionals who contributed to the advancement of my thesis project. Dr. Mathilde Vinet, a previous member of the BCBG lab who carried out the first PRMT5 project, and her work was a first step from which my PhD project emerged. From the mass spectrometry platform at Institut Curie, Dr. Loew Damarays and Florent Dingli for performing the mass spectrometry experiments and guiding me on the proper way to analyse the different experiments we performed. I am grateful to Dr. Ahmed El Marjou at the recombinant protein platform for purifying the PRMT5/MEP50 complex, and for allowing me to utilize different equipment at his platform for cloning and protein purification. I thank Vincent Crozet from the team of Dr. Anne Houdusse for performing gel filtration experiments on the proteins I purified. I am grateful for Dr. Françoise Ochsenbein at CEA (Paris Saclay) for providing me protocol for protein purification, and for the several times she welcomed me at her laboratory to perform NMR experiments. Although we did not reach our initial goals, I thank her for the time she spent with me, and I learnt a lot of new things at her team! I thank Dr. Kritika Sahni Ray and Marion Albasini from Fida Biosystems for teaching me the FIDA technique, and for their help in analysing the data I obtained. I also thank Dr. Sandrine Moutel from the recombinant antibody platform at Institute Curie for giving me access to the FIDA machine. I am also grateful to Dr. Coralie Poulard from Centre de Recherche en Cancérologie de Lyon for aiding me in analysing the ChIP-qPCR results.

A special thank you goes to my teammates at the BCBG. It was a pleasure meeting you all and working by your side. To the previous member Dr. Samyuktha Suresh, thank you for welcoming me when I first arrived with a friendly atmosphere, and for always being there whenever I had any technical and analytical questions. It was my

pleasure meeting you and I wish you all the best in your future. I thank the previous lab member Dr. Ramon Garcia Areas for giving his valuable feedback on the paper I wrote, even when he is not part of our team anymore! Virgine Maire, thank you for being a good teacher whenever I needed any help, and for creating a lovely atmosphere in the office. To my two lab mates and friends, Solène Huard and Sonia Ruggiero, thank you for being great companions and creating a friendly atmosphere at work. I have missed our “Friday lunches” and the many times we went for dinner together after long working hours in the lab. It was a delight getting to know you and sharing cultural backgrounds together, I learnt a lot on the French and Italian heritages, two of my favourite countries, from you! I wish you all the best in your personal lives and PhDs and keep up the hard work! To my lab mate, friend, and sister, Yara Hajj Younes, thank you to all the support and experimental work you provided me during your stay at the lab. I was very happy teaching you and working by your side, you are a clever and hardworking scientist and I’m sure a bright future awaits you! Thank you for the time and work you put for my project, and thank you for being an amazing companion, inside and outside the of lab, for the year and a half period we spent together.

To my friends in Lebanon and France, thank you for the continuous support and just being there! Fatima, Fatima, Aya, and Israa, you have been my closest friends since we met at university, sharing our ambitions and dreams with each other. Thank you for always believing in me, and for the many times you heard my complaints! Ghiwa, Ghalia, Zainab, and Kassem, thank you for being great lab mates during our Master 2 internships, and amazing friends whom I share a lot of “food” experiences with! Nadia, thank you for being an amazing friend whom I entrust with anything, and for always being there to hear and support me. My cousin and childhood friend Batoul, thank you for always being there for me.

To my second family in France, Hiba and Fatima, thank you to all the lovely time we spent together, and for all the trips and travelling we shared. I made amazing memories with you and visited exceptional places by your side. Thank you for being present whenever I needed help, and for sharing our thoughts and our tiring PhD experiences!

Lastly, my family, I would never be where I am today without you. I consider myself fortunate for having such a great support system by my side. To my uncle, Mohammad Dakroub, thank you for being the amazing man you are. You have helped me a lot during this journey, and I am forever grateful for you. To my siblings, Batoul, Fatima, Alaa, and Mohammad, thank you for always being there for me and for helping me whenever I needed. Our daily video calls and your presence in my life kept me going on. My sister Fatima, you are an inspiration for me. Doing a PhD is not easy by itself, and you have made it while being an amazing mother. Your ambitious and spirit inspire me to succeed, and your advice is always of great value for me. My nephew, Mohammad-Jawad, seeing your face after a long day was a source of delight for me, even if behind a screen! I love you my little man! Bilal, thank you for being the person you are, for your support, care, love, and just being there for me even from behind scenes.

My parents, thank you for everything you did and all the sacrifices you made for us. I am what I am today because of your hard work, love, and care. Thank you for raising me to believe in the power of education, and for dedicating your life for that. Dad, thank you for being the most supportive father with the greatest and kindest heart. I spent my childhood witnessing your hard work and the sacrifices you did for your family, which fuelled me to continue whenever I felt low. Mom, thank you for dedicating your life for me, thank you for your patience, love, support, hard work, prayers, and tears. *Baba and Mama*, everything I became and will ever be is owed to you.

To all, again,

Thank you

Rayan

## Table of Contents

Acknowledgments .....	4
List of Figures.....	13
List of Abbreviations .....	15
Chapter 1: Introduction.....	24
I. Breast Cancer .....	25
I.1. Generalities.....	25
I.1.1. Incidence and mortality rates .....	25
I.1.2. Breast cancer risk factors .....	25
I.1.3. Breast cancer diagnosis and screening .....	27
I.2. The Breast Anatomy .....	29
I.3. Breast cancer development and characterization .....	30
I.3.1. Histological classification of breast cancer.....	30
I.3.2. Molecular classification of breast cancer .....	33
I.4. Breast cancer treatments .....	36
I.4.1. Surgery .....	36
I.4.2. Radiotherapy .....	37
I.4.3. Chemotherapies .....	38
I.4.4. Endocrine therapy: Luminal breast tumours .....	40
I.4.5. HER2 targeted therapies .....	40
I.4.6. PARP inhibitors.....	42
I.4.7. Immunotherapy .....	44
I.4.8. Other targeted therapies .....	44
Summary.....	45
II. Triple Negative Breast Cancer .....	46
II.1. Generalities: risk factors, molecular features, and prognosis .....	46
II.2. TNBC inter-tumoral heterogeneity .....	46
II.2.1. BL1 and BL2 subtypes.....	48
II.2.2. Mesenchymal subtype .....	48
II.2.3. Luminal androgen receptor subtype .....	48
II.2.4. Prognosis of the different TNBC subtypes.....	48

II.2.5. TNBC cell line models .....	49
II.3. Approved TNBC therapies .....	49
II.4. TNBC chemoresistance .....	50
II.4.1. ATP-binding cassette (ABC) transporters .....	51
II.4.2. Breast cancer stem cells .....	51
II.5. TNBC and the EGFR pathway .....	56
Summary .....	57
III. Arginine Methylation .....	58
III.1. Biochemistry and enzymatic reaction .....	58
III.2. Metabolic regulation of arginine methylation .....	59
III.3. Writers of arginine methylation: PRMTs .....	60
III.3.1. Structure of PRMTs .....	60
III.3.2. The PRMT methylome and arginine methylation motifs .....	62
III.3.3. Crosstalk between PRMTs .....	64
III.3.4. Functions of arginine methylation .....	65
III.4. Arginine methylation readers .....	73
III.4.1. Tudor domain containing proteins .....	73
III.4.2. Readers not harbouring a Tudor domain .....	75
III.5. Arginine methylation erasers .....	77
III.6. Arginine methylation in Cancer .....	78
III.6.1. PRMT1 .....	78
III.6.2. PRMT2 .....	81
III.6.3. PRMT3 .....	81
III.6.4. PRMT4 .....	82
III.6.5. PRMT6 .....	84
III.6.6. PRMT7 .....	85
III.7. PRMT inhibitors .....	85
Summary .....	87
IV. Protein Arginine Methyltransferase 5 (PRMT5) .....	88
IV.1. Generalities .....	88
IV.2. General structure of PRMT5 .....	88
IV.3. Crystal structure of PRMT5 .....	89

IV.3.1. The active site .....	89
IV.3.2. Comparing PRMT5 structure to type I PRMTs .....	90
IV.4. PRMT5 partners .....	91
IV.4.1. The methylosome .....	91
IV.4.2. MEP50: a major PRMT5 partner .....	92
IV.4.3. pICln .....	94
IV.4.4. RIOK1 .....	94
IV.4.5. COPR5 .....	94
IV.5. The PRMT5 methylome .....	97
IV.6. PRMT5 and MEP50 localization .....	101
IV.7. PRMT5 and MEP50 PTM .....	102
IV.8. PRMT5 Functions .....	106
IV.8.1. PRMT5 in splicing regulation .....	106
IV.8.2. PRMT5 in transcriptional regulation .....	109
IV.8.3. PRMT5 and DNA damage response .....	110
IV.8.4. PRMT5 and signalling pathways .....	111
IV.8.5. PRMT5 in development, differentiation, and stem cell maintenance .....	113
IV.8.6. Hypoxia and autophagy .....	114
IV.8.7. PRMT5 and the immune system .....	115
IV.9. PRMT5 implication in cancer .....	116
IV.9.1. Breast cancer .....	116
IV.9.2. PRMT5 and MTAP depletion .....	119
IV.9.4. Leukemia .....	119
IV.9.5. Other solid tumours .....	120
IV.10. PRMT5 inhibitors .....	121
IV.11. PRMT5 as a target in combinatorial treatments .....	122
Summary .....	124
V. Far Upstream Element Binding Protein 1: FUBP1 .....	125
V.1. FUBP1 discovery and generalities .....	125
V.2. Molecular and structural features of FUBP1 .....	125
V.2.1. The Far Upstream Element Binding Protein family members .....	125
V.2.2 FUBP1 subcellular localization .....	126



V.2.3 FUBP members post-translational modifications .....	127
V.3 FUBP1 partners .....	132
V.4. FUBP1 structure .....	133
V.4.1. FUBP1 N and C terminal domains .....	133
V.4.2. NMR structure and the nucleic acid binding domain .....	134
V.5. FUBP1 Functions .....	137
V.5.1. FUBP1: a transcription factor .....	137
V.5.2. FUBP1: a pre-mRNA splicing factor .....	142
V.5.3. FUBP1 and translation .....	144
V.5.5. Global transcripts regulated by FUBP1 .....	146
V.6. FUBP1 in Cancer.....	146
Summary.....	147
Chapter 2: Objectives and results .....	148
Chapter 2: Part 1.....	149
Therapeutic advantage of targeting PRMT5 in combination with chemotherapies or EGFR/HER2 inhibitors in triple-negative breast cancers.....	149
Abstract.....	150
Introduction .....	151
Material and methods .....	153
Results .....	157
<i>Breast cancer cell lines show distinct sensitivity to PRMT5 inhibition.....</i>	<i>157</i>
<i>PRMT5 inhibition synergizes with cisplatin, doxorubicin, and camptothecin, but not with paclitaxel, to impair TNBC cell proliferation.....</i>	<i>158</i>
<i>PRMT5 inhibition synergizes with inhibitors targeting HER family members to impair the proliferation of TNBC cells.....</i>	<i>163</i>
Discussion.....	167
Conclusion .....	170
Supplementary information .....	173
Chapter 2: Part 2.....	180
Unveiling the PRMT5 interactome through immunoprecipitation and TurboID proximity labelling in TNBC .....	180
Abstract.....	181
Introduction .....	182

Materials and Methods.....	184
Results .....	193
<i>MEP50 interactome identified FUBP1 as a MEP50 partner.....</i>	193
<i>FUBP1 is overexpressed in breast cancer compared to normal breast tissues....</i>	197
<i>PRMT5 is a component of the FUBP1 interactome .....</i>	199
<i>FUBP1 is symmetrically dimethylated by PRMT5.....</i>	201
<i>The methylation of FUBP1 does not affect its localization .....</i>	202
<i>FUBP1 methylation enhances its binding to the FUSE element .....</i>	203
<i>Investigating the PRMT5 interactome by TurboID proximity labelling.....</i>	204
<i>SDCCAG3 is a novel PRMT5 interactor .....</i>	211
<i>SDCCAG3 potentially functions as a regulator of the Wnt pathway in TNBC .....</i>	212
<i>Among different PRMTs, SDCCAG3 interacts preferentially with PRMT5.....</i>	215
<i>Deciphering PRMT5 interactome by immunoprecipitation .....</i>	216
Discussion.....	220
<i>The PRMT5/MEP50 interactome .....</i>	221
<i>Functional analysis of PRMT5/MEP50 interaction with novel partners .....</i>	227
Supplementary data.....	231
Chapter 3: General Conclusions and Future Perspectives.....	251
<i>PRMT5 inhibition as a combinatorial treatment strategy in TNBC .....</i>	251
<i>Deciphering the PRMT5 interactome .....</i>	252
<i>Effect of FUBP1 methylation on its functions .....</i>	255
<i>PRMT5 interaction with DBC-1 .....</i>	256
<i>Functional analysis of the interaction between PRMT5 and SDCCAG3 .....</i>	257
References.....	259
Annexe I.....	316
Annexe II.....	317

## List of Figures

Figure 1: Cancer incidence and mortality in females worldwide (2020).....	25
Figure 2: Schematic illustration of breast cancer risk factors. ....	27
Figure 3: Anatomy of the female breast. ....	29
Figure 4: Histological subtypes of breast cancer. ....	31
Figure 5: Breast cancer stages .....	32
Figure 6: Breast cancer grades. ....	33
Figure 7: Breast cancer molecular subtypes. ....	35
Figure 8: Types of breast cancer therapies. ....	36
Figure 9: Types of breast cancer removal surgeries. ....	37
Figure 10: Synthetic lethality using PARP inhibitors in BRCA1/2 mutated cells. ....	43
Figure 11: Gene expression profile of TNBC subgroups from the Lehmann classification. .....	47
Figure 12: TNBC cell lines molecular subtypes. ....	49
Figure 13: Causes of TNBC chemoresistance. ....	51
Figure 14: BCSCs contribute to cancer relapse. ....	52
Figure 15: the TGF $\beta$ pathway.....	53
Figure 16: The Notch signalling pathway. ....	54
Figure 17: Wnt/ $\beta$ -catenin pathway.....	55
Figure 18: EGFR targeting agents. ....	56
Figure 19: Arginine methylation reaction and types. ....	59
Figure 20: Metabolic regulation of SAM. ....	60
Figure 21: The PRMT family members.....	61
Figure 22: Illustration of a PRMT homodimer. ....	62
Figure 23: PRMTs functions in transcriptional regulation. ....	66
Figure 24: PRMTs functions in pre-mRNA splicing. ....	68
Figure 25: Function of PRMTs in cell cycle regulation.....	70
Figure 26: PRMTs implication in the DNA damage response. ....	71
Figure 27: Role of PRMT1 and PRMT5 in EGFR and TGF $\beta$ signalling pathways.....	73
Figure 28: Readers of non-histone methylation.....	76
Figure 29: Readers of histone arginine methylation marks. ....	77
Figure 30: PRMT5 and MEP50 structures.....	89
Figure 31: Crystal structure of PRMT5. ....	90
Figure 32: PRMT5 methylosome.....	92
Figure 33: PRMT5:MEP50 crystal structure .....	93
Figure 34: PRMT5 localization is associated with poor prognosis.....	102
Figure 35: PRMT5 and MEP50 post-translational modifications. ....	104
Figure 36: Protein and snRNA components of the human spliceosomal snRNPs. ....	107
Figure 37: PRMT5 functions in the spliceosome assembly. ....	108
Figure 38: PRMT5 methylates and activates AKT.....	112
Figure 39: PRMT5 functions in autophagy. ....	115
Figure 40: PRMT5 implication in breast cancer.....	118
Figure 41: MTAP-deleted cancer cells are more susceptible to PRMT5 inhibition. ....	119

Figure 42: FUBP family members. ....	126
Figure 43: Post-translational modifications of FUBP1, FUBP2 and FUBP3. ....	129
Figure 44: FUBPs share conserved methylated arginine. ....	132
Figure 45: NMR structure of FUBP1 KH3 and KH4 domains bound to ssDNA ....	135
Figure 46: FUBP1/FIR/FUSE axis in the control of MYC transcription. ....	139

## List of Tables

Table 1: Breast cancer screening methods: applications and limitations. ....	28
Table 2: PRMT inhibitors.....	85
Table 3: PRMT5 partners.....	95
Table 4: PRMT5 known substrates. ....	98
Table 5: PRMT5 and MEP50 PTM.....	104
Table 6: PRMT5 inhibitors and their mechanism of action. ....	121
Table 7: PRMT5 inhibition in combination studies.....	123
Table 8: Arginine methylation sites on FUBP1, FUBP2 and FUBP3 ....	130
Table 9: FUBP1 interacting partners. ....	133
Table 10: FUBP1 DNA binding sequences ....	137
Table 11: Transcripts regulated by FUBP1 at the transcriptional level.....	141
Table 12: Transcripts regulated by FUBP1 at the pre-mRNA splicing level. ....	143
Table 13: Transcripts regulated by FUBP1 at the translational level.....	145

## List of Abbreviations

- 2OG:** 2-oxoglutarate
- 3D-CRT:** 3D-conformal radiotherapy
- 53BP1:** p53-binding protein 1
- 5-FU:** 5-fluorouracil
- ABC:** ATP-binding cassette
- ACS:** American Cancer Society
- ADCC:** antibody-dependent cell-mediated cytotoxicity
- AIs:** aromatase inhibitors
- AJCC:** American Joint Committee on Cancer
- ALDH1:** aldehyde dehydrogenase 1
- ALL:** acute lymphoblastic leukemia
- AML:** acute myeloid leukemia
- APC:** adenomatous polyposis coli
- ARE:** AU-rich elements
- ARHGAP29:** Rho GTPase-activating protein 29
- ARS:** multi-aminoacyl-tRNA synthetase
- AS:** alternative splicing events
- ASK1:** apoptosis signal-regulating kinase 1
- ATF4:** activating transcription factor 4
- AURKB:** Aurora Kinase B
- BCSC:** breast cancer stem cells
- BER:** base excision repair

**BL1:** basal-like 1

**BL2:** basal-like 2

**BMD:** becker muscular dystrophy

**CARM1:** coactivator associated arginine methyltransferase 1

**CCSST:** clear cell sarcoma of soft tissue

**CDK4:** cyclin-dependent kinase 4

**CDKI:** cyclin dependent kinase inhibitor

**CHIP:** carboxyl terminus of heat shock cognate 70-interacting protein

**CK1:** casein kinase 1

**COPR5:** cooperatoer of PRMT5

**CRC:** colorectal cancer

**CSCs:** Cancer stem cells

**DAVID:** Database for Annotation, Visualization, and Integrated Discovery

**DCIS:** ductal carcinoma in situ

**DDR:** DNA damage response

**DLBCL:** diffuse large B-cell lymphoma

**DMD:** duchenne muscular dystrophy

**DNA-PK:** DNA-dependent protein kinase

**DNMT1:** DNA methyltransferase 1

**Dvl:** Dishevelled

**EBNA2:** Epstein–Barr virus (EBV) nuclear antigen 2

**ECD:** extracellular domain

**EGFR:** epidermal growth factor receptor

**EMT:** epithelial to mesenchymal transition

**ENTR1:** endosome associated trafficking regulator 1

**ER:** Estrogen receptor

**ESC:** embryonic stem cells

**ESS:** exon splicing silencer

**EV71:** enterovirus 71

**EVI1:** ecotropic virus integration site 1

**FAD:** flavin adenine dinucleotide

**FDA:** Food and Drug Administration

**FEN1:** Flap endonuclease 1

**FGFR3:** Fibroblast Growth Factor Receptor 3

**FIR:** FUBP Interacting Repressor

**FLT3:** Fms-like receptor tyrosine kinase 3

**FOXO3a:** Forkhead Box O 3a

**FUBP:** Far upstream element binding protein

**GAR:** glycine and arginine rich motifs

**GBM:** glioblastoma

**GO:** Gene ontology

**GSK3:** glycogen synthase kinase 3

**H4:** Histone 4

**HCC:** hepatocellular carcinoma

**Hcy:** homocysteine

**HER2:** human epidermal growth factor receptor 2

**HR:** homologous recombination

**HRT:** hormone replacement therapy

**HSCs:** hematopoietic stem cells

**HSL7:** histone synthetic lethal 7

**HSP70:** heat-shock protein of 70 kDa

**ICAM1:** intercellular adhesion molecule 1

**IHC:** immunohistochemistry

**IM:** immunomodulatory

**IMAC:** immobilized-metal affinity chromatography

**IMPC:** Invasive micropapillary carcinoma

**IMRT:** intensity-modulated radiotherapy

**InsP3Rs:** inositol-1,4,5-trisphosphate receptors

**IORT:** intraoperative radiation therapy

**IRES:** internal ribosome entry site

**ISE:** intronic splicing enhancer

**ITC:** isothermal titration assay

**iTRAQ:** isobaric Tags for Relative and Absolute Quantitation

**JEV:** Japanese encephalitis virus

**JmjC:** Jumonji C domain

**JMJD6:** Jumonji domain-containing 6 protein

**KAP1:** KRAB-associated protein 1

**Kd:** dissociation constant

**KDM:** lysine demethylases



**KH:** hnRNP K homology

**KHSRP:** KH-type splicing regulatory protein

**KLF4:** Kruppel-like factor 4

**LAR:** luminal androgen receptor

**LCIS:** lobular carcinoma in situ

**LC-MS/MS:** Liquid Chromatography with tandem mass spectrometry

**LSD:** lysine specific demethylase

**M:** mesenchymal

**MAT:** methionine adenosyl-transferase

**MCL:** mantle cell lymphoma

**MDH1:** malate dehydrogenase 1

**MDM2:** mouse double minute 2

**MDR1:** multidrug resistance 1

**MED12:** mediator complex subunit 12

**MEF:** mouse embryonic fibroblasts

**MEP50:** methylosome protein 50

**MITF:** Microphthalmia-associated transcription factor

**MLOs:** membrane-less organelles

**MML:** multiple myeloid leukemia

**MMP9:** matrix metalloproteinase 9

**MP:** Myosin phosphatase

**MRI:** Magnetic resonance imaging

**MRPS23:** mitochondrial ribosomal protein S23

**MS:** mass spectrometry

**MSL:** mesenchymal stem-like

**MTA:** methylthioadenosine

**MTAP:** S-methyl-5'-thioadenosine phosphorylase

**MYPT1:** myosin phosphatase target subunit-1

**NES:** nuclear exclusion signal

**NET:** pulmonary neuroendocrine tumours

**NF90:** nuclear factor 90

**NFIB:** nuclear factor I B

**NF- $\kappa$ B:** nuclear factor  $\kappa$  of B-cells

**NHEJ:** nonhomologous end-joining

**NLS:** nuclear localization signal

**NONO:** non-POU domain-containing octamer-binding protein

**NPC:** neural progenitor cells

**NPM:** nucleophosmin

**Nrf2:** nuclear factor erythroid 2 related factor 2

**NSCLC:** non-small cell lung carcinomas

**NST:** no special type

**OPC:** oligodendrocyte progenitor cell

**OS:** overall survival

**PARP:** Poly(ADP-ribose) polymerase

**PBM:** PRMT5 binding motif

**PCBPs:** poly(C)-binding proteins

**pCR:** pathologic complete response

**PCR:** polymerase chain reaction

**PDAC:** pancreatic ductal adenocarcinoma

**PDCD4:** programmed cell death 4

**PDGF:** platelet-derived growth factor

**PELP1:** proline, glutamate, and leucine rich protein 1

**PFU60:** poly-U-binding factor

**PGC:** primordial germ cells

**PGE2:** Prostaglandin E2

**PGM:** proline-glycine-methionine

**PKD2:** polycystic kidney disease 2

**PKM2:** pyruvate kinase muscle isozyme M2

**PKMT:** protein lysine methyltransferase

**pol II:** RNA polymerase II

**pol  $\beta$ :** DNA polymerase  $\beta$

**PPI:** protein-protein interaction

**PR:** progesterone receptor

**PRC2:** polycomb repressor complex

**pri-miRNA:** primary miRNA

**PRMT:** protein arginine methyltransferase

**PTH:** parathyroid hormone

**PTM:** post-translational modification

**PXR:** pregnane x receptor

**Rb:** retinoblastoma protein

**RBP:** RNA binding proteins

**RFS:** relapse free survival

**RIOK1:** RIO kinase 1

**RISC:** RNA-induced silencing complex

**ROK:** RhoA-activated kinase

**RPA:** replication protein A

**RPS10:** ribosomal protein S10

**RPS2:** 40S ribosomal protein S2

**RRM:** RNA recognition motif

**RUVBL1:** RuvB-like 1

**SAH:** S-adenosylhomocysteine

**SAM:** S-adenosyl methionine

**SCLC:** small cell lung cancer

**SDCCAG3:** serologically defined colon cancer antigen-3

**SELEX:** systematic Evolution of Ligands by Exponential Enrichment

**SERDs:** selective modulators estrogen receptor degraders

**SERMs:** estrogen receptor modulators

**SF:** splicing factor

**SG:** sacituzumab govitecan

**SGK:** serum- and glucocorticoid-inducible kinases

**SHP1:** SH2-domain-containing protein tyrosine phosphatase 1

**SILAC:** stable isotope labeling with amino acids in cell culture

**Skb1:** Shk1 kinase-binding protein 1

**SMN:** Survival motor neuron

**SND1:** Staphylococcal nuclease domain-containing protein 1

**snRNPs:** small nuclear ribonucleoproteins

**sRNAs:** small RNAs

**TDP1:** Tyrosyl-DNA phosphodiesterase 1

**TGF $\beta$ :** transforming growth factor- $\beta$

**TGF $\beta$ R:** TGF $\beta$  receptor

**Th:** T helper

**TIC:** tumour initiating cells

**TNBC:** triple negative breast cancer

**TNM:** tumour-node-metastasis

**TOP3B:** topoisomerase IIIB

**TopIcc:** Top1 cleavage complexes

**Trop2:** trophoblast cell-surface antigen 2

**TUBB8:** Tubulin Beta 8

**ULK1:** Unc-51-like kinase 1

**USP22:** ubiquitin-specific protease 22

**USP29:** ubiquitin specific peptidase 29

**USP9X:** ubiquitin-specific protease 9 X-linked

## **Chapter 1: Introduction**

In the introduction chapter, I will outline a summary of the main topics related to the results obtained during my PhD. First, I will give an overview of breast cancer, its subtypes and treatments followed by a detailed description of the TNBC subtype. Then, I will describe the process and regulation of arginine methylation and how it is implicated in tumorigenesis, followed by a detailed description of PRMT5. Lastly, I will describe FUBP1, a protein which I identified as novel PRMT5 substrate.

# I. Breast Cancer

## I.1. Generalities

### I.1.1. Incidence and mortality rates

In 2020, breast cancer ranked first for cancer incidence and related mortality in females worldwide, accounting for 24.5% of cancer new cases (2.2 million cases) and 15.5% for cancer-related deaths (0.68 million deaths) in females globally (**Figure 1**) [1]. France ranked fourth in breast cancer rates in females worldwide, where 58,083 breast cancer cases were recorded [2]. In the Lebanese population, breast cancer accounted for 33.7% (5,802 total cases) of new cancer cases and 24.3% (2,981 total mortalities) of cancer-related mortalities in females during 2020 [2].

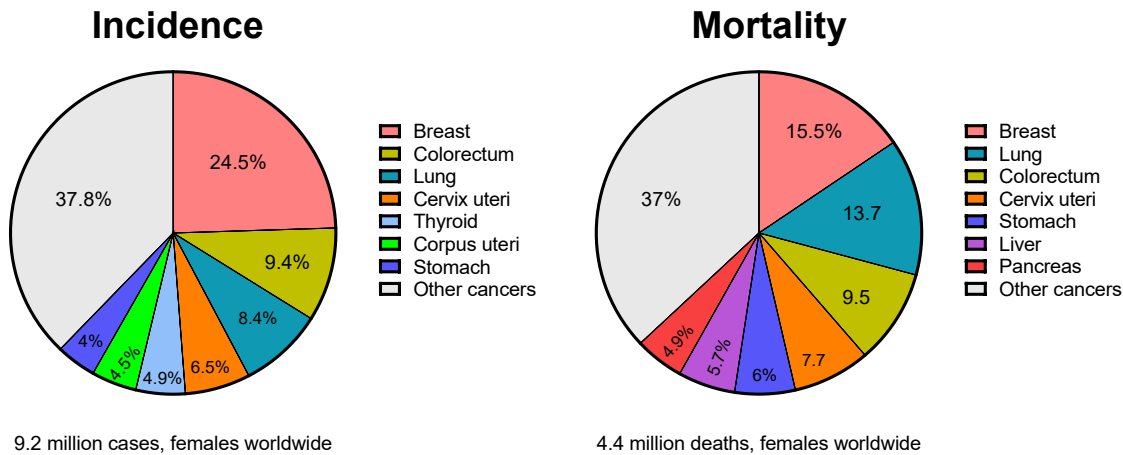


**Figure 1: Cancer incidence and mortality in females worldwide (2020).** Breast cancer is the most diagnosed cancer and causes the most cancer-related mortalities in females worldwide. Adapted and modified from [1].

### I.1.2. Breast cancer risk factors

**Figure 2** shows an illustration of the main breast cancer risk factors.

- Sex: Breast cancer is >100 times frequent in women than in men [3], hence being female itself increases the risk of getting the disease [4,5].
- Age: One of the greatest risk factors for breast cancer is age, as high percentage of breast cancer cases occur in women between the age 40-60 [5,6].
- Family history and genetics: Women with first degree relatives diagnosed with breast cancer are at a higher risk of getting the disease [6,7]. A study in the UK

showed that a woman with one first degree relative with breast cancer has a 1.75-fold increased risk of developing it. The risk increases to 2.5-fold and more in women with more than one first degree affected relatives [6]. The most common cause of this inherited susceptibility to breast cancer is mutations in *BRCA1* and *BRCA2* genes [5–8].

- d. Reproductive factors: Experiencing late menopause (after 55), early menarche (before 12), never getting pregnant, and having a first child birth at an age higher than 35 increases the risk of breast cancer [6,7,9]. However, having additional births and breastfeeding (especially for a period higher than one year) can lower the risk of getting the disease [9,10]. Having dense breasts could also increase the risk of breast cancer [10].
- e. Hormones: Taking exogenous estrogen through contraceptive pills for a period of >10 years and the administration of hormone replacement therapy (HRT) for menopausal or postmenopausal women increases the risk of breast cancer [6,10].
- f. Lifestyle: Having low physical activity, consuming excess alcohol, smoking, being overweight, and being on a high fat low fibre diet increase the chance of getting breast cancer [5–7,10].



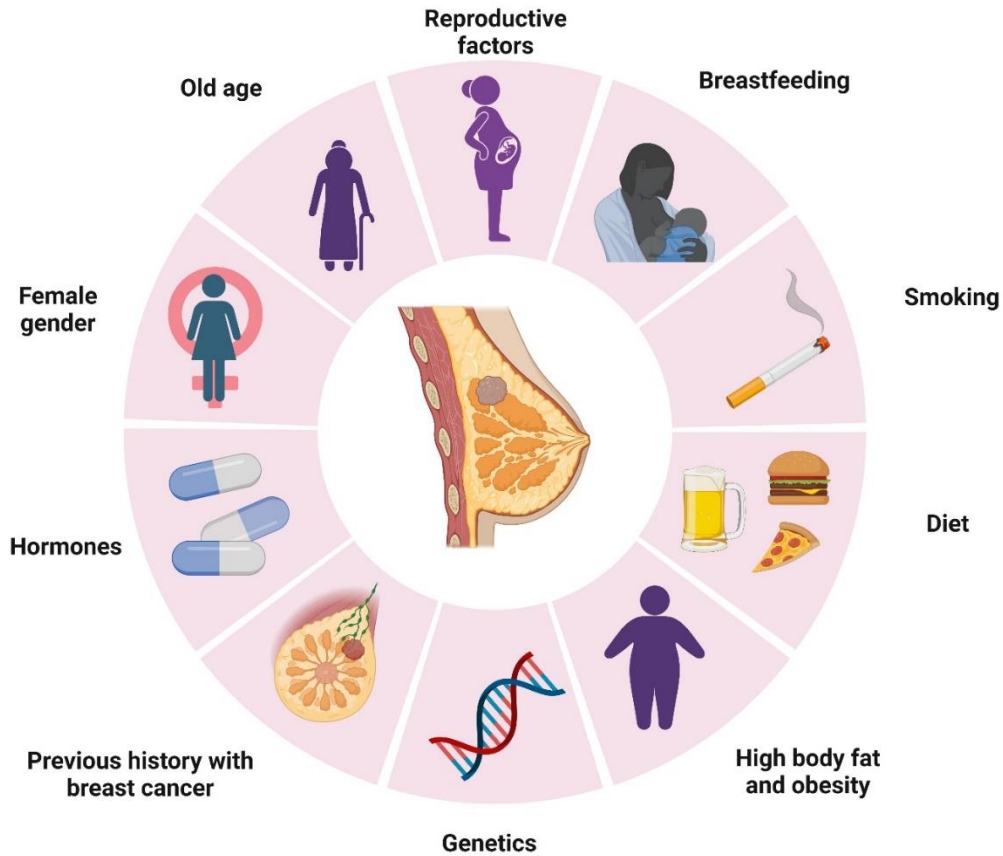


**Figure 2: Schematic illustration of breast cancer risk factors.** Breast cancer risk factors include age, family history or previous diagnosis of breast cancer, lifestyle (obesity, lack of exercise, high fat low fiber diet, alcohol intake), reproductive factors (age of first born, breastfeeding, age of menarche, dense breast), gender, and hormonal intake.

### I.1.3. Breast cancer diagnosis and screening

Imaging techniques are powerful tools to screen, diagnose, and monitor breast cancer treatment progress in patients [11]. **Table 1** summarizes the different imaging techniques used for breast cancer detection and their limitations. Mammography is an X-ray imaging technique and considered the standard method for breast cancer screening [11]. It is highly sensitive, inexpensive, and was shown to decrease breast cancer mortalities by 20% [10–12]. The American Cancer Society (ACS) recommends women between ages 45-65 to get an annual mammogram [13,14]. However, mammography has several limitations including exposure to radiation, pain, anxiety, and high false positive/negative rates especially for women with dense breasts [11,14,15]. Mammography cannot distinguish between liquid and solid lesions thus fails to accurately detect tumour masses [16]. Tomosynthesis, which provides a 3D breast study, showed better accuracy and

lesion type differentiation than mammography [16]. Ultrasound is another widely utilised detection method usually used as a complement for mammography for women with dense breasts and pregnant and breastfeeding women, as it does not involve radiation exposure. Ultrasound improves the sensitivity when used in complement to mammography, but it fails to distinguish cancerous tissues [14,16]. Magnetic resonance imaging (MRI) can detect small lesion that mammography and ultrasound fail to, but it has a low specificity and is expensive. MRI was recommended mostly for women with a high breast cancer risk, and not for the general population [10,14]. CT and PET can be employed to track breast cancer metastasis and response to therapy [14].

**Table 1: Breast cancer screening methods: applications and limitations.**

<b>Method</b>	<b>Application</b>	<b>Limitations</b>
<b>Mammography</b>	Mass screening. Image bone, soft tissues, and blood vessels all at the same time. Shadowing due to dense tissues.	Ionizing radiation, low sensitivity and specificity, sensitivity drops with tissue density increases.
<b>Ultrasound</b>	Evaluate lumps found in mammography, not suitable for bony structures.	Low sensitivity, experienced operator is required during examination, low resolution image.
<b>MRI</b>	Young women with high risk, images small details of soft tissues.	Some types of cancers cannot be detected such as ductal and lobular carcinoma, expensive.
<b>CT</b>	To determine and image distant metastasis in a single exam.	Low sensitivity, radiation risks, expensive scanner
<b>PET</b>	Functional imaging of biological processes. To image metastasis or response to therapy.	Ionizing radiation, radioactive tracer injection

Modified from [14]

Another screening method for breast cancer detection is self-examination. However, it is not scientifically investigated and has no clear benefits but can be an alternative for women in low-income countries. The ACS does not recommend clinical breast examination as a screening method for women of all ages [13].

Once a lesion is detected, the diseased tissue is obtained by biopsy, aspiration, or surgical excision. If cancer is confirmed, the samples will be evaluated for morphology (size) and predictive markers like estrogen receptor (ER), progesterone receptor (PR), and human epidermal growth factor receptor 2 (HER2). Molecular tests like DNA microarrays and polymerase chain reaction (PCR) (like 21-gene Oncotype DX® and 70-gene Mammaprint®) can be used to better diagnose breast cancer [15].

## I.2. The Breast Anatomy

Understanding the breast anatomy (**Figure 3**) is crucial to comprehend the development of breast cancer. The female breast is mainly made up of fat cells called adipose tissues. 12-20 sections of globular tissues, called the lobes, make up the breast. Each lobe is constituted of many smaller milk producing glands called lobules, and the lobes and lobules are connected to each other through the milk ducts, responsible of delivering milk to the nipples during lactation. The breast also contains blood vessels, lymphatic vessels, and lymph nodes [17,18].

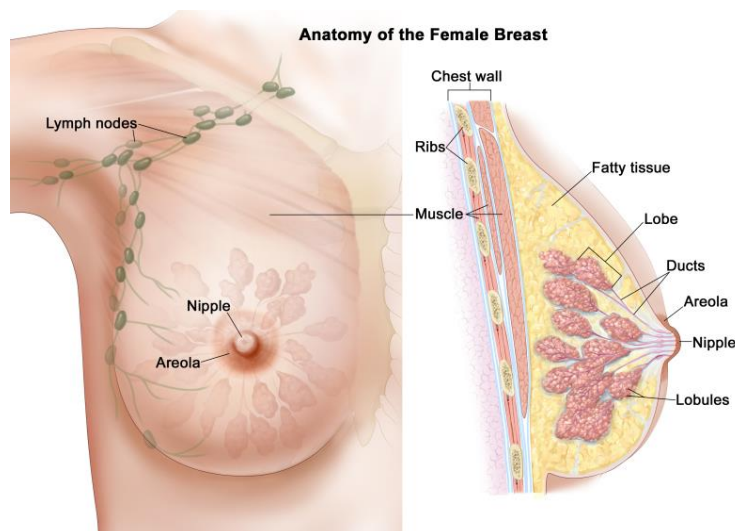


**Figure 3: Anatomy of the female breast.** From [19]

## **I.3. Breast cancer development and characterization**

### **I.3.1. Histological classification of breast cancer**

#### ***I.3.1.1. Histological subtypes***

Breast cancer can be mainly classified into in situ and invasive carcinomas. In situ carcinomas are well localized cancerous mass that do not spread to adjacent tissues and can either arise in the ducts hence termed ductal carcinoma in situ (DCIS), or in the lobules and termed lobular carcinoma in situ (LCIS) (**Figure 4**) [20]. DCIS is more frequent than LCIS, representing around 80% of total in situ carcinoma cases.

On the other hand, as the name implies, invasive breast carcinomas invade the surrounding tissue and can eventually metastasize to other body parts, most frequently to the bone, lung, brain, and liver [21]. The most common types of invasive breast carcinomas are invasive ductal carcinomas that originate in the milk ducts and invasive lobular carcinomas arising in the lobules (**Figure 4**). Invasive ductal carcinomas, now known as invasive breast cancer of no special type (NST) [5], are the most prevalent representing around 70% of invasive breast cancer cases [5,20]. Other less common types of invasive breast cancer are adenoid cystic (or adenocystic) carcinoma, low-grade adenosquamous carcinoma, medullary carcinoma, mucinous (or colloid) carcinoma, papillary carcinoma, and tubular carcinoma [22].

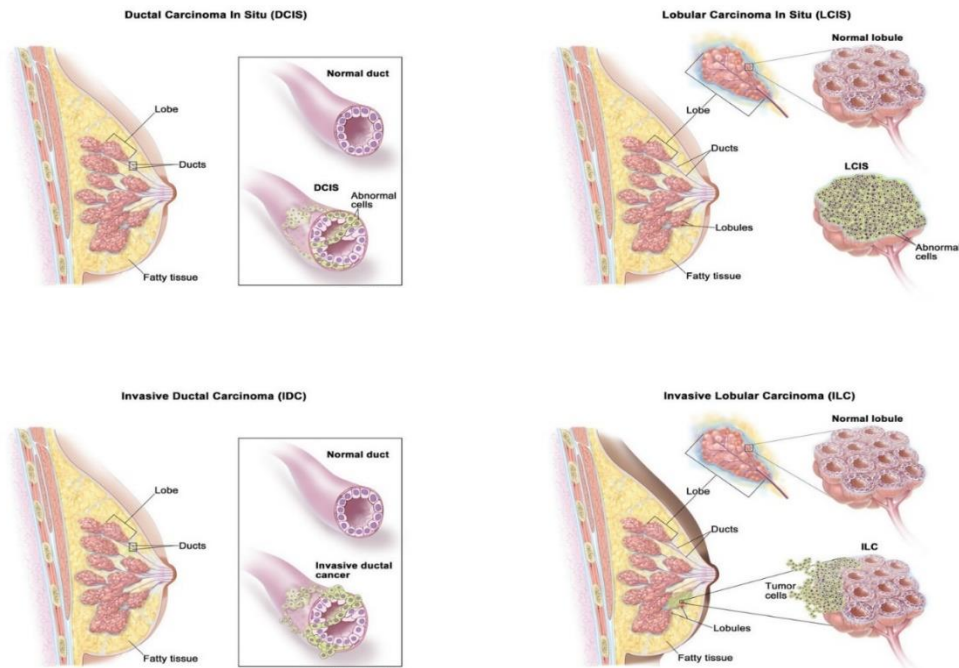


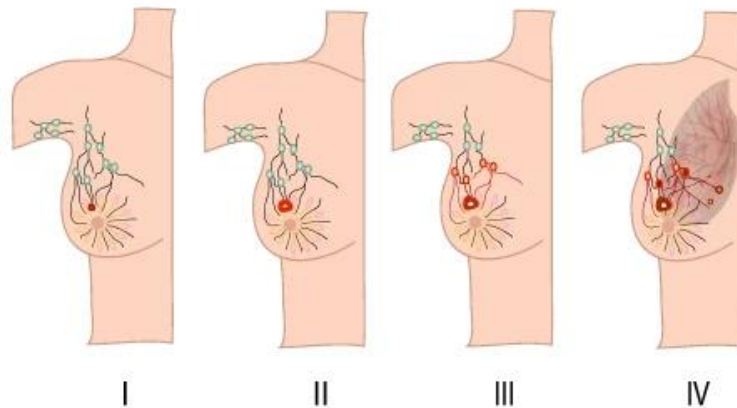
**Figure 4: Histological subtypes of breast cancer.**

### ***1.3.1.2. Breast cancer stage and grade***

Until 2018, a strictly anatomic method termed the tumour-node-metastasis (TNM) was used to evaluate breast cancer staging. The TNM method assesses tumour size (T), if it spread to the lymph nodes (N), and whether it has metastasized (M) [23]. Breast cancer stages are as follows (**Figure 5**) [24]:

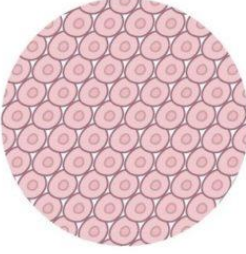
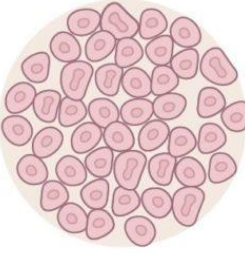
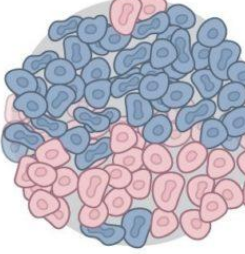
- **Stage 0:** the disease is non-invasive and restricted in the duct and lobules.
- **Stage I:** the tumour is invasive and spreading to the normal breast tissue. Stage IA represents a tumour of 2 cm size that has not spread to lymph nodes, and stage IB is when the tumour is found in the lymph node with/without cancer in the breast tissue.
- **Stage II:** the cancer is invasive. Stage IIA describes either a 2-5 cm tumour in the breast with/without spread to the lymph nodes or cancer cells present in at least 1-3 lymph nodes and not necessarily present in the breast tissue. Stage IIB represents a tumour of 2-5 cm with spread to 1-3 axillary lymph nodes, or a tumour >5 cm that has not spread to the nodes.

- **Stage III:** the cancer is invasive. Stage IIIA is when the tumour is of any size in the breast or in the nodes. It has spread to >4 lymph nodes in the breast or axilla but has not spread to other body parts. Stage IIIB represents a cancer of any size that had reached to the chest wall and could be present in up to 9 lymph nodes. This stage can cause a swelling of the breast (inflammatory breast cancer is considered a Stage IIIB). Stage IIIC is a tumour of any size, and there may be an absence of cancer signs in the breast. The cancer is spread to  $\geq 10$  axillary lymph nodes or nodes above or below the breast- or collar- bone.
- **Stage IV (metastatic):** the cancer is of any size and has spread to other tissues and organs.



**Figure 5: Breast cancer stages.** The stage of breast cancer progression is evaluated using the TNM method. When cancer starts spreading to >4 lymph nodes breast cancer is classified as stage III. Stage IV cancer is when the tumour starts metastasizing outside the breast to other body parts. From [24].

The newest update of the American Joint Committee on Cancer (AJCC) cancer staging manual (8<sup>th</sup> edition) include the integration of prognostic markers in addition to the anatomic ones (TNM) for breast cancer staging. These include the expression of biomarkers (ER, PR and HER2), gene expression profiling (ex: Onco-type DX Breast Recurrence Score [Genomic Health]), and tumour grade [25]. The grade of breast cancer defines the aggressiveness of the tumour and are summarized in **Figure 6**.

Prognosis				Grade
	Grade 1	Grade 2	Grade 3	
				
	<p><b>Glandular/Tubular Differentiation:</b> &gt;75% of tumor forms glands</p> <p><b>Nuclear Pleomorphism:</b> Uniform cells with small nuclei similar in size to normal breast epithelial cells</p> <p><b>Mitotic Count:</b> &lt; 7 mitoses per 10 high power fields</p>	<p><b>Glandular/Tubular Differentiation:</b> 10% to 75% of tumor forms glands</p> <p><b>Nuclear Pleomorphism:</b> Cells larger than normal with open vesicular nuclei, visible nucleoli, and moderate variability in size and shape</p> <p><b>Mitotic Count:</b> 8-15 mitoses per 10 high power fields</p>	<p><b>Glandular/Tubular Differentiation:</b> &lt;10% of tumor forms glands</p> <p><b>Nuclear Pleomorphism:</b> Cells with vesicular nuclei, prominent nucleoli, marked variation in size and shape</p> <p><b>Mitotic Count:</b> &gt; 16 mitoses per 10 high power fields</p>	

**Figure 6: Breast cancer grades.** As the grade of breast cancer increases the patient prognosis worsens. Grade 1 (low grade) breast cancer is when the cancer cells still look similar to normal epithelial cells and do not grow as fast as the higher grades. In grade 2 (moderate grade) breast cancer, cancer cells start looking aberrant and proliferate with faster rates than grade 1 cells. In grade 3 (high-grade) breast cancer, the cancer cells are poorly differentiated and are morphologically different from normal cells. From [26].

### I.3.2. Molecular classification of breast cancer

Perou and Sorlie classified breast cancer into five intrinsic subtypes according to the expression levels of ER, PR and HER2: luminal A, luminal B, HER2-positive, basal-like, and normal-like [5,27,28]. The luminal subtypes express ER and PR and can either carry an HER2 amplification or not. HER2-positive tumours overexpress HER2 and the triple negative breast cancer (TNBC) subtype lacks ER, PR, and *HER2* gene amplification. PAM50 is a 50-gene signature developed in 2009 to predict the intrinsic subtype of breast cancer with >90% accuracy [29]. **Figure 7** illustrates the molecular subtypes of breast cancer, their prognosis and current treatment options.



### ***1.3.2.1. Luminal A and luminal B***

Luminal subtypes correspond to the hormone-expressing breast tumours and are characterized by the expression of ER and ER-associated genes (like *CCND1*) [30].

Luminal A (ER<sup>+</sup>/PR<sup>+</sup>/HER2<sup>-</sup>) are the most common breast cancer subtype representing about 50% of all breast cancer cases [31]. What distinguishes luminal A from the luminal B subtype is the expression level of the proliferation marker Ki67 [10]. Luminal A proliferate slower than the other subtypes and have low Ki67 (<~14%) expression [32]. Therefore, this subtype is the least aggressive and has the best prognosis [31]. Luminal A is associated with high ER signalling, and 45% are mutated for *PIK3CA* [33]. Luminal B, accounting for 20-30% of breast cancer, are ER<sup>+</sup> and PR<sup>+</sup> and can either carry an *HER2* amplification or not (ER<sup>+</sup>/PR<sup>+</sup>/HER2<sup>-</sup> or ER<sup>+</sup>/PR<sup>+</sup>/HER2<sup>+</sup>) [31]. The mostly mutated genes in luminal B are *TP53* and *PIK3CA*, and this subtype shows a DNA hypermethylation phenotype [33].

### ***1.3.2.2. HER2-positive***

HER2-positive breast cancer corresponds to about 10% of breast cancer cases and lacks the expression of ER and PR (ER<sup>-</sup>/PR<sup>-</sup>/HER2<sup>+</sup>) [34]. This subtype is defined by assessing the expression of HER2 by immunohistochemistry (IHC): HER2 IHC score 3+ or IHC score of 2+ with *ERBB2* (coding HER2) gene amplification (assessed by ISH) [35]. HER2-positive breast tumours are highly mutated for the oncogenes *TP53* (72%) and *PIK3CA* (39%) [33] and have high proliferative rates and poor prognosis [35].

### ***1.3.2.3. Basal-like***

The basal-like subtype is so called as its expression pattern resembles that of basal epithelial cells: lack of ER expression, low HER2 expression, expression of basal cell keratins 5/6 and 17, and the expression of proliferation genes [27]. The majority of basal-like tumours are the high-grade TNBC (ER<sup>-</sup>/PR<sup>-</sup>/HER2<sup>-</sup>), usually associated with lower patient age and have the worst prognosis compared to the other subtypes [31]. About 10-20% of breast cancer cases are TNBC [34]. TNBC tumours are highly proliferative, have high risk of metastasis, and most cases carry *TP53* mutations [30,31]. TNBC is commonly associated with defects in the DNA repair mechanisms like *BRCA1/2* mutations. The TNBC subtype will be thoroughly discussed in section II of the thesis.



### 1.3.2.4. Normal-like

The normal-like subtype resembles luminal A IHC profile: hormone receptors-positive, no *ERBB2* gene amplification, and low Ki67. They generally have a good prognosis, but lesser than the luminal A subtype [31].

### 1.3.2.5. HER2-low

Recently, a new HER2 entity was identified, the HER2-low breast cancers. These are breast cancers, that could either be hormonal positive or negative, expressing HER2 with IHC score of 1+ or of 2+ without *ERBB2* gene amplification. Around 60% of luminal and 30% of TNBC were identified to be HER2-low. Although not being of the HER2-positive subtype, these tumours benefited from a treatment targeting HER2, suggesting new possibilities to the management of breast cancer [36–38].

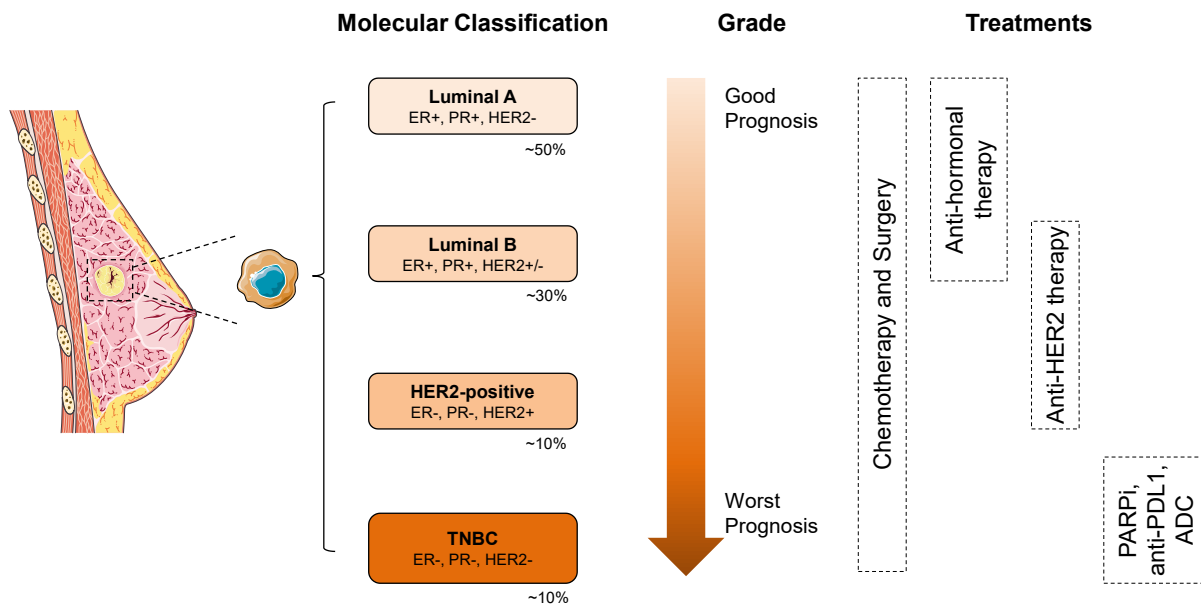


**Figure 7: Breast cancer molecular subtypes.** According to ER, PR, and HER2 expression, breast cancer is molecularly classified into four main intrinsic subtypes: luminal A, luminal B, HER2-positive, and TNBC. These subtypes vary in their grade and prognosis with luminal A having the best prognosis and TNBC having the worst. A common treatment strategy to all subtypes is surgery and chemotherapies. Depending on the subtype, specific targeted therapies like anti-hormonals are administered to breast cancer patients. ADC: antibody-drug conjugate; ER: estrogen receptor; PR: progesterone receptor; TNBC: triple negative breast cancer.

## I.4. Breast cancer treatments

Several types of breast cancer treatment exist. Primary therapy, usually being surgery, can be supplemented with neoadjuvant and/or adjuvant therapy (**Figure 8**). Neoadjuvant therapies, typically including chemo- or hormonal-therapies, help in reducing the size of the tumour and are commonly given before the primary therapy (**Figure 8**). Adjuvant therapies on the other hand are mainly administered after the primary treatment in order to eradicate residual tumour cells/tissue thus minimizing recurrence, and usually include chemotherapies, anti-hormonals, immunotherapy, targeted therapies, and radiotherapy (**Figure 8**). Tumour grade and stage, breast cancer subtype, and patients' preference can impact the choice of surgical procedure, neoadjuvant, and adjuvant therapies to follow.

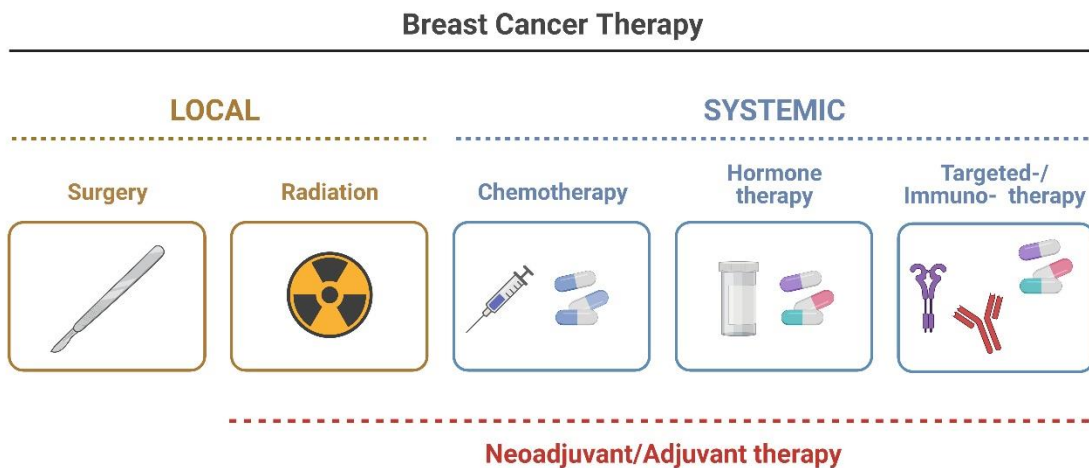


**Figure 8: Types of breast cancer therapies.**

### I.4.1. Surgery

In most breast cancer cases, the main treatment involves localized surgical procedures that have evolved over the years from more radical procedures like mastectomy to breast-conserving surgery [39]. Mastectomy involves removing all of the breast tissues followed by breast reconstruction [40]. There are two types of mastectomy, simple mastectomy referring to the surgical removal of all the breast and modified radical mastectomy where, in addition to the breast, the axillary lymph nodes are also excised (**Figure 9A**) [39,40]. Radical mastectomy is the most commonly applied form of mastectomy in modern medicine. Breast conserving surgery, also referred to as lumpectomy, quadrantectomy,

or partial mastectomy, is the removal of cancer and adjacent normal tissues while preserving the breast (**Figure 9B**) [40].

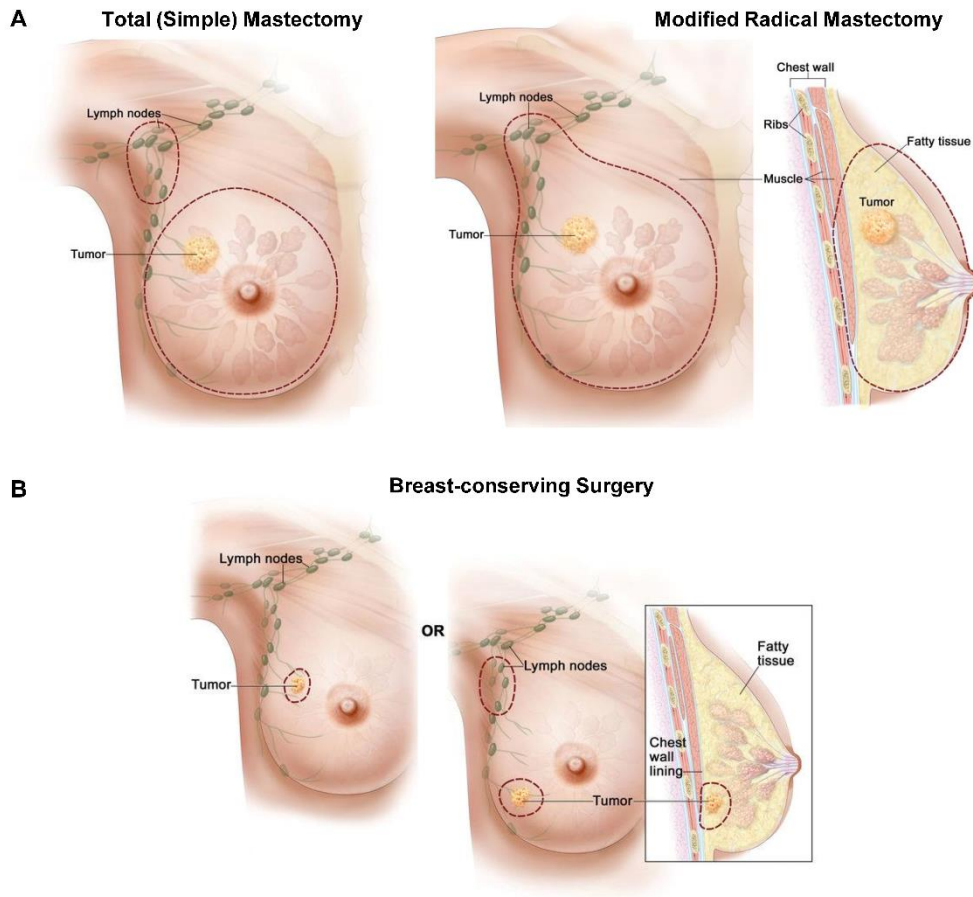


**Figure 9: Types of breast cancer removal surgeries.** (A). Mastectomy refers to the removal of all breast tissues. Modified radical mastectomy is a type of mastectomy that involves the removal of axillary lymph nodes with the breast. (B). Breast-conserving surgery removes only cancerous tissues and preserve the breast. From [19].

#### I.4.2. Radiotherapy

Radiation therapy is targeting cancer cells with high energy x-rays to eliminate them without impacting the normal tissue. It is typically performed after surgery to abolish any remaining cancer cells and prevent recurrence. The most used radiotherapy techniques include breast radiotherapy, chest-wall radiotherapy (after mastectomy), and breast boost. Breast radiotherapy types include intraoperative radiation therapy (IORT), 3D-conformal radiotherapy (3D-CRT), intensity-modulated radiotherapy (IMRT), and brachytherapy [5]. IORT, 3D-CRT, and IMRT are external-beam radiation, meaning that

the radiation is delivered through a machine outside the body and specifically targets the cancer site. Brachytherapy (internal radiation) delivers radiation in a different method. Instead of directing radiation beams, a device containing the radioactive substance is placed in the breast tissue for a short time. Radiotherapy following breast surgery decreases local recurrence and improves overall patient survival [41]. The major side effect of radiotherapy is cardiotoxicity. Minimizing exposure to the heart and lungs can be achieved via respiratory control, prone positioning, and intensity-modulated radiotherapy [34].

### **I.4.3. Chemotherapies**

#### ***I.4.3.1. Types of Chemotherapy***

Chemotherapies are drugs that typically target highly proliferative cells, like tumour cells, and are given either in the neoadjuvant or adjuvant settings. There are different classes of anticancer drugs: alkylating agents, DNA intercalating agents, purine and pyrimidine anti-metabolites, and microtubule-targeting agents. Chemotherapies are often given in combinations.

Alkylating agents cause DNA crosslinking by adding alkyl groups ( $C_nH_{2n+1}$ ) to DNA nitrogen bases thus inhibiting DNA synthesis and repair. Defects in DNA pathways cause the killing of cancer cells. The most common alkylating agent given to patients is cyclophosphamide (nitrogen mustard) [42]. Platinum salts like carboplatin and cisplatin function in a similar mechanism and are typically given to breast cancer patients [43]. Recently, several reports are suggesting that cells with defects in the DNA damage response (DDR) pathway are more sensitive to platinum agents [43]. Thus, defects in DNA repair mechanisms could be predictive biomarkers of response for platinum agent treatment.

DNA intercalating agents are molecules that insert between DNA base pairs. Intercalating agents like anthracyclines inhibit topoisomerase II leading to the inhibition of replication and transcription causing death of dividing cancer cells [44]. The most common DNA intercalating agents used for breast cancer treatment are anthracyclines like doxorubicin (also called Adriamycin) and epirubicin.

Anti-metabolites are purine/pyrimidine analogues that inhibit enzymes required for metabolism and DNA synthesis leading to apoptosis. The most widely used antimetabolites for breast cancer treatment are 5-fluorouracil (5-FU) (nucleoside analogue), methotrexate (dihydrofolate reductase inhibitor), and gemcitabine [45].

Microtubule-targeting agents cause mitotic arrest by inhibiting mitotic spindle formation and chromosomes segregation therefore impairing cell proliferation [46]. Taxanes like paclitaxel and docetaxel are a standard treatment given to breast cancer patients [46,47].

Although being a standard regimen for treating breast cancer, chemotherapies have severe side effects and drastically affect the life quality of patients. The different classes of anti-cancer drugs can cause nephrotoxicity, hepatotoxicity, neurotoxicity, cardiotoxicity, and haematological toxicities [48].

Using chemotherapies in combination improves the overall response, however, advantageous outcomes on patient survival are less investigated [49]. A traditional regimen for breast cancer is combining an alkylating agent like cyclophosphamide with antimetabolites such as methotrexate and 5-FU [49]. Other combinations between chemotherapies were assessed in clinical trials for breast cancer treatment and include docetaxel and doxorubicin (AT); docetaxel and epidoxorubicin; docetaxel after doxorubicin and cyclophosphamide; docetaxel and carboplatin; 5-FU, doxorubicin, and cyclophosphamide (FAC); doxorubicin and cyclophosphamide (AC); cyclophosphamide, methotrexate, and 5-FU (CMF); anthracycline and taxane; paclitaxel and doxorubicin [49]. Some of these combinations are approved by the Food and Drug Administration (FDA).

#### ***1.4.3.2. Neoadjuvant chemotherapy***

Administering chemotherapy before or after surgery is equally effective [34]. The NSABP-B-18 trial revealed that administering doxorubicin and cyclophosphamide in the neoadjuvant settings decreased the rate of axillary metastasis in breast cancer [50]. The subtype of breast cancer can impact the response to neoadjuvant chemotherapies. For instance, in HER2-positive and TNBC subtypes, being more likely sensitive to chemotherapies, using neoadjuvant chemotherapy could maximize the patient's pathologic complete response (pCR) [34].

### ***1.4.3.2. Adjuvant chemotherapy***

Adjuvant chemotherapy is typically given to patients with high risk of recurrence or metastasis. The standard regimen includes anthracyclines and taxanes. Two most common adjuvant chemotherapy strategies are: (i) doxorubicin and cyclophosphamide (4 cycles) followed by paclitaxel (4 cycles) and (ii) same combination as (i) followed by paclitaxel (12 weeks) or docetaxel (four cycles). Adjuvant chemotherapies are more beneficial for hormonal negative breast tumours than hormone positive ones [34]. Depending on the subtypes, adjuvant chemotherapy can be coupled to other targeted therapies like anti-hormonals and anti-HER2.

### **1.4.4. Endocrine therapy: Luminal breast tumours**

The main strategy to treat hormonal positive breast cancer is by endocrine therapy that directly targets the ER or that interferes with estrogen synthesis. The types of endocrine therapies are estrogen receptor modulators (SERMs), selective modulators estrogen receptor degraders (SERDs), and aromatase inhibitors (AIs). Endocrine therapy can either be given in the neoadjuvant or adjuvant settings. SERMs compete with estrogen for ER binding, changing its ligand-binding domain conformation and prevents co-factor recruitment therefore inhibiting the expression of ER-regulated genes like cyclin D1. Examples of SERMs include tamoxifen, toremifene, raloxifene, and bazedoxifene. The most known SERM is tamoxifen, dating back to the 1970s and approved by the FDA [34]. SERDs, like fulvestrant, entirely block the ER signalling pathway. Fulvestrant binds with a higher affinity to ER compared to tamoxifen, and it blocks ER dimerization and its nuclear translocation leading to ER degradation. AIs, that could either be steroidal or non-steroidal, inhibit the enzymatic activity of aromatase, an enzyme involved in androgens and estrogen synthesis. Exemestane is a steroidal AI that inhibits aromatase by irreversibly binding to its substrate binding site. AIs are typically given in the adjuvant therapy and can be combined with tamoxifen [34].

### **1.4.5. HER2 targeted therapies**

Since HER2-positive breast cancers overexpress HER2, therapies targeting the receptor were developed and are now essential in the management of HER2-positive breast cancer. There are three main types of anti-HER2 therapies: anti-HER2 antibodies, small

tyrosine kinase inhibitors (TKIs), and antibody-drug conjugates (ADC) directed against HER2.

#### ***1.4.5.1. monoclonal antibodies***

The first successful monoclonal antibody against HER2 is trastuzumab (Herceptin) that was FDA approved in 1998 [34,51]. Trastuzumab binds the extracellular domain (ECD) of HER2 preventing ECD cleavage and HER2 dimerization, therefore inhibiting its intracellular signalling. Trastuzumab leads to cell cycle arrest and promotes antibody-dependent cell-mediated cytotoxicity (ADCC) [52]. Trastuzumab is given in the neoadjuvant or adjuvant therapy for breast cancer treatment, either alone or in combination with chemotherapies or other anti-HER2 therapies [34,52,53]. A second antibody against HER2, pertuzumab (Perjeta), was developed. Similar to trastuzumab, pertuzumab binds the ECD of HER2 (on a different site than that of trastuzumab) inhibiting its signalling and leading to ADCC. Several clinical trials demonstrated a benefit in combining pertuzumab with trastuzumab and chemotherapies in the adjuvant and neoadjuvant settings [51]. A main disadvantage of these anti-HER2 antibodies is that patients develop resistance towards them. Hence, new approaches to target HER2 were developed.

#### ***1.4.5.2. Tyrosine kinase inhibitors***

TKIs are small molecule inhibitors that bind the catalytic domain of HER2 competing with ATP and preventing its kinase activity and downstream signalling cascade [34,51]. Lapatinib (Tykerb/Tyverb®) is a reversible dual EGFR (HER1) and HER2 TKI that could reverse the resistance to trastuzumab *in vitro* [51,54]. It was the first HER2 TKI to gain FDA approval in 2007 [55]. Chemotherapy combined with lapatinib and trastuzumab was more effective than chemotherapy combined with either lapatinib or trastuzumab alone in the neoadjuvant therapy [56]. Lapatinib can be given in combination with AIs (letrozole) in advanced or metastatic luminal breast cancer [34]. Neratinib (HKI-272; Nerlynx®) is an irreversible EGFR\HER2\HER4 inhibitor FDA approved (2017) for early stage HER2-positive breast cancer after one year of trastuzumab treatment, and for metastatic HER2-positive breast cancer patients after receiving two HER2-directed therapies [55]. Pyrotinib is another pan-HER inhibitor that is still under clinical investigation, however, is approved

by the Chinese State Drug Administration in combination with the chemotherapy capecitabine (antimetabolite) for the treatment of advanced or metastatic HER2-positive breast cancer [34,51,57]. Tucatinib (Tukysa®) is a TKI highly selective for HER2 (>1000 potency to HER2 compared with EGFR). Based on the results of the phase 3 HER2CLIMB clinical study, tucatinib gained FDA approval in 2020 for the treatment of metastatic HER2-positive breast cancer in combination with trastuzumab and capecitabine [51,55,57].

#### ***1.4.5.3. Antibody-drug conjugates***

ADCs are mono-clonal antibodies (mAbs) attached to cytotoxic molecules through synthetic linkers, hence combining the high anti-tumour potency of chemotherapies with the high selectivity of mAbs [58]. Currently, there are two FDA approved ADCs against HER2 for the treatment of breast cancer [59]. Trastuzumab-emtansine (T-DM1) is the first developed anti-HER2 ADC and is composed of trastuzumab linked to DM1 [51]. T-DM1 is approved for the treatment of metastatic HER2-positive breast cancer. Recently, T-DM1 was shown to be beneficial also for patients with recurrence risk following neoadjuvant therapy [51,59]. The second developed ADC against HER2 is Trastuzumab deruxtecan (T-DXd) that is FDA approved for the treatment of advanced-stage HER2-positive breast cancer which previously received at least two anti-HER2 therapy [59]. Importantly, HER2-low breast cancers, whether hormonal positive or negative, responded to the treatment with T-DXd leading to its FDA approval for the treatment of HER2-low breast cancer patients [36,37,59]. These results are highly important as they present HER2-targeted therapies not only for HER2-positive breast cancer, but also for the luminal and TNBC subtypes classified as HER2-low.

#### ***1.4.6. PARP inhibitors***

About 10% of breast cancer patients carry germline mutations, typically causing the loss of function of genes critical for DNA repair and cell cycle regulation [60]. *BRCA1* and *BRCA2*, two key genes in the DNA damage repair pathway, are mutated in at least 5% of breast cancer patients. Women carrying *BRCA1/BRCA2* mutations have 70% risk of contracting breast cancer compared to 10% in other women [60,61]. Germline mutations in *BRCA1* are more frequent in TNBC, while those in *BRCA2* are more common in



hormonal-positive breast cancer [61]. *BRCA* mutations are present in 23% of TNBC patients and 5% of hormonal-positive patients [60]. Poly(ADP-ribose) polymerase 1 and 2 (PARP1 and PARP2) are two enzymes important for the base excision repair (BER) pathway, initiated from DNA single strand breaks. On the contrary, *BRCA1* and *BRCA2* are involved in homologous recombination (HR) to repair double strand breaks, which form when the single breaks are not repaired [60]. A synthetic lethality concept based on targeting the DNA damage response pathway is being applied for breast cancer patients. By targeting PARP enzymes with PARP inhibitors in cells deficient in the HR pathway (*BRCA1/2* mutations for example), DNA double strand breaks accumulate and are repaired by the non-homologous end joining (NHEJ) pathway instead of the HR pathway. NHEJ is more error-prone eventually leading to the death of cancer cells (**Figure 10**). Normal cells with active HR pathway are not affected by the inhibition of PARP as they are able to repair the DNA damage caused (**Figure 10**) [60]. Based on OlympiAD and EMBRACA clinical trials, two PARP inhibitors, olaparib and talazoparib, are FDA approved for the treatment of *BRCA1/2* mutation carriers in HER2-negative breast cancer [60].

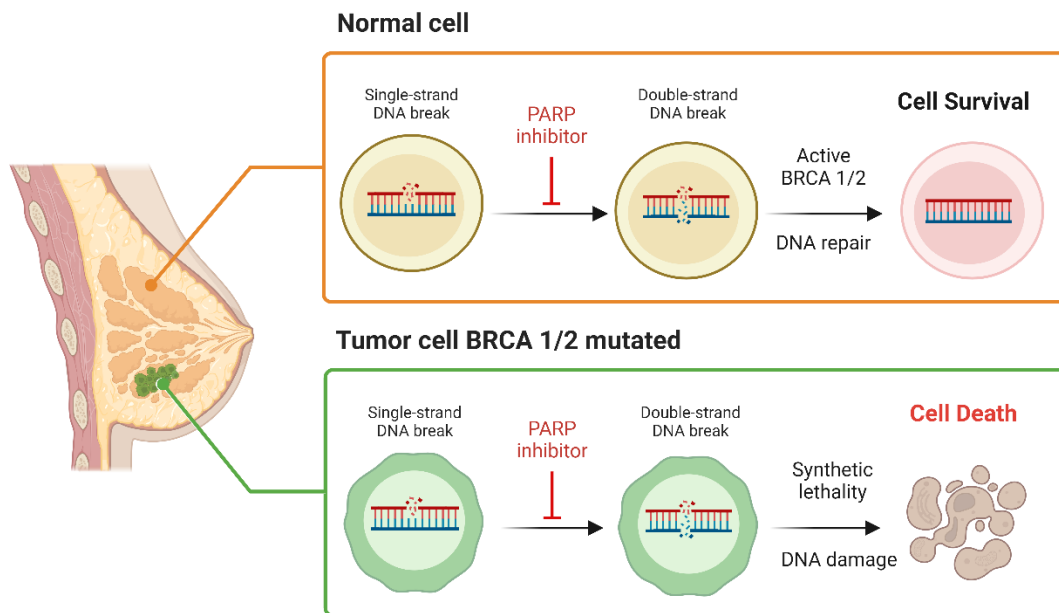


**Figure 10: Synthetic lethality using PARP inhibitors in *BRCA1/2* mutated cells.** In normal breast cells, double strand DNA breaks caused by PARP inhibitors can be repaired by the HR pathway leading to cell survival. In *BRCA1/2* mutated cancer cells, PARP inhibition causes an accumulation of double strand DNA

breaks that cannot be repaired by HR. Accumulation of DNA damage ultimately leads to the death of cancer cells.

#### **I.4.7. Immunotherapy**

Cancer immunotherapy relies on boosting the patient's immune system to kill cancer cells and can be of several types. Immune checkpoint therapy is based on targeting immune checkpoint inhibitors like the receptors PD-1 and CTLA4 to boost T cell activation towards tumour cells. Adoptive T cell therapy is based on growing tumour infiltrating lymphocytes and directing them against cancer cells, then re-infusing them to the patient. An interesting immunotherapeutic approach is the development of cancer vaccines. These could be either prophylactic to prevent or reduce the risk of cancer caused by viral infections like hepatitis B and human papillomavirus, or therapeutic vaccines that harness the immune system to eliminate cancer cells [62,63]. The PD1/PDL-1 checkpoint inhibitors, pembrolizumab and atezolizumab are FDA approved for the treatment of TNBC [63,64]. The efficiency of immunotherapy for luminal and HER2-positive subtypes is still under investigation.

#### **I.4.8. Other targeted therapies**

Targeting the cell cycle components and the mTOR/PI3K/AKT pathway is being investigated for treating breast cancer, specifically the luminal subtypes. Everolimus (an mTOR inhibitor) and Alpelisib (PI3K p110 $\alpha$  isoform inhibitor) are FDA approved for the treatment of luminal breast cancer. Pan-PI3K inhibitors that target all PI3K isoforms are highly toxic and not efficient for treating hormonal-positive breast cancer. Three CDK4/6 inhibitors palbociclib, ribociclib, and abemaciclib are approved for treating ER<sup>+</sup>/HER2<sup>-</sup> breast cancer either in combination with AIs as a first line of treatment or in combination with fulvestrant (SERD) as a second line of treatment. Although still not approved, cell cycle and mTOR/PI3K/AKT pathway inhibitors are under clinical investigation for the treatment of TNBC and HER2-positive subtypes [34].

## Summary

Breast cancer remains a leading cause of cancer incidence and related mortalities in females worldwide. According to histological and molecular features, breast cancer is classified into several subtypes differing in their prognosis and treatment strategies. At the molecular level, breast cancer subtypes include hormonal-positive (luminal) tumours, HER2-positive tumours, and TNBC. The luminal subtypes are less aggressive than HER2-positive and TNBC and are mainly treated with chemotherapies and anti-hormonals. The HER2-positive subtype is primarily treated with anti-HER2 therapies, including anti-HER2 antibodies, TKIs, and ADCs. TNBC is the most aggressive with the poorest prognosis and is primarily treated with chemotherapies.

## II. Triple Negative Breast Cancer

As previously mentioned in section I, TNBC accounts for ~15% of breast cancer and is ER<sup>-</sup>PR<sup>-</sup>HER2<sup>-</sup>. It has the worst prognosis among breast cancer subtypes and is characterized by high metastatic rates and recurrence. As this thesis is focused on TNBC, I will discuss in this section the different subtypes of TNBC, its current treatments, and the challenges facing its management.

### II.1. Generalities: risk factors, molecular features, and prognosis

Hispanic and African American women are at higher risk of contracting TNBC, and African American women have higher TNBC related mortality rates than white women [65]. Women aged less than 40 years old, those carrying *BRCA1* mutations, and women taking contraceptive pills for long durations are at higher risk of TNBC [66]. TNBC 5 years survival rate is lower than the other subtypes, and more than 50% of TNBC patients relapse after 3-5 years following diagnosis [67]. Other risk factors for TNBC include those discussed in section I (risk factors of breast cancer). In addition to *BRCA1*, TNBC is mutated for other cancer-related genes, 80% of TNBC carry *TP53* mutations and a high percentage show loss of *RB1* and *BRCA1* [33]. TNBC is also highly mutated for *PIK3CA* and have high PI3K/AKT pathway activation. PIK3CA, KRAS, BRAF and EGFR proteins are overexpressed in the basal-like subtypes [33].

### II.2. TNBC inter-tumoral heterogeneity

TNBC has been classified into six molecular subgroups by analysing gene expression profiles from breast cancer data sets [68]. Such classification sheds a light on the heterogeneity of TNBC, a characteristic that largely contributes to its complex nature and challenging treatment. These six TNBC subgroups are: basal-like 1 (BL1), basal-like 2 (BL2), mesenchymal (M), mesenchymal stem-like (MSL), immunomodulatory (IM), and luminal androgen receptor (LAR) (**Figure 11**) [68]. Few years later, in 2016, this classification was refined and excluded the IM and MSL subtypes, as the transcripts in these two subgroups were contributed from tumour infiltrating lymphocytes and stromal cells [69]. Therefore, I will only state the characteristics of the refined Lehmann TNBC classification (TNBCtype-4): BL1, BL2, M, and LAR [69]. Besides the Lehmann classification, other groups proposed different methods for TNBC subtyping [70–74].

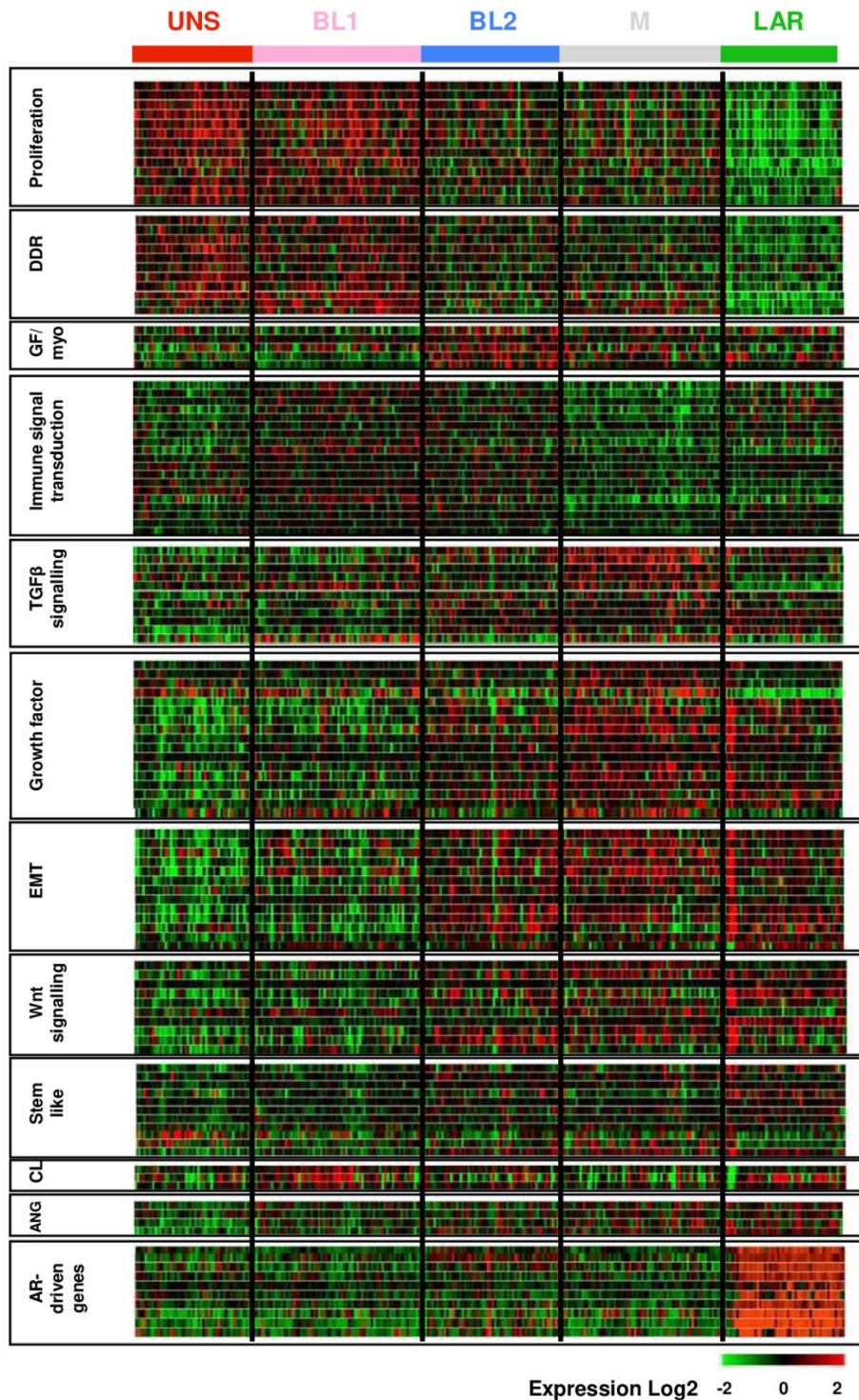


**Figure 11: Gene expression profile of TNBC subgroups from the Lehmann classification.** Heat map of relative gene expression (log<sub>2</sub>) associated with different pathways in the TNBC subgroups. UNS: unstable; BL1: basal-like 1; BL2: basal-like 2; M: mesenchymal; LAR: luminal androgen receptor; Myo: myoepithelial; CL: claudin; ANG: angiogenesis; DDR: DNA damage response; GF: growth factor; EMT: epithelial to mesenchymal transition. Modified from [68].



### **II.2.1. BL1 and BL2 subtypes**

The BL1 subtype is enriched in proliferative (like *PLK1*, *AURKA*, *AURKB*, *CCNA2*, *MYC*, *TTK* etc.) and DDR (like *CHEK1*, *RAD54BP*, *RAD51*, *RAD21* etc.) genes (**Figure 11**). BL1 is accompanied with increased DDR pathways and an elevated expression of Ki67 reflecting its highly proliferative profile.

The BL2 subtype is enriched in growth factor signalling pathways like the EGF and Wnt/ $\beta$ -catenin pathways and display elevated level of growth factor receptors like EGFR (**Figure 11**). Metabolic pathways like glycolysis and gluconeogenesis are also elevated in the BL2 subtype [68]. As they are highly proliferative, the basal-like subtypes could respond better to antimitotic drugs like taxanes (paclitaxel and docetaxel) [68].

### **II.2.2. Mesenchymal subtype**

The M subtype is enriched in genes involved in cell motility (Rho), extracellular matrix receptor interaction, and differentiation pathways (like Wnt and TGF $\beta$  pathways). Of note, these cancers are enriched in EMT-related genes and express low levels of E-cadherin, characteristic of mesenchymal cells (**Figure 11**) [68].

### **II.2.3. Luminal androgen receptor subtype**

The most distinct feature of the LAR subtype is its overexpression of the androgen receptor (AR) at both mRNA and protein levels, and therefore is enriched in AR signalling and expresses AR downstream targets and coactivators. The LAR subtype displays gene enrichment patterns similar to the luminal breast cancer subtypes, which is the reason behind its nomenclature [68]. Of note, the expression of AR positively correlates with the HER2-low TNBC entity [38].

### **II.2.4. Prognosis of the different TNBC subtypes**

The LAR subtype is diagnosed in older age women compared to the other subtypes. The overall survival (OS), pCR, and relapse free survival (RFS) of BL1 patients is the highest compared to the other three subgroups. Although the tumour size does not correlate with the different TNBC subtypes, non-basal tumours are likely to be of lower grade. Albeit basal tumours have the highest grade, non-basal tumours are more clinically advanced and have a higher stage. The LAR subtype has the highest percentage (~50%) of lymph

node metastasis, and the M and LAR subtypes have the highest frequency of lung and bone metastasis respectively [69].

### II.2.5. TNBC cell line models

Lehmann *et al.* assigned a panel of TNBC cell lines to the different TNBC subtypes described (**Figure 12**) [68]. TNBC cell lines respond differently to therapeutic agents. For instance, basal cell lines are more sensitive to PARP inhibitors [68], LAR cell lines are more sensitive to bicalutamide (AR antagonist) [68], CDK 4/6 inhibitors [75], and 17-DMAG (Hsp90 inhibitor) [68], and the M subtype are more sensitive to dasatinib (Src inhibitor) [68].

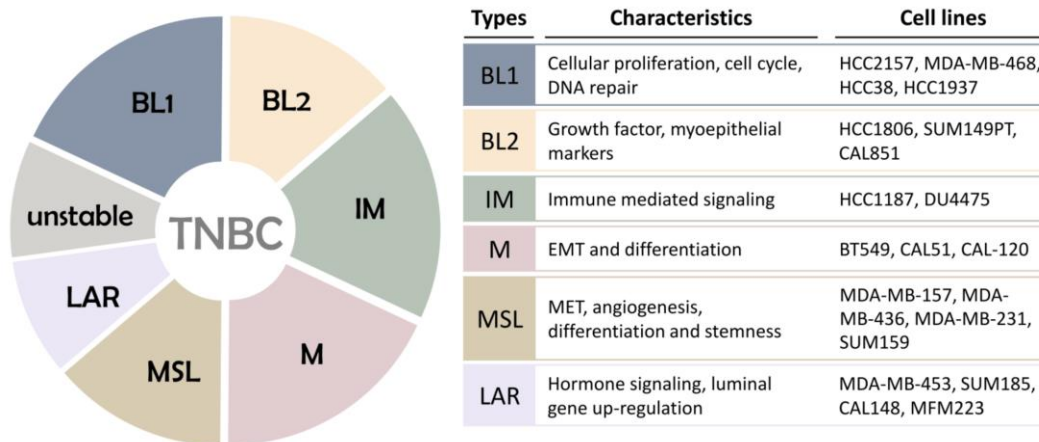


**Figure 12: TNBC cell lines molecular subtypes.** The different TNBC cell lines are associated with distinct characteristics and cellular pathways, with each encompassing several cell lines serving as in vitro models for the disease. From [76].

### II.3. Approved TNBC therapies

As TNBC lacks hormonal receptor expression and the amplification of *ERBB2*, few options to treat TNBC besides chemotherapy were available until recently.

The standard TNBC treatment option is chemotherapies like taxanes and anthracyclines. The conventional doxorubicin, cyclophosphamide, and paclitaxel (ACT) neoadjuvant chemotherapy yields a 35-45% pCR in TNBC patients [77]. As previously mentioned, (section I), breast cancers with germline *BRCA1/2* mutations are particularly sensitive to PARP inhibitors. It is therefore not surprising that the two PARP inhibitors olaparib and talazoparib are FDA approved for TNBC treatment [78–80]. Similar to PARP inhibitors,

TNBC with *BRCA1/2* mutations are more likely to benefit from a treatment regimen containing platinum salts [67,81]. Starting from 2020, immunotherapy is being implemented for TNBC treatment after the promising results of the clinical trials KEYNOTE-355 and KEYNOTE-522. FDA approved the PD-1 inhibitor pembrolizumab in combination with chemotherapy for the treatment of metastatic and early stage (at high risk) TNBC in the neoadjuvant therapy and can be continued as a single agent in the adjuvant treatment [81–83].

ADCs are paving the way for reduced treatment toxicities by directing chemotherapies specifically toward tumour cells. In 2021, the ADC sacituzumab govitecan (SG) was FDA approved for metastatic TNBC patients prior to receiving two or more systematic treatments, with at least one being for metastatic disease [81,82,84]. Till date, SG is the only ADC approved for TNBC treatment though others are under investigation. SG is composed of an antibody directed against trophoblast cell-surface antigen 2 (Trop2) linked to the chemotherapy SN-38 (topoisomerase I inhibitor). Trop2 is a  $Ca^{2+}$  signal transducer highly expressed in different cancers including the breast. SG is hence directed to cancer cells through Trop2 expression and delivers SN38 specifically to them without affecting normal tissue [81,84,85]. As mentioned in section I, the anti-HER2 ADC trastuzumab deruxtecan is approved for TNBC classified as HER2-low [36–38,81].

#### **II.4. TNBC chemoresistance**

Although TNBC responds better to chemotherapies than the other breast cancer subgroups, TNBC patients tend to develop resistance to treatments and a high percentage experience relapse 5-years following diagnosis. Therefore, extensive research has been conducted to understand the underlying mechanisms of TNBC resistance, that can aid in developing new treatment approaches. Several processes contribute to TNBC resistance such as its intra- and inter-tumoral heterogeneity, efflux mechanisms, enrichment in breast cancer stem cells (BCSC), alteration of signalling pathways, and resistance to apoptosis (**Figure 13**) [86].



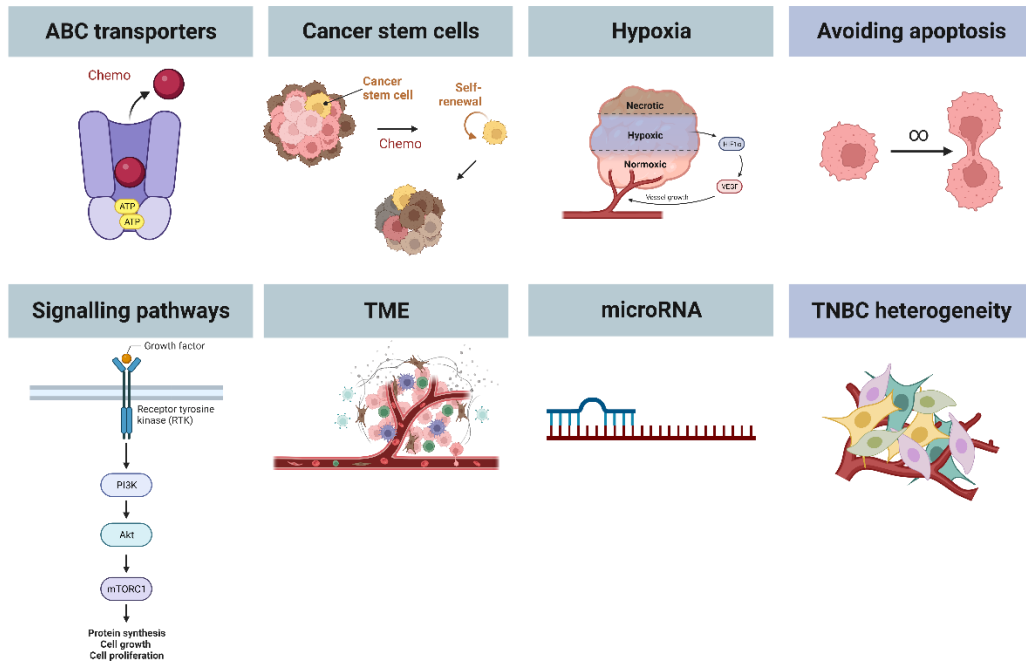


**Figure 13: Causes of TNBC chemoresistance.** TNBC chemoresistance was attributed to several factors such as drug efflux through ABC transporters, BCSCs, metabolic alterations like hypoxia, resistance to apoptosis and continuous cell division, alterations in signalling pathways, components of the tumour microenvironment, microRNAs, and the high heterogenous nature of TNBC. ABC: ATP-binding cassette; chemo: chemotherapy; TME: tumour microenvironment; TNBC: triple negative breast cancer.

#### II.4.1. ATP-binding cassette (ABC) transporters

ABC transporters use ATP to efflux compounds, including different chemotherapies, across the cell membrane contributing to chemoresistance [86]. The components of ABC transporters ABCC1, ABCG2, and ABCC11 are overexpressed in breast cancer, more frequently in TNBC [87,88]. These proteins confer TNBC resistance to a number of chemotherapies including anthracyclines, taxanes, methotrexate, 5-Fluorouracil, doxorubicin, and irinotecan [89,90]. Despite the lack of clear clinical data, pre-clinical investigations support the concept of inhibiting ABC components to reverse TNBC chemoresistance [86].

#### II.4.2. Breast cancer stem cells

Cancer stem cells (CSCs), also called tumour initiating cells (TIC), are a population of cancer cells with self-renewal abilities [91,92]. In breast cancer, three main markers identify the population of BCSCs, CD44, CD24, and aldehyde dehydrogenase 1 (ALDH1) [91–93]. The expression of these markers identifies two lineages of BCSCs, the

CD44<sup>+</sup>/CD24<sup>-</sup> or the ALDH1<sup>+</sup>. The CD44<sup>+</sup>/CD24<sup>-</sup> BCSCs usually have a mesenchymal or myoepithelial-like phenotype and as low as 100 cells are capable of initiating cancer formation. They are present at the periphery of the tumour and were found enriched at lung metastasis sites, suggesting their role in metastasis and invasion. ALDH1<sup>+</sup> BCSCs are typically located at the centre of the tumour and have a more luminal or epithelial phenotype. 500 ALDH1<sup>+</sup> cells can drive tumour formation and cancers with high ALDH1 staining are extremely aggressive. TNBC has more CD44<sup>+</sup>/CD24<sup>-</sup> and ALDH1<sup>+</sup> cells compared to luminal and HER2-positive subtypes, which could explain the aggressive nature, high metastatic potential, and treatment resistance of this subtype [93]. Chemotherapy treatment increases the population of BCSCs implying that they are resistant, and these cells can re-initiate tumour formation therefore suggested to be an important cause of cancer relapse (**Figure 14**) [92]. As TNBC is enriched in BCSCs, BCSCs largely contribute to TNBC chemoresistance, probably through different developmental and proliferative signalling pathways activated in BCSCs like TGF $\beta$ , notch, Wnt/ $\beta$ -catenin, and hedgehog pathways [86,91].

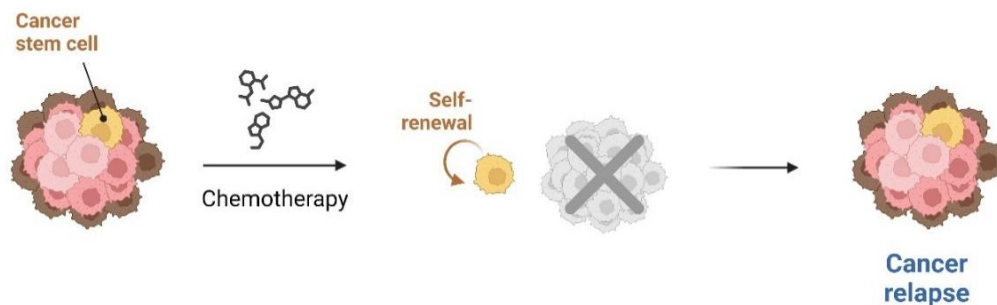


**Figure 14: BCSCs contribute to cancer relapse.** Chemotherapy treatment is able to eradicate cancer cells with the exception of BCSCs. Due to their self-renewal ability, residual BCSCs are able to re-initiate the bulk of tumour and eventually causing cancer relapse.

#### ***II.4.2.1. TGF $\beta$ pathway***

TGF $\beta$  is a cytokine that binds to the TGF $\beta$  receptor (TGF $\beta$ R). Upon TGF $\beta$  binding, TGF $\beta$ R recruits and phosphorylates the effectors SMAD2 and SMAD3. Phospho- SMAD2 and SMAD3 recruit SMAD4 forming a complex that translocates to the nucleus and regulates the transcription of target genes (**Figure 15**) [86]. TGF $\beta$  signalling pathway regulates EMT, proliferation, metastasis, chemoresistance, and the regulation of stemness [86]. It was shown that upon chemotherapy treatment in TNBC, the activity of TGF $\beta$  increases

and inhibiting TGF $\beta$  in a TNBC xenograft prevents relapse [94]. Moreover, TGF $\beta$  signalling supports BCSCs renewal and increases their population [95,96]. Inhibitors targeting the TGF $\beta$ R are still under clinical investigation for TNBC.

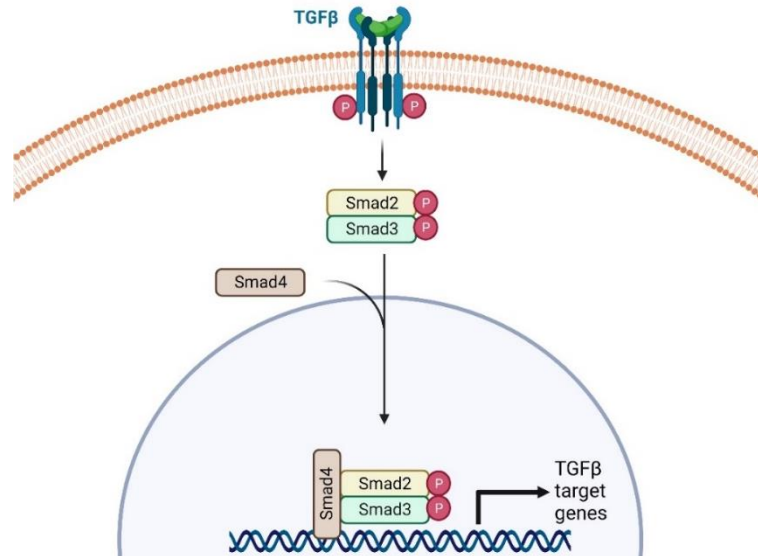


**Figure 15: the TGF $\beta$  pathway.**

#### ***II.4.2.2. Notch pathway***

Notch pathway requires cell-cell contact, where the Notch receptors comprised of four members (Notch 1-4) bind to five transmembrane ligands (Delta-like 1,3,4 and JAGGED-1,2). Binding of notch receptors to their ligands causes the cleavage of the intracellular domain of notch receptor and its nuclear translocation where it activates the transcription of target genes (**Figure 16**) [97]. Notch pathway is implicated in all hallmarks of cancer like EMT and is important for the maintenance of BCSCs and correlates with chemoresistance [86]. The different Notch receptors are overexpressed or amplified in TNBC and contribute to proliferation and invasion [86]. Monoclonal antibodies inhibiting Notch 1 enhance docetaxel anti-proliferative effects and delay recurrence in TNBC xenografts [98]. Inhibitors of the Notch pathway in combination with docetaxel are under clinical investigation for TNBC treatment [99,100].

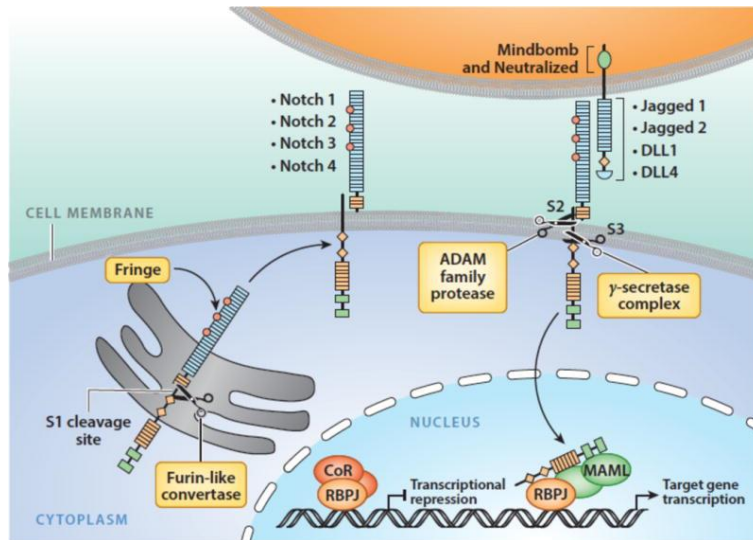


**Figure 16: The Notch signalling pathway.** Ligand binding to the Notch receptor induces its cleavage by proteases. The intracellular domain of Notch receptor translocates to the nucleus and activates the transcription of target genes. From [97].

#### ***II.4.2.3. Wnt/β-catenin pathway***

The Wnt pathway is implicated in cancer cell proliferation, metastasis, and CSCs maintenance [101]. The Wnt/β-catenin signalling is enriched in TNBC and correlates with poor clinical outcomes [102]. It drives TNBC tumorigenesis by regulating key processes like migration, proliferation, chemoresistance, and sustaining BCSCs [102]. In the absence of Wnt ligands, a complex composed of casein kinase 1 (CK1), glycogen synthase kinase 3 (GSK3), Dishevelled (Dvl), Axin, and adenomatous polyposis coli (APC) termed the destruction complex, sequesters β-catenin in the cytoplasm (**Figure 17**). β-catenin is the principal effector of the signalling pathway, and when sequestered by the destruction complex, it gets phosphorylated by GSK3 and CK1 promoting its ubiquitination and proteasomal degradation (**Figure 17**). When Wnt ligands bind to the pathway receptors Frizzled and LRP5/6, Frizzled is activated leading to Dvl recruitment and LRP5/6 phosphorylation. Phosphorylated LRP5/6 interacts with Axin, leading to the destabilization of the destruction complex preventing the degradation of β-catenin therefore its cytoplasmic accumulation and its nuclear localization, where it interacts with the transcription factors TCF/LEF activating the transcription of Wnt target genes (**Figure 17**) [101,102].

The deregulation of the Wnt/ $\beta$ -catenin pathway in TNBC is not due to mutations in the gene coding for  $\beta$ -catenin, *CTNBB1*, however, several Frizzled receptors and LRP5/6 were shown to be deregulated in TNBC and to play key roles in TNBC proliferation, metastasis, stemness, and chemoresistance [102]. LGK974, a small molecule that inhibits Wnt ligands secretion, is being clinically evaluated for TNBC treatment (NCT01351103).

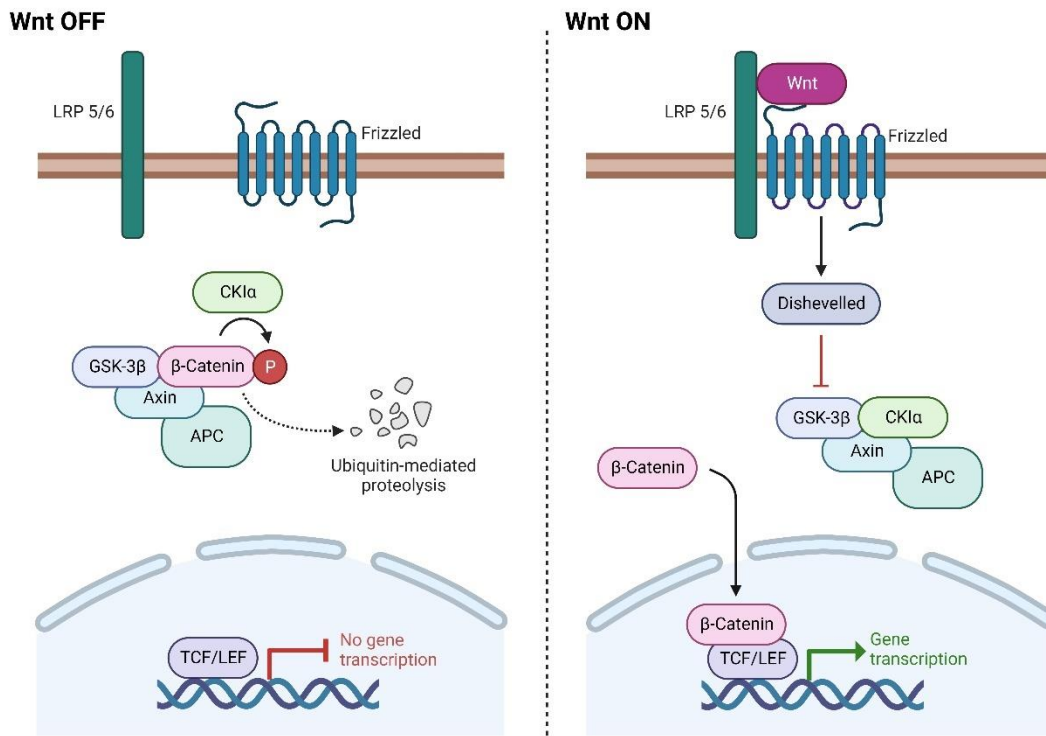


**Figure 17: Wnt/ $\beta$ -catenin pathway.** In the absence of Wnt ligands (Wnt OFF),  $\beta$ -catenin is sequestered and phosphorylated by the destruction complex leading to its proteasomal degradation, therefore the inhibition of Wnt target genes transcription. When Wnt binds to Frizzled,  $\beta$ -catenin is freed from the destruction complex and translocates to the nucleus where it interacts with TCF/LEF and activates the transcription of Wnt target genes.

#### II.4.2.4. Hedgehog pathway

The hedgehog pathway is crucial in embryonic development and tissue regeneration. Alterations in Hedgehog signalling are linked to CSC renewal and tumorigenesis. It has three secreted ligands that bind to two receptors PTCH and SMO. Pathway activation leads to the activation of the transcription factors GLIAs that are linked to proliferation,

EMT, chemoresistance, and invasion. Hedgehog pathway is activated in TNBC and promotes its aggressiveness and chemoresistance [86].

## II.5. TNBC and the EGFR pathway

EGFR belongs to the ErbB tyrosine kinase receptors family that also includes HER2, HER3, and HER4. Upon activation, they form homo- or hetero-dimers cell surface receptors and undergo autophosphorylation at tyrosine residues. EGFR controls a wide range of cellular pathways involved in proliferation, survival, and migration. EGFR is overexpressed or aberrantly activated in several cancer types and correlates with poor clinical outcomes. In TNBC, more than 50% of patients overexpress EGFR, however, inhibitors or antibodies targeting EGFR have not yet shown any promising results in the clinics. Erlotinib is a TKI targeting EGFR (**Figure 18**) that was evaluated for the treatment of breast cancer but did not present any therapeutic advantage. Gefitinib I, another EGFR kinase inhibitor similar to erlotinib (**Figure 18**), did not present any clinical advantage for ER-negative breast cancer treatment. Cetuximab is an anti-EGFR monoclonal antibody that blocks ligand binding (**Figure 18**). TNBC patients did not respond to treatment regimens including cetuximab in combination with carboplatin, anti-microtubule agents, or topoisomerase inhibitors. Another ligand-blocking anti-EGFR, panitumumab (**Figure 18**), did not improve patients' survival outcomes compared to chemotherapies alone. Although pre-clinical data strongly associate EGFR with poor outcomes in TNBC, TNBC patients failed till date to respond to any therapies targeting EGFR [103–105].

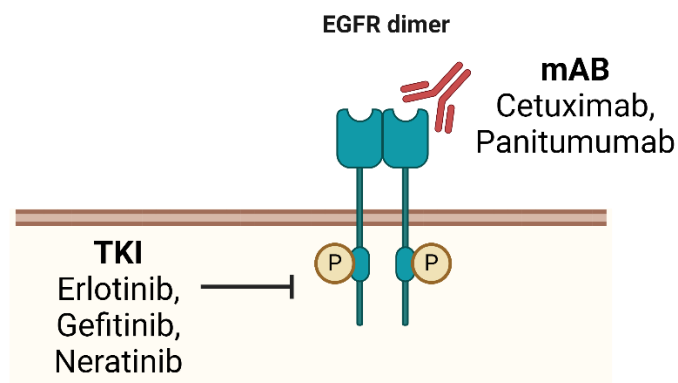


Figure 18: EGFR targeting agents.

## Summary

TNBC is the breast cancer subtype with poorest prognosis, mainly affecting women of smaller age. It is characterized with high heterogeneity, reflected by the presence of different TNBC subtypes that show distinct tumour grade and treatment sensitivity. Until date, chemotherapies remain a primary treatment option for TNBC patients, however, patients usually develop resistance to the treatment and are prone to relapse less than 5 years following the initial diagnosis. A main driver of TNBC chemoresistance and cause of relapse is its enrichment in BCSCs, that are activated for major cellular proliferation pathways like the Wnt/ $\beta$ -catenin and Hedgehog signalling pathways. Currently, three FDA-approved targeted therapies exist for TNBC treatment: immunotherapy targeting PD1/PDL1, the ADC SG, and PARP inhibitors for carriers of *BRCA1/2* mutations. A disappointing clinical data is the failure of multiple EGFR targeting agents in the management of TNBC, although more than 50% of TNBC patients overexpress EGFR.

As such, there is still an urgent need to the identification of therapeutic targets for TNBC. Being a main goal for our laboratory, proteomic and transcriptomic analysis on breast tumours of the different subtypes and normal breast tissue were performed to search for potential therapeutic candidates. This led to the identification of the family of arginine methyltransferases as attractive potential targets for TNBC.



## III. Arginine Methylation

### III.1. Biochemistry and enzymatic reaction

Protein arginine methylation is a common post-translational modification (PTM) abundant as protein phosphorylation and ubiquitination [106]. It has a high metabolic cost accounting for 12 ATP molecules per reaction and occurs on about 0.5% of arginine residues in mammalian cells [107,108]. Of all natural amino acids, arginine possesses the longest side chain and is positively charged, making it a good backbone for protein-protein and protein-nucleic acid interactions [107,109]. The guanidino group of arginine has five hydrogen bond donors favouring the interaction with hydrogen bond acceptors [110]. Actually, arginine makes the highest number of hydrogen bonds with DNA in protein-DNA complexes [110,111]. Importantly, arginine methylation does not alter the charge of the residue, however, it changes its shape and removes potential hydrogen bond donors that can ultimately interfere with protein and nucleic acid interactions [107,112,113]. This PTM is catalysed by a family of nine enzymes termed protein arginine methyltransferases (PRMT) named according to the order of their discovery (PRMT1 to PRMT9), with PRMT4 also being termed coactivator associated arginine methyltransferase 1 (CARM1). The nitrogen atom of an arginine residue can be methylated once or twice: mono-methyl arginine (MMA) or di-methyl arginine (DMA). The first step of arginine methylation reaction involves the addition of one methyl group from the universal methyl donor, S-adenosyl methionine (SAM), to the nitrogen atom of arginine side chain, creating MMA (**Figure 19**). All PRMTs can catalyse this step of methylation. The only PRMT unable to continue to the second methylation step (DMA) is PRMT7 and is classified as type III PRMT. The other PRMTs can add another methyl group and are classified as follow: Type I PRMTs (PRMT1, PRMT2, PRMT3, PRMT4, PRMT6, and PRMT8) add the second methyl group on the same nitrogen atom thus creating asymmetric di-methylation (ADMA) and type II PRMTs (PRMT5 and PRMT9) add the second methylation mark on the second terminal nitrogen creating symmetric di-methylation (SDMA) (**Figure 19**). PRMT1 is the main type I PRMT and is responsible of the majority of arginine methylation in cells, and PRMT5 is the main type II PRMT. ADMA is the most common arginine methylation mark followed by MMA then SDMA.



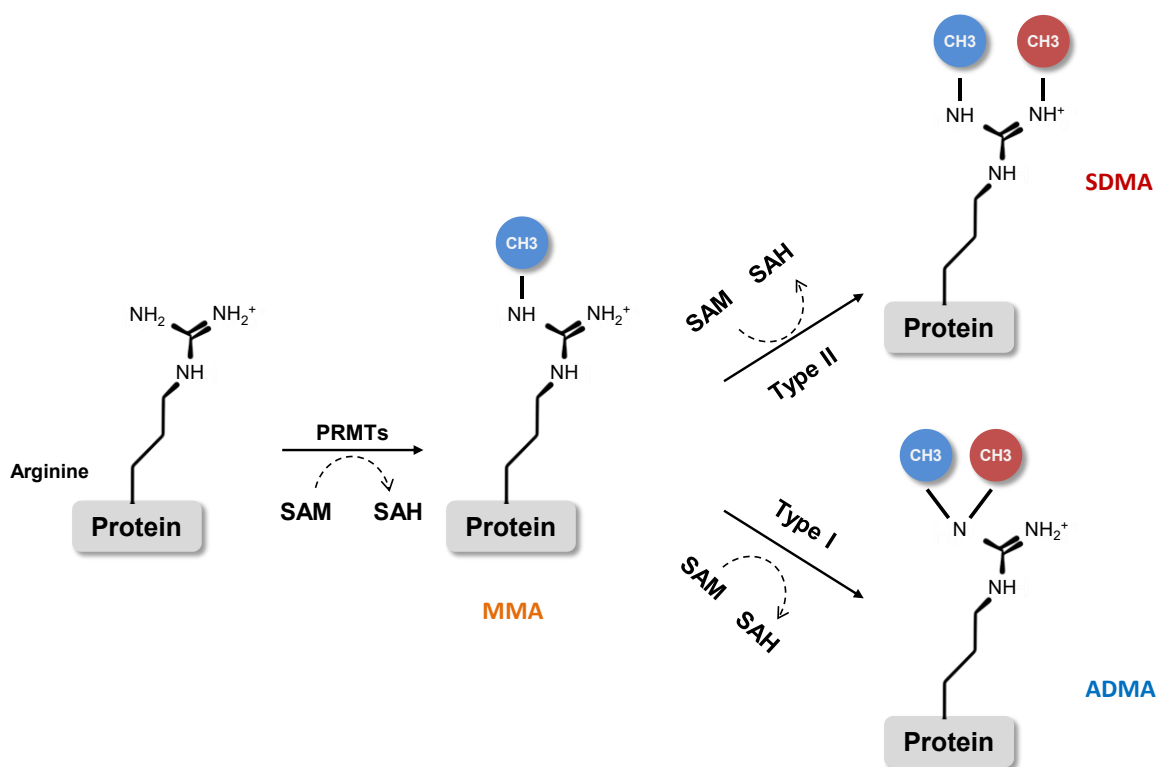


**Figure 19: Arginine methylation reaction and types.** PRMTs generate arginine methylation by transferring a methyl group from SAM to the guanidino nitrogen atom of arginine side chain creating MMA and releasing SAH as a by-product. Type I PRMTs subsequently generate ADMA and type II PRMTs generate SDMA. ADMA: asymmetric dimethyl arginine; MMA: monomethyl arginine; SAH: S-Adenosylhomocysteine; SAM: S-Adenosyl-L-methionine; SDMA: symmetric dimethyl arginine.

### III.2. Metabolic regulation of arginine methylation

SAM, the global methyl donor in cells, is generated from the amino acid methionine in an ATP-dependent process by methionine adenosyl-transferase (MAT) [114]. The by-product of methylation reaction is S-adenosylhomocysteine (SAH). SAH is converted to homocysteine (Hcy), which then regenerates methionine through the folate cycle (**Figure 20**) [114,115]. Through the methionine cycle, SAM can generate methylthioadenosine (MTA) that can in turn inhibit PRMT activity. MTA is converted to methyladenosine by S-methyl-5'-thioadenosine phosphorylase (MTAP), ultimately leading to methionine regeneration. *MTAP* gene is frequently deleted in cancers, leading to MTA accumulation and the inhibition of PRMTs [115,116]. MTAP-deleted cells possess a reduction in PRMT5 activity and are more vulnerable to PRMT5 targeting [117].

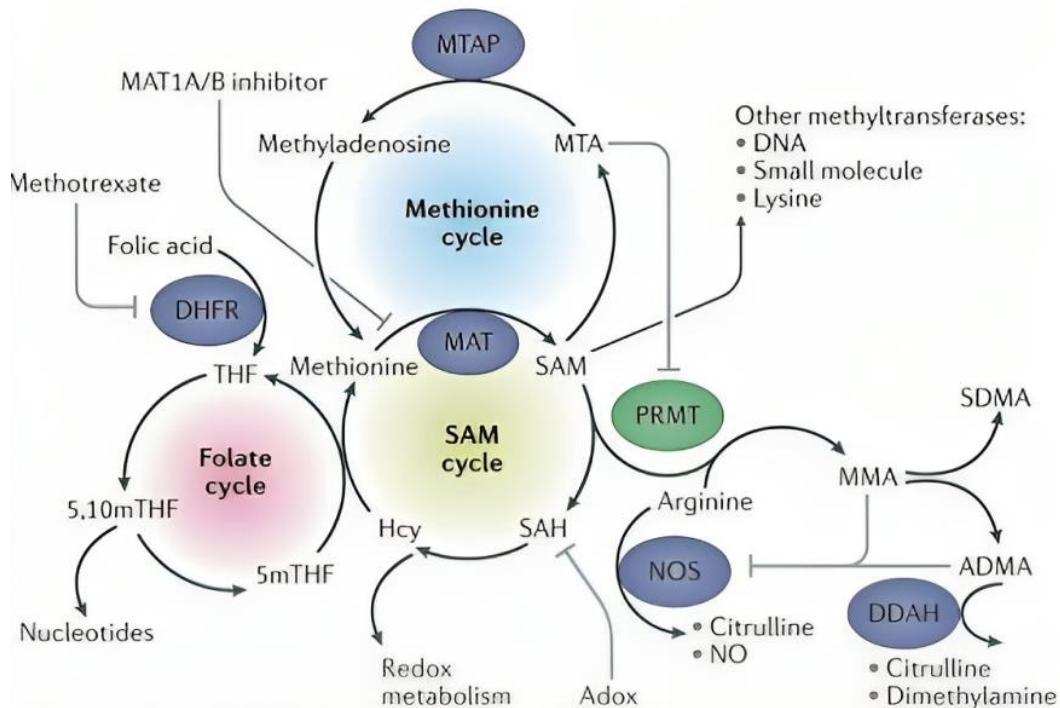


**Figure 20: Metabolic regulation of SAM.** SAM is the global methyl donor in the cells and is crucial for many methylation reactions such as protein, DNA and RNA methylation. The by-product of arginine methylation is SAH, that is further transformed into Hcy (SAM cycle). Through the folate cycle, methionine is regenerated from Hcy. Methionine is then converted into SAM by MAT (methionine cycle). SAM generates methylthioadenosine (MTA), a natural inhibitor of PRMTs. MTA is converted into methyladenosine through S-methyl-5'-thioadenosine phosphorylase (MTAP). Modified from [115].

### III.3. Writers of arginine methylation: PRMTs

#### III.3.1. Structure of PRMTs

Except for PRMT9, the crystal structure of all PRMTs has been resolved [118,119]. All PRMTs share a common architecture of the core methyltransferase domain: N-terminal Rossmann fold containing the cofactor SAM binding pocket and the C-terminal  $\beta$ -barrel (**Figure 21**) [118,119]. The distinctiveness of each PRMT comes from the N- and C-terminal regions. The N-terminal region of PRMTs sometimes harbours domains responsible for protein-protein interactions, like substrate binding, recruitment of proteins essential to form an active complex, and homo-oligomerization [119]. Such domains are present in PRMT2 (SH3 domain) [120], PRMT3 (zinc finger) [120], PRMT4 (pleckstrin homology (PH)-like) [121] and PRMT5 (TIM barrel) (**Figure 21**) [122,123].

The central methyltransferase domain of all the nine PRMTs is remarkably similar, and contains six conserved signature motifs that are indispensable for the methyltransferase activity: motif I (I) (**VLD/VGxGxG**), post-motif I (pl) (**V/I-X-G/A-X-D/E**), motif II (II) (**E/K/V/DII**), double E loop (E) (**SExMGxxLxxExM**), motif III (III) (**LK/xxGxxxP**), and the critical **THW loop** (**Figure 20**) [118,124]. An additional **YFxxF** motif is present in type I PRMTs and forms an  $\alpha$ -helical structure. Motif I contains three highly conserved glycine residues among PRMTs and forms the core of SAM-binding pocket. Through a glutamic or aspartic acid residue, the post-motif I interacts with the ribose hydroxyl group of SAM via hydrogen bonds. Motif II forms a  $\beta$ -sheet and stabilizes motif I, and motif III forms a  $\beta$ -sheet parallel to motif II. The two glutamic acid residues in the double E loop are highly crucial for PRMT activity, as they are responsible of positioning the substrate arginine. The THW loop, adjacent to the active site, binds to the substrate and is crucial for stabilizing the N-terminal helix [118].

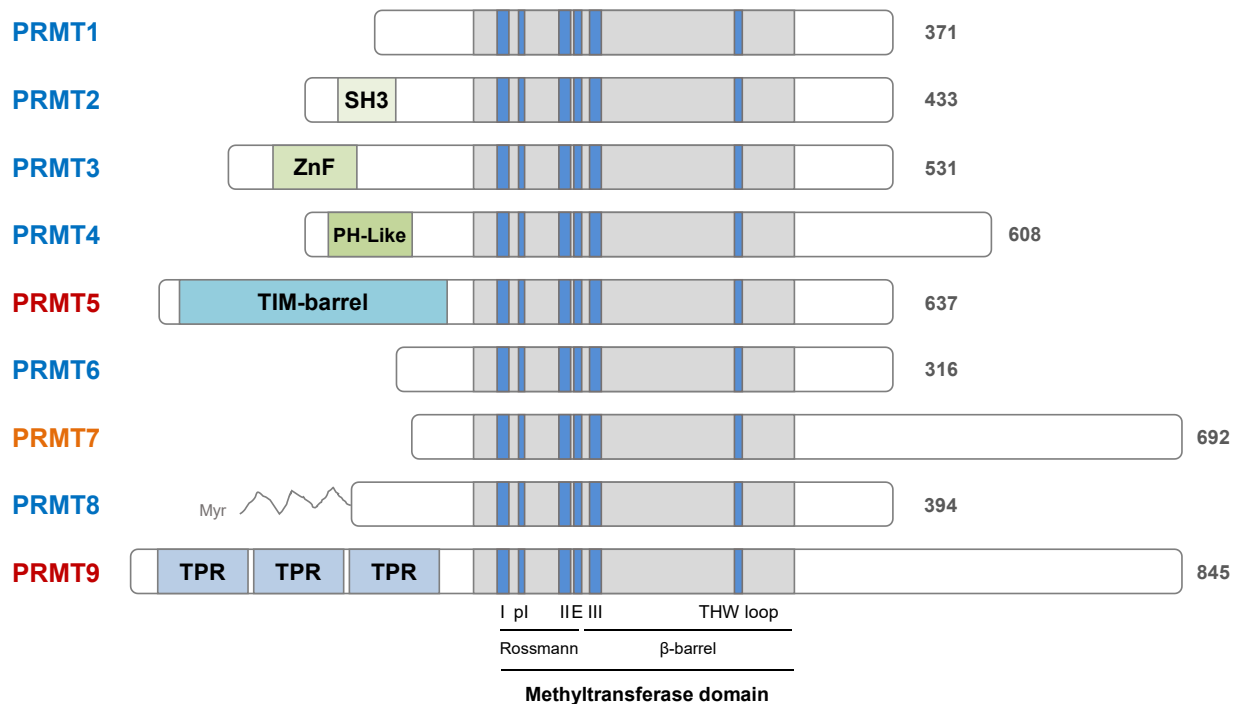


**Figure 21: The PRMT family members.** The nine PRMTs share structural homology in their central methyltransferase domain (in gray) and differ in their N- and C-terminal ones. Unique motifs in the N-terminal domain of each PRMT are labelled and marked with different colours. Signature PRMT motifs (in the catalytic domain) are indicated as blue lines: motif I (I), post I (pl), motif II (II), double E loop (E), motif III (III) and the THW loop. Type I PRMTs are indicated in blue, type II in red and type III in orange. SH3:

SRC Homology 3 Domain; ZnF: Zinc-finger; PH-like: Pleckstrin homology-like; TIM: triose phosphate isomerase; Myr: Myristoylation; TPR: Tetratricopeptide repeat.

A common feature of all PRMTs is the formation of doughnut-shaped homodimers organized in a head-to-tail orientation (**Figure 22**), with both monomers binding to SAM and the substrate [118,119]. See **Figure 22** below for details on the dimerization. Higher order oligomerizations were also seen for PRMT5 and PRMT8 [118,119,124].

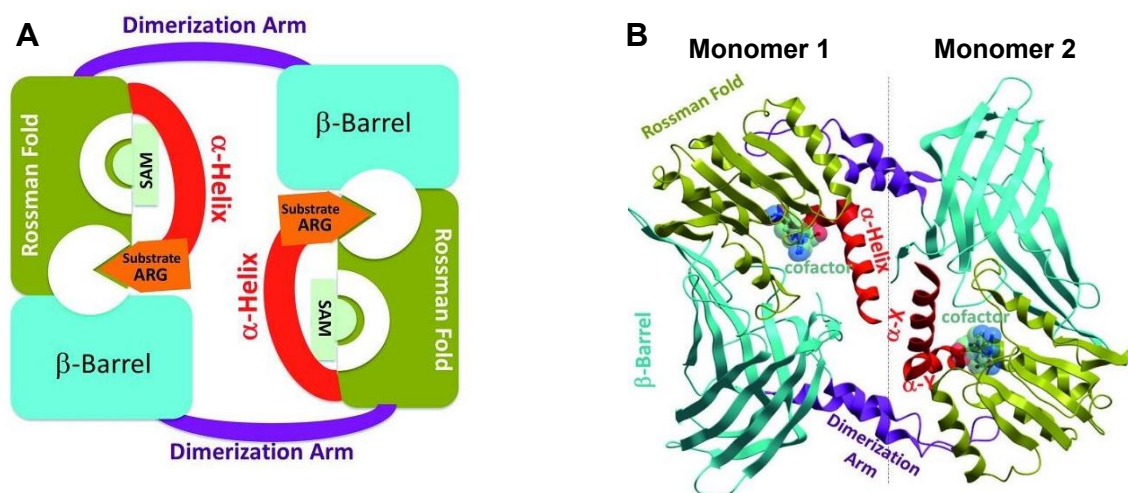


**Figure 22: Illustration of a PRMT homodimer.** (A). The PRMT homodimers adopt a doughnut-shaped head-to-tail structure, where the dimerization arm projects from the  $\beta$ -barrel of one monomer and interacts with the Rossmann fold of the other. An  $\alpha$ -helix from the N-terminal of Rossmann fold wraps onto SAM and is involved in the proper positioning and recruitment of the substrate. A substrate binding site is therefore formed between the limits of  $\beta$ -barrel, Rossmann fold, and  $\beta$ -barrel. (B). Dimeric arrangement of PRMTs represented by CARM1 structure (PDB code 3B3F). Modified from [119].

### III.3.2. The PRMT methylome and arginine methylation motifs

Classically, PRMTs methylate arginine within a glycine and arginine (GAR) rich motif in their substrates, also known as RGG/RG motifs. RNA- and DNA- binding proteins harbour RG/RGG motifs and are reported to be mono- and/or di-methylated on arginine [125], reflecting the importance of PRMTs in processes like transcription, DNA repair, and mRNA processing [106,126–134]. A unique feature of PRMT4 and PRMT7 is their preference to methylate motifs other than the GAR. PRMT4 methylates arginine in proline-glycine-methionine (PGM) rich motifs [128,135–137], and PRMT7 methylates GAR and RXR motifs [132,138]. PRMT6 methylates arginine near glycine, but they target

the RG motifs rather than the RGG [139]. PRMT5 methylates 'GRG', and its detailed methylome will be developed in a later section of the thesis.

To understand the functional relevance of arginine methylation, it is important to decipher and characterize the PRMT methylome. One of the first attempts to uncover the arginine methylome was performed in 2004 [140], where they applied for the first time the stable isotope labelling with amino acids in cell culture (SILAC) to detect and quantify *in vivo* arginine methylation sites. 59 methylation sites were identified, with the majority lying in RNA binding proteins [140]. Later studies also applied SILAC coupled with other purification methods to identify arginine methylation in T cells [126,141], revealing a role of PRMTs in endosomal trafficking, immunological synapse, and T-cell activation and differentiation [126,141]. Another method to search for the arginine methylome is by immuno-enriching methylated proteins using antibodies detecting MMA, ADMA, or SMMA followed by mass spectrometry. This method was first described in 2014 by Guo *et al.*, who identified almost 1000 MMA sites and 300-400 ADMA sites in HCT116 colon cancer cells [142]. The majority of methylated proteins identified were involved in RNA processing and transcriptional regulation [142]. In mouse tissue, arginine methylated proteins enriched from mouse brain included receptors and vesicular proteins, whereas the majority of those enriched from mouse embryo were proteins involved in RNA processing and transcriptional regulation [142]. By combining high-pH prefractionation with immune-enrichment of MMA peptides, Larsen *et al.* identified 7866 MMA sites belonging to 3086 proteins in HEK293 cells [106]. These methylation sites represent around 7% of all arginine in these proteins, reflecting the widespread occurrence of arginine methylation with levels comparable to serine phosphorylation (9%) and lysine ubiquitination (7%). Importantly, MMA sites are often close to phosphorylation sites, indicating a possible crosstalk between both PTMs [106]. Arginine methylated proteins are found both in the nucleus and in the cytoplasm, and are involved in RNA processing and transport, cell cycle, DNA replication and repair, chromatin remodelling, endocytosis, and insulin signalling. Interestingly, arginine methylated sites were enriched in the hnRNP K homology (KH) domain (ssDNA/RNA binding domain) and the RNA recognition motif (RRM) [106]. MMA was also shown to be abundant in the serum of breast cancer, acute myeloid leukemia (AML), and non-small cell lung cancer (NSCLC) patients [143], and

MMA and ADMA were identified in colorectal cancer (CRC) patient tissue samples [129]. Total DMA levels in A549 cells were examined under MS023 (type I PRMTs inhibitor) or GSK591 (PRMT5 inhibitor) treatment [131]. In non-treated cells, SDMA constituted around 3.5% of total dimethylation, was almost negligible in GSK591 treatment, and increased to ~8.5% when type I PRMTs were inhibited [131]. The increase in MMA and SDMA levels following PRMT1 loss was reported in other studies [127,144], showing a compensation of other PRMTs to PRMT1 (the major PRMT) loss or inhibition. A recent study uncovered the methylated proteins (arginine and lysine) in mouse embryonic stem cells (ESC) and mouse embryonic fibroblasts (MEF) and identified methylation events on around 4,000 arginine and 167 lysine, of which almost half were novel sites [145]. In this study, arginine methylation was mainly involved in RNA processing, and was also enriched in processes related to development, differentiation, and chromatin remodelling [145]. Large scale proteomic studies were also applied to determine the methylome of individual PRMT members like type I PRMTs [127,134], PRMT1 [106], CARM1 [106,128,132,135], PRMT3 [146], PRMT5 [106,127,132,133,147], and PRMT7 [106,132].

### **III.3.3. Crosstalk between PRMTs**

It is well established now that one substrate can be methylated by more than one PRMT, and even a single arginine residue could be a target of different PRMTs. For instance, both PRMT1 [148,149] and PRMT5 [150–153] methylate histone H4 on R3 generating H4R3me2a and H4R3me2s, respectively. CARM1 methylates H3 on R17 and R26 [154] and PRMT5 symmetrically dimethylates H3 on R8 [153]. A proteomic analysis identified 62 different proteins to be co-regulated by CARM1, PRMT5, and PRMT7 [132]. These proteins were enriched with components of the spliceosome and splicing factors like the nuclear protein hnRNPA1. CARM1, PRMT5, and PRMT7 could all methylate hnRNPA1 on different residues and enhanced its binding to RNA [132]. The pre-mRNA splicing factor SRSF2 is methylated by both CARM1 and PRMT5. CARM1 mediated methylation regulates the nuclear localization of SRSF2, whereas PRMT5 mediated methylation enhanced its binding to RNA [106]. As mentioned earlier, loss or inhibition of PRMT1 increases MMA and SDMA levels indicative of compensation among the different PRMTs and substrate scavenging [144]. On the contrary, PRMT5 inhibition did not affect basal levels of MMA and ADMA [134]

### III.3.4. Functions of arginine methylation

In this part, I will discuss the broad cellular functions of PRMTs. As this thesis focuses on PRMT5, a detailed section developing the various functions of PRMT5 and its implication in diseases will be discussed in a later section of the thesis.

#### III.3.4.1. *Transcriptional regulation*

PRMTs are involved in both transcriptional activation and repression by methylating histone tails or transcription factors. PRMT1 functions mainly as a coactivator of transcription by asymmetrically methylating histone H4 on R3 (H4R3me2a) (**Figure 23**), facilitating histone acetyltransferases (like p300) recruitment and chromatin opening [116,155]. H4R3me2a can be recognized by TDRD3, a scaffold protein that recruits DNA Topoisomerase III $\beta$  to *c-MYC* promoter and activates its transcription [156,157]. PRMT1 methylates the transcription factors Runt-related transcription factor 1 (RUNX1) and C/EBP $\alpha$  inhibiting their interaction with transcriptional corepressor and enhancing their transcriptional activity [158,159]. CARM1 was the first PRMT to be linked to transcriptional coactivation by methylating H3 on R17 and R26 (H3R26me2a) [136], but it can also be implicated in transcriptional repression [116]. CARM1 enhances the transcriptional activity of nuclear receptors by interacting with p160 coactivator family and methylating p300 and CBP (**Figure 23**) [160–163]. PRMT1 and CARM1 synergistically cooperate with and coactivate the transcription factors nuclear factor  $\kappa$  of B-cells (NF- $\kappa$ B) [164,165], NF-E2-related factor 2 (Nrf2) [166], and p53 [167] driving their transcriptional activation of target genes. CARM1 interacts also with  $\beta$ -catenin mediating its transcriptional activation [168]. Although PRMT5-dependent methylation marks on histone (H2AR3me2s, H4R3me2s, H3R8me2s, and H3R2me2s) were initially discovered to be repressive (**Figure 23**), it was later determined that these modifications could also contribute to transcriptional activation [151,169–176]. PRMT5 methylates NF- $\kappa$ B and activates it [177], the co-repressor KRAB-associated protein 1 (KAP1) [178], Epstein–Barr virus (EBV) nuclear antigen 2 (EBNA2) stimulating the EBNA2 mediated transcription [179]. PRMT6 is mostly involved in transcriptional repression by the methylation of H3R2 and H2AR29 (**Figure 23**) [116].



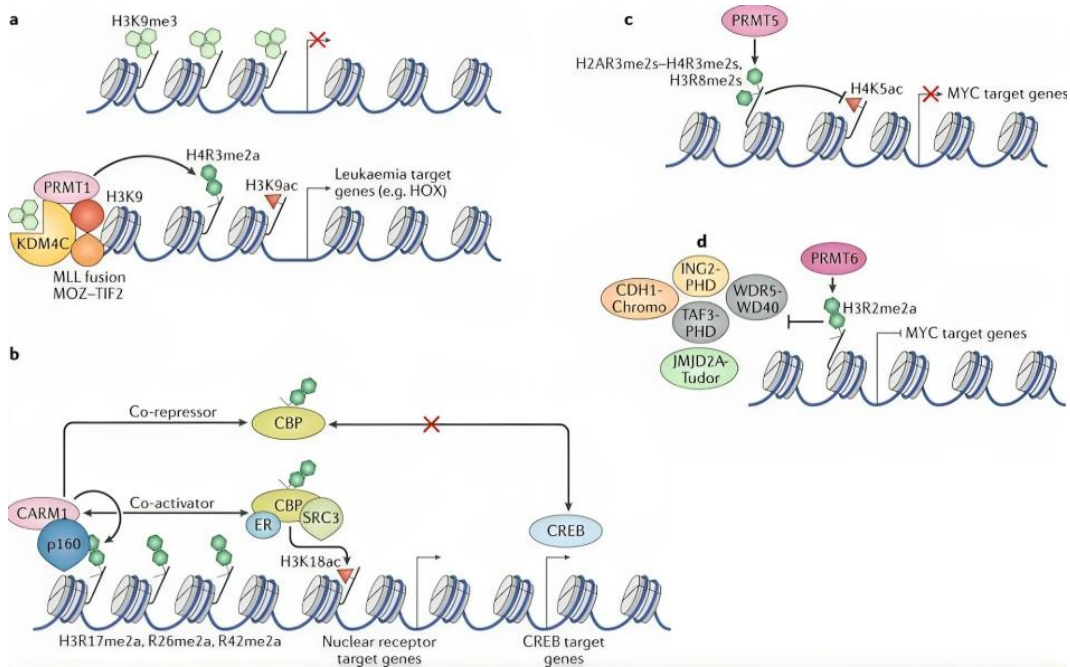


**Figure 23: PRMTs functions in transcriptional regulation.** (A). PRMT1 dependent methylation of H4R3 activates gene expression. (B). CARM1 associates with p160 and enhances nuclear receptor mediated gene transcription. (C, D). PRMT5 methylation of H2AR3, H4R3, and H3R8 (C) and PRMT6 methylation of H3R2 repress the transcription of MYC target genes. Modified from [116].

### III.3.4.2. pre-mRNA splicing

Pre-mRNA splicing is the process by which introns are removed from pre-mRNA molecules. It consists of two trans-esterification steps where each step requires a nucleophilic attack on the phosphodiester bonds of the intron [180]. The proteomic analysis of arginine methylome has revealed that the putative PRMT substrates are enriched in RNA binding proteins and proteins involved in RNA dependent processes like pre-mRNA splicing, RNA transport, and the spliceosome [106,127,129,130,132–134,142,147]. An elegant study by Fong *et al.* showed that AML cells harbouring mutations in splicing factors were sensitive to PRMT5 or type I PRMT inhibitors, and combining both inhibitors had a synergistic effect in altering alternative splicing (AS) events [127]. Similarly, Fedoriw *et al.* reported an alteration of AS events when type I PRMT were inhibited, and inhibiting PRMT5 in combination with type I PRMT aggravated this effect [134]. A recent study showed that inhibiting PRMT5 and type I PRMTs altered



the AS in A549 cells and inversely regulated intron retention [181]. The role of PRMT1 in pre-mRNA splicing has not been fully elucidated, however, it was shown that PRMT1 methylation controls the localization and functions of some RNA-binding proteins and splicing factors like Sam68 [182], hnRNP A1/2 [183,184], and FUS/TLS [185]. The only known PRMT9 substrate is the splicing factor SF3B2 (also termed SAP145), and PRMT9 is required for efficient AS in HeLa cells (**Figure 24**) [186,187]. CARM1 methylates several splicing factors like SRSF2, SmB, SF3B4, U1C, and CA150 (**Figure 24**) [136]. PRMT5 has a major role in pre-mRNA splicing by symmetrically di-methylating Sm proteins promoting spliceosome assembly (**Figure 24**). It can also methylate several splicing factors controlling their function, and its inhibition or depletion largely affects AS events (**Figure 24**) [116,133,188]. A detailed mechanism of PRMT5 roles in RNA processing is discussed in section IV of the thesis.

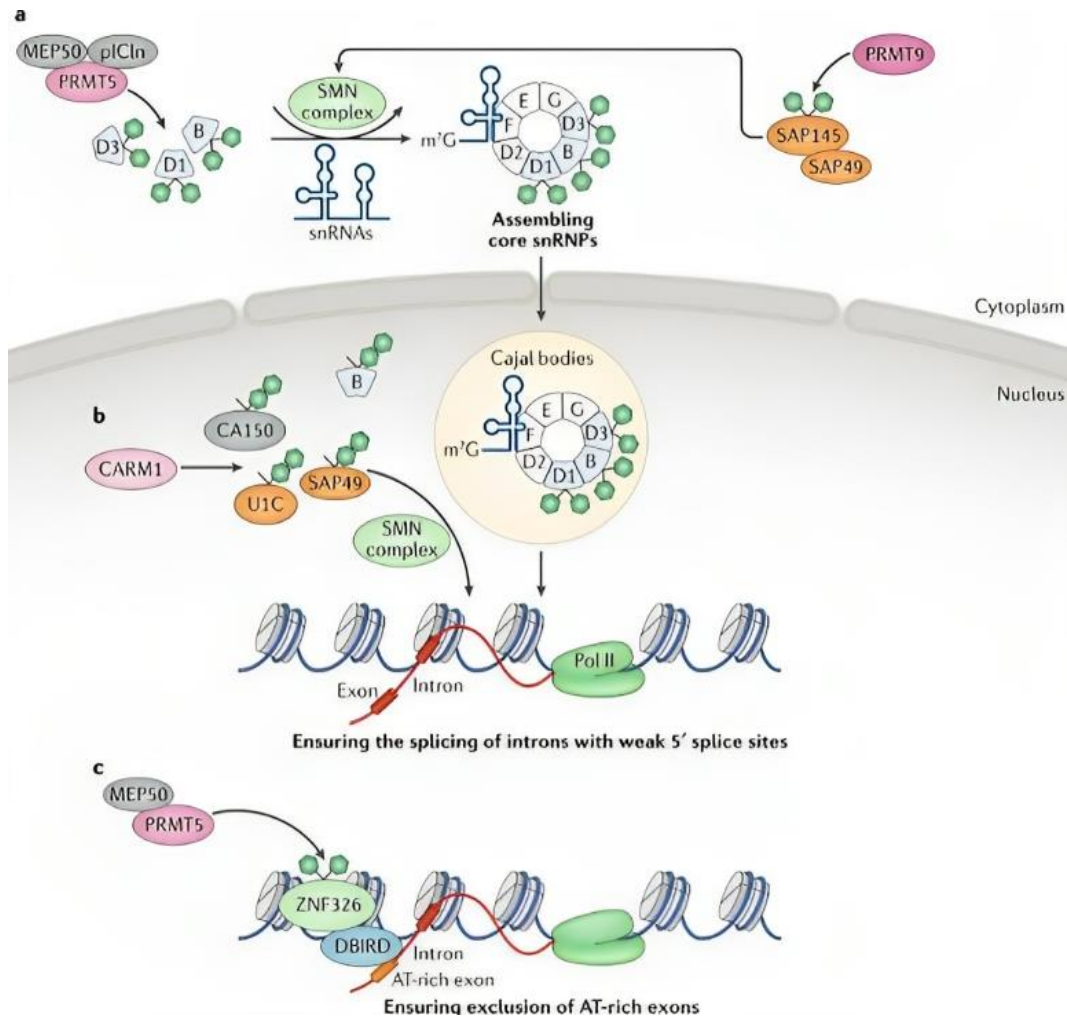


**Figure 24: PRMTs functions in pre-mRNA splicing.** (A). In the cytoplasm, PRMT5 symmetrically dimethylates Sm proteins and PRMT9 methylates SAP145 (SF3B2) to promote snRNPs assembly. The assembled snRNPs then translocate to the nucleus to carry their function in splicing. (B, C). CARM1 and PRMT5 methylate splicing factors and control alternative splicing events. From [116].

### III.3.4.3. Translation

PRMTs play roles in protein synthesis by methylating ribosomal proteins [116,125,130]. A study that identified the interactome of all PRMT members by proximity labelling in HEK293T cells revealed that the PRMT interactome is enriched in proteins involved in RNA processes including translation initiation [130]. More than half of ribosomal components and various translation elongation factors were identified in the same study, and ribosomal proteins (between 10 and 50 KDa) from different ribosome fractions were shown to be heavily methylated on arginine residues. Inhibiting or depleting PRMT1 and CARM1 caused global translation deficiency [130]. The 40S ribosomal protein S2 (RPS2) is methylated by PRMT1 [130], PRMT3 [189–191], and CARM1 [130] promoting its

assembly into the 40S ribosomal subunit. PRMT5 methylates ribosomal protein S10 (RPS10) that is required for efficient ribosome assembly and protein synthesis [192], and hnRNPA1 to promote its interaction with internal ribosome entry site (IRES) on RNA and hence facilitating IRES-dependent translation [193].

#### ***III.3.4.4. Cell cycle regulation***

PRMTs can affect the cell cycle progression by methylating cell cycle proteins and regulators, and through regulating the expression of cell cycle genes (**Figure 25**) [194]. PRMT1 methylates cyclin-dependent kinase 4 (CDK4) preventing its interaction with cyclin D3 and cell cycle progression [195]. PRMT5 interacts with CDK4 releasing it from CDKN2A and promoting cell cycle progression [196]. PRMT1 methylates INCENP, enhancing its interaction with Aurora Kinase B (AURKB), hence inhibiting AURKB activity and promoting mitosis of cancer cells [197]. CARM1 positively regulates the expression of *CCNE1* (encoding cyclin E1) and *E2F1* genes [198,199]. PRMT5 supports cell cycle progression by regulating the expression of CDK4/6, cyclin D1, cyclin D2, cyclin E1, and retinoblastoma protein (Rb) [200]. Moreover, PRMT5 represses the transcription of the microRNAs miR33b, miR96, and miR50 that targets the mRNA of cyclin D1 and myc [201]. PRMT5 inactivates the Rb proteins RB1 and RBL2 leading to the upregulation of polycomb repressor complex (PRC2) and cyclin D1 facilitating cell cycle progression [202]. PRMT6 represses the transcription of cell cycle inhibitors p21, p27, and p18 [203–205]. PRMT6 methylation mark H3R2me2a facilitates H3 phosphorylation by AURKB leading to chromatin condensation [206].

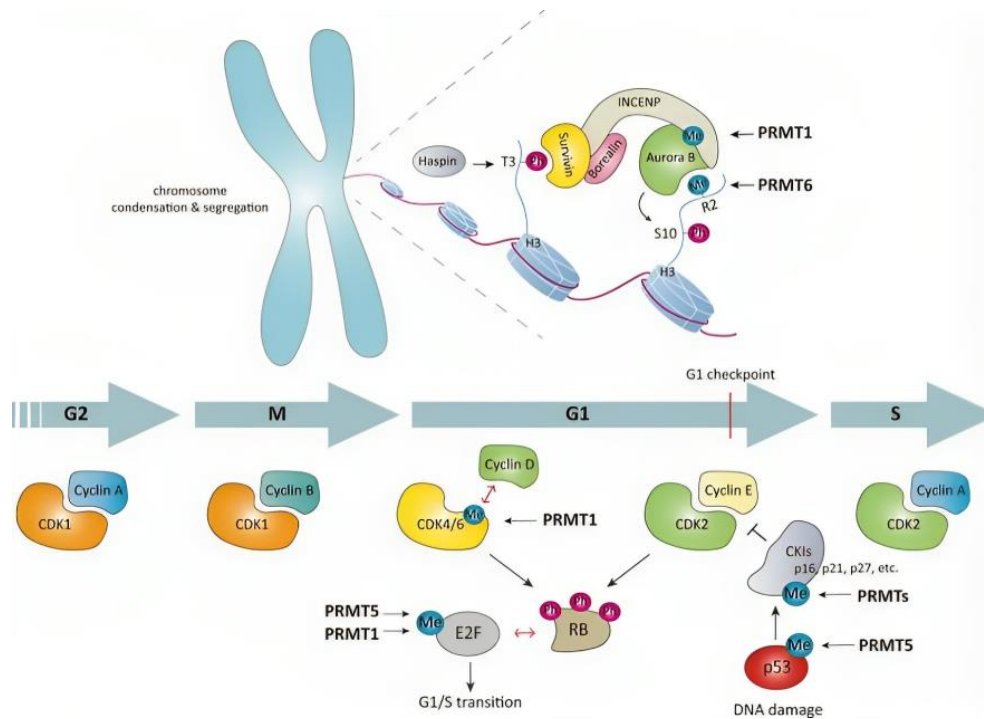


**Figure 25: Function of PRMTs in cell cycle regulation.** PRMT1 and PRMT6 mediated methylation supports Aurora B recruitment to the chromatin and phosphorylation of H3, leading to chromosome condensation and segregation during mitosis. PRMT1 methylates CDK4 preventing its interaction with cyclin D and inhibits cell cycle progression. On the contrary, PRMT1 and PRMT5 promote cell cycle progression by methylating E2F1. The CDK inhibitors p16, p21, and p27 are methylated by PRMTs regulating their interaction with CDKs. From [194].

### III.3.4.5. The DNA damage response

The two main PRMTs involved in the DDR are PRMT1 and PRMT5. PRMT1 methylates the GAR motif of the checkpoint protein MRE11 which is important for its exonuclease activity. MRE11 methylation is important for the ATR/CHK1 pathway and the recruitment of replication protein A (RPA) and RAD51 to DNA damage sites (**Figure 26**) [207–209]. p53-binding protein 1 (53BP1), an important player in the NHEJ repair pathway, is a substrate of PRMT1 and PRMT5 and its methylation is crucial to its DNA binding ability and stability (**Figure 26**) [210–212]. PRMT1 methylates DNA polymerase  $\beta$  (pol  $\beta$ ) [213], an indispensable player in the DNA BER pathway, and Flap endonuclease 1 (FEN1), a DNA repair regulator [214,215]. A main regulator of the HR pathway, BRCA1, is also methylated by PRMT1 (**Figure 26**) controlling its interaction either with SP1 or STAT1 [216]. PRMT5 plays crucial role in the HR pathway by methylating and regulating the

alternative splicing of components of the TIP60 complex (**Figure 26**) [217,218]. A detailed description of PRMT5 role in DDR is provided in section IV of the thesis.

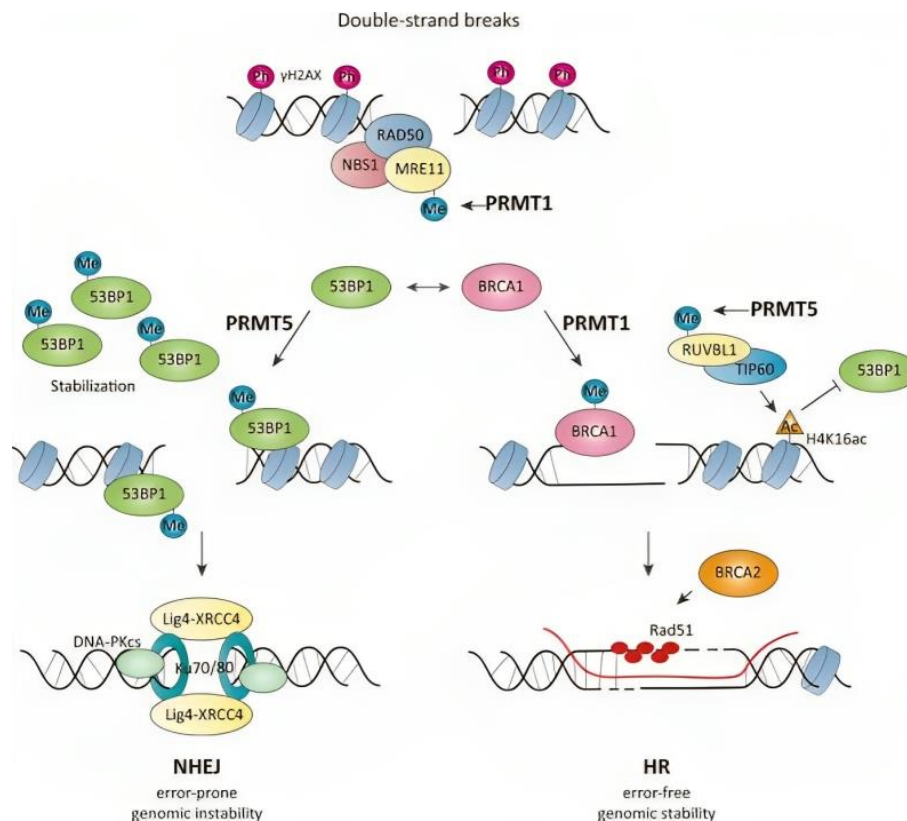


**Figure 26: PRMTs implication in the DNA damage response.** Upon DNA double breaks, PRMT1 methylation of MRE11 promotes its localization to the DNA lesion sites and is important for its exonuclease activity. PRMT5 methylates a main regulator of the NHEJ pathway 53BP1 and stabilizes it, promoting NHEJ repair mechanism. PRMT1 methylation of BRCA1 and PRMT5 regulation of the TIP60 complex facilitates the HR process. Modified from [194].

### III.3.4.6. Signalling pathways

Arginine methylation regulates several signalling pathways including EGFR, TGF $\beta$ , platelet-derived growth factor (PDGF), and the Wnt signalling pathway. SMAD proteins, the main transducers of TGF $\beta$  pathway, are methylated by PRMTs. PRMT1 methylates the inhibitory SMADs, SMAD6 and SMAD7, causing their degradation and subsequent activation of the effector SMAD3 (**Figure 27A**) [219]. SMAD6 methylation by PRMT1 also activates the bone morphogenetic protein (BMP) receptor signalling (**Figure 27A**) [220] and inhibits NF- $\kappa$ B activation [221]. PRMT5 symmetrically dimethylates the p65 subunit of NF- $\kappa$ B increasing its binding to chromatin and regulating transcription [177], and

PRMT1 and CARM1 cooperate to coactivate NF- $\kappa$ B [164,165]. PRMT1 and PRMT5 act oppositely in the BMP pathway, PRMT1 activates the BMP downstream effectors SMAD1, SMAD5, and SMAD9 (**Figure 27A**) while PRMT5 inhibits them [222,223]. PRMT5 interacts with SHARPIN and promotes the symmetric dimethylation and inhibition of the transcriptional corepressor Ski, leading to the upregulation of transcription factors SOX10, MITF, and PAX3 and the repression of TGF $\beta$  pathway [224,225].

PRMT1 and PRMT5 are linked to the EGFR pathway, and both PRMTs methylate EGFR (**Figure 27B**). PRMT5 symmetrically dimethylates R1175 on EGFR cytoplasmic domain, recruiting SH2-domain-containing protein tyrosine phosphatase 1 (SHP1) therefore attenuating the signalling pathway (**Figure 27B**) [226]. Moreover, PRMT5 methylates the RAF proteins CRAF and BRAF leading to their degradation and the inhibition of ERK1/2 signalling (**Figure 27B**) [227]. In contrast, asymmetric methylation of the extracellular domain of EGFR by PRMT1 strengthens its binding to EGF and enhances EGFR signalling (**Figure 27B**) [228–231]. PRMT1 was shown to activate the expression of EGFR, and PRMT1, PRMT5, H4R3me2a, and H4R3me2s were all found to be enriched at the EGFR promoter [232–234]. PRMT5 methylates AKT increasing its phosphorylation and translocation to the plasma membrane [235,236]. PRMT5 methylates the cytoplasmic domain of PDGF at R554 masking Y555 site from binding to the ubiquitin ligase Cbl E3 ligase, protecting it from degradation [237].

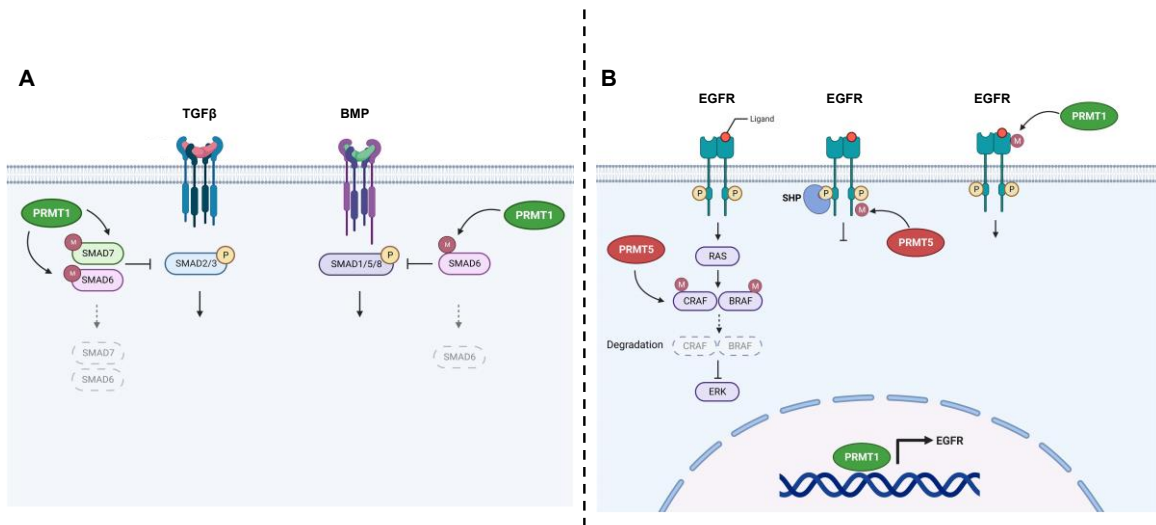


**Figure 27: Role of PRMT1 and PRMT5 in EGFR and TGF $\beta$  signalling pathways.** (A). PRMT1 effect on TGF $\beta$  and BMP pathways. PRMT1 methylates the inhibitory SMADs, SMAD6 and SMAD7, leading to their degradation and the activation of TGF $\beta$  and BMP signalling pathways. (B). PRMT1 and PRMT5 roles in EGFR signalling. PRMT5 methylates CRAF and BRAF leading to their degradation and the inactivation of the signalling cascade. PRMT5 methylates EGFR in its cytoplasmic domain facilitating the binding of SHP that inhibits EGFR activation. PRMT1 methylates the extracellular domain of EGFR promoting its activation. PRMT1 also methylates H4 (not shown in the figure) on the *EGFR* promoter or binds directly to the chromatin to activate *EGFR* gene expression.

### III.4. Arginine methylation readers

#### III.4.1. Tudor domain containing proteins

The major readers of arginine methylation are Tudor domains containing proteins [113,238]. Tudor domains can recognize and interact with both methylated arginine and lysine residues [238], however, narrower aromatic cages in Tudor domains prefer the docking of a methyl-arginine rather than a methyl-lysine [113,239]. Importantly, a Tudor domain is not able to read both arginine and lysine methylation marks [113]. Although arginine methylation preserves the positive charge, it leads to the loss of hydrogen bond donors and increases the size and hydrophobicity of the guanidinium [239]. Methylated arginine residues interact via cationic- $\pi$  interactions with aromatic rings of Tudor domains, forming an aromatic cage [109,239].

##### III.4.1.1. SMN and SPF30

Several Tudor arginine-methylation readers were previously described. Survival motor neuron (SMN) Tudor domain can bind both SDMA and ADMA, with a higher affinity

towards SDMA [240]. The symmetric dimethylation mark of Sm proteins, catalysed by PRMT5, is recognized by the Tudor domain of SMN facilitating spliceosome assembly [241,242]. SMN Tudor domain also recognizes R1810me<sub>2</sub>s in RNA polymerase II (pol II) aiding in the R-loop resolution process and influences transcriptional termination (**Figure 28**) [243]. A recent study has shown that the recognition of dimethyl arginine marks by SMN Tudor domain regulates membrane-less organelles (MLOs) assembly and composition [244]. SPF30 is an essential splicing factor sharing 50% similarity with SMN [113]. The Tudor domain of SPF30 recognizes SDMA marks and to a lesser extent ADMA [113,240], and binds methyl arginine with a lesser affinity when compared to SMN and TDRD3 [245].

#### ***III.4.1.2. SND1 (TDRD11)***

Staphylococcal nuclease domain-containing protein 1 (SND1; also known as p100, TSN or TDRD11) is a Tudor domain containing protein implicated in transcriptional co-activation and is a component of the RNA-induced silencing complex (RISC) [113]. PRMT5 methylates the RISC component AGO2 in Arabidopsis, which is recognized by SND1 promoting the degradation of AGO2 associated small RNAs (sRNAs) [246]. The Tudor domain of SND1 is not sufficient by itself to interact with methylated arginine and it requires additional residues in the SN domain for the interaction [247]. Similar to SMN and SPF30, Tudor domain of SND1 prefers SDMA over ADMA [113]. SDMA marks on E2F1 and Sm proteins are recognized by the Tudor domain of SND1 [248,249]. SND1 is a transcriptional co-activator that can bind to E2F1 [238]. PRMT5 symmetrically dimethylates E2F1 on R111 and R113 reducing its stability and transcriptional activity (**Figure 28**). SND1 reads the symmetric dimethylation mark on E2F1 affecting its half-life and inhibiting E2F1 mediated apoptosis (**Figure 28**) [250,251]. Interestingly, PRMT1 also methylates E2F1 on R109, hindering PRMT5-mediated methylation and increasing E2F1 apoptotic activity [250].

#### ***III.4.1.3. TDRD3***

TDRD3 is to-date the only Tudor domain containing protein that prefers ADMA marks over SDMA [245,252,253], and recognizes the histone methylation marks H4R3me<sub>2</sub>a (PRMT1), H3R17me<sub>2</sub>a (CARM1), and H3R2me<sub>2</sub>a (PRMT6) (**Figure 29**) [113,253].



TDRD3 forms a complex with topoisomerase IIIB (TOP3B) that can resolve both DNA and RNA entanglements [113]. By recognizing H4R3me2a mark on the *c-MYC* promoter, the TDRD3-TOP3B complex relaxes supercoiled DNA and reduces R-loops promoting *c-MYC* expression [157]. Interestingly, TOP3B is itself methylated by PRMT1, PRMT3, and PRMT6 which partially regulates its interaction with TDRD3 and enhances its activity in resolving supercoiled DNA and its localization to stress granules [254]. In breast cancer cells, the ADMA mark of ubiquitin-specific protease 9 X-linked (USP9X) is read by TDRD3 mediating its de-ubiquitination activity and localization to stress granules (**Figure 28**) [255]. CARM1 methylates R1899 of mediator complex subunit 12 (MED12) that is then read by TDRD3 promoting its interaction with non-coding RNAs [256]. Pol II R1810 is methylated by both PRMT5 [243] and CARM1 [257]. As mentioned earlier, R1810me2s is read by SMN and regulates R-loop resolving at the termination site (**Figure 28**) [243]. R1810me2a created by CARM1 on the other hand is recognized by TDRD3 and resolves R-loops at the promoter regions before transcription start site (**Figure 28**) [257].

#### **III.4.1.4. Others**

Other less studied TDRD proteins expressed in the male germ cells were described as effectors of arginine methylation [113,238]. Many of the TDRD proteins are linked to the piwi-RNA pathway and gametogenesis [258]. TDRD1 reads SDMA marks in the N-terminal of the Piwi-like RNA-binding protein PIWIL2 [259,260]. TDRD2 (also termed TDRKH) was shown to interact with PIWIL1 and PIWIL4 and that PRMT5 is required for this interaction [247,261]. However, structural analysis found that the Tudor domain of TDRD2 prefers binding to the non-methylated arginine residues in PIWIL1 rather than the methylated ones [262,263]. TDRD6 interacts with a SDMA modified peptide derived from PIWIL1 [264] and TDRD7 interacts with PIWIL2 [259].

#### **III.4.2. Readers not harbouring a Tudor domain**

Several proteins that do not have a Tudor domain were shown to interact with methylated arginine. Interestingly, most of these readers recognize non-GAR ADMA motifs that are written by CARM1 [113]. CARM1 methylation on H3, H3R17me2a, is recognized by the PAF1 transcription complex, increasing H3K4me3 levels and the transcription of estrogen responsive genes [265]. CARM1 methylates R754 of the acetyltransferase p300.

Methylated R754 is then recognized by BRCA1 which then cooperates with p53 to induce the expression of cell cycle genes like p21 in response to DNA damage [266]. The methylation of H3R4 by PRMT1 recruits SMARCA4, a subunit of the SWI/SNF complex, to the EGFR promoter enhancing its signalling and promoting CRC progression [233]. Under glucose starvation, CARM1 methylates the chromatin remodelling factor Pontin, mediating its interaction with Forkhead Box O 3a (FOXO3a) and activating autophagy genes transcription (**Figure 28**) [267]. Nuclear factor I B (NFIB) is methylated by CARM1 on R388. Only the methylated form of NFIB was able to interact with tripartite motif 29 (TRIM29) and promotes small cell lung cancer (SCLC) progression [268]. H3R2 is symmetrically and asymmetrically dimethylated by PRMT5 [172] and PRMT6 [269] respectively. H3R2me2a inhibits H3 interaction with WDR5, a subunit of lysine methyltransferase complex, and the trimethylation of H3K4 [269–271]. On the contrary, H3R2me2s recruits WDR5 and activates gene expression (**Figure 29**) [172]. Through its PHD motif, the DNA methyltransferase DNMT3A binds H4R3me2s motif generated by PRMT5 leading to chromatin methylation and gene silencing (**Figure 29**) [151,272].

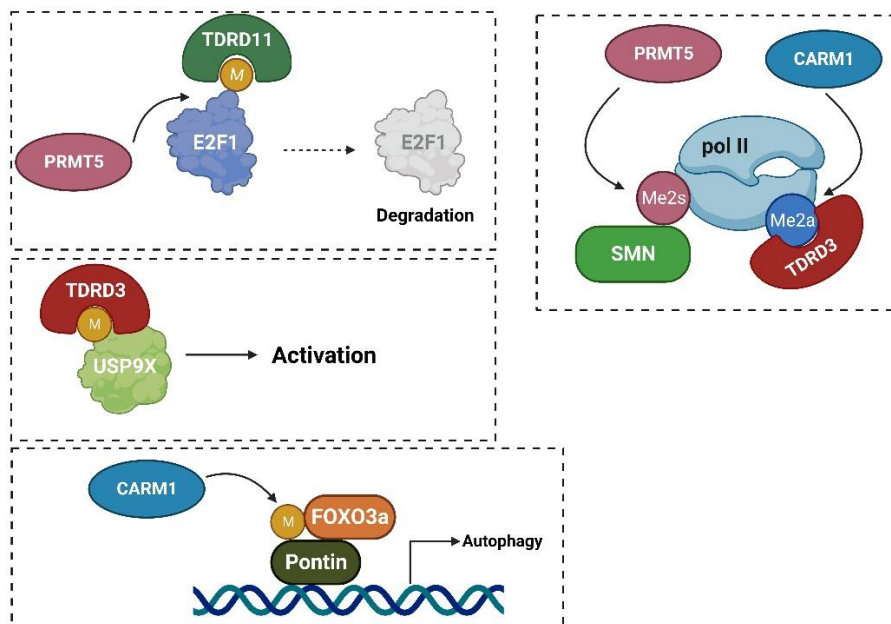


**Figure 28: Readers of non-histone methylation.** PRMT5 methylates E2F1 recruiting TDRD11 and promoting E2F1 degradation. USP9X asymmetric dimethylation marks are read by the Tudor domain of TDRD3 leading to its activation. CARM1 methylates the chromatin remodelling factor Pontin allowing its interaction with FOXO3a and the activation of autophagy genes. RNA pol II is methylated by both CARM1 and PRMT5. Symmetric dimethylation mark is recognized by SMN and the asymmetric mark recruits TDRD3. Both methylation status of pol II promotes the resolving of R-loops.

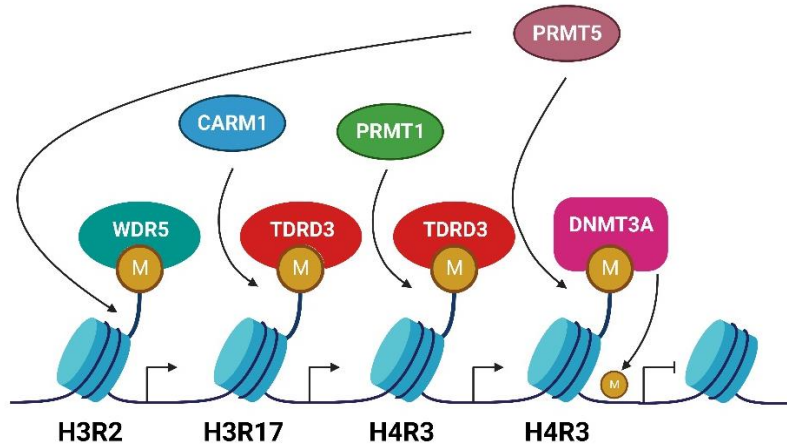


**Figure 29: Readers of histone arginine methylation marks.** TDRD3 recognizes the asymmetric dimethylation on H3R17 and H4R3 deposited by CARM1 and PRMT1 respectively leading to transcriptional activation. Symmetric dimethylation of H3R2 catalysed by PRMT5 recruits WDR5 and activates gene transcription, whereas asymmetric dimethylation of H3R2 created by PRMT6 has the opposite effect (not shown in the figure). H4R3me2s recruits DNMT3A through its PHD domain leading to DNA methylation and inhibition of transcription.

### III.5. Arginine methylation erasers

To date, the dynamic of arginine methylation is still not clear, and no specific arginine demethylase has been identified [273]. Unlike arginine demethylation, lysine demethylation is well established, with two groups of lysine demethylases (KDM) being described: (i) Class I KDMs: amine oxidase lysine specific demethylase 1 and 2 (LSD 1 and 2) also termed KDM1A and KDM1B, and (ii) Class II demethylases containing a Jumonji C domain (JmjC), consisting of 20 KDM enzymes grouped into five subfamilies KDM2-6 [274]. Class I KDMs utilise flavin adenine dinucleotide (FAD) to produce an amine intermediate that is then hydrolysed to generate demethylated lysine. Class II KDMs use Fe (II) as a cofactor and 2-oxoglutarate (2OG) to demethylate mono, di-, and tri- methyl sites [274]. Both KDM classes demethylate via oxidizing mechanisms and generate formaldehyde as a co-product [275]. The first report describing arginine demethylation was published in 2007 where the Jumonji domain-containing 6 protein (JMJD6) (class II KDM) was shown to be a 2OG oxygenase that demethylates H3R2 and H4R3 [276]. However, other studies could not replicate the demethylation activity of JMJD6 on H3 and H4 peptides using mass spectrometry methods [277], possibly due to

a weak demethylation activity that could not be detected. Later reports also supported the role of JMJD6 as an arginine demethylase of non-histone proteins. Upon oestrogen treatment, JMJD6 interacted with the arginine methylated form of ER $\alpha$  and demethylated it [278]. JMJD6 was also able to demethylate the CARM1 substrate heat-shock protein of 70 kDa (HSP70) on R469 [279]. G3BP1 is a stress granule component methylated by both PRMT1 and PRMT5. Upon oxidative stress, JMJD6 could demethylate the ADMA motif on G3BP1 promoting stress granule formation [280]. Other class II KDMs were later shown to demethylate arginine residues on histone tails and non-histone peptides *in vitro*. KDM3A, KDM4E, and KDM5C demethylated both ADMA and SDMA motifs yielding MMA or unmethylated peptides, while KDM6B was only capable of demethylating ADMA [275]. Two other members of the JmjC family, JMJD5 and JMJD7, have protease activities and could cleave the arginine methylated tails of H2, H3, and H4 [281]. More studies are needed to confirm if a dedicated arginine demethylase exists to better understand the dynamics and stability of arginine methylation.

### **III.6. Arginine methylation in Cancer**

The implication of arginine methylation in cancer has been extensively studied, and the different PRMT members are emerging as attractive targets for cancer therapy. PRMT5 is one of the most studied PRMT members in the context of tumorigenesis, and a detailed description, of its diverse functions in cancer will be discussed in section IV. The functions of other PRMTs in oncogenesis will be stated in this part.

#### **III.6.1. PRMT1**

##### **III.6.1.1. Breast cancer**

PRMT1, the major PRMT, is overexpressed in breast cancer at the mRNA and protein levels, and its expression is associated with poor survival in breast cancer patients [156,234,282]. The implication of PRMT1 in ER<sup>+</sup> breast cancer has been well described compared to the other breast cancer subtypes. In response to estrogen or IGF-1, PRMT1 methylates ER $\alpha$  at R260 regulating cell proliferation and survival in different breast cancer subtypes [283,284]. The methylated ER $\alpha$  triggers its interaction with PI3K and Src [283], forming an ER $\alpha$ /Src/PI3K complex in the cytoplasm of breast cancer cells and tumours [285]. The ER $\alpha$ /Src/PI3K complex is overexpressed in breast tumours and its high

expression correlates with the activation of AKT, low disease-free survival, and resistance to tamoxifen [285]. PRMT1 methylates BRCA1 in breast cancer cell lines regulating its protein-protein interaction and binding to chromatin, that could affect its tumour suppressor functions [216]. Depleting or inhibiting PRMT1 reduces the proliferation of TNBC cell lines [234,286,287]. The methylation of the transcription factor C/EBP $\alpha$  blocks its interaction with HDAC3 promoting the expression of cyclin D1 and the proliferation of TNBC cell lines [282]. In the TNBC cell line MDA-MB-468, PRMT1 knockdown decreased cell proliferation, sphere formation, and EGFR activation, and its inhibition sensitized the cells to the EGFR inhibitor cetuximab [230]. Our group showed that PRMT1 regulates the EGFR and Wnt signalling pathways in TNBC, and its depletion induces death of MDA-MB-468 [234]. In addition to promoting proliferation of breast cancer, several reports implicated PRMT1 in driving breast cancer metastasis and epithelial to mesenchymal (EMT) transition. By methylating H4R3 on *ZEB1* promoter and activating its expression, PRMT1 promotes EMT, invasion, and stemness of breast cancer cells [288]. EZH2 is a histone protein lysine methyltransferase (PKMT) and an inducer of EMT. PRMT1 methylates EZH2 at R342 inhibiting its phosphorylation and then subsequent ubiquitination. The stabilization of EZH2 through arginine methylation promotes breast cancer proliferation, EMT, invasion, and metastasis [289,290]. By secreting interleukin-6 (IL-6), tumour-associated macrophages (TAMs) stimulate the PRMT1-mediated methylation of EZH2 increasing breast cancer metastasis [291]. PRMT1 was suggested to contribute to drug resistance in MCF-7 breast cancer cell lines by interacting with pregnane x receptor (PXR) to activate the expression of multidrug resistance 1 (MDR1) gene [292]. PRMT1-mediated methylation of apoptosis signal-regulating kinase 1 (ASK1) enhances its interaction with its negative regulator thioredoxin. Depleting PRMT1 enhanced paclitaxel induced activation of ASK1 and apoptosis of breast cancer cells [293].

### **III.6.1.2. Other solid tumours**

PRMT1 expression levels are correlated with poor prognosis and reduced survival probability in CRC [294], and its inhibition decreased the progression of a CRC derived xenograft model [295]. Like in breast cancer, PRMT1 methylates EGFR in CRC, activating EGFR signalling and regulating the response to cetuximab treatment [228,233].

PRMT1 methylates non-POU domain-containing octamer-binding protein (NONO) promoting its oncogenic functions including CRC proliferation and metastasis [295]. Although being overexpressed in lung cancer, a little is known about the role of PRMT1 in this cancer type [296]. PRMT1 regulates EMT in lung cancer by methylating the E-cadherin repressor Twist1 [297], and mitosis through the methylation of the AURKB interactor, inner centromere protein (INCENP) [298]. In pancreatic ductal adenocarcinoma (PDAC), PRMT1 methylates the transcription factor Gli1 at R597 enhancing its binding to promoter regions, its transcriptional activity, and oncogenic functions [299]. PRMT1 can also promote the drug resistance of PDAC cells by methylating HSP70. meHSP70 binds to and stabilizes BCL2 mRNA thus increasing BCL2 protein levels and protecting cancer cells from gemcitabine-induced apoptosis [300]. PRMT1 levels are elevated in PDAC tumours and correlate with poor prognosis and survival [300]. In hepatocellular carcinoma (HCC), PRMT1 overexpression correlated with poor clinical outcomes, and its knockdown attenuated the growth of HCC cell lines [301]. PRMT1 expression predicts sensitivity to platinum-based chemotherapy, like cisplatin and carboplatin, in ovarian cancer patients [302]. An elegant study showed that PRMT1 is phosphorylated by DNA-dependent protein kinase (DNA-PK) upon cisplatin treatment, inducing its recruitment to the chromatin and activation of the senescence-associated secretory phenotype genes via H4R3 methylation, sensitizing ovarian cancer cells to cisplatin treatment [303].

### ***III.6.1.3. Leukemia***

PRMT1 levels are elevated in AML, MLL, and Hodgkin's lymphoma (HL) [304–306]. PRMT1 methylates Fms-like receptor tyrosine kinase 3 (FLT3) facilitating the recruitment of adaptor proteins and enhancing its oncogenic functions. Additionally, the type I inhibitor MS023 decreased the proliferation of AML and MLL cell lines, and it also enhanced the effect of FLT3 inhibitors in eliminating MLL and AML cells [305]. On the contrary, the tumour suppressor BTG1 recruits PRMT1 to methylate the transcription factor ATF4, activating its transcriptional activity towards pro-apoptotic genes. BTG1 is frequently deleted in leukemia leading to a shift of the activity of ATF4, which is no longer methylated by PRMT1, towards pro-survival genes expression [307]. Alterations in AS events contribute to cancer progression and could have prognostic values [308]. The splicing

factor SRSF1 is methylated by PRMT1, and both proteins are upregulated in acute lymphoblastic leukemia (ALL) patients contributing to leukemogenesis [309]. An elegant study revealed that AML cells harbouring mutations for splicing factors are more vulnerable to PRMT1 and PRMT5 inhibition. Moreover, the inhibition of both PRMTs together, or the inhibition of each PRMT in combination with a SF3B1 inhibitor, had synergistic effects in inhibiting AML cell proliferation [127].

### **III.6.2. PRMT2**

PRMT2 functions as a coactivator of nuclear receptors like ER $\alpha$  and AR, and its roles in ER $^+$  breast cancer has been investigated [310]. Full length PRMT2 and all its four splice variants are overexpressed in breast cancer and can interact with and activate ER $\alpha$  [310,311]. On the contrary, Oh *et al.* reported that PRMT2 mRNA level is lower in breast cancer compared to normal breast tissue, and that *PRMT2* and *ROR $\gamma$*  expression levels inversely correlate in ER $^+$  breast cancer [312]. PRMT2 interacts with ER $\alpha$  in its AF-1 region, DNA binding domain, and hormone binding site, acting as a transcriptional co-activator of the receptor [313]. In MCF-7 cells, PRMT2 prevented ER $\alpha$  from interacting with AP-1 on cyclin D1 promoter, resulting in a downregulation of cyclin D1 levels. The loss of nuclear PRMT2 positively correlates with cyclin D1 levels and the grade of IDC breast tumours [314]. Overexpression of PRMT2 splice variant, PRMT2 $\beta$ , arrested cell cycle progression, induced apoptosis, and inhibited cyclin D1 expression in MCF-7 cells [315]. Through its interaction with ER- $\alpha$ 36 and inhibiting its activity, PRMT2 regulates the response of breast cancer cells to tamoxifen treatment [316]. In glioblastoma (GBM), PRMT2 is highly expressed and is associated with poor prognosis [317]. PRMT2 methylates H3R8 activating the expression of oncogenic genes, and its silencing inhibits GBM cells proliferation and the self-renewal abilities of GBM stem cells [317]. Similarly, PRMT2 is overexpressed and predicts poor prognosis in HCC, and it was shown to activate Bcl2 expression in HCC cells by methylating H3R8 at its promoter [318].

### **III.6.3. PRMT3**

PRMT3 interacts with the tumour suppressor protein DAL-1/4.1B in lung and breast cancer cells, leading to an inhibition of PRMT3 catalytic activity [319]. DAL-1/4.1B also interacts with PRMT5 [319,320], and inhibiting the global methylation using Adox



significantly increased MCF-7 cells apoptosis induced by DAL-1/4.1B [321]. Invasive micropapillary carcinoma (IMPC) is a breast cancer histological subtype exhibiting higher invasiveness and metastasis incidence compared to IDC. Recently, IMPC samples were shown to have increased levels of total arginine methylation compared to IDC, and PRMT3 was identified as the main driver of this distinction [322]. The same study revealed that the methylation of H4R3 by PRMT3 regulates the endoplasmic reticulum (ER) stress signalling pathway and enhances breast cancer cells proliferation and invasion [322]. PRMT3 upregulation contributes to pancreatic cancer cell resistance to several chemotherapies by increasing the expression of the ATP-binding cassette member ABCG2, that is involved in drug resistance. Mechanistically, PRMT3 methylates hnRNPA1 at R31 promoting its binding to ABCG2 mRNA and its stabilization [323]. PRMT3 is upregulated in CRC [324,325] and its overexpression enhances CRC cells proliferation and invasion by stabilizing c-myc expression [325]. Moreover, PRMT3 methylates HIF1 $\alpha$  at R282 stabilizing its expression and enhancing its oncogenic functions in CRC [324].

#### **III.6.4. PRMT4**

##### ***III.6.4.1 Breast cancer***

CARM1 is overexpressed in the different breast cancer subtypes and its overexpression is associated with poor prognosis [326–328]. CARM1 is well studied in the context of ER<sup>+</sup> breast cancer due to its interaction with and activation of ER $\alpha$ . In ER<sup>+</sup> breast cancer cells, CARM1 is enriched on ER $\alpha$ -enhancers and essential for the activation of estrogen-induced genes [128]. Mapping of CARM1 methylome revealed that several CARM1 substrates are implicated in the regulation of ER signalling [128]. PTM of CARM1 regulates its functions in ER activation. Phosphorylation of CARM1 at S228 inhibits CARM1 activity and activation of estrogen-regulated transcription [329], and its phosphorylation by PKA on S448 is indispensable to its interaction with and subsequent activation of ER $\alpha$  [330]. CARM1 methylates LSD1 promoting its deubiquitylation and stabilization [331]. LSD1 stabilization increases the demethylation levels of H3K4me2 and H3K9me2, activating vimentin transcription and promoting metastasis of breast cancer cells. The levels of CARM1-dependent methylation of LSD1 correlates with the grade of human breast cancer samples [331]. In MCF-7 cell, CARM1 in cooperation with ER $\alpha$  and



AIB1 asymmetrically dimethylates H3R17 on the promoter of *E2F1*, activating its transcription [198]. CARM1 binds to and methylates MED12 on several arginine residues regulating its association with the chromatin and the activation of ER $\alpha$  genes [332], sensitizing breast cancer cells to chemotherapy [333]. CARM1 methylates the SWI/SNF subunit BAF155 at R1064 regulating breast cancer metastasis, and this CARM1-dependent meBAF155 is itself a prognostic marker for breast cancer relapse [334]. CARM1 switches the metabolism of breast cancer cells from oxidative phosphorylation to aerobic glycolysis by inhibiting the expression of inositol-1,4,5-trisphosphate receptors (InsP3Rs) through the methylation of the glycolytic enzyme pyruvate kinase muscle isozyme M2 (PKM2). The CARM1-dependent shift of breast cancer cells' metabolism to glycolysis promotes their tumorigenesis and invasiveness [335].

#### **III.6.4.2. Other solid tumours**

In ovarian cancer, CARM1 interacts with the transcription regulator NAC1 and both proteins are overexpressed and associated with poor prognosis in ovarian cancer patients [336]. CARM1 methylates BAF155 promoting the EZH2-mediated repression of tumour suppressor genes such as MAD2L2 [337,338]. Moreover, EZH2 inhibition reduced the proliferation of ovarian cancer cells and the growth of ovarian xenograft models specifically in cells/tumours expressing CARM1 [337], and sensitized CARM1-high ovarian cancers to PARP inhibitors [338]. CARM1 is upregulated in CRC and regulates the transcriptional targets of p53 and NF $\kappa$ B [339]. By suppressing the expression of CARM1, microRNA-195 induces death of CRC cell lines and increases their sensitivity to radiation [340,341]. CARM1 interacts with  $\beta$ -catenin and positively regulates its target genes expression promoting CRC proliferation [342]. Similarly, CARM1 cooperates with  $\beta$ -catenin to increase prostate cancer proliferation [343]. CARM1 activates AR mediated transcription by methylating H3 at AR enhancers in prostate cancer cells [344]. However, CARM1 is also implicated in the development of AR-independent prostate cancer [345]. In contrast to its cancer driving roles in other cancer types, CARM1 was proposed to suppress the proliferation of PDAC. CARM1 methylates the aspartate aminotransferase malate dehydrogenase 1 (MDH1) inhibiting its dimerization and activation, and this leads to the suppression of glutamine metabolism and cell proliferation [346].

### **III.6.4.3. Leukemia**

Although not important for normal haematopoiesis, CARM1 is required for AML oncogenesis [347]. By methylating RUNX1, CARM1 represses the expression of miR-223, blocking the differentiation of hematopoietic stem cells (HSCs) [348]. Targeting CARM1 with two small molecule inhibitors, EZM2302 and TP-064, exhibited an anti-tumour activity in multiple myeloid leukemia (MML) cell lines and xenograft model [349], and diffuse large B-cell lymphoma (DLBCL) growth [350]. Mutations in CREBBP and EP300 were suggested to be biomarkers of response to CARM1 inhibition in DLBCL, as the sensitivity to CARM1 inhibition correlates with CREBBP/EP300 mutational load, and inhibiting CARM1 globally decreases the acetyltransferase activity of CBP [350]. Interestingly, CARM1 methylates PRMT5 inhibiting its methyltransferase activity in erythroleukemia cells [351].

### **III.6.5. PRMT6**

PRMT6 is overexpressed in several cancer types including NSCLC, SCLC, bladder, and breast cancer [296]. PRMT6 regulates the expression of important cell cycle regulators like p21 and p16 [352]. Additionally, the methylation of H3R2 by PRMT6 inhibits the DNA methyltransferase 1 (DNMT1) cofactor UHRF1 recruitment to the chromatin, causing global DNA hypomethylation in cancer [353]. PRMT6 knockdown affected the global transcription and pre-mRNA splicing processes in breast cancer cells, and PRMT6 dysfunction correlated with a better relapse- and metastasis- free survival in ER<sup>+</sup> breast cancer [354]. In ER<sup>+</sup> breast cancer, PRMT6 interacts with the ligand-binding domain of ER $\alpha$  and methylates the receptor, activating both ligand dependent and independent activation of ER $\alpha$  [355]. In addition to its roles in transcriptional regulation, PRMT6 can also control AS events in breast cancer [356]. PRMT6 cooperates with the proto-oncogene proline, glutamate, and leucine rich protein 1 (PELP1) to activate ER, proliferation, and AS of cancer-related transcripts in breast cancer [357]. Recently, the complex of PRMT6, PARP, and CUL4B was shown to regulate the circadian clock supporting breast cancer progression [358]. On the contrary, PRMT6 can play a role as a tumour suppressor in ovarian, hepatocellular, and prostate cancer [359].

### III.6.6. PRMT7

PRMT7 is overexpressed in breast cancer and drives EMT and metastasis in breast cancer by downregulating E cadherin expression [360,361]. Furthermore, PRMT7 auto-methylation [362] and PRMT7-dependent activation of matrix metalloproteinase 9 (MMP9) expression [363] promotes the invasiveness of breast cancer cell lines. The methylation of mitochondrial ribosomal protein S23 (MRPS23) on R21 by PRMT7 and K108 by SETD6 controls its stabilization and subsequently breast cancer metastasis [363].

### III.7. PRMT inhibitors

Specific inhibitors targeting PRMT3, CARM1, PRMT5, PRMT6, and PRMT7 and pan-type I PRMT inhibitors have been developed, and some of these inhibitors have been evaluated in clinical trials. To date, PRMT5 has the highest number of specific inhibitors, and it is the most evaluated PRMT member in the clinical trials. **Table 2** lists the different inhibitors with their PRMT target, company, mechanism of action, and whether or not they were included in clinical trials. A separate table for PRMT5 inhibitors is found in section IV.

**Table 2: PRMT inhibitors**

Compound	Target	Company	Mechanism	Clinical trial	Ref
SGC707	PRMT3		Allosteric	-	[365]
EZM2302 (GSK3359088)	CARM1	Epizyme GlaxoSmithKline	Substrate competitive with additional contacts to the SAM binding pocket	-	[349]
TP-064	CARM1		Substrate competitive	-	[366]

MS049	CARM1 and PRMT6		Substrate competitive	-	[367]
EPZ020411	PRMT6	Epizyme	Substrate competitive	-	[368]
SGC6870	PRMT6		Allosteric	-	[369]
SGC8158	PRMT7		SAM competitive	-	[370]
	converted from the prodrug SGC3027				
DS-437	PRMT5 and PRMT7		SAM competitive	-	[371]
MS023	Type I PRMT		Substrate competitive	-	[372]
GSK3368715	Type I PRMT	Epizyme GlaxoSmithKline	Substrate competitive	NCT03666988	[134]

## Summary

Post-translational modifications are main regulators of proteins' functions, among which, arginine methylation is an abundant modification that is catalysed by the PRMT family. Arginine methylation preserves the charge of the protein but creates a bulky group that could interfere with protein-protein or protein-nucleic acid interactions. The PRMTs are classified according to their methylation mode into type I PRMT catalysing MMA and ADMA, type II PRMT catalysing MMA and SDMA, and type III PRMT catalysing only MMA. PRMTs form homodimers and are highly conserved for their central methyltransferase domains. Arginine methylation is commonly read by proteins harbouring a tudor domain, but other readers have been reported. PRMT members are implicated in diverse cellular processes and play roles in cancer progression. For that, inhibitors that target the PRMTs are developed, and several are currently under clinical evaluation. It is still not clear how the dynamics of arginine methylation work. Although some lysine demethylases were reported to remove the arginine methylation modification, no specific arginine demethylase has been discovered till now, and the extent of arginine methylation stability remains unclear.

## IV. Protein Arginine Methyltransferase 5 (PRMT5)

### IV.1. Generalities

PRMT5 is the main type II PRMT responsible for generating the majority of arginine symmetric di-methylation. PRMT5 methylates arginine in glycine rich regions, mainly within the RGG motif. It was first discovered in 1999 as a JAK2 interacting partner using the yeast two hybrid system (Y2H) and was initially termed Jak-binding protein 1 (JBP1) [152]. *PRMT5* gene is located on chromosome 14q11.2–21 [152], and the 2.5 kb PRMT5 transcript is widely expressed in tissues [152,188]. PRMT5 protein can form dimers [152]. The expression of PRMT5 is dysregulated in different cancers, either at the mRNA or/and protein levels. I will discuss in more details the involvement of PRMT5 in carcinogenesis in a later section. *PRMT5* homologues include the *S. pombe* Shk1 kinase-binding protein 1 (*Skb1*) and the *S. cerevisiae* histone synthetic lethal 7 (*HSL7*). In order to be fully active, PRMT5 associates with its main partner methylosome protein 50 (MEP50 or WDR77) in a hetero-octameric complex [122,373].

### IV.2. General structure of PRMT5

Human PRMT5 is a 72 KDa protein composed of 637 aa [188]. PRMT5 contains four main domains: a TIM-barrel domain at the N-terminal, a Rossmann-fold located in the middle of the protein, and a  $\beta$ -barrel domain at the end (**Figure 30**) [123,188]. Rossmann fold and the  $\beta$ -barrel domain constitute PRMT5 methyltransferase domain. Within the  $\beta$ -barrel domain is a ~60 residues dimerization domain, similar to other PRMTs. PRMT5 contains 3 nuclear exclusion sequences (NES). The first NES is located in the N-terminal domain (1-90) and the two other NES are in the C-terminal domain (500-560 and 576-637) (**Figure 30**) [374].

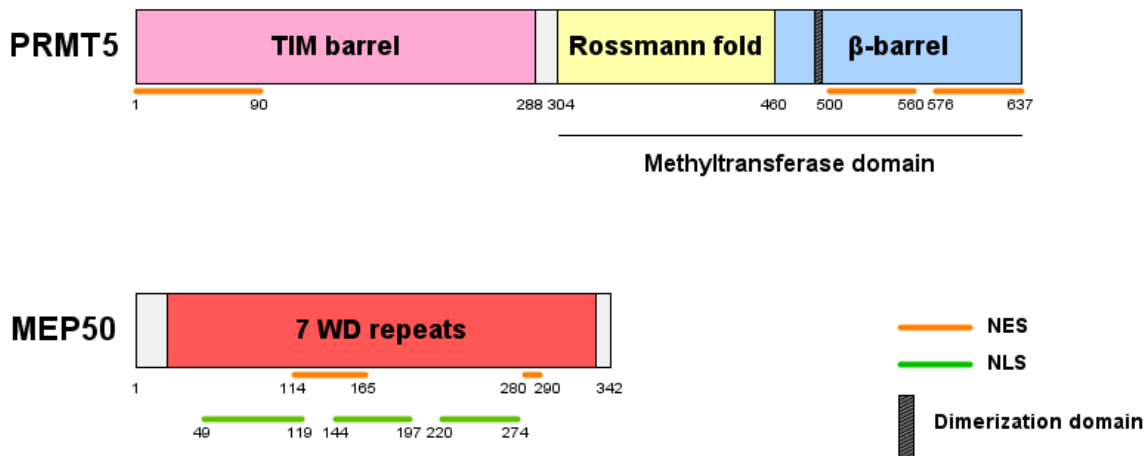


**Figure 30: PRMT5 and MEP50 structures.** PRMT5 is composed of three domains: the N-terminal TIM barrel, middle Rossmann fold and the  $\beta$ -barrel domain. The dimerization domain of PRMT5 is embedded in its  $\beta$ -barrel domain. The Rossmann fold and  $\beta$ -barrel compose the methyltransferase domain. PRMT5 harbours three NES that control its nuclear and cytoplasmic shuttling. MEP50 has 7 WD repeats, two NES and three NLS for its subcellular compartmentalization. NES: nuclear exclusion signal; NLS: nuclear localization signal.

### IV.3. Crystal structure of PRMT5

In 2011, the first crystal structure of PRMT5 from *C. elegans*, that shares high sequence homology with the human PRMT5, was determined. The oligomerization domain of PRMT5 connects the TIM-barrel and the  $\beta$ -barrel domains. The TIM, Rossmann-fold, and  $\beta$ -barrel domains are packed in a triangular fashion [123]. PRMT5 forms homodimers, where intermolecular interactions occur between the dimerization domains and between the TIM-barrel and  $\beta$ -barrel domains (**Figure 31**) [123].

#### IV.3.1. The active site

The residues F379, K385, S503, and S669 (*in C. elegans*) are conserved in the active site of PRMT5 proteins, and correspond to M, R, Y, and H respectively in type I PRMTs. Mutating most of these residues to their counterparts in type I PRMTs greatly diminishes PRMT5 enzymatic activity. However, mutating F379 to methionine (F379M) increases PRMT5 activity and confers PRMT5 the ability to both symmetrically and asymmetrically dimethylate histone H4R3. The corresponding mutation in human PRMT5 (F327M) yielded the same effects [123]. To access PRMT5 active site, H4 derived peptide binds the groove at  $\beta$ -barrel surface and inserts R3 side chain through a tight tunnel made of

L312, F327, and W579 [122]. PRMT5 active site contains the S atom of SAH and the invariant glutamate residues common to all PRMTs, E435 and E444 (corresponding to E499 and E508 in *C. elegans*). These two glutamate residues are indispensable for PRMT5 enzymatic activity and are located on the “double-E” loop bridging  $\beta$ -4 and  $\alpha$ -F [122,123]. The guanidine side chain of arginine substrate forms a pair of salt bridges with each of these two E residues, posing the  $\omega$ -NG atom for methyl transfer [122]. F327 residue plays a critical role in orienting the N atom for the transfer [122]. Y304 and Y307, which are phosphorylated by a Jak2 mutant [375], participate in substrate binding [122].

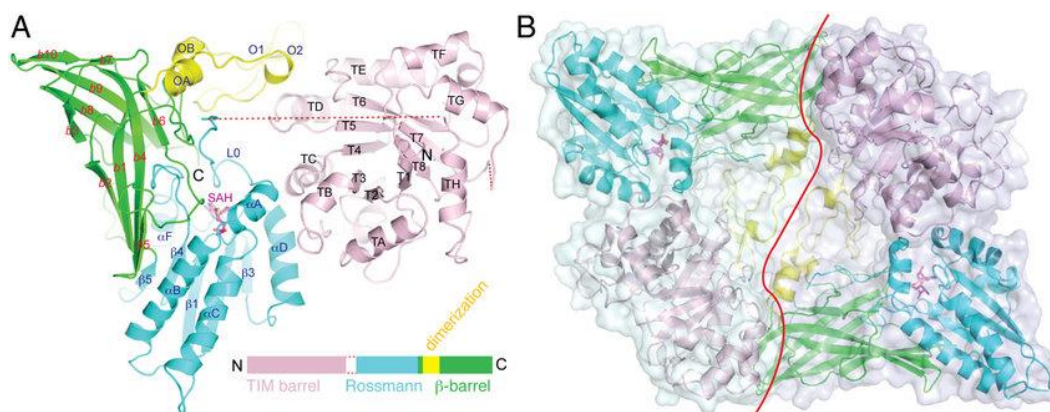


**Figure 31: Crystal structure of PRMT5.** (A). Ribbon diagram of PRMT5. TIM barrel is shown in tan, Rossmann fold in cyan,  $\beta$ -barrel in green, and oligomerization domain in yellow. SAH is shown as a stick. (B). A PRMT5 dimer in ribbon representation. The red line approximately marks the dimer interface. From [123].

### IV.3.2. Comparing PRMT5 structure to type I PRMTs

The spatial positioning and fold of the Rossmann-fold and  $\beta$ -barrel of PRMT5 are similar to PRMT1 and CARM1. Upon SAH binding, a N-terminal loop (termed L0) and a nearby  $\alpha$ -helix (termed  $\alpha$ -A) become ordered. Similar to type I PRMTs, the  $\alpha$ -A protects SAH from solvent and forms a secured catalytic active site. Y376 and F379 of PRMT5 found on  $\alpha$ -A interact with ribose via hydrogen bond and with the homocysteine via van der Waals. L0 harbours residues conserved among PRMT5 proteins in different species. The corresponding region is disordered in PRMT1 and has a helical form in CARM1. L0 of PRMT5 is responsible of contacting the SAH/SAM molecules via the residues P366, L367, and L371 (*C. elegans*) constituting a catalysis area inaccessible by solvent. The



beginning of L0 contacts the dimerization domain, thus stabilizing the loop in a form allowing it to affect substrate binding [123].

The PRMT5 catalytic domain adopts a tertiary structure similar to that of type I PRMTs. SAM binding occurs in the Rossmann fold and the substrate binding pocket lies in the  $\beta$ -barrel domain [122]. The YFxxY motif characteristic of type I PRMTs is absent in PRMT5 and the corresponding region in PRMT5 has a PLxxN motif [122,123]. Additionally, the THW motif conserved in type I PRMTs is a FSW in PRMT5 [122].

## IV.4. PRMT5 partners

### IV.4.1. The methylosome

PRMT5 is mainly present in cells as a part of multimeric complexes. To be fully active, PRMT5 needs to associate with MEP50 [122,376]. Moreover, PRMT5 interacts with additional partners known as substrate adaptors, that are required for substrate recognition and methylation [377,378]. This complex of PRMT5, MEP50 and adaptor proteins is termed the methylosome (**Figure 32A**). The most known PRMT5 adaptor proteins are RIO kinase 1 (RIOK1), pICln (also known as CLNS1A), and cooperator of PRMT5 (COPR5). A recent report revealed that these three adaptors share a common site termed PRMT5 binding motif (PBM), **GQF[D/E]DA[E/D]**, that is crucial and sufficient for interacting with PRMT5 [377]. The PBM interacts with a shallow groove in the TIM barrel domain of PRMT5 [377]. In the same year, another study with similar results was published, showing that the PRMT5 adaptors pICln, RIOK1 and COPR5 share a conserved sequence motif (**GQF[D/E]DA[E/D]**) responsible for binding with PRMT5 TIM barrel domain [378]. After these findings, compounds targeting the protein-protein interaction (PPI) of PRMT5 and its adaptor proteins are starting to emerge as a new class of PRMT5 inhibitors (**Figure 32B**) [379–381].

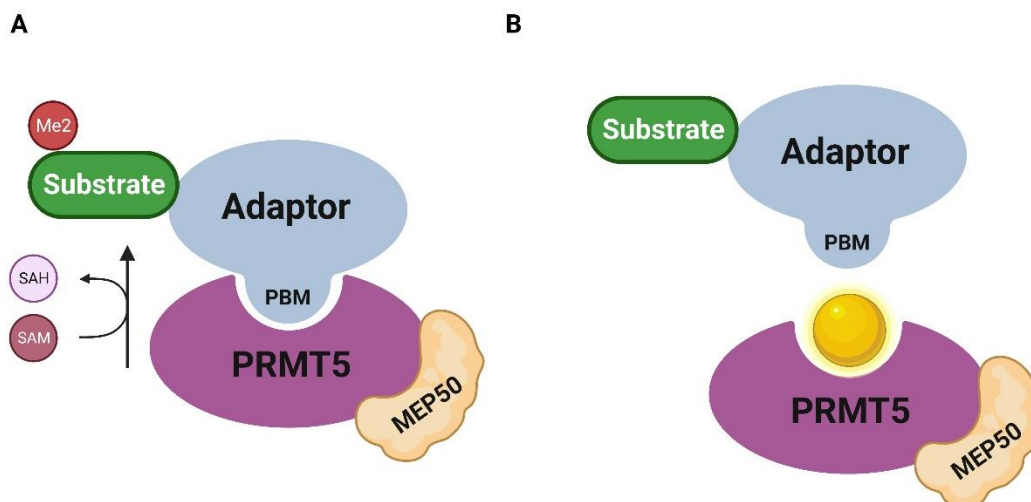


**Figure 32: PRMT5 methylosome.** (A). An adaptor protein (like RIOK1, pICln...) recruits the substrate to be methylated by PRMT5. PRMT5 adaptor proteins share a common motif termed the PBM that is responsible for the interaction with PRMT5. (B). Molecules targeting the PBM binding site in PRMT5 prevent PRMT5-adaptor interactions and hence inhibit its activity. PBM: PRMT5 binding motif; SAM: S-adenosyl methionine; SAH: S-adenosylhomocysteine.

#### IV.4.2. MEP50: a major PRMT5 partner

##### IV.4.2.i. MEP50 generalities

MEP50 is a main partner of PRMT5 that highly enhances its catalytic activity. MEP50 was initially identified by two separate groups as (i) a 50KDa WD repeat protein present in the methylosome [373], and (ii) a 44KDa androgen receptor (AR) co-activator (p44) overexpressed in prostate cancer [382]. Both studies identified MEP50 as a PRMT5 partner. MEP50 contains 7 WD repeats (**Figure 30**), and is composed of 342 aa and weighs 36.7 KDa but migrates above 45 KDa on SDS-PAGE gel [373]. MEP50 can shuttle between the nucleus and cytoplasm due to its 2 NES and 3 nuclear localization sequence (NLS). MEP50 NES1 (114-165) is not a conventional Leucine-rich NES while NES2 (280-290) is. Interestingly, NLS1 (49-119), NLS2 (144-197), and NLS3 (220-274) do not resemble any known NLS [383].

##### IV.4.2.ii. PRMT5:MEP50 crystal structure

The crystal structure of PRMT5 in complex with MEP50, H4 peptide (1-24), and A9146C (SAM analogue) was determined in 2012 (**Figure 33**) [122]. Four molecules of PRMT5 associate with four molecules of MEP50 to form a ~453 KDa hetero-octamer complex (**Figure 33A**). PRMT5 residues 13-637, covering almost the full protein, were ordered in

the structure. MEP50 residues 21-329 with the exception of loops 208–211 and 245–246 were also ordered. The four molecules of PRMT5 interact together through the TIM barrel and catalytic domain, and form a tetramer at the core of the complex (Figure 33A-C). MEP50 molecules interact only with the TIM barrel of PRMT5 and reside at the outer surface of the PRMT5<sub>4</sub>:MEP50<sub>4</sub> octamer (Figure 33A-C). Cryo-electron microscopy of the PRMT5:MEP50 complex revealed the same hetero-octamer complex structure [384].

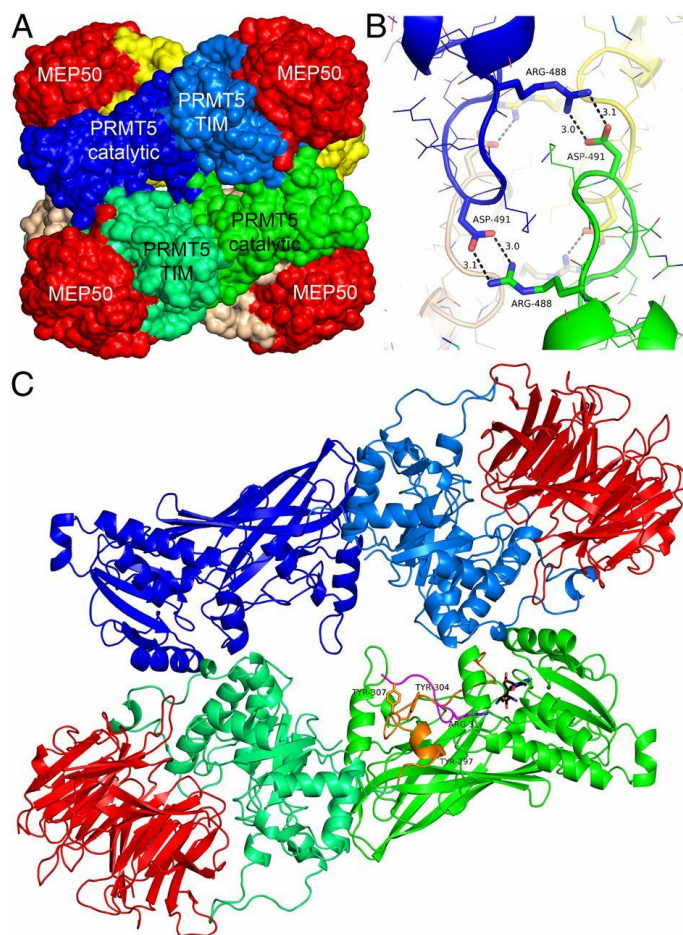


**Figure 33: PRMT5:MEP50 crystal structure.** (A). Structure of human PRMT5/MEP50 complex. The four monomers of PRMT5 are shown in green, blue, wheat, and yellow and are found at the core of the hetero-octameric complex. MEP50 four monomers, in red, are present at the periphery of the complex and only interact with the TIM barrel of PRMT5. (B). The interaction between two PRMT5 monomers, at the center of the complex, occur through their dimerization domains via salt bridges. (C). PRMT5 dimer bound to SAM analogue (in black) and H4 peptide (in magenta) with the R3 residue presented as a stick. In orange is the linker between TIM barrel domain and the C-terminal catalytic domain. From [122].

#### **IV.4.3. pICln**

The methylosome subunit pICln is a 26 KDa chaperon protein encoded by the *CLNS1A* gene and interacts with the Sm proteins in the cytoplasm. pICln is an adaptor protein of PRMT5 that enhances its activity towards specific substrates [385]. pICln brings Sm proteins Sm B/B', Sm D1, and Sm D3 to be symmetrically di-methylated by PRMT5 on their RG motifs. This methylation is essential in early steps of U snRNPs assembly, by mediating the loading of Sm protein on the SMN-complex [385–387]. A detailed mechanism of PRMT5 roles in the 6S complex and spliceosome assembly will be discussed later. pICln enhances PRMT5 mediated methylation of Sm proteins but inhibits that of histones [387]. However, a recent study showed that PRMT5 cooperates with pICln to activate AR transcription via H4R3 methylation on the AR promoter, independent of MEP50, in castration-resistant prostate cancer (CRPC) [388]. Moreover, PRMT5 and pICln activate the transcription of genes involved in the DDR [389].

#### **IV.4.4. RIOK1**

RIOK1 is a 90 KDa protein and a member of the RIO kinase family. RIOK1 is a strictly cytoplasmic PRMT5 adaptor protein and competes with pICln for binding to the N-terminal of PRMT5. RIOK1 recruits nucleolin, an RNA-binding protein involved in ribosome biogenesis, to be symmetrically di-methylated by PRMT5:MEP50 complex [390]. Nucleolin methylation is involved in its interaction with RNA [391]. RIOK1 also recruits nuclear factor 90 (NF90) to be methylated by PRMT5 in its C-terminal region [392].

#### **IV.4.5. COPR5**

COPR5 is a PRMT5 adaptor protein that regulates its nuclear functions. COPR5 binds the N terminal tail of H4 and recruits PRMT5 to the nucleosomes *in vitro*. Moreover, COPR5 can potentially regulate PRMT5 substrate specificity, as it promotes the methylation of H4R3 but not H3R8 [393]. Knockdown of COPR5 decreases H4R3 symmetric di-methylation inducing cardiomyocyte hypertrophy [394]. PRMT5 is less recruited to the promoter of *Dlk-1* (a Wnt target gene) [395] *CCNE1* (encoding cyclin E1) [393], *p21*, and *MYOG* [396] genes when COPR5 is downregulated. COPR5 interacts with RUNX1 which is suggested to recruit PRMT5-COPR5 complex to the promoter of *p21* and *MYOG* hence regulating myogenic differentiation [396].

In addition to MEP50 and its adaptors, PRMT5 interacts with a wide range of proteins involved in different cellular functions. PRMT5 partners are listed in **Table 3**, and I will discuss each separately according to the functional roles they play with PRMT5 in the “PRMT5 functions” section.

**Table 3: PRMT5 partners.**

<b>PRMT5 partner*</b>	<b>Partner interacting domain</b>	<b>PRMT5 interacting domain</b>	<b>Functional impact</b>	<b>Ref</b>
Jak1	ND	aa 268-637	ND	[152]
Murine Jak2	ND	aa 268-637	ND	[152]
Tyk2	ND	aa 268-637	ND	[152]
pICln	PBM	TIM barrel	PRMT5 adaptor	[377,378,385]
RIOK1	PBM aa 1-242	TIM barrel	PRMT5 adaptor	[377,378,390]
COPR5	PBM	TIM barrel	PRMT5 adaptor	[393]
STAT3	ND	ND	Differentiation gene repression in ESC	[169]
LCE1C	ND	ND	LCE1C translocates PRMT5 to the cytoplasm	[397]
14-3-3	ND	623-637(phosphorylated)	Viability of mice embryo	[398]
NHERF	PDZ	623-637 (unphosphorylated)	ND	[398]
MYPT-1	N-terminal	ND	MYPT-1 decreases PRMT5 activity by diminishing its phosphorylation at T80	[399]
LKB1	ND	Rossmann fold	LKB1 phosphorylates PRMT5 and inhibits its activity	[400]

Src	ND	ND	Phosphorylation of PRMT5 and inhibition of its activity	[212]
SHARPIN	UBL	TIM and $\beta$ -barrel	Facilitates the formation of PRMT complexes and increases its methyltransferase activity	[224,401]
CARM1	ND	aa 454–637	Inhibits PRMT5 homodimerization and methyltransferase activity	[351]
DAL-1/4.1B	ND	ND	Regulates PRMT5 catalytic activity	[319]
CHIP	TPR	ND	Ubiquitin-dependent degradation of PRMT5	[402]
TRAF6	ND	ND	Enhances PRMT5 binding to MEP50 and its activity	[403]
Cyclin D1			Phosphorylation of MEP50 and enhancing PRMT5 activity	
CDK4	ND	ND		[404]
FAM47E	ND	ND	Enhances PRMT5 stability and activity	[405]
EWSR1-ATF1	ND	ND	Enhances EWSR1-ATF1 transcriptional activity	[406]
SWI/SNF	ND	ND	Regulation of transcription	[153,407]
Blimp1	ND	ND	Regulates epigenetic reprogramming in primordial germ cells	[408]
CDK8 and CDK19	ND	ND	Repression of immune response genes transcription	[409]

\* Partners validated as PRMT5 substrates are listed in table 4.

## IV.5. The PRMT5 methylome

Several studies have determined the general methylome of PRMT5 in different cell types. Radzsheuskaya *et al.* applied Liquid Chromatography with tandem mass spectrometry (LC-MS/MS) to identify PRMT5 global substrates in AML [133]. KRAB cells treated either with sg-ctrl or two different sgRNA targeting PRMT5 were analysed using the TMT method, an isobaric isotope labelling quantitative technique. Profiling of proteins and of methylated peptides yielded 2962 differentially expressed proteins in the two sgPRMT5 samples, and the identified PRMT5 consensus motif in this study is **GRGRGR**. PRMT5 knockdown (KD) led to a dysregulation in RNA AS events. The splicing factor SRSF1 was identified as a PRMT5 substrate, di-methylated at R93, R97, and R109 [133]. SRSF1 methylation did not affect its localization as both wild type (wt) and lysine-mutant were nuclear. However, PRMT5 KD led to a considerable change in the proteins and mRNA transcripts that bind to SRSF1, suggesting a role of SRSF1 arginine methylation in regulating its PPI and nucleic acid binding [133]. Another study identified PRMT5 global substrates by immuno-enrichment of MMA (using PTMScan Mono-Methyl Arginine Motif [mme-RG] Kit #12235; Signaling Technology) and SDMA (using PTMScan [sdme-R] Kit #13563; Cell Signaling Technology) peptides, coupled to SILAC in HeLa cells treated or not with the PRMT5 inhibitor GSK591 [147]. PRMT5 preferred to modify arginine residues lying between two glycine residues “**GRG**” [147]. Most of the proteins whose methylation was regulated upon PRMT5 inhibition belong to the class of RNA binding proteins (RBP) and involved in RNA processing [147]. Another study used a similar approach based on immune enrichment and SILAC, and the same SDMA and MMA enrichment kits (#12235 and #13563), for PRMT5 substrate profiling in acute promyelocytic leukemia NB4 cells treated with GSK591 [127]. 391 methyl containing peptides altered upon PRMT5 inhibition were identified; of which 299 had MMA, 40 with DMA and 52 having both modifications. PRMT5 preferentially methylated arginine in the “**GRG**” motif, and most proteins were RBPs involved in RNA export, stability, and splicing [127]. The PRMT5 methylome was also determined in the mantle cell lymphoma (MCL) cell line Z-138 by immunoprecipitating SDMA containing proteins (using antibody #13222; Cell Signaling Technology), either treated or not by the PRMT5 inhibitor GSK591, followed by mass

spectrometry (MS) analysis [410]. The majority of SDMA containing proteins are involved in pre-mRNA splicing, transcription, and translation processes. Moreover, PRMT5 inhibition induced AS of MDM4, activating the p53 pathway and marking a critical role in the response to PRMT5 inhibition [410]. In MTAP-null PDAC, 408 peptides containing SDMA were identified from 107 proteins as PRMT5 substrates, with the majority of peptides methylated at the “**GRG**” motif [377]. Li *et al.* identified the methylome of PRMT4, PRMT5, and PRMT7 and revealed that these three PRMTs are important for the regulation of AS events and can methylate hnRNPA1 on different R residues enhancing its RNA binding ability [132]. Interestingly, a recent study identified PRMT5 substrates in the nuclear and cytoplasmic compartments of primary mouse oligodendrocyte progenitor cell (OPC) using isobaric Tags for Relative and Absolute Quantitation (iTRAQ) method on cells knocked down for PRMT5 [411]. Out of the 307 symmetrically di-methylated identified peptides (corresponding to 60 proteins), 77 were cytosolic, 91 were nuclear, and 139 were present in both compartments. Whether in the nucleus or cytoplasm, the identified potential PRMT5 substrates are implicated in RNA processing, splicing, stability, and translation. Nuclear substrates additionally included DNA binding proteins and histones [411].

In addition to these large-scale proteomic analyses, PRMT5 was shown to methylate proteins involved in various aspects of cellular functions. **Table 4** lists the known and validated PRMT5 substrates.

**Table 4: PRMT5 known substrates.**

Substrate	Residue	Functional impact	Ref
H2A	R3	Transcriptional regulation	[152]
H3	R8, R2	Transcriptional regulation	[153]
H4	R3	Transcriptional regulation	[123,150–153]
SmD1	R98, R100, R102, R104, R106, R108, R110, R112, R114		



SmD3	R110, R112, R114, R118	Directs Sm proteins assembly to the SMN complex	[385,386]
Sm B/B'	R108, R112, R147, R172, R181, R209		
Nucleolin	ND	Regulates RNA binding	[390,391]
NF90	C-ter (aa 640 to 655)	ND	[392]
SRSF1	R93, R97, R109	PPI and mRNA binding	[133]
hnRNPA1	R206, R218, R225	Promotes RNA binding Promotes growth of cancer cells Promotes IRES-dependent translation	[132,147,193]
hnRNPH1	R217, R224	ND	[147,410]
hnRNPK	ND	ND	[147]
SFPQ	aa 298–707	ND	[147]
KHDRBS1	ND	ND	[147]
CNBP	R25, R27	ND	[147]
ZNF326	R175	Regulates AS	[412]
FUBP1	ND	ND	[410]
53BP1	ND	Increases 53BP1 stability and the NHEJ pathway	[212]
SRSF2	ND	Promotes RNA binding	[106]
NF-κB (p65)	R30	Enhances p65 binding to DNA and its transcriptional activity	[177]
KAP1	ND	ND	[178]
EBNA2	ND	ND	[179]
RPS10	R158, R160	Mediates ribosomal assembly and protein synthesis	[192]
Ski	R8	Upregulates the expression of TFs SOX10, MITF, and PAX3 repressing TGFβ signalling	[224]

EGFR	R1175	Recruitment of SHP1 and signal inhibition	[226]
CRAF	R563	Enhances activated CRAF degradation and attenuates ERK1/2 signalling	[227]
BRAF	R671	Enhances activated CRAF degradation and attenuates ERK1/2 signaling	[227]
PDGF	R554	Prevents PDGF ubiquitination and degradation	[237]
pol II	R1810	Methylation mark is recognized by SMN that recruits senataxin, leading to R-loop resolution and controlling transcription termination	[243]
E2F1	R111, R113	Decreases E2F1 half-life and transcriptional and apoptotic activities	[250,251]
RBMX	R369, R373	Promotes assembly of RBMX-SRSF1 complex and the splicing of MDM4	[413]
SREBP	R321	Stabilization of SREBP leading to an increase in de novo lipogenesis	[414]
ULK1	R170	Promotes ULK1 autophosphorylation and subsequently autophagosome formation	[415]
	R532	Suppresses ULK1 activation and attenuates autophagy	[416]
RUVBL1	R205	Promotes DNA repair by HR	[218]
FEN1	R19, R100, R104, R192	Decreases FEN1 phosphorylation and increases its interaction with PCNA promoting the BER pathway	[214]
RAD9	R172, R174, R175	Regulation of S/M and G2/M checkpoints and sensitivity to DNA damage	[417]
TDP	R361, R586	Enhances TFP 3'- phosphodiesterase activity and enhances it DNA repair functions	[418]
P53	R333, R335, R337	Regulates p53 DNA binding and transcriptional activity and the p53 response	[419]

KLF4	R374, R376, R377	Inhibits KLF4 ubiquitination increasing its stability and breast tumorigenesis	[420]
PDCD4	R110	Enhances breast cancer progression	[421]
KLF5	R57	Inhibits KLF5 phosphorylation and ubiquitination and sustains breast cancer stemness and proliferation	[422]
AKT	R391	Promotes AKT translocation to the plasma membrane and activation	[236]
	R15		[235]

ND: not determined

#### IV.6. PRMT5 and MEP50 localization

Due to their NES and NLS, PRMT5 and MEP50 (**Figure 30**) can shuttle between the nuclear and cytoplasmic compartments [390]. One study has also reported the localization of PRMT5 to the plasma membrane of SK-CO15 via its C-terminal domain [398]. In addition to its NESs, PRMT5 was shown to translocate to the cytoplasm by interacting with LCE1C [397]. Nuclear functions of PRMT5 include transcriptional regulation and chromatin remodelling, facilitated by PRMT5 association with COPR5 [393]. The shuttling of PRMT5 between nucleus and cytoplasm determines how PRMT5 acts and can even influence cell proliferation and cancer progression (**Figure 34**). PRMT5 is upregulated in the cytoplasm of ESC where it methylates, in complex with MEP50, the cytosolic H2A hence repressing differentiation genes and maintaining pluripotency [169]. Moreover, PRMT5 translocates to the nucleus of preimplantation embryos and primordial germ cells (PGC) during DNA demethylation to suppress the transposable elements [423]. Cytoplasmic PRMT5 correlates with a higher tumour grade in NSCLC and pulmonary neuroendocrine tumours (NET) [424]. In prostate cancer cells, PRMT5 and MEP50 predominantly localize to the cytoplasm promoting cellular proliferation. Consistently, PRMT5 was present in the nucleus of normal prostate epithelium and in the cytoplasm of cancerous prostate tissue [374]. Forced PRMT5 nuclear expression decreased prostate cancer cells proliferation independent of PRMT5 enzymatic activity [374]. Similar to PRMT5, cytoplasmic MEP50 increased the proliferation of prostate epithelial cells and reduced their differentiation [383,425–427]. Translocation of MEP50 from the nucleus to the cytoplasm of prostate epithelial cells correlates with tumorigenesis [426]. Additionally,

nuclear PRMT5 was less in metastatic melanoma tissue compared to primary ones, and both PRMT5 and MEP50 were predominantly cytoplasmic in metastatic melanoma cell lines [428]. In ER-positive breast cancer, high nuclear PRMT5 associates with better prognosis and survival [400]. PRMT5, MEP50 and the symmetric di-methylation of H4R3 levels are less in TNBC compared to the other breast cancer subtypes [429,430]. In summary, the localization of PRMT5:MEP50 complex seems to determine cell fate: nuclear localization favours cell differentiation while cytoplasmic localization is associated with proliferation and poor cancer prognosis (**Figure 34**).

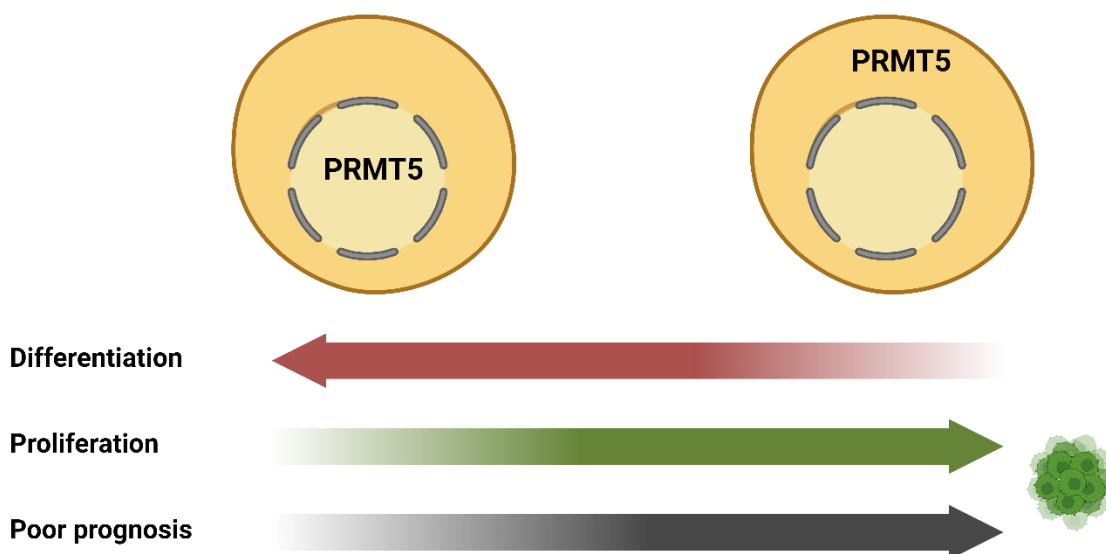


**Figure 34: PRMT5 localization is associated with poor prognosis.** When PRMT5 is enriched in the nucleus of the cell (right), cell differentiation is favoured over proliferation. On the contrary, high cytoplasmic PRMT5 (left) is associated with more proliferation and cell growth and is correlated with bad prognosis in cancer.

#### IV.7. PRMT5 and MEP50 PTM

PRMT5 C-terminal domain is phosphorylated at T634 by both AKT and serum- and glucocorticoid-inducible kinases (SGK) (**Figure 35; Table 5**). This phosphorylation event creates a switch between PRMT5 binding with 14-3-3 proteins (when phosphorylated) and PDZ domains (when unphosphorylated). Interaction of PRMT5 with 14-3-3 proteins is important for the viability of mice embryo [398]. RhoA-activated kinase (ROK) phosphorylates PRMT5 at T80 increasing its methyltransferase activity (**Figure 35; Table 5**) [399,431]. PRMT5 interacts with myosin phosphatase target subunit-1 (MYPT1),

subunit of the Myosin phosphatase (MP) holoenzyme, that dephosphorylates PRMT5 and decreases methylation of H4 and H2A [399]. PRMT5 was first discovered as a JAK2 partner, but no functional impact of this interaction was reported [152]. A constitutively active mutant of JAK2, JAK2V617F, interacts more strongly with PRMT5 and phosphorylates it at Y297, Y304 and Y307 (**Figure 35; Table 5**) impairing its interaction with MEP50 and therefore decreases its methyltransferase activity [375]. In breast cancer cell lines, PRMT5 is phosphorylated by liver kinase B1 protein (LKB1) on T132, T139, and T144 (**Figure 35; Table 5**) inhibiting its interaction with the methylosome components and hence decreasing its activity [400]. During DNA damage, Src phosphorylates PRMT5 at Y324 (**Figure 35; Table 5**) inhibiting its binding to SAM and therefore its methyltransferase activity. PRMT5 inhibition blocks the NHEJ pathway inducing cell death [212].

PRMT5 is itself methylated by CARM1 on R505 (**Figure 35; Table 5**). This methylation inhibits PRMT5 homodimerization and subsequently its methyltransferase activity, leading to diminished H4R3me2s levels on the  $\gamma$ -globin promoter activating its transcription in erythroleukemia cells [351].

The E3 ubiquitin ligase carboxyl terminus of heat shock cognate 70-interacting protein (CHIP) interacts with PRMT5 in the cytoplasm and promotes its ubiquitination at several lysine residues between aa 229 and 451 (240, 241, 248, 259, 275, 302, 329, 333, 343, 354, 380, and 387) (**Figure 35; Table 5**). PRMT5 ubiquitination leads to its downregulation via K48-linked ubiquitin-dependent proteasomal degradation [402]. Another E3 ubiquitin ligase, TRAF6, interacts with PRMT5 and promotes its K63-linked ubiquitination [403]. TRAF6 ubiquitinates PRMT5 at 6 lysine residues in its TIM barrel domain: K85, K95, K200, K227, K240, and K241. Instead of a predicted effect of ubiquitination, the proteasomal degradation, PRMT5 ubiquitination by TRAF6 enhances its binding to MEP50 and therefore its methyltransferase activity, and using TRAF6 inhibitors sensitizes breast cancer cells to PRMT5 inhibition [403]. Large-scale proteomic analysis predicts PRMT5 to be post-translationally modified on other residues [432].

The PTMs of MEP50 are less studied than PRMT5. Three residues, T5, S264, and S306 are phosphorylated by CDK4 (**Figure 35; Table 5**). T5 mutation drastically reduces

MEP50 phosphorylation. MEP50 phosphorylation on T5 and probably S264 by CDK4 increases the methyltransferase activity of PRMT5 and drives carcinogenesis [404].

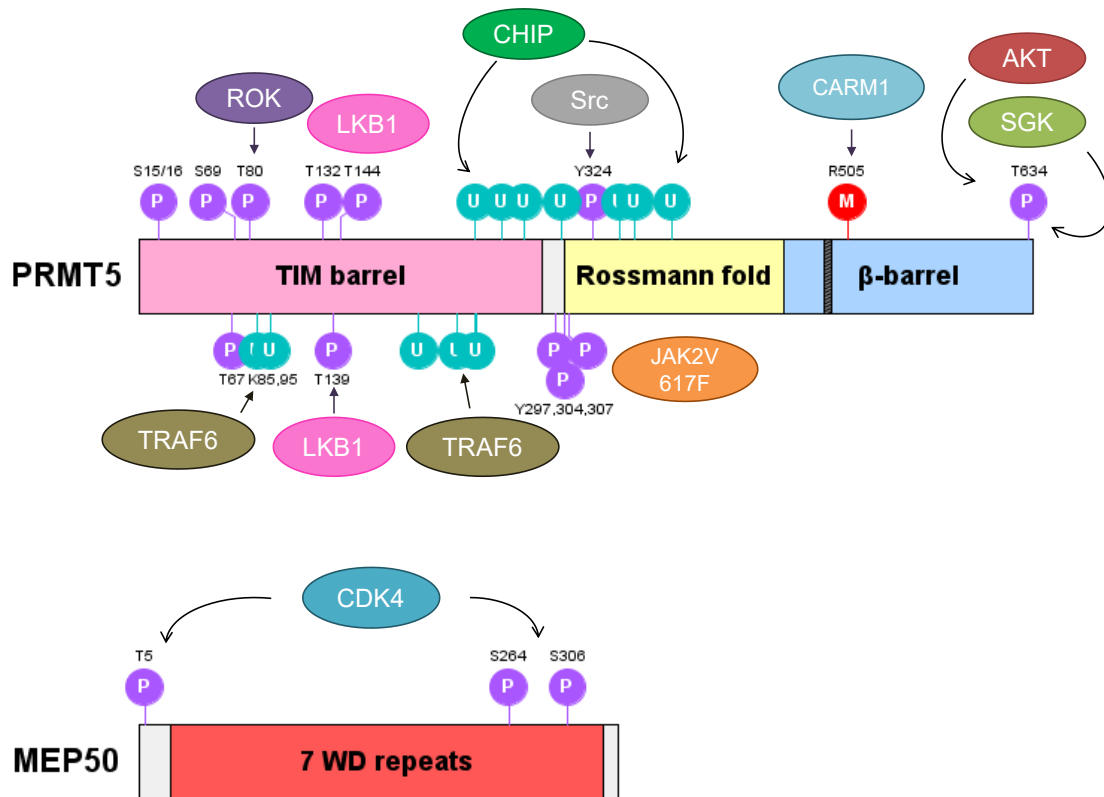


**Figure 35: PRMT5 and MEP50 post-translational modifications.** The known PTMs of human PRMT5 and MEP50 are indicated with their corresponding residues. The modifying enzyme, if identified, is also presented. M: methylation (in red); P: phosphorylation (in purple); U: ubiquitination (in blue).

**Table 5: PRMT5 and MEP50 PTM.**

Protein	PTM	Residue	PTM enzyme	Functional impact	Ref
MEP50	P	T5		Enhances PRMT5 activity	
	P	S264	CDK4		[122]
	P	S306			
	P	Y297, Y304, Y307	JAK2V617F	Impairs binding to MEP50 and decreases	[375]

				methyltransferase activity		
<b>PRMT5</b>	P	T634	AKT and SGK	switch between PRMT5 binding with 14-3-3 proteins and PDZ domains		[398]
	P	T80	ROK	Enhances PRMT5 activity		[399]
	P	S15/16	ND	ND		[399]
	P	T67	ND	ND		[399]
	P	S69	ND	ND		[399]
	P	T132, T139 and T144	LKB1	Inhibition of PRMT5 activity and interaction with methylosome		[400]
	P	Y324	Src	Inhibits PRMT5 binding to SAM and its activity		[212]
	M	R505	CARM1	Inhibits PRMT5 homodimerization		[351]
	U	Ks in 229–451 region	CHIP	PRMT5 downregulation		[402]
	U	Ks in TIM barrel	TRAF6	Enhances PRMT5 activity		[403]

M: methylation; P: phosphorylation; U: ubiquitination; ND: not determined.

## IV.8. PRMT5 Functions

### IV.8.1. PRMT5 in splicing regulation

#### *IV.8.1.1. The spliceosome assembly*

As discussed earlier, the PRMT5 interactome and methylome are enriched in spliceosomal proteins and pre-mRNA splicing factors [127,132,133,147,410]. In addition, depleting or inhibiting PRMT5 leads to global alteration in AS events, reflecting the crucial role of PRMT5 in splicing regulation [127,133]. PRMT5 promotes the assembly of the spliceosome, a large RNA-protein complex responsible for removing introns from pre-mRNA transcripts in the nucleus [433,434]. Two types of spliceosome are present in most eukaryotes, the U2-dependent spliceosome and the less abundant U12-dependent spliceosome [435]. The U2-dependent spliceosome is formed from U1, U2, U5, and U4/U6 small nuclear ribonucleoproteins (snRNPs) (**Figure 36**). Each snRNP is made of an snRNA (**Figure 36**) (2 snRNAs in case of U4/U6), the seven Sm proteins (B/B', D3, D2, D1, E, F, and G) common to all snRNPs, and a unique set of proteins specific for each snRNP (**Figure 36**) [435]. The assembly of the spliceosome occurs through the interaction of spliceosomal snRNPs with a large number of splicing factors [435]. The snRNP assembly starts in the cytoplasm and involves the SMN and its associated proteins (the SMN complex). The SMN complex recruits the snRNAs and associates them with the Sm proteins, that form a doughnut-shaped ring around the snRNAs [434].



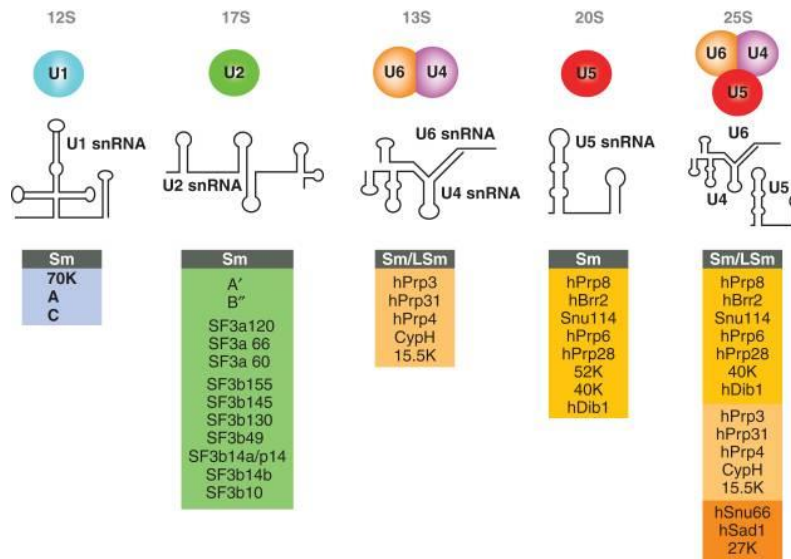


**Figure 36: Protein and snRNA components of the human spliceosomal snRNPs.** Each snRNP is composed of snRNA, the seven Sm proteins, and a specific set of proteins that vary among the different snRNPs. From [435].

PRMT5 symmetrically dimethylates the C-terminal of three Sm proteins, Sm B/D1/D3, enhancing their affinity for the SMN complex [385,386]. pICln, a component of PRMT5/MEP50 methylosome, interacts with the Sm proteins and acts as a chaperone in the assembly process [385,436–438] (**Figure 37**). As mentioned earlier (section III), the Tudor domain of SMN recognizes the PRMT5-catalyzed symmetric dimethylation motifs in Sm B/D1/D3, promoting the loading of Sm proteins onto the SMN complex and hence the spliceosome assembly [385,386,436] (**Figure 37**). PRMT5 therefore has an indispensable function in the assembly of the spliceosome, explaining the various splicing defects observed upon its loss or inhibition.

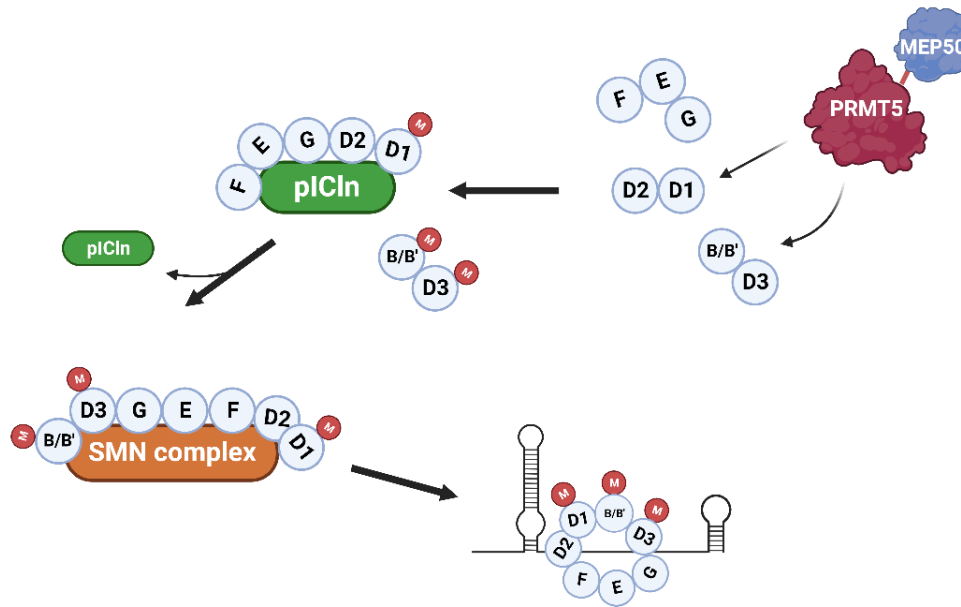


**Figure 37: PRMT5 functions in the spliceosome assembly.** The PRMT5/MEP50 complex methylates Sm proteins D1, B/B', and D3, mediating their loading on the SMN complex via the chaperon pICln therefore the spliceosome assembly.

#### ***IV.8.1.2. Global splicing regulation and methylation of splicing factors***

In addition to its roles in the spliceosome assembly, PRMT5 regulates AS by methylating known splicing factors (SF). PRMT5 methylates SRSF1 in AML regulating its binding to RNA and proteins. Consistent with that, the loss of PRMT5 caused an alteration in the AS of multiple essential genes [133]. In breast cancer cells, MEP50 interacts with the splicing factor ZNF326 (a DBIRD complex subunit) causing its symmetric dimethylation at R175 by PRMT5 [412]. The loss of PRMT5 or MEP50 causes alteration in AS events, such as the inclusion of A-T rich exons, an AS defect previously observed upon the loss of ZNF326 [412]. Despite being a transcriptional regulator, the symmetric dimethylation of E2F1, read by SND1, recruits snRNA to be assembled with E2F1, extending its role in transcription to the regulation of alternative RNA splicing [249].

Looking at its roles in the spliceosome assembly and the regulation of splicing factors' functions, it is not surprising that PRMT5 controls splicing events in the cells, and its loss or inhibition causes major splicing defects. In hematopoietic stem cell (HSC), PRMT5 regulates splicing of DNA repair genes, and its inhibition increases exon skipping and

intron retention leading to a decrease in gene expression. PRMT5 loss also increases DNA damage leading to the activation of p53 pathway and apoptosis [439]. PRMT5 regulates the splicing of activating transcription factor 4 (ATF4), and the loss of PRMT5 downregulated ATF4 protein and increased oxidative stress in AML [440]. PRMT5 depletion or inhibition causes AS of MDM4, leading to the activation of p53 pathway and apoptosis in different models [410,441]. In addition, and as stated earlier in several sections of the thesis, the repertoire of PRMT5 substrates is enriched in RNA binding proteins, splicing factors, and spliceosome components which all play roles in RNA-related processes. Moreover, PRMT5 role in splicing regulates its other cellular functions, by controlling the AS of transcripts implicated in DNA repair, cell cycle, signalling, autophagy... (refer below).

## **IV.8.2. PRMT5 in transcriptional regulation**

### ***IV.8.2.1. Histone methylation***

Histone tails undergo modifications like acetylation and methylation (R and K) that largely affects gene transcription. PRMT5 symmetrically dimethylates H2A at R3, H4 at R3, and H3 at R2 and R8, which can be linked to transcriptional activation or inhibition. PRMT5 interacts with the chromatin remodelling complex SWI/SNF, promoting H3R8 and H4R3 symmetric dimethylation, repressing the expression of tumour suppressor genes *ST7*, *cad*, and *NM23* [153,407]. PRMT5-mediated H3R8me2s and H4R3me2s also blocks the transcription of tumour suppressor genes *RB1*, *RBL1*, and *RBL2* [442] and of ribosomal proteins [170]. PRMT5 and H4R3me2s associate on the chromatin at the transcription start site at cyclin E promoter and repress its transcription [150]. PRMT5 controls the epigenetic reprogramming in primordial germ cells via interacting with Blimp1 and methylating H2AR3 and H4R3 [408]. PRMT5 interacts with CDK8 and CDK19 and dimethylates H4R3 at the promoter of immune response genes and C/EBP $\beta$  target genes to repress their expression [409]. The PRMT5 mediated symmetric dimethylation of H3R2 enhances binding to WD5 and is mainly responsible for transcriptional activation [172].

### ***IV.8.2.2. Methylation of transcription factors***

In addition to histone tail methylation, PRMT5 regulates gene transcription through the methylation of transcription factors. PRMT5 methylates R30 of the p65 subunit of NF $\kappa$ B

enhancing its binding to the  $\kappa$ B elements on DNA. Mutating R30 to A or knocking down PRMT5 resulted in the downregulation of almost 85% of NF $\kappa$ B target genes including chemokines and cytokines [177]. A separate report showed that the NF $\kappa$ B p65 subunit is rather methylated at five residues: R3, R35, R174, R304, and R330 and the depletion of PRMT5 largely decreased p65 methylation levels and decreased CXCL10 expression [443]. R30A and R35A mutants lost the ability to bind to CXCL10 promoter and activate its transcription [443]. PRMT5 methylates the tumour suppressor p53 on three residues, R333, R335, and R337 regulating its DNA binding functions and the transcription of its downstream target genes [419]. The three arginine residues are located within a region that harbours the oligomerization domain, NES, and NLS of p53 and their methylation affects p53 oligomerization and nuclear translocation [419]. E2F1 is methylated by both PRMT1 and PRMT5, and its symmetric dimethylation decreases E2F1 half-life and transcriptional and apoptotic activities [250].

#### **IV.8.3. PRMT5 and DNA damage response**

Components of the DDR pathway, like 53BP1, RAD9, and RuvB-like 1 (RUVBL1) are methylated by PRMT5 [444]. The GAR motif of 53BP1 is methylated by both PRMT1 and PRMT5, and knockdown of either PRMT increases 53BP1 methylation by the other one [444]. The PRMT5-mediated symmetric dimethylation of 53BP1 increases its stability and hence controls the NHEJ repair pathway. Importantly, under DNA damage, Src phosphorylates PRMT5 inhibiting its activity and therefore blocks NHEJ, inducing apoptosis of breast cancer cells [212]. Flap Endonuclease 1 (FEN1) is an enzyme that functions in DNA repair and replication. PRMT5 methylates FEN1 at several arginine residues, mainly at R192, leading to a decrease of FEN1 phosphorylation at S187. The methylated (unphosphorylated) form of FEN1 strongly associates with PCNA promoting the BER pathway [214]. RAD9 is an evolutionary conserved protein that functions in several pathways of the DDR, cell cycle checkpoints, and apoptosis [444]. PRMT5 methylates RAD9 on three arginine residues, which are important for the activation of the RAD9 downstream effector Chk1, important for the regulation of the cell response to DNA damage [417]. PRMT5 is a key regulator of HR pathway by methylating the TIP60 complex cofactor, RUVBL1, at R205 [218]. Methylation of RUVBL1 activates the acetyltransferase activity of TIP60 promoting the acetylation of H4K16, displacing 53BP1

from DNA double strand breaks and promoting HR [218]. Moreover, PRMT5 controls the AS of TIP60, and its inhibition or depletion leads to TIP60 aberrant splicing, decreased acetyltransferase activity, and subsequently an impairment in the HR pathway [445]. In AML, sensitivity to PRMT5 inhibition correlated with impaired DNA repair and synergized with PARP inhibitors in impairing the proliferation of AML cell lines [445]. Top1 cleavage complexes (Top1cc) are responsible of relaxing DNA supercoiling and are usually trapped by the action of some chemotherapies like camptothecin or by alterations in the DNA. Top1cc trapping generates double strand breaks and damages the genome causing cell death. Tyrosyl-DNA phosphodiesterase 1 (TDP1) is a key enzyme in repairing Top1cc and is methylated by PRMT5 on R361 and R586 that enhances its activity. In response to camptothecin, TDP1 methylation promotes its interaction with XRCC1 and its recruitment to the damaged sites. TDP1 methylation repairs Top1cc caused by camptothecin, protecting cells from its treatment [418].

#### **IV.8.4. PRMT5 and signalling pathways**

PRMT5 regulates two of the major signalling pathways involved in proliferation and survival, the PI3K (PTEN, PI3K, AKT, mTOR,) and ERK1/2 (RAS, RAF, MEK, ERK) pathways [446]. PRMT5 controls the activity of two important growth factor receptors EGFR and Fibroblast Growth Factor Receptor 3 (FGFR3).

##### ***IV.8.4.1. PRMT5 regulation of EGFR and AKT***

As mentioned earlier in section III of the thesis, PRMT5 mediated methylation of EGFR at R1175 inhibits its activity [226]. However, other recent studies showed that PRMT5 controls EMT through the EGFR/AKT pathway in lung, colorectal, and pancreatic cancer [447–449]. Two separate reports showed that PRMT5 methylates AKT and activates it [235,236]. Yin *et al.* reported that PRMT5-dependent methylation of AKT at R391 promotes its interaction with PIP3, promoting its translocation to the plasma membrane and therefore its activation by PDK1 (**Figure 38**) [236]. Importantly, PRMT5 inhibition synergized with AKT inhibitors to enhance cancer cell death [236]. Huang *et al.* reported the methylation of AKT by PRMT5 on another residue, R15 [235]. AKT R15 methylation is required for its phosphorylation at T308 and S473, plasma membrane localization,

activation, and controls the expression of the EMT transcription factors SNAIL, ZEB1, and TWIST1 [235].

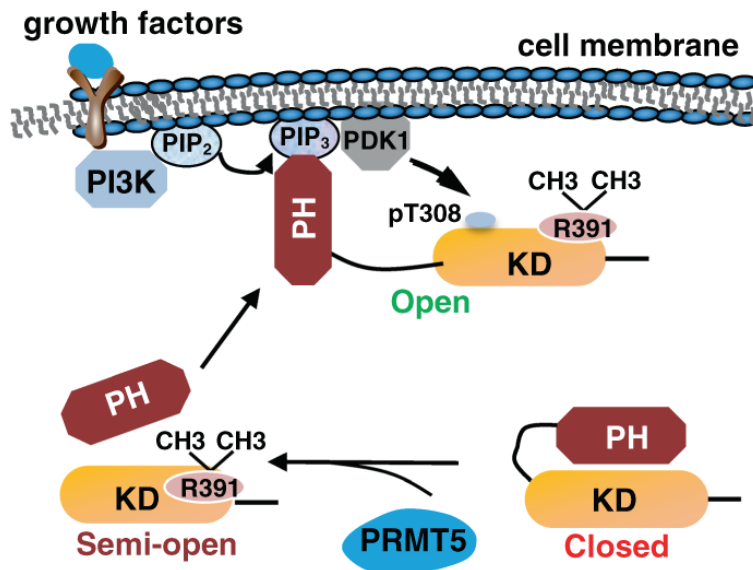


**Figure 38: PRMT5 methylates and activates AKT.** When not methylated, AKT is present in a closed conformation. Methylation of R391 by PRMT5 on AKT KD domain leads to its semi-open conformation relieving AKT PH domain. AKT is therefore translocated to the plasma membrane where it interacts with PIP3 leading to its phosphorylation by PDK1 and activation. Modified from [236].

#### IV.8.4.2. *FGFR3*

PRMT5 upregulates the expression of *FGFR3* in CRC by methylating H4R3 and H3R8 at the *FGFR3* promoter [176], in nasopharyngeal carcinoma (NPC) [450], and in lung cancer by downregulating the expression of miR-99 that targets *FGFR3* [451,452]. By methylating H4R3, PRMT5 suppresses the expression of miR-99 family therefore upregulating *FGFR3*, activating ERK and AKT and leading to cancer cell proliferation and metastasis [452].

#### IV.8.4.3. *PRMT5 and ERK1/2*

When a growth factor receptor is activated, RAS kinase is activated and phosphorylates RAF, RAF in turn phosphorylates MEK, then MEK finally phosphorylates ERK [453]. KRAS is the most mutated RAS in cancers [446,454]. In CRC patients, both PRMT5 and KRAS are upregulated and positively correlate with each other. In KRAS mutant CRC, PRMT5 is further upregulated compared to non-mutated CRC that increases the sensitivity to PRMT5 inhibition suggesting that the two proteins may crosstalk [455].

PRMT5 methylates the RAF proteins CRAF and BRAF which leads to their degradation and the inhibition of ERK pathway, shifting the cells response to EGF from proliferation to differentiation (**Figure 27** in Section III) [227]. Interestingly, treating melanoma cells with BRAF inhibitor decreased PRMT5 expression, however, when BRAF resistance was acquired, PRMT5 levels rose again [456]. In hepatocellular carcinoma, PRMT5 depletion induced ERK phosphorylation and upregulated the expression of the tumour suppressor BTG2 and a treatment with ERK1/2 inhibitor reversed the observed effect [457].

#### **IV.8.5. PRMT5 in development, differentiation, and stem cell maintenance**

PRMT5 is required in mouse early embryonic development and the loss of PRMT5 functions is lethal [169]. During the derivation of ESC, PRMT5 is upregulated and translocates to the cytoplasm in order to sustain pluripotency and repress differentiation. Depleting PRMT5 in ESC using siRNA led to the loss of pluripotency, downregulation of pluripotency and stem cell maintenance genes, and upregulation of differentiation ones [169]. PRMT5 represses differentiation genes by two mechanisms: (i) methylating in complex with MEP50 the pre-deposited histone H2A in the cytoplasm and (ii) by interacting with STAT3 in the ESCs [169]. PRMT5 is essential for the epigenetic reprogramming of PGC, where PRMT5 shuttles between the nucleus and cytoplasm to control gene expression. When DNA demethylation begins, PRMT5 moves to the nucleus and symmetrically dimethylates H2A and H4 to suppress the expression of LINE1 and AIP transposons. After DNA demethylation, PRMT5 shuttles back to the cytoplasm and methylates PIWI proteins required for pi-RNA biogenesis, that in turn silences LINE1 and AIP [423]. PRMT5 KD in CD34+ hematopoietic stem cells increased erythroid differentiation and colony formation [375]. In neuronal progenitor cells (NPC), PRMT5 knockout leads to the postnatal death of mice and is required for NPC homeostasis [441]. PRMT5 deletion causes aberrant splicing in NPCs, and one of the targets is MDM4. AS of MDM4 leads to the activation of p53 and therefore to apoptosis [441]. Similarly, PRMT5 regulates AS in HSCs, and its loss decreases the viability of HSCs, increases HSCs size, and increases mTOR pathway activation and protein synthesis. PRMT5 is therefore important for sustaining HSCs [439]. PRMT5 methylates the RGG/RG motif in the C-terminal domain of RBMX promoting its interaction with SRSF1. Loss of PRMT5 causes



a decrease in SRSF1 binding to MDM4 transcript and therefore protein levels, leading to abnormal p53 activation and differentiation of NPCs [413].

#### **IV.8.6. Hypoxia and autophagy**

The role of PRMT5 in autophagy has just been recently studied. Unc-51-like kinase 1 (ULK1) is a cytoplasmic kinase important for the process of autophagy [458]. Apart from its role in autophagy, ULK1 was found to interact with the PRMT5 methylosome complex and to phosphorylate the C-terminal of p1Cln (PRMT5 adaptor and part of the methylosome), inhibiting the transfer of Sm proteins onto the SMN complex and regulating UsnRNP biogenesis [459,460]. Then in 2022 and 2023, two separate studies reported the methylation of ULK1 by PRMT5 on two different residues (**Figure 39**) [415,416]. The symmetric dimethylation of ULK1 at R170 promotes its autophosphorylation and activation, therefore leading to the phosphorylation of Atg13 and Beclin, the formation of autophagosomes, and less oxygen consumption (**Figure 39**) [415]. The R170me<sub>2</sub>s mark is removed by the lysine demethylase KDM5C. KDM5C activity decreases upon hypoxia, causing an accumulation of ULK1 R170me<sub>2</sub>s [415]. A methylation deficient mutant of ULK1 impairs cell proliferation upon low oxygen levels [415]. On the contrary, PRMT5-mediated mono-methylation of ULK1 on R532 inhibits its activity and attenuates autophagy in TNBC cells (**Figure 39**) [416]. Moreover, an ULK1 inhibitor sensitizes TNBC cells (MDA-MB-231, BT549, and Hs 578T) to PRMT5 inhibition [416]. In lung cancer cells, PRMT5 overexpression causes a hypermethylation of ULK1 increasing autophagy activation, that can enhance cancer cell survival in hypoxic conditions [461]. Similarly, PRMT5 enhanced autophagy activation induced by EBSS or rapamycin treatment in breast cancer cells promoting tumorigenesis [462].



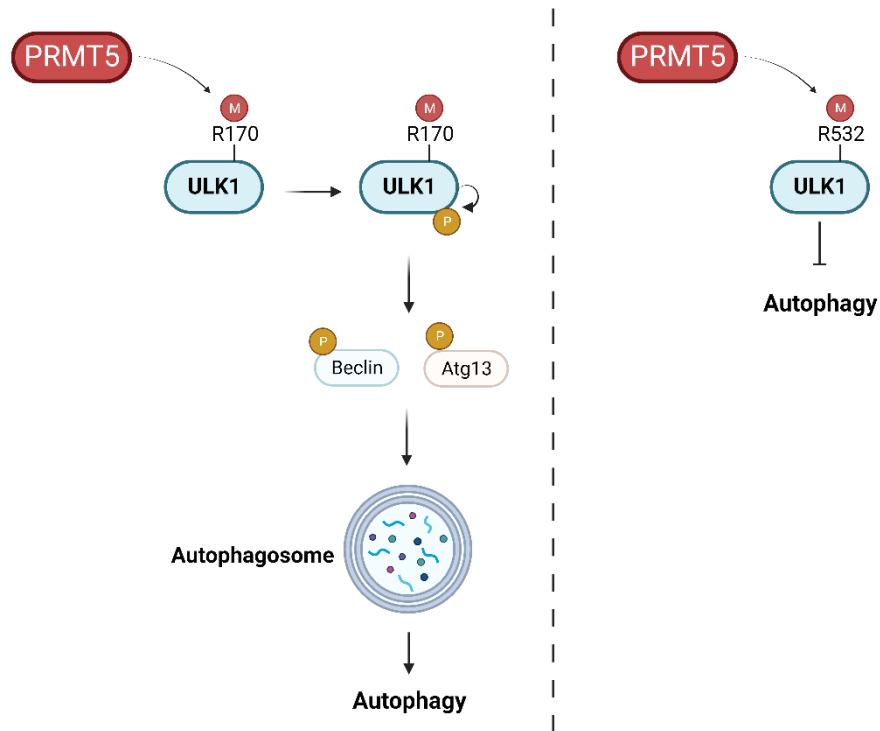


**Figure 39: PRMT5 functions in autophagy.** PRMT5 methylates ULK1 on two different residues, leading to either activation or repression of autophagy. PRMT5 symmetric di-methylation of ULK1 R170 promotes its autophosphorylation and activation, leading to Beclin and Atg13 phosphorylation, autophagosome formation, and autophagy activation. On the contrary, PRMT5-mediated monomethylation of ULK1 R532 inhibits autophagy.

#### IV.8.7. PRMT5 and the immune system

In T lymphocytes, PRMT5 inhibition alters AS and affects a set of signalling pathways including antiviral type I and type III interferon signalling [463]. Inhibiting or depleting PRMT5 in CD4 T helper (Th) cells reduces Th expansion and Il-2 production [464]. By methylating SREBP, PRMT5 promotes the induction of enzymes involved in the cholesterol biosynthesis pathway [414]. PRMT5 is important for homeostasis of Th cells, differentiation of Th17 cells, and the maintenance of CD8+ T cells [465]. During mouse T cell activation, transient transcription of *PRMT5* is induced by NFκB, and NF-κB, MYC, and mTOR drive the induction of PRMT5 protein [466]. PRMT5 also regulates AS in T cells, and one of its targets is the cation channel Trpm4 [467]. PRMT5-mediated splicing regulation of Trpm4 probably affects T cell receptor and NFAT signalling and IL-2 production [467]. PRMT5 and MEP50 interact with CDK8 and CDK19, causing the repression of C/EBPβ target genes involved in the immune response [409].

## IV.9. PRMT5 implication in cancer

### IV.9.1. Breast cancer

PRMT5 is upregulated in breast cancer tissues compared to the normal, and its high expression is associated with poor prognosis in breast cancer. Moreover, inhibiting, or depleting PRMT5 suppresses breast cancer cells proliferation, migration, and stemness properties [420,422,429,430,468–470]. PRMT5 nuclear expression is associated with luminal subtype (ER-positive) and good overall survival, while low-nuclear PRMT5 expression is associated with the more aggressive subtypes (TNBC) [400,430]. Recently, tamoxifen was shown to stimulate the methylation of ER $\alpha$  by PRMT5, promoting its binding to the corepressors SMRT and HDAC1 and therefore inhibiting ER $\alpha$  transcriptional activity. Tamoxifen triggers PRMT5 localization to the nucleus only in tamoxifen-sensitive luminal breast cancers, and nuclear PRMT5 expression presents a biomarker of response to tamoxifen (**Figure 40A**) [471]. On the contrary, a study showed that TRAF4 interacts with PRMT5 and upregulated its expression in the nucleus promoting breast cancer proliferation, and that PRMT5 nuclear expression correlates with HER2 expression [472]. In luminal breast cancer, PRMT5 expression is correlated with high nuclear LKB1 [400]. LKB1 is a kinase that can phosphorylate PRMT5 in its N-terminal domain and inhibits its methyltransferase activity, possibly by preventing its interaction with MEP50 and its adaptor proteins (**Figure 40B**) [400]. PRMT5 and MEP50 regulate AS in TNBC cell line MDA-MB-231, and their depletion causes AS defects like AT-rich exons inclusion, a phenotype previously observed upon ZNF326 (a PRMT5 substrate) depletion (**Figure 40C**) [412]. Genes that were deregulated with PRMT5 loss are involved in breast tumorigenesis, like *REPIN1/AP4*, *ST3GAL6*, *TRNAU1AP*, and *PFKM* [412]. Another PRMT5 substrate important for tumorigenesis and the regulation of breast cancer is Kruppel-like factor 4 (KLF4). PRMT5 methylates KLF4 at R374, R376, and R377 inhibiting its ubiquitylation by VHL and increasing its stability [420]. Accumulation of KLF4 reduces the transcription of tumour suppressor genes and increases that of oncogenes and stem cell renewal and metastasis genes, therefore supporting breast cancer aggressiveness (**Figure 40D**) [420]. Consistently, KLF4 and PRMT5 are elevated in aggressive breast tissues compared to the normal breast [420]. WX2–43, a molecule that inhibits PRMT5 and KLF4 interaction, suppressed TNBC tumour growth and induced cell

death of TNBC cells [473]. In addition, PRMT5 regulation of KLF4 and c-myc enhanced breast cancer stemness properties and resistance to doxorubicin [469]. PRMT5 methylates another KLF, KLF5, in basal-like breast cancer [422]. KLF5 methylation inhibits its phosphorylation and ubiquitination promoting breast cancer stem cells maintenance and proliferation (**Figure 40D**) [422]. PRMT5 sustains BCSCs that are proposed to drive breast cancer tumorigenesis and relapse. PRMT5 symmetrically dimethylates H3R2 at the *FOXP1* promoter, facilitating WD5 and H4K3 trimethylation therefore activating gene expression [468]. FOXP1 is a transcription factor involved in stem cell function. Accordingly, PRMT5 depletion or inhibition significantly reduced BCSCs both *in vitro* and *in vivo* [468]. Similarly, PRMT5 is required to sustain stemness of TNBC cells and its inhibition reduces the proliferation of a panel of breast cancer cells (ER<sup>+</sup>, HER2-positive, and TNBC) and delays the growth of TNBC PDX models [430]. PRMT5 methylates the tumour suppressor programmed cell death 4 (PDCD4) at R110 promoting breast cancer progression. High levels of PDCD4 are associated with poor prognosis in breast tumours that have elevated PRMT5 levels [421].

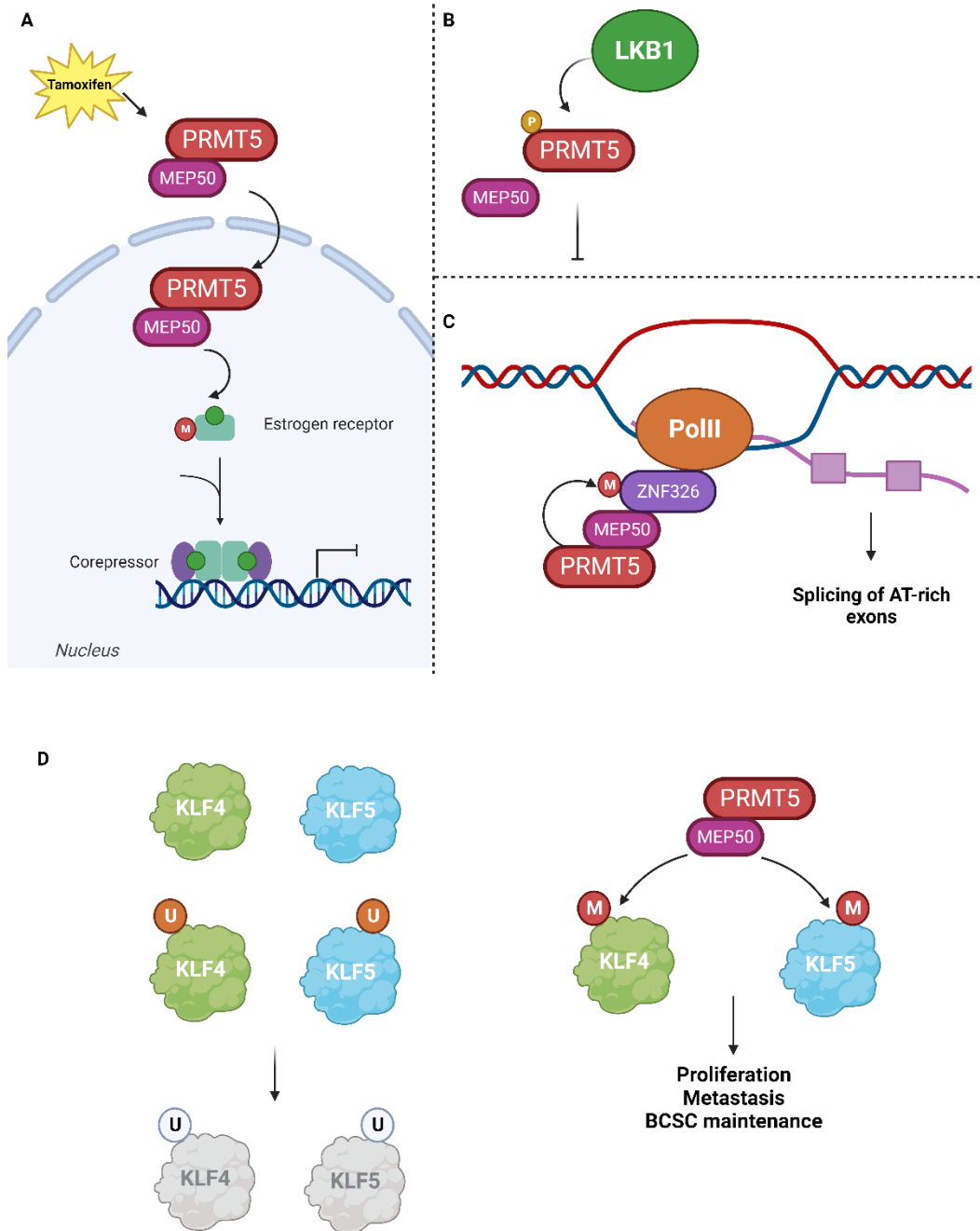


**Figure 40: PRMT5 implication in breast cancer. (A).** Tamoxifen treatment triggers PRMT5 nuclear transport, where it methylates ER $\alpha$  promoting its interaction with transcriptional corepressors. **(B).** LKB1 phosphorylates PRMT5, preventing its interaction with MEP50 and therefore inhibits its activity. **(C).** MEP50 interacts with ZNF326 causing its methylation by PRMT5 thus promoting the splicing of AT-rich exons. **(D).** PRMT5 dependent methylation of KLF4 and KLF5 prevents their ubiquitination and degradation, therefore promoting breast cancer aggressiveness and stemness.

#### IV.9.2. PRMT5 and MTAP depletion

The *MTAP* gene is often deleted in cancer due to its presence near *CDKN2A*, a frequently deleted tumour suppressor gene [474]. *MTAP* deleted cells show a remarkable increase in intracellular levels of MTA, a molecule that specifically inhibits PRMT5 activity. *MTAP* deleted cells therefore show less PRMT5 activity, which correlates with an increased sensitivity to PRMT5 depletion or inhibition [474], and sensitizes cells to type I PRMT inhibitor [134]. Consequently, inhibitors targeting PRMT5 in the presence of MTA have been developed and evaluated for treating cancer with *MTAP* deletions [475].

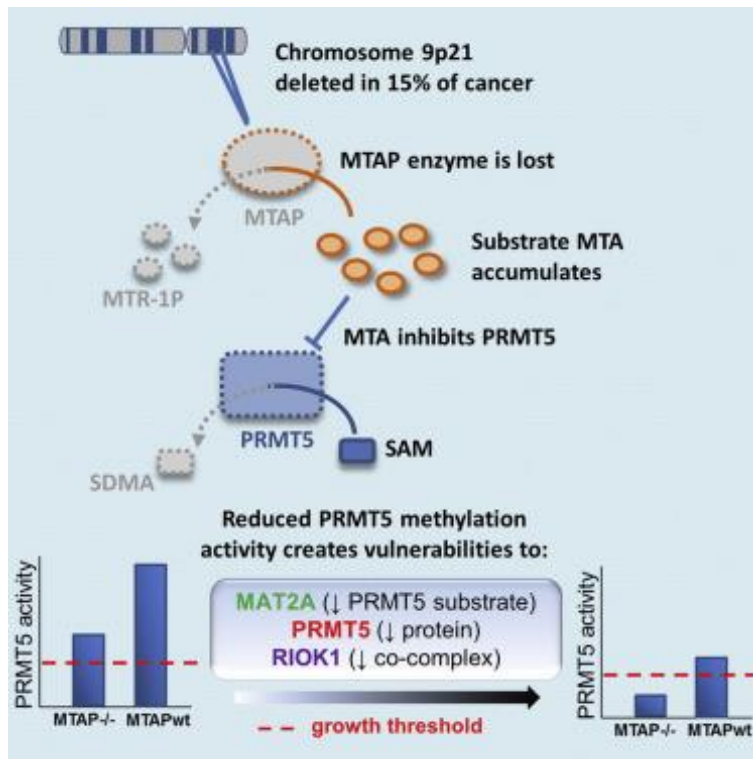


**Figure 41: MTAP-deleted cancer cells are more susceptible to PRMT5 inhibition.** Cancer cells carrying *MTAP* deletion accumulate MTA which is an inhibitor of PRMT5 enzymatic activity, creating a vulnerability to PRMT5 inhibition or depletion. From [117].

#### IV.9.4. Leukemia

Methylation of PRMT5 by CARM1 inhibits PRMT5 methyltransferase activity and increases  $\gamma$ -globin expression in erythroleukemia cells [351]. In AML, PRMT5 inhibition resulted in aberrant splicing of ATF4, producing an intron retaining ATF4 transcript that is unstable and stuck in the nucleus [440]. This leads to the loss of ATF4 protein and subsequently downregulation of its target genes, resulting in an increase in oxidative

stress, growth arrest, and cellular senescence [440]. One class of AML is dependent on ecotropic virus integration site 1 (EVI1) driven gene expression that affects stemness and apoptosis. AML cells overexpressing EVI1 had lower ATF4 expression, increased oxidative stress, and sensitized the cells to PRMT5 inhibition [440]. In lymphoma, PRMT5 inactivates the retinoblastoma proteins RB1 and RBL2 therefore upregulating polycomb repressor complex (PRC2) expression and favouring tumorigenesis [202]. PRMT5 epigenetically inhibits the expression of RBL2 [442] and indirectly enhances RB1 phosphorylation through activating cyclin D1 expression [202].

#### **IV.9.5. Other solid tumours**

PRMT5 is upregulated in hepatocellular carcinoma (HCC) and correlates with poor prognosis in HCC patients, and PRMT5 knockdown decreases HCC proliferation and tumour growth [457]. PRMT5 methylates the transcription factor SREBP at R321 and prevents its phosphorylation by GSK3 $\beta$  leading to its stabilization [414]. Stabilization of SREBP causes an increase in de novo lipogenesis promoting hepatocellular cancer cells proliferation. Interestingly, R321 methylation of SREBP is associated with poor prognosis in hepatocellular carcinoma [414]. Sachamitr *et al.* showed that using two different PRMT5 inhibitors decreases the growth of 46 patient derived glioblastoma stem cells and causes a global disruption of AS, with a particular effect on cell cycle transcripts [476]. Interestingly, the same study identified a GBM splicing signature that correlates with PRMT5 sensitivity, implying that the response of GBM cells to PRMT5 is dependent upon pre-mRNA splicing [476]. PRMT5 is upregulated at the mRNA and protein levels, in addition to its methylation mark H4R3, in lung tumour compared to normal lung tissue, and its cytoplasmic localization is associated with tumour grade in lung cancer [424]. PRMT5 protein is upregulated in melanoma, including malignant and metastatic tumours, compared to normal epidermis [428]. PRMT5 depletion using siRNA decreased the proliferation of melanoma cell lines but increased that of other subsets. PRMT5 depletion also decreased the expression of microphthalmia-associated transcription factor (MITF), a melanoma oncogene, while increased that of p27<sup>Kip1</sup> [428]. Clear cell sarcoma of soft tissue (CCSST) is a rare sarcoma that lacks any therapy, characterized by the expression of EWSR1-ATF1, a genes fusion product. PRMT5 interacts with EWSR1-ATF1 enhancing

its transcriptional activity and supporting CCSST cells proliferation, and PRMT5 inhibitor decreased the proliferation of CCSST in vitro and in vivo [406].

#### IV.10. PRMT5 inhibitors

For its involvement in crucial cellular functions, and as increasing reports are validating its roles in oncogenesis, several PRMT5 inhibitors have been developed, and a number of which were evaluated in clinical trials [477,478]. **Table 6** lists the different PRMT5 inhibitors developed and by which company, their mechanism of actions, and whether or not were evaluated in the clinical trials.

**Table 6: PRMT5 inhibitors and their mechanism of action.**

Compound	Company	Mechanism of action	Evaluated in clinical trials	Ref
BRD0639	-	PBM competitive	No	[379]
macrocyclic peptide (50)	-	PBM competitive	No	[380]
WX2-43	-	Inhibits PRMT5-KLF4 interaction	No	[473]
EPZ015666	Epizyme	Substrate competitive	No	[479]
GSK3235025	GSK			
EPZ015938	Epizyme	Substrate competitive	NCT04676516	
GSK3326595	GSK		NCT03614728 NCT02783300	[410]
EPZ015866	Epizyme	Substrate competitive	No	[410]
GSK3203591	GSK			
DC_Y134	-	Substrate competitive	No	[480]

JNJ-64619178	Janssen Research and Development	Dual SAM/substrate site	NCT03573310	[481]
PF-06939999	Pfizer	SAM competitive	NCT03854227	[482]
T1551	-	Substrate competitive	No	[483]
LLY-283	Eli Lilly and Company	SAM competitive	No	[484]
MRTX1719	Mirati Therapeutics	PRMT5-MTA inhibitor	NCT05245500	[475]
TNG908	Tango Therapeutics	PRMT5-MTA inhibitor	NCT05275478	[485]
PRT543	Prelude Therapeutics	Substrate competitive	NCT03886831	[478]
PRT811	Prelude Therapeutics	SAM competitive	NCT04089449	[478]
AMG 193	Amgen	PRMT5-MTA inhibitor	NCT05094336	[478]

#### IV.11. PRMT5 as a target in combinatorial treatments

Recently, the use of PRMT5 in combination with other targeted therapies or chemotherapies is being evaluated in different cancer models and appears to be promising. Drug combinations are gaining interest in cancer research, as they can increase the efficacy of treatment while reducing toxicities and side effects. In **Table 7**, drug combination studies performed between PRMT5 inhibitors and chemo- or targeted-



therapies are listed, along with the model they have been tested in. Only combinations that showed a therapeutic benefit are included in the table.

**Table 7: PRMT5 inhibition in combination studies**

<b>PRMT5 inhibitor</b>	<b>Combinatorial compound</b>	<b>Combinatorial target</b>	<b>Model</b>	<b>Reference</b>
EPZ015666	Erlotinib	EGFR	TNBC cells	[430]
GSK3186000	Olaparib	PARP	AML cell lines	[445]
GSK3326595	EPZ5676	DOT1L	MLL	[486]
GSK3203591	anti-PDL1	PDL-1	Lung cancer	[487]
GSK3326595	abemaciclib	CDK4/6	MCL	[488]
GSK3326595	AZD6738	ATR	MCL	[488]
GSK3326595	palbociclib	CDK4/6	Breast, esophageal, and pancreatic cancer cells	[489]
GSK3203591	GSK2816126	EZH2	CRC	[490]
GSK3326595	GSK3368715	Type I PRMT	Pancreatic cancer, DLBCL cells	[134]
GSK3203591	MS023	Type I PRMT	AML	[127]
GSK3203591	E7107	Spliceosome	AML	[127]
EPZ015666	PP242	mTOR	Glioblastoma	[491]
T1-44	Vactosertib	TGF $\beta$	Pancreatic cancer	[492]
GSK3326595	MRT68921	ULK1/2	TNBC cells	[416]
GSK332659	Niraparib	PARP	Breast and ovarian cancer	[493]

EPZ015666	Paclitaxel	-	Lung, breast, liver, and colon cancer cells	[494]
-----------	------------	---	---	-------

## Summary

PRMT5 is responsible for the majority of arginine symmetric dimethylation in the cells and prefers the 'GRG' motif for methylation. Unlike other PRMT members, PRMT5 is mostly present in protein complexes, and its interaction with MEP50 is indispensable for its full enzymatic activity. The two proteins form a hetero-octameric complex, where four PRMT5 monomers interact together at the core of the complex, and four MEP50 molecules are present at the periphery. The PRMT5/MEP50 complex activity can be modulated by PTMs occurring either at PRMT5 or at MEP50. Another way to regulate the activity of PRMT5 and MEP50 is through their subcellular localization. Interestingly, the subcellular compartmentalization of the complex is linked to oncogenesis, as the higher levels of cytoplasmic PRMT5 and MEP50 are associated with tumour aggressiveness. The methylome of PRMT5 was identified in various models, and all support the enrichment of PRMT5 substrates with RNA binding proteins involved in processes of RNA metabolism. The PRMT5/MEP50 complex functions in a wide range of cellular processes, and is deregulated in several cancer types, including the breast. In breast cancer, PRMT5 expression is associated with poor patient prognosis, and its inhibition or depletion reduces the proliferation of breast cancer cells, stemness properties, and tumour growth of *in vivo* breast cancer models. Inhibitors that target PRMT5 substrate binding pocket, SAM binding site, or sites of protein-protein interactions have been developed and several are under clinical evaluation. Recently, the use of PRMT5 inhibitors in combination with chemo- or targeted- therapies is emerging and has yielded promising data in the preclinical settings.

## V. Far Upstream Element Binding Protein 1: FUBP1

### V.1. FUBP1 discovery and generalities

The Far Upstream Element (FUSE) is a DNA sequence located 1.5 kb upstream the P1 promoter of the *MYC* oncogene, capable of efficiently regulating its transcription. It was first reported in 1990, in a study demonstrating that the FUSE element and its unidentified “binding factor” are positive regulators of *MYC* transcription, however, this regulation is lost upon differentiation [495]. Later, in 1994, this 70 KDa “binding factor” was isolated by Duncan *et al.* and termed Fuse Upstream Element Binding Protein (FUBP) [496].

We are particularly interested in FUBP1 as it was identified during my thesis as a PRMT5 substrate. In this section, I will discuss the general features of FUBP1, its diverse functions, and then its role in tumorigenesis.

### V.2. Molecular and structural features of FUBP1

#### V.2.1. The Far Upstream Element Binding Protein family members

FUBP1 belongs to a conserved family of nucleic acid binding regulators, also including FUBP2 (known as KHSRP; KH-type splicing regulatory protein) and FUBP3 (**Figure 42**). A fourth FBP member expressed in *Caenorhabditis elegans* was described, revealing the high homology in this ancient family [497]. *FBP1* gene is located on chromosome 1p31.1, *FBP2* on 19p13.3, and *FBP3* on 9q34.11 [498]. The three proteins share high sequence homology and the same general structure of three distinct domains: amino-terminal, C-terminal, and a central nucleic acid binding domain. The central domain is formed of four KH motifs similarly spaced in the three proteins (**Figure 42**). Though structurally similar, different functions were attributed to the three members. FUBP1 is well known as a transcription factor regulating *MYC* expression, however, it has been also described later as a splicing and a translation factor [499]. FUBP2 is best known in regulating RNA processes, such as pre-mRNA splicing, microRNA biogenesis and mRNA decay [500]. Unlike its homologs, FUBP3 functions are poorly described, but has been reported to function in transcriptional and post-transcriptional processes [499]. Interestingly, FUBP1, FUBP2, and FUBP3 are components of the spliceosome [501], implying they are present in same functional complexes as PRMT5 and MEP50.

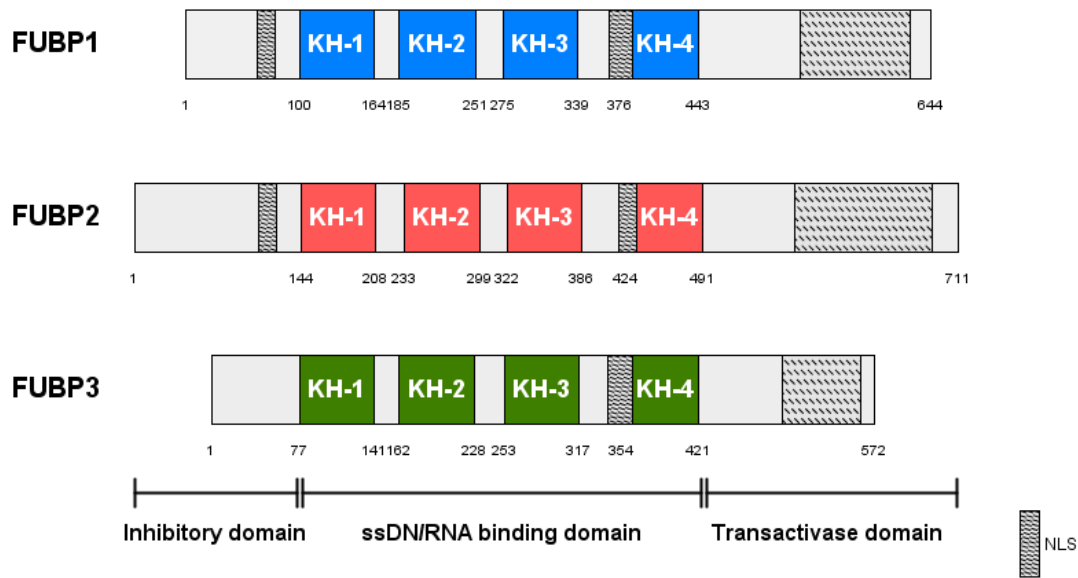


**Figure 42: FUBP family members.** The FUBP family is composed of three members, FUBP1, FUBP2 (KHSRP), and FUBP3. The three members share conserved structure of an N-terminal self-inhibitory domain, central nucleic acid binding domain, and a C-terminal transactivation domain. Their nucleic acid binding domains are formed of four equally spaced KH motifs, responsible of direct contact with ssDNA/RNA. The three members share two conserved NLS in their central and C-terminal domains. FUBP1 and FUBP2 share a bipartite NLS at their N-terminal, which is lacking in FUBP3.

### V.2.2 FUBP1 subcellular localization

FUBP1 is primarily a nuclear protein [502–505], in accordance with its role in transcriptional regulation. The translocation of FUBP1 to the nucleus is driven by three NLS located in its N-terminal, central, and C-terminal domains. In HeLa cells, both endogenous and ectopically expressed GFP-FUBP1 localize to the nucleus. Interestingly, each of the three FUBP1 domains alone fused to GFP localizes to the nucleus suggesting the presence of an NLS in each [502]. The N-terminal NLS is a canonical bipartite NLS located at residues 63-78 (**Figure 42**). The two other NLS are atypical, located at amino acids 366-386 and 531-644 in the central and C-terminal domains respectively (**Figure 42**) [502]. Upon cell death, oxidative stress, and viral infection, FUBP1 localizes to the cytoplasm [503–505]. When cells are undergoing apoptosis, FUBP1 is cleaved by caspases 3 and 7 at the consensus site DQPD located in the bipartite N-terminal NLS, thus mediating FUBP1 transport from the nucleus [503]. During Japanese encephalitis virus (JEV) and Enterovirus 71 (EV71) infection, FUBP1 translocates to the cytoplasm

probably to regulate viral replication and translation [504,505]. Under stress induction like heat shock, FUBP1 was also shown to localize to the stress granules [505].

### **V.2.3 FUBP members post-translational modifications**

#### **V.2.3.1. Ubiquitination**

Ubiquitination is the most reported modification of FUBP1. FUBP1 was found to be ubiquitinated by Parkin promoting its degradation [506]. Moreover, FUBP1 interacts with AIMP2/p38 (also known as JTV1), a component of tRNA synthetase complex, promoting its ubiquitination and degradation, leading to a downregulation of c-myc levels and enhancing lung cell differentiation [507]. In another study, Prostaglandin E2 (PGE2) was shown to activate the EP3 receptor that in turn inhibits TGF $\beta$  [508]. TGF $\beta$  suppression downregulates AIMP2/p38, decreasing FUBP1 ubiquitination levels leading to its stabilization and promoting liver cancer progression [508]. However, AIMP2/p38 is not itself a ubiquitin ligase. It was later reported that AIMP2/p38 interacts with Smurf2, and the latter is responsible for FUBP1 ubiquitination [509]. Another study also reported the ubiquitination of FUBP1 by Smurf2 in CRC, particularly CRC carrying *KRAS* mutations [510]. Though several studies showed FUBP1 ubiquitination, the exact ubiquitination sites were not investigated. The lysine residues illustrated in **Figure 43** were obtained from large scale proteomic analysis reported on PhosphoSitePlus and none was confirmed [432]. Ubiquitin-specific protease 22 (USP22) was shown to deubiquitinate FUBP1 [511].

One study found that FUBP2/KHSRP is ubiquitinated on K109, K121 and K122 (**Figure 43**) [512] and large-scale analysis predicted other ubiquitination sites (**Figure 43**) [432]. No study specifically reports the ubiquitination of FUBP3, however, like the other two members, FUBP3 is predicted to be potentially ubiquitinated on different residues (**Figure 43**) [432].

#### **V.2.3.2. Phosphorylation**

Though the phosphorylation of FUBP1 was not deeply investigated, the protein is reported to be potentially phosphorylated on different residues by large-scale proteomic analysis, especially on its N-terminal domain (**Figure 43**; PhosphoSitePlus website [432]). One study reported that c-src phosphorylates FUBP1 on Y58, Y126, Y268, and Y625 (**Figure 43**) [513]. Apart from c-src, the kinases responsible for FUBP1 phosphorylation

on other residues are not known. Interestingly, the phosphorylation level of FUBP1 varies between normal and cancer tissues [514]. Phosphorylation of S120 in the KH-1 domain is significantly elevated in lung and clear cell renal carcinoma, and that at S630 and T153 is increased in uterine corpus endometrial carcinoma (UCEC) [514]. In breast tumours, FUBP1 is more phosphorylated at Y126 and T174 sites compared to the normal tissues [514]. This variation in the phosphorylation levels of FUBP1 between normal and malignant tissues is important, as it implies that the functions of FUBP1 can be modulated through post-translational modifications. Nevertheless, the exact implication of FUBP1 phosphorylation in cancer development/progression is yet to be explored.

The phosphorylation of FUBP2/KHSRP has been more studied. Like FUBP1, FUBP2 is phosphorylated by c-src on Y317, Y583, and Y688 (**Figure 43**) [513]. During muscle differentiation, p38 phosphorylates FUBP2 at T692 (**Figure 43**) inhibiting its interaction with AU-rich elements (ARE) containing mRNA and preventing their decay by FUBP2 [515]. FUBP2 was shown to be phosphorylated by AKT at S193 (**Figure 43**) promoting its interaction with 14-3-3 protein and impairing the mRNA decay of  $\beta$ -catenin [516], but this study was later retracted [517]. However, other studies also reported this phosphorylation event on FUBP2. Moreno *et. al* showed that the phosphorylation of FUBP2 at S193 creates a binding site for 14-3-3 driving its nuclear translocation [518], and Ruggiero *et al.* reported that some FUBP2 target transcripts are regulated by the AKT pathway [519]. In breast cancer, FUBP2 can be phosphorylated through the AKT pathway promoting its nuclear localization, enhancing breast cancer progression and drug resistance [520]. Additionally, PI3K/AKT pathway activation was shown to activate FUBP2 function in promoting miRNA maturation while inhibiting its functions in miRNA decay [521]. FUBP2 is phosphorylated at S395 (**Figure 43**) by p70S6K inhibiting its binding with a precursor RNA pre-let-7a [522]. The ATM kinase interacts with FUBP2 and phosphorylates it at S132, S274, and S670 (**Figure 43**) enhancing its interaction with primary miRNA (pri-miRNA) and hence miRNA processing [523]. FUBP2 phosphorylation at S181 increases in response to 2 hours stimulation by parathyroid hormone (PTH) [524].

No data has been reported for the phosphorylation of FUBP3, but the protein was predicted to be phosphorylated by proteomic analysis (**Figure 43**; PhosphoSite website [432]).

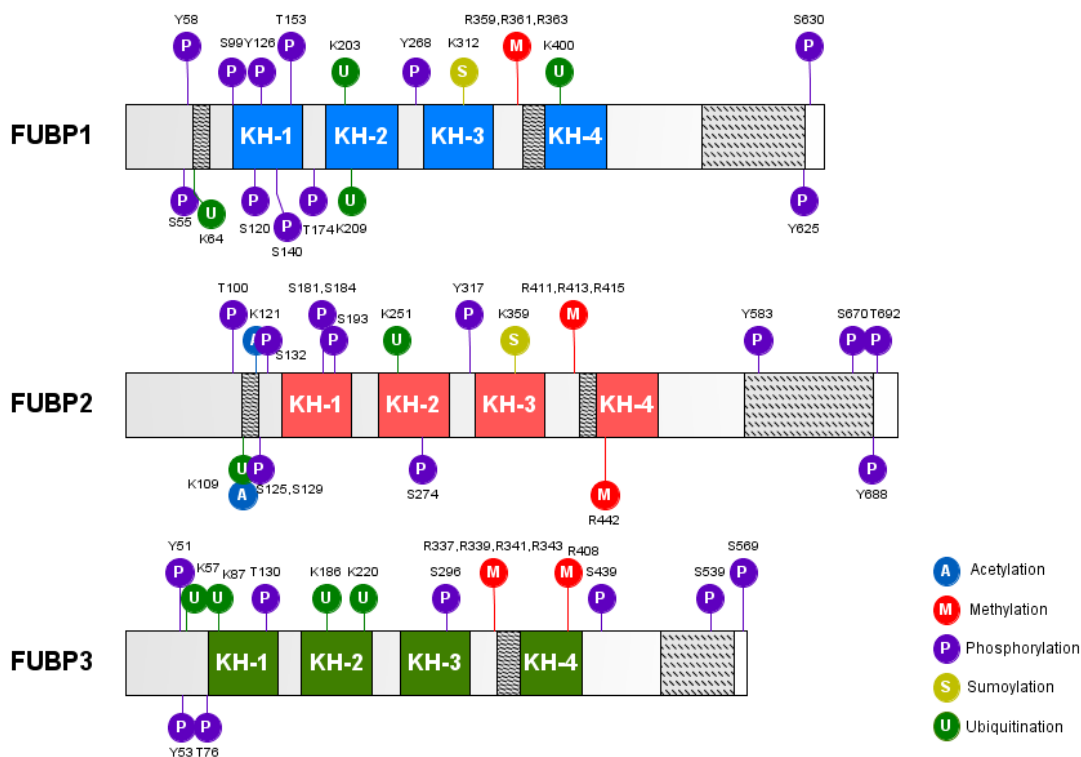


**Figure 43: Post-translational modifications of FUBP1, FUBP2, and FUBP3.** The known PTMs of human FUBP1, FUBP2, and FUBP3 are indicated with their corresponding residues. A: acetylation (in blue); M: methylation (in red); P: phosphorylation (in purple); S: sumoylation (in yellow); U: ubiquitination (in green).

### V.2.3.3. Methylation

Several large-scale proteomic data have reported the methylation of all FUBPs on arginine residues (**Table 8**). Interestingly, three potentially methylated arginine residues found in the three FUBPs lie in the linker region between KH3 and KH4 domains (**Figure 44**; **Table 8**) and have the RGRG PRMT5 consensus methylation motif [106]. The sequence of these three residues is conserved between FUBP1 (R359, R361, R363; PGPGRGRGRGQGN) and FUBP2 (R411, R413, R415; MPPGRGRGRGQGN) but differs in FUBP3 (R337, R339, R341, R343; GLAAARGRGRGRGD) (**Figure 44**; **Table 8**). A fourth arginine is reported to be methylated by several studies on FUBP2 (R422) and FUBP3 (R408) but not on FUBP1 (**Table 8**; **Figure 44**). Interestingly, the three

FUBPs were reported to be potential PRMT5 substrates [133,147], and Gerhart *et al.* have shown that the methylation of FUBP1 and FUBP2 small peptides, that include the linker region between KH3 and KH4 domains, decreases upon PRMT5 inhibition [410]. A recent study shows that FUBP1 and FUBP3 are symmetrically dimethylated in HT1080 fibrosarcoma cell lines which express MTAP, and this methylation is absent in MTAP-negative cell lines [525]. The same study reports that adding MTA, that inhibits PRMT5, to the medium of MTAP-positive cells reduces the total symmetric dimethylation levels [525]. Using reporter plasmid containing FUSE sequence, MTA addition reduced the transcription of GFP, implying that FUBP1 and FUBP3 methylation could potentially have a functional impact on their transcriptional activity [525]. FUBP2 was reported to be methylated in N<sub>2a</sub> cells on 14 arginine residues, seven of which are not RG motifs [526]. The same study shows that depleting CARM1 inhibited the interaction between FUBP2 and SMN and induced FUBP2 localization to the cytoplasm. The authors suggested that CARM1 is the PRMT responsible for FUBP2 methylation, however, no experiments were performed to validate this hypothesis [526].

**Table 8: Arginine methylation sites on FUBP1, FUBP2 and FUBP3**

Protein	Methylated Arg	Sequence	Methylation	Ref
FUBP1	R359	GGPGPGG <b>R</b> GRG RGQG	MMA/DMA	[106,128,134,141– 144,146,377,411,527]
	R361	PGPGGRG <b>R</b> GRG QGNW	MMA/DMA	[106,126,128,134,144,147, 377]
	R363	PGGRGRG <b>R</b> GQG NWNM	MMA/DMA	[106,126,128,134,147,377, 411,527]
FUBP2	R411	PGMPPGG <b>R</b> GRG RGQG	MMA/DMA	[106,128,134,143,144,147, 377,411]
	R413	MPPGGRG <b>R</b> GRG QGNW	MMA/DMA	[106,142,144,147,377,411, 527]
	R415	PGGRGRG <b>R</b> GQG NWGP	MMA/DMA	[106,126,147,377,411,527]



	R442	KCGLVIGRGGEN VKA	MMA/DMA	[106,134,141,143,144,527]
FUBP3	R337	FGGLAAARGRGR GRG	MMA	[106,134,143,147,377]
	R339	GLAAARGRGR GDW	MMA	[106,377]
	R341	AAARGRGRG DWSV	MMA	[106,377]
	R343	ARGRGRGDW SVG A	MMA	[106]
	R408	NLRRFTIRGVPQQ IE	MMA	[128,142]

---

MMA: mono-methyl arginine; DMA: di-methyl arginine

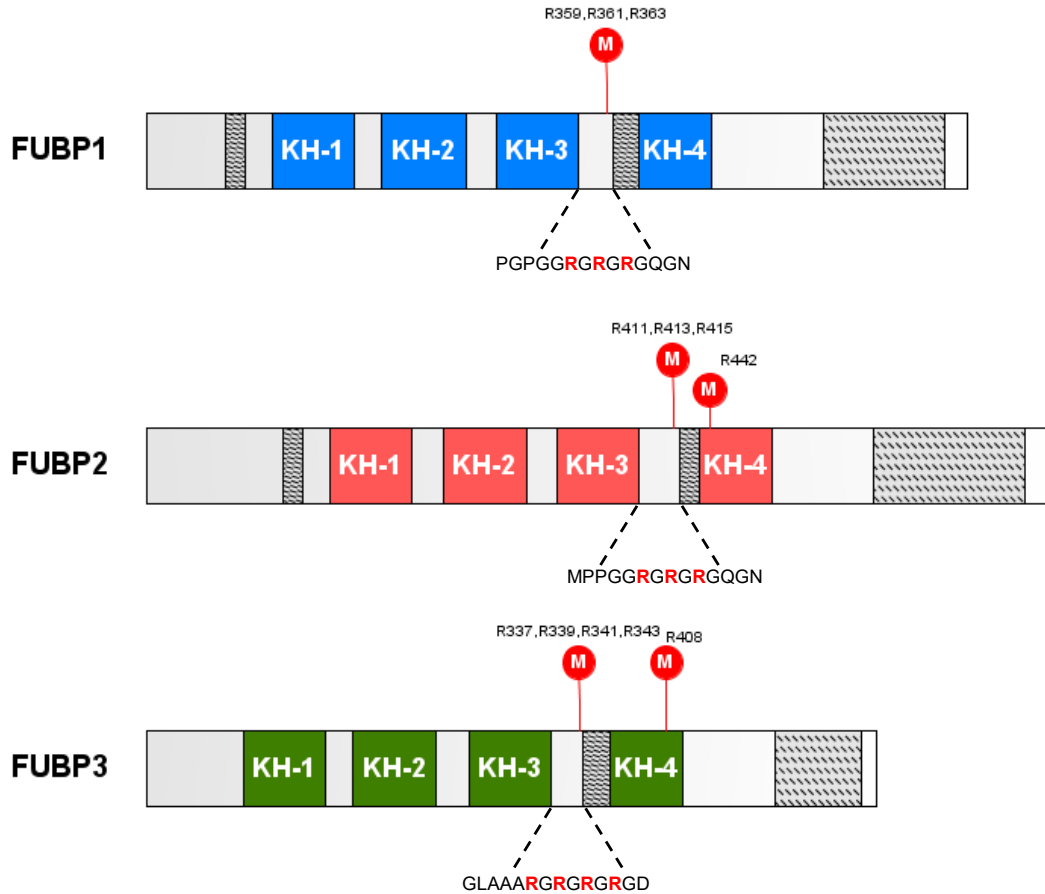


**Figure 44: FUBPs share conserved methylated arginine.** FUBP1, FUBP2, and FUBP3 are methylated on arginine residues (marked in red) between their KH3 and KH4 domains, whose sequence is conserved between FUBP1 and FUBP2.

### V.3 FUBP1 partners

Proteomic analysis aiming to identify FUBP1 partners indicate that it interacts with proteins involved in pre-mRNA splicing, translation, mRNA processing and transport, and spliceosome components [528,529], similar to the processes involving PRMT substrates, particularly PRMT5 (discussed in sections III and IV). FUBP1 interacting partners were identified in HEK293T cells, and PRMT1, PRMT5, MEP50, and CHTOP (PRMT1 and PRMT5 partner) were identified as potential FUBP1 partners. **Table 9** lists the known partners of FUBP1. A description of the functional interaction between FUBP1 and its different partners will be discussed in later in this section.

**Table 9: FUBP1 interacting partners.**

Partner	FUBP1 domain	Partner domain	Reference
FIR	CD	ND	[530]
(PUF60 isoform)	N-ter and CD	RRM1 and RRM2 motifs	[531]
TFIIH subunits: p62, p89, Cyc H	C-ter (449–644)	ND	[532]
JTV1 (FL) and JA (JTV1 lacking E2)	ND	ND	[533]
p53	ND	ND	[534]
BCCIP (TOK-1)	ND	ND	[534]
TCTP	ND	ND	[534]
RUNX1	ND	ND	[535]
4EBP1	CD	ND	[536]
PTBP2	ND	ND	[529]
NOVA1/NOVA2	ND	ND	[529]
SRRM4	ND	ND	[529]
eIF3 $\eta$	ND	ND	[537]
USP22	ND	ND	[511]
GCN5	ND	ND	[511]
P38	C-ter	ND	[507]
AIMP2	ND	MT1 (84–119) and MT2 (120–155)	[509]
Smurf2	ND	HECT domain	[509]

CD: central domain; ND: not determined

## V.4. FUBP1 structure

### V.4.1. FUBP1 N and C terminal domains

The N terminal domain of FUBP1 extends from aa 1 to 106 (**Figure 42**), bearing at the beginning a stretch of 11 repeated glycine residues followed by an amphipathic  $\alpha$ -helix. After the helix, the remaining residues of the N terminal domain are enriched in glutamine.

Similarly, the C terminal domain of FUBP1 (448-644) is rich in glutamine residues in addition to tyrosine. Some tyrosine residues form repeated tyrosine-dyad motifs, representing potential phosphorylation sites [496].

Classical transcription factors contain a DNA binding domain and a trans-activating domain that drives gene transcription. To understand the exact mechanism of FUBP1 transcriptional function, Duncan *et al.* utilised GAL4-FUBP1 domains constructs chimeras. The study revealed that the C-terminal domain of FUBP1 was sufficient by itself to drive transcription activation, unlike the other two domains, marking it as FUBP1 transactivation domain. However, it had no sequence homology with other known trans-activation domains, rising questions about its mechanism of action. The beginning of the C-terminal domain is rich in proline, histidine, and glycine and is marked by a three-time repetition of “PHGP” sequence. A discern feature in the rest of the domain is the presence of five pairs of tyrosine dyads (YY) in a novel sequence motif. The motifs containing these tyrosine dyads were termed YM1, YM2, and YM3. YM1 and YM3 bear 2 sets of tyrosine pairs and YM2 contains one. Each motif alone was capable of driving transcription, and the deletion of all the three together completely abolished the C-terminal domain trans-activating activity [538]. Several mutations in the tyrosine residues augmented transactivation, emphasizing the importance of the presence of at least one of the motifs for transcriptional activation [538]. The authors unravelled the role of the N-terminal domain in auto-repressing the transcriptional activity of FUBP1, as co-expressing two chimeras of the separate domains drastically augmented the activity of the C-terminal one [538].

#### **V.4.2. NMR structure and the nucleic acid binding domain**

The central domain of FUBP1 is the largest of the three domains and is responsible of nucleic acid binding. It is comprised of four KH domains consisting of 30 residues each, separated by equal spacers. The four domains share similar structures: a  $\beta$ -sheet followed by a turn at glycine 13 and 14, separating the sheet from the adjacent  $\alpha$ -helix. Each domain is then followed by an amphipathic  $\alpha$ -helix and share sequence homology to those of hnRNP K. FUBP1 binds to the non-coding strand of the FUSE element, an AT-rich 29 nucleotide sequence (5'-TATATTCCCTCGGGATTTTTTATTTTGTG-3')

located 1500 nct upstream *MYC* P1 promoter (or 1700 upstream P2 promoter) [495,496]. Truncated constructs of the central domain uncovered the importance of the last two repeats, where in between FUBP1's methylation sites are present (**Figure 44**), in binding to ssDNA [496].

KH domains are ssDNA and RNA binding motifs present on some nucleic acid binding proteins, and one domain can generally bind up to 4 nucleotides. In eukaryotic KH motifs, the  $\beta$ -sheet is composed of three anti-parallel  $\beta$ -strands of the order  $\beta 1$ ,  $\beta'$  and  $\beta 2$ , and three  $\alpha$ -helices pack on the surface of the  $\beta$ -sheet. Binding to nucleic acids is mediated by a hydrophobic cleft (or groove) formed between  $\alpha 1$ ,  $\alpha 2$ , and GxxG loop on one end, and the  $\beta$ -sheet and variable loop on the other end [539,540].

The NMR structure of FUBP1 KH3 and KH4 domains in complex with FUSE has been resolved in 2002 (**Figure 45**) [541]. On FUSE, KH3 and KH4 respectively bind to the short sequences 5'-TATTCCC-3' and 5'-ATTTT-3' separated by a 6-nucleotide spacer that does not contact FUBP1 [541]. Additionally, KH3 and KH4 domains do not interact together and are connected by a flexible, highly disordered glycine rich 30 residue linker [541].

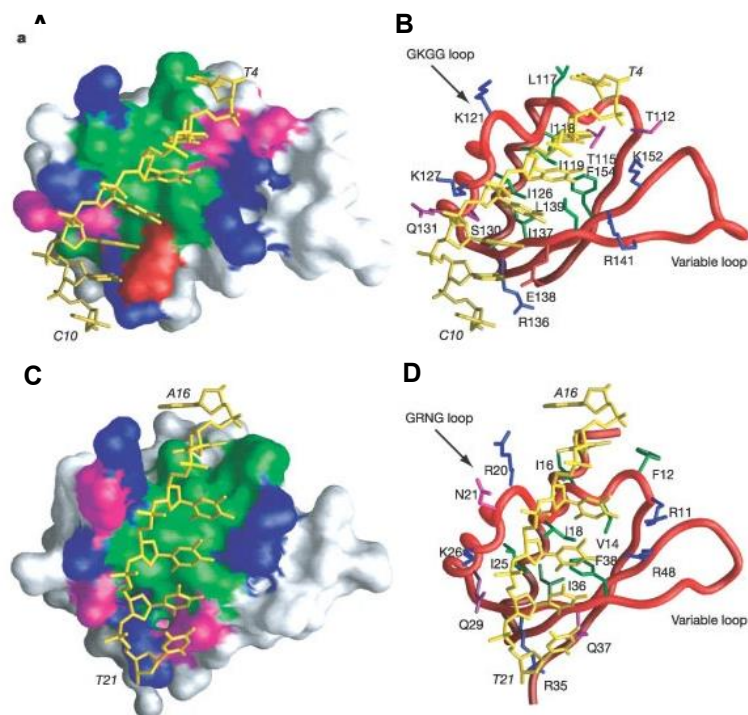


**Figure 45: NMR structure of FUBP1 KH3 and KH4 domains bound to ssDNA.** (A, B) KH4 and (C, D) KH3 domains FUSE. In A and C the domains are presented as a molecular surface, with hydrophobic

(green), uncharged hydrophilic (pink), positively charged (blue), and negatively charged (red) residues comprising the ssDNA (yellow) binding sites. In B and D, the protein backbone is represented as a red tube.

Systematic Evolution of Ligands by Exponential Enrichment (SELEX) method was adapted to ssDNA binding proteins and employed to characterize the binding of full length FUBP1 to FUSE [542]. SELEX revealed that FUBP1 KH1 preferentially bound (T/G)TG(T/C), and the other three KH domains' optimal binding sequence is T(T/C)GT. Furthermore, EMSA assay was used to define an ideal spacing between KH binding tetrads and unveiled the importance of the nucleotide spacers lengths and compositions in FUBP1 binding to FUSE [542].

The early NMR and SELEX studies of FUBP1 KH domains have added to the understanding of FUBP1 ssDNA binding ability. However, they did not provide sufficient data on the contribution of each KH domain alone. Recently, the crystal structure of each FUBP1 KH domain was obtained, in an attempt to characterize their nucleic acid binding properties [543]. To assess the binding capabilities of each domain, a series of EMSA and isothermal titration assay (ITC) experiments were performed. All KH domains were alone capable to moderately bind to the FUSE sequence [543]. Random deletions in the FUSE sequence showed the preference of KH1 and KH3 domains to a core "TGT" sequence while KH2 and KH4 preferred a core "TTT". Interestingly, KH3 domain had the strongest FUSE binding potency, with a 5-fold increase compared to the other domains [543]. Moreover, the binding strength of different pairs of KH domains was assessed. KH1-2, KH2-3, and KH3-4 all showed an increased but still moderate affinity to FUSE compared to individual domains [543]. The different pairing combinations had almost equal binding affinities, in contrast with the early report showing the importance of KH3 and KH4 in DNA binding [496]. Interestingly, the presence of all KH domains showed a remarkable increase in the binding affinity to FUSE, unveiling a possible orchestration between the four domains for ssDNA binding [543]. Since FUBP1-FUSE interaction was reported, several "FUSE-like" sequences have been discovered that FUBP1 can interact with and are summarized in **Table 10**.

**Table 10: FUBP1 DNA binding sequences**

Gene	FUBP1 DNA binding sequence	Reference
	<u>GAUUUUUUUA</u>	[541]
<i>MYC</i>	<u>AUAUUC</u> CCUC	
(FUSE)	TTGT	[542]
	GTGT; GTGC	
	5'-TATATTCCTCGGGATTTTTTATTTTGTG-3'	[496,543]
<i>USP29</i>	5' <u>AGTTTGC</u> ATTACTTTTTTTTTT <u>TTGTTTGT</u> TTTTGAGATGGAGTT TTGCT <u>CTTGT</u> TGCCCAGGC 3'	[533]
<i>P21</i>	5'-TTTTGTTTTTCATTTTGTTTTTTTGTTT-3'	[511,535,544]
	+30kb enhancer	[535]
<i>c-KIT</i>	5'-TTT <u>ATTC</u> TATGGGGATATAAAAGTGTGT-3'	
	<b>KH4</b> <b>KH3</b>	
<i>HK1</i>	3 promoter regions	[545]
<i>HK2</i>	promoter distal and proximal regions	
<i>CCNA1</i>	2 promoter regions	[546]
<i>DVL1</i>	5'-TTCCCCTGATTT-3'	[510]

## V.5. FUBP1 Functions

### V.5.1. FUBP1: a transcription factor

#### V.5.1.1. FUSE/FUBP1/FIR and MYC activation

Numerous studies have studied the FUSE-FUBP1 interaction and the regulation of *MYC* expression by FUBP1 [496,531,547–549]. *MYC* is a proto-oncogene that drives global transcription, regulating the expression of 10-15% of the human genome and is reported to be deregulated in ~70% of human cancers [499,550,551]. Noteworthy, FUBP1 alone is not sufficient to activate *MYC* transcription, but is required for its maximum activation [552]. However, some studies report the failure of FUBP1 in inducing *MYC* expression or binding upstream its promoter, raising a possibility that this activation is cell line

dependent [511,535,544]. FUBP1 regulation of *MYC* transcription activation involves two other crucial players, TFIIH and FUBP Interacting Repressor (FIR).

TFIIH is a multi-protein RNA polymerase II transcription initiation factor composed of ten subunits forming two main sub-complexes [553]. FIR is a splice variant of the essential splicing factor 60-kDa poly-U-binding factor (PFU60). FIR is composed of a repression domain at its N terminal that interacts with TFIIH and inhibit its 3'-5' helicase activity [530], a central domain encompassing two RRM able to interact with RNA and to a lesser extent ssDNA, and an U2AF homology domain at its C terminus [498,499]. FIR can interact with the FUSE element as a dimer [530,531] and with FUBP1 and FUBP2 central domains, but not with FUBP3. Both RRM1 and RRM2 motifs of FIR are responsible for its interaction with FUBP1, that is highly enhanced in the presence of FUSE nucleotide sequence [531].

**Figure 46** summarizes the mechanism of *MYC* regulation by the FUBP1/FUSE/FIR system. When *MYC* transcription is initiated, binding of factors and chromatin remodelling exerts torsional stress on the FUSE element, leading to its melting and the recruitment of FUBP1 to the non-coding strand. At the meantime, TFIIH is also recruited and binds FUBP1 C-terminal activation domain, activating its 3'-5' helicase activity leading to maximum *MYC* transcription activation [532,552]. However, c-myc levels should be critically controlled and monitored, as even a transient increase in c-myc levels can elevate tumorigenicity [550,554]. After *MYC* transcription reaches a peak, FIR is recruited and interacts with the central domain of FUBP1, allowing the interaction of FIR with FUSE and forming a FUSE/FUBP1/FIR tripartite complex. This puts FIR in a proximity to TFIIH -still interacting with FUBP1- and subsequently inhibits TFIIH p89/XPB helicase activity. Inhibition of TFIIH exerts a torsional stress on FUSE, leading to conformational changes and finally allowing FUSE renaturation. This ejects FUBP1 from the complex, allowing FIR to homo-dimerize on FUSE. The stabilization of the FUSE/FIR interaction allows *MYC* transcription to reach basal levels [531,532,552,555].



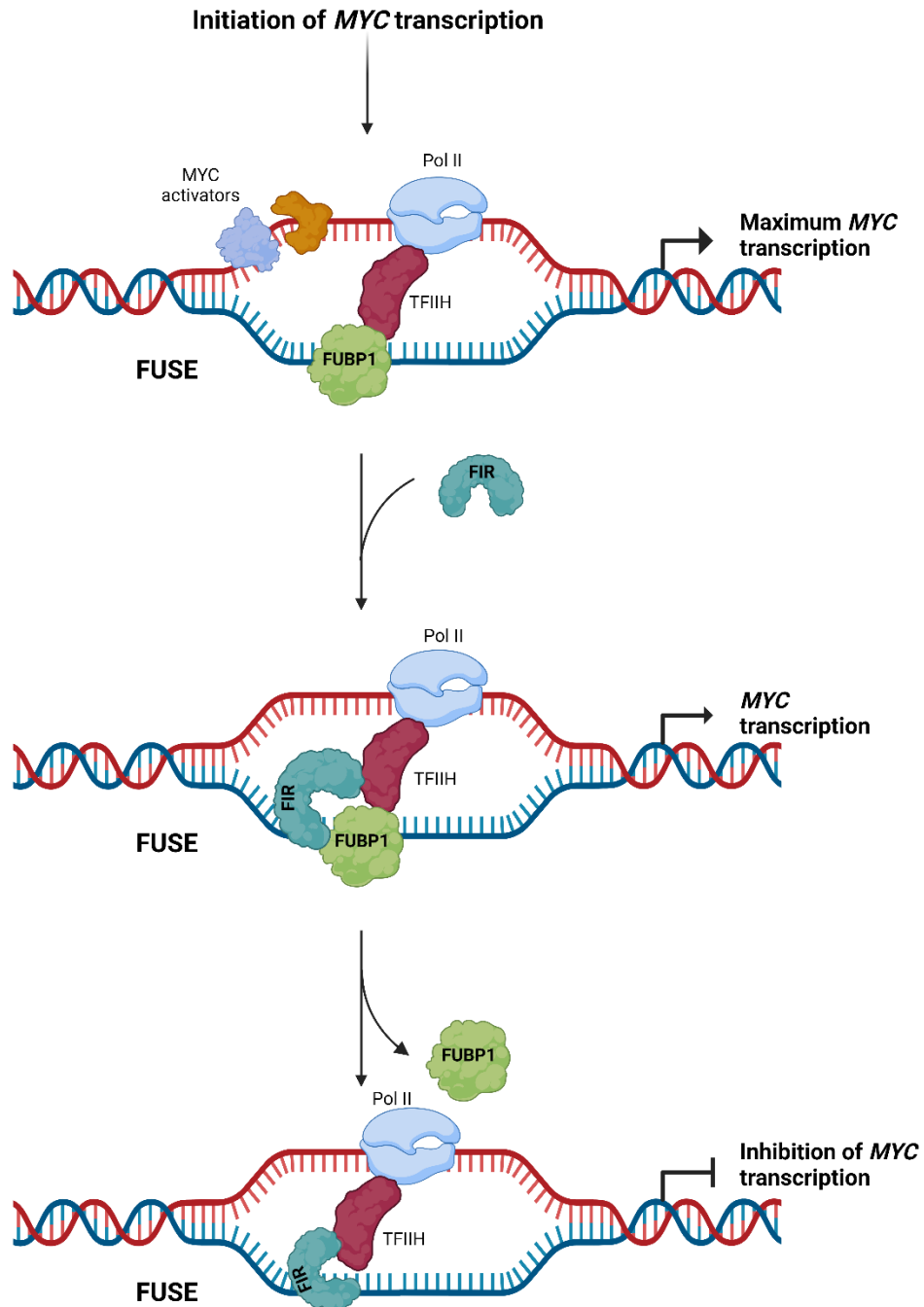


**Figure 46: FUBP1/FIR/FUSE axis in the control of MYC transcription.** When MYC transcription is initiated, binding of activation factors causes torsional stress, leading to DNA unwinding and the recruitment of FUBP1 to the non-coding strand of FUSE. FUBP1 interacts with the transcriptional machinery on the FUSE element, leading to maximum MYC transcription. FIR is then recruited and interacts with both FUBP1 and FUSE, forming a FUSE/FUBP1/FIR tripartite complex. FIR interacts with TFIID and inhibits its activity, which causes a conformational change in the chromatin leading to the ejection of FUBP1 and terminating MYC transcription.

### **V.5.1.2. Regulation of cell cycle and apoptotic genes**

Apart from *MYC*, FUBP1 can up- or down-regulate the expression of genes implicated in cell cycle, proliferation, differentiation, apoptosis, and metabolism. **Table 11** includes the different genes found to be regulated by FUBP1 at the transcriptional level.

P21 (encoded by *CDKN1A*), a cell cycle inhibitor, is regulated by FUBP1 through the direct binding of FUBP1 to its promoter [511,535,544]. FUBP1 is required in S phase of the cell cycle more than the mitotic one (M) and is enriched more in G1/S than in G2/M. Knockdown of FUBP1 in NIH3T3 fibroblasts diminished the expression of cyclin A1 and cyclin A2 (encoded by *CCNA1* and *CCNA2* respectively) mRNA expression levels. Consistently, cyclin A protein levels decreased after FUBP1 knockdown. Regulation of cyclin A1 transcription was directly mediated by FUBP1, as FUBP1 is significantly enriched at two regions of *CCNA1* promoter (**Table 10**) [546]. Stathmins are a family of four proteins: stathmin, stathmin-like 2 (SCG10), stathmin-like 3 (SCLIP), and stathmin-like 4 (RB3) encoded by different genes. Stathmins play critical roles in regulating microtubule organization and cell cycle, and their overexpression is associated with oncogenesis [556,557]. Depleting FUBP1 using siRNA decreased the expression of stathmin in Calu-1 and both stathmin and SCLIP in Calu-6 lung cancer cells. Additionally, analysing FUBP1, stathmin, SCG10, and SCLIP mRNA levels in NSCLC tissues showed a correlation between FUBP1 overexpression and all three stathmins in cancerous tissue [557]. An elegant study published in 2011 revealed a cooperation between FUBP1 and JTV1 in activating ubiquitin specific peptidase 29 (USP29) transcription [533]. In response to oxidative stress, JTV1 - a component of a multi-aminoacyl-tRNA synthetase (ARS) complex - dissociates from ARS and translocates to the nucleus. Nuclear JTV1 then associates with FUBP1, and the latter binds to the USP29 promoter activating its transcription [533]. USP29 then binds to p53 and deubiquitinates it, stabilizing p53 expression. The same study identified a 54 bp FUSE-like sequence located 2.5 kb upstream the USP29 TSS (**Table 10**). Surprisingly, this FUSE-like sequence matches FUBP1 predicted optimal binding site better than the FUSE element [533]. Another FUSE-like sequence was identified using structural modelling and molecular biology in the +30 kb enhancer upstream the *c-KIT* gene (**Table 10**) [535]. *c-kit* is a tyrosine kinase receptor expressed primarily on progenitors of hematopoietic, melanogenesis and reproductive

systems. It is involved in cell growth and stimulation of differentiation and is classified as an oncogene [558]. Debaize *et al.* reported an interaction and cooperation between FUBP1 and RUNX1 in driving *c-KIT* expression [535]. The two transcription factors bind two regulatory regions, +700 bp and +30 kb in the *c-KIT* first intron. Overexpressing both FUBP1 and RUNX1 increased *c-kit* mRNA and protein expression levels, amplified *c-kit* signalling pathway, and led to proliferation and resistance to imatinib mesylate (a *c-kit* inhibitor) in Nalm6 pre-B cell line [535]. Hk1 and Hk2 are two hexokinases that play roles in glycolysis. FUBP1 was shown to bind to three and two regions of *HK1* and *HK2* promoters, respectively (**Table 10**), thus activating their expression and mediating lactate production [545]. Recently, FUBP1 was shown to enhance the Wnt signalling pathway in CRC by directly binding to *DVL1* promoter and activating its transcription, promoting CRC cell migration and invasion [510].

**Table 11: Transcripts regulated by FUBP1 at the transcriptional level.**

Target	FUBP1 Effect	Reference
c-myc	Activation	[496,548]
Cyclin E/H/I	Activation	[548]
L32	Activation	[548]
Stathmin and SCLIP	Activation	[557]
USP29	Activation	[533]
p21	Repression	[544]
p15		
p21	Repression	[534]
PDL-1	Activation	[559]
c-Kit	Activation	[535]
Hk1	Activation	[545]
Hk2	Activation	[545]
PKM1	Activation	[545]

Ccna1 and Ccna2	Activation	[546]
DVL1	Activation	[510]

### V.5.2. FUBP1: a pre-mRNA splicing factor

Although FUBP1 has been found to be present in the spliceosome [501], and though FUBP1's close family member FUBP2 is a well-studied pre-mRNA splicing factor, the first report implicating FUBP1 in splicing was only lately demonstrated [560]. FUBP1 has been shown to mediate the second step splicing inhibition of tridian exon 10 by binding to an AU rich exon splicing silencer (ESS) [560]. Adding increasing amounts of recombinant FUBP1 in an *in-vitro* splicing assay caused 50-80% splicing inhibition and depleting endogenous FUBP1 by siRNA increased exon inclusion of tridian exon 10. In the same report, the splicing pattern of 51 additional transcripts was examined upon FUBP1 depletion, and four out of the 51 analysed transcripts were regulated by FUBP1. FUBP1 increases the inclusion of *PTBP2* exon 10 and *ENAH/MENA* exon 11 and decreases the inclusion of exons 4-7 of *caspase 9* and exon 14 of *ACLY* [560]. This was the first report proving the role of FUBP1 in pre-mRNA splicing and presented it as either a positive or negative splicing regulator [560]. In another study, it was shown that in the presence of SMN-C2, a small molecule regulating AS, FUBP1 and FUBP2 bind with a higher efficiency to SMN2 mRNA regulating the splicing of SMN2 exon 7 [561]. FUBP1 was also demonstrated to be a positive regulator of Mouse double minute 2 (MDM2) splicing. MDM2 is a negative regulator of p53, causing its ubiquitination and subsequent degradation in the cytoplasm [562]. *MDM2* has been reported to be spliced into malignant isoforms under stress conditions [563,564]. By using a MDM2 minigene, FUBP1 was shown to bind to regions both upstream and downstream of intron 11 of MDM2 and positively regulate its splicing. The same study showed the emergence of a shorter isoform of FUBP1 under stress inducing conditions (cisplatin treatment). Surprisingly, both the long and short isoforms of FUBP1 were able to regulate MDM2 splicing, under normal and stress conditions [563]. Moreover, FUBP1 binds to a UG rich intronic splicing enhancer (ISE) upstream exon 39 of *DMD* gene [565]. *DMD* encodes dystrophin, and loss of function mutations leading to the absence of dystrophin in muscle cells cause

Duchenne muscular dystrophy (DMD). *DMD* mutations causing a non-functional, truncated, or lower level of dystrophin in muscle cells causes Becker muscular dystrophy (BMD), a milder variant of DMD. By binding to intron 38 of *ISE*, FUBP1 increases E39 inclusion of DMD, and enhances normal splicing of the transcript [565]. Mass spectrometry analysis of immunoprecipitated FUBP1 in neural progenitor cells (NPC) retrieved FUBP1 partners present in the spliceosome like PTBP2, NOVA1/2 and SRRM4. *LSD1* gene contains 19 exons. Mature *LSD1* transcript can contain an extra mini exon 8a, generating LSD1+8a isoform that is exclusively expressed in the nervous system. Loss of LSD1+8a strongly inhibits neuronal differentiation. FUBP1 and SRRM4 bind to different regions of LSD1 introns 8 and 8+, promoting exon 8+ inclusion and subsequently neuronal differentiation [529]. In an elegant study, FUBP1 was shown to regulate the splicing of different transcripts involved in tumorigenesis like caspase 8 and BRCA1 [528]. Caspase 8 can experience A3' AS giving rise to a non-functional transcript unable to produce caspase 8 protein, and FUBP1 null cells exhibited a complete loss of caspase 8. BRCA1 was highly expressed in FUBP1 null cells as an aberrantly spliced form missing most of exon 11, termed BRCA1<sup>Δ11b</sup>. In addition, FUBP1 KO cells expressed a truncated and oncogenic form of *MAGI3*, a Hippo signalling regulator, MAGI3<sup>pPA</sup>. The same altered AS events were assessed in a different breast cell line upon FUBP1 depletion, MCF10A. Similar to MCF10F, FUBP1-null MCF10A cells exhibited a complete loss of caspase 8 protein, however, there was no effect on *BRCA1* or *MAGI3* AS [528].

**Table 12** summarizes the different transcripts for which pre-mRNA splicing is regulated by FUBP1 and the corresponding FUBP1 RNA binding motifs.

**Table 12: Transcripts regulated by FUBP1 at the pre-mRNA splicing level.**

Target	Splicing event	FUBP1 binding site/motif	Reference
Tridian E10	Exon skipping	Tridian exon 10 ESS: AUAUAUGAU	
ACLY	Exon 14 skipping	ND	[560]
Caspase 9	Exon 4-7 skipping	ND	

PTBP2	Exon 10 inclusion	ND	
ENAH/MENA	Exon 11 inclusion	ND	
MDM2	Exon inclusion	MDM2 intron 11	[563]
DMD	Exon 39 inclusion	DMD intron 38	[565]
LSD1	Exon 8+ inclusion	two regions in introns 8 and 8a of LSD1	[529]
MAGI3	Cleavage and polyadenylation in intron 10	ND	
BRCA1	Exon 11 skipping	ND	[528]
Caspase 8	Alternative A3' splicing	ND	

### V.5.3. FUBP1 and translation

As an RNA binding protein, FUBP1 is implicated in regulating the translation of some transcripts, which are summarized in **Table 13**.

#### V.5.3.1. Translation regulation via 3'UTR binding

Both FUBP1 and FUBP2 were found to bind the 3'UTR of nucleophosmin (*NPM*), coding for a protein involved in ribosome biogenesis and cell proliferation [566]. By binding to the 3'UTR, FUBP1 represses the translation of NPM in MEF stably depleted of Tsc1 and p53. FUBP1 depletion in this cell line increased the fraction of polysomes associated transcripts, elevating the translation of NPM. As NPM promotes cell growth, FUBP1 depletion enhanced proliferation, marking it as a tumour suppressor in the context of the study [566]. FUBP1 binding site on NPM UTR is still not described.

Similar to NPM, FUBP1 binds to an AU rich region in the 3'UTR of polycystic kidney disease 2 (*PKD2*) and represses its translation [536]. PKD2 is an integral membrane cation channel expressed on a wide range of tissues. By controlling PKD2 protein levels, FUBP1 regulates disease-associated phenotypes in larval zebrafish like tail curling and pronephric cyst induction [536].

### V.5.3.2. Translation regulation via 5'UTR binding

P27, also known as KIP1, is a cyclin dependent kinase inhibitor (CDKI) that inhibits cell cycle progression. Reduction of p27 levels is detected in different tumours and is associated with poor clinical outcomes [567]. Using RNA pulldown from MCF7 cytosolic extracts, FUBP1 was identified to associate with the 5'UTR of p27. The interaction is strong and direct, requiring nucleotides 431-439 (5'-GCGAAGAG-3) situated at the 3' end of p27 5'UTR. FUBP1 stimulates p27 IRES activity promoting its translation both *in vitro* and in MCF7 cell line. Accordingly, overexpressing or depleting FUBP1 in MCF7 cells respectively increased and decreased endogenous p27 protein levels [568].

Nuclear factor erythroid 2 related factor 2 (Nrf2) is a transcription factor regulating the expression of antioxidant proteins in response to oxidative stress [537]. Upon H<sub>2</sub>O<sub>2</sub> treatment, FUBP1 associates with the 5'UTR of Nrf2 mRNA and activates its IRES-mediated translation. FUBP1 was present in the 40/43S fraction and showed a H<sub>2</sub>O<sub>2</sub> dose-dependent increase in the total ribosome fraction. Interestingly, it interacts with eIF3 $\eta$ , a subunit of the eIF3 complex responsible for 43S pre-initiation complex assembly. The interaction between both proteins was also enhanced upon H<sub>2</sub>O<sub>2</sub> treatment. This reinforces a function of FUBP1 in promoting 43S complex attachment to Nrf2 mRNA for translational initiation [569].

**Table 13: Transcripts regulated by FUBP1 at the translational level.**

Gene	Regulation Mechanism	FUBP1 binding site/motif	Reference
P27	Activation	5'-GCGAAGAG-3' on the 5'UTR (Important, but not direct contact)	[568]
NPM	Repression	3'UTR	[566]
PKD2	Repression	3'UTR	[536]
Nrf2	Activation upon H <sub>2</sub> O <sub>2</sub> treatment	5'UTR	[569]

EV71 viral RNA	FUBP1 positively regulates EV71 IRES activity	5'UTR; linker region through KH3+KH4	[504]
----------------------	--	---	-------

### V.5.5. Global transcripts regulated by FUBP1

FUBP1 impacts the global transcription and splicing mechanisms in cells [528,529]. RNA-seq analysis in NPC FUBP1 KO cells revealed an increase in exon skipping events upon FUBP1 loss in differentiating NPCs [529]. Additionally, depleting FUBP1 from MCF10F cells caused a dysregulation in AS events [528]. Compared to the control, FUBP1 null cells presented more than 10,000 differential alternative splicing events, with exon skipping being the most prevalent one (70% of total events). Differentially spliced genes affected by FUBP1 depletion are implicated in mRNA processing, DNA repair, and cell cycle, linking FUBP1 splicing regulation to tumour formation [528]. Furthermore, cancers having FUBP1 loss of function mutations and an additional glioma cell line U87MG depleted from FUBP1 by siRNA were assessed for splicing alterations. Interestingly, an overlap of FUBP1 alternatively spliced events was observed between human brain cancers, U87MG, and MCF10F cells. Several altered alternative splicing events included A3SS, A5SS, and SE events [528].

### V.6. FUBP1 in Cancer

Conflicting roles of FUBP1 were reported in cancer progression. In oligodendrogliomas, homolog of *Drosophila capicua* (CIC) and *FUBP1* genes are mutated, leading to the loss of FUBP1 and CIC proteins in oligodendroglial tumours [570–572]. The loss of FUBP1 expression correlated with unfavourable progression-free survival and overall survival, implying the role of FUBP1 as a tumour suppressor in this cancer [573]. By analysing whole-exome sequencing data in 33 tumours from the TCGA database, Seiler *et al.* identified 119 mutated splicing factor genes, including loss of function mutations in *FUBP1* gene [574]. In neuronal progenitors, FUBP1 enhances the splicing of LSD1+8a isoform, favouring neuronal cells differentiation and suppresses tumorigenesis [529].

On the contrary, FUBP1 is reported to be overexpressed, drives oncogenesis, and correlates with poor patient prognosis in NSCLC [557,575], CRC [576], HCC [577],



leukemia [578–580], ovarian [514], and breast cancer [528,581]. The involvement of FUBP1 in oncogenesis is linked to a deregulation of its target genes expression like *MYC*.

In breast cancer, the circular RNA circACTN4 binds competitively to FUBP1 preventing its association with FIR, therefore elevating *MYC* transcription and promoting breast cancer tumorigenesis [582]. FUBP1 and *myc* protein levels were higher in breast cancer tumour tissue compared to the normal breast, and their expression decreases upon cisplatin treatment [583]. Furthermore, FUBP1 knockdown in TNBC cell lines arrests cell cycle progression, decreases proliferation and cyclin A2 levels, reduces cell migration, and enhances the sensitivity of TNBC cells to cisplatin treatment [583]. In HER2-positive breast cancer, trastuzumab and lapatinib treatment upregulates the expression of the microRNA miR-16. By targeting FUBP1, miR-16 inhibits breast cancer proliferation even in cells resistant to trastuzumab and lapatinib [581]. In accordance, high miR-16 and low FUBP1 expression levels correlate with the response of HER2-positive breast tumours to trastuzumab [581]. In MCF7 luminal breast cancer cell lines, induction of apoptosis causes the cleavage of FUBP1 by caspases at its NLS, promoting its export from the nucleus leading to the downregulation of *MYC* levels [503].

## Summary

FUBP1 is a protein involved in transcription, translation, and pre-mRNA splicing, processes similar to those enriched in the PRMT5 methylome and regulated by PRMT5. FUBP1 is present in the spliceosome, a complex that PRMT5 is crucial in its assembly. FUBP1 functions are largely regulated by its central domain, encompassing four KH domains responsible for ssDNA and RNA binding. Between KH3 and KH4 domains, three arginine residues are reported to be mono- and di- methylated in all three FUBP members, reflecting an importance of their methylation in regulating FUBP functions. Although having contradictory roles in cancer, FUBP1 acts primarily as an oncogene in breast cancer and regulates breast cancer sensitivity to some therapies like cisplatin and HER2-targeted therapies.

## Chapter 2: Objectives and results

During my thesis, I mainly worked on two projects pertaining the role of PRMT5 in TNBC. This chapter will be divided into two parts, each part consisting of the results, discussion, and conclusions for each project.

The first part is the manuscript entitled “Therapeutic advantage of targeting PRMT5 in combination with chemotherapies or EGFR/HER2 inhibitors in triple-negative breast cancers”, where the aim was to test different combinations of PRMT5 inhibitor with targeted or chemotherapies on a panel of TNBC cell line. This project was entirely performed during this thesis, and this manuscript has been published in the *Breast Cancer: Targets and Therapy* journal.

The second part is the manuscript entitled “Unveiling the PRMT5 interactome through immunoprecipitation and TurboID proximity labelling in TNBC”, that aimed to decipher the interactome of PRMT5 and study the functional interaction between PRMT5 and some of the partners retrieved. This project started before the start of my thesis by a previous PhD student, where she carried out the experiments of MEP50 mass spectrometry. The rest of the data was obtained during this thesis.

## Chapter 2: Part 1

*ORIGINAL RESEARCH*

*Dakroub et al*

### **Therapeutic advantage of targeting PRMT5 in combination with chemotherapies or EGFR/HER2 inhibitors in triple-negative breast cancers**

Rayan Dakroub <sup>1,2</sup>, Solène Huard <sup>1</sup>, Yara Hajj-Younes <sup>1</sup>, Samyuktha Suresh<sup>1</sup>, Bassam Badran <sup>2</sup>, Hussein Fayyad-Kazan <sup>2</sup>, and Thierry Dubois <sup>1</sup>

<sup>1</sup> Breast Cancer Biology Group, Translational Research Department, Institute Curie-PSL Research University, 75005 Paris, France

<sup>2</sup> Laboratory of Cancer Biology and Molecular Immunology, Faculty of Sciences-I, Lebanese University, Hadath 1003, Lebanon

Correspondence: Thierry Dubois

Breast Cancer Biology Group, Translational Research Department, Institute Curie-PSL Research University, 75005 Paris, France

Te+33 156246250

Email: [thierry.dubois@curie.fr](mailto:thierry.dubois@curie.fr)

## Abstract

Purpose: Triple-negative breast cancer (TNBC) is the most aggressive breast cancer subgroup characterized by a high risk of resistance to chemotherapies and high relapse potential. TNBC shows inter-and intra-tumoral heterogeneity; more than half expresses high EGFR levels and about 30% are classified as HER2-low breast cancers. High PRMT5 mRNA levels are associated with poor prognosis in TNBC and inhibiting PRMT5 impairs the viability of subsets of TNBC cell lines and delays tumour growth in TNBC mice models. TNBC patients may therefore benefit from a treatment targeting PRMT5. The aim of this study was to assess the therapeutic benefit of combining a PRMT5 inhibitor with different chemotherapies used in the clinics to treat TNBC patients, or with FDA-approved inhibitors targeting the HER family members.

Methods: The drug combinations were performed using proliferation and colony formation assays on TNBC cell lines that were sensitive or resistant to EPZ015938, a PRMT5 inhibitor that has been evaluated in clinical trials. The chemotherapies analyzed were cisplatin, doxorubicin, camptothecin, and paclitaxel. The targeted therapies tested were erlotinib (EGFR inhibitor), neratinib (EGFR/HER2/HER4 inhibitor) and tucatinib (HER2 inhibitor).

Results: We found that PRMT5 inhibition synergized mostly with cisplatin, and to a lesser extent with doxorubicin or camptothecin, but not with paclitaxel, to impair TNBC cell proliferation. PRMT5 inhibition also synergized with erlotinib and neratinib in TNBC cell lines, especially in those overexpressing EGFR. Additionally, a synergistic interaction was observed with neratinib and tucatinib in a HER2-low TNBC cell line as well as in a HER2-positive breast cancer cell line. We noticed that synergy can be obtained in TNBC cell lines that were resistant to PRMT5 inhibition alone.

Conclusion: Altogether, our data highlight the therapeutic potential of targeting PRMT5 using combinatorial strategies for the treatment of subsets of TNBC patients.

Keywords: TNBC; erlotinib; neratinib; cisplatin; drug combination

## Introduction

Breast cancer is a heterogeneous disease with distinct subgroups categorized according to the expression level of estrogen receptor (ER), progesterone receptor (PR), and human epidermal growth factor receptor 2 (HER2). Luminal breast cancers express ER and PR; HER2-positive tumours carry an amplification of the *HER2* gene; and triple-negative breast cancers (TNBC) do not express ER and PR and have no *HER2* gene amplification [10,584]. Recently, about 65% of luminal breast cancers and 35% of TNBC were found to be HER2-low breast tumours [38,585], defined as tumours expressing HER2 with immunohistochemical (IHC) scores of 1+ and 2+ without *HER2* gene amplification. Breast cancer subgroups differ in their grade and prognosis, with TNBC being the most aggressive. TNBC is an invasive tumour usually associated with drug resistance, high metastatic potential, and poor prognosis [66,67,80,81]. A high percentage of TNBC patients experience relapse within 3-5 years following treatment [67]. Compared to the other breast cancer subgroups, TNBC is enriched in a subpopulation of cells with self-renewal ability, termed breast cancer stem cells (BCSC) or tumour-initiating cells (TIC) that are drug-resistant and thought to be involved in the high relapse rate of TNBC patients [67,586,587]. Another major concern in TNBC is its inherent inter-tumoral heterogeneity with different TNBC subtypes: basal-like 1 (BL1), basal-like 2 (BL2), mesenchymal (M), and luminal androgen receptor (LAR) [68,69]. Interestingly, HER2-low breast cancer is associated with the expression of androgen receptor (AR) in luminal and in TNBC [38]. The high inter- and intra-tumoral heterogeneity poses a considerable challenge in TNBC treatment options as one specific target/drug may not be beneficial to all TNBC but rather to a subset of them. Although chemotherapies such as platinum agents (cisplatin, carboplatin), taxanes (paclitaxel and docetaxel), and anthracyclines (doxorubicin, epirubicin), remain the standard treatment option [584,588,589], a few new treatments have been recently approved by the Food and Drug Administration (FDA) for selected TNBC patients: poly (ADP-ribose) polymerase (PARP) inhibitors for patients with *BRCA1/2* mutations [78–80], anti-PDL-1 antibodies for metastatic and early disease [67,590], and the antibody-drug conjugate sacituzumab govitecan [591]. Although more than half of TNBC overexpress the epidermal growth factor receptor (EGFR) [104,105,592], early clinical trials failed to demonstrate the clinical benefit of its inhibition

[81]. It is possible that the patients were not selected for high EGFR expression, or the pathway was not stimulated or was activated by downstream effectors such as AKT [81,592]. By screening an FDA-approved drug library in TNBC cells, we have reported that erlotinib, a reversible EGFR inhibitor, acts in synergy with the first described PRMT5 inhibitor (EPZ015666 [479]), to impair the proliferation of TNBC cells [430].

Arginine methylation is a common post-translational modification catalyzed by nine protein arginine methyltransferases (PRMT1-9), regulating transcription, pre-mRNA splicing, cell signaling, DNA repair, and stem cell maintenance [106,109,115,593,594]. Several PRMTs are overexpressed in different cancer types [115,116,136,234,287,595]. High PRMT5 mRNA expression is associated with poor prognosis in TNBC [429,430,470,473]. Inhibitors specifically targeting PRMT5 have been developed and are currently being evaluated in clinical trials [115,478,593]. Using the first described PRMT5 inhibitor (EPZ015666), we showed that inhibiting PRMT5 impairs cell proliferation of TNBC cell lines, reduces mammosphere formation, and slows tumour growth in a TNBC patient-derived xenograft (PDX) mice model [430]. By methylating and stabilizing KLF4 and KLF5, PRMT5 sustains stemness in TNBC, and its inhibition reduces tumour growth in xenograft models derived from TNBC cell lines [422,473]. These data suggest that PRMT5 could be an attractive therapeutic target for TNBC [422,430].

In this study, we used a more potent PRMT5 inhibitor, EPZ015938, optimized from EPZ015666, to improve pharmacokinetic properties, yielding a more drug-like molecule that has been evaluated in a clinical trial [410,478]. We assessed its antiproliferative effects on several breast cancer cell lines and non-cancerous breast cells. We evaluated the therapeutic benefit of combining it with different chemotherapies currently used in the clinic to treat TNBC patients [589]. We also combined EPZ015938 with different FDA-approved inhibitors targeting the HER family members: erlotinib [596,597], neratinib (EGFR, HER2, and HER4 inhibitor) [598], and tucatinib (HER2 inhibitor) [55]. Our results showed that inhibiting PRMT5 in combination with some chemotherapies or with inhibitors targeting the HER family could be a promising therapeutic strategy to treat subsets of TNBC patients.

## **Material and methods**

### ***Cell Culture***

The MDA-MB-231 cell line was a kind gift from Dr. Mina Bissell (University of California, Berkeley, CA, USA) and its use was approved by our institute with the establishment of a material transfer agreement. All other cell lines were purchased from the American Type Culture Collection (ATCC, LGC Promochem). All cell lines were authenticated by short tandem repeat profiling in 2021 and tested for mycoplasma by the MycoAlert Mycoplasma Detection Kit (Lonza Biosciences, Durham, NC, USA). MDA-MB-468, BT474, and T47D cells were cultured in RPMI-1640 GlutaMAX™ (LifeTechnologies) supplemented with 10% (vol/vol) fetal bovine serum (FBS, LifeTechnologies), 100 U/mL penicillin, and 100 µg/mL streptomycin (P/S, LifeTechnologies). HCC38, HCC70, and HCC1954 cells were cultured in RPMI-1640 GlutaMAX™ supplemented with 10% (vol/vol) FBS, 100 U/mL P/S, 1.5 g/L sodium bicarbonate (LifeTechnologies), 10 mmol/L Hepes (LifeTechnologies), and 1 mmol/L sodium pyruvate (LifeTechnologies). MCF-10A cells were cultured in DMEM-F12 (LifeTechnologies) supplemented with 0.01 mg/mL insulin, 100 ng/mL cholera toxin (Sigma), 500 ng/mL hydrocortisone (SERB Laboratories), and 20 ng/mL epidermal growth factor (Sigma). MDA-MB-453 and MDA-MB-231 cells were cultured in DMEM-F12 (LifeTechnologies) supplemented with 10% FBS and 1% P/S. BT-20 and MCF-7 cells were cultured in MEM (Sigma-Aldrich) containing 10% FBS, 1% P/S, 1.5 g/L sodium bicarbonate, 0.1 mmol/L non-essential amino-acids (NEAA, LifeTechnologies) and 1 mmol/L sodium pyruvate. All cell lines were maintained at 37°C with 5% CO<sub>2</sub>.

### ***Inhibitors***

EPZ015938 (PRMT5 inhibitor; ref: HY-101563), neratinib (HER1/2/4 inhibitor; ref: HY-32721), and tucatinib (HER2 inhibitor; ref: HY-16069) were purchased from MedChemExpress. Erlotinib (EGFR inhibitor; ref: S7786), cisplatin (ref: S1166), and paclitaxel (ref: S1150) were obtained from Selleckchem. Camptothecin (ref: C9911) and doxorubicin (ref: D1515) were purchased from Sigma-Aldrich. Cisplatin was resuspended in water and the other inhibitors in DMSO.

### ***Proliferation assay***

To determine the half-maximal inhibitory concentration (IC<sub>50</sub>) of the PRMT5 inhibitor on the eleven breast cell lines, cells were seeded in 96 well plates and then treated after 48 hours with 0.05% DMSO or 1 μM maximal concentration of EPZ015938 followed by two-fold serial dilutions. Cell proliferation was then assessed using MTT (M2128-1G, Sigma-Aldrich, St. Louis, MO, USA), WST-1 (11644807001, Sigma-Aldrich), or CellTiterGlo (G7572, Promega, Madison, WI, USA) after four doubling times (3-7 days depending on the cell line) (**Table S1**).

For combination analyses, four TNBC cell lines (BT20, MDA-MB-231, MDA-MB-453, and MDA-MB-468) were seeded in 96-well plates and treated with 0.05% DMSO or varying concentrations of inhibitors, either on their own or in combination. For combinations, the two inhibitors were added simultaneously. Cell proliferation was measured after four doubling times by MTT or CellTiterGlo assays (**Table S1**). Inhibitors were used at a maximal concentration of ~2xIC<sub>50</sub> (or 5 μM if the cell line was resistant to the inhibitor) (**Tables S2 and S3**), followed by two-fold serial dilutions. Drug interactions were assessed using the Loewe model and calculated on the Combenefit software [599]. The combination index (CI) was calculated using the formula  $CI = \frac{Cax}{ICax} + \frac{Cbx}{ICbx}$ , where Cax and Cbx are the concentrations of drugs A and B that produce an effect “x” (such as 50% cell death), and ICax and ICbx are the concentrations of drugs A and B that yield the same effect “x” when used alone [600]. CI = 1 indicates additivity, CI > 1 indicates antagonism and CI < 1 indicates synergism. Combination experiments were done in triplicates, and a minimum of three independent experiments were performed.

### ***Colony formation assay***

For colony formation assay (CFA), two TNBC cell lines were seeded at low density in 6-well plates and treated 24 hours later with vehicle or one single concentration of each drug alone or in combination and incubated until colonies formed (~9 days for MDA-MB-468 and ~12 days for BT20). For combinations, the two inhibitors were added simultaneously. As a vehicle, 0.05% DMSO was used for all the combinations except when cisplatin was examined (0.05% DMSO + H<sub>2</sub>O). Different doses of inhibitors (cisplatin, EPZ015938, erlotinib, neratinib) were first tested on these cell lines, and



concentrations that decreased colony number to a maximum of 50% were chosen. The colonies were then fixed and stained with 0.05% Coomassie Brilliant Blue in 50% methanol and 10% acetic acid solution for 20 minutes then rinsed with ultrapure water. Colonies were imaged using the ChemiDoc MP imager (Bio-rad Laboratories, Hercules, CA, USA) and quantified by ImageJ 1.43u software [601].

### ***Western Blotting***

Western blotting was performed as previously described [602] with few modifications. The cells were lysed in Laemmli buffer containing 50 mmol/L Tris pH 6.8, 2% sodium dodecyl sulfate (SDS), 5% glycerol, 2 mmol/L 1,4-dithio-dl-threitol (DTT), 2.5 mmol/L ethylenediaminetetraacetic acid (EDTA), 2.5 mmol/L ethylene glycol tetraacetic acid (EGTA), 2 mmol/L sodium orthovanadate, and 10 mmol/L sodium fluoride (Sigma-Aldrich), a cocktail of protease (Roche) and phosphatase (Thermo Scientific) inhibitors, and then boiled at 100°C for 10 minute. The protein concentration in each sample was determined with the reducing agent-compatible version of the BCA Protein Assay kit (Thermo Scientific, 23227). Equal amounts of total protein (20 µg) were fractionated by SDS-PAGE under reducing conditions (4%-12% TGX gels, Bio-Rad, Marnes la Coquette, France) and blotted onto nitrocellulose membranes (Bio-Rad). The membranes were blocked with 5% BSA in TBS containing 0.1% Tween 20 (TBS-T) and hybridized with anti-PRMT5 (Cell Signaling Technology #79998) or anti-actin (Sigma-Aldrich #A5441) antibodies overnight at 4°C. Membranes were washed in TBS-T and then hybridized with the secondary antibody for 1 hour at room temperature. Antibodies were diluted in TBS-T containing 5% BSA. The membranes were washed with TBS-T, and immune complexes were revealed by enhanced chemiluminescence (SuperSignal West Pico Chemiluminescent Substrate, Thermo Scientific) and imaged using a ChemiDoc™ XRS+ System (Bio-Rad Laboratories, Inc.).

### ***Transcriptomic microarray***

Total RNA was purified with miRNeasy kit from Qiagen (Qiagen, Courtaboeuf, France) according to the supplier recommendations. A quality control of total RNA was carried out with a Nanodrop ND1000 spectrophotometer (Thermo Fisher) to monitor the concentration and purity of samples, and integrity of total RNA was controlled using

RNA6000 Lab-on-a-chip with a Bioanalyzer (Agilent technologies) as described [603]. Samples were then hybridized with the GeneChip Human Exon 1.0 ST arrays (Affymetrix) following the manufacturer's instructions. Data quality control was performed using Affymetrix Expression Console. The data were analyzed as described elsewhere [603].

### ***Statistical Analysis***

GraphPad Prism 8.4.3 was used for statistical analysis. Data are presented as mean  $\pm$  standard deviation (SD) and p-values were calculated using the Student t-test.  $P < 0.05$  was considered statistically significant.

## Results

### *Breast cancer cell lines show distinct sensitivity to PRMT5 inhibition*

We treated ten breast cancer cell lines from the different breast cancer subgroups (six TNBC, two HER2-positive, and two luminal) and one non-cancerous breast cell line with nanomolar concentrations (3.9 nM – 1000 nM) of EPZ015938 (**Table S2**). To take into account the well-established TNBC inter-tumoral heterogeneity [68,69], cell lines representing different TNBC subtypes were tested (**Table S2**). Among the TNBC cell lines, HCC38 cells were the most sensitive ( $IC_{50} = 21.9 \text{ nM} \pm 8.7 \text{ nM}$ ) to PRMT5 inhibition, followed by MDA-MB-453 ( $IC_{50} = 109.4 \text{ nM} \pm 13.4 \text{ nM}$ ) and MDA-MB-468 ( $IC_{50} = 319.3 \text{ nM} \pm 226.2 \text{ nM}$ ) cells (**Figure 1, Table S2**). The three other TNBC cell lines (BT20, HCC70, and MDA-MB-231) were resistant to PRMT5 inhibition as the treatment did not permit the calculation of an  $IC_{50}$  (**Figure 1, Table S2**). EPZ015938 also impaired the proliferation of the two luminal cell lines T47D ( $IC_{50} = 303.9 \text{ nM} \pm 244.8 \text{ nM}$ ) and MCF-7 ( $IC_{50} = 191.5 \text{ nM} \pm 47 \text{ nM}$ ) (**Figure 1, Table S2**). Out of the two HER2-positive cell lines, HCC1954 ( $IC_{50} = 54.2 \text{ nM} \pm 19.4 \text{ nM}$ ) was more sensitive to PRMT5 inhibition than BT474 ( $IC_{50} = 625.5 \text{ nM} \pm 217.6 \text{ nM}$ ) (**Figure 1, Table S2**). Importantly, EPZ015938 was less effective in inhibiting the proliferation of the non-cancerous cell line MCF10A ( $IC_{50} = 722.8 \text{ nM} \pm 122 \text{ nM}$ ) compared to the sensitive breast cancer cell lines (**Figure 1, Table S2**). These results show that the cells respond differently to PRMT5 inhibition, and this is independent of the PRMT5 expression level (**Figure S1**).

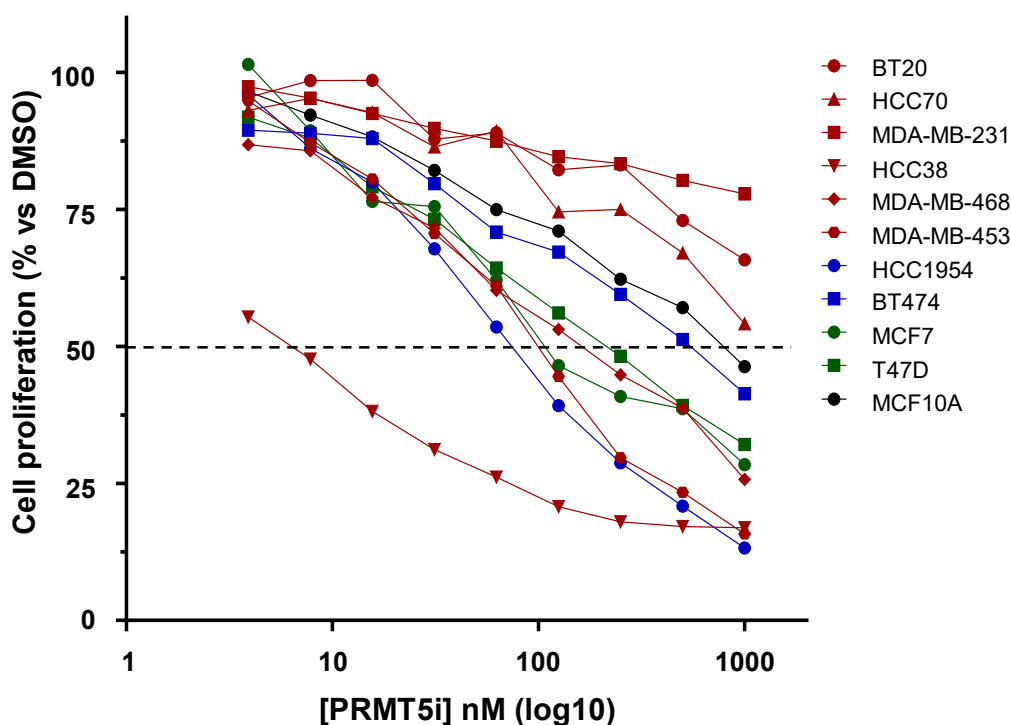


**Figure 1: Evaluation of the sensitivity of various breast cell lines to PRMT5 inhibition (EPZ015938).** Six TNBC (red), two HER2-positive (blue), two luminal (green) breast cancer cell lines, and one non-tumorigenic breast cell line (black) were treated with nanomolar doses (3.9 nM – 1000 nM) of EPZ015938 (PRMT5i). Cell proliferation was determined after four mitotic cycles. The percentage of viable cells was normalized to DMSO-treated cells. The mean of at least three independent experiments is presented for each cell line (error bars are not shown to better visualize the different cell lines but  $IC_{50} \pm SD$  are indicated in Table S2).

***PRMT5 inhibition synergizes with cisplatin, doxorubicin, and camptothecin, but not with paclitaxel, to impair TNBC cell proliferation***

Drug combinations have gained increasing interest as a means to overcome resistance, increase treatment efficacy, and reduce relapse, all representing concerns in TNBC management. Therefore, we tested the antiproliferative effects of inhibiting PRMT5 in combination with different chemotherapies used in the clinics to treat TNBC patients [589]. The drug combinations were assessed in four TNBC cell lines: two sensitive (MDA-MB-453 and MDA-MB-468) and two resistant (BT20 and MDA-MB-231) to PRMT5 inhibition with EPZ015938 (**Figure 1, Table S2**). Cells were treated with varying concentrations of both drugs starting with a dose corresponding to  $\sim 2 \times IC_{50}$  for sensitive

cells and to 5  $\mu$ M for resistant cells, then viability was quantified after four mitotic cycles. To assess the nature of drug interactions (synergy, additivity, antagonism), we employed the widely used Loewe additivity model which assumes there is no interaction when a compound is combined with itself [604,605].

PRMT5 inhibition acted synergistically with cisplatin to inhibit the proliferation of BT20, MDA-MB-453 and MDA-MB-468 (**Figure 2A**) cells; additivity was observed in MDA-MB-231 cells (**Figure S2**). The highest synergy scores ( $>30$ ) and lowest CI values were obtained in BT20 and MDA-MB-468 cells, and importantly, at doses lower than the  $IC_{50}$  for both PRMT5 inhibitor and cisplatin in MDA-MB-468 cells. Remarkably, synergy was observed at low doses (125-250 nM) of EPZ015938 in BT20 cells (**Figure 2A**), a cell line resistant to PRMT5 inhibition alone (**Figure 1**). Next, we examined whether the EPZ015938 plus cisplatin combination affected the ability of TNBC cell lines to form colonies. At the tested doses, the EPZ015938 plus cisplatin combination decreased the colony number by  $63.7\% \pm 1.9\%$  in BT20 (**Figure 2B**) and  $77.8\% \pm 3.9\%$  in MDA-MB-468 (**Figure 2C**) cells. This reduction is more pronounced compared to cisplatin alone in BT20 ( $20.4\% \pm 2.7\%$ ) and in MDA-MB-468 ( $35.4\% \pm 2.1\%$ ) or compared to EPZ015938 alone in BT20 ( $46.7\% \pm 2.9\%$ ) and in MDA-MB-468 ( $45.6\% \pm 8.8\%$ ) cells (**Figure 2B-C**). These results suggest that targeting TNBC with PRMT5 inhibitors in combination with cisplatin may offer a promising therapeutic option by using lower doses of each drug, hence potentially lowering toxicity in patients.

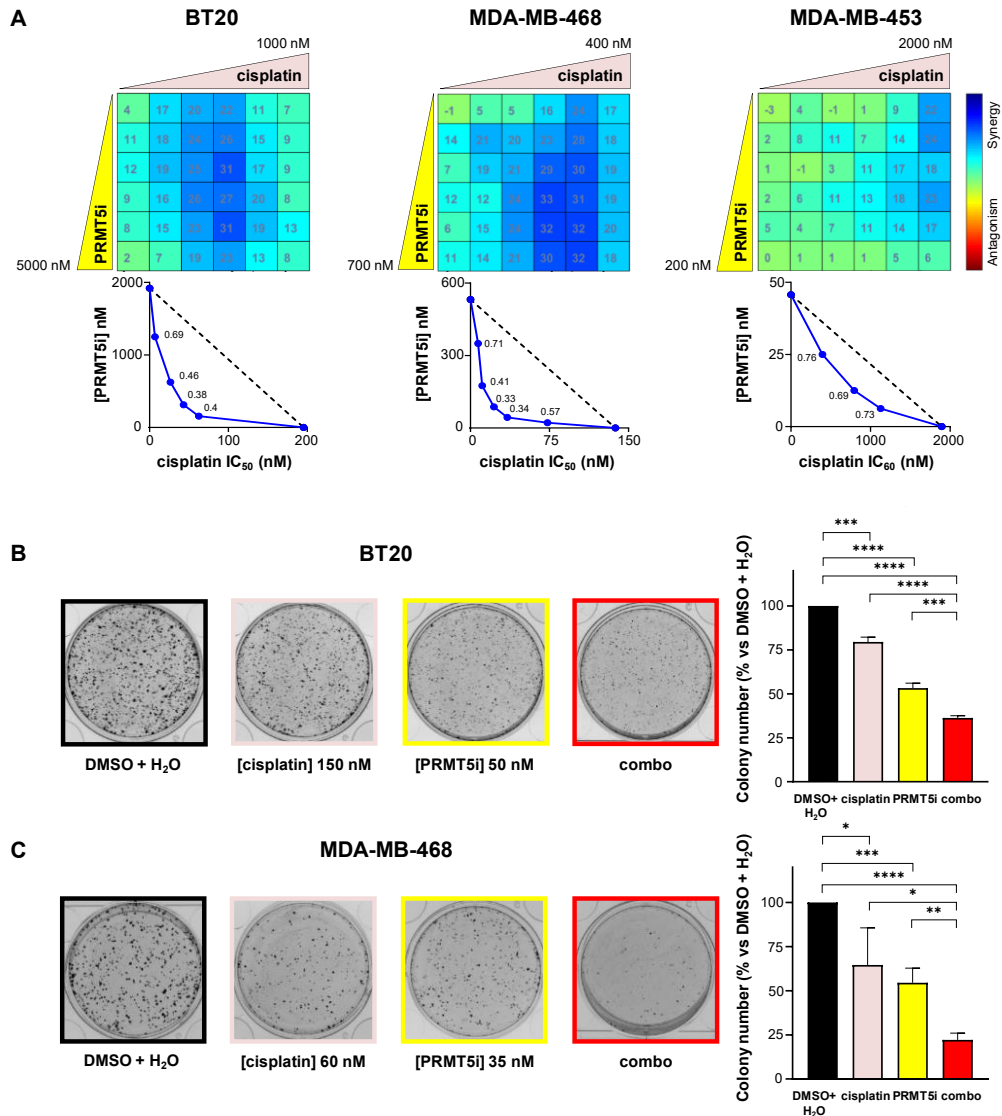


**Figure 2: Effect of the inhibition of PRMT5 in combination with cisplatin on the proliferation (A) and colony formation (B, C) of TNBC cell lines.** (A) BT20, MDA-MB-468, and MDA-MB-453 TNBC cells were seeded in 96-well plates and treated with varying concentrations of EPZ015938 (PRMT5i) and/or cisplatin, then cell proliferation was measured after four mitotic cycles (7 days). The percentage of viable cells was normalized to (DMSO + H<sub>2</sub>O)-treated cells. Each drug was used at a maximal concentration of 2xIC<sub>50</sub> for sensitive cell lines (5 μM maximum for resistant cells), followed by two-fold serial dilutions. The nature of drug interaction between EPZ015938 and cisplatin was assessed using the Loewe model on the Combenefit software. The synergy matrix (upper panel) and isobologram (bottom panel) for each cell line are shown. Isobolograms represent the IC<sub>50</sub> (BT20, MDA-MB-468) or IC<sub>60</sub> (MDA-MB-453) of cisplatin (X-axis) obtained at various EPZ015938 concentrations (Y-axis). CI were calculated at the different EPZ015938 concentrations used and are shown on the isobolograms. Data are representative of at least three independent experiments. (B, C) BT20 (B) and MDA-MB-468 (C) cells were seeded at low densities and then treated with DMSO + H<sub>2</sub>O, EPZ015938 (PRMT5i), cisplatin, or a combination (combo) of the two drugs. The colony number was quantified using ImageJ software. An image for each condition is shown and is representative of three independent experiments. Quantification of colony number is expressed as a percentage relative to (DMSO + H<sub>2</sub>O)-treated cells and represented as the mean ± SD from at least three independent experiments (right panels). P values were calculated using a student t-test and presented as: \*p<0.05, \*\*p<0.01, \*\*\*p<0.001, \*\*\*\*p<0.0001.

Moreover, we found that doxorubicin synergized with PRMT5 inhibition to impair cell proliferation in BT20 and MDA-MB-453 cell lines (**Figure 3A**); additivity was observed in MDA-MB-468 (**Figure 3A**) cells and weak antagonism in MDA-MB-231 cells (**Figure S2**). Camptothecin synergized with PRMT5 inhibition in BT20 and MDA-MB-468 cell lines (**Figure 3B**); additivity was observed in MDA-MB-453 (Figure 3B) and weak antagonism in MDA-MB-231 (**Figure S2**). The paclitaxel/EPZ015938 combination had an additive effect on all the tested cell lines except on MDA-MB-453 cells in which the drug combination exhibited antagonism (**Figure S2; Figure S3**). These results showed that a particular drug combination could show synergy, additivity, or antagonism depending on the TNBC cell line.

Taken together, analyzing the effects on cell viability of PRMT5 inhibition combined with different clinically relevant chemotherapies to treat TNBC patients revealed that (i) there is a heterogeneity of response to a particular combination between TNBC cell lines, (ii) the most effective synergistic interaction was obtained with cisplatin, and (iii) the response of a cell line to a particular combination is independent of its sensitivity to PRMT5 inhibitor when used alone.

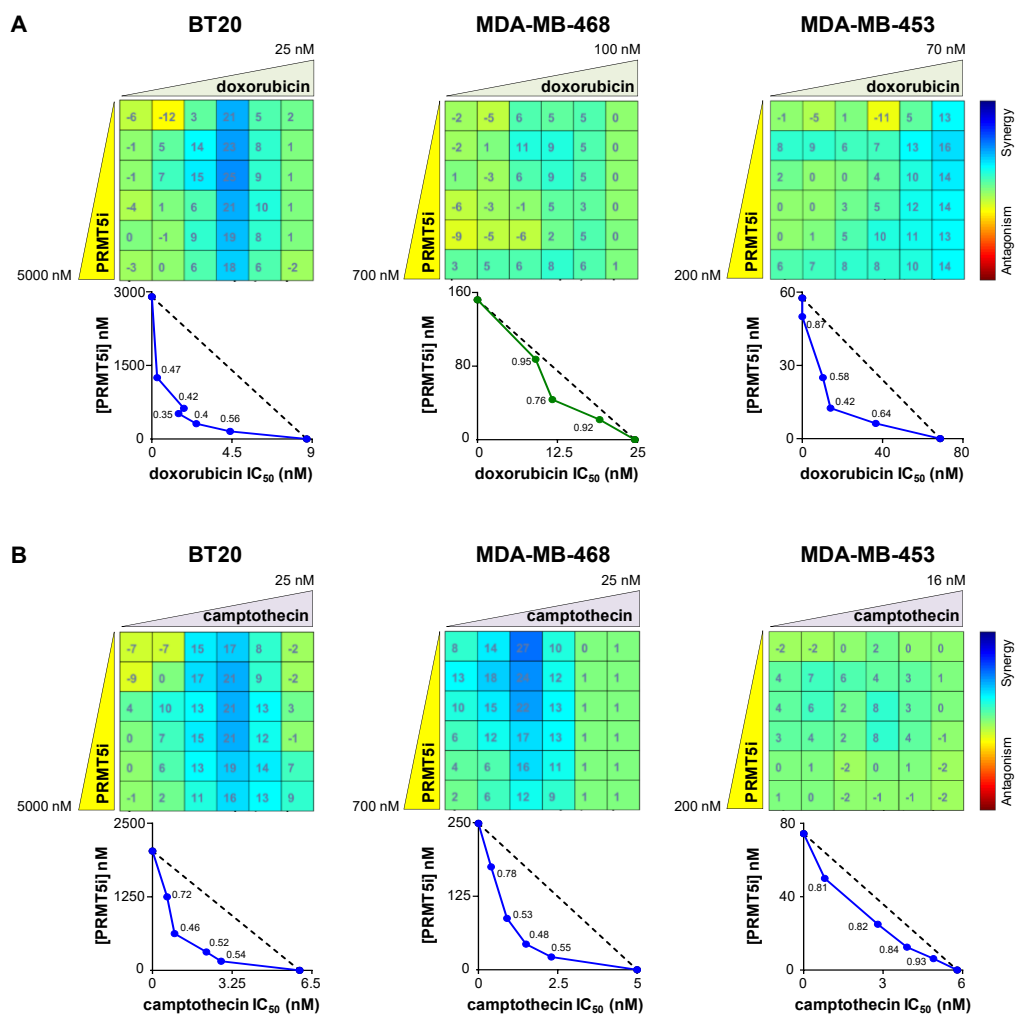


**Figure 3: Effect of the inhibition of PRMT5 in combination with doxorubicin (A) or camptothecin (B) on TNBC cell proliferation.** BT20, MDA-MB-468, and MDA-MB-453 TNBC cells were seeded in 96-well plates and treated with varying concentrations of EPZ015938 (PRMT5i) and/or doxorubicin (A) or camptothecin (B), then cell proliferation was measured after four mitotic cycles (7 days). The percentage of viable cells was normalized to DMSO-treated cells. Each drug was used at a maximal concentration of  $2 \times IC_{50}$  for sensitive cell lines ( $5 \mu M$  maximum for resistant cells), followed by two-fold serial dilutions. The nature of drug interaction between EPZ015938 and doxorubicin (A) or camptothecin (B) was assessed using the Loewe model on the Combenefit software. The synergy matrix (upper panel) and isobologram (bottom panel) for each cell line are shown. Isobolograms represent the  $IC_{50}$  of doxorubicin (A) or camptothecin (B) (X-axis) obtained at various EPZ015938 concentrations (Y-axis). CI were calculated at the different EPZ015938 concentrations used and are shown on the isobolograms. Data are representative of at least three independent experiments.



***PRMT5 inhibition synergizes with inhibitors targeting HER family members to impair the proliferation of TNBC cells***

As more than half of TNBC tumours overexpress EGFR and approximately a third of TNBC are classified as HER2-low breast cancers, we tested the combination between EPZ015938 and FDA-approved inhibitors that target different HER family members (EGFR/HER1, HER2, and HER4). We performed the analyses in the same four TNBC cell lines used for the combination with chemotherapies. Among them, MDA-MB-468 and BT20 express high levels of EGFR (**Figure S4**). MDA-MB-453 expresses AR as well as higher levels of HER2 (with no *HER2* amplification) compared to other TNBC cell lines [606] (**Figure S4**) and could be considered as a HER2-low breast cancer cell line.

Erlotinib synergized with EPZ015938 in the two EGFR-high expressing cell lines, BT20 and MDA-MB-468, to impair their proliferation (**Figure 4A**). BT20 cells were the most responsive to the combination with synergistic scores reaching 36 (**Figure 4A**). This combination was additive in MDA-MB-453 cells (**Figure 4A**) and varied between additivity or weak antagonism in MDA-MB-231 cells (**Figure S2**). The erlotinib/EPZ015938 combination also significantly decreased the ability of BT20 and MDA-MB-468 cells to form colonies by  $62.2\% \pm 3.7\%$  and  $69.4\% \pm 13.4\%$ , respectively (**Figure 4B-C**), compared to an  $8.7\% \pm 0.2\%$  (BT20) and  $25.1\% \pm 6.7\%$  (MDA-MB-468) reduction caused by erlotinib treatment alone and a  $49.9\% \pm 3.2\%$  (BT20) and  $40.5\% \pm 9.7\%$  (MDA-MB-468) reduction by EPZ015938 treatment alone (**Figure 4B-C**).

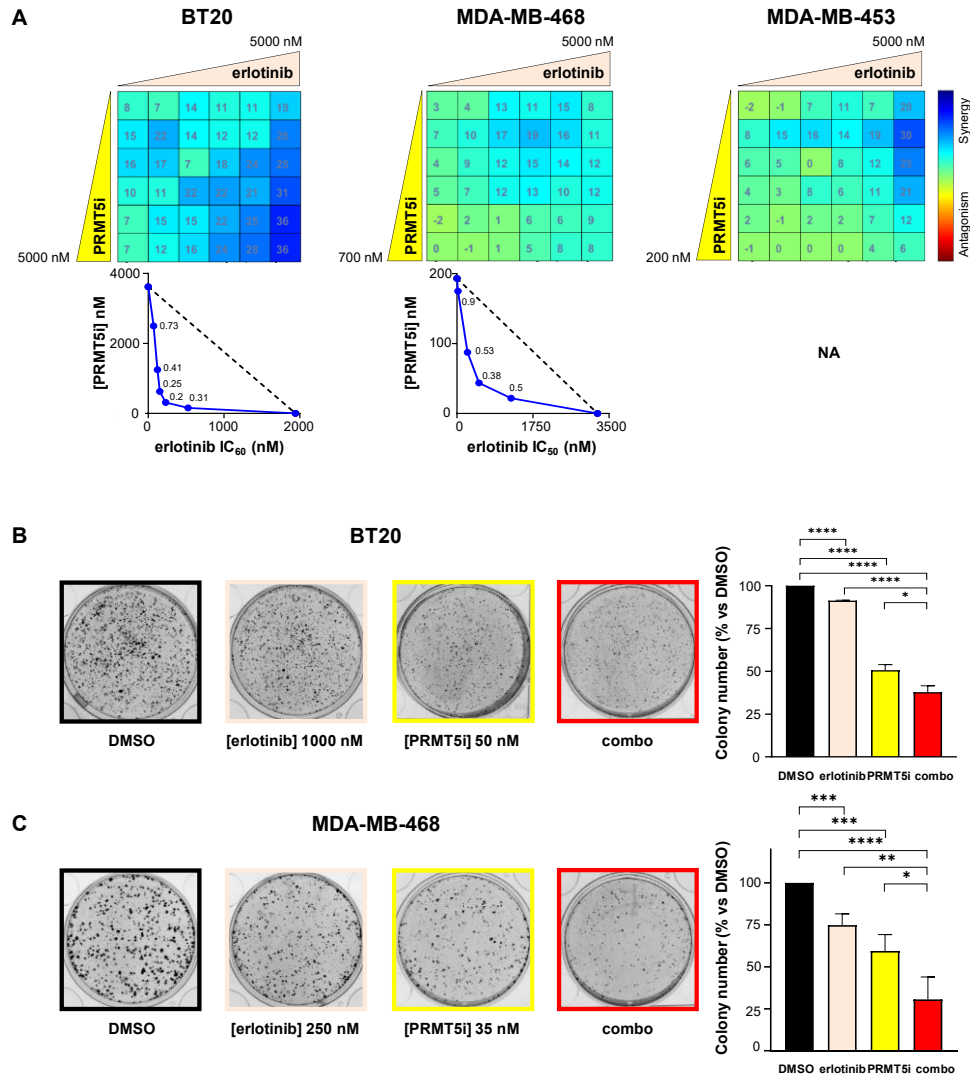


**Figure 4: Effect of PRMT5i/erlotinib combination on the proliferation (A) and colony formation (B, C) of TNBC cell lines.** (A) BT20, MDA-MB-453, and MDA-MB-468 cells were seeded in 96-well plates and treated with varying concentrations of EPZ015938 (PRMT5i) and/or erlotinib, then cell proliferation was measured after four mitotic cycles (7 days). The percentage of viable cells was normalized to DMSO-treated cells. Cells were treated with a 5  $\mu$ M maximal concentration of erlotinib, and EPZ015938 was used at a maximal concentration of 2xIC<sub>50</sub> for sensitive cell lines (5  $\mu$ M for resistant cells). Both drugs were then two-fold serially diluted. The nature of drug interaction between EPZ015938 and erlotinib was assessed using the Loewe model on the Combenefit software. The synergy matrix (upper panel) and isobologram (bottom panel) for each cell line are shown. Isobolograms represent the IC<sub>50</sub> of erlotinib (X-axis) obtained at various EPZ015938 concentrations (Y-axis). CI were calculated at the different EPZ015938 concentrations used and are shown on the isobolograms. Isobologram for MDA-MB-453 cells (A) was not plotted as erlotinib alone did not impair cell viability by more than 20% and is indicated as NA (not applicable). Data are representative of at least three independent experiments. (B, C) BT20 (B) and MDA-MB-468 (C) cells were seeded at low densities and then treated with DMSO, EPZ015938 (PRMT5i), erlotinib, or a combination (combo) of the two inhibitors. Colonies were quantified using ImageJ software. An image for each condition is shown and is representative of three independent experiments (left panel). Quantification of colony number is expressed as a percentage relative to DMSO-treated cells and represented as mean  $\pm$  SD of three independent experiments (right panel). P values were calculated using a student t-test and presented as: \*p<0.05, \*\*p<0.01, \*\*\*p<0.001, \*\*\*\*p<0.0001.

Neratinib synergized with EPZ015938 to impair the proliferation of both MDA-MB-468 and BT20 cells (**Figure 5**) expressing high EGFR levels (**Figure S4**) and in MDA-MB-453 cells (**Figure 5**) which express HER2 (**Figure S4**). The highest synergistic scores (> 30) were observed at low PRMT5 doses (~ 25-50 nM) in MDA-MB-453 cells (**Figure 5**). Of note, the highest synergistic scores in BT20 cells were obtained at the lowest concentrations of both neratinib (120 nM) and PRMT5 inhibitor (150 nM) (**Figure 5**). Compared to the drugs used alone, the neratinib/EPZ015938 combination did not further reduce the colony number in BT20 (**Figure S5**). Although not significant, this combination tended to decrease colony formation in MDA-MB-468 cells compared to EPZ015938 alone (**Figure S5**).

We then tested the combination between EPZ015938 and tucatinib or neratinib on the HER2-positive breast cancer cell line HCC1954 and found synergistic interactions between EPZ015938 and both inhibitors (**Figure 5**). The tucatinib/EPZ015938 combination also yielded a synergistic effect in reducing MDA-MB-453 cell proliferation (**Figure 5**).

Altogether, our data highlight the potential of targeting PRMT5 in combination with inhibitors targeting the HER family members in EGFR-high TNBC, HER2-low breast cancer (LAR-TNBC), and HER2-positive breast cancer.

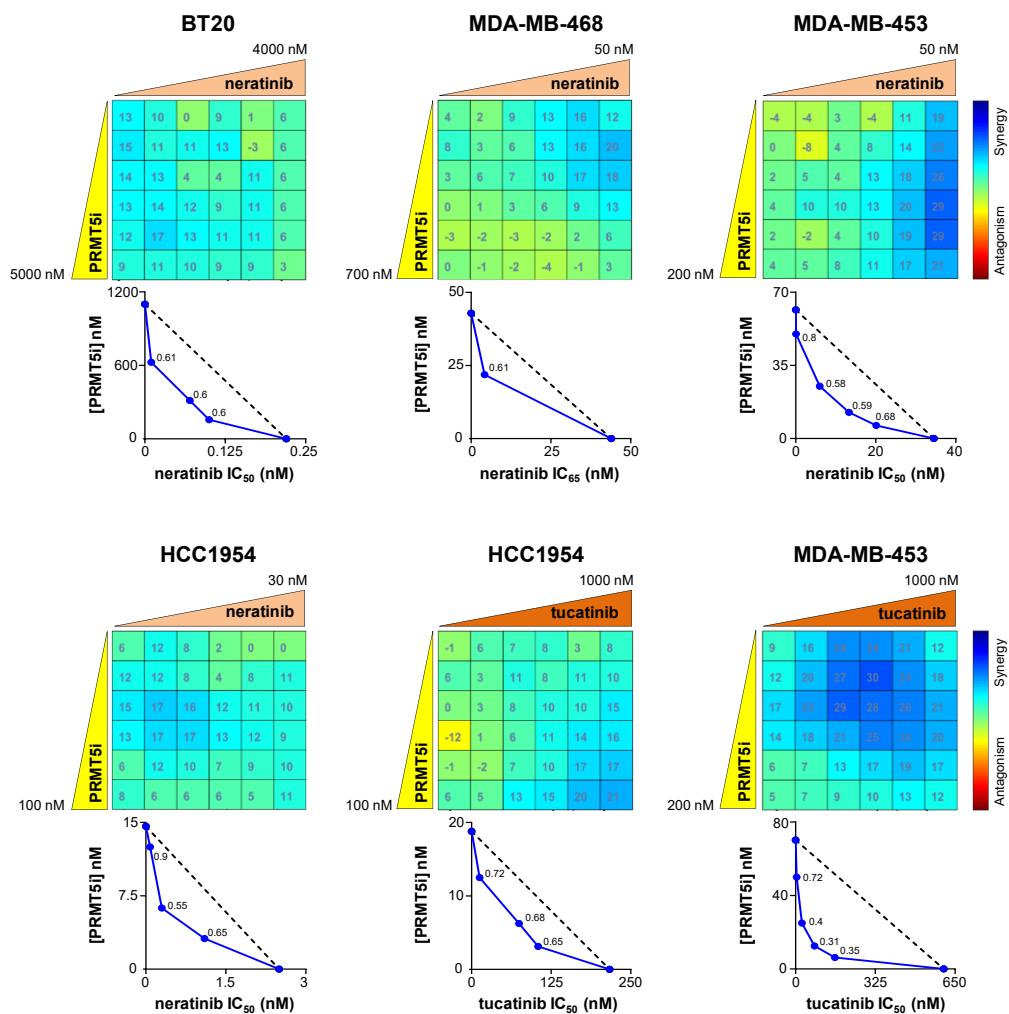


**Figure 5. Effect of PRMT5/neratinib and PRMT5/tucatinib combinations on the proliferation of TNBC and HER2-positive breast cancer cell lines.** BT20, MDA-MB-468, MDA-MB-453, and HCC1954 cells were seeded in 96-well plates and treated with varying concentrations of EPZ015938 (PRMT5i) and/or neratinib or tucatinib as indicated, then cell proliferation was measured after four mitotic cycles (7 days). The percentage of viable cells was normalized to DMSO-treated cells. Each drug was used at a maximal concentration of  $2 \times IC_{50}$  for sensitive cell lines (5  $\mu$ M maximum for resistant cells), followed by two-fold serial dilutions. The nature of drug interaction between EPZ015938 and neratinib or tucatinib was assessed using the Loewe model on the Combenefit software. The synergy matrix (upper panel) and isobologram (bottom panel) for each cell line are shown. Isobolograms represent the  $IC_{50}$  (BT20, MDA-MB-453, and HCC1954) or  $IC_{65}$  (MDA-MB-468) of neratinib or the  $IC_{50}$  of tucatinib (X-axis) obtained at various EPZ015938 concentrations (Y-axis). CI were calculated at the different EPZ015938 concentrations used and are shown on the isobolograms. Data are representative of at least three independent experiments.

## Discussion

TNBC is the most aggressive breast cancer subgroup associated with a high relapse rate and metastatic potential. Although a few targeted therapies have recently been approved for subsets of TNBC patients [78,79,590,591], chemotherapies remain the main treatment option for these patients [10,584]. Due to their high expression in several cancer types, PRMTs have emerged as attractive therapeutic targets and PRMT inhibitors have been developed [115]. More specifically, different PRMT5 inhibitors have been characterized and several are currently under evaluation in phase I clinical trials [478]. High levels of PRMT5 are associated with poor prognosis in TNBC [429,430,473] and PRMT5 inhibition impairs tumour growth in a TNBC PDX model [430] and xenograft models derived from TNBC cell lines [422,473]. TNBC patients may therefore benefit from a treatment targeting PRMT5.

As expected, similar to EPZ015666 [430], we found a heterogeneity of response to EPZ015938 in breast cancer cell lines (**Table S2**). Importantly, the cell lines that were sensitive to EPZ015938 were also sensitive to EPZ015666, but with a ~10-fold lower IC<sub>50</sub> (**Table S2**). Among the six TNBC cell lines examined, only the two BL1-TNBC (HCC38 and MDA-MB-468) and the LAR-TNBC (MDA-MB-453) cell lines were sensitive to both EPZ015938 and EPZ015666 (**Table S2**). To generalize whether BL1- and LAR-TNBC subtypes are the most sensitive to PRMT5 inhibition remains to be examined by analysing additional TNBC cell lines. Previous studies also found that MDA-MB-468, MDA-MB-453, MCF7, and T47D cells were sensitive to EPZ015938, whereas HCC70 (BL2-TNBC), MDA-MB-231 (M-TNBC), BT549 (M-TNBC), Hs578T (M-TNBC) and MCF10A cells were resistant [236,416]. The heterogeneity of response to EPZ015938 is not restricted to breast cancer cell lines but to cell lines of different cancer types [410]. The variable sensitivity of breast cancer cell lines to PRMT5 inhibition was also highlighted using GSK3203591 (later called GSK591) [287], another PRMT5 inhibitor also optimized from EPZ015666 [410]. Understanding the reasons why some cell lines are sensitive and others resistant to PRMT5 inhibition would help to identify biomarkers of response, which then could aid in stratifying patients who could benefit from a treatment targeting PRMT5.

In this study, we assessed in four TNBC cell lines (two sensitive and two resistant to EPZ015938) whether there is a benefit of combining EPZ015938 with different chemotherapies currently given in the clinic to treat TNBC patients. We observed a heterogeneous response to the different combinations among the cell lines. Synergy was observed with the EPZ015938/doxorubicin combination in BT20 and MDA-MB-453 cells, and with the EPZ015938/camptothecin combination in BT20 and MDA-MB-468 cells. Our results show that synergy can be observed in the BT20 cell line which is resistant to EPZ015938. In contrast, we did not find synergy when the PRMT5 inhibitor was combined with paclitaxel. Nevertheless, a previous study has reported a synergistic interaction between EPZ015666 and paclitaxel in MDA-MB-231 cells [494].

The most striking result was observed when EPZ015938 was combined with cisplatin, with synergy seen in three out of the four TNBC cell lines. The highest synergy scores (>30) were reached in BT20 (resistant to EPZ015938) and in MDA-MB-468 (sensitive to EPZ015938) cells, importantly, at low doses of the drugs. Being resistant to PRMT5 inhibition alone does not predict that a cell line will not respond to the combination treatment. Our findings are in agreement with a study reporting that PRMT5 inhibition (EPZ015938) sensitizes breast cancer cells to cisplatin, even in BT549 cells that were resistant to PRMT5 inhibition alone [236]. Altogether, these results imply that therapeutic strategies combining PRMT5 inhibition with cisplatin could be useful for a larger number of TNBC patients, regardless of their response to PRMT5 inhibition used as a monotherapy. Combining cisplatin and a PRMT5 inhibitor, at low doses, may reduce toxicity and achieve better clinical outcomes. Cisplatin also sensitizes TNBC [234] and ovarian cancer [303] cells to PRMT1 inhibitors. In the ovarian cancer study, it was shown that cisplatin treatment induces DNA-PK-dependent phosphorylation of PRMT1, leading to the methylation of histone H4 and the activation of genes involved in the senescence-associated secretory phenotype (SASP), protecting cells from apoptosis [303]. Whether a similar PRMT1-dependent mechanism occurs in cisplatin-treated TNBC cells has not yet been reported. Moreover, whether cisplatin induces the expression of SASP genes in a PRMT5-dependent manner remains to be explored.

Although more than half of the TNBC patients overexpress EGFR, targeting EGFR as monotherapy in TNBC patients did not achieve the expected results [105,592]. The screening of an FDA-approved drug library permitted us to uncover a synergistic interaction between the first described PRMT5 inhibitor (EPZ015666) and erlotinib in several TNBC cell lines [430]. Here, to be more clinically relevant, we wanted to confirm these results with EPZ015938, a more drug-like PRMT5 inhibitor already being evaluated in clinical trials [478]. As expected, we found that EPZ015938 synergizes with erlotinib in the two TNBC cell lines expressing high levels of EGFR (MDA-MB-468 and BT20). We further show that inhibiting PRMT5 activity sensitizes these two cell lines to erlotinib to reduce their ability to form colonies. Next, we wanted to strengthen these findings by assessing the combination between EPZ015938 and neratinib, an EGFR/HER2/HER4 inhibitor. We found that EPZ015938 also acts in synergy with neratinib in BT20 and MDA-MB-468 cell lines. Importantly, synergy with both neratinib and erlotinib was observed at low doses of EPZ015938, avoiding potential undesirable effects. Synergy with EGFR inhibitors was observed in BT20 which are resistant to PRMT5 alone. Together, these results suggest that combining a PRMT5 inhibitor with erlotinib or neratinib could be beneficial for TNBC patients expressing high levels of EGFR and/or having an activated EGFR signalling pathway. We also reported that PRMT1 inhibition synergized with erlotinib in MDA-MB-468 cells [234]. The molecular mechanisms underlying the synergistic interaction between EGFR and PRMT inhibitors remain to be understood. Nevertheless, previous studies have reported a relationship between PRMTs and EGFR. Indeed, PRMT1 controls the expression of EGFR, and EGFR is methylated by PRMT1 and PRMT5 affecting downstream signalling pathways [226,228–231,233,234]. PRMT5 methylates and activates AKT [235,236], a downstream effector of EGFR. Moreover, AKT inhibition sensitizes breast cancer cells (luminal and TNBC) to PRMT5 inhibition [236]. AKT can be activated by different signalling pathways, not only by EGFR, which could explain the synergy observed when combining EGFR and PRMT5 inhibitors.

The evaluation in a clinical trial of an antibody-drug conjugate (ADC) targeting HER2 coupled to a topoisomerase I inhibitor (Trastuzumab-deruxtecan) revealed a therapeutic benefit not only in HER2-positive but also in HER2-low breast cancers (all breast cancer subgroups including TNBC) [36]. This ADC has recently been FDA-approved for HER2-

low breast cancer patients, independently of the expression of hormone receptors [37]. Interestingly, being HER2-low positively correlates with AR expression in TNBC and luminal breast cancer [38]. We found that EPZ015938 synergizes with neratinib and tucatinib in MDA-MB-453, a LAR-TNBC cell line, and in HCC1954, a HER2-positive breast cancer cell line. High synergistic scores were obtained at low doses of the PRMT5 inhibitor (~10-20 nM) in MDA-MB-453 cells. These results uncover for the first time the therapeutic potential of combining PRMT5 and HER2 inhibitors in HER2-low and HER2-positive breast cancers.

Combination strategies with PRMT5 inhibition appear to be promising therapeutic approaches with high translational impact. Indeed, other laboratories have also shown that PRMT5 inhibition sensitizes cancer cells to targeted therapies: anti-PDL1 in lung cancer [487], ATR inhibitor in mantle cell lymphoma (MCL) [488], CDK4/6 inhibitors in MCL [488] and melanoma [489], EZH2 inhibitor in colorectal cancer [490], type I PRMT inhibitors in pancreatic cancer [607] and in acute myeloid leukemia (AML) [127], mTOR inhibitor in glioblastoma [491], spliceosome inhibitor in AML [127], TGF- $\beta$  inhibitor in pancreatic cancer [492], ULK1 inhibitor in M-TNBC cell lines [416], and PARP inhibitors in ovarian and breast cancer [493]. In addition, PRMT5 inhibition in combination with gemcitabine leads to synthetic lethality in pancreatic cancer [608].

## **Conclusion**

Our study highlights the benefit of targeting PRMT5 in combination with some chemotherapies and with inhibitors targeting the HER family members. The most promising combinations with PRMT5 inhibition were obtained with (i) cisplatin in TNBC cells, (ii) EGFR inhibition in EGFR-high TNBC cells, and (iii) HER2 inhibition in HER2-low breast cancer (MDA-MB-453) and in HER2-positive breast cancer cells. In future studies, we will further evaluate the combination of inhibitors targeting PRMT5 with HER family members in additional cell lines, to strengthen our findings. These studies may identify EGFR and HER2 as biomarkers of response to these drug combinations, aiding in the stratification of patients who will most likely respond to the treatment. To translate these *in vitro* results to preclinical studies, we will assess the therapeutic advantage of the most



promising combinations on tumour growth in various TNBC PDX models, chosen based on the expression of the appropriate biomarker of response.

## **Abbreviations**

ADC, antibody-drug conjugate; AML, acute myeloid leukemia; AR, androgen receptor; BCSC, breast cancer stem cells; BL1, basal-like 1; BL2, basal-like 2; CFA, colony formation assay; EGFR, epidermal growth factor receptor; ER, estrogen receptor; FDA, Food and Drug Administration; HER2, human epidermal growth factor receptor 2; IC<sub>50</sub>, half-maximal inhibitory concentration; IHC, immunohistochemistry; LAR, luminal androgen receptor; M, mesenchymal; MCL, mantle cell lymphoma; PARP, poly (ADP-ribose) polymerase; PDX, patient-derived xenograft; PR, progesterone receptor; PRMT, protein arginine methyltransferase; SASP, senescence-associated secretory phenotype; SD, standard deviation; TIC, tumour-initiating cells; TNBC, Triple-negative breast cancer.

## **Disclosure**

The author reports no conflicts of interest in this work.

## **Consent for publication**

All authors read and approved the final manuscript.

## **Funding**

This work was supported by the Institut Curie. S.S. was funded by the European Union's Horizon 2020 Research and Innovation Program (Marie Skłodowska-Curie grant agreement No 666003). R.D. was financed by the French Embassy of Lebanon and the Lebanese University (Safar Volet 1).

## **Competing interests**

The authors declare that they have no competing interests.

## **Authors' contributions**

All authors made a significant contribution to the work reported, whether that is in the conception, study design, execution, acquisition of data, analysis and interpretation, or in all these areas; took part in drafting, revising or critically reviewing the article; gave final

approval of the version to be published; have agreed on the journal to which the article has been submitted; and agree to be accountable for all aspects of the work.

## **Acknowledgments**

We thank Dylan Payet (BCBG lab, Institut Curie) for performing some experiments and Dr. David Gentien (Genomics platform, Institut Curie) for performing the microarrays on the cell lines. We are grateful to Virginie Maire (BCBG, Institut Curie) and Dr. Ramón García-Areas (BCBG, Institut Curie) for critical reading of the manuscript. We also thank Dr. Lisa McPherson (Division of Oncology, Stanford University School of Medicine, USA) for verifying the English language of the manuscript.

## Supplementary information

**Table S1: Doubling time of the breast cell lines, and the assays used to measure proliferation**

<b>Cell line</b>	<b>Doubling Time (hours)</b>	<b>Treatment duration (days)</b>	<b>Proliferation assay</b>
MCF10A	16	3	MTT
T47D	43	7	MTT
MCF7	45	7	MTT
HCC1954	40	7	MTT
BT474	40	7	MTT
HCC38	60	7	WST-1
MDA-MB-453	55	7	MTT
MDA-MB-468	45	7	MTT
BT20	50	7	MTT
HCC70	50	7	MTT
MDA-MB-231	25	4	CTG

CTG: CellTiter-Glo luminescent cell viability assay; MTT: 3-(4,5-dimethylthiazol-2-yl)-2,5 diphenyltetrazolium bromide-based assay; WST-1: water-soluble tetrazolium salt based assay.

**Table S2: Sensitivity of breast cell lines to EPZ015938 and EPZ015666**

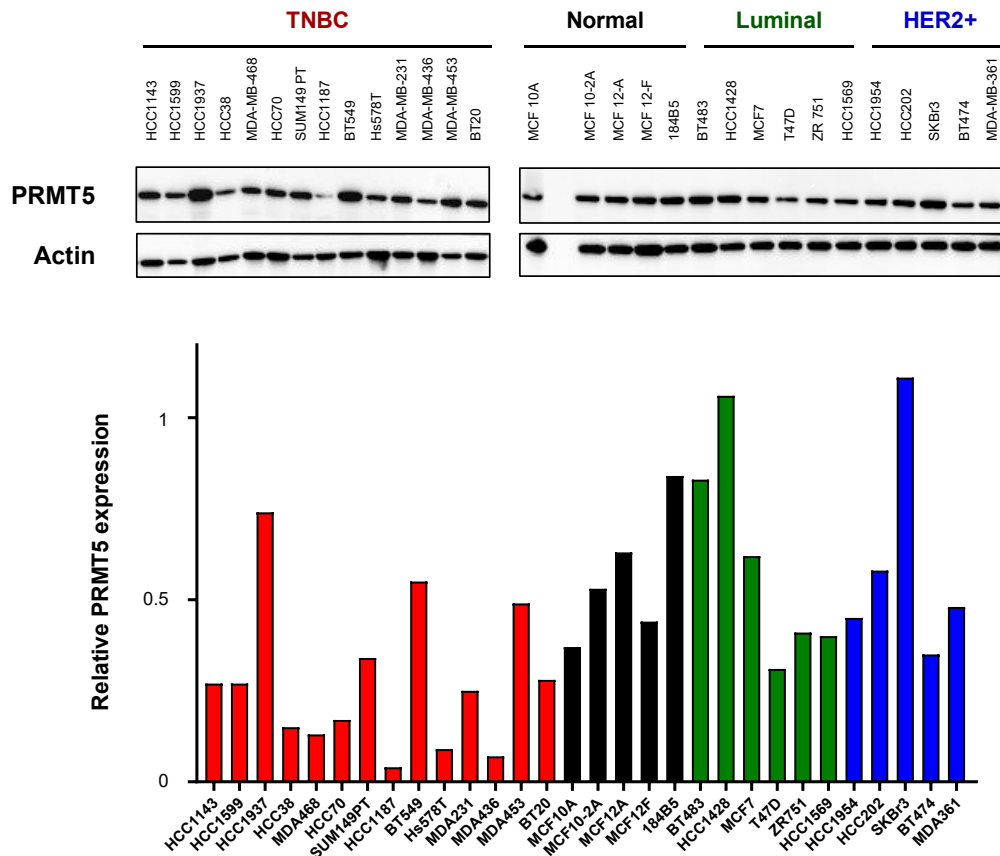
Cell line	Classification	EPZ015938 IC <sub>50</sub> (nM ± SD) This study	EPZ015666 IC <sub>50</sub> (nM ± SD) From Ref. [430]
MCF10A	Normal epithelial	722.8 ± 122	42684 ± 14200
MCF12A	Normal epithelial	ND	47078 ± 11200
T47D	Luminal	304 ± 244.8	ND
MCF7	Luminal	191.5 ± 47	2642 ± 1010
HCC1954	HER2-positive	54.2 ± 19.4	812 ± 140
SKBr3	HER2-positive	ND	3939 ± 1930
BT474	HER2-positive	625.5 ± 217.6	ND
HCC38	TNBC (BL1)	21.9 ± 8.7	2770 ± 1430
MDA-MB-453	TNBC (LAR)	109.4 ± 13.4	985 ± 256
MDA-MB-468	TNBC (BL1)	319.3 ± 226.2	2224 ± 909
BT20	TNBC (unclassified)	>1000	12316 ± 7800
HCC70	TNBC (BL2)	>1000	29852 ± 5650
MDA-MB-231	TNBC (M)	>1000	ND
MDA-MB-157	TNBC (M)	ND	33365 ± 1729
Hs578T	TNBC (M)	ND	67847 ± 17600

BL1: basal-like 1; BL2: basal-like 2; IC<sub>50</sub>: half-maximal inhibitory concentration; LAR: luminal androgen receptor; M: mesenchymal; ND: not determined; SD: Standard deviation; TNBC: Triple-negative breast cancer.

**Table S3: IC<sub>50</sub> of the inhibitors used in the study**

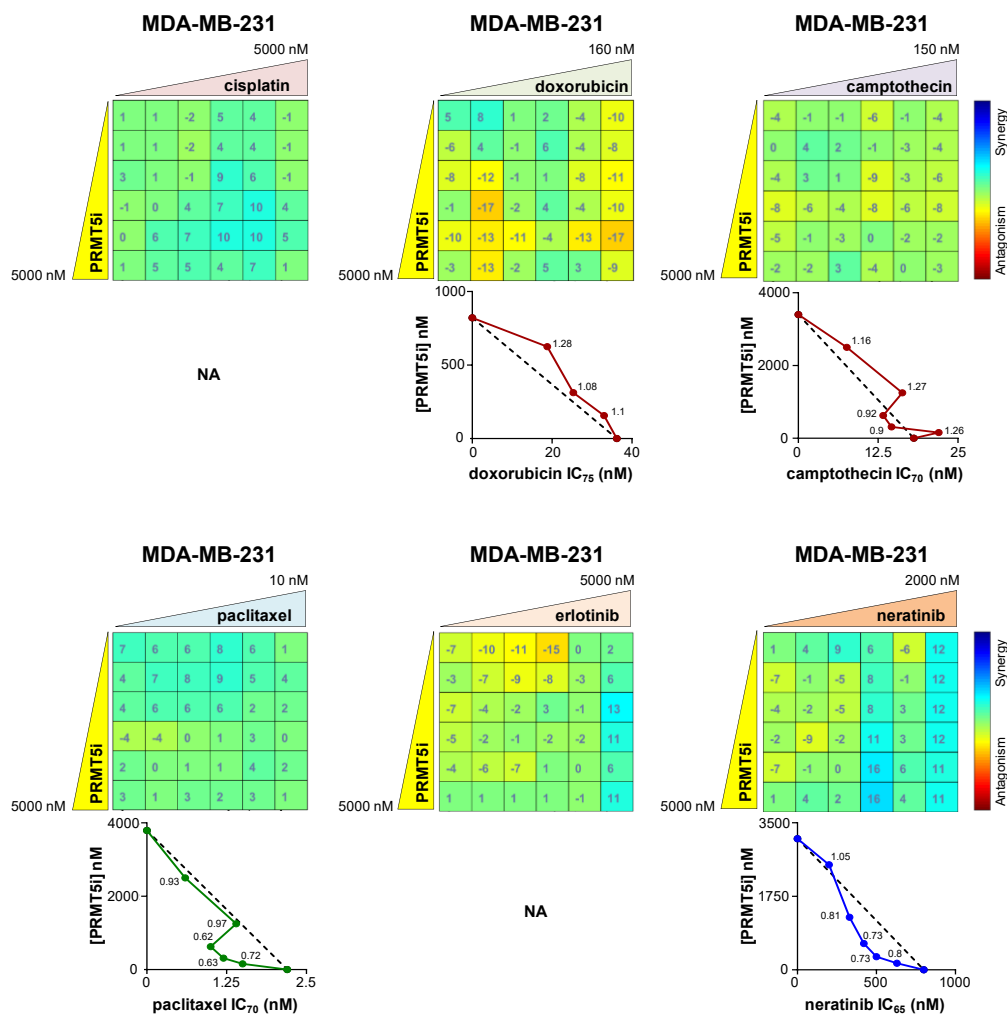
	IC <sub>50</sub> (nM ± SD)				
	BT20	MDA-MB-231	MDA-MB-468	MDA-MB-453	HCC1954
Neratinib	1502 ± 519	918.3 ± 478	30.9 ± 14	22.6 ± 10	14.2 ± 1.8
Tucatinib	>5000	ND	>5000	431.2 ± 162	508.6 ± 61
Erlotinib	2379 ± 911	>5000	1950 ± 490	>5000	ND
Cisplatin	155.7 ± 56.5	>5000	133.8 ± 49.5	949.1 ± 340	ND
Camptothecin	6.2 ± 2.1	53.8 ± 15	7.7 ± 2.9	6.9 ± 0.4	ND
Paclitaxel	1.39 ± 0.5	5.8 ± 3	5.4 ± 0.4	1.05 ± 0.2	ND
Doxorubicin	7.08 ± 1.2	0.07 ± 0.03	19.9 ± 6.7	0.04 ± 0.01	ND

IC<sub>50</sub>: half-maximal inhibitory concentration; ND: not determined; SD: Standard deviation.

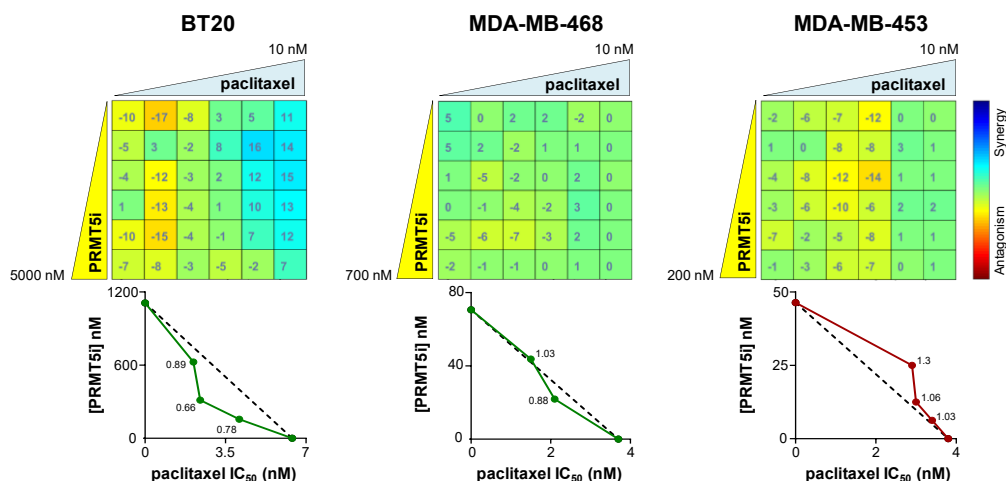


**Supplementary figure 1. PRMT5 expression in breast cell lines.** PRMT5 expression was assessed in breast cancer cells of the different subtypes (TNBC, luminal, HER2-positive) and normal breast cell lines

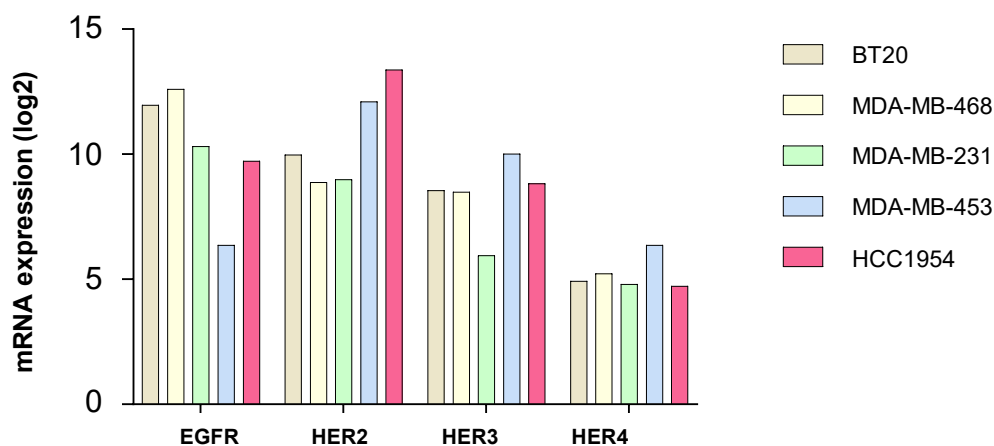
by western blotting. Actin was used as a loading control. The graphs represent the relative amount of PRMT5 normalized to actin. Noteworthy, the levels of actin may vary across the different cell lines.



**Supplementary figure 2. Effect of the inhibition of PRMT5 in combination with chemotherapies, erlotinib and neratinib on MDA-MB-231 cell proliferation.** MDA-MB-231 TNBC cells were seeded in 96-well plates and treated with varying concentrations of EPZ015938 (PRMT5i) and/or cisplatin, doxorubicin, camptothecin, paclitaxel, erlotinib, or neratinib, then cell proliferation was measured after four mitotic cycles (4 days). Percentage of viable cells was normalized to DMSO or DMSO + H<sub>2</sub>O (when cisplatin was used)-treated cells. Each drug was used at a maximal concentration of 2xIC<sub>50</sub> or 5  $\mu$ M maximum when MDA-MB-231 are resistant to the inhibitor, followed by two-fold serial dilutions. The nature of drug interaction between EPZ015938 and the different inhibitors was assessed using the Loewe model on the Combobenefit software. The synergy matrix (upper panel) and isobologram (bottom panel) for each combination are shown. The isobolograms represent the IC<sub>60</sub> of neratinib, IC<sub>70</sub> of paclitaxel and camptothecin or IC<sub>75</sub> of doxorubicin (X-axis) obtained at various EPZ015938 concentrations (Y-axis). CI were calculated at the different EPZ015938 concentrations used and are shown on the isobolograms. Isobolograms of the combination between EPZ015938 and cisplatin or erlotinib could not be plotted as the treatment with cisplatin or erlotinib alone did not impair cell viability more than 20% and are indicated as NA (not applicable). Data are representative of at least three independent experiments.

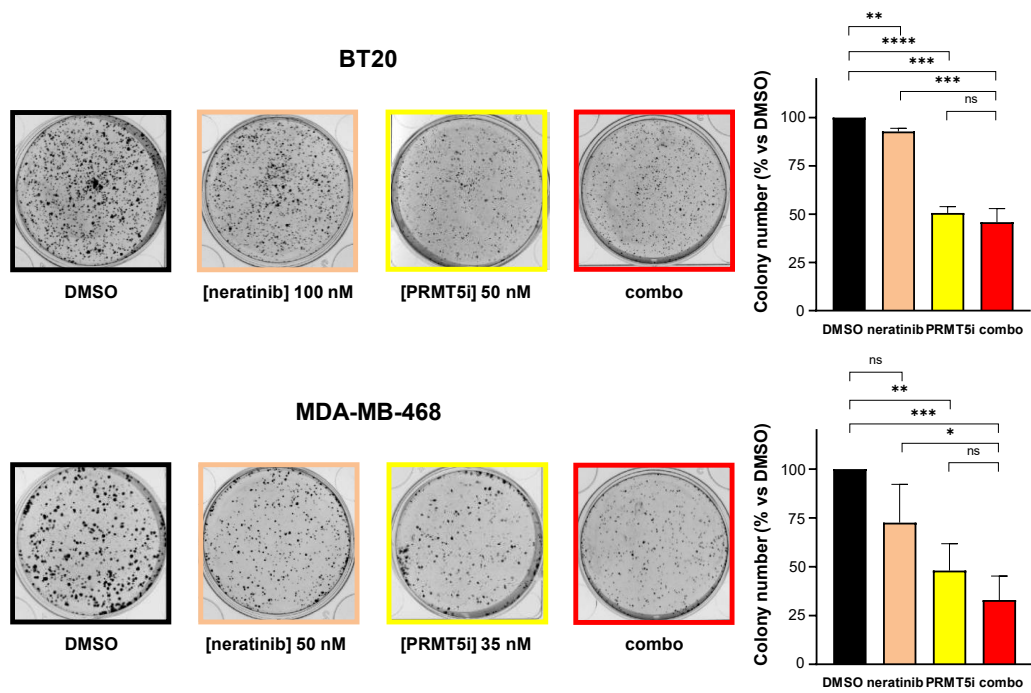


**Supplementary figure 3. Effect of the inhibition of PRMT5 in combination with paclitaxel on TNBC cell proliferation.** BT20, MDA-MB-468, and MDA-MB-453 TNBC cells were seeded in 96-well plates and treated with varying concentrations of EPZ015938 (PRMT5i) and/or paclitaxel, then cell proliferation was measured after four mitotic cycles (7 days). Percentage of viable cells was normalized to DMSO-treated cells. Each drug was used at a maximal concentration of  $2 \times IC_{50}$  for sensitive cell lines (5  $\mu$ M maximum for resistant cells), followed by two-fold serial dilutions. The nature of drug interaction between EPZ015938 and paclitaxel was assessed using the Loewe model on the Combenefit software. The synergy matrix (upper panel) and isobologram (bottom panel) for each cell line are shown. The isobolograms represent the  $IC_{50}$  of paclitaxel (X-axis) obtained at various EPZ015938 concentrations (Y-axis). CI calculated at the different EPZ015938 concentrations used are shown on the isobolograms. CI were calculated at the different EPZ015938 concentrations used and are shown on the isobolograms. Data are representative of at least three independent experiments.



**Supplementary figure 4. mRNA expression of the four HER family members in breast cancer cell lines.** mRNA expression (log<sub>2</sub> transformed) of EGFR, HER2, HER3 and HER4 in BT20, MDA-MB-468, MDA-MB-231, MDA-MB-453, and HCC1954 cells.





**Supplementary figure 5. Effect of the inhibition of PRMT5 in combination with neratinib on TNBC cell colony formation.** BT20 and MDA-MB-468 cells were seeded at low densities then treated with DMSO, EPZ015938 (PRMT5i), neratinib, or a combination (combo) of the two inhibitors. Colonies were quantified using ImageJ software. An image for each condition is shown and is representative of three independent experiments (left panel). Quantification of colony number is expressed as a percentage relative to DMSO-treated cells and represented as a mean  $\pm$  SD of three independent experiments (right panel). P values were calculated using student t-test and presented as: \* $p < 0.05$ , \*\* $p < 0.01$ , \*\*\* $p < 0.001$ , \*\*\*\* $p < 0.0001$ , ns: not significant.

## Chapter 2: Part 2

# Unveiling the PRMT5 interactome through immunoprecipitation and TurboID proximity labelling in TNBC

Rayan Dakroub <sup>1,2</sup>, Mathilde Vinet <sup>1</sup>, Yara Hajj-Younes <sup>1</sup>, Virginie Maire <sup>1</sup>, Florent Dingli <sup>3</sup>, Loew Damarys <sup>3</sup>, Bassam Badran <sup>2</sup>, Hussein Fayyad-Kazan <sup>2</sup>, Thierry Dubois <sup>1, \*</sup>

<sup>1</sup> Breast Cancer Biology Group, Translational Research Department, Institute Curie-PSL Research University, 75005 Paris, France

<sup>2</sup> Laboratory of Cancer Biology and Molecular Immunology, Faculty of Sciences-I, Lebanese University, Hadat 1003, Lebanon

<sup>3</sup> Mass-spectrometry platform, Institute Curie-PSL Research University, Institute Curie-PSL Research University, 75005 Paris, France

\* Correspondence: [thierry.dubois@curie.fr](mailto:thierry.dubois@curie.fr); Tel.: +33 156246250

## Abstract

TNBC is an aggressive tumour known for its high heterogeneity, treatment resistance, elevated recurrence rates, and poor prognosis. We previously found that high *PRMT5* mRNA levels are associated with poor prognosis in TNBC. Moreover, using a specific inhibitor targeting PRMT5, we observed reduced viability in TNBC cells and delayed tumour growth in a TNBC PDX model. In this study, we aimed to characterize the PRMT5 interactome in TNBC through two distinct approaches. First, we conducted immunoprecipitation of endogenous PRMT5 or its co-factor MEP50 from TNBC cell lysates. This enabled us to identify FUBP1, a protein involved in transcription and pre-mRNA splicing, as a partner of the PRMT5/MEP50 complex. We additionally demonstrated that PRMT5 methylates FUBP1, thereby promoting its binding to the FUSE element of the *MYC* promoter. Second, we employed a proximity labelling technique (TurboID) that uncovered numerous potential new interactors of PRMT5, primarily implicated in protein transport, cell division, and endocytosis. Among these, SDCCAG3 that has established roles in cytokinesis and receptor trafficking emerged as a key PRMT5 interactor. Further validation confirmed the interaction between PRMT5 and SDCCAG3, both of which we showed to interact with the Wnt pathway receptor LRP6. Notably, depleting SDCCAG3 led to decreased expression of specific Wnt target genes in the TNBC cell line MDA-MB-468. However, the precise involvement of SDCCAG3 and PRMT5 in LRP6 trafficking or regulation has yet to be demonstrated. Additional research is necessary to establish a clearer understanding of the functional association between PRMT5 and SDCCAG3.

**Keywords:** TNBC, PRMT5, MEP50, protein-protein interaction, arginine methylation, FUBP1, SDCCAG3

## Introduction

Post-translational modifications (PTM) play a significant role in modulating protein functions and could contribute to oncogenesis [609]. Among these modifications, arginine methylation is a prevalent PTM catalysed by protein arginine methyltransferases (PRMT), the expression of which is dysregulated in diverse cancers [115]. PRMT5 is the main type II PRMT catalysing symmetric arginine dimethylation (SDMA). Operating in tandem with its cofactor MEP50, PRMT5 forms a hetero-octameric complex that augments its activity [122]. This PRMT5/MEP50 complex engages in multiple cellular processes including transcription, pre-mRNA splicing, DNA repair, signal transduction, ribosome biogenesis and translation, cell proliferation, and the maintenance of stem cells [188]. Demonstrating oncogenic properties, PRMT5 exhibits heightened expression in various cancers, notably in breast cancer [194,610,611]. High PRMT5 expression is associated with poor prognosis in breast cancer patients, and its inhibition or depletion has shown to reduce breast cancer cells proliferation, migration, and stemness properties [420,422,429,430,468–470].

Breast cancer, the leading cause of cancer related mortalities in females worldwide [1], is classified into distinct molecular subtypes according to the expression of estrogen receptor (ER), progesterone receptor (PR), and human epidermal growth receptor (HER2). Luminal breast cancers express ER and PR; HER2-positive tumours carry an amplification of the *HER2* gene; and triple-negative breast cancers (TNBC) do not express ER and PR and have no *HER2* gene amplification [10,584]. TNBC is the most aggressive subtype of breast cancer and continues to be treated primarily with chemotherapies. In previous studies, we reported a correlation between elevated *PRMT5* mRNA levels and poor prognosis in TNBC [429,430]. Additionally, we demonstrated the therapeutic potential of targeting PRMT5 in TNBC, showing that its inhibition impaired the growth of some TNBC cell lines and tumour growth in a TNBC patient-derived xenograft (PDX) model [430].

This study aims to better understand the oncogenic functions of the PRMT5/MEP50 complex in TNBC by characterizing its interactome. Through immunoprecipitation (IP) of endogenous MEP50 from the TNBC cell line HCC38 coupled to liquid chromatography with tandem mass spectrometry (LC-MS/MS) analysis, we uncovered a novel MEP50 partner: the far upstream element binding protein 1 (FUBP1), a

transcription factor that activates the oncogene *MYC* expression [499]. Our findings further revealed that PRMT5 methylates FUBP1, enhancing the interaction between FUBP1 and the FUSE element located upstream of the *MYC* promoter. Considering the limited efficacy of commercial antibodies in immunoprecipitating PRMT5, we opted for TurboID proximity labelling [612] followed by LC-MS/MS analysis to unveil the PRMT5 interactome. This approach led to the identification of novel PRMT5 interactors, enriched in proteins associated with protein transport, cell division, and endocytosis, cellular pathways not previously linked to PRMT5. Notably, our study identified SDCCAG3, a protein involved in cytokinesis and receptor trafficking, as a PRMT5 interactor and confirmed their interaction by conducting co-IP experiments in HEK293T cells. Further investigation is necessary to understand the functional consequences of the interaction between PRMT5 and SDCCAG3.

## **Materials and Methods**

### ***Cell Culture, transfection, and siRNA treatment***

All cell lines were purchased from the American Type Culture Collection (ATCC, LGC Promochem), authenticated by short tandem repeat profiling in 2021, and tested for mycoplasma by the MycoAlert Mycoplasma Detection Kit (Lonza Biosciences, Durham, NC, USA). MDA-MB-468 cells were cultured in RPMI-1640 GlutaMAX™ (LifeTechnologies) supplemented with 10% (vol/vol) foetal bovine serum (FBS, LifeTechnologies), 100 U/mL penicillin, and 100 µg/mL streptomycin (P/S, LifeTechnologies). HCC38 cells were cultured in RPMI-1640 GlutaMAX™ supplemented with 10% (vol/vol) FBS, 100 U/mL P/S, 1.5 g/L sodium bicarbonate (LifeTechnologies), 10 mmol/L HEPES (LifeTechnologies), and 1 mmol/L sodium pyruvate (LifeTechnologies). HEK293T and Hela cells were cultured in DMEM GlutaMAX™ (LifeTechnologies) supplemented with 10% FBS and 1% P/S. All cell lines were maintained at 37°C with 5% CO<sub>2</sub>. For overexpression assays, DNA vectors were transfected into cells using Xtremegene-HP (Sigma) according to the manufacturer's instructions. For knock down experiments, 20 nM siRNA were transfected into cells using INTERFERin (Polyplus, 101000016) following the manufacturer's guidelines.

### ***Human samples and transcriptome microarray***

The Curie cohort has been previously described [234,429,430]. Transcriptome microarray (U133 Plus 2.0 Affymetrix chips, Thermo Fisher Scientific, Waltham, MA, USA) was performed on TNBC (n = 41), HER2 (n = 30), luminal A (n = 29), luminal B (n = 30), and normal breast tissue from plastic surgery (n = 11) as previously described [234,429,430]. Experiments were conducted in accordance with Bioethics Law No. 2004–800 and the Ethics Charter from the French National Institute of Cancer (INCa), and after approval from the ethics committee of our Institution. The RNA-SeqV2 Level 3 data (Jan 2015) were downloaded from the publicly available TCGA breast invasive carcinoma (TCGA-BRCA) cohort (<http://cancergenome.nih.gov/>) [33] and integrated into a platform in knowledge data integration (KDI) at Institut Curie (<https://bioinfo-portal.curie.fr>). TCGA-BRCA included TNBC (n = 106), HER2 (n = 36), luminal A (n = 415), and luminal B (n = 118). The TCGA database includes 113 referenced normal breast tissue samples.

### *Immunoprecipitation*

All immunoprecipitations were performed at 4°C. Cells were washed once with cold 1X PBS and scraped with IP lysis buffer (50 mM Tris-HCl pH 7.4, 100 mM NaCl, 1 mM EDTA, 1 mM EGTA, and freshly supplemented with 0.1% NP-40, 1mM DTT, 10% glycerol, and protease inhibitor cocktail). Cells were lysed by rotation (40 rpm) for 30 minutes then centrifuged at maximum speed for 15 minutes to remove cell debris. Total proteins were then quantified using the Pierce™ BCA Protein Assay Kit (ThermoFisher, 23227), and the lysates were diluted to obtain a final amount of 1mg proteins per IP reaction. 2 µg antibodies (**Table S1**) were added per IP reaction, and the samples were then incubated with rotation (40 rpm) for two hours or overnight in the cold room. 20µl protein G agarose beads (ThermoFisher, 20399) were added per IP and incubated with rotation (40 rpm) for 1 hour in the cold room. The beads were then washed three times and proteins were eluted using laemmli 1X sample buffer and analysed by immunoblotting. For IP of ectopic proteins, HEK293T cells were harvested 48 hours following transfection, and proteins were immunoprecipitated as before.

### *Immunoblotting*

Cells were lysed in laemmli 1X (50 mM Tris pH=6.8, 2% SDS, 5% glycerol, 2mM DTT, 2.5 mM EDTA, 2.5mM EGTA and freshly supplemented with 4 mM Sodium Orthovanadate, 20 mM Sodium Fluoride and protease inhibitor cocktail). Protein concentration was determined using the Pierce™ BCA Protein Assay Kit (ThermoFisher, 23227) then 10µg proteins were loaded on 4–15% Mini-PROTEAN® TGX™ precast gels (Biorad) and transferred to Trans-Blot Turbo 0.2 µm nitrocellulose membrane (Biorad). Membranes were blocked using 5% BSA in 1X TBS and 0.1% Tween-20 (TBST) for 1 hour at room temperature then incubated with the appropriate primary antibody (**Table S1**) at 4°C overnight. Membranes were washed three times 5 minutes each, followed by incubation with the secondary antibody for 1 hour at room temperature. Membranes were washed three times then revealed using the SuperSignal West Pico PLUS Chemiluminescent Substrate (ThermoFisher, 34580) and imaged using the ChemiDoc MP system (Biorad).

## ***Plasmids***

pcDNA 3.1-Flag-PRMT5 and pcDNA 3.1-Flag-PRMT4 were synthesized by GENEWIZ. pcDNA 3.1 Flag-PRMT3 (Plasmid #164695) and pcDNA 3.1-Flag-PRMT6 (Plasmid #164697) were purchased from Addgene. pcDNA 3.1-V5-PRMT5 was a gift from Dr Muriel Le Romancer, Centre de Recherche en Cancérologie de Lyon. pcDNA 3.1-Flag-FUBP1 was a kind gift from Dr Marie-Bérengrère Troadec, Institut de Génétique et Développement de Rennes. pFastBac-Flag-PRMT5 and pFastBac-His-MEP50 were received from Dr Karl Syson, AstraZeneca, Cambridge. pcDNA-GFP-SDCCAG3 was a kind gift from Dr Kai S Erdmann, University of Sheffield. pcDNA 3.1-Flag-TurboID-PRMT5 was generated by inserting TurboID sequence in pcDNA 3.1-Flag-PRMT5, and pcDNA 3.1-Flag-PRMT1 was generated by replacing PRMT5 by PRMT1 in the pcDNA 3.1-Flag-PRMT5 vector using NEBuilder HiFi DNA Assembly Cloning Kit (New England BioLabs, E5520). pcDNA 3.1-Flag-TurboID-PRMT5 was mutated using the QuikChange Lightning Site-Directed Mutagenesis Kit (Agilent, 210518) to insert a stop codon after TurboID to translate only Flag-TurboID for use as a negative control in biotin pulldown experiments. pcDNA 3.1-Flag-FUBP1 R359,361,363K (FUBP1 3K) was generated by mutating the coding sequence of R359, R361, and R363 to substitute with lysine residues in pcDNA 3.1-Flag-FUBP1 using the QuikChange Lightning Site-Directed Mutagenesis Kit. FUBP1 KH1-4 and FUBP1 KH3-4 were PCR amplified either from wild type or mutated pcDNA 3.1-Flag-FUBP1 and inserted into pET28 b+ plasmid by HindIII and XhoI digestion to generate pET28 His-FUBP1 KH1-KH4, pET28 His-FUBP1 KH1-KH4 3K, pET28 His-FUBP1 KH3-KH4, and pET28 His-FUBP1 KH3-KH4 3K for protein purification. pcDNA 3.1 LRP6-Flag was generated using Gibson assembly. All plasmids, whether received, purchased, or cloned, were verified by sequencing with Eurofins genomics, France. Cloning and mutagenesis primers are listed in **Table S2**.

## ***Recombinant protein expression and purification***

FUBP1 KH domains (wild type and mutated) were transformed in BL21(DE3) competent *E. coli* (New England BioLabs, C25271). Transformed BL21 bacteria were induced with 0.5 mM IPTG for 14 hours at 20°C then harvested by centrifugation at 2000 rpm for 30 minutes at 4°C. All purification steps were done at 4°C. Cells were resuspended in lysis buffer (50 mM Tris pH 8, 1% Triton, 500mM NaCl, 5% glycerol, 10 mM imidazole, 1 µg/ml Leupeptin, 1 µg/ml Aprotinin, 1 mM PMSF, and protease



inhibitor cocktail) and incubated for 30 minutes at 4°C then further lysed by sonication. Crude lysates were centrifuged for 30 minutes at 4°C and the supernatant was collected and transferred to a new tube. His tagged proteins were purified using Nickel beads (Ni-NTA Agarose, Qiagen, 30210) and eluted using 50 mM Tris pH 8, 150 mM NaCl and 300 mM imidazole. Purified proteins were dialysed using dialysis cassette (ThermoFisher) in 20 mM Tris pH 8, 150 mM NaCl, 10% glycerol, and 1 mM DTT overnight then quantified using Nanodrop.

The human PRMT5/MEP50 complex was produced using the Bac-to-Bac Baculovirus expression system (ThermoFisher). pFastBac-Flag-PRMT5 and pFastBac-His-MEP50 were transformed into DH10Bac E.Coli to generate recombinant bacmids. Bacmids containing the gene of interest were then purified and transfected into Sf9 insect cells to generate a virus for each clone. Flag-PRMT5 and His-MEP50 were co-expressed by infecting Hi5 insect cells with the two baculoviruses using a 1:2 (PRMT5:MEP50) virus ratio. Cells were then harvested and resuspended in lysis buffer (50 mM Tris pH 8, 10 % glycerol, 500 mM NaCl, 10 mM MGCl<sub>2</sub>, 0.5 mM TCEP, Benzonase + PIC). The PRMT5:MEP50 complex was purified using Ni-NTA beads. The immobilized-metal affinity chromatography (IMAC) elution fractions were loaded on the superdex 200 16/600 column equilibrated in a buffer containing 20 mM Hepes pH 8, 5 % glycerol, 150 mM NaCl, 0,5 mM TCEP. The fractions were stored at -80°C.

#### ***In vitro methylation assay***

1-2 µg of recombinant FUBP1 domains were incubated with purified PRMT5/MEP50 complex (1:20 molar ratio) and 0.5 µCi SAM[<sup>3</sup>H] (PerkinElmer) in buffer containing 50 mM Tris pH 7.4, 100 mM NaCl, and 1 mM DTT at 30°C for 1 hour. The reaction was then stopped with laemmli 4X sample buffer (Biorad) and incubating the mixtures at 95°C for 5 minutes, then resolved by SDS-PAGE and transferred to PVDF membrane. The membrane was first stained with Coomassie then revealed by autoradiography after 48 hours.

#### ***Flow Induced Dispersion Analysis (FIDA)***

FIDA experiments were done using a Fida 1 machine (Fida Biosystems ApS, Copenhagen, Denmark), that employs LED detection with excitation wavelength of 480 nm. Standard capillaries (75 µm inner diameter) were coated with high sensitivity (HS) coating reagent (Fida Biosystems ApS, Copenhagen, Denmark) before use to

decrease protein adherence to the capillaries. The indicator, Alexa 488 labelled FUSE (5' **ATGTATATTCCCTCGGGATTTTTATTTTGTGTTATTCCACGGCATG** 3') (Eurofins genomics, France), was used at 10 nM fixed concentration. The analytes, FUBP1 KH1-4 and FUBP1 KH1-4 3K, were used at a maximum concentration of 2 $\mu$ M then 2-fold serially diluted with the assay buffer (PBS, 0.05% Tween 20). The indicator was mixed with the analyte and incubated for 10 minutes at 37°C to allow the domains binding to DNA before proceeding to the Fida measurements. First, the column was washed and equilibrated with assay buffer. Then, the analyte sample was injected into the capillary, followed by the indicator sample. In the final step, the indicator was mobilized to the detector with the analyte. Tylograms are recorded at the final step. All samples are measured in triplicates, and the experiments were performed in three independent replicates. The analysis was done at 25°C, and the obtained data (tylograms) were analysed using FIDA software version 2.34 (Fida Biosystems ApS, Copenhagen, Denmark) to calculate the hydrodynamic radius (Rh) of the indicator at different analyte concentrations.

#### ***Chromatin immunoprecipitation (ChIP)***

MDA-MB-468 cells were treated with 1  $\mu$ M EPZ015938 (PRMT5 inhibitor; MedChemExpress, HY-101563) or DMSO for 48 hours. ChIP was then performed using the simple ChIP plus enzymatic chromatin IP Kit (9004, Cell signalling Technology, Danvers, MA, USA), according to the manufacturer's protocol. Briefly, 5-10  $\times$  10<sup>6</sup> cells from each condition were crosslinked with 1% PFA for 10 minutes, then glycine was added for 5 minutes followed by two washes with cold 1X PBS. Cells were then scraped with cold 1X PBS freshly supplemented with protease inhibitor cocktail (from the kit). The chromatin was digested using micrococcal nuclease (provided by the kit) followed by sonication to obtain chromatin fragments of 100-900 bp. Chromatin was immunoprecipitated using anti-FUBP1 (**Table S1**) or anti-IgG (provided by the kit) antibodies overnight, then protein G agarose beads (provided by the kit) were added to pull down the chromatin/antibody complex. After several washing steps, the DNA-protein cross links were reversed by proteinase K and the DNA was purified using spin columns provided with the kit. Lastly, qPCR was performed using the SimpleChIP® Universal qPCR Master Mix (Cell signalling technologies, #88989) on the FUSE region of the *MYC* promoter. The primers used were *MYC* -1.5 kb F: 5'

CCCACACATGATTTGTTTGC 3' and MYC -1.5 kb R: 5'  
TTTTTCATGCCGTGGAATAAC 3' obtained from a previous study [535].

### *Immunofluorescence*

Hela cells were cultured on glass coverslips and transfected with the indicated DNA. 48 hours after transfection, cells were fixed with 4% PFA for 15 minutes at room temperature, then permeabilized in PBS 0.1% Triton X-100 for 5 minutes at room temperature. After three washing steps, the coverslips were blocked using PBS 1% BSA for 30 minutes at room temperature. The primary antibodies (**Table S1**) were then added either for 1 hour at room temperature or for overnight at 4°C. After three washes, the coverslips were incubated with the appropriate secondary antibody for 1 hour at room temperature, followed by three washing steps and then with 0.1 µg/ml Dapi incubation for 5 minutes at room temperature. Three washing steps were performed before mounting the coverslips with Mowiol 4-88 (Sigma-Aldrich) solution. Images were acquired using an Upright Epifluorescence widefield microscope (Zeiss) at 40X (NA=1.3) or 63X (NA =1.4) and a CoolSnap HQ2 camera.

### *Biotin assays and biotin pulldown*

Flag-TurboID-PRMT5 and Flag-TurboID were first checked for their activity and expression. HEK293T cells were transfected with either DNA construct, then treated 48 after transfection with either 50µM or 500µM biotin (Thermofisher, B20656) for 10 or 30 minutes. After the indicated time, cells were placed on ice and washed three times with cold 1X PBS to stop the biotinylation reaction. Cells were then scraped with laemmli 1X and proteins were analysed by western blotting as previously mentioned. Anti-Flag (**Table S1**) was used to check the recombinant proteins' expression and streptavidin-HRP (Thermofisher) was used to reveal the total biotinylated proteins.

For biotin pulldown experiments, HEK293T cells were treated as mentioned above, then were scraped using RIPA buffer (25 mM Tris pH 7.4, 0.1% SDS, 0.5% DOC, 1% NP-40, 150 Mm NaCl) and lysed by rotation (40 rpm) for 30 minutes at 4°C. Total proteins were quantified using Pierce™ BCA Protein Assay Kit (Thermofisher, 23227) Before proceeding with the protein pulldown, WB analysis was done to check for the recombinant proteins expression and activity. 1 mg proteins were used per pulldown. 40 µl of chemically modified (see below for the modification method) streptavidin sepharose beads (Sigma, GE17-5113-01) were added to the samples and incubated

overnight at 4°C. The beads were then washed twice with RIPA buffer, once with KCl, then twice with RIPA buffer. Beads were then resuspended with 1 ml RIPA buffer by gentle tapping, and 100 µl were removed for WB analysis. The remaining 900 µl, for mass spectrometry analysis, were washed three times with 5M urea in 200 mM ammonium bicarbonate, then five times with 25mM ammonium bicarbonate to remove urea. Lastly, the beads were resuspended in 100 µl ammonium bicarbonate and analysed by mass spectrometry.

### ***Chemical modification of the streptavidin beads***

Streptavidin sepharose beads (Sigma, GE17-5113-01) were chemically modified to prevent the digestion of streptavidin by trypsin during mass spectrometry analysis. The protocol is adapted from [613]. Streptavidin beads were first centrifuged to remove the storage buffer then washed with PBS 0.1% Tween 20 (PBST). The beads were then resuspended in CHD solution (120 mg cyclohexanedione dissolved in 14 ml PBST pH 13) and incubated for 4 hours with rotation (40 rpm) at room temperature. Then, the beads were washed once with PBST and resuspended in PFA 4% in PBST followed by adding 0.2 M sodium cyanoborohydride in PBST. The beads were incubated for 2 hours at room temperature with rotation (40 rpm) then washed once with 0.1M Tris pH 7.5 and once with PBST. Lastly, the beads were resuspended in PBST and stored at 4°C for several months.

### ***Mass-spectrometry***

For mass-spectrometry (MS) analysis, beads were washed three times with 25 mM ammonium bicarbonate, then resuspended with 100 µl of 25 mM ammonium bicarbonate and digested with 0.2 µg of trypsin/LysC (Promega) for 1 hour at 37°C. Samples were then loaded into custom-made C18 StageTips packed by stacking one AttractSPE disk (Affinisep) and 2 mg of beads (Cartridge Waters) into a 200-µl micropipette tip for desalting. Peptides were eluted using a ratio of 40:60 MeCN:H<sub>2</sub>O + 0.1% formic acid and vacuum-concentrated to dryness. Peptides were reconstituted in injection buffer (2:98 MeCN:H<sub>2</sub>O + 0.3% trifluoroacetic acid) before liquid chromatography tandem MS (LC-MS/MS) analysis.

Online chromatography was performed with an RSLCnano system (Ultimate 3000, Thermo Scientific) coupled to an Orbitrap Exploris 480 mass spectrometer (Thermo Scientific). Peptides were trapped on a C18 column (75 µm inner diameter × 2 cm;

nanoViper Acclaim PepMap™ 100, Thermo Scientific) with buffer A (2/98 CH<sub>3</sub>CN/H<sub>2</sub>O in 0.1% formic acid) at a flow rate of 3.0 µL/min over 4 min. Separation was performed on a 50 cm x 75 µm C18 column (nanoViper Acclaim PepMap™ RSLC, 2 µm, 100Å, Thermo Scientific) regulated to a temperature of 40°C with a linear gradient of 3% to 29% buffer B (100% CH<sub>3</sub>CN in 0.1% formic acid) at a flow rate of 300 nL/min over 91 min. Full scans MS were performed in the ultrahigh-field Orbitrap mass analyzer in ranges m/z 375–1500 with a resolution of 120 000 at m/z 200.

### ***Data processing of LC-MS/MS***

For protein identification, the data were searched against the Homo sapiens (UP000005640) UniProt database using SequestHT Proteome Discoverer (version 2.4). Enzyme specificity was set to trypsin and a maximum of two missed cleavage sites were allowed. Maximum allowed mass deviation was set to 10 ppm for monoisotopic precursor ions and 0.02 Da for MS/MS peaks. The resulting files were further processed using myProMS v3.9.3 (<https://github.com/bioinfo-pf-curie/myproms>) [614]. The maximum false discovery rate (FDR) calculation was set to 1% at the peptide level (Percolator or QUALITY algorithm). Label-free quantification was performed using peptide extracted ion chromatograms (XICs) computed with MassChroQ v.2.2.21. For protein quantification, XICs from proteotypic peptides shared between compared conditions (TopN matching) with missed cleavages were used. Experiments that were not performed in replicates were analysed manually. For the experiments performed in biological replicates, median and scale normalization at peptide level were applied on the total signal to correct the XICs for each biological replicate (n=3 for MEP50 IP, and n=5 for FUBP1 IP). To estimate the significance of the change in protein abundance, a linear model (adjusted on peptides and biological replicates) was performed, and p-values were adjusted using the Benjamini-Hochberg FDR procedure. Proteins with at least three total peptides in all three independent replicates, a 2-fold (MEP50 IP) or 1.5-fold (FUBP1 IP) enrichment, and an adjusted p-value ≤ 0.05 were considered significantly enriched in sample comparisons. Unique proteins were considered with at least three total peptides in all three replicates.

### ***Real time qPCR for Wnt target genes***

MDA-MB-468 cells were transfected with siRNA then serum starved overnight and stimulated with 100 ng/mL Wnt3a conditioned media for 6 hours. RNA was then

extracted using the RNeasy Mini Kit (74106, Qiagen, Hilden, Germany) according to the manufacturer's protocol. Reverse transcription and qPCR were done in a single reaction using the QuantiTect SYBR Green RT-PCR Kit (204245, Qiagen), according to the manufacturer's protocol. The acquisition was made using a QuantStudio™ 12K Flex Real-Time PCR System (Applied Biosystems, Waltham, MA, USA).

### ***Statistical Analysis***

GraphPad Prism 8.4.3 was used for statistical analysis. Data are presented as mean  $\pm$  standard deviation (SD) and p-values were calculated using the Student t-test or one way ANOVA.  $P < 0.05$  was considered statistically significant.

## Results

### *MEP50 interactome identified FUBP1 as a MEP50 partner*

To identify PRMT5 partners in TNBC, PRMT5 was attempted to be immunoprecipitated from the TNBC cell line HCC38. However, efficient IP of PRMT5 was unsuccessful, and only few PRMT5 partners were retrieved (**Table S3**). These data were generated before my arrival in the lab, and at that time none of the commercially available anti-PRMT5 antibodies could efficiently IP PRMT5.

As MEP50 is a main PRMT5 partner that forms a stable complex with it, and since its IP poses no problems, we focused our investigations on the MEP50 interactome. We performed IP of MEP50 in 3 replicates using the antibody #A301-561A (**Table S1**), referred to as Ab1, from the TNBC cell line HCC38 and identified the potential partners by LC-MS/MS (**Table S4**). Proteins with a  $\geq 2$ -fold enrichment in the MEP50 IP compared to the IgG, having at least 3 total peptides in the three independent replicates, and an adjusted p-value  $\leq 0.05$  were considered significantly enriched in the MEP50 IP (**Table S4**). Proteins that had 0 peptides in all IgG replicates, referred to as distinct or unique proteins, were considered enriched when having at least 3 total peptides in the three replicates. PRMT5 was retrieved as one of the top MEP50 interactors (**Figure 1A; Table S4**) and we identified known PRMT5/MEP50 partners (**Figure 1A-B; Figure 2; Table S4**), validating our approach. Gene ontology (GO) analysis performed on the proteins enriched in MEP50 IP revealed an enrichment of RNA binding and ribosomal proteins involved in translation, RNA processing, and ribosomal biogenesis (**Figure 1B; Figure 2**). Among the unique MEP50 partners, the top identified protein was FUBP1 (**Figure 1A; left panel**), a ssDNA/RNA binding protein that is involved in transcription and RNA processing [499]. To validate the specificity of this finding, we repeated the LC-MS/MS experiment in HCC38 cell line using Ab1 and an additional anti-MEP50 antibody, #A301-562A (referred to as Ab2), that binds to the C-terminal domain of MEP50, unlike Ab1 that binds to its N-terminal domain (**Figure 1C**). We found 42 common proteins (**Figure 1C; Table S5**) retrieved with the two antibodies, including PRMT5, MEP50, and known PRMT5 interactors like some methylosome components (**Figure 1D; Table S5**). Interestingly, we retrieved again FUBP1 as a top hit among the MEP50 partners, with 0 peptides retrieved in the IgG condition (**Figure 1D; left panel**). FUBP1 belongs to the FUBP family that includes FUBP2 and FUBP3, which we also retrieved in the MEP50 interactome

(**Figure 1A,D; Figure 2; Table S4 and S5**), implying that there could be a functional association between the FUBP family members and the PRMT5/MEP50 complex. We performed a functional interaction analysis using the STRING database on both MEP50 IP experiments, and found that the MEP50 interactors, including FUBP1, FUBP2, and FUBP3, are mostly present in spliceosomal complexes (**Figure 2A,B**). Interestingly, FUBP1, FUBP2, and FUBP3 were all present in the same functional clusters as PRMT5 and MEP50, the spliceosome (**Figure 2A,B**). In addition to the methylosome and spliceosome complexes, MEP50 partners were also clustered in translational and cell cycle regulator complexes (**Figure 2A,B**).

Given that FUBP1 emerged as a prominent MEP50 interactor in both experiments employing two distinct anti-MEP50 antibodies, and considering its involvement in processes regulated by PRMT5, we opted to further investigate the relation between FUBP1 and the PRMT5/MEP50 complex within the context of TNBC.



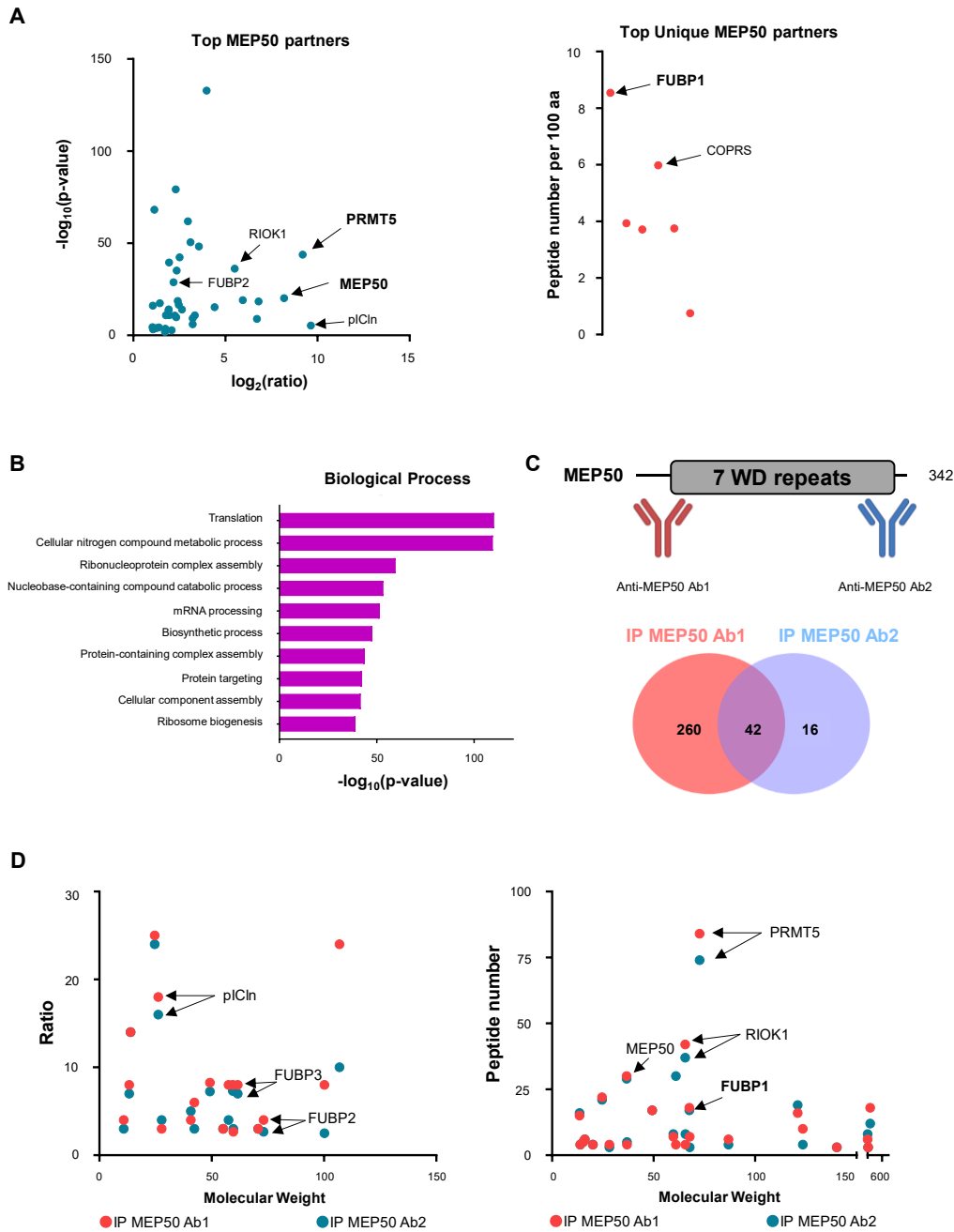


**Figure 1: The characterization of the MEP50 interactome identifies FUBP1 as a top partner.** MEP50 was immunoprecipitated from the TNBC cell line HCC38 using either Ab1 in 3 replicates (A-B) or Ab1 and Ab2 in 1 replicate (C-D). **(A)** Volcano plot (right panel) of proteins enriched with immunoprecipitated MEP50 compared to the IgG control identified by LC-MS/MS. The graph represents  $-\log_{10}(p\text{-value})$  (y-axis) versus the enrichment ratio in MEP50 IP versus IgG ( $\log_2(\text{ratio})$ ; x-axis). The left panel represents uniquely identified proteins (0 peptides in IgG), where the y-axis indicates the number of peptides in MEP50 IP per 100 amino acids. Each dot represents a protein. **(B)** Biological processes of the identified MEP50 partners. Gene ontology analysis was performed using myProMS software developed at Institute Curie (<https://github.com/bioinfo-pf-curie/myproms>). **(C)** A scheme (upper panel) showing the binding regions of the two anti-MEP50 antibodies on MEP50. Venn diagram (lower panel) showing the number of common proteins identified with both MEP50 antibodies IP. **(D)** The MEP50 interactome was represented by plotting the ratio of peptide number obtained in MEP50 IP versus IgG (right panel; y-axis) or the peptide number retrieved in MEP50 IP for unique proteins (left panel; y-axis) of the proteins retrieved with Ab1 (in red) and Ab2 (in blue) with respect to the molecular weight (kDa) (x-axis). Each dot represents a protein.

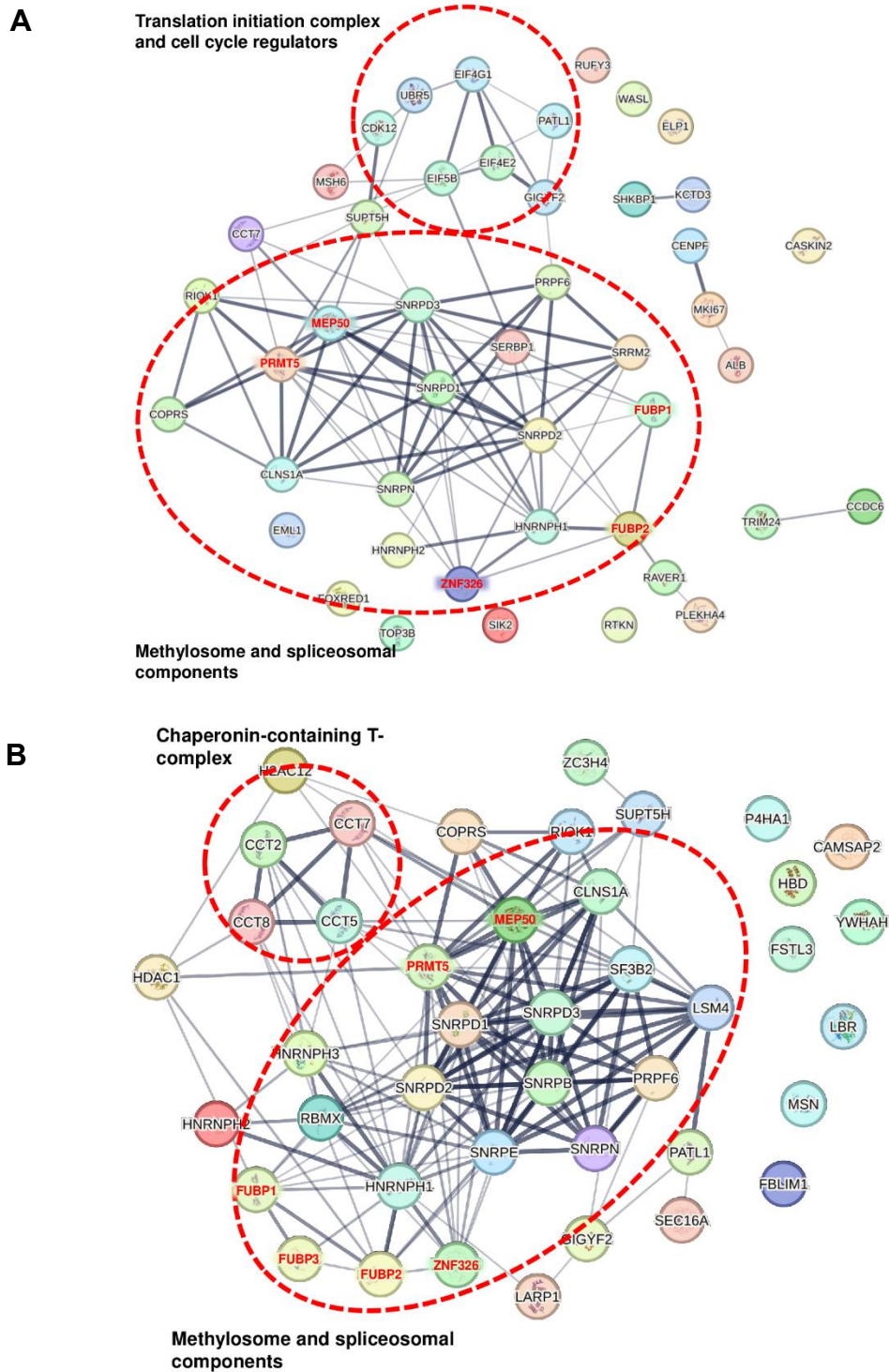


**Figure 2: Functional interactions among the identified MEP50 partners.** Functional associations among the 45 partners identified through MEP50 IP in 3 replicates (A) or the 42 partners identified in common between MEP50 IP using Ab1 and Ab2 (B) were assessed using the STRING database (<http://string-db.org/>). Each node represents a protein, and the lines connecting two nodes represent an association between two proteins.

### ***FUBP1 is overexpressed in breast cancer compared to normal breast tissues***

To test if FUBP1 levels are dysregulated in breast cancer, we examined the expression of FUBP1 across diverse breast cancer cells belonging to the different breast cancer subtypes and two normal breast cell lines. We found a differential expression of FUBP1 protein among these cell lines (**Figure 3A**), however, the level of FUBP1 expression did not appear to correlate with specific breast cancer subtypes (**Figure 3A**). Subsequently, we examined the mRNA expression of FUBP1 within our Curie cohort [234,429,430] and found that FUBP1 is overexpressed in breast tumours, with the exception of the luminal B subtype, in comparison to normal breast tissue (**Figure 3B**; right panel). In addition, FUBP1 is overexpressed in TNBC when compared to the other three breast cancer subtypes (**Figure 3B**; right panel). In order to validate these findings, we examined FUBP1 mRNA expression in the publicly available TCGA cohort (**Figure 3B**; left panel). Similarly, we noticed an overexpression of FUBP1 in breast cancer compared to normal breast tissue (**Figure 3B**), however, unlike the Curie cohort, no variation in FUBP1 mRNA levels was observed among the various breast cancer subtypes (**Figure 3B**; left panel).

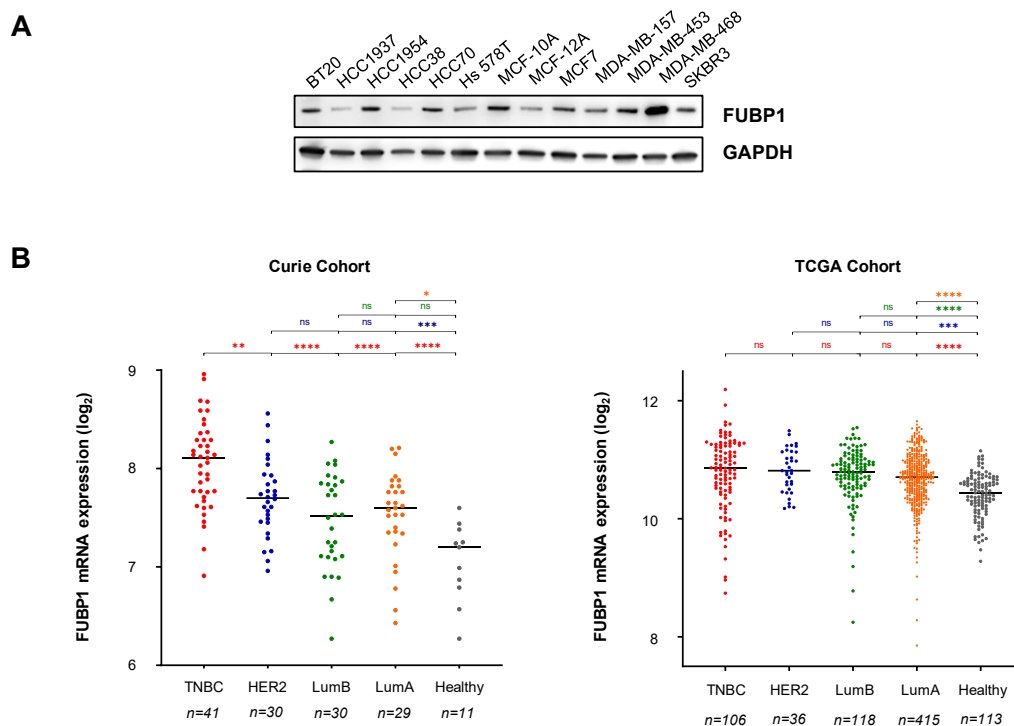


**Figure 3: FUBP1 is overexpressed in breast cancer. (A).** Evaluation of FUBP1 protein expression across a range of breast cancer and normal breast cell lines by western blotting. GAPDH was used as a loading control. **(B).** The mRNA levels of FUBP1 were evaluated in TNBC (red), HER2-positive (blue), luminal B (LumB; green), and luminal A (LumA; orange) breast cancers, as well as in healthy breast tissue (grey) within both the Curie cohort (right panel) and the TCGA cohort (left panel). The graphs indicate the respective sample numbers for each breast cancer subtype and for normal breast tissue in both cohorts. The RNA quantifications were logarithmically transformed ( $\log_2$ ) and are presented as scatter plots, where each coloured closed circle corresponds to one sample. The mean RNA expression is represented by a black line. Statistical analysis was conducted using one-way ANOVA, yielding the following significance indicators: “ns” denotes not significant; \* $p < 0.05$ ; \*\* $p < 0.01$ ; \*\*\* $p < 0.001$ ; \*\*\*\* $p < 0.0001$ .

To assess whether FUBP1 is required for breast cancer cell proliferation, we depleted FUBP1 using two distinct siRNA in MDA-MB-468 TNBC cells, which express high levels of FUBP1 (**Figure 3A**), and then monitored cell proliferation at various time points (**Figure 4**). From 120 hours post-transfection with the siRNA, we observed a significant decline in the proliferation of MDA-MB-468 cells upon FUBP1 depletion, indicating that FUBP1 plays a role in maintaining their viability.

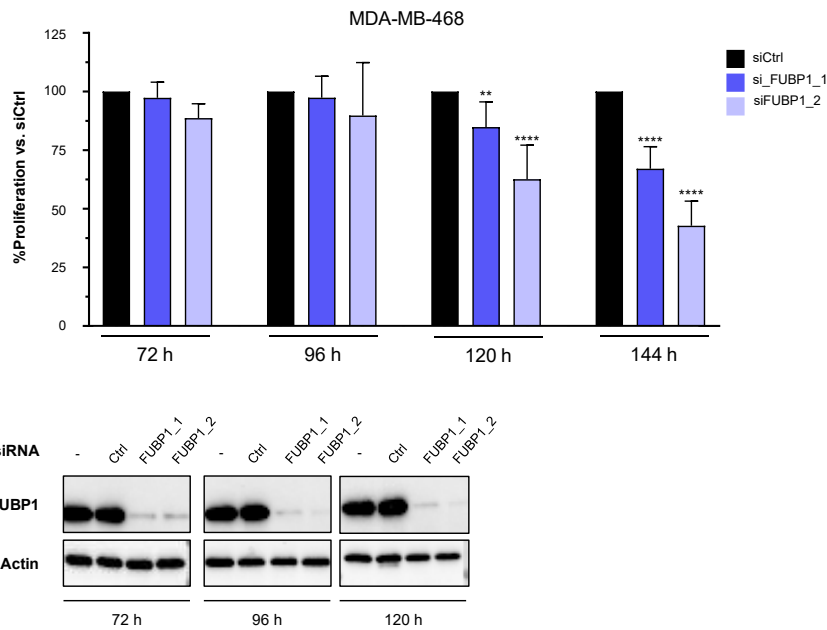


**Figure 4: FUBP1 depletion impairs the proliferation of MDA-MB-468 TNBC cells.** MDA-MB-468 cells were transfected with control siRNA (siCtrl) or two distinct siRNA targeting FUBP1 (FUBP1\_1 and FUBP1\_2). Subsequently, cell proliferation was assessed using the MTT assay at time points of 72-, 96-, 120-, and 144-hours post-transfection. FUBP1 depletion was confirmed by western blotting and actin was used as a loading control.

### ***PRMT5 is a component of the FUBP1 interactome***

To ascertain the interaction between FUBP1 and the PRMT5/MEP50 complex, we immunoprecipitated endogenous FUBP1 in five biological replicates from MDA-MB-468 cells, followed by LC-MS/MS analysis (**Figure 5A**). As we employed 5 biological replicates for this experiment, we considered proteins having  $\geq 1.5$ -fold enrichment in the FUBP1 IP compared to the IgG, with at least 3 total peptides in three independent replicates, and an adjusted p-value  $\leq 0.05$ , to be significantly enriched in the FUBP1 IP (**Figure 5A; Table S6**). Potential FUBP1 partners included the other FUBP family members FUBP2 and FUBP3, components of the spliceosome, and translation and splicing factors (**Table S6**). While FUBP1 emerged as a prominent partner of MEP50 in HCC38 cells (**Figure 1A, C**), MEP50 was not significantly enriched in FUBP1 IP in MDA-MB-468 cells (**Figure 5C**). Nevertheless, PRMT5 as well as PRMT1 were identified within the FUBP1 interactome with an enrichment ratio of 1.59 and 3.56 respectively (**Figure 5C; Table S6**).

Upon conducting GO analysis on the FUBP1 interactome, we found a significant enrichment in RNA binding proteins and ribosomal components, as well as proteins

involved in RNA processing and translation (**Figure 5B**). This enrichment pattern mirrors that of the MEP50 interactome (**Figure 1B**) and the previously described PRMT5 methylome [106,127,132,133,147]. Consistent with our findings, the FUBP1 partners retrieved in HEK293T cells were involved in RNA processing, and included PRMT1, PRMT5, MEP50, and CHTOP (PRMT1 and PRMT5 partners) [528].

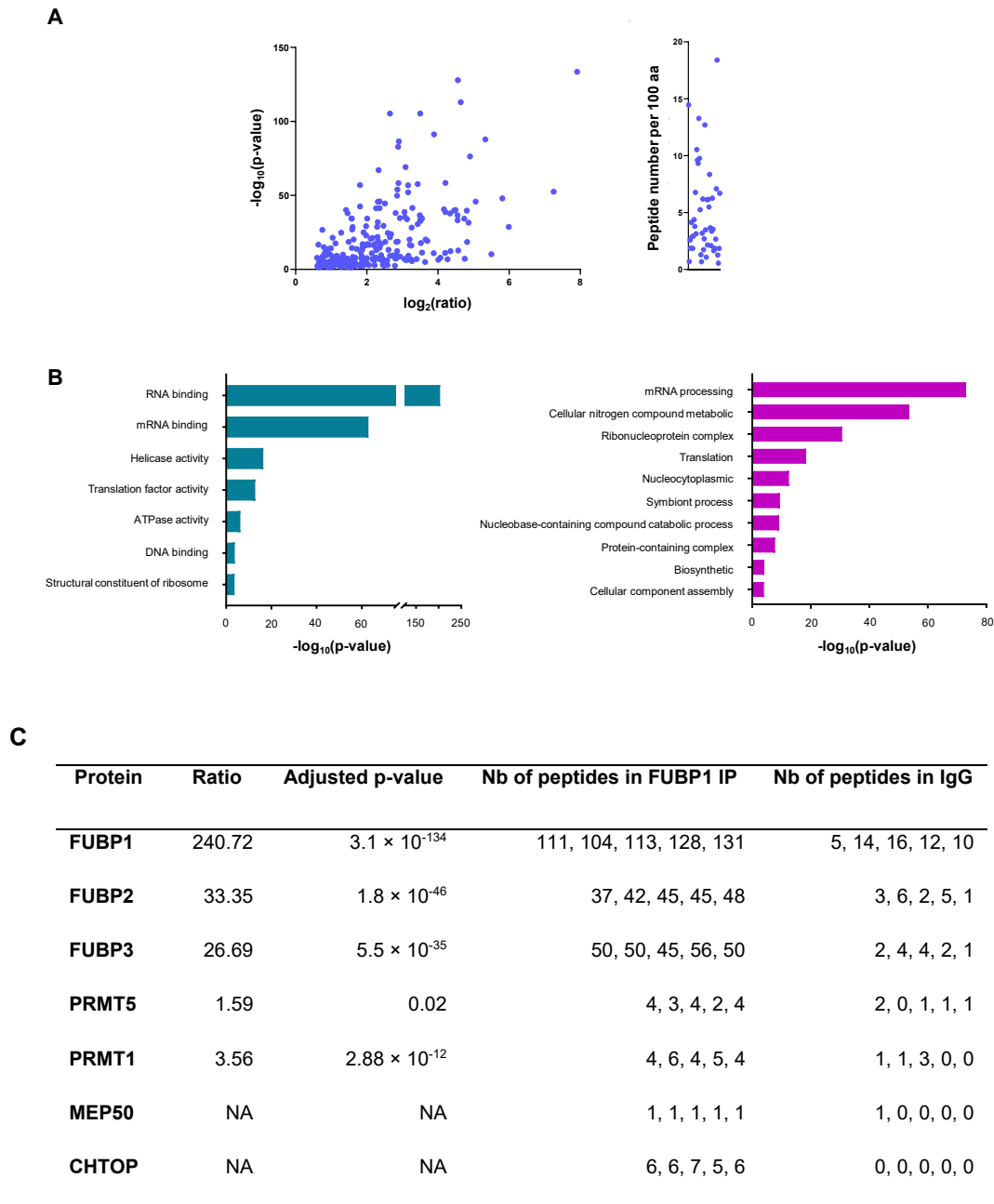


**Figure 5: Both PRMT5 and PRMT1 are detected in the FUBP1 interactome.** Endogenous FUBP1 was immunoprecipitated from MDA-MB-468 cells, followed by LC-MS/MS analysis (five biological replicates) (**A**). Volcano plot of proteins enriched in the five replicates of immunoprecipitated FUBP1 compared to the IgG control identified by LC-MS/MS. The graph represents  $-\log_{10}(\text{p-value})$  (y-axis) versus the enrichment ratio in FUBP1 IP compared to IgG ( $\log_2(\text{ratio})$ ); x-axis). On the right is the plot of the number of peptides per 100 amino acids of unique proteins present in FUBP1 IP and not in the IgG.

Each protein is presented as a dot. **(B)**. GO enrichment analysis was performed with the significantly enriched FUBP1 partners using the myProMS software developed at Institute Curie (<https://github.com/bioinfo-pf-curie/myproms>). The upper panel illustrates the molecular functions, while the lower panel presents the biological processes. **(C)** Table showing the ratio, adjusted p-value, and the number of retrieved peptides in FUBP1 or IgG replicates of the indicated proteins. NA: not applicable.

### ***FUBP1 is symmetrically dimethylated by PRMT5***

FUBP1 has four KH domains which are accountable for binding to ssDNA and RNA, and three nuclear localization signals (**Figure 6A**). Several comprehensive proteomic analyses have provided evidence of FUBP1 undergoing mono- and di-methylation, predominantly on three arginine residues located between KH3 and KH4, which are close to one of the FUBP1 NLS: R359, R361, and R363 [106,128,134,141–144,146,377,411,527] (**Figure 6A**). These three arginine residues fall within a PRMT5 methylation motif (**Figure 6A**). We next examined whether PRMT5 was responsible for the methylation occurring at these specific sites in FUBP1. For this purpose, we purified two fragments of FUBP1, comprising the KH1-KH4 (KH1 to KH4) and the KH3-KH4 domains. Both fragments were subjected to mutation, where lysine replaced arginine on the three potential arginine methylation sites (FUBP1 3K). Through *in vitro* methylation assays, we found that FUBP1 is a substrate for PRMT5 *in vitro*, and that R359, R361, and R363 represent the primary PRMT5 methylation sites within the FUBP1 central nucleic acid binding domain (KH1-KH4) (**Figure 6B**).

To examine whether endogenous FUBP1 is indeed methylated by PRMT5 in TNBC cells, FUBP1 was immunoprecipitated from MDA-MB-468 cells preincubated or not with a specific PRMT5 inhibitor (EPZ015938) for 48 hours (**Figure 6C**). Western-blot analysis using a pan-SDMA antibody revealed that immunoprecipitated FUBP1 was symmetrically dimethylated in MDA-MB-468 cells, and its methylation was reduced upon PRMT5 inhibition (**Figure 6C**). Altogether, these data show that FUBP1 is symmetrically dimethylated by PRMT5 in cells, and mainly on R359, R361, and R363 *in vitro*.



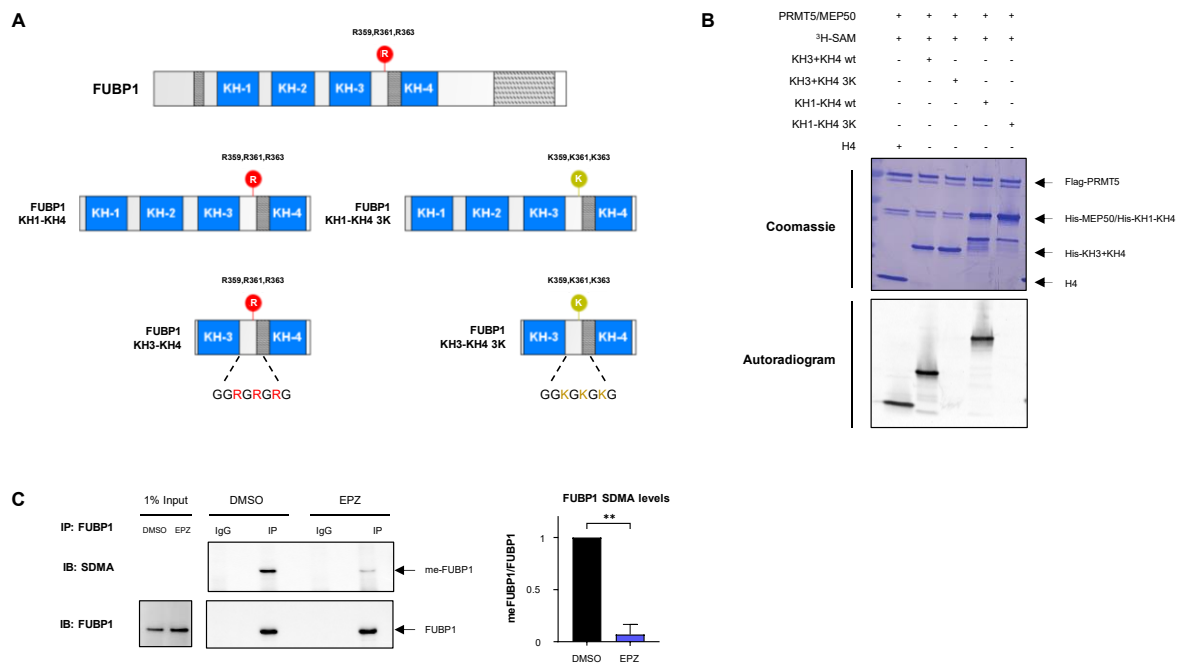


**Figure 6: PRMT5 symmetrically dimethylates FUBP1. (A).** Illustration depicting FUBP1 full length, KH1-KH4 and KH3-KH4 domains wild type and triple lysine mutants (3K). FUBP1 three potential methylation sites (in red) and their corresponding mutations to lysine (in yellow), positioned between FUBP1's KH3 and KH4 domains are shown. FUBP1 NLSs are shown in grey, dashed boxes. **(B).** PRMT5 methylates FUBP1 central domain (KH1-KH4) on R359, R361, and R363. The wild-type (wt) or triple lysine mutants (3K) of KH1-KH4 and KH3-KH4 domains were incubated with recombinant PRMT5/MEP50 in the presence of radioactive S-adenosyl methionine (<sup>3</sup>H-SAM) for 1 hour at 30°C. The samples were then loaded onto SDS-PAGE and transferred onto a PVDF membrane. Coomassie staining (upper panel) confirmed the presence of all recombinant proteins, and the autoradiography results are presented (lower panel). Histone H4, a known PRMT5 substrate, was employed as a control for *in vitro* methylation. The images originate from a single experiment, representative of a minimum of three independent experiments **(C).** PRMT5 symmetrically dimethylates FUBP1 in MDA-MB-468 cells. Cells were treated with 1 μM PRMT5 inhibitor (EPZ015938; EPZ) or DMSO for 48 hours, followed by IP of FUBP1. Western blot was performed using an antibody targeting pan-symmetric dimethylation (SDMA). FUBP1 was probed to confirm the efficacy of the IP and to serve as a loading control. Western blot images were obtained from a single experiment representative of three independent experiments. The bands corresponding to methylated FUBP1 (meFUBP1) and total FUBP1 were quantified across these three independent experiments, and the average ratio of meFUBP1/FUBP1 was plotted as a bar graph (left panel). The p-value was determined using a Student's t-test; \*\*p<0.01.

### *The methylation of FUBP1 does not affect its localization*

Due to the presence of three NLSs, FUBP1 is primarily located in the nucleus. Considering that the methylation sites of FUBP1 are situated near one of its NLS (**Figure 6A**), we investigated whether FUBP1 methylation influences its subcellular localization. We introduced exogenous expression of Flag-tagged FUBP1 wild type (FUBP1 wt) or a triple lysine mutant (FUBP1 3K) in HeLa cells, followed by immunofluorescence staining using anti-Flag antibody. We found that both FUBP1 wt and FUBP1 3K localize to the nucleus (**Figure 7**), thus excluding the possibility that



arginine methylation of FUBP1 regulates its subcellular localization, in the experimental conditions used.

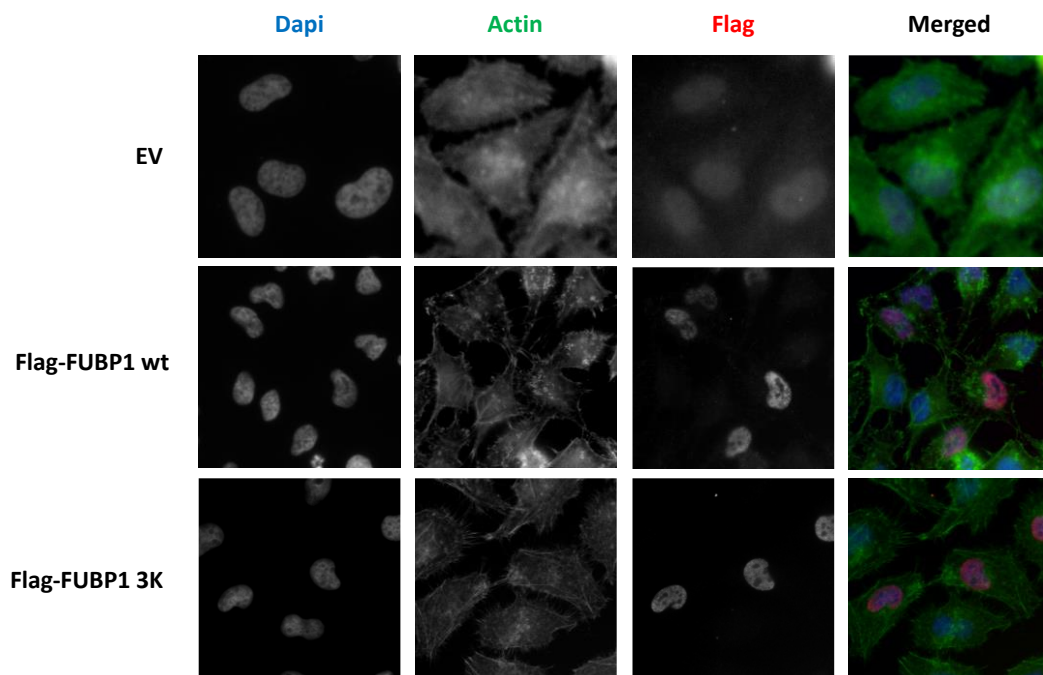


**Figure 7: Arginine methylation of FUBP1 does not regulate its subcellular localization.** HeLa cells were transfected with an empty vector (EV), Flag-FUBP1 wild type (wt) or a triple lysine mutant (3K). 48 hours post-transfection, the cells were fixed with PFA and stained for Dapi (blue), Flag (red), and actin (green). Images were acquired using an Apotome microscope at 40X magnification and are representative of three independent experiments.

### ***FUBP1 methylation enhances its binding to the FUSE element***

Next, we aimed to investigate the functional implication of FUBP1 methylation by PRMT5. Since the methylation sites reside within the nucleic acid binding domain of FUBP1, we questioned whether this methylation influences its interaction with ssDNA, potentially affecting its transcriptional activity. The FUSE element is a well characterized FUBP1 binding site, located approximately 1.5 Kb upstream of the *MYC* promoter. A previous study delineated the binding of individual KH domains of FUBP1 to the FUSE sequence and concluded that all four domains are necessary for robust and efficient binding [543]. To assess the impact of FUBP1 methylation on its interaction with FUSE, we employed flow-Induced dispersion analysis (FIDA) to assess the binding between FUSE with FUBP1 KH1-KH4 wt or with FUBP1 KH1-KH4 3K (**Figure 8A**). FIDA is based on measuring the change in the hydrodynamic radius (size) of a ligand (FUSE in this case) as it interacts with a target protein (FUBP1 KH1-KH4 wild type or triple lysine mutant) [615]. The binding curves indicated that FUBP1

KH1-KH4 wt exhibits a more robust binding to FUSE compared to FUBP1 KH1-KH4 3K (**Figure 8A**). This is enforced by a smaller dissociation constant ( $K_d$ ) for FUSE and FUBP1 KH1-KH4 wt ( $K_d = 9.47 \text{ nM} \pm 2.82 \text{ nM}$ ) compared to FUSE and FUBP1 KH1-KH4 3K ( $K_d = 93.45 \text{ nM} \pm 26.23 \text{ nM}$ ). In order to validate the modulation of FUBP1/FUSE interaction *in vivo*, we evaluated the enrichment of FUBP1 at the *MYC* promoter (FUSE element) following PRMT5 inhibition (**Figure 8B**) and observed a reduction in FUBP1 recruitment to the *MYC* promoter in cells treated with the PRMT5 inhibitor (**Figure 8B**). These data suggest that FUBP1 symmetric dimethylation by PRMT5 enhances the interaction between FUBP1 and the FUSE element.

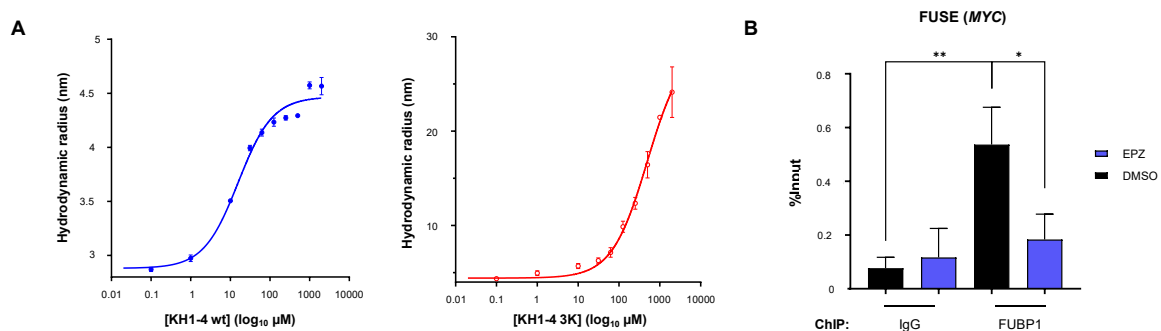


**Figure 8: The arginine methylation of FUBP1 enhances its interaction with the FUSE element.** **(A)** Binding curves of the association between FUSE with FUBP1 KH1-4 wt (blue; right panel) or with FUBP1 KH1-KH4 3K (red; left panel). The curves represent the complex hydrodynamic radius (nm; y-axis) plotted against the  $\log_{10}$  transformed concentration ( $\mu\text{M}$ ; x-axis) of analyte (FUBP1 KH1-KH4 wt or 3K), that were obtained through Fida at  $25^\circ\text{C}$  with pre-incubated samples. The data are representative of three separate experiments, each of them involving the measurement of technical triplicates. **(B)** MDA-MB-468 cells were treated with DMSO (black bar) or  $1 \mu\text{M}$  PRMT5 inhibitor (EPZ015938; EPZ; blue bar) for 48 hours, followed by ChIP using anti-FUBP1 antibodies or IgG as a control. The FUSE element upstream the *MYC* promoter was then amplified by qPCR. The mean of three independent experiments  $\pm$  SD is represented. Student t-test was used to determine p-values and are represented as \*  $p < 0.05$ ; \*\*  $p < 0.01$ .

### *Investigating the PRMT5 interactome by TurboID proximity labelling*

As previously mentioned, the conventional IP method was not successful in determining the PRMT5 interactome, therefore, we opted to unravel it through biotin proximity labelling using TurboID. This technique involves the fusion of PRMT5 with TurboID, a biotin ligase that can add biotin molecules onto proteins in the vicinity of PRMT5 (biotinylation radius up to 35 nm [616]) (**Figure 9A**). As the biotinylation reaction catalysed by TurboID is fast (occurring within 10 minutes; [612]), this approach has the potential to capture transient protein-protein interactions (**Figure 9A**), unlike the classical IP method. The protein in close proximity to PRMT5-TurboID, representing a potential PRMT5 partner, will be biotinylated then captured using

streptavidin conjugated beads, and can be further identified by LC-MS/MS analysis (**Figure 9A**). We first generated Flag-TurboID-PRMT5 and a negative control, Flag-TurboID, then verified their expression and their ability to biotinylate proteins in HEK293T cells (**Figure 9B**). After transfection, cells were incubated with 50  $\mu$ M or 500  $\mu$ M biotin for 10 (**Figure 9B**) or 30 (data not shown) minutes. We found that TurboID was functional under the examined conditions. Notably, Flag-TurboID-PRMT5 exhibited a slightly higher activity when cells were exposed to 500  $\mu$ M biotin in comparison to 50  $\mu$ M (**Figure 9B**). Moreover, it is noteworthy that TurboID was able to biotinylate proteins even in the absence of external biotin supplementation (**Figure 9B**; middle panel lane 2). To determine the localization of the Flag-TurboID-PRMT5 and Flag-TurboID proteins, we expressed them in HeLa cells then performed immunofluorescence staining using anti-Flag antibodies and found that both proteins localized primarily to the cytoplasm (**Figure 9C**).

Next, we attempted to optimize the partners pulldown protocol. We first conducted a pulldown experiment using 500  $\mu$ M exogenous biotin and allowing the biotinylation reaction to proceed for 30 minutes. While we successfully identified both established and potential novel PRMT5 partners (data not shown), we encountered a notable issue involving a high number of non-specific biotinylated peptides, as approximately 800 proteins were identified to be enriched in the Flag-TurboID control. This could be due to an extended reaction time and/or elevated concentration of biotin employed, or due to an increased expression of TurboID alone compared to TurboID-PRMT5. In addition, we faced another technical challenge that is the presence of large peaks corresponding to streptavidin in the LC-MS/MS spectra, that result from the tryptic digestion of the streptavidin coupled to the beads used during the pulldown experiments (**Figure 9D**). The presence of these peaks in the MS spectra may mask the identification of potential PRMT5 partners, hence we decided to follow a protocol to chemically modify the beads to render streptavidin resistant to the digestion by trypsin (**Figure 9D**; [613]). The chemical modification is based on lysine dimethylation and arginine condensation, that create bulk groups on the lysine and arginine residues of streptavidin preventing trypsin from digesting them (**Figure 9D**) [613]. After treating the streptavidin-conjugated beads, we tested them by performing a biotin pulldown experiment followed by LC-MS/MS and found that the saturated streptavidin peaks were absent in the chromatograms (**Figure 9D**).

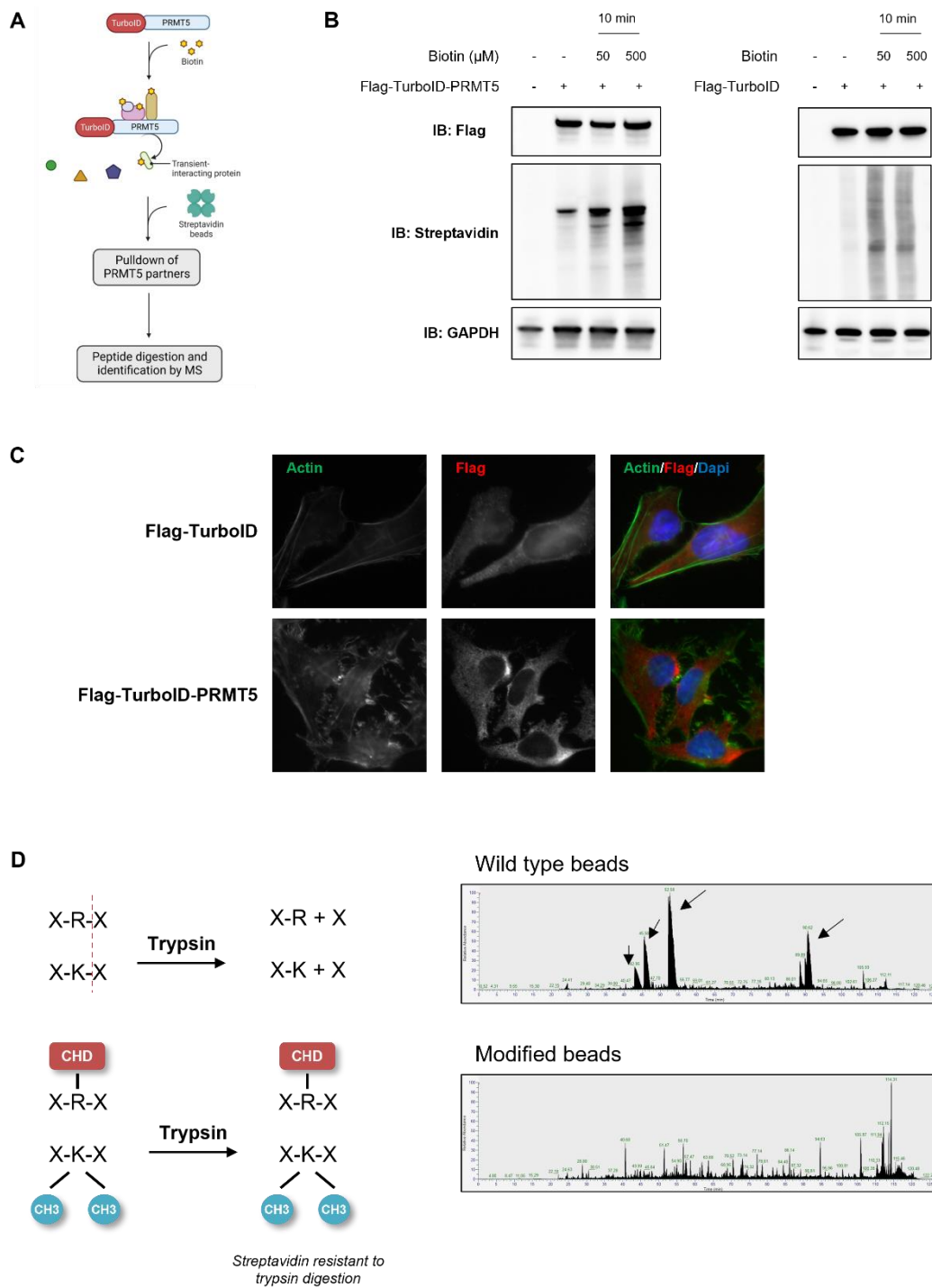


**Figure 9: TurboID proximity labelling method setup. (A).** Illustration outlining the experimental workflow. **(B).** Forty-eight hours post-transfection with Flag-TurboID-PRMT5 or Flag-TurboID, HEK293T cells were treated with 50  $\mu$ M or 500  $\mu$ M biotin for 10 minutes at 37°C. Western blotting was used to assess the fusion protein expression using an anti-Flag antibody, and the total biotinylated proteins utilizing an HRP-conjugated streptavidin. GAPDH was used as a loading control. **(C).** HeLa cells were transfected with Flag-TurboID or Flag-TurboID-PRMT5. 48 hours post-transfection, the cells were fixed with PFA and stained for Dapi (blue), Flag (red), and actin (green). Images were acquired using an Apotome microscope at 40X magnification. **(D).** Chemical modification of streptavidin sepharose beads prevents tryptic digestion of streptavidin. The streptavidin-conjugated beads were chemically modified on lysine and arginine residues by dimethylation and condensation respectively (right panel), which prevents streptavidin proteolysis by trypsin. Chromatograms (left panel) of the LS-MS/MS acquired from pull-down of biotinylated proteins using wild type streptavidin sepharose beads

(upper panel) or the chemically modified ones (lower panel). Black arrows are used to mark the streptavidin peak.

Next, we performed a proximity ligation assay to identify PRMT5 partners. HEK293T cells were transfected with Flag-TurboID or Flag-TurboID-PRMT5. Forty-eight hours post-transfection, cells were either not treated, or treated with 50  $\mu$ M biotin for 2 or 10 minutes. The biotinylated proteins were then pulled-down with the trypsin-resistant streptavidin beads and identified using LC-MS/MS analysis (**Table S7**). We considered proteins with a ratio of peptide number in TurboID-PRMT5 versus TurboID greater than 2 as enriched in TurboID-PRMT5 pulldown. Unique proteins (0 peptides in TurboID) were considered enriched when having a peptide number of  $\geq 2$  in the TurboID-PRMT5 pulldown. Even without adding biotin to the medium, we retrieved 128 proteins enriched in the TurboID-PRMT5 sample, meaning that TurboID-PRMT5 fusion protein is active without biotin supplementation, consistent with what we previously observed (**Figure 9B**). Upon adding 50  $\mu$ M biotin, the number of identified proteins increased to 279 (2 minutes biotin treatment) and 203 (10 minutes biotin treatment), meaning that a reaction time of just 2 minutes is sufficient for partners identification using TurboID (**Table S7**). Among the potential PRMT5 interactors, several are known PRMT5 partners including components of the methylosome like MEP50, RIOK1, and COPRS, validating the efficiency of the TurboID approach. By conducting a GO analysis on PRMT5 potential partners using the Database for Annotation, Visualization and Integrated Discovery (DAVID; <https://david.ncifcrf.gov/>), we observed a significant enrichment of proteins involved in intracellular protein transport and localization to the plasma membrane, of the proteins identified after 2 minutes biotin treatment (**Figure 10A**), while those enriched after 10 minutes treatment were involved in processes of cilium assembly, endocytosis, and cell division (**Figure 10A**). All these processes were not previously described to be regulated by PRMT5. By comparing the enriched partners retrieved in the three conditions tested, we found 60 proteins in common between 2 and 10 minutes treatment (**Figure 10C,D; Table S8**), and 10 proteins in common between all three tested conditions (**Figure 10C; Table 1**). The 60 proteins common between the 2 and 10 minutes biotinylation time points included PRMT5, MEP50, and RIOK1 (**Figure 10D**). Among the most enriched proteins shared between these conditions, which had not been previously validated as partners of PRMT5, were serologically defined colon

cancer antigen-3 (SDCCAG3), HERC1, and tubulin beta 8 (TUBB8) (**Figure 10D**). SDCCAG3 and HERC1 were found to be common across all three conditions tested (**Table 1**). STRING analysis of the 60 proteins common to both the 2- and 10-minutes biotin pulldown did not reveal network clusters, apart from the methylosome, among the retrieved PRMT5 interactors (**Figure 11**). However, upon individual analysis of the proteins retrieved at each time point, we found that the PRMT5 potential interactors identified at 2 minutes of biotinylation time were associated with proteasomal complexes, desmosome junctions, and a number of them were mitochondrial components (**Figure S1**). On the other hand, the proteins identified after 10 minutes of biotin treatment were found to be part of network clusters related to centrosome cycle, and included components associated to the ER membrane and intracellular transport (**Figure S2**).

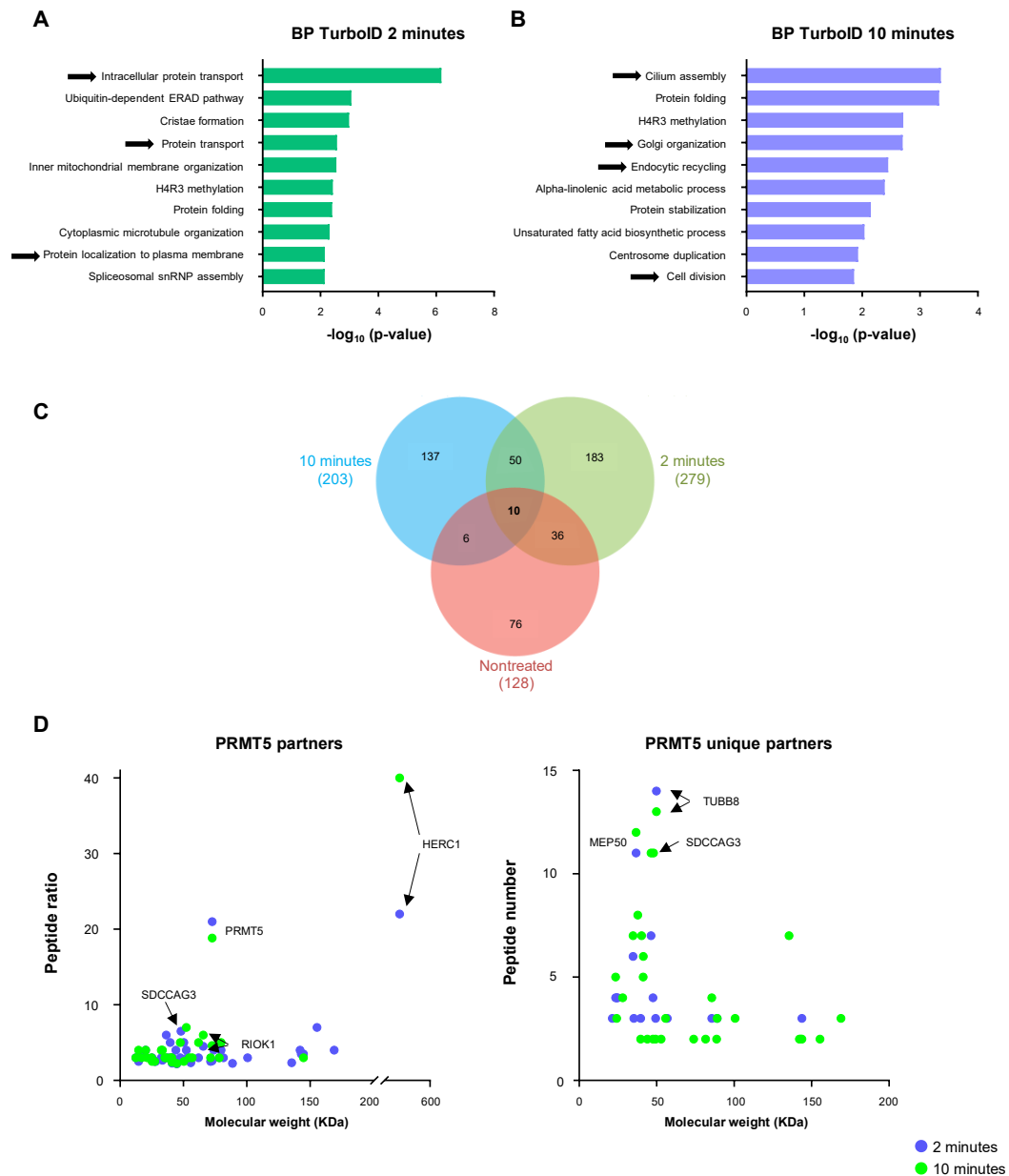


**Figure 10: Identifying PRMT5 interactome by TurboID proximity labelling.** HEK293T cells were transfected with pcDNA3.1-Flag-TurboID or pcDNA3.1-Flag-TurboID-PRMT5. 48 hours later, cells were either not treated, or treated with 50  $\mu$ M biotin for 2 or 10 minutes. Cells were then lysed and biotinylated proteins were pulled down using trypsin-resistant streptavidin-conjugated beads and identified by LC-MS/MS. **(A, B)** GO analysis by DAVID (<https://david.ncifcrf.gov/>) of the top 10 biological processes (BP) of the proteins retrieved after 2 minutes (A) and 10 minutes (B) biotin treatment. **(C)** Venn diagram showing the retrieved proteins common to the three conditions used for TurboID proximity labelling of PRMT5 neighbouring proteins. **(D)** Presentation of the PRMT5 neighbours identified through TurboID proximity labelling, common to the 2 (blue) and 10 (green) minutes biotin labelling time, presented as the peptide number ratio retrieved in Flag-TurboID-PRMT5 versus Flag-TurboID (y-axis) with respect to the molecular weight (x-axis; KDa) (right panel). Unique proteins are presented as the peptide number in Flag-TurboID-PRMT5 pull-down as it is not possible to calculate a ratio (0 peptides in TurboID). Each protein is depicted as a circle.

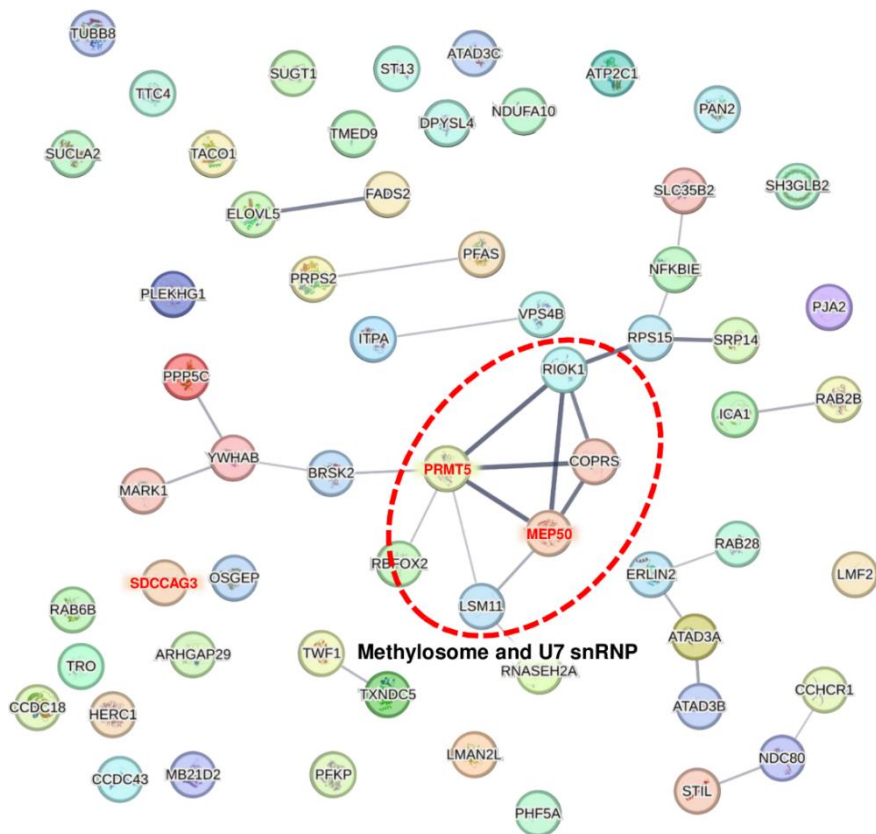


**Figure 11: Functional interactions among the 60 PRMT5 neighbouring proteins identified with TurboID during 2- and 10-minutes biotin treatment.** Functional associations were determined using the STRING database (<http://string-db.org/>). Each node represents a protein, and the lines represent an association between two proteins.

**Table 1: Proteins common to the three conditions used in the TurboID proximity labelling method**

Protein	TurboID			TurboID-PRMT5		
	NT	2 minutes	10 minutes	NT	2 minutes	10 minutes
<b>PRMT5</b>	0	6	5	88	113	105
<b>MEP50</b>	0	0	0	9	12	11
<b>RIOK1</b>	4	12	16	61	72	72
<b>COPRS</b>	0	1	1	3	4	4
<b>HERC1</b>	0	1	2	22	40	44
<b>SDCCAG3</b>	0	0	2	2	11	13
<b>PPP5C</b>	0	1	0	3	3	3
<b>RAB6B</b>	0	0	0	6	5	4
<b>CCDC43</b>	0	2	2	2	5	6
<b>PFKP</b>	0	0	0	4	4	3

NT: nontreated.



### ***SDCCAG3 is a novel PRMT5 interactor***

Among the novel potential PRMT5 partners, the protein SDCCAG3 emerged as a robust and prominent candidate in all three conditions tested (**Figure 10D; Table 1**). Additionally, we consistently found SDCCAG3 as a potential PRMT5 partner throughout our optimization experiments, when evaluating various biotin concentrations (such as 500  $\mu\text{M}$ ), and durations of biotinylation reactions (30 minutes) (data not shown). SDCCAG3, also referred to as endosome associated trafficking regulator 1 (ENTR1), is a relatively understudied protein that plays roles in various cellular processes such as cytokinesis [617], ciliogenesis [618], receptor endocytosis, and protein trafficking [619–621]. Given the consistent presence of SDCCAG3 as a neighbouring protein to PRMT5, along with its involvement in PRMT5-dependent enriched biological pathways (**Figure 10A, B**), we chose to dig deeper into the relationship between PRMT5 and SDCCAG3.

We first examined the mRNA expression level of SDCCAG3 in the Curie and TCGA cohorts (**Figure 12**) to investigate whether SDCCAG3 is dysregulated in breast cancer. In the Curie cohort, SDCCAG3 mRNA level was not significantly differential between the different breast cancer subtypes and the normal breast tissue (**Figure 12**). On the contrary, SDCCAG3 mRNA expression was significantly higher in the different breast cancer tumours compared to the normal tissue in the TCGA cohort (**Figure 12**)

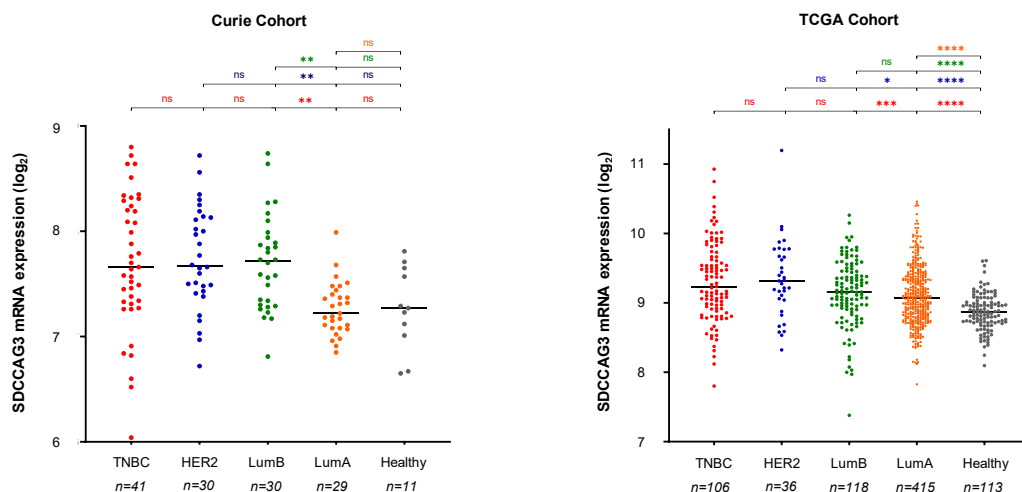


**Figure 12: SDCCAG3 mRNA expression level in breast tumours and normal breast tissue.** SCDDAG3 mRNA levels were analysed in TNBC (red), HER2-positive (blue), luminal B (LumB; green), and luminal A (LumA; orange) breast cancers and in healthy breast tissue (grey) in the curie (right panel) and TCGA (left panel) cohorts. The respective sample numbers for each breast cancer subtype and for normal breast tissue are indicated on the graphs in both cohorts. The RNA quantifications were

logarithmically transformed (log<sub>2</sub>) and are presented as scatter plots, where each coloured closed circle corresponds to one sample. The mean RNA expression is represented by a black line. Statistical analysis was conducted using one-way ANOVA, yielding the following significance indicators: “ns” denotes not significant; \*p < 0.05; \*\*p<0.01; \*\*\*p < 0.001; \*\*\*\*p < 0.0001.

Next, to examine whether SDCCAG3 interacted with PRMT5, we transfected HEK293T cells with Flag-PRMT5 and GFP-SDCCAG3 followed by co-IP experiments. Immunoprecipitating Flag-PRMT5 using an anti-Flag antibody revealed the presence of GFP-SDCCAG3 in complex with Flag-PRMT5 (**Figure 13A**). Similarly, Flag-PRMT5 was detected in the GFP-SDCCAG3 IP (**Figure 13B**), validating that the two proteins precipitate together. Due to the absence antibodies capable to IP endogenous SDCCAG3, it was not possible to investigate the interaction between endogenous PRMT5 and SDCCAG3 by co-IP.

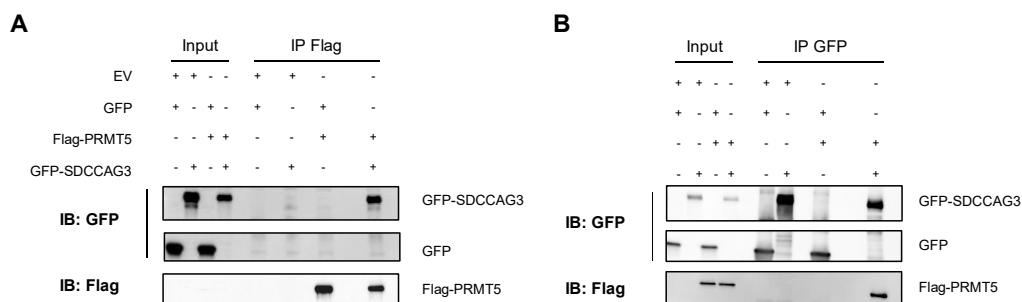


**Figure 13: PRMT5 and SDCCAG3 form a complex.** HEK293T cells were transfected with pcDNA 3.1-Flag-PRMT5 and/or with pcDNA 3.1-GFP-SDCCAG3 for 48 hours. Flag-PRMT5 was immunoprecipitated (A) using anti-Flag antibody and subsequent immunoblotting was performed first using anti-GFP (to visualize GFP-SDCCAG3), then using an anti-Flag antibody (to verify Flag-PRMT5 was indeed immunoprecipitated). Reciprocally, GFP-SDCCAG3 was immunoprecipitated using an anti-GFP antibody (B), followed by immunoblotting with anti-Flag and anti-GFP antibodies. Input samples consisted of 1% of total protein lysate. Images are representative of at least three independent experiments.

### ***SDCCAG3 potentially functions as a regulator of the Wnt pathway in TNBC***

As the Wnt signalling pathway is activated in TNBC and promotes its progression [102], our group previously investigated the modulation of the Wnt pathway within the context of TNBC [622,623]. Notably, our recent findings have revealed that PRMT1 positively regulates the Wnt pathway in MDA-MB-468 cells [234]. Among the numerous IP experiments followed by LC-MS/MS analysis performed in the laboratory,

SDCCAG3 was identified only when using an anti-LRP6 antibody (**Figure 14A**). This result suggested that SDCCAG3 may interact with the Wnt pathway receptor LRP6. First, we validated the interaction between LRP6 and SDCCAG3 by co-IP of ectopically expressed LRP6-Flag and GFP-SDCCAG3 in HEK293T cells (**Figure 14B**). IP of LRP6-Flag captured GFP-SDCCAG3, and conversely, IP of GFP-SDCCAG3 pulled down LRP6-Flag (**Figure 14B**). Since SDCCAG3 interacts with LRP6 (**Figure 14B**) and PRMT5 (**Figure 13**), we explored the potential interaction between PRMT5 and LRP6 (**Figure 14C**). Although not completely convincing, IP of PRMT5-GFP seemed to pulldown LRP6-Flag in HEK293T cells (**Figure 14B**).

Since SDCCAG3 has been reported to participate in the endocytosis of TNF and Fas receptors [620,621], we hypothesized that SDCCAG3 could control LRP6 trafficking, thereby impacting the Wnt pathway. To investigate the potential impact of SDCCAG3 on the Wnt pathway, we evaluated the expression of Wnt target genes through qPCR analysis following SDCCAG3 depletion in MDA-MB-468 cells (**Figure 14D**). We examined the expression of Wnt target genes that had been previously reported by our laboratory to be upregulated upon Wnt3a activation in MDA-MB-468 cells [623]. We found that SDCCAG3 depletion caused a decrease in the expression of *APCDD1* and *DDIT4L*, but not *NKD1* and *Axin2*, compared to the siRNA control condition (**Figure 14D**). LRP6 depletion was used as a positive control for the assay (**Figure 14D**). Intriguingly, we made an unexpected observation: when LRP6 was depleted, SDCCAG3 expression was also decreased, suggesting that the expression of SDCCAG3 itself could be regulated by the Wnt pathway.

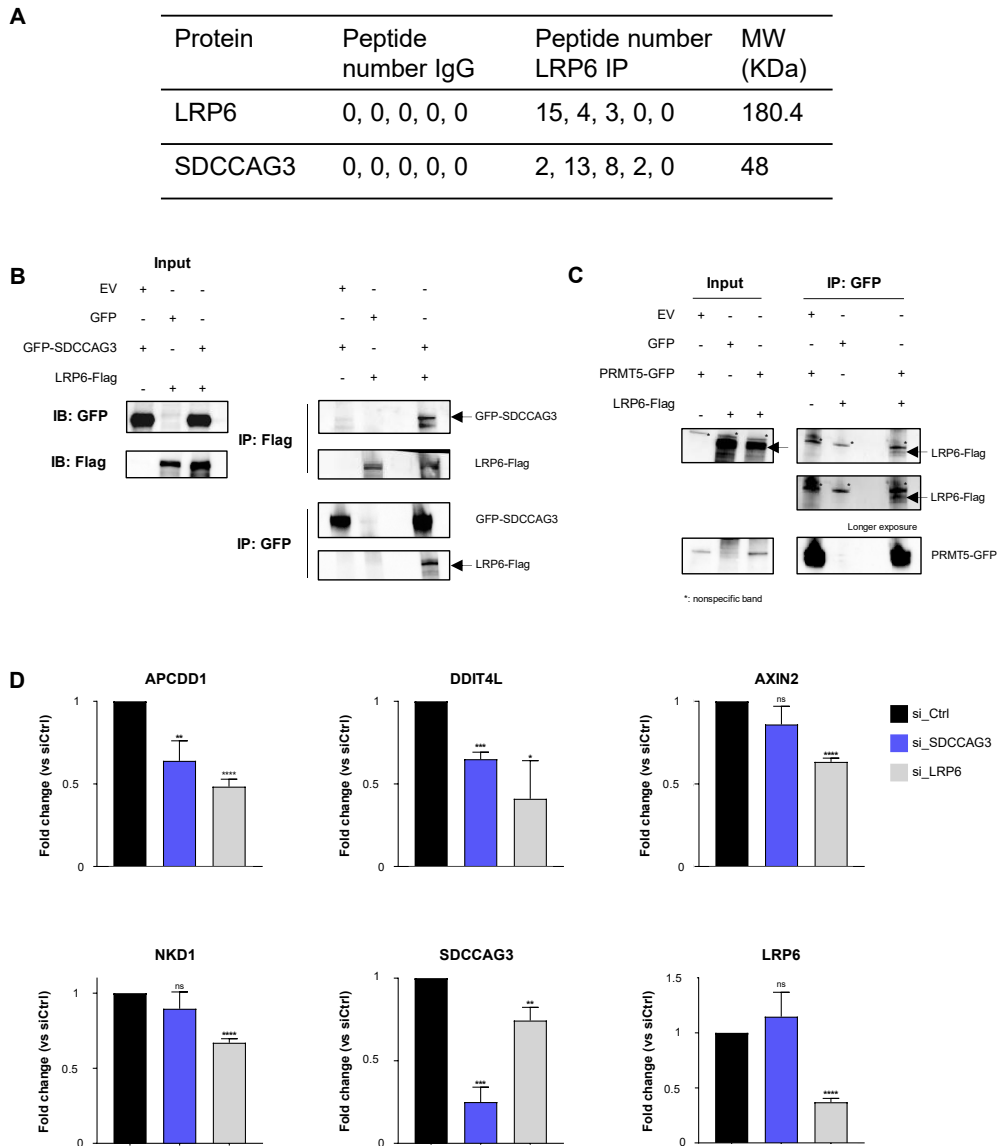


**Figure 14: SDCCAG3 interacts with LRP6 and regulates the Wnt pathway. (A).** Table including the number of LRP6 and SDCCAG3 peptides retrieved from LRP6 or IgG IP followed by LC-MS/MS. **(B, C).** Co-IP assays were conducted to explore the interactions between LRP6 and SDCCAG3 (B) or PRMT5 (C) in HEK293T cells. HEK293T cells were transfected with vectors encoding LRP6-Flag along with GFP-SDCCAG3 (B) or GFP-PRMT5 (C). IP was performed using anti-Flag or anti-GFP antibodies as indicated in the figure. Western blotting analysis was then performed using anti-Flag and anti-GFP antibodies. Input samples constituting 1% of the total protein lysate were loaded as controls. Images are representative of at least three independent experiments. **(D).** Impact of SDCCAG3 depletion on the expression of Wnt target genes in MDA-MB-468 cells. Cells were transfected with control siRNA (Ctrl), or with siRNA targeting SDCCAG3 or LRP6. After 48 hours, the cells were exposed to Wnt3a-conditioned media for 6h. qPCR was employed to determine the mRNA expression levels of the Wnt target genes, as well as *SDCCAG3* and *LRP6* as controls. The quantification is presented as a fold change relative to the control (siRNA control with Wnt3a), and the values are expressed as the mean  $\pm$  SD originating from three independent experiments. Statistical analysis was conducted employing the Student t-test, with significance levels (p-values) presented as \* $p < 0.05$ , \*\* $p < 0.01$ , \*\*\* $p < 0.001$ , and  $p > 0.05$  marked as ns (not significant).

***Among different PRMTs, SDCCAG3 interacts preferentially with PRMT5***

We tested whether SDCCAG3 could interact with other PRMT members, given the common occurrence of proteins interacting with or being methylated by various PRMTs. Through co-IP experiments, we found that SDCCAG3 interacts with PRMT5, PRMT1, PRMT3, and weakly with PRMT6, while no association was observed with PRMT4 (**Figure 15A,B**). However, it is important to note that Flag-PRMT5 is less expressed compared to the other Flag-PRMTs (lanes 4 and 7 in comparison to lanes 2, 3, 5, and 6 in the input samples). This reduced expression level of Flag-PRMT5 could potentially be attributed to a difficulty to ectopically express PRMT5 in cells, especially since it is always present in protein complexes. Another contributing factor might be the exclusive expression of PRMT5 without MEP50, as these two proteins mutually stabilize each other's expression levels. Altogether, these data suggest that SDCCAG3 interacts preferentially with PRMT5 among the tested PRMT members.

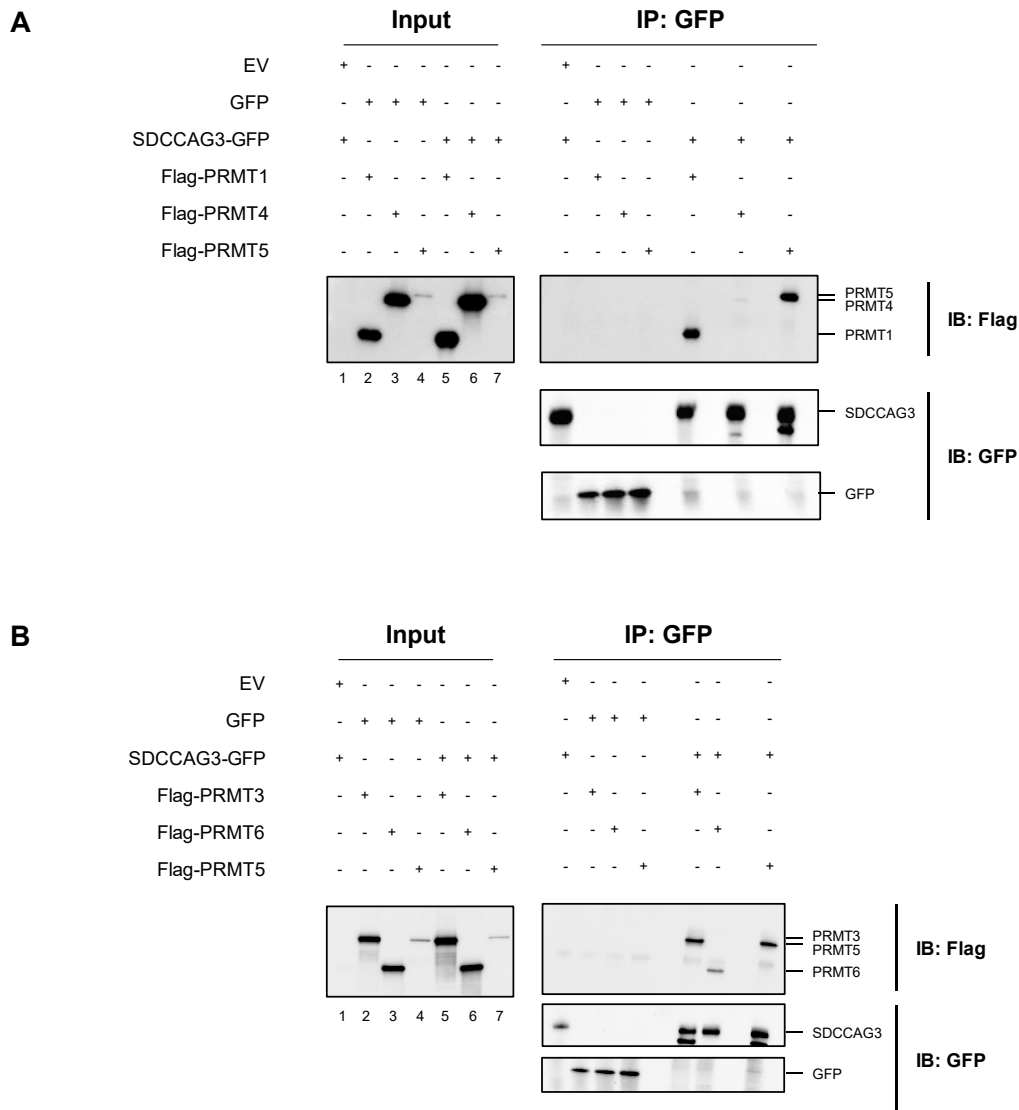


**Figure 15: Among different PRMTs, SDCCAG3 interacts preferentially with PRMT5.** HEK293T cells were transfected with pcDNA 3.1-Flag-PRMT and/or pcDNA 3.1-GFP-SDCCAG3 for 48 hours. GFP-SDCCAG3 was then immunoprecipitated using anti-GFP antibodies, followed by immunoblotting of the membranes with first anti-GFP then anti-Flag antibodies. Flag-PRMT5 was used as a positive control for the interaction between SDCCAG3 and a PRMT. Input samples constituting 1% of the total protein lysate were loaded as controls. Images are representative of three independent experiments.

### *Deciphering PRMT5 interactome by immunoprecipitation*

During our study, novel commercial anti-PRMT5 antibodies became available, Ab1 (ThermoFisher #PA5-78323), Ab2 (CST #79998), and Ab3 (Bethyl #A300-849A). We tested the abilities of Ab1, Ab2, Ab3, and an anti-PRMT5 antibody (Ab4) received from the team of Dr. Jocelyn Coté (University of Ottawa) to IP endogenous PRMT5 and found that Ab1 could efficiently pull down PRMT5 from MDA-MB-468 cells (**Figure 16A**). We then used Ab1 to IP endogenous PRMT5 from MDA-MB-468 cells and

identified the co-immunoprecipitated proteins by LC-MS/MS analysis (**Figure 16B**). We considered proteins with a ratio of peptide number retrieved in PRMT5 IP versus IgG >2 as enriched in PRMT5 IP (**Table S8**). Our analysis identified 82 proteins as potential PRMT5 interactors (**Table S8**), which included known PRMT5 partners like RIOK1 and MEP50 (**Figure 16B**; **Table S8**). The partners we retrieved were significantly enriched in proteins involved in actin organization, cell division, and RNA related processes such as pre-mRNA splicing and spliceosomal assembly (**Figure 16C**). Interestingly, the identified PRMT5 interactome includes network clusters of Golgi to ER transport, adherens junction, and Striatin family members (**Figure 17**), which are different than those identified for the MEP50 interactome, and PRMT5 partners identified by TurboID. One of the top novel potential PRMT5 partners was the DBIRD complex subunit, deleted in breast cancer 1 (DBC-1) also termed KIAA1967 (**Figure 16B**). The DBIRD complex is involved in the splicing regulation of exons present in AT-rich regions [624]. The interaction between endogenous PRMT5 and DBC-1 was confirmed by IP in MDA-MB-468 cells (**Figure 16D**). Remarkably, DBC-1 was found to be enriched in the PRMT5 IP sample compared to the input samples, similar to what is expected for MEP50 (**Figure 16D**). Interestingly, DBC-1 is also present in the interactome of FUBP1 (**Table S6**) but not in the MEP50 interactome (**Table 4 and 5**). Our data therefore (i) validated the success in efficiently immunoprecipitating endogenous PRMT5 for proteomic analysis, and (ii) identified DBC-1 as a novel PRMT5 partner.

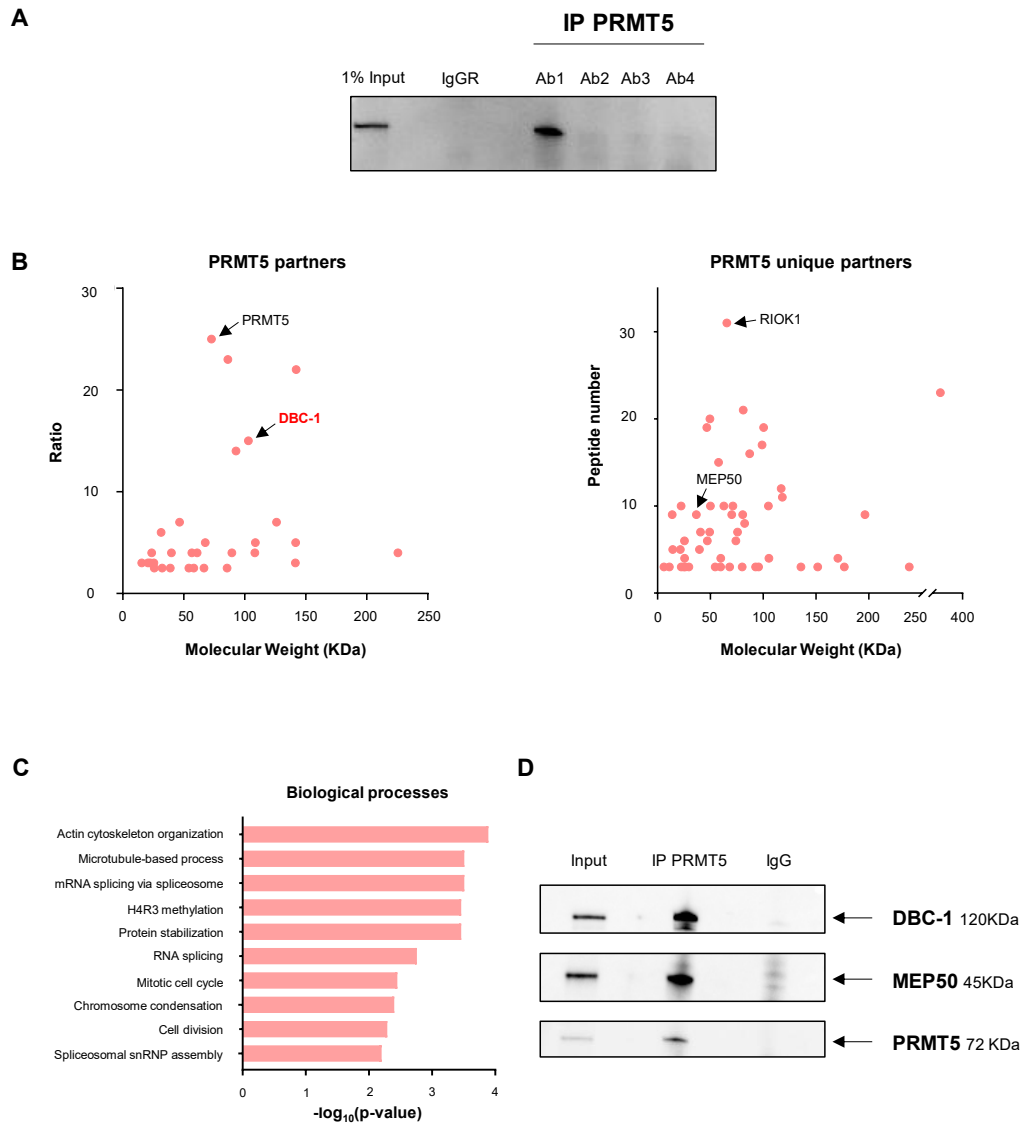


**Figure 16: Unveiling the PRMT5 interactome via endogenous PRMT5 IP in TNBC. (A).** Assessment of different PRMT5 antibodies for their ability to IP endogenous PRMT5. Endogenous PRMT5 was immunoprecipitated from MDA-MB-468 cells using four different anti-PRMT5 antibodies: Ab1 (Thermofisher #PA5-78323), Ab2 (CST #79998), Ab3 (Bethyl #A300-849A), and Ab4 (Jocelyn Coté). Immunoprecipitated samples were subsequently probed through Western blot analysis utilizing an anti-PRMT5 antibody (sc-376937; Table S1). Input samples constituting 1% of the total protein lysate were loaded as controls. **(B).** Representation of the PRMT5 interacting partners: peptide ratio versus molecular weight (KDa), or peptide number versus molecular weight (KDa) for unique PRMT5 partners (0 peptides in IgG). Each identified PRMT5 partner is visualized as an individual circle. **(C)** Analysis of Biological processes associated with the identified PRMT5 partners. GO analysis was performed using DAVID database (<https://david.ncifcrf.gov/>). **(D)** PRMT5 interacts with DBC-1. PRMT5 was immunoprecipitated using Ab1 from MDA-MB-468 cells and western blotting was performed using anti-DBC-1 antibodies. To validate the effectiveness of the IP, the presence of PRMT5 and its cofactor MEP50 was analysed. Input samples constituting 1% of the total protein lysate were loaded as controls.



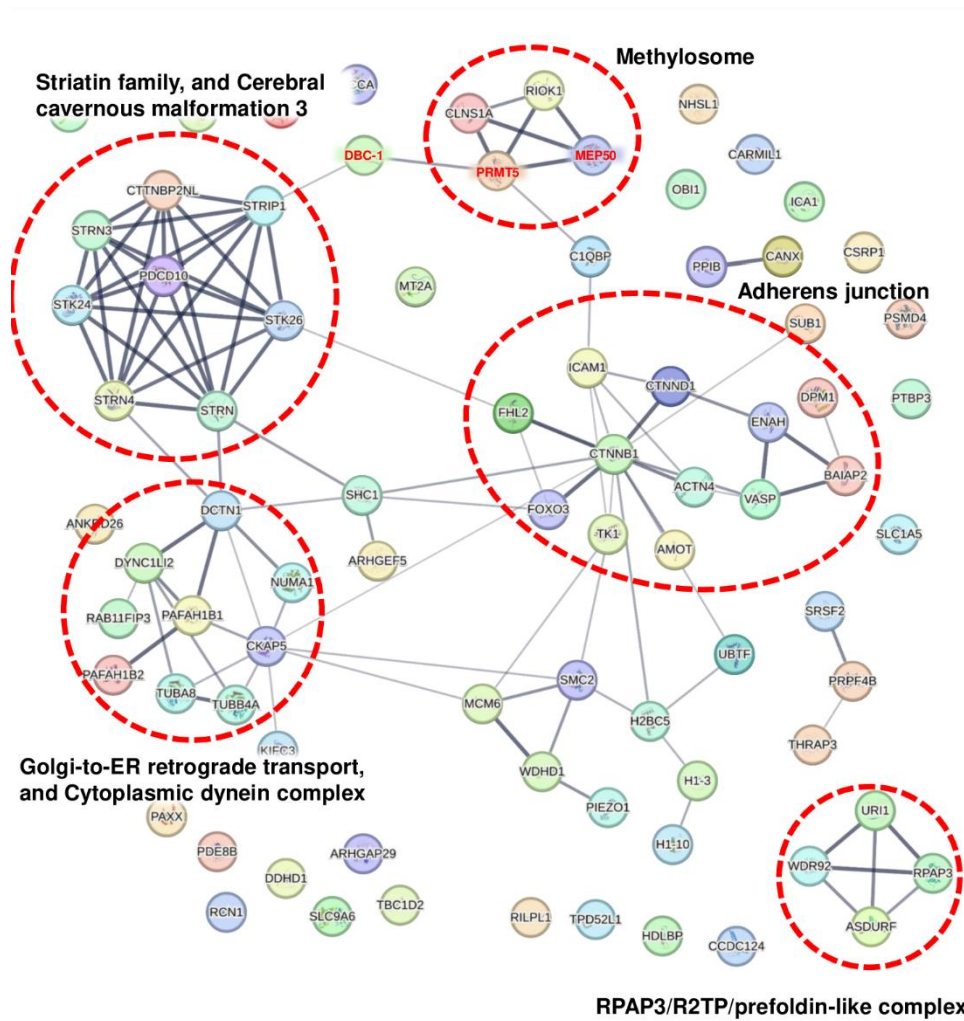


**Figure 17: Functional interactions among the 82 partners identified in PRMT5 IP.** Functional associations were determined using the STRING database (<http://string-db.org/>). Each node represents a protein, and the lines connecting the nodes represent an association between the two proteins.

## Discussion

PRMT5 is responsible of most of the arginine symmetric dimethylation marks in cells. Over the years, PRMT5 has been extensively studied in cancer development and progression, and evidence continues to emerge confirming its roles as an oncogenic driver.

In the breast, malignant tissues display higher levels of both PRMT5 mRNA and protein compared to their normal counterparts, a factor correlated with poor prognosis. The oncogenic role of PRMT5 in breast cancer is further supported by the decrease in cancer cells' growth, migration, and stemness upon PRMT5 depletion or inhibition [420,422,429,430,468–470]. Interestingly, the localization of PRMT5/MEP50 complex appears important and linked to cancer progression: high nuclear PRMT5/MEP50 expression associates with better prognosis in prostate, ovarian, and breast cancers [374,383,425–427,429,430,471,625]. Therefore, PRMT5 stands as an appealing therapeutic target, and small molecules targeting PRMT5 have been developed. Several PRMT5 inhibitors are undergoing evaluation in clinical trials [478], marking PRMT5 as the most studied PRMT in the clinical settings. Our laboratory has previously reported a link between high *PRMT5* mRNA expression levels and unfavourable prognosis in TNBC patients, the most aggressive breast cancer subtype, and specifically within the mesenchymal TNBC subtype [429,430]. At the protein level, we did not detect any significant difference in the expression of PRMT5 between normal and cancerous breast tissue. Instead, we observed variations in the intracellular localization of PRMT5 and MEP50 between cancer and healthy tissue. Both PRMT5 and MEP50 showed lower nuclear localization in TNBC compared to breast tumours of other subgroups and to normal breast tissue [429,430]. Accordingly, symmetrically dimethylation of Histone H4 on arginine 3 (H4R3me<sub>2</sub>s), a modification dependent on PRMT5, is predominantly observed in normal breast tissues and luminal A breast cancers [429]. Moreover, we found that inhibiting PRMT5 led to apoptosis in TNBC cell lines, reduced their stemness properties, and delayed tumour growth in a TNBC-derived PDX mice model [430]. We also found that combining a PRMT5 inhibitor with specific chemotherapies or EGFR/HER2 inhibitors yielded a synergistic effect in inhibiting the proliferation of TNBC cells [626]. Therefore, our findings support the idea that PRMT5 represents a promising therapeutic target for TNBC.

Subsequently, we opted to delve deeper into the molecular mechanisms governed by PRMT5 in TNBC cells.

### ***The PRMT5/MEP50 interactome***

To understand the molecular functions of PRMT5, we aimed to decipher the PRMT5 interactome in TNBC, and uncover potential PRMT5 partners that might contribute to its roles in TNBC oncogenesis. Although the PRMT5 methylome has been characterized in various models [127,132,133,147,410], little effort has been dedicated to unravelling the complete repertoire of PRMT5 partners. This could be due to the difficulty of immunoprecipitating PRMT5, as it is primarily located at the core of the octameric complex it forms with MEP50 [122]. In contrast, MEP50, which is present at the periphery of the PRMT5/MEP50 complex, can be efficiently immunoprecipitated. The MEP50 interactome in breast cancer cells has been previously reported [412]. In our study, we characterized the PRMT5 interactome by immunoprecipitating endogenous PRMT5 or MEP50 and by proximity labelling using TurboID-PRMT5, followed by LC-MS/MS.

The immunoprecipitation of MEP50 coupled with LC-MS/MS revealed a significant enrichment of RNA binding proteins among MEP50 partners, involved in biological processes related to translation and RNA processing. Employing a similar approach and the same anti-MEP50 antibody (Ab1; #A301-561A), Rengasamy *et al.* characterized both nuclear and cytoplasmic MEP50 partners in MDA-MB-231 cells following subcellular fractionation [412]. Surprisingly, most MEP50 partners were detected across both the nuclear and cytoplasmic compartments [412]. Consistent with our findings, the MEP50 interactome identified by Rengasamy *et al.* was enriched in proteins involved in RNA processing and pre-mRNA splicing. Seventeen proteins, mainly involved in RNA-related processes, were found in common between the two studies and are listed below (**Figure 18**).

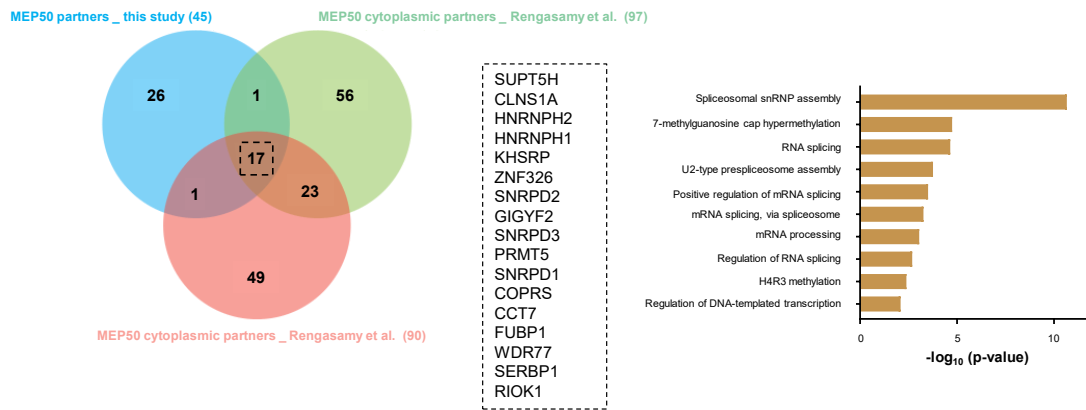


**Figure 18: MEP50 partners commonly identified in our study and Rengasamy et al.** [412]. A Venn diagram (right panel) illustrates the number of shared proteins among our study (MEP50 3 replicates; 45 proteins) and Rengasamy et al.'s work [412] (97 nuclear partners and 90 cytoplasmic partners). The 17 proteins found in common across all three sets are listed. Analysis of Biological processes (left panel) associated with the identified common partners. GO analysis was performed using DAVID database (<https://david.ncifcrf.gov/>).

Characterizing directly the PRMT5 interactome using a similar approach has been challenging due to the lack of commercially available antibodies capable of efficiently immunoprecipitating endogenous PRMT5. Previous attempts in the group, before my arrival in the laboratory, were unsuccessful due to this technical limitation. However, over the course of my thesis, additional anti-PRMT5 antibodies became available, and one of them proved suitable for PRMT5 immunoprecipitation. Similar to the MEP50 interactome, and as expected, the PRMT5 interactome was significantly enriched in RNA binding proteins and proteins involved in RNA processing, spliceosome, and translation. Indeed, the PRMT5/MEP50 complex plays a critical role in pre-mRNA splicing by symmetrically di-methylating Sm proteins, a modification crucial for their incorporation into the SMN complex, a pivotal step in spliceosome assembly [385,386]. Moreover, the PRMT5 methylome is known to be enriched in spliceosomal proteins and pre-mRNA splicing factors [127,132,133,147,410]. Depleting or inhibiting PRMT5 has been shown to induce global alterations in alternative splicing events [127,133]. Importantly, our analysis highlighted the involvement of pathways related to cytoskeleton organization and microtubule-related processes specifically associated with PRMT5 partners, not MEP50 partners. In a study on oligodendrocyte progenitor cells (OPC), PRMT5 immunoprecipitation was conducted using the antibody # ab109451 (Abcam) [411]. While this antibody was found by our team to be ineffective for PRMT5 immunoprecipitation from HCC38 cells (Table S3), Dansu et al.'s study identified over 1000 proteins as potential PRMT5 partners, primarily

involved in processes related to RNA binding, ribosomes, actin binding, GTPase activity, and cadherins [411]. When we compared the partners we identified in our LC-MS/MS experiment (Table S8) with those retrieved by Dansu *et al.* [411], we found only 20 proteins in common between both studies, that are involved in RNA-related processes, mitosis, and actin cytoskeleton (**Figure 19**).

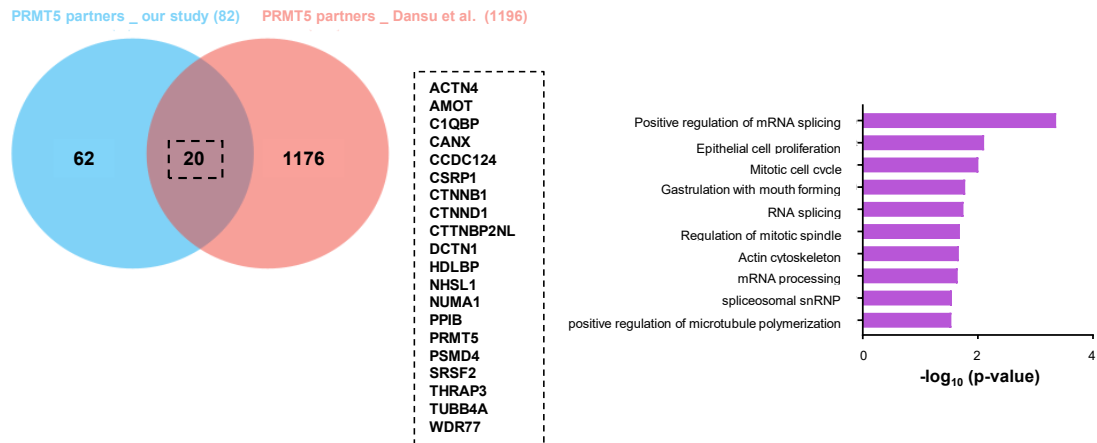


**Figure 19: PRMT5 potential interactors retrieved in common between our study and Dansu *et al.*** [411]. Venn diagram (right panel) showing the number of common proteins retrieved between our study (PRMT5 IP; 82 proteins) and Dansu *et al.* [411] (1196 proteins). The 20 common proteins between the two sets are listed. Analysis of Biological processes (left panel) associated with the identified common partners. GO analysis was performed using DAVID database (<https://david.ncifcrf.gov/>).

We identified distinct network clusters associated with the partners obtained from PRMT5 and MEP50 immunoprecipitations. While MEP50 partners were mainly found in the spliceosome and translation initiation complexes, PRMT5 partners were additionally present in protein transport complexes and adherens junctions. Surprisingly, only PRMT5, MEP50, RIOK1, and pICln (the methylosome components) were retrieved in common between the immunoprecipitations of PRMT5 and MEP50 (**Figure 20**). These findings suggest that PRMT5 and MEP50 may have distinct repertoires of partners and could have independent functions, beyond their roles within the hetero-octameric complex. Another explanation could be that MEP50 serves as an adaptor protein, bringing the substrates to be methylated by PRMT5. Consequently, the interactome of MEP50 may better represent PRMT5 substrates rather than direct interactors of PRMT5. Supporting this notion, the MEP50 partners we retrieved were enriched in RNA binding proteins, mainly present in the spliceosomal complex, and involved in RNA processing, mirroring the PRMT5 methylome identified in several studies [127,132,133,147,410]. Upon direct

investigation of the PRMT5 interactome through the immunoprecipitation of endogenous PRMT5 (our study and [411]), potential PRMT5 interactors were found to be involved not only in RNA-related processes, but also in activities related to actin and cytoskeleton organization, cadherin binding, and cell division. This suggests that PRMT5 may engage with other proteins, potentially outside the context of the PRMT5/MEP50 complex, to regulate additional cellular processes.

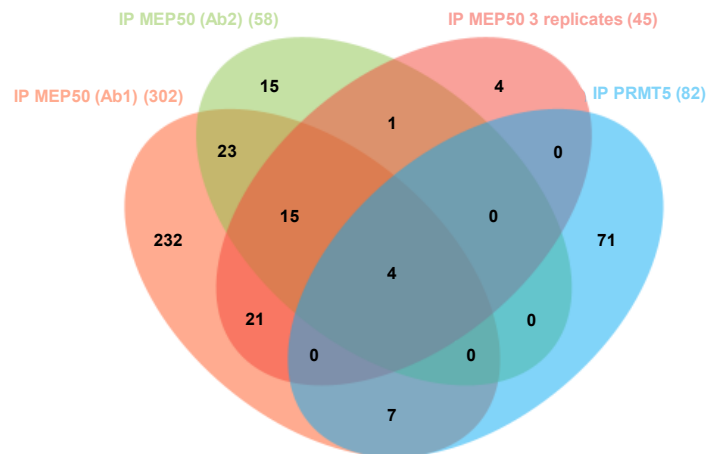


**Figure 20: Venn diagram illustrating the number of common proteins between PRMT5 and MEP50 immunoprecipitations identified in our study.**

In parallel, we characterized the PRMT5 interactome using an alternative method, TurboID proximity labelling coupled to LC-MS/MS analysis. TurboID, derived from BirA, is a bacterial biotin ligase that exhibits an accelerated biotinylation rate compared to BirA [612]. By creating a fusion protein of TurboID with PRMT5, we enabled the biotinylation of proteins in proximity (up to 35 nm) to PRMT5, including even transient interactions. The biotinylated proteins, considered as potential PRMT5 partners, were then captured using streptavidin beads and identified by LC-MS/MS analysis. We validated this proximity labelling approach by identifying established PRMT5/MEP50 interactors (**Table S7**) and uncovering numerous novel potential PRMT5 partners. The proteins identified through the TurboID method included components of the ER membrane, mitochondria, and intracellular transport machinery. They were also found in proteasomal complexes, desmosome junctions, centrosome cycle, and participated in various biological processes such as endocytosis, protein transport, cell division, and metabolic processes. A similar approach using BioID, another biotin ligase but with a slower biotinylation rate (~16 hours) compared to TurboID, was recently

employed to reveal the interactome of all nine PRMTs in HEK293T cells [130]. By comparing their study (BioID) and ours (TurboID), only 21 proteins were found in common (**Figure 21A**), including PRMT5 and MEP50, and are involved in spliceosomal assembly and mRNA splicing (**Figure 21A**). Although TurboID and BioID employ the same concept of proximity labelling, the biotinylation rate is highly different between both (10 minutes for TurboID compared to 16 hours for BioID), that could explain the low number of common partners identified between our study and Wei *et al.* Compared to the partners we identified by immunoprecipitating PRMT5, we found 15 proteins in common with those retrieved in the BioID study (**Figure 21B**), mainly functioning in spliceosomal assembly, pre-mRNA splicing, transcription, and cell adhesion (**Figure 21B**).

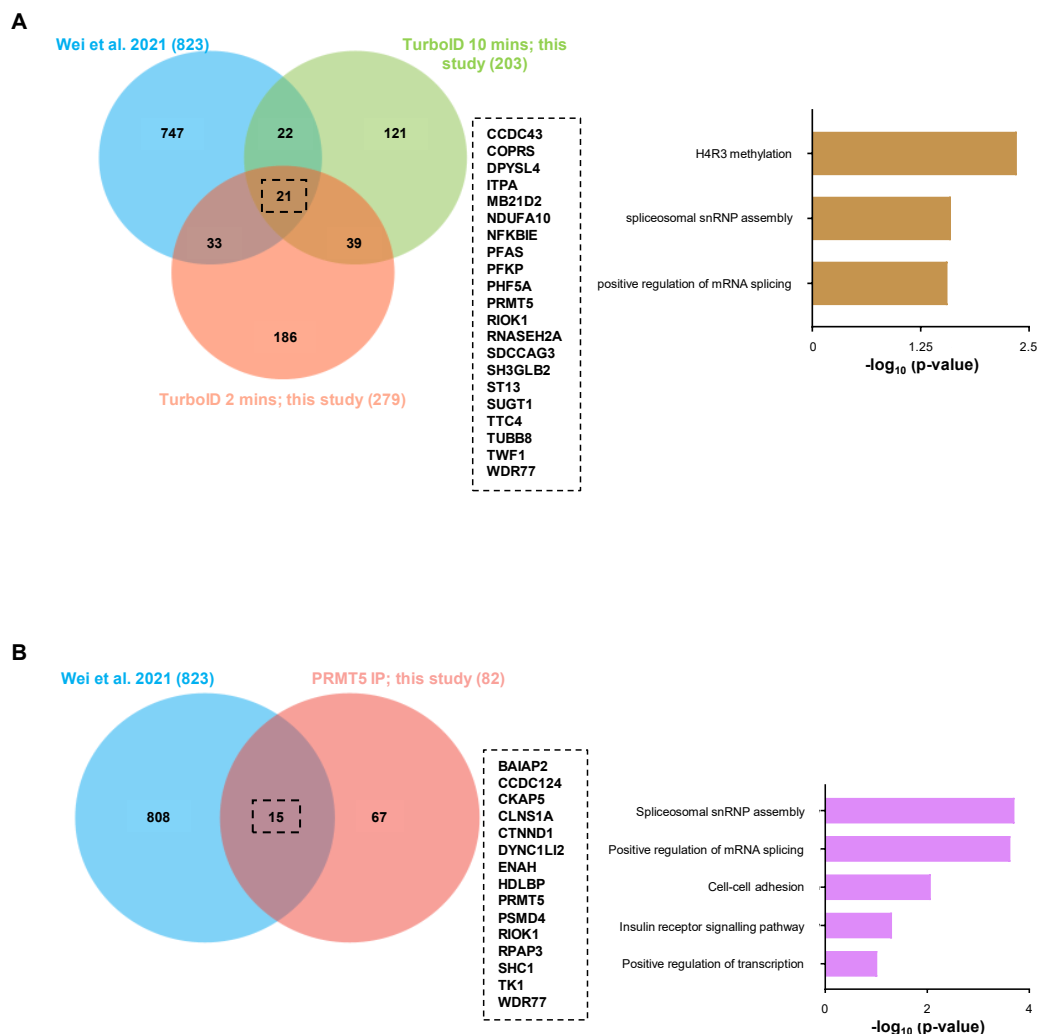


**Figure 21: PRMT5 potential interactors retrieved in common between our study and Wei *et al.* [130]. (A).** Venn diagram (right panel) illustrating the number of common proteins between our study (TurboID, 2 minutes and 10 minutes; 279 and 203 proteins, respectively) and Wei *et al.* (BioID; 823 proteins) [130]. The 21 common proteins across all three sets are listed. Analysis of Biological



processes (left panel) associated with the identified common partners. GO analysis was performed using DAVID database (<https://david.ncifcrf.gov/>). **(B)**. Venn diagram (right panel) showing the number of common proteins retrieved between our study (PRMT5 IP; 82 proteins) and Wei *et al.*'s study (BioID; 823 proteins) [130]. The 15 common proteins between the two sets are listed. Analysis of Biological processes (left panel) associated with the identified common partners. GO analysis was performed using DAVID database (<https://david.ncifcrf.gov/>).

Between the proteins identified through endogenous PRMT5 immunoprecipitation and TurboID, only 5 proteins were found in common (**Figure 22**), which included PRMT5, MEP50, and RIOK1. The other two common proteins were intercellular adhesion molecule 1 (ICAM1) and Rho GTPase-activating protein 29 (ARHGAP29). The substantial difference in the retrieved PRMT5 partners using the two methods could be attributed to several factors. Firstly, it may stem from the concept of the techniques themselves. Immunoprecipitation typically captures stable protein-protein interactions and may not be suitable for detecting transient interactions. In contrast, proximity labelling with TurboID has the capacity to pulldown transiently interacting proteins due to its rapid labelling kinetics. A second possible factor could be related to conformational changes caused by fusing TurboID to the N-terminus of PRMT5 or by the antibody binding to the central domain of PRMT5, which could interfere with protein-protein interactions. Another possibility would be the transient transfection of TurboID-PRMT5, leading to its expression in levels distinct to the endogenous protein that could affect partners identification. Indeed, it was shown that the endogenous tagging of TurboID to the AP-1 complex subunit identified interactors of the complex that simple overexpression of the enzyme could not [627]. Additionally, the choice of the cell lines used for each technique could have played a role. Since the TurboID method was not previously employed in the laboratory, we first optimized the protocol using HEK293T cells that are easy to transfect. Conversely, a TNBC cell line, MDA-MB-468, was chosen for partner identification using endogenous PRMT5 immunoprecipitation. Finally, false positives retrieved by the TurboID method might have contributed to the differences between the two approaches. With TurboID, a protein that is not a genuine PRMT5 interactor, but happens to be within the biotinylation radius of TurboID-PRMT5 (more than 35 nm [616]), will be biotinylated and captured, leading to potential false positive identification.



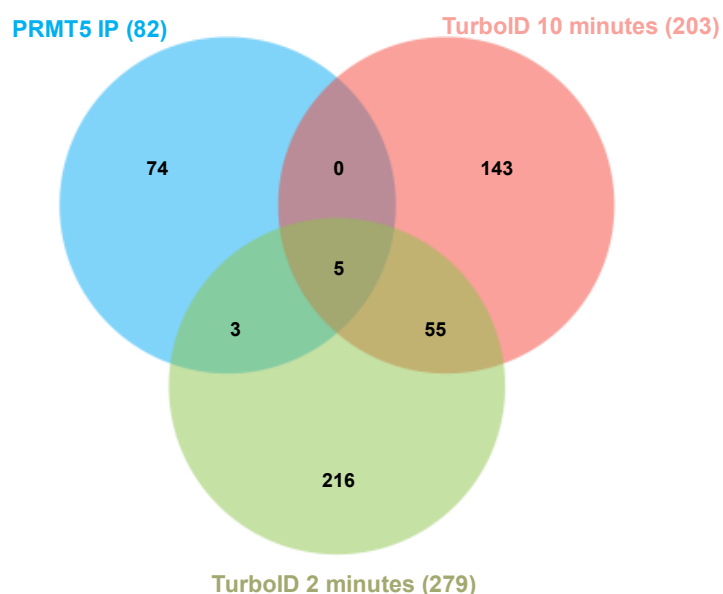


**Figure 22: Venn diagram illustrating the overlapped proteins identified through PRMT5 endogenous immunoprecipitation (IP) and the TurboID method identified in our study.**

### ***Functional analysis of PRMT5/MEP50 interaction with novel partners***

We identified FUBP1, a protein involved in RNA processing and transcription, as a top hit among MEP50's potential novel interactors. Notably, FUBP1 and FUBP2 (KHSRP) were identified as MEP50 partners by us and in both nuclear and cytoplasmic compartments by Rengasamy *et al.* [412] (**Figure 18**). This suggests a potential functional association between the FUBP members and the PRMT5/MEP50 complex. Indeed, the STRING analysis performed on the MEP50 partners revealed that the FUBP members are present in the same complex with both PRMT5 and MEP50 (**Figure 2**). FUBP1 comprises four KH domains giving it the ability to bind to ssDNA and RNA [499]. It was initially discovered as a protein that binds to the FUSE DNA element located 1.5 kb upstream of the oncogene *MYC* promoter [496]. The interaction between FUBP1 and the FUSE element, as well as the FUBP1-mediated activation of *MYC* transcription, are well characterized [496,531,547–549]. Large-scale proteomic analyses of the arginine methylome revealed that FUBP1 can be mono- and dimethylated on arginine located at positions R359, R361, and R363 [106,128,134,141–144,146,377,411,527]. These post-translational modifications lie within a “GRG” motif, which PRMT5 prefers, between the third and fourth KH domains of FUBP1. Interestingly, FUBP2 and FUBP3 are also predicted to be mono- and di-methylated on three arginines located in the same position as in FUBP1, between KH3 and KH4

domains [106,128,134,141–144,146,377,411,527]. This suggests that methylation of arginine residues between the KH3 and KH4 domains may regulate the functions of FUBP members. We first showed that PRMT5 symmetrically di-methylates FUBP1 in MDA-MB-468 cells, and confirmed that the three predicted arginine residues, R359, R361, and R363, are the main methylation sites within FUBP1 central domain *in vitro*. In accordance with our observations, FUBP1 was identified in proteomic analysis specifically identifying the PRMT5 methylome as a potential PRMT5 substrate [133,147], and Gerhart *et al.* have shown a decrease in the methylation of a small peptide derived from FUBP1 (aa 349-369) which includes the three potential methylation sites upon the inhibition of PRMT5 [410]. A recent study showed that FUBP1 and its close family member FUBP3 are symmetrically di-methylated in HT1080 fibrosarcoma cell lines and this methylation decreases upon the addition of MTA, previously reported to inhibit PRMT5 activity [525]. However, the study did not ascertain the specific methylation sites on FUBP1, nor did it validate PRMT5 as the enzyme responsible for its methylation. The same study revealed that adding MTA decreased the transcription of GFP using a reporter plasmid containing the FUSE element [525]. However, the authors did not provide evidence that the transcriptional regulation of the reporter plasmid is FUBP dependent, nor did they demonstrate a direct link between the decrease in GFP transcription and a decrease in FUBPs methylation levels [525]. However, this observation suggests that the methylation of FUBPs could participate to their transcriptional activity. Using FIDA, we found that the central DNA binding domain of FUBP1 exhibits reduced binding efficiency to FUSE when the arginine residues at positions R359, R361, and R363 are substituted with lysine, reflected by an increased dissociation constant between the triple lysine mutant domain and FUSE. While our findings do not establish that FUBP1 methylation directly enhances its binding to FUSE, they do demonstrate the involvement of these three arginine residues in the association between FUBP1 and FUSE, as modifications to these residues lead to a weakening of the interaction. Using ChIP-qPCR, we confirmed that symmetric dimethylation of FUBP1 enhances its interaction with FUSE. Notably, upon inhibiting PRMT5 with doses resulting in a reduction in FUBP1 SDMA levels (**Figure 5C**), we observed a decrease in FUBP1 enrichment on the FUSE element in MDA-MB-468 cells. When we investigated the expression of FUBP1 in TNBC, we found that its mRNA levels are elevated in TNBC tumour samples compared to normal breast tissue, and its depletion using siRNA reduces the

proliferation of MDA-MB-468 cells. Similar to our findings, a study reported that FUBP1 protein levels are higher in breast cancer tissue compared to the normal breast, and FUBP1 knockdown in the TNBC cell line MDA-MB-231 reduces proliferation and colony formation, downregulates the expression of matrix metalloproteinase 2 thus decreasing migration, and increases the sensitivity of MDA-MB-231 cells to cisplatin treatment [583]. We have recently reported a synergistic interaction between PRMT5 inhibition and cisplatin in TNBC cell lines [626], especially in MDA-MB-468 cells that overexpress FUBP1.

In MDA-MB-231 cells, Rengasamy *et al.* identified the splicing regulator ZNF326 as a main MEP50 partner and showed it is a PRMT5 substrate [412]. ZNF326 is part of the DBIRD complex which regulates the splicing of AT-rich exons and consists of ZNF326 and the protein DBC-1 [624]. Although we did not identify ZNF326 in our PRMT5 interactome, we retrieved DBC-1 as a main PRMT5 partner and validated the interaction in MDA-MB-468 cells (**Figure 16**). An investigation into protein-protein interaction network among spliceosomal proteins using yeast two-hybrid system also found that PRMT5, and not MEP50, associates with DBC-1 [628]. DBC-1 was not found when searching for MEP50 partners (our study and [412]).

Using the TurboID method, we identified SDCCAG3 (also known as ENTR1) as a novel PRMT5 partner. This finding was consistently observed across different experimental setups, underscoring the strength of this association. SDCCAG3 was also identified as a potential PRMT5 partner using the BioID method in two different studies (**Figure 21**; [130,629]). Importantly, they also reported that SDCCAG3 specifically interacted with PRMT5, and not with the other PRMTs [130,629]. The later study identified 8 potential PRMT5 partners that were in common with our TurboID analysis (CCDC43, COPRS, HERC1, PRMT5, RIOK1, RNASEH2A, **SDCCAG3**, WDR77) [629]. While BioID and TurboID approaches consistently identified SDCCAG3 as a robust PRMT5 interactor of PRMT5 (our study and [130,629]), we did not detect SDCCAG3 following immunoprecipitation of PRMT5 or MEP50. Nevertheless, co-immunoprecipitation experiments confirmed that SDCCAG3 associates with PRMT5, and more efficiently with PRMT5 compared to other PRMTs.

Remarkably, among numerous immunoprecipitation experiments coupled to MS analysis, SDCCAG3 was additionally found as a potential LRP6 partner. LRP6 is a

receptor of the Wnt/ $\beta$ -catenin signalling pathway that is activated in TNBC and correlates with poor clinical outcomes, by regulating key processes like migration, proliferation, chemoresistance, and sustaining BCSCs [102,622,623]. Frizzled receptors and LRP5/6 were shown to be deregulated in TNBC, and to play key roles in TNBC proliferation, metastasis, stemness, and chemoresistance [102]. LGK974 is a small molecule that inhibits Wnt signalling and is being clinically evaluated for TNBC treatment (NCT01351103). We confirmed by co-IP the interaction between LRP6 and both SDCCAG3 and PRMT5 in HEK293T cells. Our experiments also demonstrated that depleting SDCCAG3 from MDA-MB-468 cells resulted in the decreased expression of certain Wnt target genes, suggesting that SDCCAG3 has the capacity to activate the Wnt pathway. Interestingly, in bone marrow mesenchymal stem cells (BMSCs), the expression levels of LRP5, LRP6, Wnt5a, Wnt5b, and  $\beta$ -catenin positively correlated with the expression of SDCCAG3 [630]. PRMT5 also regulates the Wnt pathway through diverse mechanisms. PRMT5 activates the Wnt/ $\beta$ -catenin pathway in hematopoietic, liver, laryngeal, and breast cancer [631–635], by silencing the expression of different pathway inhibitors like *DVL3*, *Axin2*, *WIF1*, *DKK1*, and *DKK3* [631,632,635]. In laryngeal carcinoma, PRMT5 activates the Wnt pathway promoting laryngeal cancer cells proliferation and migration, and lymphatic metastasis *in vivo* [634]. Through COPRS, PRMT5 and  $\beta$ -catenin are recruited to the promoter of *Dlk-1* inhibiting its transcription and regulating adipogenesis [395]. It is therefore conceivable that the PRMT5/SDCCAG3 interaction could modulate Wnt pathway activation, albeit the precise mechanism behind this effect remains to be explored.

## Supplementary data

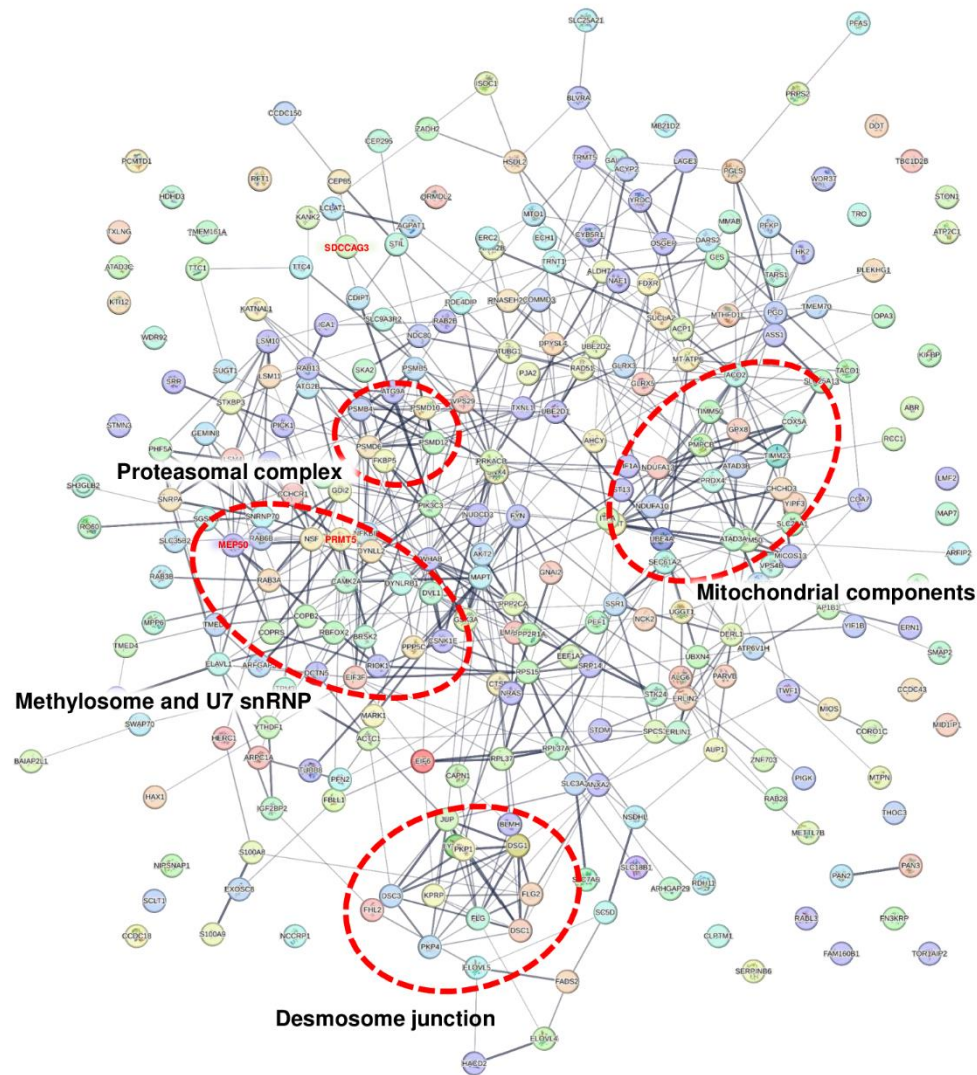


**Figure S1: Functional interactions among the PRMT5 neighbouring proteins identified with TurboID-PRMT5 for 2 minutes biotinylation.** Functional associations were determined using the STRING database (<http://string-db.org/>). Each node represents a protein, and the lines connecting the nodes represent an association between the two proteins.

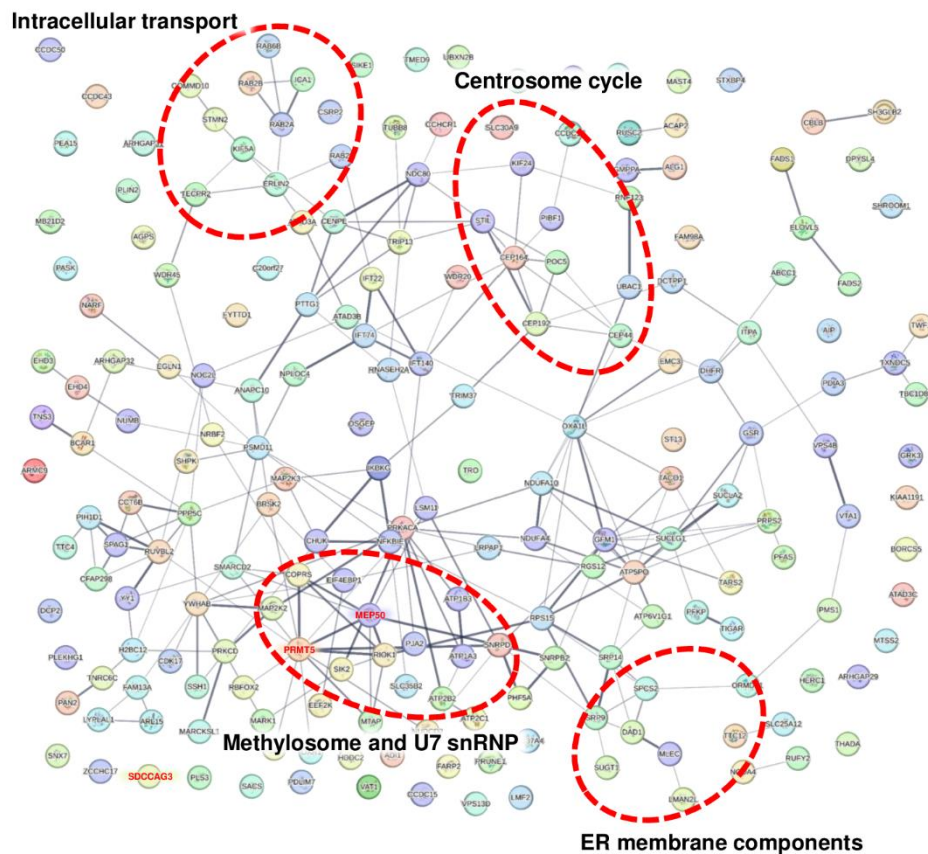


**Figure S2: Functional interactions among the PRMT5 neighbouring proteins identified with TurboID-PRMT5 for 10 minutes biotinylation.** Functional associations were determined using the STRING database (<http://string-db.org/>). Each node represents a protein, and the lines connecting the nodes represent an association between the two proteins.

**Table S1: List of antibodies used in the study**

Target	Supplier	Reference	Application
PRMT5	Thermofisher	PA5-78323	IP, MS
PRMT5	Santa-Cruz Biotechnology	sc-376937	WB
PRMT5	Sigma- Aldrich	07-405	WB
SDMA	Cell Signaling Technology	13222	WB
MEP50	Bethyl	A301-561A	IP, MS
MEP50	Bethyl	A301-562A	IP, MS
FUBP1	Abcam	ab181111	IP, MS, ChIP
FUBP1	Novus Biologicals	NBP2-59448	WB
Flag	Sigma-Aldrich	F3165	IP, WB, IF
GFP	Institut Curie	A-P-R#06	IP, WB
LRP6	Cell Signaling Technology	2560	IP, MS, WB
GAPDH	Cell Signaling Technology	2118	WB
Actin	Sigma- Aldrich	A5441	WB

IF: immunofluorescence; IP: immunoprecipitation; MS: mass spectrometry; WB: western blot.

**Table S2: List of DNA oligos used in the study**

Oligo	Target	Sequence (5' - 3')	Application
pcDNA3,1 (+)_R	pcDNA	AAGCTTAAGTTTAAACGCTAGCCA	Cloning
Flag_pcDNA3,1 (+)_F	pcDNA	GATTACAAGGACGACGACGATAAGTGACTCGAGTCTAGAGG GCCCGTT	Cloning
pcDNA3,1_LRP6_F	LRP6	TGGCTAGCGTTTAAACTTAAGCTTATGGGGGCCGTCCTGAG G	Cloning
Flag_LRP6_R	LRP6	AACGGGCCCTCTAGACTCGAGTCACTTATCGTCGTCGTCCTT GTAATC	Cloning
KH1 HindIII F	FUBP1	GCGCAAGCTTGGAACACAGTTACCACCGATG	Cloning
KH3 HindIII F	FUBP1	GCGCAAGCTTTTCAGAGAAGTTCGGAATGAGTATG	Cloning
KH4 XhoI R	FUBP1	GCGCCTCGAGTTACCCTAAAGGATTTACTGGGCC	Cloning
TurboID F	TurboID	TTCATGGACTACAAAGACGATGACGACAAGGCTAGCAAAGAC AATACTGTGCC	Cloning
TurboID R	TurboID	CCCACCAGCACCCCGACCGCCATCGCCGCCTCGAGCTTTT CGGCAGACCGCAGAC	Cloning
Flag-PRMT5 F	pcDNA PRMT5	Flag-CTCGAGGCGGCGATGGCGGTGGGGG	Cloning
Flag-PRMT5 R	pcDNA PRMT5	Flag-CTTGTCGTCATCGTCTTTGTAG	Cloning
pcDNA-Flag-PRMT5 F	pcDNA PRMT5	Flag-CTAGAGGGCCCCGTTTAAACC	Cloning
pcDNA-Flag-PRMT5 R	pcDNA PRMT5	Flag-CTTGTCGTCATCGTCTTTG	Cloning
PRMT1 F	PRMT1	CATGGACTACAAAGACGATGACGACAAGATGGCGGCAGCCG AGGCC	Cloning
PRMT1 R	PRMT1	GATCAGCGGGTTTAAACGGGCCCTCTAGATCAGCGCATCCG GTAGTCGG	Cloning
FUBP1 F	FUBP1	GTGGACCTGGACCTGGTGGTAAAGGAAAAGGTAAAGGTCAA GGCAACTG	Mutagenesis
FUBP1 R	FUBP1	CAGTTGCCTTGACCTTTACCTTTTCTTTACCACCAGGTCCA GGTCC	Mutagenesis
TurboID-PRMT5 F	TurboID-PRMT5	GCCGAAAAGCTCGAATAGGCGATGGCGGTC	Mutagenesis
TurboID-PRMT5 R	TurboID-PRMT5	GACCGCCATCGCCTATTTCGAGCTTTTCGGC	Mutagenesis

**Table S3: List of proteins retrieved from PRMT5 MS using antibody #ab109451**

Protein ID	Gene	Enrichment ratio	p-value	MW (KDa)
A0FGR8	ESYT2	2.98	$1.48 \times 10^{-11}$	102.4
O14744	PRMT5	24.69	$1.42 \times 10^{-05}$	72.7
O60869	EDF1	3.38	$1.00 \times 10^{-03}$	16.4
P62314	SNRPD1	2.92	$1.20 \times 10^{-03}$	13.3
P62316	SNRPD2	2.40	$4.83 \times 10^{-03}$	13.5
Q9NYU2	UGGT1	6.74	$5.22 \times 10^{-03}$	177.2
P22314	UBA1	3.08	$1.00 \times 10^{-02}$	117.8

**Table S4: List of proteins retrieved from MEP50 MS (in 3 replicates)**

Protein ID	Gene	Ratio	Adj. p-value	MW (kDa)	Peptide number per 100 aa
O00423	EML1	NA	NA	89.90	3.93
P63162	SNRPN	NA	NA	24.60	3.75
Q8WXE0	CASKIN2	NA	NA	126.80	0.75
Q96AE4	FUBP1	NA	NA	67.60	8.54
Q96CU9	FOXRED1	NA	NA	53.80	3.70
Q9NQ92	COPRS	NA	NA	20.10	5.98
P54105	CLNS1A	796.19	$5.09 \times 10^{-06}$	26.20	
O14744	PRMT5	583.94	$1.54 \times 10^{-44}$	72.70	
Q9BQA1	WDR77	290.55	$7.25 \times 10^{-21}$	36.70	
P62314	SNRPD1	111.41	$4.24 \times 10^{-19}$	13.30	
P62318	SNRPD3	104.38	$1.12 \times 10^{-09}$	13.90	
P62316	SNRPD2	61.19	$7.77 \times 10^{-20}$	13.50	
Q9BRS2	RIOK1	45.20	$6.86 \times 10^{-37}$	65.60	
Q9BST9	RTKN	21.26	$5.42 \times 10^{-16}$	62.70	
O95071	UBR5	15.83	$1.53 \times 10^{-133}$	309.40	
O95163	ELP1	11.76	$5.72 \times 10^{-49}$	150.30	
O00267	SUPT5H	10.11	$1.60 \times 10^{-11}$	121.00	
Q7L099	RUFY3	9.31	$9.34 \times 10^{-07}$	53.00	
Q9H4M7	PLEKHA4	9.30	$5.59 \times 10^{-10}$	85.40	
Q99832	CCT7	8.56	$3.27 \times 10^{-51}$	59.40	
Q9UQ35	SRRM2	7.79	$1.36 \times 10^{-62}$	299.60	
Q9NYV4	CDK12	6.23	$1.03 \times 10^{-14}$	164.20	
Q16204	CCDC6	5.69	$4.58 \times 10^{-43}$	53.30	
P55795	HNRNPH2	5.53	$2.70 \times 10^{-17}$	49.30	
P46013	MKI67	5.31	$2.17 \times 10^{-19}$	358.70	
P31943	HNRNPH1	5.09	$6.90 \times 10^{-36}$	49.20	
O15164	TRIM24	5.03	$1.56 \times 10^{-10}$	116.80	
O60841	EIF5B	4.93	$5.67 \times 10^{-80}$	138.80	
O60573	EIF4E2	4.76	$1.93 \times 10^{-11}$	28.40	
Q92945	KHSRP	4.54	$1.68 \times 10^{-29}$	73.10	
O00401	WASL	4.21	$1.65 \times 10^{-03}$	54.80	
Q86TB9	PATL1	3.85	$1.30 \times 10^{-11}$	86.90	
Q8NC51	SERBP1	3.83	$3.03 \times 10^{-40}$	45.00	
Q6Y7W6	GIGYF2	3.78	$8.09 \times 10^{-15}$	150.10	
Q5BKZ1	ZNF326	3.77	$3.92 \times 10^{-14}$	65.70	
Q8TBC3	SHKBP1	3.42	$1.23 \times 10^{-11}$	76.30	
Q9H0K1	SIK2	3.35	$2.73 \times 10^{-04}$	103.90	
P49454	CENPF	3.30	$1.56 \times 10^{-02}$	367.80	
P52701	MSH6	2.71	$3.52 \times 10^{-18}$	152.80	
Q9Y597	KCTD3	2.62	$4.89 \times 10^{-05}$	89.00	
P02768	ALB	2.37	$1.23 \times 10^{-04}$	69.40	
Q04637	EIF4G1	2.21	$6.49 \times 10^{-69}$	175.50	
Q8IY67	RAVER1	2.10	$5.35 \times 10^{-04}$	63.90	
O94906	PRPF6	2.08	$8.44 \times 10^{-17}$	106.90	
O95985	TOP3B	2.06	$3.83 \times 10^{-05}$	96.70	



**Table S5: List of common proteins retrieved from MEP50 IP using Ab1 and Ab2**

Protein ID	Protein	# Peptide in IgG	# Peptide in MEP50 IP Ab1	Ratio MEP50 Ab1/IgG	IP	# Peptide in MEP50 IP Ab2	Ratio MEP50 Ab2/IgG	IP	MW (KDa)
Q08AD1	CAMSAP2	-	3	NA		3	NA		168.1
P48643	CCT5	-	7	NA		8	NA		59.7
Q9NQ92	COPRS	-	4	NA		4	NA		20.1
Q96AE4	FUBP1	-	18	NA		18	NA		67.6
Q6Y7W6	GIGYF2	-	6	NA		8	NA		150.1
Q96KK5	H2AC12	-	4	NA		4	NA		13.9
P02042	HBD	-	6	NA		6	NA		16.1
P55795	HNRNPH2	-	17	NA		17	NA		49.3
P31942	HNRNPH3	-	4	NA		5	NA		36.9
Q6PKG0	LARP1	-	10	NA		4	NA		123.5
Q9Y4Z0	LSM4	-	5	NA		5	NA		15.3
P26038	MSN	-	7	NA		3	NA		67.8
P13674	P4HA1	-	4	NA		30	NA		61.0
Q86TB9	PATL1	-	6	NA		4	NA		86.9
O14744	PRMT5	-	84	NA		74	NA		72.7
Q9BRS2	RIOK1	-	42	NA		37	NA		65.6
O15027	SEC16A	-	18	NA		12	NA		233.5
P62316	SNRPD2	-	15	NA		16	NA		13.5
P63162	SNRPN	-	22	NA		21	NA		24.6
O00267	SUPT5H	-	16	NA		19	NA		121.0
Q9BQA1	WDR77	-	30	NA		29	NA		36.7
Q04917	YWHAH	-	4	NA		3	NA		28.2
Q9UPT8	ZC3H4	-	3	NA		3	NA		140.3
Q5BKZ1	ZNF326	-	4	NA		8	NA		65.7
P14678	SNRPB	1	25	25.00		24	24.00		24.6
O94906	PRPF6	1	24	24.00		10	10.00		106.9
P54105	CLNS1A	1	18	18.00		16	16.00		26.2
P62318	SNRPD3	1	14	14.00		14	14.00		13.9
P31943	HNRNPH1	4	33	8.25		29	7.25		49.2
P78371	CCT2	1	8	8.00		4	4.00		57.5
Q99832	CCT7	3	24	8.00		22	7.33		59.4
Q96I24	FUBP3	1	8	8.00		7	7.00		61.6
Q13435	SF3B2	2	16	8.00		5	2.50		100.2
P62314	SNRPD1	1	8	8.00		7	7.00		13.3
P38159	RBMX	1	6	6.00		3	3.00		42.3
Q8WUP2	FBLIM1	1	4	4.00		5	5.00		40.7
Q92945	KHSRP	3	12	4.00		8	2.67		73.1
P62304	SNRPE	1	4	4.00		3	3.00		10.8
O95633	FSTL3	1	3	3.00		4	4.00		27.7
Q13547	HDAC1	1	3	3.00		3	3.00		55.1
Q14739	LBR	1	3	3.00		3	3.00		70.7
P50990	CCT8	3	8	2.67		9	3.00		59.6

NA: not applicable

**Table S6: List of proteins retrieved from FUBP1 IP (in 5 replicates)**

Gene	Ratio	Adj. p-value	MW (KDa)	Peptide number per 100 aa
ANXA11	NA	NA	54.40	14.46
ARID1A	NA	NA	242.00	0.7
C17orf85	NA	NA	70.60	2.58
CDC5L	NA	NA	92.30	1.87
CHERP	NA	NA	103.70	4.15
DDX42	NA	NA	103.00	2.88
EFTUD2	NA	NA	109.40	1.85
ETV3	NA	NA	57.00	2.93
FIP1L1	NA	NA	66.50	4.38
GPATCH2	NA	NA	58.90	3.79
GPBP1	NA	NA	53.30	6.77
IFIT1	NA	NA	55.40	3.14
LSM1	NA	NA	15.20	10.53
MBNL3	NA	NA	38.50	9.6
MRPL4	NA	NA	34.90	9.32
MRPL51	NA	NA	15.10	13.28
MRPS26	NA	NA	24.20	9.76
MS1	NA	NA	39.10	5.25
MST1R	NA	NA	152.20	1.29
N4BP2	NA	NA	198.80	0.68
NFIX	NA	NA	55.10	3.19
NGRN	NA	NA	32.40	6.19
NKRF	NA	NA	77.70	1.74
NYNRIN	NA	NA	208.40	2.69
PARP12	NA	NA	79.10	12.7
PLK1	NA	NA	68.30	3.48
PRRC2B	NA	NA	243.00	1.08
PTCD1	NA	NA	78.90	6.14
R3HDM2	NA	NA	107.00	2.15
RBFOX2	NA	NA	41.40	6.15
RBM17	NA	NA	45.00	5.49
RBMS2	NA	NA	44.00	8.35
SF3A1	NA	NA	88.90	3.66
SMARCAL1	NA	NA	105.90	2.1
SNRNP40	NA	NA	39.30	3.36
SNRPA1	NA	NA	28.40	6.27
SREK1	NA	NA	59.40	3.54
SUPV3L1	NA	NA	88.00	1.65
TCAF1	NA	NA	102.10	1.85
TNRC6C	NA	NA	176.00	1.83
TOP3B	NA	NA	96.70	2.67
TRA2A	NA	NA	32.70	7.09
TRA2B	NA	NA	33.70	18.4
WDR33	NA	NA	145.90	1.27
YLPM1	NA	NA	241.60	0.56
ZC3H11A	NA	NA	89.10	1.85
ZCCHC3	NA	NA	43.50	6.7
FUBP1	240.72	$3.07 \times 10^{-134}$	67.60	
ZNF185	152.50	$3.03 \times 10^{-53}$	73.50	

DAZAP1	63.53	$1.72 \times 10^{-29}$	43.40
ELAVL1	55.97	$1.19 \times 10^{-48}$	36.10
RALY	45.28	$5.98 \times 10^{-11}$	32.50
IGF2BP3	40.27	$1.49 \times 10^{-88}$	63.70
KHSRP	33.35	$1.84 \times 10^{-46}$	73.10
FAM120A	29.83	$4.98 \times 10^{-77}$	121.90
STAU2	29.12	$2.98 \times 10^{-32}$	62.60
HNRNPC	28.33	$3.41 \times 10^{-19}$	33.70
PABPC1	27.99	$2.06 \times 10^{-40}$	70.70
RBMS1	26.86	$7.27 \times 10^{-08}$	44.50
FUBP3	26.69	$5.53 \times 10^{-35}$	61.60
LARP1	24.93	$9.98 \times 10^{-114}$	123.50
YBX2	23.83	$1.70 \times 10^{-13}$	38.50
HNRNPA2B1	23.60	$1.39 \times 10^{-128}$	37.40
HNRNPDL	23.49	$3.28 \times 10^{-37}$	46.40
FMR1	23.41	$6.19 \times 10^{-34}$	71.20
KHDRBS1	22.44	$8.02 \times 10^{-41}$	48.20
HNRNPR	21.86	$2.19 \times 10^{-40}$	70.90
CELF1	20.39	$5.26 \times 10^{-13}$	52.10
MOV10	20.22	$1.71 \times 10^{-38}$	113.70
QKI	19.35	$1.41 \times 10^{-07}$	37.70
HNRNPUL1	18.55	$1.86 \times 10^{-39}$	95.70
PABPC4	18.46	$3.91 \times 10^{-59}$	70.80
FXR1	18.43	$8.67 \times 10^{-12}$	69.70
NUFIP2	18.01	$2.69 \times 10^{-41}$	76.10
MSI2	16.77	$1.36 \times 10^{-08}$	35.20
FXR2	16.08	$3.59 \times 10^{-07}$	74.20
UPF1	14.82	$6.37 \times 10^{-92}$	124.30
EIF4ENIF1	14.73	$1.25 \times 10^{-11}$	108.20
PCBP2	13.02	$6.66 \times 10^{-20}$	38.60
KPNA2	12.53	$6.79 \times 10^{-21}$	57.90
TIAL1	12.51	$1.13 \times 10^{-05}$	41.60
IGF2BP2	11.75	$4.64 \times 10^{-12}$	66.10
HNRNPA0	11.69	$3.55 \times 10^{-35}$	30.80
ESRP1	11.50	$1.59 \times 10^{-18}$	75.60
DHX36	11.36	$1.57 \times 10^{-33}$	114.80
SF1	11.34	$3.71 \times 10^{-34}$	68.30
ILF3	11.33	$4.74 \times 10^{-106}$	95.30
CSDA	11.27	$2.74 \times 10^{-37}$	40.10
HNRNPK	10.81	$2.20 \times 10^{-58}$	51.00
HNRNPL	10.81	$2.85 \times 10^{-31}$	64.10
PURA	10.58	$1.06 \times 10^{-07}$	34.90
PRRC2C	9.74	$2.95 \times 10^{-42}$	316.90
TARDBP	9.67	$2.32 \times 10^{-06}$	44.70
EWSR1	9.60	$5.55 \times 10^{-29}$	68.50
THRAP3	9.57	$2.80 \times 10^{-07}$	108.70
HECA	9.49	$8.38 \times 10^{-17}$	58.80
HNRNPA3	9.27	$3.77 \times 10^{-17}$	39.60
HNRNPH1	9.16	$6.71 \times 10^{-21}$	49.20
HNRNPUL2	8.99	$6.07 \times 10^{-10}$	85.10
ILF2	8.96	$9.44 \times 10^{-53}$	43.10
RTCB	8.92	$1.67 \times 10^{-57}$	55.20

NCBP1	8.88	$1.99 \times 10^{-07}$	91.80
HNRNPA1	8.76	$1.17 \times 10^{-34}$	38.70
CPSF7	8.60	$5.42 \times 10^{-07}$	52.10
PTBP1	8.50	$7.73 \times 10^{-70}$	57.20
SFPQ	8.39	$4.25 \times 10^{-36}$	76.10
HNRNPF	8.34	$1.64 \times 10^{-39}$	45.70
PUF60	8.31	$9.04 \times 10^{-08}$	59.90
MBNL1	7.65	$2.67 \times 10^{-09}$	41.80
YBX1	7.60	$2.06 \times 10^{-35}$	35.90
EIF4G1	7.45	$3.46 \times 10^{-87}$	175.50
LRPPRC	7.43	$5.33 \times 10^{-59}$	157.90
SYNCRIP	7.34	$1.57 \times 10^{-83}$	69.60
GEMIN5	7.30	$1.73 \times 10^{-19}$	168.60
DDX6	7.28	$1.03 \times 10^{-54}$	54.40
LARP4B	7.21	$4.73 \times 10^{-13}$	80.60
DDX1	7.19	$1.46 \times 10^{-50}$	82.40
SRSF7	7.14	$4.45 \times 10^{-10}$	27.40
EIF4E	7.12	$2.59 \times 10^{-19}$	25.10
ATXN2	7.07	$5.66 \times 10^{-08}$	140.30
PATL1	7.01	$9.16 \times 10^{-39}$	86.90
MATR3	6.93	$1.98 \times 10^{-08}$	94.60
RBM47	6.92	$3.90 \times 10^{-03}$	64.10
U2AF1	6.65	$3.79 \times 10^{-10}$	27.90
EIF3H	6.39	$1.46 \times 10^{-24}$	39.90
RAVER1	6.29	$2.11 \times 10^{-22}$	63.90
STAU1	6.27	$4.74 \times 10^{-106}$	63.20
PTBP3	6.26	$7.94 \times 10^{-10}$	59.70
DHX30	6.11	$5.54 \times 10^{-14}$	133.90
HNRNPAB	6.01	$2.64 \times 10^{-25}$	36.20
PUM2	5.99	$1.28 \times 10^{-03}$	114.20
HNRNPH2	5.93	$1.19 \times 10^{-06}$	49.30
SRSF11	5.84	$1.13 \times 10^{-06}$	53.50
PLOD1	5.73	$2.62 \times 10^{-19}$	83.60
HNRNPM	5.68	$2.98 \times 10^{-45}$	77.50
GNAO1	5.56	$3.27 \times 10^{-03}$	40.10
DDX17	5.55	$3.36 \times 10^{-30}$	80.30
EIF4A3	5.46	$8.51 \times 10^{-04}$	46.90
ADAR	5.41	$1.58 \times 10^{-06}$	136.10
C14orf166	5.41	$3.27 \times 10^{-08}$	28.10
SLIRP	5.33	$4.14 \times 10^{-09}$	12.30
PRRC2A	5.27	$2.07 \times 10^{-10}$	228.90
YTHDF1	5.26	$4.56 \times 10^{-18}$	60.90
USP10	5.23	$2.27 \times 10^{-17}$	87.10
MRPL3	5.17	$1.49 \times 10^{-07}$	38.60
DHX15	5.15	$2.42 \times 10^{-15}$	90.90
MID1IP1	5.14	$1.25 \times 10^{-46}$	20.20
YTHDF2	5.14	$3.88 \times 10^{-42}$	62.30
G3BP1	5.04	$9.36 \times 10^{-68}$	52.20
PRKRA	4.98	$4.58 \times 10^{-20}$	34.40
NONO	4.97	$2.11 \times 10^{-46}$	54.20
CSDE1	4.95	$1.23 \times 10^{-32}$	88.90
SEC31A	4.92	$1.17 \times 10^{-22}$	133.00

UNK	4.88	$1.77 \times 10^{-29}$	88.10
STRAP	4.84	$1.59 \times 10^{-14}$	38.40
ATXN2L	4.83	$8.63 \times 10^{-14}$	113.40
DHX9	4.79	$4.79 \times 10^{-42}$	141.00
FAM120C	4.75	$1.02 \times 10^{-08}$	120.60
KIF1C	4.66	$1.54 \times 10^{-03}$	122.90
EIF3F	4.66	$9.00 \times 10^{-18}$	37.60
NELFE	4.61	$1.03 \times 10^{-06}$	43.20
HMMR	4.57	$3.38 \times 10^{-17}$	84.10
RBM14	4.47	$9.86 \times 10^{-08}$	69.50
UPF2	4.47	$5.83 \times 10^{-22}$	147.80
EIF3G	4.42	$1.36 \times 10^{-11}$	35.60
EIF3I	4.32	$1.66 \times 10^{-21}$	36.50
HNRNPH3	4.21	$2.63 \times 10^{-17}$	36.90
U2AF2	4.17	$1.29 \times 10^{-03}$	53.50
G3BP2	4.04	$8.48 \times 10^{-18}$	54.10
EIF3D	4.03	$4.77 \times 10^{-35}$	64.00
EDC4	4.00	$2.51 \times 10^{-08}$	151.70
XRN2	4.00	$5.63 \times 10^{-05}$	108.60
NUDT21	3.96	$3.93 \times 10^{-04}$	26.20
DDX5	3.94	$6.62 \times 10^{-30}$	69.10
GRSF1	3.94	$1.09 \times 10^{-23}$	53.10
ALYREF	3.92	$2.11 \times 10^{-17}$	26.90
LSM14A	3.91	$6.52 \times 10^{-17}$	50.50
LSM14B	3.84	$4.09 \times 10^{-05}$	42.10
TFAM	3.76	$1.07 \times 10^{-25}$	29.10
RC3H1	3.71	$3.05 \times 10^{-03}$	125.70
CC2D1A	3.67	$7.89 \times 10^{-18}$	104.10
UPF3B	3.65	$6.03 \times 10^{-14}$	57.80
EIF3L	3.65	$5.69 \times 10^{-15}$	66.70
SRSF3	3.63	$8.06 \times 10^{-10}$	19.30
CMTR1	3.61	$1.43 \times 10^{-04}$	95.30
FUS	3.60	$1.97 \times 10^{-08}$	53.40
CPSF6	3.60	$8.19 \times 10^{-08}$	59.20
PRMT1	3.56	$2.88 \times 10^{-12}$	42.50
PHF6	3.54	$2.12 \times 10^{-03}$	41.30
HNRNPD	3.51	$3.20 \times 10^{-43}$	38.40
HNRNPU	3.50	$1.18 \times 10^{-57}$	90.60
LARP4	3.49	$2.86 \times 10^{-03}$	80.60
SEC13	3.33	$8.43 \times 10^{-04}$	35.50
ANKHD1	3.28	$1.41 \times 10^{-14}$	269.50
FAM98A	3.27	$1.06 \times 10^{-03}$	55.30
MRPS17	3.20	$1.47 \times 10^{-08}$	14.50
ZNF593	3.18	$2.21 \times 10^{-05}$	15.20
HNRNPLL	3.16	$4.16 \times 10^{-03}$	60.10
CIRBP	3.12	$1.44 \times 10^{-04}$	18.60
KIAA1967	3.10	$1.67 \times 10^{-06}$	102.90
PKP3	3.10	$7.11 \times 10^{-21}$	87.10
AGO2	3.08	$5.57 \times 10^{-05}$	97.20
PURB	3.08	$9.05 \times 10^{-06}$	33.20
KIAA1522	3.07	$6.39 \times 10^{-04}$	107.10
RBM39	3.06	$3.53 \times 10^{-09}$	59.40

YWHAG	3.05	$1.60 \times 10^{-04}$	28.30
EIF3A	3.04	$2.46 \times 10^{-29}$	166.60
MKRN2	3.04	$9.31 \times 10^{-05}$	46.90
CAPRIN1	3.01	$1.07 \times 10^{-27}$	78.40
MEX3D	2.99	$2.26 \times 10^{-02}$	64.90
MARK2	2.98	$3.25 \times 10^{-15}$	87.90
ZC3HAV1	2.98	$4.77 \times 10^{-35}$	101.40
PPFIA1	2.97	$3.99 \times 10^{-35}$	135.80
SRP68	2.93	$2.70 \times 10^{-02}$	70.70
POP7	2.93	$1.14 \times 10^{-03}$	15.70
ITIH2	2.91	$4.34 \times 10^{-02}$	106.50
DHX29	2.88	$8.95 \times 10^{-07}$	155.20
KRT4	2.83	$1.67 \times 10^{-02}$	57.30
UBAP2L	2.82	$2.54 \times 10^{-19}$	114.50
SRPK1	2.78	$5.70 \times 10^{-07}$	74.30
SF3B2	2.75	$1.24 \times 10^{-38}$	100.20
FAM111B	2.74	$5.08 \times 10^{-08}$	84.70
PABPN1	2.74	$2.62 \times 10^{-02}$	32.70
VAPA	2.71	$6.96 \times 10^{-05}$	27.90
TRIM25	2.67	$7.59 \times 10^{-41}$	71.00
SRSF5	2.65	$9.80 \times 10^{-04}$	31.30
DDX3X	2.65	$1.52 \times 10^{-07}$	73.20
PTBP2	2.56	$4.00 \times 10^{-05}$	57.50
PEG10	2.51	$1.12 \times 10^{-10}$	80.20
EIF2AK2	2.43	$1.71 \times 10^{-25}$	62.10
PUM1	2.43	$2.00 \times 10^{-02}$	126.50
CDC20	2.41	$3.94 \times 10^{-08}$	54.70
EIF3B	2.40	$1.77 \times 10^{-05}$	92.50
RNMT	2.37	$4.32 \times 10^{-03}$	54.80
MRPL14	2.34	$1.74 \times 10^{-04}$	15.90
BAIAP2	2.25	$7.94 \times 10^{-08}$	60.90
TRIM56	2.24	$1.65 \times 10^{-06}$	81.50
FBL	2.24	$6.86 \times 10^{-10}$	33.80
EIF4A1	2.24	$9.42 \times 10^{-04}$	46.20
YTHDF3	2.21	$7.28 \times 10^{-09}$	63.90
EIF4G2	2.20	$6.87 \times 10^{-07}$	102.40
GNB2L1	2.19	$1.74 \times 10^{-09}$	35.10
MAP7D1	2.18	$6.95 \times 10^{-04}$	92.80
LTV1	2.18	$2.80 \times 10^{-18}$	54.90
RPS10	2.17	$1.06 \times 10^{-06}$	18.90
RDX	2.15	$4.56 \times 10^{-08}$	68.60
SNRPD3	2.15	$2.21 \times 10^{-05}$	13.90
TYK2	2.14	$4.47 \times 10^{-07}$	133.70
EIF3E	2.12	$2.08 \times 10^{-07}$	52.20
PNO1	2.10	$4.06 \times 10^{-03}$	27.90
LLGL2	2.10	$2.95 \times 10^{-04}$	113.40
NEMF	2.07	$3.45 \times 10^{-08}$	123.00
EIF2A	2.06	$4.03 \times 10^{-22}$	65.00
PPFIBP2	2.01	$1.63 \times 10^{-04}$	98.50
DHX57	2.01	$3.09 \times 10^{-02}$	155.60
WIBG	1.99	$5.85 \times 10^{-15}$	22.70
RPL22L1	1.98	$1.65 \times 10^{-06}$	14.60

GTPBP1	1.98	$1.48 \times 10^{-10}$	72.50
SPAG5	1.97	$2.94 \times 10^{-02}$	134.40
HLTF	1.94	$8.00 \times 10^{-05}$	113.90
SOGA2	1.89	$1.80 \times 10^{-14}$	209.50
AP2A1	1.87	$6.71 \times 10^{-04}$	107.50
NAV1	1.87	$4.46 \times 10^{-12}$	202.50
OTUD4	1.86	$2.94 \times 10^{-02}$	124.00
SFRP1	1.85	$2.21 \times 10^{-05}$	35.40
REEP4	1.84	$6.81 \times 10^{-04}$	29.40
TSR1	1.80	$5.59 \times 10^{-10}$	91.80
FAM83D	1.79	$1.14 \times 10^{-05}$	64.40
ASCC3	1.79	$2.06 \times 10^{-12}$	251.50
POLDIP3	1.76	$1.90 \times 10^{-03}$	46.10
RPS17	1.75	$2.13 \times 10^{-11}$	15.60
RPL22	1.74	$2.95 \times 10^{-05}$	14.80
MAP7	1.73	$9.08 \times 10^{-16}$	84.10
H1-5	1.72	$1.22 \times 10^{-04}$	22.60
YTHDC2	1.71	$5.23 \times 10^{-03}$	160.20
CSNK1A1	1.70	$3.45 \times 10^{-03}$	38.90
BYSL	1.69	$1.40 \times 10^{-06}$	49.60
RC3H2	1.69	$3.11 \times 10^{-03}$	131.70
RASAL2	1.68	$3.16 \times 10^{-04}$	128.60
XRCC5	1.68	$2.02 \times 10^{-27}$	82.70
AP2M1	1.68	$2.93 \times 10^{-09}$	49.70
MYO9B	1.68	$4.03 \times 10^{-05}$	243.40
RPS7	1.66	$3.89 \times 10^{-07}$	22.10
MAP7D3	1.66	$2.27 \times 10^{-04}$	98.40
DNAJC9	1.60	$1.05 \times 10^{-07}$	29.90
IQGAP3	1.60	$2.28 \times 10^{-02}$	184.70
PRMT5	1.59	$2.33 \times 10^{-02}$	72.70
NSUN2	1.59	$2.79 \times 10^{-05}$	86.50
SRP14	1.57	$8.34 \times 10^{-03}$	14.60
RPS21	1.56	$3.08 \times 10^{-02}$	9.10
XRCC6	1.56	$1.82 \times 10^{-17}$	69.80
CCDC124	1.52	$5.20 \times 10^{-03}$	25.80
MSN	1.52	$1.54 \times 10^{-08}$	67.80

**Table S7: List of proteins retrieved after biotin pulldown (proximity labelling by TurboID)**

no treatment			50 $\mu$ M biotin, 2 minutes			50 $\mu$ M biotin, 10 minutes		
Protein ID	Protein	Enrichment ratio	Protein ID	Protein	Enrichment ratio	Protein ID	Protein	Enrichment ratio
O14744	PRMT5	NA	P68032	ACTC1	NA	Q3ZCM7	TUBB8	NA
Q15751	HERC1	NA	Q05639	EEF1A2	NA	Q9BQA1	WDR77	NA
Q9BQE3	TUBA1C	NA	Q3ZCM7	TUBB8	NA	P13637	ATP1A3	NA
P68032	ACTC1	NA	Q9BQA1	WDR77	NA	Q5T2N8	ATAD3C	NA
Q05639	EEF1A2	NA	Q96C92	SDCCAG3	NA	Q12840	KIF5A	NA
Q9BQA1	WDR77	NA	Q5T2N8	ATAD3C	NA	P11908	PRPS2	NA
P62987	UBA52	NA	Q12979	ABR	NA	P35626	GRK3	NA
P42357	HAL	NA	O94905	ERLIN2	NA	Q92526	CCT6B	NA
P06899	H2BC11	NA	Q12792	TWF1	NA	O60814	H2BC12	NA
Q9NRW1	RAB6B	NA	P11908	PRPS2	NA	Q92925	SMARCD2	NA

P58107	EPPK1	NA	Q504Q3	PAN2	NA	Q93045	STMN2	NA
P52789	HK2	NA	Q58FF8	HSP90AB2 P	NA	Q96RG2	PASK	NA
Q01813	PFKP	NA	O43251	RBFOX2	NA	P30533	LRPAP1	NA
P11166	SLC2A1	NA	P49674	CSNK1E	NA	P17612	PRKACA	NA
P28070	PSMB4	NA	P50502	ST13	NA	P30101	PDIA3	NA
P25786	PSMA1	NA	Q9NRW1	RAB6B	NA	Q8WUD1	RAB2B	NA
Q92997	DVL3	NA	Q13162	PRDX4	NA	O15111	CHUK	NA
Q9Y6A5	TACC3	NA	Q9H9S3	SEC61A2	NA	P51157	RAB28	NA
Q93052	LPP	NA	Q9UQM7	CAMK2A	NA	Q9NRW1	RAB6B	NA
Q9NQ92	COPRS	NA	Q53FV1	ORMDL2	NA	Q8NBS9	TXNDC5	NA
O00767	SCD	NA	Q10567	AP1B1	NA	O94887	FARP2	NA
Q5TFE4	NT5DC1	NA	P52789	HK2	NA	O94972	TRIM37	NA
Q96F07	CYFIP2	NA	P22694	PRKACB	NA	P25490	YY1	NA
O00186	STXBP3	NA	P31946	YWHAB	NA	Q15057	ACAP2	NA
Q9UBV8	PEF1	NA	Q01813	PFKP	NA	Q9P0S3	ORMDL1	NA
P60763	RAC3	NA	P05109	S100A8	NA	Q01814	ATP2B2	NA
P53041	PPP5C	NA	P07339	CTSD	NA	Q13126	MTAP	NA
Q96MG8	PCMTD1	NA	Q9Y2Z2	MTO1	NA	Q6PML9	SLC30A9	NA
Q9UHQ1	NARF	NA	Q8WUD1	RAB2B	NA	Q96IJ6	GMPPA	NA
Q08426	EHHADH	NA	Q5HYI8	RABL3	NA	Q14165	MLEC	NA
Q13243	SRSF5	NA	Q99943	AGPAT1	NA	Q9BY32	ITPA	NA
Q9H853	TUBA4B	NA	P28074	PSMB5	NA	Q9NYP7	ELOVL5	NA
Q05397	PTK2	NA	P06753	TPM3	NA	P08579	SNRPB2	NA
Q9Y5Z9	UBIAD1	NA	O00303	EIF3F	NA	Q9P0I2	EMC3	NA
P09132	SRP19	NA	Q8IYB1	MB21D2	NA	P53041	PPP5C	NA
Q9C0F1	CEP44	NA	Q9BW62	KATNAL1	NA	Q01813	PFKP	NA
Q9Y2T2	AP3M1	NA	Q7LG56	RRM2B	NA	Q14CS0	UBXN2B	NA
O95674	CDS2	NA	O14640	DVL1	NA	Q9UHQ1	NARF	NA
Q9H3N1	TMX1	NA	Q6ZVX7	NCCRP1	NA	Q9P0L2	MARK1	NA
Q96EK5	KIFBP	NA	Q9Y6I3	EPN1	NA	O75351	VPS4B	NA
O75348	ATP6V1G 1	NA	Q9UBQ0	VPS29	NA	O94988	FAM13A	NA
Q96MW1	CCDC43	NA	P98194	ATP2C1	NA	Q12816	TRO	NA
Q9BWH6	RPAP1	NA	Q5BJH7	YIF1B	NA	Q9H0V9	LMAN2L	NA
Q9UFF9	CNOT8	NA	Q5T9S5	CCDC18	NA	Q765P7	MTSS1L	NA
Q6R327	RICTOR	NA	Q9P0L2	MARK1	NA	Q8TBZ3	WDR20	NA
Q8WU79	SMAP2	NA	O75845	SC5D	NA	Q969J3	LOH12CR 1	NA
O95336	PGLS	NA	P43307	SSR1	NA	Q9UNH6	SNX7	NA
P50570	DNM2	NA	O75477	ERLIN1	NA	O15021	MAST4	NA
Q9BV44	THUMPD3	NA	P62837	UBE2D2	NA	Q0P6D6	CCDC15	NA
Q9UH65	SWAP70	NA	P61927	RPL37	NA	Q8WXA3	RUFY2	NA
Q8TDJ6	DMXL2	NA	P56537	EIF6	NA	Q9BRV8	SIKE1	NA
P08579	SNRPB2	NA	Q9NZ72	STMN3	NA	Q9NZN3	EHD3	NA
P20337	RAB3B	NA	Q86U90	YRDC	NA	Q15751	HERC1	22.00
Q99808	SLC29A1	NA	Q9BQT8	SLC25A21	NA	O14744	PRMT5	21.00
O14772	FPGT	NA	Q9GZR5	ELOVL4	NA	Q02224	CENPE	9.00
Q06609	RAD51	NA	O00221	NFKBIE	NA	Q9NZJ4	SACS	8.00
Q9P2S5	WRAP73	NA	P00966	ASS1	NA	Q9GZN8	C20orf27	7.00
Q8NI77	KIF18A	NA	P20337	RAB3B	NA	Q9Y6K9	IKBKG	7.00
Q96BR5	SELRC1	NA	P35237	SERPINB6	NA	Q9ULL1	PLEKHG1	7.00
Q9BV38	WDR18	NA	Q99808	SLC29A1	NA	Q96C92	SDCCAG3	6.50
Q3SY69	ALDH1L2	NA	Q9GZT4	SRR	NA	Q9NPF4	OSGEP	6.00



P00390	GSR	NA	Q14192	FHL2	NA	Q15005	SPCS2	6.00
Q9NQX3	GPHN	NA	Q7Z7H5	TMED4	NA	P54709	ATP1B3	5.00
Q9UBW7	ZMYM2	NA	Q96EK9	KTI12	NA	Q9NQ88	TIGAR	5.00
Q96C92	SDCCAG3	NA	Q9HBI1	PARVB	NA	Q96QD9	FYTTD1	5.00
Q14562	DHX8	NA	Q9NYU2	UGGT1	NA	Q9P2R7	SUCLA2	5.00
Q15599	SLC9A3R2	NA	Q06609	RAD51	NA	P83369	LSM11	5.00
Q92536	SLC7A6	NA	O00186	STXBP3	NA	Q8TAT6	NPLOC4	5.00
Q9UBQ0	VPS29	NA	Q9UBV8	PEF1	NA	Q9UPV0	CEP164	5.00
Q9H6K4	OPA3	NA	Q99798	ACO2	NA	Q7Z3E5	ARMC9	5.00
O75683	SURF6	NA	Q96NL6	SCLT1	NA	Q9H892	TTC12	5.00
Q96SZ5	ADO	NA	Q15468	STIL	NA	Q9BRS2	RIOK1	4.50
Q9BQP7	MGME1	NA	Q9Y6E0	STK24	NA	P56945	BCAR1	4.50
O75845	SC5D	NA	O43639	NCK2	NA	P62314	SNRPD1	4.00
Q96Q11	TRNT1	NA	Q8NBS9	TXNDC5	NA	Q8WVJ2	NUDCD2	4.00
O75874	IDH1	NA	O15083	ERC2	NA	Q96F24	NRBF2	4.00
P50995	ANXA11	NA	Q96MG8	PCMTD1	NA	Q6YHU6	THADA	4.00
Q9Y2V2	CARHSP1	NA	Q15599	SLC9A3R2	NA	P48047	ATP5PO	4.00
Q9Y3E2	BOLA1	NA	Q8IVD9	NUDCD3	NA	O00116	AGPS	4.00
P29218	IMPA1	NA	Q8IWQ3	BRSK2	NA	O00170	AIP	4.00
P50452	SERPINB8	NA	Q92536	SLC7A6	NA	P33527	ABCC1	4.00
Q00534	CDK6	NA	Q9Y6M1	IGF2BP2	NA	Q9GZT9	EGLN1	4.00
Q6P582	MZT2A	NA	Q13011	ECH1	NA	O95864	FADS2	4.00
Q9P031	CCDC59	NA	Q14139	UBE4A	NA	Q9BU23	LMF2	4.00
Q9BRS2	RIOK1	15.25	Q5W0V3	FAM160B1	NA	Q9C0F1	CEP44	4.00
Q13867	BLMH	11.00	Q5XKP0	QIL1	NA	Q9NQ92	COPRS	4.00
Q01469	FABP5	7.00	Q9BUN8	DERL1	NA	Q13191	CBLB	4.00
Q9HD45	TM9SF3	5.00	Q9H6K4	OPA3	NA	P00390	GSR	4.00
Q969N2	PIGT	5.00	Q9UBI1	COMMD3	NA	Q8NA72	POC5	4.00
Q96QA5	GSDMA	5.00	Q9Y4Z0	LSM4	NA	Q07617	SPAG1	4.00
Q5D862	FLG2	4.50	P01111	NRAS	NA	Q0IIM8	TBC1D8B	4.00
Q13835	PKP1	4.50	P52209	PGD	NA	Q8N2Y8	RUSC2	4.00
P04040	CAT	4.33	Q6Y1H2	HACD2	NA	O14777	NDC80	4.00
O14828	SCAMP3	4.00	Q8TED1	GPX8	NA	Q52LW3	ARHGAP29	4.00
Q9NUL7	DDX28	4.00	Q9NP97	DYNLRB1	NA	Q9NR46	SH3GLB2	4.00
O75947	ATP5PD	4.00	Q9Y3C8	UFC1	NA	Q5T9S5	CCDC18	4.00
Q8IV63	VRK3	4.00	O14777	NDC80	NA	Q5T7B8	KIF24	4.00
Q9BTE3	MCMBP	4.00	Q52LW3	ARHGAP29	NA	Q99536	VAT1	4.00
O15127	SCAMP2	4.00	Q9NR46	SH3GLB2	NA	Q05655	PRKCD	3.50
Q99614	TTC1	4.00	Q8TD31	CCHCR1	NA	O15067	PFAS	3.50
Q9Y2Z2	MTO1	4.00	Q9ULL1	PLEKHG1	NA	P62841	RPS15	3.50
Q9H2U2	PPA2	4.00	O75351	VPS4B	NA	Q8IWS0	PHF6	3.50
P0CG12	CHTF8	4.00	P53677	AP3M2	NA	Q8WXW3	PIBF1	3.50
P22735	TGM1	4.00	Q12816	TRO	NA	O43314	PPIP5K2	3.50
O43583	DENR	3.50	Q9H0V9	LMAN2L	NA	Q15468	STIL	3.50
P08621	SNRNP70	3.00	O96005	CLPTM1	NA	Q99541	PLIN2	3.50
P61758	VBP1	3.00	P06241	FYN	NA	Q8IVM0	CCDC50	3.33
Q15813	TBCE	3.00	P20674	COX5A	NA	Q9NR12	PDLIM7	3.00
P10155	RO60	3.00	P61009	SPCS3	NA	Q96A73	KIAA1191	3.00
Q63ZY3	KANK2	3.00	Q92575	UBXN4	NA	Q9NP64	ZCCHC17	3.00
Q8TC12	RDH11	3.00	Q969L4	LSM10	NA	O60427	FADS1	3.00
P09661	SNRPA1	2.75	Q96Q11	TRNT1	NA	P53597	SUCLG1	3.00

P55786	NPEPPS	2.75	Q9BPW8	NIPSNAP1	NA	Q86TP1	PRUNE	3.00
Q9NRK6	ABCB10	2.67	O94925	GLS	NA	Q9BSH4	TACO1	3.00
Q96P63	SERPINB1 2	2.50	P30046	DDT	NA	O94905	ERLIN2	3.00
Q99816	TSG101	2.50	Q32P41	TRMT5	NA	Q96MW1	CCDC43	3.00
Q86TP1	PRUNE	2.50	Q6NT16	SLC18B1	NA	O14531	DPYSL4	3.00
P23258	TUBG1	2.50	Q7Z3C6	ATG9A	NA	Q6ZWJ1	STXBP4	3.00
Q6UB35	MTHFD1L	2.50	Q9BSH5	HDHD3	NA	Q9H223	EHD4	3.00
Q8ND56	LSM14A	2.50	Q9NRD5	PICK1	NA	O43164	PJA2	3.00
P23526	AHCY	2.50	Q9Y512	SAMM50	NA	O00483	NDUFA4	3.00
O76003	GLRX3	2.50	Q9Y672	ALG6	NA	Q8NCA5	FAM98A	3.00
P19367	HK1	2.50	A6NHQ2	FBLL1	NA	P61803	DAD1	3.00
Q8WVV4	POF1B	2.50	P06702	S100A9	NA	Q9UHJ6	SHPK	3.00
Q86YZ3	HRNR	2.38	P20336	RAB3A	NA	Q9UM13	ANAPC10	3.00
Q02413	DSG1	2.27	P67775	PPP2CA	NA	Q13541	EIF4EBP1	3.00
Q15031	LARS2	2.14	Q86SX6	GLRX5	NA	Q9BV57	ADI1	3.00
P07355	ANXA2	2.11	Q96EY8	MMAB	NA	Q9NP79	VTA1	3.00
			Q15751	HERC1	40.00	P49458	SRP9	3.00
			O14744	PRMT5	18.83	O75746	SLC25A12	3.00
			O95864	FADS2	7.00	O95299	NDUFA10	3.00
			P20930	FLG	7.00	Q7RTV0	PHF5A	3.00
			O95336	PGLS	7.00	O43826	SLC37A4	3.00
			Q9H1K0	RBSN	7.00	Q7Z4H3	HDDC2	3.00
			Q9BRS2	RIOK1	6.00	Q9Y3T9	NOC2L	3.00
			Q9P0J0	NDUFA13	6.00	Q15070	OXA1L	3.00
			Q6PI48	DARS2	6.00	O00231	PSMD11	3.00
			Q9Y679	AUP1	5.00	P46734	MAP2K3	3.00
			O14735	CDIPT	5.00	P36507	MAP2K2	3.00
			Q8TB61	SLC35B2	5.00	Q13686	ALKBH1	3.00
			P18754	RCC1	5.00	Q9Y6G5	COMMD1 0	3.00
			Q9BU23	LMF2	5.00	Q8TB61	SLC35B2	3.00
			Q9UHQ9	CYB5R1	5.00	O00221	NFKBIE	3.00
			Q14574	DSC3	5.00	O75348	ATP6V1G 1	3.00
			P14621	ACYP2	5.00	Q9BT22	ALG1	3.00
			O14531	DPYSL4	5.00	O95997	PTTG1	3.00
			Q96HU1	SGSM3	5.00	Q8IU60	DCP2	3.00
			Q5T9A4	ATAD3B	4.60	Q9Y484	WDR45	3.00
			Q99614	TTC1	4.00	Q13772	NCOA4	3.00
			Q5D862	FLG2	4.00	Q15121	PEA15	3.00
			Q9NX63	CHCHD3	4.00	Q68CZ2	TNS3	3.00
			P37108	SRP14	4.00	Q9BSL1	UBAC1	3.00
			O75832	PSMD10	4.00	Q9NW68	BSDC1	3.00
			P49419	ALDH7A1	4.00	Q8IWQ3	BRSK2	3.00
			Q9NZW5	MPP6	4.00	O15040	TECPR2	3.00
			Q96B26	EXOSC8	4.00	Q2M1Z3	ARHGAP3 1	3.00
			Q9BSH4	TACO1	4.00	Q2M3G4	SHROOM 1	3.00
			Q6YN16	HSDL2	4.00	Q5THJ4	VPS13D	3.00
			Q96EK5	KIFBP	4.00	Q96RY7	IFT140	3.00
			Q8TC12	RDH11	4.00	Q9H7X7	IFT22	3.00
			P30153	PPP2R1A	4.00	P98194	ATP2C1	3.00
			Q9NQ92	COPRS	4.00	O43251	RBFOX2	3.00
			O75792	RNASEH2 A	4.00	O00418	EEF2K	3.00

			P49840	GSK3A	4.00	O14924	RGS12	3.00
			P58546	MTPN	4.00	Q8N573	OXR1	3.00
			Q9C0D2	KIAA1731	4.00	Q9HCJ0	TNRC6C	2.75
			Q8NEB9	PIK3C3	4.00	Q15645	TRIP13	2.67
			Q14244	MAP7	3.50	O75792	RNASEH2 A	2.67
			Q08554	DSC1	3.50	Q12792	TWF1	2.67
			Q16891	IMMT	3.33	Q05084	ICA1	2.67
			Q9NP61	ARFGAP3	3.33	P50502	ST13	2.67
			Q02413	DSG1	3.00	Q5T9A4	ATAD3B	2.57
			Q9NVI7	ATAD3A	3.00	Q9NVI7	ATAD3A	2.50
			P46459	NSF	3.00	Q5VWZ2	LYPLAL1	2.50
			P24666	ACP1	3.00	Q9H773	DCTPP1	2.50
			Q96J01	THOC3	3.00	Q9BVK6	TMED9	2.50
			Q15717	ELAVL1	3.00	Q9NXU5	ARL15	2.50
			P23526	AHCY	3.00	P37108	SRP14	2.50
			Q92643	PIGK	3.00	Q00537	CDK17	2.50
			Q9NPF4	OSGEP	3.00	P61019	RAB2A	2.50
			Q8N1B4	VPS52	3.00	P49006	MARCKSL 1	2.50
			O75439	PMPCB	3.00	P57076	C21orf59	2.50
			O15067	PFAS	3.00	P49757	NUMB	2.50
			P10636	MAPT	3.00	A7KAX9	ARHGAP3 2	2.50
			Q99569	PKP4	3.00	Q9H0K1	SIK2	2.50
			P62841	RPS15	3.00	P31946	YWHAB	2.50
			Q58A45	PAN3	3.00	Q5XPI4	RNF123	2.50
			P50395	GDI2	3.00	Q504Q3	PAN2	2.33
			O95299	NDUFA10	3.00	Q96RP9	GFM1	2.33
			P51570	GALK1	3.00	Q9BW92	TARS2	2.33
			Q7RTV0	PHF5A	3.00	Q9NWS0	PIH1D1	2.33
			Q92747	ARPC1A	3.00	Q8IYB1	MB21D2	2.33
			Q9UI12	ATP6V1H	3.00	Q8WYL5	SSH1	2.33
			O00232	PSMD12	3.00	P00374	DHFR	2.29
			Q6UX53	METTL7B	3.00	Q9Y2Z0	SUGT1	2.29
			P61513	RPL37A	3.00	Q16527	CSRP2	2.25
			Q9NWZ8	GEMIN8	3.00	P54277	PMS1	2.25
			Q9NX61	TMEM161A	3.00	Q8TD31	CCHCR1	2.25
			O43396	TXNL1	3.00	Q9Y230	RUVBL2	2.22
			P27105	STOM	3.00	Q96LB3	IFT74	2.20
			Q9BTE1	DCTN5	3.00	P13797	PLS3	2.17
			O75608	LYPLA1	3.00	O95801	TTC4	2.17
			Q5T749	KPRP	3.00	Q8TEP8	CEP192	2.14
			Q9GZM5	YIPF3	3.00			
			Q9UHR4	BAIAP2L1	3.00			
			Q8NCX0	CCDC150	3.00			
			P28070	PSMB4	3.00			
			Q8NMQ8	TOR1AIP2	3.00			
			Q14657	LAGE3	3.00			
			P22570	FDXR	3.00			
			P31751	AKT2	3.00			
			Q9BY32	ITPA	3.00			
			Q8N4Q0	ZADH2	3.00			
			Q9NYP7	ELOVL5	3.00			

			Q15008	PSMD6	3.00			
			P83369	LSM11	3.00			
			Q96BR5	SELRC1	3.00			
			P51668	UBE2D1	3.00			
			Q96AA3	RFT1	3.00			
			P26639	TARS1	3.00			
			P53041	PPP5C	3.00			
			Q9Y6Q2	STON1	3.00			
			O95219	SNX4	3.00			
			O43164	PJA2	3.00			
			Q05084	ICA1	3.00			
			Q9Y2I8	WDR37	3.00			
			P51157	RAB28	3.00			
			Q13835	PKP1	3.00			
			Q13564	NAE1	3.00			
			P09012	SNRPA	2.67			
			Q13867	BLMH	2.67			
			Q9UPU7	TBC1D2B	2.67			
			Q6P2H3	CEP85	2.54			
			P08621	SNRNP70	2.50			
			Q9BYJ9	YTHDF1	2.50			
			P00846	MT-ATP6	2.50			
			Q9BUB7	TMEM70	2.50			
			P51153	RAB13	2.50			
			Q9BVK6	TMED9	2.50			
			Q9NPA3	MID1IP1	2.50			
			O14925	TIMM23	2.50			
			O95070	YIF1A	2.50			
			O76003	GLRX3	2.50			
			Q9H7S9	ZNF703	2.50			
			Q96CN7	ISOC1	2.50			
			Q9P2R7	SUCLA2	2.50			
			P04899	GNAI2	2.50			
			Q9ULV4	CORO1C	2.50			
			Q96MW1	CCDC43	2.50			
			Q5VU43	PDE4DIP	2.50			
			Q9NXC5	MIOS	2.50			
			Q8WU79	SMAP2	2.50			
			P53365	ARFIP2	2.50			
			Q13451	FKBP5	2.50			
			Q8WVK7	SKA2	2.50			
			Q96MX6	WDR92	2.50			
			Q96FJ2	DYNLL2	2.50			
			P14923	JUP	2.45			
			Q63ZY3	KANK2	2.40			
			Q9Y2Z0	SUGT1	2.40			
			P35080	PFN2	2.33			
			Q6UWP7	LCLAT1	2.33			
			O00165	HAX1	2.33			
			P10155	RO60	2.33			
			P23258	TUBG1	2.33			
			Q6UB35	MTHFD1L	2.33			

			P35606	COPB2	2.33			
			Q9UH65	SWAP70	2.33			
			Q96BY7	ATG2B	2.31			
			P53004	BLVRA	2.29			
			P07355	ANXA2	2.29			
			Q9HA64	FN3KRP	2.25			
			Q3ZCQ8	TIMM50	2.25			
			P07384	CAPN1	2.25			
			Q15738	NSDHL	2.25			
			O95801	TTC4	2.25			
			Q9UJS0	SLC25A13	2.20			
			Q9NUQ3	TXLNG	2.20			
			P08195	SLC3A2	2.14			

NA: not applicable

**Table S8: List of proteins common between 2 minutes and 10 minutes treatment**

Protein ID	Protein	50 $\mu$ M biotin, 2 minutes		50 $\mu$ M biotin, 10 minutes		MW (KDa)
		Enrichment ratio	Peptide number*	Enrichment ratio	Peptide number*	
Q52LW3	ARHGAP29	NA	2	4.00		142.1
Q9NV17	ATAD3A	3.00		2.50		71.4
Q5T9A4	ATAD3B	4.60		2.57		72.6
Q5T2N8	ATAD3C	NA	11	NA	7	46.4
P98194	ATP2C1	NA	3	3.00		100.6
Q8IWK3	BRSK2	NA	2	3.00		81.6
Q5T9S5	CCDC18	NA	3	4.00		169
Q96MW1	CCDC43	2.50		3.00		25.2
Q8TD31	CCHCR1	NA	2	2.25		88.7
Q9NQ92	COPRS	4.00		4.00		20.1
O14531	DPYSL4	5.00		3.00		61.9
Q9NYP7	ELOVL5	3.00		NA	3	35.3
O94905	ERLIN2	NA	8	3.00		37.8
O95864	FADS2	7.00		4.00		52.3
Q15751	HERC1	40.00		22.00		532.2
Q05084	ICA1	3.00		2.67		54.6
Q9BY32	ITPA	3.00		NA	3	21.4
Q9H0V9	LMAN2L	NA	2	NA	3	39.7
Q9BU23	LMF2	5.00		4.00		79.7
P83369	LSM11	3.00		5.00		39.5
Q9P0L2	MARK1	NA	3	NA	3	89
Q8IYB1	MB21D2	NA	3	2.33		55.8
O14777	NDC80	NA	2	4.00		73.9
O95299	NDUFA10	3.00		3.00		40.8
O00221	NFKBIE	NA	2	3.00		52.9
Q9NPF4	OSGEP	3.00		6.00		36.4
Q504Q3	PAN2	NA	7	2.33		135.4
O15067	PFAS	3.00		3.50		144.7
Q01813	PFKP	NA	4	NA	3	85.6
Q7RTV0	PHF5A	3.00		3.00		12.4
O43164	PJA2	3.00		3.00		78.2
Q9ULL1	PLEKHG1	NA	2	7.00		155.4

P53041	PPP5C	3.00		NA	3	56.9
O14744	PRMT5	18.83		21.00		72.7
P11908	PRPS2	NA	7	NA	6	34.8
P51157	RAB28	3.00		NA	4	24.8
Q8WUD1	RAB2B	NA	3	NA	4	24.2
Q9NRW1	RAB6B	NA	5	NA	4	23.5
O43251	RBFOX2	NA	6	3.00		41.4
Q9BRS2	RIOK1	6.00		4.50		65.6
O75792	RNASEH2 A	4.00		2.67		33.4
P62841	RPS15	3.00		3.50		17
Q96C92	SDCCAG3	NA	11	6.50		48
Q9NR46	SH3GLB2	NA	2	4.00		44
Q8TB61	SLC35B2	5.00		3.00		47.5
P37108	SRP14	4.00		2.50		14.6
P50502	ST13	NA	5	2.67		41.3
Q15468	STIL	NA	2	3.50		143
Q9P2R7	SUCLA2	2.50		5.00		50.3
Q9Y2Z0	SUGT1	2.40		2.29		41
Q9BSH4	TACO1	4.00		3.00		32.5
Q9BVK6	TMED9	2.50		2.50		27.3
Q12816	TRO	NA	2	NA	3	143.7
O95801	TTC4	2.25		2.17		44.7
Q3ZCM7	TUBB8	NA	13	NA	14	49.8
Q12792	TWF1	NA	7	2.67		40.3
Q8NBS9	TXNDC5	NA	2	NA	4	47.6
O75351	VPS4B	NA	2	NA	3	49.3
Q9BQA1	WDR77	NA	12	NA	11	36.7
P31946	YWHAB	NA	4	2.50		28.1

\*: Peptide number was indicated instead of the ratio for proteins that had 0 peptides in the control condition (TurboID only); NA: not applicable

**Table S9: List of proteins retrieved with PRMT5 LC-MS/MS using antibody #PA5-78323**

Protein ID	Gene	MW	Ratio (PRMT5 IP/IgG)	Peptide number
O43707	ACTN4	104.9	NA	10
Q4VCS5	AMOT	118.1	NA	11
Q9UPS8	ANKRD26	196.4	NA	9
Q12774	ARHGEF5	176.8	NA	3
L0R819	ASDURF	11.2	NA	3
Q676U5	ATG16L1	68.3	NA	3
Q9BUH6	C9orf142	21.6	NA	5
P54105	CLNS1A	26.2	NA	3
Q9P2B4	CTTNBP2NL	70.2	NA	9
Q8NEL9	DDHD1	100.4	NA	19
O60762	DPM1	29.6	NA	3
O43524	FOXO3	71.3	NA	10
P16402	H1-3	22.3	NA	10
P58876	H2BC5	13.9	NA	9
Q05084	ICA1	54.6	NA	3
P05362	ICAM1	57.8	NA	15
Q5VZK9	LRRC16A	151.6	NA	3
Q14566	MCM6	92.9	NA	3

P02795	MT2A	6	NA	3
Q5SYE7	NHSL1	170.7	NA	4
Q14980	NUMA1	238.3	NA	3
P43034	PAFAH1B1	46.6	NA	19
P68402	PAFAH1B2	25.6	NA	4
P05165	PCCA	80.1	NA	3
Q9BUL8	PDCD10	24.7	NA	3
O95263	PDE8B	99	NA	17
Q92508	PIEZO1	286.8	NA	23
Q13523	PRPF4B	117	NA	12
P55036	PSMD4	40.7	NA	7
O95758	PTBP3	59.7	NA	3
O75154	RAB11FIP3	82.4	NA	8
Q5EBL4	RILPL1	47.1	NA	6
Q9BRS2	RIOK1	65.6	NA	31
Q5W0B1	RNF219	81.1	NA	21
Q9H6T3	RPAP3	75.7	NA	7
P29353	SHC1	62.8	NA	10
Q92581	SLC9A6	74.2	NA	6
O95347	SMC2	135.7	NA	3
Q9Y6E0	STK24	49.3	NA	7
Q5VSL9	STRIP1	95.6	NA	3
Q13033	STRN3	87.2	NA	16
Q9NRL3	STRN4	80.6	NA	9
P53999	SUB1	14.4	NA	5
Q9BYX2	TBC1D2	105.4	NA	4
P04183	TK1	25.5	NA	6
Q16890	TPD52L1	22.4	NA	3
Q9NY65	TUBA8	50.1	NA	10
P04350	TUBB4A	49.6	NA	20
O94763	URI1	59.8	NA	4
Q9BQA1	WDR77	36.7	NA	9
Q96MX6	WDR92	39.7	NA	5
O14744	PRMT5	72.7	25	
O43815	STRN	86.1	23	
Q52LW3	ARHGAP29	142.1	22	
Q8N163	KIAA1967	102.9	15	
Q9BVG8	KIFC3	92.8	14	
Q9P289	MST4	46.5	7	
O75717	WDHD1	126	7	
Q07021	C1QBP	31.4	6	
P27824	CANX	67.6	5	
Q14203	DCTN1	141.7	5	
Q9Y2W1	THRAP3	108.7	5	
Q9UQB8	BAIAP2	60.9	4	
Q14008	CKAP5	225.5	4	
O60716	CTNND1	108.2	4	
P23284	PPIB	23.7	4	
Q15758	SLC1A5	56.6	4	
P17480	UBTF	89.4	4	
P50552	VASP	39.8	4	
Q5T1J5	CHCHD2P9	15.5	3	

P21291	CSRP1	20.6	3	
Q92522	H1-10	22.5	3	
Q00341	HDLBP	141.5	3	
Q01130	SRSF2	25.5	3	
Q9UHF7	TRPS1	141.5	3	
Q96CT7	CCDC124	25.8	2.5	
P35222	CTNNB1	85.5	2.5	
O43237	DYNC1LI2	54.1	2.5	
Q8N8S7	ENAH	66.5	2.5	
Q14192	FHL2	32.2	2.5	
P05166	PCCB	58.2	2.5	
Q15293	RCN1	38.9	2.5	

\*: Peptide number was indicated instead of the ratio for proteins that had 0 peptides in the control condition (TurboID only); NA: not applicable



## Chapter 3: General Conclusions and Future Perspectives

### ***PRMT5 inhibition as a combinatorial treatment strategy in TNBC***

In this study, we explored the advantage of combining the inhibition of PRMT5 with several chemotherapies and with inhibitors targeting the HER family members in TNBC. We observed a synergistic interaction between the PRMT5 inhibitor EPZ015938 and chemotherapies, with the strongest effect observed in the EPZ015938/cisplatin combination. The combination of EPZ015938 with EGFR inhibitor (erlotinib) and with the EGFR/HER2/HER4 inhibitor (neratinib) yielded synergistic advantages when applied on the EGFR-overexpressing TNBC cells MDA-MB-468 and BT20. In addition, the combinations of EPZ015938 with neratinib or with the HER2 inhibitor tucatinib showed high synergism in the HER2-low TNBC cell line, MDA-MB-453 and in the HER2-positive cell line HCC1954. Next, it is important to test the combination of PRMT5 inhibition with other HER2-targeted therapies (antibodies or ADC) on additional HER2-low TNBC and HER2-positive breast cancer cell lines, to examine if we can extend our findings. Future experiments that address the efficacy of the different combination *in vivo* will be performed, employing various TNBC PDX models. The EPZ015938/cisplatin combination could be tested on PDX models derived from patients that developed resistance to chemotherapies to address if this combination is effective in overcoming TNBC resistance, a major concern in its treatment. Moreover, biomarkers of response could be evaluated for these combinations. The EPZ015938/cisplatin combination can be performed on models with defects in the DNA damage response pathways, like *BRCA1/2* mutations, as these tumours were reported to be more sensitive to platinum agents [43]. The combination of PRMT5 inhibition with EGFR inhibitors could be tested on PDX models with EGFR overexpression, and those with HER2 inhibitors could be employed on HER2-low PDX models.

Another concern for TNBC is its high relapse rates, that could originate from its enrichment in BCSCs. The efficiency of combining PRMT5 inhibitors with chemotherapies in decreasing the population of BCSCs can be evaluated *in vitro* by performing mammosphere formation assays, or by examining BCSCs markers like ALDH1 and CD44 by flowcytometry. *In vivo*, we can examine if the drug combinations could diminish the population of BCSCs by flowcytometry performed on mice cells

extracted from the treated tumours. Tumour relapse can also be tested *in vivo*, to examine if the drug combinations could decrease tumour recurrence compared to the individual treatments.

In addition to these translational studies, the molecular effects underlying the different combinations could be investigated. DNA damage upon combining PRMT5 inhibition with cisplatin can be examined by assessing the DNA damage marker  $\gamma$ H2AX by WB and IF, to test if it is increased upon the combinatorial treatment. Additionally, the effect of combinations between PRMT5 inhibitor and the EGFR inhibitors on the EGFR pathway could be examined by WB analysis of phosphorylated downstream effectors of the signalling pathway like AKT and MAPK. It would also be interesting to test whether these combinations impact the trafficking of EGFR, another regulator of its activity. Similar experiments can be performed regarding HER2. The activity HER2 pathway could be evaluated after combining HER2 and PRMT5 inhibitors. In addition, it would be interesting to check whether HER2 is a PRMT5 substrate, similar to what has been reported for EGFR, and if this contributes to its signalling cascade regulation.

To identify the downstream effectors/targets of the various combinations, proteomic and/or transcriptomic analysis could be performed. In the proteomic analysis, the PRMT5 methylome and interactome could be identified by mass-spectrometry, and differential PRMT5 partners and/or substrates between the drug combinations and individual treatments could be identified. Moreover, RNA-seq analysis upon the combinatorial treatment can be employed to identify differentially expressed or differentially spliced transcripts, considering the pivotal role of PRMT5 in transcription and pre-mRNA splicing regulation.

### ***Deciphering the PRMT5 interactome***

In this study, our primary goal was to elucidate the interactome of PRMT5 in TNBC cells using a combination of immunoprecipitation and proximity labelling approaches. Initially, due to the lack of an anti-PRMT5 antibody suitable for PRMT5 immunoprecipitation, we first characterized the MEP50 interactome by immunoprecipitating MEP50 from HCC38 cells, which are BL1 TNBC cells. Subsequently, upon validating a PRMT5 antibody for efficient immunoprecipitation, we identified the PRMT5 interactome in MDA-MB-468 cells, another BL1 TNBC cell line. In future studies, it will be important to replicate these experiments in the same cell

lines with a minimum of 3 biological replicates to ensure robust and statistically significant data. Additionally, it is advisable to extend this investigation to other TNBC cell lines, ideally encompassing different TNBC subtypes to take into consideration the heterogeneity of the disease, and to non-cancerous cell lines. A main limitation of the classical immunoprecipitation lies in its challenge to detect transient protein-protein interactions. Although it may not be the case, PRMT5 is an enzyme which may engage in transient interactions with its substrates, as it is observed for kinases. This is one of the reasons why we employed the TurboID proximity labelling method which can be valuable in uncovering these dynamic interactions. Choosing HEK293T cells, which are easily to transfect, allowed us to establish and optimize the TurboID protocol before applying it to TNBC cells. With the method now optimized, it is possible to perform a similar procedure to capturing PRMT5 partners in TNBC cell lines. TurboID, being a protein of approximately 36 KDa, may potentially interfere with PRMT5-protein interactions. To address this issue, future experiments could utilize TurboID fused to the C-terminus of PRMT5 (**Figure 1A**; PRMT5-TurboID, clone generated during my thesis) and compare the PRMT5 neighbours obtained in both conditions.

Given that PRMT5 forms a stable hetero-octameric complex with MEP50, with 4 PRMT5 monomers situated at the core and 4 MEP50 molecules at the periphery [122], it could be insightful to co-transfect both TurboID-PRMT5 and TurboID-MEP50 (or PRMT5-TurboID and MEP50-TurboID) to identify the partners of the complex. Constructs for TurboID-MEP50 were also generated during my thesis (**Figure 1A**). Lastly, rather than overexpressing the TurboID fusion proteins, an alternative approach would be to introduce the TurboID sequence upstream or downstream the *PRMT5* gene using CRISPR-Cas9 knock-in in a TNBC cell line [627]. This would result in the expression of the TurboID-PRMT5 protein at levels comparable to the endogenous PRMT5.

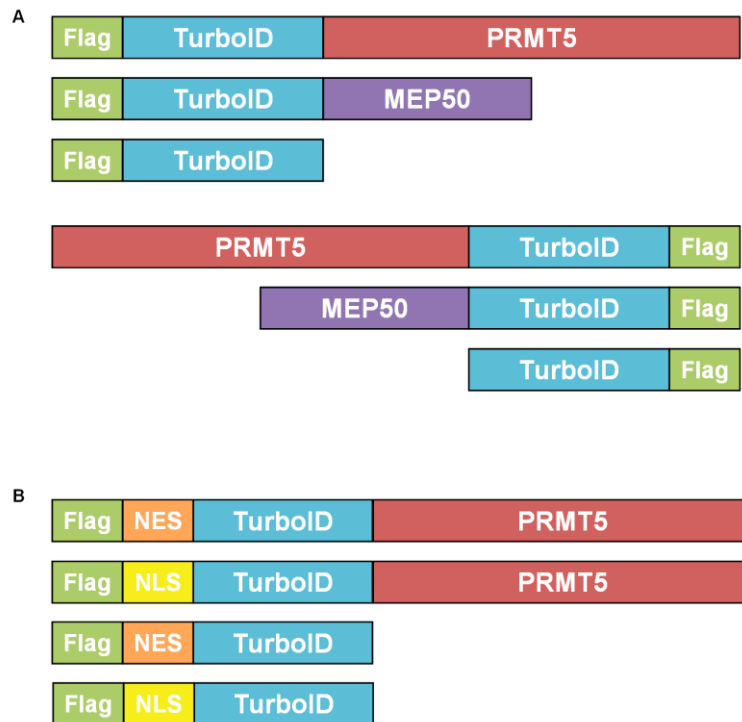


**Figure 1: TurboID constructs schemes.**

The dynamic shuttling of PRMT5 between the nucleus and cytoplasm emerges as a critical aspect of its role in oncogenesis. As highlighted in the discussion, low levels of nuclear PRMT5 and MEP50 are associated with poor prognosis and aggressive tumours, such as TNBC. What are the PRMT5 partners both in the cytosol and in the nucleus? Among these partners, which ones may be involved in promoting malignant transformation? Furthermore, what mechanisms govern the controlled translocation of PRMT5 between these cellular compartments? In order to gain comprehensive insights, it will be crucial to determine the PRMT5 interactome in both compartments. The TurboID technique holds potential for this purpose, achieved through the insertion of an NES or NLS (**Figure 1B**), forcing in theory the expression of PRMT5 in the cytoplasm and the nucleus respectively, to capture its partners in both compartments. The experiments could be performed in a TNBC cell line and in a non-cancerous breast cell line (like MCF10A) for comparative analysis. Constructs encoding TurboID-NES-PRMT5 and TurboID-NLS-PRMT5 fusion proteins were also generated during my thesis (**Figure 1B**); however, due to time and prioritization constraints, these investigations were not further pursued. The initial step in the future would be to validate the proper subcellular localization of the fused proteins (Flag-NES-TurboID-PRMT5, Flag-NLS-TurboID-PRMT5) through IF. Subsequently, partner identification

would be carried out in cells expressing Flag-NES-TurboID-PRMT5 or Flag-NLS-TurboID-PRMT5 (transient transfection or CRISPR/Cas9 knock-in). Alternatively, PRMT5 could be immunoprecipitated following subcellular fractionation, similar to the study performed by Rengasamy *et al.* using MEP50 antibodies [412]. However, they detected the same proteins in both the nucleus and cytoplasm and found RIOK1 which is a strictly cytoplasmic interactor of the PRMT5/MEP50 complex as a nuclear partner, raising questions about the of purity of their nuclear and cytosolic fractions. Thus, careful fractionation and validation steps would be essential for reliable results.

### ***Effect of FUBP1 methylation on its functions***

Among the identified MEP50 interactors, FUBP1 emerged as a top candidate. Subsequent studies demonstrated that FUBP1 is a substrate of PRMT5, and that symmetric di-methylation plays a pivotal role in regulating its binding to the FUSE element. However, this modification did not appear to impact FUBP1's cellular localization. Additional work will be required to better understand the functional impact of the PRMT5/MEP50-FUBP1 interaction. While our study highlighted that FUBP1 methylation enhances its interaction with the FUSE element, we have yet to explore its impact on other chromatin sequences. This could be addressed by conducting a ChIP-seq analysis of FUBP1 in TNBC cells following PRMT5 inhibition, which would provide insights into the chromatin regions where FUBP1 exhibits altered binding due to its methylation status. This could unravel a broader understanding of how FUBP1's methylation contributes to its chromatin interactions and transcriptional functions. Furthermore, identifying the RNA molecules that differentially interact with FUBP1 upon its methylation status represents another avenue of exploration. This could be achieved through RNA IP (RIP) followed by sequencing (RIP-seq) in TNBC cells after PRMT5 inhibition, which would shed light on how FUBP1's methylation influences its interactions with RNA transcripts.

Given FUBP1's dual roles in regulating both transcription and pre-mRNA splicing, coupled with our discovery that its methylation modulates its binding to FUSE, it would be interesting to investigate whether FUBP1 methylation influences gene expression and alternative splicing events. One approach could involve the stable expression of FUBP1 wild-type and a triple lysine mutant (mimicking the methylation-deficient state) in a TNBC cell line (both resistant to FUBP1 siRNA). Subsequently, endogenous FUBP1 will be depleted using siRNA before the RNA-seq analysis, to uncover

differentially expressed and spliced transcripts between cells expressing mutant and wild-type FUBP1. This same approach could be applied before performing ChIP-seq or RIP-seq, instead of inhibiting PRMT5, to investigate the effects of these three arginine residues in regulating FUBP1 interaction with nucleic acids.

Given our findings that FUBP1 is overexpressed in TNBC compared to normal tissue, and its depletion impairs the proliferation of MDA-MB-468 cells, it would be interesting to investigate the impact of its methylation on TNBC tumorigenesis. This study would involve both *in vitro* and *in vivo* experiments. To examine whether the methylation of FUBP1 correlates with clinical parameters in breast cancer, antibodies targeting the symmetrically dimethylated form of FUBP1 could be generated. Subsequently, immunohistochemical staining of normal breast and breast cancer tumours belonging to the different subtypes, could be performed. Additionally, since we showed that inhibiting PRMT5 decreases the proliferation of a subset of TNBC cell lines, investigating the effects of FUBP1 depletion together with PRMT5 inhibition, could determine whether this combination exerts a synergistic effect on inhibiting TNBC cells proliferation. This concept could be extended to *in vivo* studies, utilizing TNBC xenografts models generated from TNBC cells depleted or KO for FUBP1, followed by PRMT5 inhibition, to assess the potential therapeutic benefits.

### ***PRMT5 interaction with DBC-1***

DBC-1 was identified among the top PRMT5 partners using the IP method. DBC-1 is a subunit of the DBIRD complex, which also includes ZNF326, a validated PRMT5 substrate [412]. Since the function of the interaction between PRMT5 and ZNF326 was already demonstrated, we did not analyse the functional impact of the interaction between PRMT5 and DBC-1, as it will be most likely similar to ZNF326. Of note, DBC-1 is predicted to be methylated by large scale proteomic analysis on several arginine residues (PhosphoSitePlus; [432]). Subsequent experiments could aim to confirm these methylation events and establish their dependency on PRMT5 activity. This would contribute valuable insights into the regulatory mechanisms governing DBC-1 and its potential role in PRMT5-mediated processes.

## ***Functional analysis of the interaction between PRMT5 and SDCCAG3***

Extensive research is still needed to elucidate the functional interaction between SDCCAG3 and PRMT5. Unfortunately, the unavailability of an antibody capable of specifically detecting SDCCAG3 via western blotting hindered the validation of the interaction between endogenous PRMT5 and SDCCAG3 using immunoprecipitation. We could examine whether SDCCAG3 undergoes methylation in TNBC cells. If methylation is detected, it will be essential to ascertain whether PRMT5 is the enzyme responsible for this modification. Analysing proteomic data of the PRMT5 methylome, potential monomethylation of SDCCAG3 on R7 and 15 were identified in the study performed by Larsen *et al.* [106]. To validate if SDCCAG3 is indeed methylated and determine if it is mediated by PRMT5, *in vitro* methylation assays could be envisaged using recombinant SDCCAG3 protein and PRMT5/MEP50 complex. If methylation event(s) is(are) observed, a subsequent step would entail identifying the specific methylation sites through mass spectrometry analysis, followed by validation using site-directed mutagenesis and methylation assays. Furthermore, comprehensive biochemical analysis could be conducted to determine which domains of PRMT5 interact with SDCCAG3, and conversely, using co-immunoprecipitation assays with deleted mutants of the 2 proteins. To examine in which cellular compartments PRMT5 and SDCCAG3 interact, Proximity Ligation Assay (PLA) could be performed.

As arginine methylation can affect subcellular localisation and stability, we could investigate whether PRMT5 exerts influence on SDCCAG3's localization and stability. This can be achieved by depleting or inhibiting PRMT5 followed by monitoring SDCCAG3 localization and levels. Reciprocally, exploring whether SDCCAG3 impacts PRMT5 activity could also be explored. This can be addressed by depleting SDCCAG3 and examining the total symmetric dimethylation levels (SDMA) in the cells.

We found that SDCCAG3, and possibly PRMT5, interacts with LRP6, and regulates the Wnt signalling pathway. As PRMT5 was shown to regulate the Wnt pathway [631,632,634,635], it raises an intriguing possibility: Could SDCCAG3 be involved in the intracellular trafficking of LRP6? Moreover, does PRMT5 also participate in this process? While previous research has not established a link between PRMT5 and

endocytosis or protein trafficking, it is noteworthy that these pathways emerged prominently in the analysis of the PRMT5 interactome using TurboID. This potential intersection between PRMT5 and cellular trafficking mechanisms presents a promising avenue for further exploration.

What about the other functions of SDCCAG3? Is PRMT5 involved? Previous research has indicated that SDCCAG3 is present at the midbody during cytokinesis, and alterations in its expression levels can lead to cytokinetic defects revealed by multinucleated cells [617]. However, the exact functions of SDCCAG3 during cell division remain to be fully elucidated. Interestingly, proteomic analysis of midbody remnants has revealed the presence of both PRMT5 and SDCCAG3 [636], and our study identified cell division as one of the significantly enriched pathways among PRMT5 interactors using both PRMT5 IP and TurboID. These findings suggest a potential role for PRMT5 in cytokinesis, possibly through its interaction with SDCCAG3. Therefore, future studies could be made to investigate first if PRMT5 is indeed required for cell division, and then if it is through its interaction with SDCCAG3.

While our current data does not provide definitive answers to these questions, it lays the foundation for further investigations into PRMT5's involvement in pathways that have not been extensively studied in the context of PRMT5. This preliminary data offers a valuable starting point for future projects in the laboratory.



## References

- [1] Sung H, Ferlay J, Siegel RL, Laversanne M, Soerjomataram I, Jemal A, et al. Global Cancer Statistics 2020: GLOBOCAN Estimates of Incidence and Mortality Worldwide for 36 Cancers in 185 Countries. *CA Cancer J Clin* 2021;71:209–49. <https://doi.org/10.3322/CAAC.21660>.
- [2] Global Cancer Observatory n.d. <https://gco.iarc.fr/> (accessed April 3, 2023).
- [3] Makki J. Diversity of Breast Carcinoma: Histological Subtypes and Clinical Relevance. *Clin Med Insights Pathol* 2015;8:23. <https://doi.org/10.4137/CPATH.S31563>.
- [4] Ginsburg O, Bray F, Coleman MP, Vanderpuye V, Eniu A, Kotha SR, et al. The global burden of women's cancers: a grand challenge in global health. *Lancet* 2017;389:847–60. [https://doi.org/10.1016/S0140-6736\(16\)31392-7](https://doi.org/10.1016/S0140-6736(16)31392-7).
- [5] Łukasiewicz S, Czezelewski M, Forma A, Baj J, Sitarz R, Stanisławek A. Breast Cancer-Epidemiology, Risk Factors, Classification, Prognostic Markers, and Current Treatment Strategies-An Updated Review 2021. <https://doi.org/10.3390/cancers13174287>.
- [6] Sun YS, Zhao Z, Yang ZN, Xu F, Lu HJ, Zhu ZY, et al. Risk Factors and Preventions of Breast Cancer. *Int J Biol Sci* 2017;13:1387. <https://doi.org/10.7150/IJBS.21635>.
- [7] Washbrook E. Risk factors and epidemiology of breast cancer. *Women's Health Medicine* 2006;3:8–14. <https://doi.org/10.1383/WOHM.2006.3.1.8>.
- [8] KB K, JL H, DR B, KA P, TM M, MJ R-B, et al. Risks of Breast, Ovarian, and Contralateral Breast Cancer for BRCA1 and BRCA2 Mutation Carriers. *JAMA* 2017;317:2402–16. <https://doi.org/10.1001/JAMA.2017.7112>.
- [9] What Are the Risk Factors for Breast Cancer? | CDC n.d. [https://www.cdc.gov/cancer/breast/basic\\_info/risk\\_factors.htm](https://www.cdc.gov/cancer/breast/basic_info/risk_factors.htm) (accessed April 3, 2023).
- [10] Loibl S, Poortmans P, Morrow M, Denkert C, Curigliano G. Breast cancer. *The Lancet* 2021;397:1750–69. [https://doi.org/10.1016/S0140-6736\(20\)32381-3](https://doi.org/10.1016/S0140-6736(20)32381-3).
- [11] Jafari SH, Saadatpour Z, Salmaninejad A, Momeni F, Mokhtari M, Nahand JS, et al. Breast cancer diagnosis: Imaging techniques and biochemical markers. *J Cell Physiol* 2018;233:5200–13. <https://doi.org/10.1002/JCP.26379>.
- [12] Mammography n.d. <https://www.nibib.nih.gov/science-education/science-topics/mammography#pid-1061> (accessed April 4, 2023).
- [13] Oeffinger KC, Fontham ETH, Etzioni R, Herzig A, Michaelson JS, Shih YCT, et al. Breast Cancer Screening for Women at Average Risk: 2015 Guideline Update from the American Cancer Society. *JAMA* 2015;314:1599. <https://doi.org/10.1001/JAMA.2015.12783>.

- [14] Wang L. Early Diagnosis of Breast Cancer. *Sensors* 2017, Vol 17, Page 1572 2017;17:1572. <https://doi.org/10.3390/S17071572>.
- [15] McDonald ES, Clark AS, Tchou J, Zhang P, Freedman GM. Clinical Diagnosis and Management of Breast Cancer. *J Nucl Med* 2016;57:9–16. <https://doi.org/10.2967/jnumed.115.157834>.
- [16] Alcantara D, Leal MP, García-Bocanegra I, García-Martín ML. Molecular imaging of breast cancer: present and future directions. *Front Chem* 2014;2. <https://doi.org/10.3389/FCHEM.2014.00112>.
- [17] Breast Anatomy - National Breast Cancer Foundation n.d. <https://www.nationalbreastcancer.org/breast-anatomy/> (accessed April 4, 2023).
- [18] Hassiotou F, Geddes D. Anatomy of the Human Mammary Gland: Current Status of Knowledge n.d. <https://doi.org/10.1002/ca.22165>.
- [19] Terese Winslow LLC, Medical and Scientific Illustration n.d. <https://www.teresewinslow.com/> (accessed April 4, 2023).
- [20] Types of breast cancer and related conditions | Cancer Research UK n.d. <https://www.cancerresearchuk.org/about-cancer/breast-cancer/stages-types-grades/types> (accessed April 5, 2023).
- [21] Jin X, Mu P. Targeting Breast Cancer Metastasis. *Breast Cancer (Auckl)* 2015;9:23. <https://doi.org/10.4137/BCBCR.S25460>.
- [22] Invasive Breast Cancer (IDC/ILC) n.d. <https://www.cancer.org/cancer/breast-cancer/about/types-of-breast-cancer/invasive-breast-cancer.html> (accessed April 7, 2023).
- [23] Zhu H, Doğan BE. American Joint Committee on Cancer’s Staging System for Breast Cancer, Eighth Edition: Summary for Clinicians. *Eur J Breast Health* 2021;17:234. <https://doi.org/10.4274/EJBH.GALENOS.2021.2021-4-3>.
- [24] Breast Cancer Staging | ACS n.d. <https://www.facs.org/for-patients/home-skills-for-patients/breast-cancer-surgery/breast-cancer-types/breast-cancer-staging/> (accessed April 8, 2023).
- [25] Teichgraeber DC, Guirguis MS, Whitman GJ. Breast Cancer Staging: Updates in the AJCC Cancer Staging Manual, 8th Edition, and Current Challenges for Radiologists, From the AJR Special Series on Cancer Staging. <https://doi.org/10.2214/AJR.20.25223> 2021;217:278–90. <https://doi.org/10.2214/AJR.20.25223>.
- [26] Staging & Grade - Breast Pathology | Johns Hopkins Pathology n.d. <https://pathology.jhu.edu/breast/staging-grade/> (accessed April 9, 2023).
- [27] Perou CM, Sørile T, Eisen MB, Van De Rijn M, Jeffrey SS, Renshaw CA, et al. Molecular portraits of human breast tumours. *Nature* 2000 406:6797–800. <https://doi.org/10.1038/35021093>.

- [28] Harbeck N, Penault-Llorca F, Cortes J, Gnant M, Houssami N, Poortmans P, et al. Breast cancer. *Nature Reviews Disease Primers* 2019 5:1 2019;5:1–31. <https://doi.org/10.1038/s41572-019-0111-2>.
- [29] Parker JS, Mullins M, Cheang MCU, Leung S, Voduc D, Vickery T, et al. Supervised Risk Predictor of Breast Cancer Based on Intrinsic Subtypes. *J Clin Oncol* 2009;27:1160–7. <https://doi.org/10.1200/JCO.2008.18.1370>.
- [30] Brenton JD, Carey LA, Ahmed A, Caldas C. Molecular classification and molecular forecasting of breast cancer: ready for clinical application? *J Clin Oncol* 2005;23:7350–60. <https://doi.org/10.1200/JCO.2005.03.3845>.
- [31] Dai X, Li T, Bai Z, Yang Y, Liu X, Zhan J, et al. Breast cancer intrinsic subtype classification, clinical use and future trends. *Am J Cancer Res* 2015;5:2929.
- [32] Feeley LP, Mulligan AM, Pinnaduwage D, Bull SB, Andrulis IL. Distinguishing luminal breast cancer subtypes by Ki67, progesterone receptor or TP53 status provides prognostic information. *Mod Pathol* 2014;27:554–61. <https://doi.org/10.1038/MODPATHOL.2013.153>.
- [33] Koboldt DC, Fulton RS, McLellan MD, Schmidt H, Kalicki-Veizer J, McMichael JF, et al. Comprehensive molecular portraits of human breast tumours. *Nature* 2012;490:61–70. <https://doi.org/10.1038/NATURE11412>.
- [34] Burguin A, Diorio C, Durocher F. Breast Cancer Treatments: Updates and New Challenges. *J Pers Med* 2021;11:808. <https://doi.org/10.3390/JPM11080808>.
- [35] Felip Falgas E, Sirven Milana Arantza B, Florencia Mercogliano M, Bruni S, Luciana Mauro F, Schillaci R. Emerging Targeted Therapies for HER2-Positive Breast Cancer. *Cancers* 2023, Vol 15, Page 1987 2023;15:1987. <https://doi.org/10.3390/CANCERS15071987>.
- [36] Modi S, Jacot W, Yamashita T, Sohn J, Vidal M, Tokunaga E, et al. Trastuzumab Deruxtecan in Previously Treated HER2-Low Advanced Breast Cancer. *New England Journal of Medicine* 2022;387:9–20. [https://doi.org/10.1056/NEJMOA2203690/SUPPL\\_FILE/NEJMOA2203690\\_DATA-SHARING.PDF](https://doi.org/10.1056/NEJMOA2203690/SUPPL_FILE/NEJMOA2203690_DATA-SHARING.PDF).
- [37] FDA Approves First Targeted Therapy for HER2-Low Breast Cancer | FDA n.d. <https://www.fda.gov/news-events/press-announcements/fda-approves-first-targeted-therapy-her2-low-breast-cancer> (accessed May 30, 2023).
- [38] Li Y, Tsang JY, Tam F, Loong T, Tse GM. Comprehensive characterization of HER2-low breast cancers: implications in prognosis and treatment. *EBioMedicine* 2023;91:104571. <https://doi.org/10.1016/j.ebiom.2023.104571>.
- [39] Czajka ML, Pfeifer C. Breast Cancer Surgery. *Breast Cancer and Gynecologic Cancer Rehabilitation* 2023:99–107. <https://doi.org/10.1016/B978-0-323-72166-0.00010-4>.
- [40] Arbuckle JD, Wilke LG. Mastectomy. *Illustrative Handbook of General Surgery: Second Edition* 2022:107–14. [https://doi.org/10.1007/978-3-319-24557-7\\_10](https://doi.org/10.1007/978-3-319-24557-7_10).

- [41] Polgár C, Kahán Z, Ivanov O, Chorváth M, Ligačová A, Csejtei A, et al. Radiotherapy of Breast Cancer—Professional Guideline 1st Central-Eastern European Professional Consensus Statement on Breast Cancer. *Pathology and Oncology Research* 2022;28. <https://doi.org/10.3389/PORE.2022.1610378>.
- [42] Lehmann F, Wennerberg J. Evolution of Nitrogen-Based Alkylating Anticancer Agents. *Processes* 2021, Vol 9, Page 377 2021;9:377. <https://doi.org/10.3390/PR9020377>.
- [43] Garutti M, Pelizzari G, Bartoletti M, Malfatti MC, Gerratana L, Tell G, et al. Platinum Salts in Patients with Breast Cancer: A Focus on Predictive Factors. *International Journal of Molecular Sciences* 2019, Vol 20, Page 3390 2019;20:3390. <https://doi.org/10.3390/IJMS20143390>.
- [44] Avendaño C, Menéndez JC. DNA Intercalators and Topoisomerase Inhibitors. *Medicinal Chemistry of Anticancer Drugs* 2008:199–228. <https://doi.org/10.1016/B978-0-444-52824-7.00007-X>.
- [45] Kaye SB. New antimetabolites in cancer chemotherapy and their clinical impact. *Br J Cancer* 1998;78 Suppl 3:1–7. <https://doi.org/10.1038/BJC.1998.747>.
- [46] Čermák V, Dostál V, Jelínek M, Libusová L, Kovář J, Rösel D, et al. Microtubule-targeting agents and their impact on cancer treatment. *Eur J Cell Biol* 2020;99. <https://doi.org/10.1016/J.EJCB.2020.151075>.
- [47] Nabholz JM, Gligorov J. The role of taxanes in the treatment of breast cancer. *Expert Opin Pharmacother* 2005;6:1073–94. <https://doi.org/10.1517/14656566.6.7.1073>.
- [48] van den Boogaard WMC, Komninos DSJ, Vermeij WP. Chemotherapy Side-Effects: Not All DNA Damage Is Equal. *Cancers* 2022, Vol 14, Page 627 2022;14:627. <https://doi.org/10.3390/CANCERS14030627>.
- [49] Fisusi FA, Akala EO. Drug Combinations in Breast Cancer Therapy. *Pharm Nanotechnol* 2019;7:3. <https://doi.org/10.2174/2211738507666190122111224>.
- [50] Fisher B, Bryant J, Wolmark N, Mamounas E, Brown A, Fisher ER, et al. Effect of preoperative chemotherapy on the outcome of women with operable breast cancer. *J Clin Oncol* 1998;16:2672–85. <https://doi.org/10.1200/JCO.1998.16.8.2672>.
- [51] Swain SM, Shastry M, Hamilton E. Targeting HER2-positive breast cancer: advances and future directions. *Nature Reviews Drug Discovery* 2022 22:2 2022;22:101–26. <https://doi.org/10.1038/s41573-022-00579-0>.
- [52] Baselga J. Treatment of HER2-overexpressing breast cancer. *Annals of Oncology* 2010;21:vii36–40. <https://doi.org/10.1093/annonc/mdq421>.
- [53] Moo TA, Sanford R, Dang C, Morrow M. Overview of Breast Cancer Therapy. *PET Clin* 2018;13:339. <https://doi.org/10.1016/J.CPET.2018.02.006>.

- [54] Nahta R, Yuan LXH, Du Y, Esteva FJ. Lapatinib induces apoptosis in trastuzumab-resistant breast cancer cells: effects on insulin-like growth factor I signaling. *Mol Cancer Ther* 2007;6:667–74. <https://doi.org/10.1158/1535-7163.MCT-06-0423>.
- [55] Conlon NT, Kooijman JJ, van Gerwen SJC, Mulder WR, Zaman GJR, Diala I, et al. Comparative analysis of drug response and gene profiling of HER2-targeted tyrosine kinase inhibitors. *Br J Cancer* 2021;124:1249–59. <https://doi.org/10.1038/s41416-020-01257-x>.
- [56] Guarneri V, Frassoldati A, Bottini A, Cagossi K, Bisagni G, Sarti S, et al. Preoperative chemotherapy plus trastuzumab, lapatinib, or both in human epidermal growth factor receptor 2-positive operable breast cancer: results of the randomized phase II CHER-LOB study. *J Clin Oncol* 2012;30:1989–95. <https://doi.org/10.1200/JCO.2011.39.0823>.
- [57] Schlam I, Swain SM. HER2-positive breast cancer and tyrosine kinase inhibitors: the time is now. *Npj Breast Cancer* 2021 7:1 2021;7:1–12. <https://doi.org/10.1038/s41523-021-00265-1>.
- [58] Beck A, Goetsch L, Dumontet C, Corvaia N. Strategies and challenges for the next generation of antibody–drug conjugates. *Nature Reviews Drug Discovery* 2017 16:5 2017;16:315–37. <https://doi.org/10.1038/nrd.2016.268>.
- [59] Ferraro E, Drago JZ, Modi S. Implementing antibody-drug conjugates (ADCs) in HER2-positive breast cancer: state of the art and future directions. *Breast Cancer Research* 2021;23:1–11. <https://doi.org/10.1186/S13058-021-01459-Y/TABLES/4>.
- [60] Cortesi L, Rugo HS, Jackisch C. An Overview of PARP Inhibitors for the Treatment of Breast Cancer. *Target Oncol* 2021;16:255–82. <https://doi.org/10.1007/S11523-021-00796-4>.
- [61] KB K, JL H, DR B, KA P, TM M, MJ R-B, et al. Risks of Breast, Ovarian, and Contralateral Breast Cancer for BRCA1 and BRCA2 Mutation Carriers. *JAMA* 2017;317:2402–16. <https://doi.org/10.1001/JAMA.2017.7112>.
- [62] Waldman AD, Fritz JM, Lenardo MJ. A guide to cancer immunotherapy: from T cell basic science to clinical practice. *Nature Reviews Immunology* 2020 20:11 2020;20:651–68. <https://doi.org/10.1038/s41577-020-0306-5>.
- [63] Debien V, De Caluwé A, Wang X, Piccart-Gebhart M, Tuohy VK, Romano E, et al. Immunotherapy in breast cancer: an overview of current strategies and perspectives. *Npj Breast Cancer* 2023 9:1 2023;9:1–10. <https://doi.org/10.1038/s41523-023-00508-3>.
- [64] Valencia GA, Rioja P, Morante Z, Ruiz R, Fuentes H, Castaneda CA, et al. Immunotherapy in triple-negative breast cancer: A literature review and new advances. *World J Clin Oncol* 2022;13:219. <https://doi.org/10.5306/WJCO.V13.I3.219>.

- [65] DeSantis CE, Fedewa SA, Goding Sauer A, Kramer JL, Smith RA, Jemal A. Breast cancer statistics, 2015: Convergence of incidence rates between black and white women. *CA Cancer J Clin* 2016;66:31–42. <https://doi.org/10.3322/CAAC.21320>.
- [66] Almansour NM. Triple-Negative Breast Cancer: A Brief Review About Epidemiology, Risk Factors, Signaling Pathways, Treatment and Role of Artificial Intelligence. *Front Mol Biosci* 2022;9:836417. <https://doi.org/10.3389/fmolb.2022.836417>.
- [67] Li Y, Zhang H, Merkher Y, Chen L, Liu N, Leonov S, et al. Recent advances in therapeutic strategies for triple-negative breast cancer. *J Hematol Oncol* 2022;15:121. <https://doi.org/10.1186/s13045-022-01341-0>.
- [68] Lehmann BD, Bauer JA, Chen X, Sanders ME, Chakravarthy AB, Shyr Y, et al. Identification of human triple-negative breast cancer subtypes and preclinical models for selection of targeted therapies. *J Clin Invest* 2011;121:2750–67. <https://doi.org/10.1172/jci45014>.
- [69] Lehmann BD, Jovanović B, Chen X, Estrada M V, Johnson KN, Shyr Y, et al. Refinement of Triple-Negative Breast Cancer Molecular Subtypes: Implications for Neoadjuvant Chemotherapy Selection. *PLoS One* 2016;11:e0157368. <https://doi.org/10.1371/journal.pone.0157368>.
- [70] Ensenyat-Mendez M, Llinàs-Arias P, Orozco JIJ, Íñiguez-Muñoz S, Salomon MP, Sesé B, et al. Current Triple-Negative Breast Cancer Subtypes: Dissecting the Most Aggressive Form of Breast Cancer. *Front Oncol* 2021;11. <https://doi.org/10.3389/fonc.2021.681476>.
- [71] Jézéquel P, Kerdraon O, Hondermarck H, Guérin-Charbonnel C, Lasla H, Gouraud W, et al. Identification of three subtypes of triple-negative breast cancer with potential therapeutic implications. *Breast Cancer Research* 2019;21. <https://doi.org/10.1186/s13058-019-1148-6>.
- [72] Liu YR, Jiang YZ, Xu XE, Yu K Da, Jin X, Hu X, et al. Comprehensive transcriptome analysis identifies novel molecular subtypes and subtype-specific RNAs of triple-negative breast cancer. *Breast Cancer Research* 2016;18. <https://doi.org/10.1186/s13058-016-0690-8>.
- [73] Burstein MD, Tsimelzon A, Poage GM, Covington KR, Contreras A, Fuqua SAW, et al. Comprehensive genomic analysis identifies novel subtypes and targets of triple-negative breast cancer. *Clinical Cancer Research* 2015;21:1688–98. <https://doi.org/10.1158/1078-0432.CCR-14-0432>.
- [74] Quist J, Mirza H, Cheang MCU, Telli ML, O’Shaughnessy JA, Lord CJ, et al. A four-gene decision tree signature classification of triple-negative breast cancer: Implications for targeted therapeutics. *Mol Cancer Ther* 2019;18:204–12. <https://doi.org/10.1158/1535-7163.MCT-18-0243>.
- [75] Asghar US, Barr AR, Cutts R, Beaney M, Babina I, Sampath D, et al. Single-Cell Dynamics Determines Response to CDK4/6 Inhibition in Triple-Negative Breast

- Cancer. *Clin Cancer Res* 2017;23:5561–72. <https://doi.org/10.1158/1078-0432.CCR-17-0369>.
- [76] Li CJ, Tzeng YDT, Chiu YH, Lin HY, Hou MF, Chu PY. Pathogenesis and potential therapeutic targets for triple-negative breast cancer. *Cancers (Basel)* 2021;13. <https://doi.org/10.3390/cancers13122978>.
- [77] Lee JS, Yost SE, Yuan Y. Neoadjuvant Treatment for Triple Negative Breast Cancer: Recent Progresses and Challenges. *Cancers (Basel)* 2020;12. <https://doi.org/10.3390/CANCERS12061404>.
- [78] Tung N, Garber JE. PARP inhibition in breast cancer: progress made and future hopes. *NPJ Breast Cancer* 2022;8:47. <https://doi.org/10.1038/s41523-022-00411-3>.
- [79] Singh DD, Parveen A, Yadav DK. Role of PARP in TNBC: Mechanism of Inhibition, Clinical Applications, and Resistance. *Biomedicines* 2021;9. <https://doi.org/10.3390/biomedicines9111512>.
- [80] Barchiesi G, Roberto M, Verrico M, Vici P, Tomao S, Tomao F. Emerging Role of PARP Inhibitors in Metastatic Triple Negative Breast Cancer. Current Scenario and Future Perspectives. *Front Oncol* 2021;11:769280. <https://doi.org/10.3389/fonc.2021.769280>.
- [81] Zagami P, Carey LA. Triple negative breast cancer: Pitfalls and progress. *NPJ Breast Cancer* 2022;8:95. <https://doi.org/10.1038/s41523-022-00468-0>.
- [82] Cortes J, Rugo HS, Cescon DW, Im S-A, Yusof MM, Gallardo C, et al. Pembrolizumab plus Chemotherapy in Advanced Triple-Negative Breast Cancer. *N Engl J Med* 2022;387:217–26. <https://doi.org/10.1056/NEJMOA2202809>.
- [83] Shah M, Osgood CL, Amatya AK, Fiero MH, Pierce WF, Nair A, et al. FDA Approval Summary: Pembrolizumab for Neoadjuvant and Adjuvant Treatment of Patients with High-Risk Early-Stage Triple-Negative Breast Cancer. *Clin Cancer Res* 2022;28:5249–53. <https://doi.org/10.1158/1078-0432.CCR-22-1110>.
- [84] Nonneville A de, Goncalves A, Mamessier E, Bertucci F. Sacituzumab govitecan in triple-negative breast cancer. *Ann Transl Med* 2022;10:647–647. <https://doi.org/10.21037/ATM-22-813>.
- [85] Bardia A, Hurvitz SA, Tolaney SM, Loirat D, Punie K, Oliveira M, et al. Sacituzumab Govitecan in Metastatic Triple-Negative Breast Cancer. *New England Journal of Medicine* 2021;384:1529–41. [https://doi.org/10.1056/NEJMOA2028485/SUPPL\\_FILE/NEJMOA2028485\\_DATA-SHARING.PDF](https://doi.org/10.1056/NEJMOA2028485/SUPPL_FILE/NEJMOA2028485_DATA-SHARING.PDF).
- [86] Nedeljković M, Damjanović A. Mechanisms of Chemotherapy Resistance in Triple-Negative Breast Cancer—How We Can Rise to the Challenge. *Cells* 2019;8. <https://doi.org/10.3390/CELLS8090957>.

- [87] Yamada A, Ishikawa T, Ota I, Kimura M, Shimizu D, Tanabe M, et al. High expression of ATP-binding cassette transporter ABCC11 in breast tumors is associated with aggressive subtypes and low disease-free survival. *Breast Cancer Res Treat* 2013;137:773–82. <https://doi.org/10.1007/S10549-012-2398-5>.
- [88] Xu L, Zhao Z, Wang K, Zhou H, Xing C. Expression of aldehyde dehydrogenase 1 and ATP-binding cassette superfamily G member 2 is enhanced in primary foci and metastatic lymph node from patients with triple-negative breast cancer. *Biomedical Research* n.d.;28.
- [89] Sissung TM, Baum CE, Kirkland CT, Gao R, Gardner ER, Figg WD. Pharmacogenetics of Membrane Transporters: An Update on Current Approaches. *Mol Biotechnol* 2010;44:152. <https://doi.org/10.1007/S12033-009-9220-6>.
- [90] Oguri T, Bessho Y, Achiwa H, Ozasa H, Maeno K, Maeda H, et al. MRP8/ABCC11 directly confers resistance to 5-fluorouracil. *Mol Cancer Ther* 2007;6:122–7. <https://doi.org/10.1158/1535-7163.MCT-06-0529>.
- [91] Fultang N, Chakraborty M, Peethambaran B. Regulation of cancer stem cells in triple negative breast cancer. *Cancer Drug Resistance* 2021;4:321. <https://doi.org/10.20517/CDR.2020.106>.
- [92] O’Conor CJ, Chen T, González I, Cao D, Peng Y. Cancer stem cells in triple-negative breast cancer: a potential target and prognostic marker. *Biomark Med* 2018;12:813–20. <https://doi.org/10.2217/BMM-2017-0398>.
- [93] He L, Wick N, Germans SK, Peng Y. The Role of Breast Cancer Stem Cells in Chemoresistance and Metastasis in Triple-Negative Breast Cancer. *Cancers* 2021, Vol 13, Page 6209 2021;13:6209. <https://doi.org/10.3390/CANCERS13246209>.
- [94] Bholra NE, Balko JM, Dugger TC, Kuba MG, Sánchez V, Sanders M, et al. TGF- $\beta$  inhibition enhances chemotherapy action against triple-negative breast cancer. *J Clin Invest* 2013;123:1348–58. <https://doi.org/10.1172/JCI65416>.
- [95] Woosley AN, Dalton AC, Hussey GS, Howley B V., Mohanty BK, Grelet S, et al. TGF $\beta$  promotes breast cancer stem cell self-renewal through an ILEI/LIFR signaling axis. *Oncogene* 2019 38:20 2019;38:3794–811. <https://doi.org/10.1038/s41388-019-0703-z>.
- [96] Nie Z, Wang C, Zhou Z, Chen C, Liu R, Wang D. Transforming growth factor-beta increases breast cancer stem cell population partially through upregulating PMEPA1 expression. *Acta Biochim Biophys Sin (Shanghai)* 2016;48:194–201. <https://doi.org/10.1093/ABBS/GMV130>.
- [97] Aster JC, Pear WS, Blacklow SC. The Varied Roles of Notch in Cancer. *Annu Rev Pathol* 2017;12:245. <https://doi.org/10.1146/ANNUREV-PATHOL-052016-100127>.



- [98] Qiu M, Peng Q, Jiang I, Carroll C, Han G, Rymer I, et al. Specific inhibition of Notch1 signaling enhances the antitumor efficacy of chemotherapy in triple negative breast cancer through reduction of cancer stem cells. *Cancer Lett* 2013;328:261–70. <https://doi.org/10.1016/J.CANLET.2012.09.023>.
- [99] Locatelli MA, Aftimos P, Claire Dees E, LoRusso PM, Pegram MD, Awada A, et al. Phase I study of the gamma secretase inhibitor PF-03084014 in combination with docetaxel in patients with advanced triple-negative breast cancer. *Oncotarget* 2017;8:2320–8. <https://doi.org/10.18632/ONCOTARGET.13727>.
- [100] Schott AF, Landis MD, Dontu G, Griffith KA, Layman RM, Krop I, et al. Preclinical and clinical studies of gamma secretase inhibitors with docetaxel on human breast tumors. *Clin Cancer Res* 2013;19:1512–24. <https://doi.org/10.1158/1078-0432.CCR-11-3326>.
- [101] Liu J, Xiao Q, Xiao J, Niu C, Li Y, Zhang X, et al. Wnt/ $\beta$ -catenin signalling: function, biological mechanisms, and therapeutic opportunities. *Signal Transduction and Targeted Therapy* 2021 7:1 2022;7:1–23. <https://doi.org/10.1038/s41392-021-00762-6>.
- [102] Pohl SG, Brook N, Agostino M, Arfuso F, Kumar AP, Dharmarajan A. Wnt signaling in triple-negative breast cancer. *Oncogenesis* 2017;6:e310. <https://doi.org/10.1038/ONCSIS.2017.14>.
- [103] Ali R, Wendt MK. The paradoxical functions of EGFR during breast cancer progression. *Signal Transduct Target Ther* 2017;2. <https://doi.org/10.1038/SIGTRANS.2016.42>.
- [104] Nakai K, Hung MC, Yamaguchi H. A perspective on anti-EGFR therapies targeting triple-negative breast cancer. *Am J Cancer Res* 2016;6:1609–23.
- [105] Maennling AE, Tur MK, Niebert M, Klockenbring T, Zeppernick F, Gattenlöhner S, et al. Molecular Targeting Therapy against EGFR Family in Breast Cancer: Progress and Future Potentials. *Cancers (Basel)* 2019;11. <https://doi.org/10.3390/cancers11121826>.
- [106] Larsen SC, Sylvestersen KB, Mund A, Lyon D, Mullari M, Madsen M V, et al. Proteome-wide analysis of arginine monomethylation reveals widespread occurrence in human cells. *Sci Signal* 2016;9:rs9. <https://doi.org/10.1126/scisignal.aaf7329>.
- [107] Gayatri S, Bedford MT. Readers of Histone Methylarginine Marks. *Biochim Biophys Acta* 2014;1839:702. <https://doi.org/10.1016/J.BBAGRM.2014.02.015>.
- [108] Gary JD, Clarke S. RNA and protein interactions modulated by protein arginine methylation. *Prog Nucleic Acid Res Mol Biol* 1998;61:65–131. [https://doi.org/10.1016/S0079-6603\(08\)60825-9](https://doi.org/10.1016/S0079-6603(08)60825-9).
- [109] Blanc RS, Richard S. Arginine Methylation: The Coming of Age. *Mol Cell* 2017;65:8–24. <https://doi.org/10.1016/j.molcel.2016.11.003>.

- [110] Bedford MT, Clarke SG. Protein arginine methylation in mammals: who, what, and why. *Mol Cell* 2009;33:1–13. <https://doi.org/10.1016/J.MOLCEL.2008.12.013>.
- [111] Luscombe NM, Laskowski RA, Thornton JM. Amino acid–base interactions: a three-dimensional analysis of protein–DNA interactions at an atomic level. *Nucleic Acids Res* 2001;29:2860. <https://doi.org/10.1093/NAR/29.13.2860>.
- [112] Fuhrmann J, Clancy KW, Thompson PR. Chemical biology of protein arginine modifications in epigenetic regulation. *Chem Rev* 2015;115:5413–61. <https://doi.org/10.1021/ACS.CHEMREV.5B00003>.
- [113] Wang Y, Bedford MT. Effectors and effects of arginine methylation. *Biochem Soc Trans* 2023;51:725–34. <https://doi.org/10.1042/BST20221147>.
- [114] Ouyang Y, Wu Q, Li J, Sun S, Sun S. S-adenosylmethionine: A metabolite critical to the regulation of autophagy. *Cell Prolif* 2020;53. <https://doi.org/10.1111/CPR.12891>.
- [115] Wu Q, Schapira M, Arrowsmith CH, Barsyte-Lovejoy D. Protein arginine methylation: from enigmatic functions to therapeutic targeting. *Nat Rev Drug Discov* 2021;20:509–30. <https://doi.org/10.1038/s41573-021-00159-8>.
- [116] Guccione E, Richard S. The regulation, functions and clinical relevance of arginine methylation. *Nat Rev Mol Cell Biol* 2019;20:642–57. <https://doi.org/10.1038/s41580-019-0155-x>.
- [117] Marjon K, Cameron MJ, Quang P, Clasquin MF, Mandley E, Kunii K, et al. MTAP Deletions in Cancer Create Vulnerability to Targeting of the MAT2A/PRMT5/RIOK1 Axis. *Cell Rep* 2016;15:574–87. <https://doi.org/10.1016/J.CELREP.2016.03.043>.
- [118] Tewary SK, Zheng YG, Ho MC. Protein arginine methyltransferases: insights into the enzyme structure and mechanism at the atomic level. *Cell Mol Life Sci* 2019;76:2917. <https://doi.org/10.1007/S00018-019-03145-X>.
- [119] Schapira M, Ferreira De Freitas R. Structural biology and chemistry of protein arginine methyltransferases. *Medchemcomm* 2014;5:1779. <https://doi.org/10.1039/C4MD00269E>.
- [120] Frankel A, Clarke S. PRMT3 Is a Distinct Member of the Protein Arginine N-Methyltransferase Family. *Journal of Biological Chemistry* 2000;275:32974–82. <https://doi.org/10.1074/jbc.m006445200>.
- [121] Troffer-Charlier N, Cura V, Hassenboehler P, Moras D, Cavarelli J. Functional insights from structures of coactivator-associated arginine methyltransferase 1 domains. *EMBO J* 2007;26:4391–401. <https://doi.org/10.1038/SJ.EMBOJ.7601855>.
- [122] Antonysamy S, Bonday Z, Campbell RM, Doyle B, Druzina Z, Gheyi T, et al. Crystal structure of the human PRMT5:MEP50 complex. *Proc Natl Acad Sci U S A* 2012;109:17960–5.

- [https://doi.org/10.1073/PNAS.1209814109/SUPPL\\_FILE/PNAS.201209814SI.PDF](https://doi.org/10.1073/PNAS.1209814109/SUPPL_FILE/PNAS.201209814SI.PDF).
- [123] Sun L, Wang M, Lv Z, Yang N, Liu Y, Bao S, et al. Structural insights into protein arginine symmetric dimethylation by PRMT5. *Proc Natl Acad Sci U S A* 2011;108:20538–43. [https://doi.org/10.1073/PNAS.1106946108/SUPPL\\_FILE/PNAS.1106946108\\_SI.PDF](https://doi.org/10.1073/PNAS.1106946108/SUPPL_FILE/PNAS.1106946108_SI.PDF).
- [124] Morales Y, Cáceres T, May K, Hevel JM. Biochemistry and regulation of the protein arginine methyltransferases (PRMTs). *Arch Biochem Biophys* 2016;590:138–52. <https://doi.org/10.1016/J.ABB.2015.11.030>.
- [125] Chowdhury MN, Jin H. The RGG motif proteins: Interactions, functions, and regulations. *Wiley Interdiscip Rev RNA* 2023;14. <https://doi.org/10.1002/WRNA.1748>.
- [126] Uhlmann T, Geoghegan VL, Thomas B, Ridlova G, Trudgian DC, Acuto O. A method for large-scale identification of protein arginine methylation. *Mol Cell Proteomics* 2012;11:1489–99. <https://doi.org/10.1074/MCP.M112.020743>.
- [127] Fong JY, Pignata L, Goy PA, Kawabata KC, Lee SC, Koh CM, et al. Therapeutic Targeting of RNA Splicing Catalysis through Inhibition of Protein Arginine Methylation. *Cancer Cell* 2019;36:194-209.e9. <https://doi.org/10.1016/j.ccell.2019.07.003>.
- [128] Peng BL, Li WJ, Ding JC, He YH, Ran T, Xie BL, et al. A hypermethylation strategy utilized by enhancer-bound CARM1 to promote estrogen receptor  $\alpha$ -dependent transcriptional activation and breast carcinogenesis. *Theranostics* 2020;10:3451–73. <https://doi.org/10.7150/THNO.39241>.
- [129] Lim Y, Lee JY, Ha SJ, Yu S, Shin JK, Kim HC. Proteome-wide identification of arginine methylation in colorectal cancer tissues from patients. *Proteome Sci* 2020;18. <https://doi.org/10.1186/S12953-020-00162-8>.
- [130] Wei HH, Fan XJ, Hu Y, Tian XX, Guo M, Mao MW, et al. A systematic survey of PRMT interactomes reveals the key roles of arginine methylation in the global control of RNA splicing and translation. *Sci Bull (Beijing)* 2021;66:1342–57. <https://doi.org/10.1016/J.SCIB.2021.01.004>.
- [131] Maron MI, Lehman SM, Gayatri S, DeAngelo JD, Hegde S, Lorton BM, et al. Independent transcriptomic and proteomic regulation by type I and II protein arginine methyltransferases. *IScience* 2021;24. <https://doi.org/10.1016/J.ISCI.2021.102971>.
- [132] Li Wjuan, He Yhui, Yang Jjing, Hu Gsheng, Lin Y an, Ran T, et al. Profiling PRMT methylome reveals roles of hnRNPA1 arginine methylation in RNA splicing and cell growth. *Nat Commun* 2021;12. <https://doi.org/10.1038/S41467-021-21963-1>.
- [133] Radzisheuskaya A, Shliaha P V., Grinev V, Lorenzini E, Kovalchuk S, Shlyueva D, et al. PRMT5 methylome profiling uncovers a direct link to splicing regulation

- in acute myeloid leukemia. *Nat Struct Mol Biol* 2019;26:999–1012. <https://doi.org/10.1038/S41594-019-0313-Z>.
- [134] Fedoriw A, Rajapurkar SR, O'Brien S, Gerhart S V., Mitchell LH, Adams ND, et al. Anti-tumor Activity of the Type I PRMT Inhibitor, GSK3368715, Synergizes with PRMT5 Inhibition through MTAP Loss. *Cancer Cell* 2019;36:100-114.e25. <https://doi.org/10.1016/J.CCELL.2019.05.014>.
- [135] Shishkova E, Zeng H, Liu F, Kwiecien NW, Hebert AS, Coon JJ, et al. Global mapping of CARM1 substrates defines enzyme specificity and substrate recognition. *Nat Commun* 2017;8. <https://doi.org/10.1038/NCOMMS15571>.
- [136] Suresh S, Huard S, Dubois T. CARM1/PRMT4: Making Its Mark beyond Its Function as a Transcriptional Coactivator. *Trends Cell Biol* 2021;31:402–17. <https://doi.org/10.1016/j.tcb.2020.12.010>.
- [137] Gayatri S, Cowles MW, Vemulapalli V, Cheng D, Sun ZW, Bedford MT. Using oriented peptide array libraries to evaluate methylarginine-specific antibodies and arginine methyltransferase substrate motifs. *Sci Rep* 2016;6. <https://doi.org/10.1038/SREP28718>.
- [138] Feng Y, Maity R, Whitelegge JP, Hadjikyriacou A, Li Z, Zurita-Lopez C, et al. Mammalian protein arginine methyltransferase 7 (PRMT7) specifically targets RXR sites in lysine- and arginine-rich regions. *J Biol Chem* 2013;288:37010–25. <https://doi.org/10.1074/JBC.M113.525345>.
- [139] Hamey JJ, Rakow S, Bouchard C, Senst JM, Kolb P, Bauer UM, et al. Systematic investigation of PRMT6 substrate recognition reveals broad specificity with a preference for an RG motif or basic and bulky residues. *FEBS J* 2021;288:5668–91. <https://doi.org/10.1111/FEBS.15837>.
- [140] Ong SE, Mittler G, Mann M. Identifying and quantifying in vivo methylation sites by heavy methyl SILAC. *Nature Methods* 2004 1:2 2004;1:119–26. <https://doi.org/10.1038/nmeth715>.
- [141] Geoghegan V, Guo A, Trudgian D, Thomas B, Acuto O. Comprehensive identification of arginine methylation in primary T cells reveals regulatory roles in cell signalling. *Nat Commun* 2015;6. <https://doi.org/10.1038/NCOMMS7758>.
- [142] Guo A, Gu H, Zhou J, Mulhern D, Wang Y, Lee KA, et al. Immunoaffinity enrichment and mass spectrometry analysis of protein methylation. *Mol Cell Proteomics* 2014;13:372–87. <https://doi.org/10.1074/MCP.O113.027870>.
- [143] Gu H, Ren JM, Jia X, Levy T, Rikova K, Yang V, et al. Quantitative Profiling of Post-translational Modifications by Immunoaffinity Enrichment and LC-MS/MS in Cancer Serum without Immunodepletion. *Mol Cell Proteomics* 2016;15:692–702. <https://doi.org/10.1074/MCP.O115.052266>.
- [144] Dhar S, Vemulapalli V, Patananan AN, Huang GL, Di Lorenzo A, Richard S, et al. Loss of the major Type I arginine methyltransferase PRMT1 causes substrate scavenging by other PRMTs. *Sci Rep* 2013;3. <https://doi.org/10.1038/SREP01311>.

- [145] Sayago C, Sánchez-Wandelmer J, García F, Hurtado B, Lafarga V, Prieto P, et al. Decoding protein methylation function with thermal stability analysis. *Nat Commun* 2023;14. <https://doi.org/10.1038/S41467-023-38863-1>.
- [146] Ma M, Zhao X, Chen S, Zhao Y, Yang L, Feng Y, et al. Strategy Based on Deglycosylation, Multiprotease, and Hydrophilic Interaction Chromatography for Large-Scale Profiling of Protein Methylation. *Anal Chem* 2017;89:12909–17. <https://doi.org/10.1021/ACS.ANALCHEM.7B03673>.
- [147] Musiani D, Bok J, Massignani E, Wu L, Tabaglio T, Ippolito MR, et al. Proteomics profiling of arginine methylation defines PRMT5 substrate specificity. *Sci Signal* 2019;12. <https://doi.org/10.1126/SCISIGNAL.AAT8388>.
- [148] Strahl BD, Briggs SD, Brame CJ, Caldwell JA, Koh SS, Ma H, et al. Methylation of histone H4 at arginine 3 occurs in vivo and is mediated by the nuclear receptor coactivator PRMT1. *Current Biology* 2001;11:996–1000. [https://doi.org/10.1016/S0960-9822\(01\)00294-9](https://doi.org/10.1016/S0960-9822(01)00294-9).
- [149] Strahl BD, Briggs SD, Brame CJ, Caldwell JA, Koh SS, Ma H, et al. Methylation of histone H4 at arginine 3 occurs in vivo and is mediated by the nuclear receptor coactivator PRMT1. *Curr Biol* 2001;11:996–1000. [https://doi.org/10.1016/S0960-9822\(01\)00294-9](https://doi.org/10.1016/S0960-9822(01)00294-9).
- [150] Fabbrizio E, El Messaoudi S, Polanowska J, Paul C, Cook JR, Lee JH, et al. Negative regulation of transcription by the type II arginine methyltransferase PRMT5. *EMBO Rep* 2002;3:641–5. <https://doi.org/10.1093/EMBO-REPORTS/KVF136>.
- [151] Zhao Q, Rank G, Tan YT, Li H, Moritz RL, Simpson RJ, et al. PRMT5-mediated methylation of histone H4R3 recruits DNMT3A, coupling histone and DNA methylation in gene silencing. *Nature Structural & Molecular Biology* 2009 16:3 2009;16:304–11. <https://doi.org/10.1038/nsmb.1568>.
- [152] Pollack BP, Kotenko S V., He W, Izotova LS, Barnoski BL, Pestka S. The human homologue of the yeast proteins Skb1 and Hsl7p interacts with Jak kinases and contains protein methyltransferase activity. *J Biol Chem* 1999;274:31531–42. <https://doi.org/10.1074/JBC.274.44.31531>.
- [153] Pal S, Vishwanath SN, Erdjument-Bromage H, Tempst P, Sif S. Human SWI/SNF-associated PRMT5 methylates histone H3 arginine 8 and negatively regulates expression of ST7 and NM23 tumor suppressor genes. *Mol Cell Biol* 2004;24:9630–45. <https://doi.org/10.1128/MCB.24.21.9630-9645.2004>.
- [154] Schurter BT, Koh SS, Chen D, Bunick GJ, Harp JM, Hanson BL, et al. Methylation of Histone H3 by Coactivator-Associated Arginine Methyltransferase 1†. *Biochemistry* 2001;40:5747–56. <https://doi.org/10.1021/BI002631B>.
- [155] Huang S, Litt M, Felsenfeld G. Methylation of histone H4 by arginine methyltransferase PRMT1 is essential in vivo for many subsequent histone modifications. *Genes Dev* 2005;19:1885. <https://doi.org/10.1101/GAD.1333905>.

- [156] Thiebaut C, Eve L, Poulard C, Le Romancer M. Structure, Activity, and Function of PRMT1. *Life* 2021;11. <https://doi.org/10.3390/LIFE11111147>.
- [157] Yang Y, McBride KM, Hensley S, Lu Y, Chedin F, Bedford MT. Arginine methylation facilitates the recruitment of TOP3B to chromatin to prevent R loop accumulation. *Mol Cell* 2014;53:484–97. <https://doi.org/10.1016/J.MOLCEL.2014.01.011>.
- [158] Zhao X, Jankovic V, Gural A, Huang G, Pardnani A, Menendez S, et al. Methylation of RUNX1 by PRMT1 abrogates SIN3A binding and potentiates its transcriptional activity. *Genes Dev* 2008;22:640. <https://doi.org/10.1101/GAD.1632608>.
- [159] Liu LM, Sun WZ, Fan XZ, Xu YL, Cheng M Bin, Zhang Y. Methylation of C/EBPa by PRMT1 inhibits its tumor-suppressive function in breast cancer. *Cancer Res* 2019;79:2865–77. <https://doi.org/10.1158/0008-5472.CAN-18-3211/662408/AM/METHYLATION-OF-C-EBP-BY-PRMT1-INHIBITS-ITS-TUMOR>.
- [160] Xu W, Chen H, Du K, Asahara H, Tini M, Emerson BM, et al. A transcriptional switch mediated by cofactor methylation. *Science* 2001;294:2507–11. <https://doi.org/10.1126/SCIENCE.1065961>.
- [161] Yi P, Wang Z, Feng Q, Chou CK, Pintilie GD, Shen H, et al. Structural and Functional Impacts of ER Coactivator Sequential Recruitment. *Mol Cell* 2017;67:733-743.e4. <https://doi.org/10.1016/J.MOLCEL.2017.07.026>.
- [162] Ceschin DG, Walia M, Wenk SS, Duboé C, Gaudon C, Xiao Y, et al. Methylation specifies distinct estrogen-induced binding site repertoires of CBP to chromatin. *Genes Dev* 2011;25:1132–46. <https://doi.org/10.1101/GAD.619211>.
- [163] Chen D, Ma M, Hong H, Koh SS, Huang SM, Schurter BT, et al. Regulation of Transcription by a Protein Methyltransferase. *Science* (1979) 1999;284:2174–7. <https://doi.org/10.1126/SCIENCE.284.5423.2174>.
- [164] Hassa PO, Covic M, Bedford MT, Hottiger MO. Protein Arginine Methyltransferase 1 Coactivates NF-κB-Dependent Gene Expression Synergistically with CARM1 and PARP1. *J Mol Biol* 2008;377:668–78. <https://doi.org/10.1016/J.JMB.2008.01.044>.
- [165] Covic M, Hassa PO, Sacconi S, Buerki C, Meier NI, Lombardi C, et al. Arginine methyltransferase CARM1 is a promoter-specific regulator of NF-κB-dependent gene expression. *EMBO J* 2005;24:85. <https://doi.org/10.1038/SJ.EMBOJ.7600500>.
- [166] Lin W, Shen G, Yuan X, Jain MR, Yu S, Zhang A, et al. Regulation of Nrf2 transactivation domain activity by p160 RAC3/SRC3 and other nuclear co-regulators. *J Biochem Mol Biol* 2006;39:304–10. <https://doi.org/10.5483/BMBREP.2006.39.3.304>.

- [167] An W, Kim J, Roeder RG. Ordered cooperative functions of PRMT1, p300, and CARM1 in transcriptional activation by p53. *Cell* 2004;117:735–48. <https://doi.org/10.1016/j.cell.2004.05.009>.
- [168] Koh SS, Li H, Lee YH, Widelitz RB, Chuong CM, Stallcup MR. Synergistic coactivator function by coactivator-associated arginine methyltransferase (CARM) 1 and beta-catenin with two different classes of DNA-binding transcriptional activators. *J Biol Chem* 2002;277:26031–5. <https://doi.org/10.1074/JBC.M110865200>.
- [169] Tee WW, Pardo M, Theunissen TW, Yu L, Choudhary JS, Hajkova P, et al. Prmt5 is essential for early mouse development and acts in the cytoplasm to maintain ES cell pluripotency. *Genes Dev* 2010;24:2772–7. <https://doi.org/10.1101/GAD.606110>.
- [170] Majumder S, Alinari L, Roy S, Miller T, Datta J, Sif S, et al. Methylation of Histone H3 and H4 by PRMT5 Regulates Ribosomal RNA Gene Transcription. *J Cell Biochem* 2010;109:553. <https://doi.org/10.1002/JCB.22432>.
- [171] Pal S, Vishwanath SN, Erdjument-Bromage H, Tempst P, Sif S. Human SWI/SNF-associated PRMT5 methylates histone H3 arginine 8 and negatively regulates expression of ST7 and NM23 tumor suppressor genes. *Mol Cell Biol* 2004;24:9630–45. <https://doi.org/10.1128/MCB.24.21.9630-9645.2004>.
- [172] Migliori V, Müller J, Phalke S, Low D, Bezzi M, Mok WC, et al. Symmetric dimethylation of H3R2 is a newly identified histone mark that supports euchromatin maintenance. *Nat Struct Mol Biol* 2012;19:136–45. <https://doi.org/10.1038/NSMB.2209>.
- [173] Chung JH, Sloan S, Scherle P, Vaddi K, Sif S, Lapalombella R, et al. PRMT5 Is a Key Epigenetic Regulator That Promotes Transcriptional Activation in Mantle Cell Lymphoma By Regulating the Lysine Methyltransferase SETD7 and MLL1 Activity. *Blood* 2019;134:2777. <https://doi.org/10.1182/BLOOD-2019-131020>.
- [174] Deng X, Shao G, Zhang HT, Li C, Zhang D, Cheng L, et al. Protein arginine methyltransferase 5 functions as an epigenetic activator of the androgen receptor to promote prostate cancer cell growth. *Oncogene* 2017;36:1223–31. <https://doi.org/10.1038/ONC.2016.287>.
- [175] Zheng Y, Chen Z, Zhou B, Chen S, Han L, Chen N, et al. PRMT5 Deficiency Enforces the Transcriptional and Epigenetic Programs of Klrp1+CD8+ Terminal Effector T Cells and Promotes Cancer Development. *J Immunol* 2022;208:501–13. <https://doi.org/10.4049/JIMMUNOL.2100523>.
- [176] Zhang B, Dong S, Zhu R, Hu C, Hou J, Li Y, et al. Targeting protein arginine methyltransferase 5 inhibits colorectal cancer growth by decreasing arginine methylation of eIF4E and FGFR3. *Oncotarget* 2015;6:22799–811. <https://doi.org/10.18632/ONCOTARGET.4332>.

- [177] Wei H, Wang B, Miyagi M, She Y, Gopalan B, Huang D Bin, et al. PRMT5 dimethylates R30 of the p65 subunit to activate NF- $\kappa$ B. *Proc Natl Acad Sci U S A* 2013;110:13516–21. <https://doi.org/10.1073/PNAS.1311784110>.
- [178] di Caprio R, Ciano M, Montano G, Costanzo P, Cesaro E. KAP1 is a Novel Substrate for the Arginine Methyltransferase PRMT5. *Biology (Basel)* 2015;4:41–9. <https://doi.org/10.3390/BIOLOGY4010041>.
- [179] Liu C Der, Cheng CP, Fang JS, Chen LC, Zhao B, Kieff E, et al. Modulation of Epstein-Barr virus nuclear antigen 2-dependent transcription by protein arginine methyltransferase 5. *Biochem Biophys Res Commun* 2013;430:1097–102. <https://doi.org/10.1016/J.BBRC.2012.12.032>.
- [180] Chen M, Manley JL. Mechanisms of alternative splicing regulation: insights from molecular and genomics approaches. *Nat Rev Mol Cell Biol* 2009;10:741. <https://doi.org/10.1038/NRM2777>.
- [181] Maron MI, Casill AD, Gupta V, Roth JS, Sidoli S, Query CC, et al. Type I and II PRMTs inversely regulate post-transcriptional intron detention through Sm and CHTOP methylation. *Elife* 2022;11:72867. <https://doi.org/10.7554/ELIFE.72867>.
- [182] Côté J, Boisvert FM, Boulanger MC, Bedford MT, Richard S. Sam68 RNA Binding Protein Is an In Vivo Substrate for Protein Arginine N-Methyltransferase 1. *Mol Biol Cell* 2003;14:274. <https://doi.org/10.1091/MBC.E02-08-0484>.
- [183] Nichols RC, Wang XW, Tang J, Hamilton BJ, High FA, Herschman HR, et al. The RGG Domain in hnRNP A2 Affects Subcellular Localization. *Exp Cell Res* 2000;256:522–32. <https://doi.org/10.1006/EXCR.2000.4827>.
- [184] Wall ML, Lewis SM. Methylarginines within the RGG-Motif Region of hnRNP A1 Affect Its IRES Trans-Acting Factor Activity and Are Required for hnRNP A1 Stress Granule Localization and Formation. *J Mol Biol* 2017;429:295–307. <https://doi.org/10.1016/J.JMB.2016.12.011>.
- [185] Tradewell ML, Yu Z, Tibshirani M, Boulanger MC, Durham HD, Richard S. Arginine methylation by PRMT1 regulates nuclear-cytoplasmic localization and toxicity of FUS/TLS harbouring ALS-linked mutations. *Hum Mol Genet* 2012;21:136–49. <https://doi.org/10.1093/HMG/DDR448>.
- [186] Hadjikyriacou A, Yang Y, Espejo A, Bedford MT, Clarke SG. Unique features of human protein arginine methyltransferase 9 (PRMT9) and its substrate RNA splicing factor SF3B2. *Journal of Biological Chemistry* 2015;290:16723–43. <https://doi.org/10.1074/jbc.M115.659433>.
- [187] Yang Y, Hadjikyriacou A, Xia Z, Gayatri S, Kim D, Zurita-Lopez C, et al. PRMT9 is a Type II methyltransferase that methylates the splicing factor SAP145. *Nat Commun* 2015;6:6428. <https://doi.org/10.1038/NCOMMS7428>.
- [188] Stopa N, Krebs JE, Shechter D. The PRMT5 arginine methyltransferase: many roles in development, cancer and beyond. *Cell Mol Life Sci* 2015;72:2041–59. <https://doi.org/10.1007/S00018-015-1847-9>.



- [189] Dionne KL, Bergeron D, Landry-Voyer AM, Bachand F. The 40S ribosomal protein uS5 (RPS2) assembles into an extraribosomal complex with human ZNF277 that competes with the PRMT3– uS5 interaction. *Journal of Biological Chemistry* 2019;294:1944–55. <https://doi.org/10.1074/JBC.RA118.004928/ATTACHMENT/6C4FE769-3DB4-4F77-9EC3-A5CB1E995C30/MMC1.ZIP>.
- [190] Swiercz R, Cheng D, Kim D, Bedford MT. Ribosomal protein rpS2 is hypomethylated in PRMT3-deficient mice. *Journal of Biological Chemistry* 2007;282:16917–23. <https://doi.org/10.1074/jbc.M609778200>.
- [191] Bachand F, Silver PA. PRMT3 is a ribosomal protein methyltransferase that affects the cellular levels of ribosomal subunits. *EMBO J* 2004;23:2641. <https://doi.org/10.1038/SJ.EMBOJ.7600265>.
- [192] Ren J, Wang Y, Liang Y, Zhang Y, Bao S, Xu Z. Methylation of ribosomal protein S10 by protein-arginine methyltransferase 5 regulates ribosome biogenesis. *J Biol Chem* 2010;285:12695–705. <https://doi.org/10.1074/JBC.M110.103911>.
- [193] Gao G, Dhar S, Bedford MT. PRMT5 regulates IRES-dependent translation via methylation of hnRNP A1. *Nucleic Acids Res* 2017;45:4359. <https://doi.org/10.1093/NAR/GKW1367>.
- [194] Hwang JW, Cho Y, Bae GU, Kim SN, Kim YK. Protein arginine methyltransferases: promising targets for cancer therapy. *Exp Mol Med* 2021;53:788. <https://doi.org/10.1038/S12276-021-00613-Y>.
- [195] Dolezal E, Infantino S, Drepper F, Börsig T, Singh A, Wossning T, et al. The BTG2-PRMT1 module limits pre-B cell expansion by regulating the CDK4-Cyclin-D3 complex. *Nature Immunology* 2017 18:8 2017;18:911–20. <https://doi.org/10.1038/ni.3774>.
- [196] Yang H, Zhao X, Zhao L, Liu L, Li J, Jia W, et al. PRMT5 competitively binds to CDK4 to promote G1-S transition upon glucose induction in hepatocellular carcinoma. *Oncotarget* 2016;7:72131–47. <https://doi.org/10.18632/ONCOTARGET.12351>.
- [197] Deng X, Keudell G Von, Suzuki T, Dohmae N, Nakakido M, Piao L, et al. PRMT1 promotes mitosis of cancer cells through arginine methylation of INCENP. *Oncotarget* 2015;6:35173–82. <https://doi.org/10.18632/ONCOTARGET.6050>.
- [198] Frieze S, Lupien M, Silver PA, Brown M. CARM1 Regulates Estrogen-Stimulated Breast Cancer Growth through Up-regulation of E2F1. *Cancer Res* 2008;68:301–6. <https://doi.org/10.1158/0008-5472.CAN-07-1983>.
- [199] El Messaoudi S, Fabrizio E, Rodriguez C, Chuchana P, Fauquier L, Cheng D, et al. Coactivator-associated arginine methyltransferase 1 (CARM1) is a positive regulator of the Cyclin E1 gene. *Proc Natl Acad Sci U S A* 2006;103:13351–6. [https://doi.org/10.1073/PNAS.0605692103/SUPPL\\_FILE/05692FIG9.PDF](https://doi.org/10.1073/PNAS.0605692103/SUPPL_FILE/05692FIG9.PDF).
- [200] Wei TYW, Juan CC, Hisa JY, Su LJ, Lee YCG, Chou HY, et al. Protein arginine methyltransferase 5 is a potential oncoprotein that upregulates G1

- cyclins/cyclin-dependent kinases and the phosphoinositide 3-kinase/AKT signaling cascade. *Cancer Sci* 2012;103:1640. <https://doi.org/10.1111/J.1349-7006.2012.02367.X>.
- [201] Karkhanis V, Alinari L, Ozer HG, Chung J, Zhang X, Sif S, et al. Protein arginine methyltransferase 5 represses tumor suppressor miRNAs that down-regulate CYCLIN D1 and c-MYC expression in aggressive B-cell lymphoma. *J Biol Chem* 2020;295:1165. <https://doi.org/10.1074/JBC.RA119.008742>.
- [202] Chung J, Karkhanis V, Tae S, Yan F, Smith P, Ayers LW, et al. Protein arginine methyltransferase 5 (PRMT5) inhibition induces lymphoma cell death through reactivation of the retinoblastoma tumor suppressor pathway and polycomb repressor complex 2 (PRC2) Silencing. *Journal of Biological Chemistry* 2013;288:35534–47. <https://doi.org/10.1074/jbc.M113.510669>.
- [203] Tang J, Meng Q, Shi R, Xu Y. PRMT6 serves an oncogenic role in lung adenocarcinoma via regulating p18. *Mol Med Rep* 2020;22:3161–72. <https://doi.org/10.3892/MMR.2020.11402>.
- [204] Kleinschmidt MA, de Graaf P, van Teeffelen HAAM, Timmers HTM. Cell cycle regulation by the PRMT6 arginine methyltransferase through repression of cyclin-dependent kinase inhibitors. *PLoS One* 2012;7. <https://doi.org/10.1371/JOURNAL.PONE.0041446>.
- [205] Phalke S, Mzoughi S, Bezzi M, Jennifer N, Mok WC, Low DHP, et al. p53-Independent regulation of p21Waf1/Cip1 expression and senescence by PRMT6. *Nucleic Acids Res* 2012;40:9534–42. <https://doi.org/10.1093/NAR/GKS858>.
- [206] Kim S, Kim NH, Park JE, Hwang JW, Myung N, Hwang KT, et al. PRMT6-mediated H3R2me2a guides Aurora B to chromosome arms for proper chromosome segregation. *Nat Commun* 2020;11. <https://doi.org/10.1038/S41467-020-14511-W>.
- [207] Yu Z, Vogel G, Yan C, Dubeau D, Spehalski E, Hébert J, et al. The MRE11 GAR motif regulates DNA double-strand break processing and ATR activation. *Cell Res* 2012;22:305–20. <https://doi.org/10.1038/CR.2011.128>.
- [208] Boisvert FM, Déry U, Masson JY, Richard S. Arginine methylation of MRE11 by PRMT1 is required for DNA damage checkpoint control. *Genes Dev* 2005;19:671–6. <https://doi.org/10.1101/GAD.1279805>.
- [209] Boisvert FM, Hendzel MJ, Masson JY, Richard S. Methylation of MRE11 regulates its nuclear compartmentalization. *Cell Cycle* 2005;4:981–9. <https://doi.org/10.4161/CC.4.7.1830>.
- [210] Boisvert FM, Rhie A, Richard S, Doherty AJ. The GAR motif of 53BP1 is arginine methylated by PRMT1 and is necessary for 53BP1 DNA binding activity. *Cell Cycle* 2005;4:1834–41. <https://doi.org/10.4161/CC.4.12.2250>.

- [211] Adams MM, Wang B, Xia Z, Morales JC, Lu X, Donehower LA, et al. 53BP1 oligomerization is independent of its methylation by PRMT1. *Cell Cycle* 2005;4:1854–61. <https://doi.org/10.4161/CC.4.12.2282>.
- [212] Hwang JW, Kim SN, Myung N, Song D, Han G, Bae GU, et al. PRMT5 promotes DNA repair through methylation of 53BP1 and is regulated by Src-mediated phosphorylation. *Commun Biol* 2020;3. <https://doi.org/10.1038/S42003-020-01157-Z>.
- [213] El-Andaloussi N, Valovka T, Toueille M, Hassa PO, Gehrig P, Covic M, et al. Methylation of DNA polymerase beta by protein arginine methyltransferase 1 regulates its binding to proliferating cell nuclear antigen. *FASEB J* 2007;21:26–34. <https://doi.org/10.1096/FJ.06-6194COM>.
- [214] Guo Z, Zheng L, Xu H, Dai H, Zhou M, Pascua MR, et al. Methylation of FEN1 suppresses nearby phosphorylation and facilitates PCNA binding. *Nat Chem Biol* 2010;6:766–73. <https://doi.org/10.1038/NCHEMBIO.422>.
- [215] He L, Hu Z, Sun Y, Zhang M, Zhu H, Jiang L, et al. PRMT1 is critical to FEN1 expression and drug resistance in lung cancer cells. *DNA Repair (Amst)* 2020;95:102953. <https://doi.org/10.1016/J.DNAREP.2020.102953>.
- [216] Guendel I, Carpio L, Pedati C, Schwartz A, Teal C, Kashanchi F, et al. Methylation of the Tumor Suppressor Protein, BRCA1, Influences Its Transcriptional Cofactor Function. *PLoS One* 2010;5. <https://doi.org/10.1371/JOURNAL.PONE.0011379>.
- [217] Hamard PJ, Santiago GE, Liu F, Karl DL, Martinez C, Man N, et al. PRMT5 Regulates DNA Repair by Controlling the Alternative Splicing of Histone-Modifying Enzymes. *Cell Rep* 2018;24:2643–57. <https://doi.org/10.1016/J.CELREP.2018.08.002>.
- [218] Clarke TL, Sanchez-Bailon MP, Chiang K, Reynolds JJ, Herrero-Ruiz J, Bandejas TM, et al. PRMT5-Dependent Methylation of the TIP60 Coactivator RUVBL1 Is a Key Regulator of Homologous Recombination. *Mol Cell* 2017;65:900-916.e7. <https://doi.org/10.1016/J.MOLCEL.2017.01.019>.
- [219] Katsuno Y, Qin J, Osés-Prieto J, Wang H, Jackson-Weaver O, Zhang T, et al. Arginine methylation of SMAD7 by PRMT1 in TGF $\beta$ -induced epithelial–mesenchymal transition and epithelial stem-cell generation. *Journal of Biological Chemistry* 2018;293:13059–137072. <https://doi.org/10.1074/jbc.RA118.002027>.
- [220] Xu J, Wang AH, Osés-Prieto J, Makhijani K, Katsuno Y, Pei M, et al. Arginine methylation initiates BMP-induced Smad signaling. *Mol Cell* 2013;51:5–19. <https://doi.org/10.1016/j.molcel.2013.05.004>.
- [221] Zhang T, Wu J, Ungvijanpunya N, Jackson-Weaver O, Gou Y, Feng J, et al. Smad6 Methylation Represses NF $\kappa$ B Activation and Periodontal Inflammation. *J Dent Res* 2018;97:810. <https://doi.org/10.1177/0022034518755688>.

- [222] Gou Y, Li J, Jackson-Weaver O, Wu J, Zhang T, Gupta R, et al. Protein Arginine Methyltransferase PRMT1 Is Essential for Palatogenesis. *J Dent Res* 2018;97:1510–8. <https://doi.org/10.1177/0022034518785164>.
- [223] Li Q, Jiao J, Li H, Wan H, Zheng C, Cai J, et al. Histone arginine methylation by Prmt5 is required for lung branching morphogenesis through repression of BMP signaling. *J Cell Sci* 2018;131. <https://doi.org/10.1242/JCS.217406>.
- [224] Tamiya H, Kim H, Klymenko O, Kim H, Feng Y, Zhang T, et al. SHARPIN-mediated regulation of protein arginine methyltransferase 5 controls melanoma growth. *J Clin Invest* 2018;128:517–30. <https://doi.org/10.1172/JCI95410>.
- [225] Tabata T, Kokura K, ren Dijke P, Ishii S. Ski co-repressor complexes maintain the basal repressed state of the TGF- $\beta$  target gene, SMAD7, via HDAC3 and PRMT5. *Genes to Cells* 2009;14:17–28. <https://doi.org/10.1111/J.1365-2443.2008.01246.X>.
- [226] Hsu JM, Chen CT, Chou CK, Kuo HP, Li LY, Lin CY, et al. Crosstalk between Arg 1175 methylation and Tyr 1173 phosphorylation negatively modulates EGFR-mediated ERK activation. *Nat Cell Biol* 2011;13:174–81. <https://doi.org/10.1038/ncb2158>.
- [227] Andreu-Pérez P, Esteve-Puig R, De Torre-Minguela C, López-Fauqued M, Bech-Serra JJ, Tenbaum S, et al. Protein Arginine Methyltransferase 5 Regulates ERK1/2 Signal Transduction Amplitude and Cell Fate Through CRAF. *Sci Signal* 2011;4:ra58. <https://doi.org/10.1126/SCISIGNAL.2001936>.
- [228] Liao HW, Hsu JM, Xia W, Wang HL, Wang YN, Chang WC, et al. PRMT1-mediated methylation of the EGF receptor regulates signaling and cetuximab response. *J Clin Invest* 2015;125:4529–43. <https://doi.org/10.1172/jci82826>.
- [229] Epstein DM, Buck E. Old dog, new tricks: extracellular domain arginine methylation regulates EGFR function. *J Clin Invest* 2015;125:4320–2. <https://doi.org/10.1172/jci85001>.
- [230] Nakai K, Xia W, Liao HW, Saito M, Hung MC, Yamaguchi H. The role of PRMT1 in EGFR methylation and signaling in MDA-MB-468 triple-negative breast cancer cells. *Breast Cancer* 2018;25:74–80. <https://doi.org/10.1007/s12282-017-0790-z>.
- [231] Wang WJ, Hsu JM, Wang YN, Lee HH, Yamaguchi H, Liao HW, et al. An essential role of PRMT1-mediated EGFR methylation in EGFR activation by ribonuclease 5. *Am J Cancer Res* 2019;9:180–5.
- [232] Takai H, Masuda K, Sato T, Sakaguchi Y, Suzuki T, Suzuki T, et al. 5-Hydroxymethylcytosine plays a critical role in glioblastomagenesis by recruiting the CHTOP-Methylosome complex. *Cell Rep* 2014;9:48–60. <https://doi.org/10.1016/j.celrep.2014.08.071>.
- [233] Yao B, Gui T, Zeng X, Deng Y, Wang Z, Wang Y, et al. PRMT1-mediated H4R3me2a recruits SMARCA4 to promote colorectal cancer progression by

- enhancing EGFR signaling. *Genome Med* 2021;13:58. <https://doi.org/10.1186/s13073-021-00871-5>.
- [234] Suresh S, Huard S, Brisson A, Némati F, Dakroub R, Poulard C, et al. PRMT1 Regulates EGFR and Wnt Signaling Pathways and Is a Promising Target for Combinatorial Treatment of Breast Cancer. *Cancers (Basel)* 2022;14. <https://doi.org/10.3390/cancers14020306>.
- [235] Huang L, Zhang XO, Rozen EJ, Sun X, Sallis B, Verdejo-Torres O, et al. PRMT5 activates AKT via methylation to promote tumor metastasis. *Nat Commun* 2022;13:3955. <https://doi.org/10.1038/s41467-022-31645-1>.
- [236] Yin S, Liu L, Brobbey C, Palanisamy V, Ball LE, Olsen SK, et al. PRMT5-mediated arginine methylation activates AKT kinase to govern tumorigenesis. *Nat Commun* 2021;12:3444. <https://doi.org/10.1038/s41467-021-23833-2>.
- [237] Calabretta S, Vogel G, Yu Z, Choquet K, Darbelli L, Nicholson TB, et al. Loss of PRMT5 Promotes PDGFR $\alpha$  Degradation during Oligodendrocyte Differentiation and Myelination. *Dev Cell* 2018;46:426-440.e5. <https://doi.org/10.1016/j.devcel.2018.06.025>.
- [238] Park IG, Jeon M, Kim H, Lee JM. Coordinated methyl readers: Functional communications in cancer. *Semin Cancer Biol* 2022;83:88–99. <https://doi.org/10.1016/J.SEMCANCER.2021.03.015>.
- [239] Beaver JE, Waters ML. Molecular Recognition of Lys and Arg Methylation. *ACS Chem Biol* 2016;11:643–53. [https://doi.org/10.1021/ACSCHEMPIO.5B00996/ASSET/IMAGES/LARGE/CB-2015-00996F\\_0010.JPEG](https://doi.org/10.1021/ACSCHEMPIO.5B00996/ASSET/IMAGES/LARGE/CB-2015-00996F_0010.JPEG).
- [240] Tripsianes K, Madl T, MacHyna M, Fessas D, Englbrecht C, Fischer U, et al. Structural basis for dimethylarginine recognition by the Tudor domains of human SMN and SPF30 proteins. *Nat Struct Mol Biol* 2011;18:1414–20. <https://doi.org/10.1038/NSMB.2185>.
- [241] Brahms H, Meheus L, De Brabandere V, Fischer U, Lührmann R. Symmetrical dimethylation of arginine residues in spliceosomal Sm protein B/B' and the Sm-like protein LSm4, and their interaction with the SMN protein. *RNA* 2001;7:1531–42. <https://doi.org/10.1017/S135583820101442X>.
- [242] Friesen WJ, Massenet S, Paushkin S, Wyce A, Dreyfuss G. SMN, the product of the spinal muscular atrophy gene, binds preferentially to dimethylarginine-containing protein targets. *Mol Cell* 2001;7:1111–7. [https://doi.org/10.1016/S1097-2765\(01\)00244-1](https://doi.org/10.1016/S1097-2765(01)00244-1).
- [243] Yanling Zhao D, Gish G, Braunschweig U, Li Y, Ni Z, Schmitges FW, et al. SMN and symmetric arginine dimethylation of RNA polymerase II C-terminal domain control termination. *Nature* 2016;529:48–53. <https://doi.org/10.1038/NATURE16469>.
- [244] Courchaine EM, Barentine AES, Straube K, Lee DR, Bewersdorf J, Neugebauer KM. DMA-tudor interaction modules control the specificity of in vivo

condensates. *Cell* 2021;184:3612-3625.e17.  
<https://doi.org/10.1016/J.CELL.2021.05.008>.

- [245] Liu K, Guo Y, Liu H, Bian C, Lam R, Liu Y, et al. Crystal structure of TDRD3 and methyl-arginine binding characterization of TDRD3, SMN and SPF30. *PLoS One* 2012;7. <https://doi.org/10.1371/JOURNAL.PONE.0030375>.
- [246] Hu P, Zhao H, Zhu P, Xiao Y, Miao W, Wang Y, et al. Dual regulation of Arabidopsis AGO2 by arginine methylation. *Nat Commun* 2019;10. <https://doi.org/10.1038/S41467-019-08787-W>.
- [247] Chen C, Jin J, James DA, Adams-Cioaba MA, Park JG, Guo Y, et al. Mouse Piwi interactome identifies binding mechanism of Tdrkh Tudor domain to arginine methylated Miwi. *Proc Natl Acad Sci U S A* 2009;106:20336–41. <https://doi.org/10.1073/PNAS.0911640106>.
- [248] Gao X, Zhao X, Zhu Y, He J, Shao J, Su C, et al. Tudor staphylococcal nuclease (Tudor-SN) participates in small ribonucleoprotein (snRNP) assembly via interacting with symmetrically dimethylated Sm proteins. *J Biol Chem* 2012;287:18130–41. <https://doi.org/10.1074/JBC.M111.311852>.
- [249] Roworth AP, Carr SM, Liu G, Barczak W, Miller RL, Munro S, et al. Arginine methylation expands the regulatory mechanisms and extends the genomic landscape under E2F control. *Sci Adv* 2019;5. <https://doi.org/10.1126/SCIADV.AAW4640>.
- [250] Zheng S, Moehlenbrink J, Lu YC, Zalmas LP, Sagum CA, Carr S, et al. Arginine Methylation-Dependent Reader-Writer Interplay Governs Growth Control by E2F-1. *Mol Cell* 2013;52:37–51. <https://doi.org/10.1016/J.MOLCEL.2013.08.039>.
- [251] Cho EC, Zheng S, Munro S, Liu G, Carr SM, Moehlenbrink J, et al. Arginine methylation controls growth regulation by E2F-1. *EMBO J* 2012;31:1785–97. <https://doi.org/10.1038/EMBOJ.2012.17>.
- [252] Sikorsky T, Hobor F, Krizanova E, Pasulka J, Kubicek K, Stefl R. Recognition of asymmetrically dimethylated arginine by TDRD3. *Nucleic Acids Res* 2012;40:11748–55. <https://doi.org/10.1093/NAR/GKS929>.
- [253] Yang Y, Lu Y, Espejo A, Wu J, Xu W, Liang S, et al. TDRD3 is an Effector Molecule for Arginine Methylated Histone Marks. *Mol Cell* 2010;40:1016. <https://doi.org/10.1016/J.MOLCEL.2010.11.024>.
- [254] Huang L, Wang Z, Narayanan N, Yang Y. Arginine methylation of the C-terminus RGG motif promotes TOP3B topoisomerase activity and stress granule localization. *Nucleic Acids Res* 2018;46:3061–74. <https://doi.org/10.1093/NAR/GKY103>.
- [255] Narayanan N, Wang Z, Li L, Yang Y. Arginine methylation of USP9X promotes its interaction with TDRD3 and its anti-apoptotic activities in breast cancer cells. *Cell Discov* 2017;3:16048. <https://doi.org/10.1038/CELLDISC.2016.48>.

- [256] Cheng D, Vemulapalli V, Lu Y, Shen J, Aoyagi S, Fry CJ, et al. CARM1 methylates MED12 to regulate its RNA-binding ability. *Life Sci Alliance* 2018;1. <https://doi.org/10.26508/LSA.201800117>.
- [257] Sims RJ, Rojas LA, Beck D, Bonasio R, Schüller R, Drury WJ, et al. The C-Terminal Domain of RNA Polymerase II Is Modified by Site-Specific Methylation. *Science* 2011;332:99. <https://doi.org/10.1126/SCIENCE.1202663>.
- [258] Chen C, Nott TJ, Jin J, Pawson T. Deciphering arginine methylation: Tudor tells the tale. *Nat Rev Mol Cell Biol* 2011;12:629–42. <https://doi.org/10.1038/NRM3185>.
- [259] Vagin V V., Wohlschlegel J, Qu J, Jonsson Z, Huang X, Chuma S, et al. Proteomic analysis of murine Piwi proteins reveals a role for arginine methylation in specifying interaction with Tudor family members. *Genes Dev* 2009;23:1749. <https://doi.org/10.1101/GAD.1814809>.
- [260] Reuter M, Chuma S, Tanaka T, Franz T, Stark A, Pillai RS. Loss of the Mili-interacting Tudor domain-containing protein-1 activates transposons and alters the Mili-associated small RNA profile. *Nature Structural & Molecular Biology* 2009 16:6 2009;16:639–46. <https://doi.org/10.1038/nsmb.1615>.
- [261] Saxe JP, Chen M, Zhao H, Lin H. Tdrkh is essential for spermatogenesis and participates in primary piRNA biogenesis in the germline. *EMBO Journal* 2013;32:1869–85. <https://doi.org/10.1038/emboj.2013.121>.
- [262] Zhang H, Liu K, Izumi N, Huang H, Ding D, Ni Z, et al. Structural basis for arginine methylation-independent recognition of PIWIL1 by TDRD2 2017. <https://doi.org/10.5281/zenodo.1021859>.
- [263] Chen S, Zhang W, Min J, Liu K. Lesson from a Fab-enabled co-crystallization study of TDRD2 and PIWIL1. *Methods* 2020;175:72–8. <https://doi.org/10.1016/J.YMETH.2019.07.002>.
- [264] Kirino Y, Vourekas A, Sayed N, De Lima Alves F, Thomson T, Lasko P, et al. Arginine methylation of Aubergine mediates Tudor binding and germ plasm localization. *RNA* 2010;16:70–8. <https://doi.org/10.1261/RNA.1869710>.
- [265] Wu J, Xu W. Histone H3R17me2a mark recruits human RNA polymerase-associated factor 1 complex to activate transcription. *Proc Natl Acad Sci U S A* 2012;109:5675–80. <https://doi.org/10.1073/PNAS.1114905109>.
- [266] Lee YH, Bedford MT, Stallcup MR. Regulated recruitment of tumor suppressor BRCA1 to the p21 gene by coactivator methylation. *Genes Dev* 2011;25:176–88. <https://doi.org/10.1101/GAD.1975811>.
- [267] Yu YS, Shin HR, Kim D, Baek SA, Choi SA, Ahn H, et al. Pontin arginine methylation by CARM1 is crucial for epigenetic regulation of autophagy. *Nat Commun* 2020;11. <https://doi.org/10.1038/S41467-020-20080-9>.

- [268] Gao G, Hausmann S, Flores NM, Benitez AM, Shen J, Yang X, et al. The NFIB/CARM1 partnership is a driver in preclinical models of small cell lung cancer. *Nat Commun* 2023;14. <https://doi.org/10.1038/S41467-023-35864-Y>.
- [269] Iberg AN, Espejo A, Cheng D, Kim D, Michaud-Levesque J, Richard S, et al. Arginine methylation of the histone H3 tail impedes effector binding. *J Biol Chem* 2008;283:3006–10. <https://doi.org/10.1074/JBC.C700192200>.
- [270] Hyllus D, Stein C, Schnabel K, Schiltz E, Imhof A, Dou Y, et al. PRMT6-mediated methylation of R2 in histone H3 antagonizes H3 K4 trimethylation. *Genes Dev* 2007;21:3369–80. <https://doi.org/10.1101/GAD.447007>.
- [271] Guccione E, Bassi C, Casadio F, Martinato F, Cesaroni M, Schuchlantz H, et al. Methylation of histone H3R2 by PRMT6 and H3K4 by an MLL complex are mutually exclusive. *Nature* 2007;449:933–7. <https://doi.org/10.1038/NATURE06166>.
- [272] Liu X, Zhang J, Liu L, Jiang Y, Ji J, Yan R, et al. Protein arginine methyltransferase 5-mediated epigenetic silencing of IRX1 contributes to tumorigenicity and metastasis of gastric cancer. *Biochimica et Biophysica Acta (BBA) - Molecular Basis of Disease* 2018;1864:2835–44. <https://doi.org/10.1016/J.BBADIS.2018.05.015>.
- [273] Zhang J, Jing L, Li M, He L, Guo Z. Regulation of histone arginine methylation/demethylation by methylase and demethylase. *Mol Med Rep* 2019;19:3963. <https://doi.org/10.3892/MMR.2019.10111>.
- [274] Punnia-Moorthy G, Hersey P, Emran A Al, Tiffen J. Lysine Demethylases: Promising Drug Targets in Melanoma and Other Cancers. *Front Genet* 2021;12:680633. <https://doi.org/10.3389/FGENE.2021.680633/BIBTEX>.
- [275] Walport LJ, Hopkinson RJ, Chowdhury R, Schiller R, Ge W, Kawamura A, et al. Arginine demethylation is catalysed by a subset of JmJc histone lysine demethylases. *Nat Commun* 2016;7. <https://doi.org/10.1038/NCOMMS11974>.
- [276] Chang B, Chen Y, Zhao Y, Bruick RK. JMJD6 is a histone arginine demethylase. *Science* 2007;318:444–7. <https://doi.org/10.1126/SCIENCE.1145801>.
- [277] Kwok J, O'Shea M, Hume DA, Lengeling A. Jmjd6, a JmJc dioxygenase with many interaction partners and pleiotropic functions. *Front Genet* 2017;8. <https://doi.org/10.3389/FGENE.2017.00032/FULL>.
- [278] Poulard C, Rambaud J, Hussein N, Corbo L, Le Romancer M. JMJD6 regulates ER $\alpha$  methylation on arginine. *PLoS One* 2014;9. <https://doi.org/10.1371/JOURNAL.PONE.0087982>.
- [279] Gao WW, Xiao RQ, Peng BL, Xu HT, Shen HF, Huang MF, et al. Arginine methylation of HSP70 regulates retinoid acid-mediated RAR $\beta$ 2 gene activation. *Proc Natl Acad Sci U S A* 2015;112:E3327–36. <https://doi.org/10.1073/PNAS.1509658112>.



- [280] Tsai WC, Reineke LC, Jain A, Jung SY, Lloyd RE. Histone arginine demethylase JMJD6 is linked to stress granule assembly through demethylation of the stress granule-nucleating protein G3BP1. *J Biol Chem* 2017;292:18886–96. <https://doi.org/10.1074/JBC.M117.800706>.
- [281] Liu H, Wang C, Lee S, Deng Y, Wither M, Oh S, et al. Clipping of arginine-methylated histone tails by JMJD5 and JMJD7. *Proc Natl Acad Sci U S A* 2017;114:E7717–26. [https://doi.org/10.1073/PNAS.1706831114/SUPPL\\_FILE/PNAS.201706831SI.PDF](https://doi.org/10.1073/PNAS.1706831114/SUPPL_FILE/PNAS.201706831SI.PDF).
- [282] Liu LM, Sun WZ, Fan XZ, Xu YL, Cheng M Bin, Zhang Y. Methylation of C/EBP $\alpha$  by PRMT1 Inhibits Its Tumor-Suppressive Function in Breast Cancer. *Cancer Res* 2019;79:2865–77. <https://doi.org/10.1158/0008-5472.CAN-18-3211>.
- [283] Le Romancer M, Treilleux I, Leconte N, Robin-Lespinasse Y, Sentis S, Bouchekioua-Bouzaghrou K, et al. Regulation of estrogen rapid signaling through arginine methylation by PRMT1. *Mol Cell* 2008;31:212–21. <https://doi.org/10.1016/J.MOLCEL.2008.05.025>.
- [284] Choucair A, Pham TH, Omarjee S, Jacquemetton J, Kassem L, Trédan O, et al. The arginine methyltransferase PRMT1 regulates IGF-1 signaling in breast cancer. *Oncogene* 2019;38:4015–27. <https://doi.org/10.1038/S41388-019-0694-9>.
- [285] Poulard C, Treilleux I, Lavergne E, Bouchekioua-Bouzaghrou K, Goddard-Léon S, Chabaud S, et al. Activation of rapid oestrogen signalling in aggressive human breast cancers. *EMBO Mol Med* 2012;4:1200–13. <https://doi.org/10.1002/EMMM.201201615>.
- [286] Sharieh EA, Awidi AS, Ahram M, Zihlif MA. Alteration of gene expression in MDA-MB-453 breast cancer cell line in response to continuous exposure to Trastuzumab. *Gene* 2016;575:415–20. <https://doi.org/10.1016/j.gene.2015.09.019>.
- [287] Wu Q, Nie DY, Ba-alawi W, Ji Y, Zhang Z, Cruickshank J, et al. PRMT inhibition induces a viral mimicry response in triple-negative breast cancer. *Nat Chem Biol* 2022;18:821–30. <https://doi.org/10.1038/s41589-022-01024-4>.
- [288] Gao Y, Zhao Y, Zhang J, Lu Y, Liu X, Geng P, et al. The dual function of PRMT1 in modulating epithelial-mesenchymal transition and cellular senescence in breast cancer cells through regulation of ZEB1. *Sci Rep* 2016;6. <https://doi.org/10.1038/SREP19874>.
- [289] Li Z, Wang D, Chen X, Wang W, Wang P, Hou P, et al. PRMT1-mediated EZH2 methylation promotes breast cancer cell proliferation and tumorigenesis. *Cell Death Dis* 2021;12. <https://doi.org/10.1038/S41419-021-04381-5>.
- [290] Li Z, Wang D, Lu J, Huang B, Wang Y, Dong M, et al. Methylation of EZH2 by PRMT1 regulates its stability and promotes breast cancer metastasis. *Cell*

- Death & Differentiation 2020 27:12 2020;27:3226–42.  
<https://doi.org/10.1038/s41418-020-00615-9>.
- [291] Li Z, Wang D, Wang W, Chen X, Tang A, Hou P, et al. Macrophages-stimulated PRMT1-mediated EZH2 methylation promotes breast cancer metastasis. *Biochem Biophys Res Commun* 2020;533:679–84. <https://doi.org/10.1016/J.BBRC.2020.10.037>.
- [292] Li T, Kong ANT, Ma Z, Liu H, Liu P, Xiao Y, et al. Protein arginine methyltransferase 1 may be involved in pregnane x receptor-activated overexpression of multidrug resistance 1 gene during acquired multidrug resistant. *Oncotarget* 2016;7:20236–48. <https://doi.org/10.18632/ONCOTARGET.7752>.
- [293] Cho JH, Lee MK, Yoon KW, Lee J, Cho SG, Choi EJ. Arginine methylation-dependent regulation of ASK1 signaling by PRMT1. *Cell Death Differ* 2012;19:859–70. <https://doi.org/10.1038/CDD.2011.168>.
- [294] Mathioudaki K, Papadokostopoulou A, Scorilas A, Xynopoulos D, Agnanti N, Talieri M. The PRMT1 gene expression pattern in colon cancer. *Br J Cancer* 2008;99:2094–9. <https://doi.org/10.1038/SJ.BJC.6604807>.
- [295] Yin XK, Wang YL, Wang F, Feng WX, Bai SM, Zhao WW, et al. PRMT1 enhances oncogenic arginine methylation of NONO in colorectal cancer. *Oncogene* 2021;40:1375–89. <https://doi.org/10.1038/S41388-020-01617-0>.
- [296] Yoshimatsu M, Toyokawa G, Hayami S, Unoki M, Tsunoda T, Field HI, et al. Dysregulation of PRMT1 and PRMT6, Type I arginine methyltransferases, is involved in various types of human cancers. *Int J Cancer* 2011;128:562–73. <https://doi.org/10.1002/IJC.25366>.
- [297] Avasarala S, Van Scoyk M, Rathinam MKK, Zerayesus S, Zhao X, Zhang W, et al. PRMT1 Is a Novel Regulator of Epithelial-Mesenchymal-Transition in Non-small Cell Lung Cancer. *J Biol Chem* 2015;290:13479–89. <https://doi.org/10.1074/JBC.M114.636050>.
- [298] Deng X, von Keudell G, Suzuki T, Dohmae N, Nakakido M, Piao L, et al. PRMT1 promotes mitosis of cancer cells through arginine methylation of INCENP. *Oncotarget* 2015;6:35173–82. <https://doi.org/10.18632/ONCOTARGET.6050>.
- [299] Wang Y, Hsu JM, Kang Y, Wei Y, Lee PC, Chang SJ, et al. Oncogenic Functions of Gli1 in Pancreatic Adenocarcinoma Are Supported by Its PRMT1-Mediated Methylation. *Cancer Res* 2016;76:7049–58. <https://doi.org/10.1158/0008-5472.CAN-16-0715>.
- [300] Wang L, Jia Z, Xie D, Zhao T, Tan Z, Zhang S, et al. Methylation of HSP70 Orchestrates Its Binding to and Stabilization of BCL2 mRNA and Renders Pancreatic Cancer Cells Resistant to Therapeutics. *Cancer Res* 2020;80:4500–13. <https://doi.org/10.1158/0008-5472.CAN-19-1738>.
- [301] Ryu JW, Kim SK, Son MY, Jeon SJ, Oh JH, Lim JH, et al. Novel prognostic marker PRMT1 regulates cell growth via downregulation of CDKN1A in HCC.

- [302] MATSUBARA H, FUKUDA T, AWAZU Y, NANNO S, SHIMOMURA M, INOUE Y, et al. PRMT1 expression predicts sensitivity to platinum-based chemotherapy in patients with ovarian serous carcinoma. *Oncol Lett* 2021;21. <https://doi.org/10.3892/OL.2020.12423>.
- [303] Musiani D, Giambruno R, Massignani E, Ippolito MR, Maniaci M, Jammula S, et al. PRMT1 Is Recruited via DNA-PK to Chromatin Where It Sustains the Senescence-Associated Secretory Phenotype in Response to Cisplatin. *Cell Rep* 2020;30:1208-1222.e9. <https://doi.org/10.1016/j.celrep.2019.12.061>.
- [304] He X, Zhu Y, Lin YC, Li M, Du J, Dong H, et al. PRMT1-mediated FLT3 arginine methylation promotes maintenance of FLT3-ITD+ acute myeloid leukemia. *Blood* 2019;134:548–60. <https://doi.org/10.1182/BLOOD.2019001282>.
- [305] Zhu Y, He X, Lin YC, Dong H, Zhang L, Chen X, et al. Targeting PRMT1-mediated FLT3 methylation disrupts maintenance of MLL-rearranged acute lymphoblastic leukemia. *Blood* 2019;134:1257–68. <https://doi.org/10.1182/BLOOD.2019002457>.
- [306] Leonard S, Gordon N, Smith N, Rowe M, Murray PG, Woodman CB. Arginine Methyltransferases Are Regulated by Epstein-Barr Virus in B Cells and Are Differentially Expressed in Hodgkin's Lymphoma. *Pathogens* 2012;1:52–64. <https://doi.org/10.3390/PATHOGENS1010052>.
- [307] Yuniati L, van der Meer LT, Tijchon E, Schenau D van I, van Emst L, Levers M, et al. Tumor suppressor BTG1 promotes PRMT1-mediated ATF4 function in response to cellular stress. *Oncotarget* 2016;7:3128–43. <https://doi.org/10.18632/ONCOTARGET.6519>.
- [308] Bonnal SC, López-Oreja I, Valcárcel J. Roles and mechanisms of alternative splicing in cancer — implications for care. *Nature Reviews Clinical Oncology* 2020 17:8 2020;17:457–74. <https://doi.org/10.1038/s41571-020-0350-x>.
- [309] Zou L, Zhang H, Du C, Liu X, Zhu S, Zhang W, et al. Correlation of SRSF1 and PRMT1 expression with clinical status of pediatric acute lymphoblastic leukemia. *J Hematol Oncol* 2012;5. <https://doi.org/10.1186/1756-8722-5-42>.
- [310] Cura V, Cavarelli J. Structure, Activity and Function of the PRMT2 Protein Arginine Methyltransferase. *Life* 2021;11. <https://doi.org/10.3390/LIFE11111263>.
- [311] Zhong J, Cao RX, Zu XY, Hong T, Yang J, Liu L, et al. Identification and characterization of novel spliced variants of PRMT2 in breast carcinoma. *FEBS J* 2012;279:316–35. <https://doi.org/10.1111/J.1742-4658.2011.08426.X>.
- [312] Oh TG, Bailey P, Dray E, Smith AG, Goode J, Eriksson N, et al. PRMT2 and ROR $\alpha$  expression are associated with breast cancer survival outcomes. *Molecular Endocrinology* 2014;28:1166–85. [https://doi.org/10.1210/ME.2013-1403/SUPPL\\_FILE/ME-13-1403.PDF](https://doi.org/10.1210/ME.2013-1403/SUPPL_FILE/ME-13-1403.PDF).

- [313] Qi C, Chang J, Zhu Y, Yeldandi A V., Rao SM, Zhu YJ. Identification of protein arginine methyltransferase 2 as a coactivator for estrogen receptor alpha. *J Biol Chem* 2002;277:28624–30. <https://doi.org/10.1074/JBC.M201053200>.
- [314] Zhong J, Cao RX, Liu JH, Liu YB, Wang J, Liu LP, et al. Nuclear loss of protein arginine N-methyltransferase 2 in breast carcinoma is associated with tumor grade and overexpression of cyclin D1 protein. *Oncogene* 2014;33:5546–58. <https://doi.org/10.1038/ONC.2013.500>.
- [315] Zhong J, Chen YJ, Chen L, Shen YY, Zhang QH, Yang J, et al. PRMT2 $\beta$ , a C-terminal splice variant of PRMT2, inhibits the growth of breast cancer cells. *Oncol Rep* 2017;38:1303–11. <https://doi.org/10.3892/OR.2017.5786>.
- [316] Shen Y, Zhong J, Liu J, Liu K, Zhao J, Xu T, et al. Protein arginine N-methyltransferase 2 reverses tamoxifen resistance in breast cancer cells through suppression of ER- $\alpha$ 36. *Oncol Rep* 2018;39:2604–12. <https://doi.org/10.3892/OR.2018.6350>.
- [317] Dong F, Li Q, Yang C, Huo D, Wang X, Ai C, et al. PRMT2 links histone H3R8 asymmetric dimethylation to oncogenic activation and tumorigenesis of glioblastoma. *Nat Commun* 2018;9. <https://doi.org/10.1038/S41467-018-06968-7>.
- [318] Hu G, Yan C, Xie P, Cao Y, Shao J, Ge J. PRMT2 accelerates tumorigenesis of hepatocellular carcinoma by activating Bcl2 via histone H3R8 methylation. *Exp Cell Res* 2020;394. <https://doi.org/10.1016/J.YEXCR.2020.112152>.
- [319] Singh V, Branscombe Miranda T, Jiang W, Frankel A, Roemer ME, Robb VA, et al. DAL-1/4.1B tumor suppressor interacts with protein arginine N-methyltransferase 3 (PRMT3) and inhibits its ability to methylate substrates in vitro and in vivo. *Oncogene* 2004;23:7761–71. <https://doi.org/10.1038/SJ.ONC.1208057>.
- [320] Jiang W, Roemer ME, Newsham IF. The tumor suppressor DAL-1/4.1B modulates protein arginine N-methyltransferase 5 activity in a substrate-specific manner. *Biochem Biophys Res Commun* 2005;329:522–30. <https://doi.org/10.1016/J.BBRC.2005.01.153>.
- [321] Jiang W, Newsham IF. The tumor suppressor DAL-1/4.1B and protein methylation cooperate in inducing apoptosis in MCF-7 breast cancer cells. *Mol Cancer* 2006;5. <https://doi.org/10.1186/1476-4598-5-4>.
- [322] Zhi R, Wu K, Zhang J, Liu H, Niu C, Li S, et al. PRMT3 regulates the progression of invasive micropapillary carcinoma of the breast. *Cancer Sci* 2023;114. <https://doi.org/10.1111/CAS.15724>.
- [323] Hsu MC, Pan MR, Chu PY, Tsai YL, Tsai CH, Shan YS, et al. Protein Arginine Methyltransferase 3 Enhances Chemoresistance in Pancreatic Cancer by Methylating hnRNPA1 to Increase ABCG2 Expression. *Cancers* 2019, Vol 11, Page 8 2018;11:8. <https://doi.org/10.3390/CANCERS11010008>.

- [324] Zhang X, Wang K, Feng X, Wang J, Chu Y, Jia C, et al. PRMT3 promotes tumorigenesis by methylating and stabilizing HIF1 $\alpha$  in colorectal cancer. *Cell Death & Disease* 2021 12:11 2021;12:1–13. <https://doi.org/10.1038/s41419-021-04352-w>.
- [325] Hu Y, Su Y, He Y, Liu W, Xiao B. Arginine methyltransferase PRMT3 promote tumorigenesis through regulating c-MYC stabilization in colorectal cancer. *Gene* 2021;791:145718. <https://doi.org/10.1016/J.GENE.2021.145718>.
- [326] Cheng H, Qin Y, Fan H, Su P, Zhang X, Zhang H, et al. Overexpression of CARM1 in breast cancer is correlated with poorly characterized clinicopathologic parameters and molecular subtypes. *Diagn Pathol* 2013;8. <https://doi.org/10.1186/1746-1596-8-129>.
- [327] Davis MB, Liu X, Wang S, Reeves J, Khramtsov A, Huo D, et al. Expression and sub-cellular localization of an epigenetic regulator, co-activator arginine methyltransferase 1 (CARM1), is associated with specific breast cancer subtypes and ethnicity. *Mol Cancer* 2013;12. <https://doi.org/10.1186/1476-4598-12-40>.
- [328] Habashy HO, Rakha EA, Ellis IO, Powe DG. The oestrogen receptor coactivator CARM1 has an oncogenic effect and is associated with poor prognosis in breast cancer. *Breast Cancer Res Treat* 2013;140:307–16. <https://doi.org/10.1007/S10549-013-2614-Y>.
- [329] Higashimoto K, Kuhn P, Desai D, Cheng X, Xu W. Phosphorylation-mediated inactivation of coactivator-associated arginine methyltransferase 1. *Proc Natl Acad Sci U S A* 2007;104:12318–23. <https://doi.org/10.1073/PNAS.0610792104/ASSET/64CE475C-B85D-4FC6-AAA1-647406257537/ASSETS/GRAPHIC/ZPQ0300770810006.JPEG>.
- [330] Carascossa S, Dudek P, Cenni B, Briand PA, Picard D. CARM1 mediates the ligand-independent and tamoxifen-resistant activation of the estrogen receptor alpha by cAMP. *Genes Dev* 2010;24:708–19. <https://doi.org/10.1101/GAD.568410>.
- [331] Liu J, Feng J, Li L, Lin L, Ji J, Lin C, et al. Arginine methylation-dependent LSD1 stability promotes invasion and metastasis of breast cancer. *EMBO Rep* 2020;21. <https://doi.org/10.15252/EMBR.201948597>.
- [332] Gao W wei, Xiao R quan, Zhang W juan, Hu Y ren, Peng B ling, Li W juan, et al. JMJD6 Licenses ER $\alpha$ -Dependent Enhancer and Coding Gene Activation by Modulating the Recruitment of the CARM1/MED12 Co-activator Complex. *Mol Cell* 2018;70:340-357.e8. <https://doi.org/10.1016/J.MOLCEL.2018.03.006>.
- [333] Wang L, Zeng H, Wang Q, Zhao Z, Boyer TG, Bian X, et al. MED12 methylation by CARM1 sensitizes human breast cancer cells to chemotherapy drugs. *Sci Adv* 2015;1. <https://doi.org/10.1126/SCIADV.1500463>.
- [334] Wang L, Zhao Z, Meyer MB, Saha S, Yu M, Guo A, et al. CARM1 methylates chromatin remodeling factor BAF155 to enhance tumor progression and

- metastasis. *Cancer Cell* 2014;25:21–36. <https://doi.org/10.1016/J.CCR.2013.12.007>.
- [335] Liu F, Ma F, Wang Y, Hao L, Zeng H, Jia C, et al. PKM2 methylation by CARM1 activates aerobic glycolysis to promote tumorigenesis. *Nat Cell Biol* 2017;19:1358–70. <https://doi.org/10.1038/NCB3630>.
- [336] Nakayama N, Sakashita G, Nariai Y, Kato H, Sinmyozu K, Nakayama JI, et al. Cancer-related transcription regulator protein NAC1 forms a protein complex with CARM1 for ovarian cancer progression. *Oncotarget* 2018;9:28408–20. <https://doi.org/10.18632/ONCOTARGET.25400>.
- [337] Karakashev S, Zhu H, Wu S, Yokoyama Y, Bitler BG, Park PH, et al. CARM1-expressing ovarian cancer depends on the histone methyltransferase EZH2 activity. *Nat Commun* 2018;9. <https://doi.org/10.1038/S41467-018-03031-3>.
- [338] Karakashev S, Fukumoto T, Zhao B, Lin J, Wu S, Fatkhutdinov N, et al. EZH2 Inhibition Sensitizes CARM1-High, Homologous Recombination Proficient Ovarian Cancers to PARP Inhibition. *Cancer Cell* 2020;37:157-167.e6. <https://doi.org/10.1016/J.CCELL.2019.12.015>.
- [339] Kim YR, Lee BK, Park RY, Nguyen NTX, Bae JA, Kwon DD, et al. Differential CARM1 expression in prostate and colorectal cancers. *BMC Cancer* 2010;10. <https://doi.org/10.1186/1471-2407-10-197>.
- [340] Zheng L, Chen J, Zhou Z, He Z. miR-195 enhances the radiosensitivity of colorectal cancer cells by suppressing CARM1. *Onco Targets Ther* 2017;10:1027–38. <https://doi.org/10.2147/OTT.S125067>.
- [341] Zhang M, Wu W, Gao M, Zhang J, Ding X, Zhu R, et al. Coactivator-associated arginine methyltransferase 1 promotes cell growth and is targeted by microRNA-195-5p in human colorectal cancer. *Tumour Biol* 2017;39. <https://doi.org/10.1177/1010428317694305>.
- [342] Ou CY, LaBonte MJ, Manegold PC, So AYL, Ianculescu I, Gerke DS, et al. A coactivator role of CARM1 in the dysregulation of  $\beta$ -catenin activity in colorectal cancer cell growth and gene expression. *Mol Cancer Res* 2011;9:660–70. <https://doi.org/10.1158/1541-7786.MCR-10-0223>.
- [343] Lee E, Madar A, David G, Garabedian MJ, Gupta R Das, Logan SK. Inhibition of androgen receptor and  $\beta$ -catenin activity in prostate cancer. *Proc Natl Acad Sci U S A* 2013;110:15710–5. <https://doi.org/10.1073/PNAS.1218168110>.
- [344] Majumder S, Liu Y, Ford OH, Mohler JL, Whang YE. Involvement of arginine methyltransferase CARM1 in androgen receptor function and prostate cancer cell viability. *Prostate* 2006;66:1292–301. <https://doi.org/10.1002/PROS.20438>.
- [345] Hong H, Kao C, Jeng MH, Eble JN, Koch MO, Gardner TA, et al. Aberrant expression of CARM1, a transcriptional coactivator of androgen receptor, in the development of prostate carcinoma and androgen-independent status. *Cancer* 2004;101:83–9. <https://doi.org/10.1002/CNCR.20327>.

- [346] Wang YP, Zhou W, Wang J, Huang X, Zuo Y, Wang TS, et al. Arginine Methylation of MDH1 by CARM1 Inhibits Glutamine Metabolism and Suppresses Pancreatic Cancer. *Mol Cell* 2016;64:673–87. <https://doi.org/10.1016/J.MOLCEL.2016.09.028>.
- [347] Greenblatt SM, Man N, Hamard PJ, Asai T, Karl D, Martinez C, et al. CARM1 Is Essential for Myeloid Leukemogenesis but Dispensable for Normal Hematopoiesis. *Cancer Cell* 2018;33:1111-1127.e5. <https://doi.org/10.1016/J.CCELL.2018.05.007>.
- [348] Vu LP, Perna F, Wang L, Voza F, Figueroa ME, Tempst P, et al. PRMT4 blocks myeloid differentiation by assembling a methyl-RUNX1-dependent repressor complex. *Cell Rep* 2013;5:1625–38. <https://doi.org/10.1016/J.CELREP.2013.11.025>.
- [349] Drew AE, Moradei O, Jacques SL, Rioux N, Boriack-Sjodin AP, Allain C, et al. Identification of a CARM1 Inhibitor with Potent In Vitro and In Vivo Activity in Preclinical Models of Multiple Myeloma. *Scientific Reports* 2017 7:1 2017;7:1–13. <https://doi.org/10.1038/s41598-017-18446-z>.
- [350] Veazey KJ, Cheng D, Lin K, Villarreal OD, Gao G, Perez-Oquendo M, et al. CARM1 inhibition reduces histone acetyltransferase activity causing synthetic lethality in CREBBP/EP300-mutated lymphomas. *Leukemia* 2020;34:3269–85. <https://doi.org/10.1038/S41375-020-0908-8>.
- [351] Nie M, Wang Y, Guo C, Li X, Wang Y, Deng Y, et al. CARM1-mediated methylation of protein arginine methyltransferase 5 represses human  $\gamma$ -globin gene expression in erythroleukemia cells. *J Biol Chem* 2018;293:17454–63. <https://doi.org/10.1074/JBC.RA118.004028>.
- [352] Stein C, Riedl S, R uthnick D, N told RR, Bauer UM. The arginine methyltransferase PRMT6 regulates cell proliferation and senescence through transcriptional repression of tumor suppressor genes. *Nucleic Acids Res* 2012;40:9522–33. <https://doi.org/10.1093/NAR/GKS767>.
- [353] Veland N, Hardikar S, Zhong Y, Gayatri S, Dan J, Strahl BD, et al. The Arginine Methyltransferase PRMT6 Regulates DNA Methylation and Contributes to Global DNA Hypomethylation in Cancer. *Cell Rep* 2017;21:3390–7. <https://doi.org/10.1016/J.CELREP.2017.11.082>.
- [354] Dowhan DH, Harrison MJ, Eriksson NA, Bailey P, Pearen MA, Fuller PJ, et al. Protein arginine methyltransferase 6-dependent gene expression and splicing: association with breast cancer outcomes. *Endocr Relat Cancer* 2012;19:509–26. <https://doi.org/10.1530/ERC-12-0100>.
- [355] Sun Y, Chung HH, Woo ARE, Lin VCL. Protein arginine methyltransferase 6 enhances ligand-dependent and -independent activity of estrogen receptor  $\alpha$  via distinct mechanisms. *Biochim Biophys Acta* 2014;1843:2067–78. <https://doi.org/10.1016/J.BBAMCR.2014.04.008>.

- [356] Harrison MJ, Tang YH, Dowhan DH. Protein arginine methyltransferase 6 regulates multiple aspects of gene expression. *Nucleic Acids Res* 2010;38:2201–16. <https://doi.org/10.1093/NAR/GKP1203>.
- [357] Mann M, Zou Y, Chen Y, Brann D, Vadlamudi R. PELP1 oncogenic functions involve alternative splicing via PRMT6. *Mol Oncol* 2014;8:389–400. <https://doi.org/10.1016/J.MOLONC.2013.12.012>.
- [358] Yang T, Huang W, Ma T, Yin X, Zhang J, Huo M, et al. The PRMT6/PARP1/CRL4B Complex Regulates the Circadian Clock and Promotes Breast Tumorigenesis. *Adv Sci (Weinh)* 2023;10. <https://doi.org/10.1002/ADVS.202202737>.
- [359] Chen Z, Gan J, Wei Z, Zhang M, Du Y, Xu C, et al. The Emerging Role of PRMT6 in Cancer. *Front Oncol* 2022;12. <https://doi.org/10.3389/FONC.2022.841381>.
- [360] Halabelian L, Barsyte-Lovejoy D. Structure and Function of Protein Arginine Methyltransferase PRMT7. *Life* 2021;11. <https://doi.org/10.3390/LIFE11080768>.
- [361] Yao R, Jiang H, Ma Y, Wang L, Wang L, Du J, et al. PRMT7 induces epithelial-to-mesenchymal transition and promotes metastasis in breast cancer. *Cancer Res* 2014;74:5656–67. <https://doi.org/10.1158/0008-5472.CAN-14-0800>.
- [362] Geng P, Zhang Y, Liu X, Zhang N, Liu Y, Liu X, et al. Automethylation of protein arginine methyltransferase 7 and its impact on breast cancer progression. *FASEB J* 2017;31:2287–300. <https://doi.org/10.1096/FJ.201601196R>.
- [363] Mitchell Baldwin R, Haghbandish N, Daneshmand M, Amin S, Paris G, Falls TJ, et al. Protein arginine methyltransferase 7 promotes breast cancer cell invasion through the induction of MMP9 expression. *Oncotarget* 2015;6:3013–32. <https://doi.org/10.18632/ONCOTARGET.3072>.
- [364] Liu L, Zhang X, Ding H, Liu X, Cao D, Liu Y, et al. Arginine and lysine methylation of MRPS23 promotes breast cancer metastasis through regulating OXPHOS. *Oncogene* 2021;40:3548–63. <https://doi.org/10.1038/S41388-021-01785-7>.
- [365] Kaniskan HÜ, Szewczyk MM, Yu Z, Eram MS, Yang X, Schmidt K, et al. A potent, selective and cell-active allosteric inhibitor of protein arginine methyltransferase 3 (PRMT3). *Angew Chem Int Ed Engl* 2015;54:5166–70. <https://doi.org/10.1002/ANIE.201412154>.
- [366] Nakayama K, Szewczyk MM, dela Sena C, Wu H, Dong A, Zeng H, et al. TP-064, a potent and selective small molecule inhibitor of PRMT4 for multiple myeloma. *Oncotarget* 2018;9:18480–93. <https://doi.org/10.18632/ONCOTARGET.24883>.
- [367] Shen Y, Szewczyk MM, Eram MS, Smil D, Kaniskan HÜ, Ferreira De Freitas R, et al. Discovery of a Potent, Selective, and Cell-Active Dual Inhibitor of Protein Arginine Methyltransferase 4 and Protein Arginine Methyltransferase 6. *J Med Chem* 2016;59:9124–39. <https://doi.org/10.1021/ACS.JMEDCHEM.6B01033>.



- [368] Mitchell LH, Drew AE, Ribich SA, Rioux N, Swinger KK, Jacques SL, et al. Aryl Pyrazoles as Potent Inhibitors of Arginine Methyltransferases: Identification of the First PRMT6 Tool Compound. *ACS Med Chem Lett* 2015;6:655. <https://doi.org/10.1021/ACSMEDCHEMLETT.5B00071>.
- [369] Shen Y, Li F, Szewczyk MM, Halabelian L, Chau I, Eram MS, et al. A First-in-Class, Highly Selective and Cell-Active Allosteric Inhibitor of Protein Arginine Methyltransferase 6. *J Med Chem* 2021;64:3697–706. <https://doi.org/10.1021/ACS.JMEDCHEM.0C02160>.
- [370] Szewczyk MM, Ishikawa Y, Organ S, Sakai N, Li F, Halabelian L, et al. Pharmacological inhibition of PRMT7 links arginine monomethylation to the cellular stress response. *Nature Communications* 2020 11:1 2020;11:1–15. <https://doi.org/10.1038/s41467-020-16271-z>.
- [371] Smil D, Eram MS, Li F, Kennedy S, Szewczyk MM, Brown PJ, et al. Discovery of a dual PRMT5-PRMT7 inhibitor. *ACS Med Chem Lett* 2015;6:408–12. [https://doi.org/10.1021/ML500467H/SUPPL\\_FILE/ML500467H\\_SI\\_001.PDF](https://doi.org/10.1021/ML500467H/SUPPL_FILE/ML500467H_SI_001.PDF).
- [372] Eram MS, Shen Y, Szewczyk MM, Wu H, Senisterra G, Li F, et al. A Potent, Selective, and Cell-Active Inhibitor of Human Type I Protein Arginine Methyltransferases. *ACS Chem Biol* 2016;11:772–81. <https://doi.org/10.1021/ACSCHEMBIO.5B00839>.
- [373] Friesen WJ, Wyce A, Paushkin S, Abel L, Rappsilber J, Mann M, et al. A novel WD repeat protein component of the methylosome binds Sm proteins. *Journal of Biological Chemistry* 2002;277:8243–7. <https://doi.org/10.1074/jbc.M109984200>.
- [374] Gu Z, Li Y, Lee P, Liu T, Wan C, Wang Z. Protein Arginine Methyltransferase 5 Functions in Opposite Ways in the Cytoplasm and Nucleus of Prostate Cancer Cells. *PLoS One* 2012;7:44033. <https://doi.org/10.1371/JOURNAL.PONE.0044033>.
- [375] Liu F, Zhao X, Perna F, Wang L, Koppikar P, Abdel-Wahab O, et al. JAK2V617F-mediated phosphorylation of PRMT5 downregulates its methyltransferase activity and promotes myeloproliferation. *Cancer Cell* 2011;19:283–94. <https://doi.org/10.1016/J.CCR.2010.12.020>.
- [376] Ho MC, Wilczek C, Bonanno JB, Xing L, Seznec J, Matsui T, et al. Structure of the arginine methyltransferase PRMT5-MEP50 reveals a mechanism for substrate specificity. *PLoS One* 2013;8. <https://doi.org/10.1371/JOURNAL.PONE.0057008>.
- [377] Mulvaney KM, Blomquist C, Acharya N, Li R, Ranaghan MJ, O’Keefe M, et al. Molecular basis for substrate recruitment to the PRMT5 methylosome. *Mol Cell* 2021;81:3481-3495.e7. <https://doi.org/10.1016/J.MOLCEL.2021.07.019>.
- [378] Krzyzanowski A, Gasper R, Adihou H, Hart P t., Waldmann H. Biochemical Investigation of the Interaction of pICln, RioK1 and COPR5 with the PRMT5-

- MEP50 Complex. *Chembiochem* 2021;22:1908–14. <https://doi.org/10.1002/CBIC.202100079>.
- [379] Mckinney DC, Mcmillan BJ, Ranaghan MJ, Moroco JA, Brousseau M, Mullin-Bernstein Z, et al. Discovery of a First-in-Class Inhibitor of the PRMT5–Substrate Adaptor Interaction. *Cite This: J Med Chem* 2021;64:11148–68. <https://doi.org/10.1021/acs.jmedchem.1c00507>.
- [380] Krzyzanowski A, Esser LM, Willaume A, Prudent R, Peter C, T’Hart P, et al. Development of Macrocyclic PRMT5-Adaptor Protein Interaction Inhibitors. *J Med Chem* 2022;65:15300–11. [https://doi.org/10.1021/ACS.JMEDCHEM.2C01273/SUPPL\\_FILE/JM2C01273\\_SI\\_002.CSV](https://doi.org/10.1021/ACS.JMEDCHEM.2C01273/SUPPL_FILE/JM2C01273_SI_002.CSV).
- [381] Sims HS, Dai M. Taming PRMT5–adaptor protein interactions. *Trends Pharmacol Sci* 2023;44:134–6. <https://doi.org/10.1016/j.tips.2023.01.002>.
- [382] Hosohata K, Li P, Hosohata Y, Qin J, Roeder RG, Wang Z. Purification and Identification of a Novel Complex Which Is Involved in Androgen Receptor-Dependent Transcription. *Mol Cell Biol* 2003;23:7019. <https://doi.org/10.1128/MCB.23.19.7019-7029.2003>.
- [383] Gu Z, Zhou L, Gao S, Wang Z. Nuclear Transport Signals Control Cellular Localization and Function of Androgen Receptor Cofactor p44/WDR77. *PLoS One* 2011;6:22395. <https://doi.org/10.1371/JOURNAL.PONE.0022395>.
- [384] Timm DE, Bowman V, Madsen R, Rauch C. Cryo-electron microscopy structure of a human PRMT5:MEP50 complex. *PLoS One* 2018;13. <https://doi.org/10.1371/JOURNAL.PONE.0193205>.
- [385] Friesen WJ, Paushkin S, Wyce A, Massenet S, Pesiridis GS, Van Duyne G, et al. The methylosome, a 20S complex containing JBP1 and pICln, produces dimethylarginine-modified Sm proteins. *Mol Cell Biol* 2001;21:8289–300. <https://doi.org/10.1128/MCB.21.24.8289-8300.2001>.
- [386] Meister G, Eggert C, Bühler D, Brahms H, Kambach C, Fischer U. Methylation of Sm proteins by a complex containing PRMT5 and the putative U snRNP assembly factor pICln. *Curr Biol* 2001;11:1990–4. [https://doi.org/10.1016/S0960-9822\(01\)00592-9](https://doi.org/10.1016/S0960-9822(01)00592-9).
- [387] Pesiridis GS, Diamond E, Van Duyne GD. Role of pICln in methylation of Sm proteins by PRMT5. *Journal of Biological Chemistry* 2009;284:21347–59. <https://doi.org/10.1074/jbc.M109.015578>.
- [388] Beketova E, Fang S, Owens JL, Liu S, Chen X, Zhang Q, et al. Protein Arginine Methyltransferase 5 Promotes pICln-Dependent Androgen Receptor Transcription in Castration-Resistant Prostate Cancer. *Cancer Res* 2020;80:4904–17. <https://doi.org/10.1158/0008-5472.CAN-20-1228>.
- [389] Owens JL, Beketova E, Liu S, Tinsley SL, Asberry AM, Deng X, et al. PRMT5 Cooperates with pICln to Function as a Master Epigenetic Activator of DNA

- Double-Strand Break Repair Genes. *IScience* 2020;23. <https://doi.org/10.1016/J.ISCI.2019.100750>.
- [390] Guderian G, Peter C, Wiesner J, Sickmann A, Schulze-Osthoff K, Fischer U, et al. RioK1, a New Interactor of Protein Arginine Methyltransferase 5 (PRMT5), Competes with pICln for Binding and Modulates PRMT5 Complex Composition and Substrate Specificity. *J Biol Chem* 2011;286:1976. <https://doi.org/10.1074/JBC.M110.148486>.
- [391] Raman B, Guarnaccia C, Nadassy K, Zakhariyev S, Pintar A, Zanuttin F, et al. N $\omega$ -arginine dimethylation modulates the interaction between a Gly/Arg-rich peptide from human nucleolin and nucleic acids. *Nucleic Acids Res* 2001;29:3377. <https://doi.org/10.1093/NAR/29.16.3377>.
- [392] Cox J, Esser LM, Jüdt M, Schmitz K, Reiffert K, Grimmmler M, et al. NF90/NFAR (nuclear factors associated with dsRNA) - a new methylation substrate of the PRMT5-WD45-RioK1 complex. *Biol Chem* 2022;403:907–15. <https://doi.org/10.1515/HSZ-2022-0136>.
- [393] Lacroix M, El Messaoudi S, Rodier G, Le Cam A, Sardet C, Fabrizio E. The histone-binding protein COPR5 is required for nuclear functions of the protein arginine methyltransferase PRMT5. *EMBO Rep* 2008;9:452–8. <https://doi.org/10.1038/EMBOR.2008.45>.
- [394] Cai S, Wang P, Xie T, Li Z, Li J, Lan R, et al. Histone H4R3 symmetric dimethylation by Prmt5 protects against cardiac hypertrophy via regulation of Filip1L/ $\beta$ -catenin. *Pharmacol Res* 2020;161. <https://doi.org/10.1016/J.PHRS.2020.105104>.
- [395] Paul C, Sardet C, Fabrizio E. The Wnt-target gene Dlk-1 is regulated by the Prmt5-associated factor Copr5 during adipogenic conversion. *Biol Open* 2015;4:312–6. <https://doi.org/10.1242/BIO.201411247>.
- [396] Paul C, Sardet C, Fabrizio E. The histone- and PRMT5-associated protein COPR5 is required for myogenic differentiation. *Cell Death Differ* 2012;19:900–8. <https://doi.org/10.1038/CDD.2011.193>.
- [397] Yabuta N, Ota C, Sasakura T, Naito Y, Okuzaki D, Fukushima K, et al. Late cornified envelope 1C (LCE1C), a transcriptional target of TAp63 phosphorylated at T46/T281, interacts with PRMT5. *Sci Rep* 2018;8. <https://doi.org/10.1038/S41598-018-23045-7>.
- [398] Espejo AB, Gao G, Black K, Gayatri S, Veland N, Kim J, et al. PRMT5 C-terminal Phosphorylation Modulates a 14-3-3/PDZ Interaction Switch. *J Biol Chem* 2017;292:2255–65. <https://doi.org/10.1074/JBC.M116.760330>.
- [399] Sipos A, Iván J, Bécsi B, Darula Z, Tamás I, Horváth D, et al. Myosin phosphatase and RhoA-activated kinase modulate arginine methylation by the regulation of protein arginine methyltransferase 5 in hepatocellular carcinoma cells. *Sci Rep* 2017;7. <https://doi.org/10.1038/SREP40590>.

- [400] Lattouf H, Kassem L, Jacquemetton J, Choucair A, Poulard C, Trédan O, et al. LKB1 regulates PRMT5 activity in breast cancer. *Int J Cancer* 2019;144:595–606. <https://doi.org/10.1002/IJC.31909>.
- [401] Fu T, Lv X, Kong Q, Yuan C. A novel SHARPIN-PRMT5-H3R2me1 axis is essential for lung cancer cell invasion. *Oncotarget* 2017;8:54809–20. <https://doi.org/10.18632/ONCOTARGET.18957>.
- [402] Zhang HT, Zeng LF, He QY, Tao WA, Zha ZG, Hu CD. The E3 ubiquitin ligase CHIP mediates ubiquitination and proteasomal degradation of PRMT5. *Biochim Biophys Acta* 2016;1863:335. <https://doi.org/10.1016/J.BBAMCR.2015.12.001>.
- [403] Liu L, Yin S, Gan W. TRAF6 Promotes PRMT5 Activity in a Ubiquitination-Dependent Manner. *Cancers (Basel)* 2023;15:2501. <https://doi.org/10.3390/CANCERS15092501/S1>.
- [404] Aggarwal P, Vaites LP, Kim JK, Mellert H, Gurung B, Nakagawa H, et al. Nuclear cyclin D1/CDK4 kinase regulates CUL4 expression and triggers neoplastic growth via activation of the PRMT5 methyltransferase. *Cancer Cell* 2010;18:329–40. <https://doi.org/10.1016/J.CCR.2010.08.012>.
- [405] Chakrapani B, Khan MIK, Kadumuri RV, Gupta S, Verma M, Awasthi S, et al. The uncharacterized protein FAM47E interacts with PRMT5 and regulates its functions. *Life Sci Alliance* 2020;4. <https://doi.org/10.26508/LSA.202000699>.
- [406] Li BX, David LL, Davis LE, Xiao X. Protein arginine methyltransferase 5 is essential for oncogene product EWSR1-ATF1-mediated gene transcription in clear cell sarcoma. *J Biol Chem* 2022;298. <https://doi.org/10.1016/J.JBC.2022.102434>.
- [407] Pal S, Yun R, Datta A, Lacomis L, Erdjument-Bromage H, Kumar J, et al. mSin3A/histone deacetylase 2- and PRMT5-containing Brg1 complex is involved in transcriptional repression of the Myc target gene cad. *Mol Cell Biol* 2003;23:7475–87. <https://doi.org/10.1128/MCB.23.21.7475-7487.2003>.
- [408] Ancelin K, Lange UC, Hajkova P, Schneider R, Bannister AJ, Kouzarides T, et al. Blimp1 associates with Prmt5 and directs histone arginine methylation in mouse germ cells. *Nat Cell Biol* 2006;8:623–30. <https://doi.org/10.1038/NCB1413>.
- [409] Tsutsui T, Fukasawa R, Shinmyozu K, Nakagawa R, Tobe K, Tanaka A, et al. Mediator Complex Recruits Epigenetic Regulators via Its Two Cyclin-dependent Kinase Subunits to Repress Transcription of Immune Response Genes. *J Biol Chem* 2013;288:20955. <https://doi.org/10.1074/JBC.M113.486746>.
- [410] Gerhart S V, Kellner WA, Thompson C, Pappalardi MB, Zhang XP, Montes de Oca R, et al. Activation of the p53-MDM4 regulatory axis defines the anti-tumour response to PRMT5 inhibition through its role in regulating cellular splicing. *Sci Rep* 2018;8:9711. <https://doi.org/10.1038/s41598-018-28002-y>.

- [411] Dansu DK, Liang J, Selcen I, Zheng H, Moore DF, Casaccia P. PRMT5 Interacting Partners and Substrates in Oligodendrocyte Lineage Cells. *Front Cell Neurosci* 2022;16. <https://doi.org/10.3389/FNCEL.2022.820226>.
- [412] Rengasamy M, Zhang F, Vashisht A, Song WM, Aguilo F, Sun Y, et al. The PRMT5/WDR77 complex regulates alternative splicing through ZNF326 in breast cancer. *Nucleic Acids Res* 2017;45:11106–20. <https://doi.org/10.1093/NAR/GKX727>.
- [413] Cai T, Cinkornpumin JK, Yu Z, Villarreal OD, Pastor WA, Richard S. Deletion of RBMX RGG/RG motif in Shashi-XLID syndrome leads to aberrant p53 activation and neuronal differentiation defects. *Cell Rep* 2021;36. <https://doi.org/10.1016/J.CELREP.2021.109337>.
- [414] Liu L, Zhao X, Zhao L, Li J, Yang H, Zhu Z, et al. Arginine Methylation of SREBP1a via PRMT5 Promotes De Novo Lipogenesis and Tumor Growth. *Cancer Res* 2016;76:1260–72. <https://doi.org/10.1158/0008-5472.CAN-15-1766>.
- [415] Li J, Zhang T, Ren T, Liao X, Hao Y, Lim JS, et al. Oxygen-sensitive methylation of ULK1 is required for hypoxia-induced autophagy. *Nature Communications* 2022 13:1 2022;13:1–11. <https://doi.org/10.1038/s41467-022-28831-6>.
- [416] Brobbey C, Yin S, Liu L, Ball LE, Howe PH, Delaney JR, et al. Autophagy dictates sensitivity to PRMT5 inhibitor in breast cancer. *Scientific Reports* 2023 13:1 2023;13:1–13. <https://doi.org/10.1038/s41598-023-37706-9>.
- [417] He W, Ma X, Yang X, Zhao Y, Qiu J, Hang H. A role for the arginine methylation of Rad9 in checkpoint control and cellular sensitivity to DNA damage. *Nucleic Acids Res* 2011;39:4719–27. <https://doi.org/10.1093/NAR/GKQ1264>.
- [418] Rehman I, Basu SM, Das SK, Bhattacharjee S, Ghosh A, Pommier Y, et al. PRMT5-mediated arginine methylation of TDP1 for the repair of topoisomerase I covalent complexes. *Nucleic Acids Res* 2018;46:5601–17. <https://doi.org/10.1093/NAR/GKY291>.
- [419] Jansson M, Durant ST, Cho EC, Sheahan S, Edelmann M, Kessler B, et al. Arginine methylation regulates the p53 response. *Nat Cell Biol* 2008;10:1431–9. <https://doi.org/10.1038/NCB1802>.
- [420] Hu D, Gur M, Zhou Z, Gamper A, Hung MC, Fujita N, et al. Interplay between arginine methylation and ubiquitylation regulates KLF4-mediated genome stability and carcinogenesis. *Nat Commun* 2015;6. <https://doi.org/10.1038/NCOMMS9419>.
- [421] Powers MA, Fay MM, Factor RE, Welm AL, Ullman KS. Protein arginine methyltransferase 5 accelerates tumor growth by arginine methylation of the tumor suppressor programmed cell death 4. *Cancer Res* 2011;71:5579–87. <https://doi.org/10.1158/0008-5472.CAN-11-0458>.
- [422] Wang X, Qiu T, Wu Y, Yang C, Li Y, Du G, et al. Arginine methyltransferase PRMT5 methylates and stabilizes KLF5 via decreasing its phosphorylation and

- ubiquitination to promote basal-like breast cancer. *Cell Death Differ* 2021;28:2931–45. <https://doi.org/10.1038/s41418-021-00793-0>.
- [423] Kim S, Günesdogan U, Zylicz JJ, Hackett JA, Cougot D, Bao S, et al. PRMT5 Protects Genomic Integrity during Global DNA Demethylation in Primordial Germ Cells and Preimplantation Embryos. *Mol Cell* 2014;56:564. <https://doi.org/10.1016/J.MOLCEL.2014.10.003>.
- [424] Shilo K, Wu X, Sharma S, Welliver M, Duan W, Villalona-Calero M, et al. Cellular localization of protein arginine methyltransferase-5 correlates with grade of lung tumors. *Diagn Pathol* 2013;8:1–9. <https://doi.org/10.1186/1746-1596-8-201/TABLES/4>.
- [425] Gao S, Wang Z. Subcellular localization of p44/WDR77 determines proliferation and differentiation of prostate epithelial cells. *PLoS One* 2012;7. <https://doi.org/10.1371/JOURNAL.PONE.0049173>.
- [426] Zhou L, Wu H, Lee P, Wang Z. Roles of the androgen receptor cofactor p44 in the growth of prostate epithelial cells. *J Mol Endocrinol* 2006;37:283–300. <https://doi.org/10.1677/JME.1.02062>.
- [427] O’Bryant D, Wang Z. The essential role of WD repeat domain 77 in prostate tumor initiation induced by Pten loss. *Oncogene* 2018;37:4151–63. <https://doi.org/10.1038/S41388-018-0254-8>.
- [428] Nicholas C, Yang J, Peters SB, Bill MA, Baiocchi RA, Yan F, et al. PRMT5 Is Upregulated in Malignant and Metastatic Melanoma and Regulates Expression of MITF and p27Kip1. *PLoS One* 2013;8:e74710. <https://doi.org/10.1371/JOURNAL.PONE.0074710>.
- [429] Suresh S, Vinet M, Dakroub R, Lesage L, Ye M, Fayyad-Kazan H, et al. Expression, Localization and Prognosis Association of MEP50 in Breast Cancer. *Cancers (Basel)* 2022;14. <https://doi.org/10.3390/cancers14194766>.
- [430] Vinet M, Suresh S, Maire V, Monchecourt C, Némati F, Lesage L, et al. Protein arginine methyltransferase 5: A novel therapeutic target for triple-negative breast cancers. *Cancer Med* 2019;8:2414–28. <https://doi.org/10.1002/cam4.2114>.
- [431] Börzsei R, Bayarsaikhan B, Zsidó BZ, Lontay B, Hetényi C. The Structural Effects of Phosphorylation of Protein Arginine Methyltransferase 5 on Its Binding to Histone H4. *Int J Mol Sci* 2022;23:11316. <https://doi.org/10.3390/IJMS231911316/S1>.
- [432] Hornbeck P V., Zhang B, Murray B, Kornhauser JM, Latham V, Skrzypek E. PhosphoSitePlus, 2014: mutations, PTMs and recalibrations. *Nucleic Acids Res* 2015;43:D512–20. <https://doi.org/10.1093/NAR/GKU1267>.
- [433] Lamond AI. The spliceosome. *Bioessays* 1993;15:595–603. <https://doi.org/10.1002/BIES.950150905>.

- [434] Matera AG, Wang Z. A day in the life of the spliceosome. *Nature Reviews Molecular Cell Biology* 2014 15:2 2014;15:108–21. <https://doi.org/10.1038/nrm3742>.
- [435] Will CL, Lührmann R. Spliceosome structure and function. *Cold Spring Harb Perspect Biol* 2011;3:1–2. <https://doi.org/10.1101/CSHPERSPECT.A003707>.
- [436] Chari A, Golas MM, Klingenhäger M, Neuenkirchen N, Sander B, Englbrecht C, et al. An assembly chaperone collaborates with the SMN complex to generate spliceosomal SnRNPs. *Cell* 2008;135:497–509. <https://doi.org/10.1016/J.CELL.2008.09.020>.
- [437] Meister G, Fischer U. Assisted RNP assembly: SMN and PRMT5 complexes cooperate in the formation of spliceosomal UsnRNPs. *EMBO J* 2002;21:5853–63. <https://doi.org/10.1093/EMBOJ/CDF585>.
- [438] Grimm C, Chari A, Pelz JP, Kuper J, Kisker C, Diederichs K, et al. Structural Basis of Assembly Chaperone-Mediated snRNP Formation. *Mol Cell* 2013;49:692–703. <https://doi.org/10.1016/j.molcel.2012.12.009>.
- [439] Tan DQ, Li Y, Yang C, Li J, Tan SH, Chin DWL, et al. PRMT5 Modulates Splicing for Genome Integrity and Preserves Proteostasis of Hematopoietic Stem Cells. *Cell Rep* 2019;26:2316–2328.e6. <https://doi.org/10.1016/J.CELREP.2019.02.001>.
- [440] Szewczyk MM, Luciani GM, Vu V, Murison A, Dilworth D, Barghout SH, et al. PRMT5 regulates ATF4 transcript splicing and oxidative stress response. *Redox Biol* 2022;51. <https://doi.org/10.1016/j.redox.2022.102282>.
- [441] Bezzi M, Teo SX, Muller J, Mok WC, Sahu SK, Vardy LA, et al. Regulation of constitutive and alternative splicing by PRMT5 reveals a role for Mdm4 pre-mRNA in sensing defects in the spliceosomal machinery. *Genes Dev* 2013;27:1903–16. <https://doi.org/10.1101/GAD.219899.113>.
- [442] Wang L, Pal S, Sif S. Protein arginine methyltransferase 5 suppresses the transcription of the RB family of tumor suppressors in leukemia and lymphoma cells. *Mol Cell Biol* 2008;28:6262–77. <https://doi.org/10.1128/MCB.00923-08>.
- [443] Harris DP, Bandyopadhyay S, Maxwell TJ, Willard B, DiCorleto PE. Tumor Necrosis Factor (TNF)- $\alpha$  Induction of CXCL10 in Endothelial Cells Requires Protein Arginine Methyltransferase 5 (PRMT5)-mediated Nuclear Factor (NF)- $\kappa$ B p65 Methylation. *J Biol Chem* 2014;289:15328. <https://doi.org/10.1074/JBC.M114.547349>.
- [444] Brobbey C, Liu L, Yin S, Gan W. The Role of Protein Arginine Methyltransferases in DNA Damage Response. *International Journal of Molecular Sciences* 2022, Vol 23, Page 9780 2022;23:9780. <https://doi.org/10.3390/IJMS23179780>.
- [445] Hamard PJ, Santiago GE, Liu F, Karl DL, Martinez C, Man N, et al. PRMT5 regulates DNA repair by controlling the alternative splicing of key histone-

- modifying enzymes. *Cell Rep* 2018;24:2643. <https://doi.org/10.1016/J.CELREP.2018.08.002>.
- [446] Sapir T, Shifteh D, Pahmer M, Goel S, Maitra R. Protein Arginine Methyltransferase 5 (PRMT5) and the ERK1/2 & PI3K Pathways: A Case for PRMT5 Inhibition and Combination Therapies in Cancer. *Mol Cancer Res* 2021;19:388. <https://doi.org/10.1158/1541-7786.MCR-20-0745>.
- [447] Ge L, Wang H, Xu X, Zhou Z, He J, Peng W, et al. PRMT5 promotes epithelial-mesenchymal transition via EGFR- $\beta$ -catenin axis in pancreatic cancer cells. *J Cell Mol Med* 2020;24:1969–79. <https://doi.org/10.1111/JCMM.14894>.
- [448] Yan Y, Zhao P, Wang Z, Liu Z, Wang Z, Zhang J, et al. PRMT5 regulates colorectal cancer cell growth and EMT via EGFR/Akt/GSK3 $\beta$  signaling cascades. *AGING* 2021;13:4468–81. <https://doi.org/10.18632/AGING.202407>.
- [449] Huang J, Zheng Y, Zheng X, Qian B, Yin Q, Lu J, et al. PRMT5 Promotes EMT Through Regulating Akt Activity in Human Lung Cancer. *Cell Transplant* 2021;30. <https://doi.org/10.1177/09636897211001772>.
- [450] Yang D, Liang T, Gu Y, Zhao Y, Shi Y, Zuo X, et al. Protein N-arginine methyltransferase 5 promotes the tumor progression and radioresistance of nasopharyngeal carcinoma. *Oncol Rep* 2016;35:1703–10. <https://doi.org/10.3892/OR.2015.4513>.
- [451] Zheng Y, Lu J, Hu X, Hu X, Gao X, Zhou J. PRMT5/FGFR3/AKT Signaling Axis Facilitates Lung Cancer Cell Metastasis. *Technol Cancer Res Treat* 2023;22:153303382311611. <https://doi.org/10.1177/15330338231161139>.
- [452] Jing P, Zhao N, Ye M, Zhang Y, Zhang Z, Sun J, et al. Protein arginine methyltransferase 5 promotes lung cancer metastasis via the epigenetic regulation of miR-99 family/FGFR3 signaling. *Cancer Lett* 2018;427:38–48. <https://doi.org/10.1016/J.CANLET.2018.04.019>.
- [453] Dhillon AS, Hagan S, Rath O, Kolch W. MAP kinase signalling pathways in cancer. *Oncogene* 2007;26:3279–90. <https://doi.org/10.1038/SJ.ONC.1210421>.
- [454] Kranenburg O. The KRAS oncogene: past, present, and future. *Biochim Biophys Acta* 2005;1756:81–2. <https://doi.org/10.1016/J.BBCAN.2005.10.001>.
- [455] Shifteh D, Sapir T, Pahmer M, Haimowitz A, Goel S, Maitra R. Protein Arginine Methyltransferase 5 as a Therapeutic Target for KRAS Mutated Colorectal Cancer. *Cancers (Basel)* 2020;12:1–17. <https://doi.org/10.3390/CANCERS12082091>.
- [456] Grigore F, Yang H, Hanson ND, VanBrocklin MW, Sarver AL, Robinson JP. BRAF inhibition in melanoma is associated with the dysregulation of histone methylation and histone methyltransferases. *Neoplasia* 2020;22:376. <https://doi.org/10.1016/J.NEO.2020.06.006>.
- [457] Jiang H, Zhu Y, Zhou Z, Xu J, Jin S, Xu K, et al. PRMT5 promotes cell proliferation by inhibiting BTG2 expression via the ERK signaling pathway in



hepatocellular carcinoma. *Cancer Med* 2018;7:869.  
<https://doi.org/10.1002/CAM4.1360>.

- [458] Liu L, Yan L, Liao N, Wu WQ, Shi JL. A Review of ULK1-Mediated Autophagy in Drug Resistance of Cancer. *Cancers* 2020, Vol 12, Page 352 2020;12:352. <https://doi.org/10.3390/CANCERS12020352>.
- [459] Schmitz K, Cox J, Esser LM, Voss M, Sander K, Löffler A, et al. An essential role of the autophagy activating kinase ULK1 in snRNP biogenesis. *Nucleic Acids Res* 2021;49:6437–55. <https://doi.org/10.1093/NAR/GKAB452>.
- [460] Esser LM, Schmitz K, Hillebrand F, Erkelenz S, Schaal H, Stork B, et al. Phosphorylation of pICln by the autophagy activating kinase ULK1 regulates snRNP biogenesis and splice activity of the cell. *Comput Struct Biotechnol J* 2023;21:2100–9. <https://doi.org/10.1016/J.CSBJ.2023.03.015>.
- [461] Fan J, Li H, Ruan Q, Zhu X, Jing P, Gu Z. The PRMT5 inhibitor C9 mitigates hypoxia-induced carboplatin resistance in lung cancer by inducing autophagy. *Cell Biol Int* 2023. <https://doi.org/10.1002/CBIN.12066>.
- [462] Kong J, Wang Z, Zhang Y, Wang T, Ling R. Protein Arginine Methyltransferases 5 (PRMT5) affect Multiple Stages of Autophagy and Modulate Autophagy-related Genes in Controlling Breast Cancer Tumorigenesis. *Curr Cancer Drug Targets* 2023;23:242–50. <https://doi.org/10.2174/1568009622666220922093059>.
- [463] Metz PJ, Ching KA, Xie T, Delgado Cuenca P, Niessen S, Tatlock JH, et al. Symmetric Arginine Dimethylation Is Selectively Required for mRNA Splicing and the Initiation of Type I and Type III Interferon Signaling. *Cell Rep* 2020;30:1935-1950.e8. <https://doi.org/10.1016/J.CELREP.2020.01.054>.
- [464] Webb LM, Amici SA, Jablonski KA, Savardekar H, Panfil AR, Li L, et al. PRMT5-Selective Inhibitors Suppress Inflammatory T Cell Responses and Experimental Autoimmune Encephalomyelitis. *J Immunol* 2017;198:1439–51. <https://doi.org/10.4049/JIMMUNOL.1601702>.
- [465] Webb LM, Sengupta S, Edell C, Piedra-Quintero ZL, Amici SA, Miranda JN, et al. Protein arginine methyltransferase 5 promotes cholesterol biosynthesis-mediated Th17 responses and autoimmunity. *J Clin Invest* 2020;130:1683–98. <https://doi.org/10.1172/JCI1131254>.
- [466] Webb LM, Miranda JN, Amici SA, Sengupta S, Nagy G, Guerau-De-Arellano M. NF-κB/mTOR/MYC Axis Drives PRMT5 Protein Induction after T Cell Activation via Transcriptional and Non-transcriptional Mechanisms. *Front Immunol* 2019;10. <https://doi.org/10.3389/FIMMU.2019.00524/FULL>.
- [467] Sengupta S, West KO, Sanghvi S, Laliotis G, Agosto LM, Lynch KW, et al. PRMT5 promotes symmetric dimethylation of RNA processing proteins and modulates activated T cell alternative splicing and Ca<sup>2+</sup>/NFAT signaling. *Immunohorizons* 2021;5:884. <https://doi.org/10.4049/IMMUNOHORIZONS.2100076>.

- [468] Chiang K, Zielinska AE, Shaaban AM, Sanchez-Bailon MP, Jarrold J, Clarke TL, et al. PRMT5 Is a Critical Regulator of Breast Cancer Stem Cell Function via Histone Methylation and FOXP1 Expression. *Cell Rep* 2017;21:3498–513. <https://doi.org/10.1016/j.celrep.2017.11.096>.
- [469] Wang Z, Kong J, Wu Y, Zhang J, Wang T, Li N, et al. PRMT5 determines the sensitivity to chemotherapeutics by governing stemness in breast cancer. *Breast Cancer Res Treat* 2018;168:531–42. <https://doi.org/10.1007/s10549-017-4597-6>.
- [470] Wu Y, Wang Z, Zhang J, Ling R. Elevated expression of protein arginine methyltransferase 5 predicts the poor prognosis of breast cancer. *Tumour Biol* 2017;39:1010428317695917. <https://doi.org/10.1177/1010428317695917>.
- [471] Poulard C, Pham TH, Drouet Y, Jacquemetton J, Surmielova A, Kassem L, et al. Nuclear PRMT5 is a biomarker of sensitivity to tamoxifen in ERα+ breast cancer. *EMBO Mol Med* 2023;15:e17248. <https://doi.org/10.15252/EMMM.202217248>.
- [472] Yang F, Wang J, Ren H yan, Jin J, Wang A lian, Sun L li, et al. Proliferative role of TRAF4 in breast cancer by upregulating PRMT5 nuclear expression. *Tumor Biology* 2015;36:5901–11. <https://doi.org/10.1007/S13277-015-3262-0/METRICS>.
- [473] Zhou Z, Feng Z, Hu D, Yang P, Gur M, Bahar I, et al. A novel small-molecule antagonizes PRMT5-mediated KLF4 methylation for targeted therapy. *EBioMedicine* 2019;44:98–111. <https://doi.org/10.1016/j.ebiom.2019.05.011>.
- [474] Kryukov G V., Wilson FH, Ruth JR, Paulk J, Tsherniak A, Marlow SE, et al. MTAP deletion confers enhanced dependency on the arginine methyltransferase PRMT5 in human cancer cells. *Science* 2016;351:1214. <https://doi.org/10.1126/SCIENCE.AAD5214>.
- [475] Smith CR, Aranda R, Bobinski TP, Briere DM, Burns AC, Christensen JG, et al. Fragment-Based Discovery of MRTX1719, a Synthetic Lethal Inhibitor of the PRMT5•MTA Complex for the Treatment of MTAP-Deleted Cancers. *J Med Chem* 2022;65:1749–66. [https://doi.org/10.1021/ACS.JMEDCHEM.1C01900/SUPPL\\_FILE/JM1C01900\\_SI\\_002.PDF](https://doi.org/10.1021/ACS.JMEDCHEM.1C01900/SUPPL_FILE/JM1C01900_SI_002.PDF).
- [476] Sachamitr P, Ho JC, Ciamponi FE, Ba-Alawi W, Coutinho FJ, Guilhamon P, et al. PRMT5 inhibition disrupts splicing and stemness in glioblastoma. *Nat Commun* 2021;12:979. <https://doi.org/10.1038/s41467-021-21204-5>.
- [477] Fu S, Zheng Q, Zhang D, Lin C, Ouyang L, Zhang J, et al. Medicinal chemistry strategies targeting PRMT5 for cancer therapy. *Eur J Med Chem* 2022;244. <https://doi.org/10.1016/J.EJMECH.2022.114842>.
- [478] Feustel K, Falchook GS. Protein Arginine Methyltransferase 5 (PRMT5) Inhibitors in Oncology Clinical Trials: A review. *J Immunother Precis Oncol* 2022;5:58–67. <https://doi.org/10.36401/jipo-22-1>.

- [479] Chan-Penebre E, Kuplast KG, Majer CR, Boriack-Sjodin PA, Wigle TJ, Johnston LD, et al. A selective inhibitor of PRMT5 with in vivo and in vitro potency in MCL models. *Nature Chemical Biology* 2015 11:6 2015;11:432–7. <https://doi.org/10.1038/nchembio.1810>.
- [480] Ye F, Zhang W, Ye X, Jin J, Lv Z, Luo C. Identification of Selective, Cell Active Inhibitors of Protein Arginine Methyltransferase 5 through Structure-Based Virtual Screening and Biological Assays. *J Chem Inf Model* 2018;58:1066–73. [https://doi.org/10.1021/ACS.JCIM.8B00050/SUPPL\\_FILE/C18B00050\\_SI\\_001.PDF](https://doi.org/10.1021/ACS.JCIM.8B00050/SUPPL_FILE/C18B00050_SI_001.PDF).
- [481] Brehmer D, Beke L, Wu T, Millar HJ, Moy C, Sun W, et al. Discovery and pharmacological characterization of JNJ-64619178, a novel small-molecule inhibitor of PRMT5 with potent antitumor activity. *Mol Cancer Ther* 2021;20:2317–28. <https://doi.org/10.1158/1535-7163.MCT-21-0367/665882/AM/DISCOVERY-AND-PHARMACOLOGICAL-CHARACTERIZATION-OF>.
- [482] Jensen-Pergakes K, Tatlock J, Maegley KA, McAlpine IJ, McTigue M, Xie T, et al. SAM-Competitive PRMT5 Inhibitor PF-06939999 Demonstrates Antitumor Activity in Splicing Dysregulated NSCLC with Decreased Liability of Drug Resistance. *Mol Cancer Ther* 2022;21:3–15. <https://doi.org/10.1158/1535-7163.MCT-21-0620>.
- [483] Wang Q, Xu J, Li Y, Huang J, Jiang Z, Wang Y, et al. Identification of a novel protein arginine methyltransferase 5 inhibitor in non-small cell lung cancer by structure-based virtual screening. *Front Pharmacol* 2018;9:325810. <https://doi.org/10.3389/FPHAR.2018.00173/BIBTEX>.
- [484] Bonday ZQ, Cortez GS, Grogan MJ, Antonysamy S, Weichert K, Bocchinfuso WP, et al. LLY-283, a Potent and Selective Inhibitor of Arginine Methyltransferase 5, PRMT5, with Antitumor Activity. *ACS Med Chem Lett* 2018;9:612–7. [https://doi.org/10.1021/ACSMEDCHEMLETT.8B00014/SUPPL\\_FILE/ML8B00014\\_SI\\_001.PDF](https://doi.org/10.1021/ACSMEDCHEMLETT.8B00014/SUPPL_FILE/ML8B00014_SI_001.PDF).
- [485] Briggs K, Cottrell K, Tsai A, Zhang M, Tonini M, Yoda S, et al. TNG908 is a brain-penetrant, MTA-cooperative PRMT5 inhibitor for the treatment of MTAP-deleted cancer. *Eur J Cancer* 2022;174:S84. [https://doi.org/10.1016/S0959-8049\(22\)01021-8](https://doi.org/10.1016/S0959-8049(22)01021-8).
- [486] Secker KA, Keppeler H, Duerr-Stoerzer S, Schmid H, Schneidawind D, Hentrich T, et al. Inhibition of DOT1L and PRMT5 promote synergistic anti-tumor activity in a human MLL leukemia model induced by CRISPR/Cas9. *Oncogene* 2019;38:7181–95. <https://doi.org/10.1038/S41388-019-0937-9>.
- [487] Hu R, Zhou B, Chen Z, Chen S, Chen N, Shen L, et al. PRMT5 Inhibition Promotes PD-L1 Expression and Immuno-Resistance in Lung Cancer. *Front Immunol* 2021;12:722188. <https://doi.org/10.3389/fimmu.2021.722188>.

- [488] Che Y, Liu Y, Yao Y, Hill HA, Li Y, Cai Q, et al. Exploiting PRMT5 as a target for combination therapy in mantle cell lymphoma characterized by frequent ATM and TP53 mutations. *Blood Cancer J* 2023;13:27. <https://doi.org/10.1038/s41408-023-00799-6>.
- [489] AbuHammad S, Cullinane C, Martin C, Bacolas Z, Ward T, Chen H, et al. Regulation of PRMT5-MDM4 axis is critical in the response to CDK4/6 inhibitors in melanoma. *Proc Natl Acad Sci U S A* 2019;116:17990–8000. <https://doi.org/10.1073/pnas.1901323116>.
- [490] Yang L, Ma DW, Cao YP, Li DZ, Zhou X, Feng JF, et al. PRMT5 functionally associates with EZH2 to promote colorectal cancer progression through epigenetically repressing CDKN2B expression. *Theranostics* 2021;11:3742–59. <https://doi.org/10.7150/thno.53023>.
- [491] Holmes B, Benavides-Serrato A, Saunders JT, Landon KA, Schreck AJ, Nishimura RN, et al. The protein arginine methyltransferase PRMT5 confers therapeutic resistance to mTOR inhibition in glioblastoma. *J Neurooncol* 2019;145:11–22. <https://doi.org/10.1007/s11060-019-03274-0>.
- [492] Hong E, Barczak W, Park S, Heo JS, Ooshima A, Munro S, et al. Combination treatment of T1-44, a PRMT5 inhibitor with Vactosertib, an inhibitor of TGF- $\beta$  signaling, inhibits invasion and prolongs survival in a mouse model of pancreatic tumors. *Cell Death Dis* 2023;14:93. <https://doi.org/10.1038/s41419-023-05630-5>.
- [493] O'Brien S, Butticello M, Thompson C, Wilson B, Wyce A, Mahajan V, et al. Inhibiting PRMT5 induces DNA damage and increases anti-proliferative activity of Niraparib, a PARP inhibitor, in models of breast and ovarian cancer. *BMC Cancer* 2023;23:775. <https://doi.org/10.1186/S12885-023-11260-Z>.
- [494] Mueller HS, Fowler CE, Dalin S, Moiso E, Udomlumleart T, Garg S, et al. Acquired resistance to PRMT5 inhibition induces concomitant collateral sensitivity to paclitaxel. *Proc Natl Acad Sci U S A* 2021;118. <https://doi.org/10.1073/pnas.2024055118>.
- [495] Avigan MI, Strober B, Levens D. A far upstream element stimulates c-myc expression in undifferentiated leukemia cells. *Journal of Biological Chemistry* 1990;265:18538–45. [https://doi.org/10.1016/s0021-9258\(17\)44785-5](https://doi.org/10.1016/s0021-9258(17)44785-5).
- [496] Duncan R, Bazar L, Michelotti G, Tomonaga T, Krutzsch H, Avigan M, et al. A sequence-specific, single-strand binding protein activates the far upstream element of c-myc and defines a new DNA-binding motif. *Genes Dev* 1994;8:465–80. <https://doi.org/10.1101/gad.8.4.465>.
- [497] Davis-Smyth T, Duncan RC, Zheng T, Michelotti G, Levens D. The far upstream element-binding proteins comprise an ancient family of single-strand DNA-binding transactivators. *J Biol Chem* 1996;271:31679–87. <https://doi.org/10.1074/JBC.271.49.31679>.

- [498] Zhang J, Chen QM. Far upstream element binding protein 1: A commander of transcription, translation and beyond. *Oncogene* 2013;32:2907–16. <https://doi.org/10.1038/ONC.2012.350>.
- [499] Debaize L, Troadec MB. The master regulator FUBP1: its emerging role in normal cell function and malignant development. *Cellular and Molecular Life Sciences* 2019;76:259–81. <https://doi.org/10.1007/S00018-018-2933-6>.
- [500] Briata P, Bordo D, Puppo M, Gorlero F, Rossi M, Perrone-Bizzozero N, et al. Diverse roles of the nucleic acid-binding protein KHSRP in cell differentiation and disease. *Wiley Interdiscip Rev RNA* 2016;7:227–40. <https://doi.org/10.1002/wrna.1327>.
- [501] Rappsilber J, Ryder U, Lamond AI, Mann M. Large-scale proteomic analysis of the human spliceosome. *Genome Res* 2002;12:1231–45. <https://doi.org/10.1101/GR.473902>.
- [502] He L, Weber A, Levens D. Nuclear targeting determinants of the far upstream element binding protein, a c-myc transcription factor. *Nucleic Acids Res* 2000;28:4558–65. <https://doi.org/10.1093/NAR/28.22.4558>.
- [503] Jang M, Park BC, Kang S, Chi SW, Cho S, Chung SJ, et al. Far upstream element-binding protein-1, a novel caspase substrate, acts as a cross-talker between apoptosis and the c-myc oncogene. *Oncogene* 2009;28:1529–36. <https://doi.org/10.1038/ONC.2009.11>.
- [504] Huang PN, Lin JY, Locker N, Kung YA, Hung CT, Lin JY, et al. Far upstream element binding protein 1 binds the internal ribosomal entry site of enterovirus 71 and enhances viral translation and viral growth. *Nucleic Acids Res* 2011;39:9633–48. <https://doi.org/10.1093/NAR/GKR682>.
- [505] Chien H-L, Liao C-L, Lin Y-L. FUSE Binding Protein 1 Interacts with Untranslated Regions of Japanese Encephalitis Virus RNA and Negatively Regulates Viral Replication. *J Virol* 2011;85:4698–706. <https://doi.org/10.1128/JVI.01950-10>.
- [506] Han SK, Seong WK, Sriram SR, Dawson VL, Dawson TM. Identification of far upstream element-binding protein-1 as an authentic Parkin substrate. *Journal of Biological Chemistry* 2006;281:16193–6. <https://doi.org/10.1074/JBC.C600041200>.
- [507] Kim MJ, Park BJ, Kang YS, Kim HJ, Park JH, Kang JW, et al. Downregulation of FUSE-binding protein and c-myc by tRNA synthetase cofactor p38 is required for lung cell differentiation. *Nat Genet* 2003;34:330–6. <https://doi.org/10.1038/NG1182>.
- [508] Ma J, Chen M, Xia SK, Shu W, Guo Y, Wang YH, et al. Prostaglandin E2 promotes liver cancer cell growth by the upregulation of FUSE-binding protein 1 expression. *Int J Oncol* 2013;42:1093–104. <https://doi.org/10.3892/ijo.2013.1782>.

- [509] Kim DG, Lee JY, Lee JH, Cho HY, Kang BS, Jang SY, et al. Oncogenic mutation of AIMP2/p38 inhibits its tumor-suppressive interaction with Smurf2. *Cancer Res* 2016;76:3422–36. <https://doi.org/10.1158/0008-5472.CAN-15-3255>.
- [510] Yin H, Gao T, Xie J, Huang Z, Zhang X, Yang F, et al. FUBP1 promotes colorectal cancer stemness and metastasis via DVL1-mediated activation of Wnt/ $\beta$ -catenin signaling. *Mol Oncol* 2021;15:3490–512. <https://doi.org/10.1002/1878-0261.13064>.
- [511] Atanassov BS, Dent SYR. USP22 regulates cell proliferation by deubiquitinating the transcriptional regulator FBP1. *EMBO Rep* 2011;12:924–30. <https://doi.org/10.1038/EMBOR.2011.140>.
- [512] Kung YA, Hung CT, Chien KY, Shih SR. Control of the negative IRES trans-acting factor KHSRP by ubiquitination. *Nucleic Acids Res* 2017;45:271. <https://doi.org/10.1093/NAR/GKW1042>.
- [513] Amanchy R, Zhong J, Molina H, Chaerkady R, Iwahori A, Kalume DE, et al. Identification of c-Src tyrosine kinase substrates using mass spectrometry and peptide microarrays. *J Proteome Res* 2008;7:3900–10. <https://doi.org/10.1021/PR800198W>.
- [514] Wang H, Zhang R, Li E, Yan R, Ma B, Ma Q. Pan-Cancer Transcriptome and Immune Infiltration Analyses Reveal the Oncogenic Role of Far Upstream Element-Binding Protein 1 (FUBP1). *Front Mol Biosci* 2022;9. <https://doi.org/10.3389/FMOLB.2022.794715>.
- [515] Briata P, Forcales SV, Ponassi M, Corte G, Chen CY, Karin M, et al. p38-dependent phosphorylation of the mRNA decay-promoting factor KSRP controls the stability of select myogenic transcripts. *Mol Cell* 2005;20:891–903. <https://doi.org/10.1016/J.MOLCEL.2005.10.021>.
- [516] Gherzi R, Trabucchi M, Ponassi M, Ruggiero T, Corte G, Moroni C, et al. The RNA-binding protein KSRP promotes decay of beta-catenin mRNA and is inactivated by PI3K-AKT signaling. *PLoS Biol* 2006;5:0082–95. <https://doi.org/10.1371/JOURNAL.PBIO.0050005>.
- [517] Gherzi R, Trabucchi M, Ponassi M, Ruggiero T, Corte G, Moroni C, et al. Retraction: The RNA-Binding Protein KSRP Promotes Decay of  $\beta$ -Catenin mRNA and Is Inactivated by PI3K-AKT Signaling. *PLoS Biol* 2015;13. <https://doi.org/10.1371/JOURNAL.PBIO.1002314>.
- [518] Díaz-Moreno I, Hollingworth D, Frenkiel TA, Kelly G, Martin S, Howell S, et al. Phosphorylation-mediated unfolding of a KH domain regulates KSRP localization via 14-3-3 binding. *Nat Struct Mol Biol* 2009;16:238–46. <https://doi.org/10.1038/NSMB.1558>.
- [519] Ruggiero T, Trabucchi M, Ponassi M, Corte G, Chen CY, al-Haj L, et al. Identification of a set of KSRP target transcripts upregulated by PI3K-AKT signaling. *BMC Mol Biol* 2007;8:28. <https://doi.org/10.1186/1471-2199-8-28>.

- [520] Wang YY, Gu XL, Wang C, Wang H, Ni QC, Zhang CH, et al. The far-upstream element-binding protein 2 is correlated with proliferation and doxorubicin resistance in human breast cancer cell lines. *Tumour Biol* 2016;37:9755–69. <https://doi.org/10.1007/S13277-016-4819-2>.
- [521] Briata P, Lin WJ, Giovarelli M, Pasero M, Chou CF, Trabucchi M, et al. PI3K/AKT signaling determines a dynamic switch between distinct KSRP functions favoring skeletal myogenesis. *Cell Death Differ* 2012;19:478–87. <https://doi.org/10.1038/CDD.2011.117>.
- [522] Chen H, Zhao L, Meng Y, Qian X, Fan Y, Zhang Q, et al. Sulfonylurea receptor 1-expressing cancer cells induce cancer-associated fibroblasts to promote non-small cell lung cancer progression. *Cancer Lett* 2022;536. <https://doi.org/10.1016/J.CANLET.2022.215611>.
- [523] Zhang X, Wan G, Berger FG, He X, Lu X. The ATM kinase induces microRNA biogenesis in the DNA damage response. *Mol Cell* 2011;41:371–83. <https://doi.org/10.1016/J.MOLCEL.2011.01.020>.
- [524] Murray RD, Merchant ML, Hardin E, Clark B, Khundmiri SJ, Lederer ED. Identification of an RNA-binding protein that is phosphorylated by PTH and potentially mediates PTH-induced destabilization of Npt2a mRNA. *Am J Physiol Cell Physiol* 2016;310:C205–15. <https://doi.org/10.1152/AJPCELL.00192.2015>.
- [525] Tang B, Lee HO, Gupta S, Wang L, Kurimchak AM, Duncan JS, et al. Extracellular 5'-methylthioadenosine inhibits intracellular symmetric dimethylarginine protein methylation of FUSE-binding proteins. *Journal of Biological Chemistry* 2022;298. <https://doi.org/10.1016/J.JBC.2022.102367>.
- [526] Tadesse H, Deschênes-Furry J, Boisvenue S, Côté J. KH-type splicing regulatory protein interacts with survival motor neuron protein and is misregulated in spinal muscular atrophy. *Hum Mol Genet* 2008;17:506–24. <https://doi.org/10.1093/HMG/DDM327>.
- [527] Papanikolaou NA, Nikolaidis M, Amoutzias GD, Fouza A, Papaioannou M, Pandey A, et al. The Dynamic and Crucial Role of the Arginine Methylproteome in Myoblast Cell Differentiation. *Int J Mol Sci* 2023;24. <https://doi.org/10.3390/IJMS24032124>.
- [528] Elman JS, Ni TK, Mengwasser KE, Jin D, Wronski A, Elledge SJ, et al. Identification of FUBP1 as a Long Tail Cancer Driver and Widespread Regulator of Tumor Suppressor and Oncogene Alternative Splicing. *Cell Rep* 2019;28:3435-3449.e5. <https://doi.org/10.1016/J.CELREP.2019.08.060>.
- [529] Hwang I, Cao D, Na Y, Kim DY, Zhang T, Yao J, et al. Far Upstream Element-Binding Protein 1 Regulates LSD1 Alternative Splicing to Promote Terminal Differentiation of Neural Progenitors. *Stem Cell Reports* 2018;10:1208–21. <https://doi.org/10.1016/J.STEMCR.2018.02.013>.

- [530] Liu J, He L, Collins I, Ge H, Libutti D, Li J, et al. The FBP interacting repressor targets TFIIH to inhibit activated transcription. *Mol Cell* 2000;5:331–41. [https://doi.org/10.1016/S1097-2765\(00\)80428-1](https://doi.org/10.1016/S1097-2765(00)80428-1).
- [531] Chung H-J, Liu J, Dundr M, Nie Z, Sanford S, Levens D. FBPs Are Calibrated Molecular Tools To Adjust Gene Expression. *Mol Cell Biol* 2006;26:6584–97. <https://doi.org/10.1128/MCB.00754-06>.
- [532] Liu J, Akoulitchev S, Weber A, Ge H, Chuikov S, Libutti D, et al. Defective interplay of activators and repressors with TFIIH in xeroderma pigmentosum. *Cell* 2001;104:353–63. [https://doi.org/10.1016/S0092-8674\(01\)00223-9](https://doi.org/10.1016/S0092-8674(01)00223-9).
- [533] Liu J, Chung HJ, Vogt M, Jin Y, Malide D, He L, et al. JTV1 co-activates FBP to induce USP29 transcription and stabilize p53 in response to oxidative stress. *EMBO Journal* 2011;30:846–58. <https://doi.org/10.1038/EMBOJ.2011.11>.
- [534] Dixit U, Liu Z, Pandey AK, Kothari R, Pandey VN. Fuse binding protein antagonizes the transcription activity of tumor suppressor protein p53. *BMC Cancer* 2014;14. <https://doi.org/10.1186/1471-2407-14-925>.
- [535] Debaize L, Jakobczyk H, Avner S, Gaudichon J, Rio AG, Sérandour AA, et al. Interplay between transcription regulators RUNX1 and FUBP1 activates an enhancer of the oncogene c-KIT and amplifies cell proliferation. *Nucleic Acids Res* 2018;46:11214–28. <https://doi.org/10.1093/NAR/GKY756>.
- [536] Zheng W, Shen F, Hu R, Roy B, Yang J, Wang Q, et al. Far upstream element-binding protein 1 binds the 39 untranslated region of PKD2 and suppresses its translation. *Journal of the American Society of Nephrology* 2016;27:2645–57. <https://doi.org/10.1681/ASN.2015070836>.
- [537] Zgorzynska E, Dzedzic B, Walczewska A. An Overview of the Nrf2/ARE Pathway and Its Role in Neurodegenerative Diseases. *International Journal of Molecular Sciences* 2021, Vol 22, Page 9592 2021;22:9592. <https://doi.org/10.3390/IJMS22179592>.
- [538] Duncan R, Collins I, Tomonaga T, Zhang T, Levens D. A unique transactivation sequence motif is found in the carboxyl-terminal domain of the single-strand-binding protein FBP. *Mol Cell Biol* 1996;16:2274–82. <https://doi.org/10.1128/MCB.16.5.2274>.
- [539] Valverde R, Edwards L, Regan L. Structure and function of KH domains. *FEBS J* 2008;275:2712–26. <https://doi.org/10.1111/J.1742-4658.2008.06411.X>.
- [540] Hollingworth D, Candel AM, Nicastro G, Martin SR, Briata P, Gherzi R, et al. KH domains with impaired nucleic acid binding as a tool for functional analysis. *Nucleic Acids Res* 2012;40:6873. <https://doi.org/10.1093/NAR/GKS368>.
- [541] Braddock DT, Louis JM, Baber JL, Levens D, Clore GM. Structure and dynamics of KH domains from FBP bound to single-stranded DNA. *Nature* 2002;415:1051–6. <https://doi.org/10.1038/4151051A>.



- [542] Benjamin LR, Chung HJ, Sanford S, Kouzine F, Liu J, Levens D. Hierarchical mechanisms build the DNA-binding specificity of FUSE binding protein. *Proc Natl Acad Sci U S A* 2008;105:18296–301. <https://doi.org/10.1073/PNAS.0803279105>.
- [543] Ni X, Knapp S, Chaikuad A. Comparative structural analyses and nucleotide-binding characterization of the four KH domains of FUBP1. *Sci Rep* 2020;10. <https://doi.org/10.1038/S41598-020-69832-Z>.
- [544] Rabenhorst U, Beinoraviciute-Kellner R, Brezniceanu ML, Joos S, Devens F, Lichter P, et al. Overexpression of the far upstream element binding protein 1 in hepatocellular carcinoma is required for tumor growth. *Hepatology* 2009;50:1121–9. <https://doi.org/10.1002/HEP.23098>.
- [545] Kang M, Lee SM, Kim W, Lee KH, Kim DY. Fubp1 supports the lactate-Akt-mTOR axis through the upregulation of Hk1 and Hk2. *Biochem Biophys Res Commun* 2019;512:93–9. <https://doi.org/10.1016/J.BBRC.2019.03.005>.
- [546] Kang M, Kim HJ, Kim TJ, Byun JS, Lee JH, Lee DH, et al. Multiple Functions of Fubp1 in Cell Cycle Progression and Cell Survival. *Cells* 2020;9. <https://doi.org/10.3390/CELLS9061347>.
- [547] Bazar L, Meighen D, Harris V, Duncan R, Levens D, Avigan M. Targeted melting and binding of a DNA regulatory element by a transactivator of c-myc. *J Biol Chem* 1995;270:8241–8. <https://doi.org/10.1074/JBC.270.14.8241>.
- [548] He L, Liu J, Collins I, Sanford S, O'Connell B, Benham CJ, et al. Loss of FBP function arrests cellular proliferation and extinguishes c-myc expression. *EMBO Journal* 2000;19:1034–44. <https://doi.org/10.1093/EMBOJ/19.5.1034>.
- [549] Zheng Y, Dubois W, Benham C, Batchelor E, Levens D. FUBP1 and FUBP2 enforce distinct epigenetic setpoints for MYC expression in primary single murine cells. *Commun Biol* 2020;3. <https://doi.org/10.1038/S42003-020-01264-X>.
- [550] Llombart V, Mansour MR. Therapeutic targeting of “undruggable” MYC. *EBioMedicine* 2022;75. <https://doi.org/10.1016/J.EBIOM.2021.103756>.
- [551] Das SK, Lewis BA, Levens D. MYC: a complex problem. *Trends Cell Biol* 2023;33:235–46. <https://doi.org/10.1016/J.TCB.2022.07.006>.
- [552] Liu J, Kouzine F, Nie Z, Chung HJ, Elisha-Feil Z, Weber A, et al. The FUSE/FBP/FIR/TFIIH system is a molecular machine programming a pulse of c-myc expression. *EMBO J* 2006;25:2119. <https://doi.org/10.1038/SJ.EMBOJ.7601101>.
- [553] Compe E, Egly JM. TFIIH: when transcription met DNA repair. *Nat Rev Mol Cell Biol* 2012;13:343–54. <https://doi.org/10.1038/NRM3350>.
- [554] Felsher DW, Bishop JM. Transient excess of MYC activity can elicit genomic instability and tumorigenesis. *Proc Natl Acad Sci U S A* 1999;96:3940–4.

<https://doi.org/10.1073/PNAS.96.7.3940/ASSET/B281D973-9DCB-4720-B3CF-A50F7DC927CF/ASSETS/GRAPHIC/PQ0690316004.JPEG>.

- [555] Crichlow G V., Zhou H, Hsiao HH, Frederick KB, Debrosse M, Yang Y, et al. Dimerization of FIR upon FUSE DNA binding suggests a mechanism of c-myc inhibition. *EMBO Journal* 2008;27:277–89. <https://doi.org/10.1038/SJ.EMBOJ.7601936>.
- [556] Gagliardi D, Pagliari E, Meneri M, Melzi V, Rizzo F, Comi G Pietro, et al. Stathmins and Motor Neuron Diseases: Pathophysiology and Therapeutic Targets. *Biomedicines* 2022, Vol 10, Page 711 2022;10:711. <https://doi.org/10.3390/BIOMEDICINES10030711>.
- [557] Singer S, Malz M, Herpel E, Warth A, Bissinger M, Keith M, et al. Coordinated expression of stathmin family members by far upstream sequence element-binding protein-1 increases motility in non-small cell lung cancer. *Cancer Res* 2009;69:2234–43. <https://doi.org/10.1158/0008-5472.CAN-08-3338/654749/P/COORDINATED-EXPRESSION-OF-STATHMIN-FAMILY-MEMBERS>.
- [558] Tsai M, Valent P, Galli SJ. KIT as a master regulator of the mast cell lineage. *J Allergy Clin Immunol* 2022;149:1845–54. <https://doi.org/10.1016/J.JACI.2022.04.012>.
- [559] Fan P, Ma J, Jin X. Far upstream element-binding protein 1 is up-regulated in pancreatic cancer and modulates immune response by increasing programmed death ligand 1. *Biochem Biophys Res Commun* 2018;505:830–6. <https://doi.org/10.1016/J.BBRC.2018.10.009>.
- [560] Li H, Wang Z, Zhou X, Cheng Y, Xie Z, Manley JL, et al. Far upstream element-binding protein 1 and rna secondary structure both mediate second-step splicing repression. *Proc Natl Acad Sci U S A* 2013;110. <https://doi.org/10.1073/PNAS.1310607110>.
- [561] Wang J, Schultz PG, Johnson KA. Mechanistic studies of a small-molecule modulator of SMN2 splicing. *Proc Natl Acad Sci U S A* 2018;115:E4604–12. <https://doi.org/10.1073/PNAS.1800260115>.
- [562] Hou H, Sun D, Zhang X. The role of MDM2 amplification and overexpression in therapeutic resistance of malignant tumors. *Cancer Cell Int* 2019;19. <https://doi.org/10.1186/S12935-019-0937-4>.
- [563] Jacob AG, Singh RK, Mohammad F, Bebee TW, Chandler DS. The splicing factor FUBP1 is required for the efficient splicing of oncogene MDM2 pre-mRNA. *Journal of Biological Chemistry* 2014;289:17350–64. <https://doi.org/10.1074/JBC.M114.554717>.
- [564] Jacob AG, Singh RK, Comiskey DF, Rouhier MF, Mohammad F, Bebee TW, et al. Stress-Induced Alternative Splice Forms of MDM2 and MDMX Modulate the p53-Pathway in Distinct Ways. *PLoS One* 2014;9:e104444. <https://doi.org/10.1371/JOURNAL.PONE.0104444>.

- [565] Miro J, Laaref AM, Rofidal V, Lagrafeuille R, Hem S, Thorel D, et al. FUBP1: A new protagonist in splicing regulation of the DMD gene. *Nucleic Acids Res* 2015;43:2378–89. <https://doi.org/10.1093/NAR/GKV086>.
- [566] Olanich ME, Moss BL, Piwnica-Worms D, Townsend RR, Weber JD. Identification of FUSE-binding protein 1 as a regulatory mRNA-binding protein that represses nucleophosmin translation. *Oncogene* 2011;30:77–86. <https://doi.org/10.1038/ONC.2010.404>.
- [567] Abbastabar M, Kheyrollah M, Azizian K, Bagherlou N, Tehrani SS, Maniati M, et al. Multiple functions of p27 in cell cycle, apoptosis, epigenetic modification and transcriptional regulation for the control of cell growth: A double-edged sword protein. *DNA Repair (Amst)* 2018;69:63–72. <https://doi.org/10.1016/J.DNAREP.2018.07.008>.
- [568] Zheng Y, Miskimins WK. Far upstream element binding protein 1 activates translation of p27 Kip1 mRNA through its internal ribosomal entry site. *International Journal of Biochemistry and Cell Biology* 2011;43:1641–8. <https://doi.org/10.1016/J.BIOCEL.2011.08.001>.
- [569] Dai W, Qu H, Zhang J, Thongkum A, Dinh TN, Kappeler K V., et al. Far Upstream Binding Protein 1 (FUBP1) participates in translational regulation of Nrf2 protein under oxidative stress. *Redox Biol* 2021;41. <https://doi.org/10.1016/J.REDOX.2021.101906>.
- [570] Komotar RJ, Starke RM, Sisti MB, Connolly E. CIC and FUBP1 mutations in oligodendroglioma. *Neurosurgery* 2012;70. <https://doi.org/10.1227/01.NEU.0000414948.56225.36>.
- [571] Bettgowda C, Agrawal N, Jiao Y, Sausen M, Wood LD, Hruban RH, et al. Mutations in CIC and FUBP1 contribute to human oligodendroglioma. *Science (1979)* 2011;333:1453–5. <https://doi.org/10.1126/SCIENCE.1210557>.
- [572] Sahm F, Koelsche C, Meyer J, Pusch S, Lindenberg K, Mueller W, et al. CIC and FUBP1 mutations in oligodendrogliomas, oligoastrocytomas and astrocytomas. *Acta Neuropathol* 2012;123:853–60. <https://doi.org/10.1007/S00401-012-0993-5>.
- [573] Chan AKY, Pang JCS, Chung NYF, Li KKW, Poon WS, Chan DTM, et al. Loss of CIC and FUBP1 expressions are potential markers of shorter time to recurrence in oligodendroglial tumors. *Modern Pathology* 2014;27:332–42. <https://doi.org/10.1038/MODPATHOL.2013.165>.
- [574] Seiler M, Peng S, Agrawal AA, Palacino J, Teng T, Zhu P, et al. Somatic Mutational Landscape of Splicing Factor Genes and Their Functional Consequences across 33 Cancer Types. *Cell Rep* 2018;23:282-296.e4. <https://doi.org/10.1016/J.CELREP.2018.01.088>.
- [575] Müller B, Bovet M, Yin Y, Stichel D, Malz M, González-Vallinas M, et al. Concomitant expression of far upstream element (FUSE) binding protein (FBP) interacting repressor (FIR) and its splice variants induce migration and invasion

- of non-small cell lung cancer (NSCLC) cells. *Journal of Pathology* 2015;237:390–401. <https://doi.org/10.1002/path.4588>.
- [576] Jia MY, Wang YJ. Far upstream element-binding protein 1(FUBP1) expression differs between human colorectal cancer and non-cancerous tissue. *Neoplasma* 2014;61:533–9. [https://doi.org/10.4149/NEO\\_2014\\_065](https://doi.org/10.4149/NEO_2014_065).
- [577] Zubaidah RM, Gek ST, Tan SBE, Seng GL, Lin Q, Chung MCM. 2-D DIGE profiling of hepatocellular carcinoma tissues identified isoforms of far upstream binding protein (FUBP) as novel candidates in liver carcinogenesis. *Proteomics* 2008;8:5086–96. <https://doi.org/10.1002/PMIC.200800322>.
- [578] Hoang VT, Verma D, Godavarthy PS, Llavona P, Steiner M, Gerlach K, et al. The transcriptional regulator FUBP1 influences disease outcome in murine and human myeloid leukemia. *Leukemia* 2019;33:1700–12. <https://doi.org/10.1038/S41375-018-0358-8>.
- [579] Steiner M, Schneider L, Yillah J, Gerlach K, Kuvardina ON, Meyer A, et al. FUSE binding protein 1 (FUBP1) expression is upregulated by T-cell acute lymphocytic leukemia protein 1 (TAL1) and required for efficient erythroid differentiation. *PLoS One* 2019;14. <https://doi.org/10.1371/JOURNAL.PONE.0210515>.
- [580] Hoang VT, Gerlach K, Kuller-Müller U, Weissenberger E, Krause D, Zörnig M. FUBP1 promotes leukemia progression by regulation of cell cycle and apoptosis. *Exp Hematol* 2017;53:S98. <https://doi.org/10.1016/j.exphem.2017.06.234>.
- [581] Venturutti L, Cordo Russo RI, Rivas MA, Mercogliano MF, Izzo F, Oakley RH, et al. MiR-16 mediates trastuzumab and lapatinib response in ErbB-2-positive breast and gastric cancer via its novel targets CCNJ and FUBP1. *Oncogene* 2016;35:6189–202. <https://doi.org/10.1038/ONC.2016.151>.
- [582] Wang X, Xing L, Yang R, Chen H, Wang M, Jiang R, et al. The circACTN4 interacts with FUBP1 to promote tumorigenesis and progression of breast cancer by regulating the expression of proto-oncogene MYC. *Mol Cancer* 2021;20. <https://doi.org/10.1186/S12943-021-01383-X>.
- [583] Liu W, Xiong X, Chen W, Li X, Hua X, Liu Z, et al. High expression of FUSE binding protein 1 in breast cancer stimulates cell proliferation and diminishes drug sensitivity. *Int J Oncol* 2020;57:488–99. <https://doi.org/10.3892/ijo.2020.5080>.
- [584] Denkert C, Liedtke C, Tutt A, von Minckwitz G. Molecular alterations in triple-negative breast cancer—the road to new treatment strategies. *The Lancet* 2017;389:2430–42. [https://doi.org/10.1016/S0140-6736\(16\)32454-0](https://doi.org/10.1016/S0140-6736(16)32454-0).
- [585] Popović M, Silovski T, Križić M, Dedić Plavetić N. HER2 Low Breast Cancer: A New Subtype or a Trojan for Cytotoxic Drug Delivery? *Int J Mol Sci* 2023;24. <https://doi.org/10.3390/IJMS24098206>.

- [586] Park SY, Choi JH, Nam JS. Targeting Cancer Stem Cells in Triple-Negative Breast Cancer. *Cancers (Basel)* 2019;11. <https://doi.org/10.3390/cancers11070965>.
- [587] Kumar H, Gupta N V, Jain R, Madhunapantula S V, Babu CS, Kesharwani SS, et al. A review of biological targets and therapeutic approaches in the management of triple-negative breast cancer. *J Adv Res* 2023. <https://doi.org/10.1016/j.jare.2023.02.005>.
- [588] Lee J. Current Treatment Landscape for Early Triple-Negative Breast Cancer (TNBC). *Journal of Clinical Medicine* 2023, Vol 12, Page 1524 2023;12:1524. <https://doi.org/10.3390/JCM12041524>.
- [589] Denduluri N, Somerfield MR, Eisen A, Holloway JN, Hurria A, King TA, et al. Selection of Optimal Adjuvant Chemotherapy Regimens for Human Epidermal Growth Factor Receptor 2 (HER2) -Negative and Adjuvant Targeted Therapy for HER2-Positive Breast Cancers: An American Society of Clinical Oncology Guideline Adaptation of the Cancer Care Ontario Clinical Practice Guideline. *J Clin Oncol* 2016;34:2416–27. <https://doi.org/10.1200/JCO.2016.67.0182>.
- [590] Tarantino P, Corti C, Schmid P, Cortes J, Mittendorf EA, Rugo H, et al. Immunotherapy for early triple negative breast cancer: research agenda for the next decade. *NPJ Breast Cancer* 2022;8:23. <https://doi.org/10.1038/s41523-022-00386-1>.
- [591] Jeong JH, Kim SB. Antibody-drug conjugates targeting Trop-2: Clinical developments in early breast cancer therapy. *Breast* 2022;66:199–203. <https://doi.org/10.1016/j.breast.2022.10.015>.
- [592] You KS, Yi YW, Cho J, Park JS, Seong YS. Potentiating Therapeutic Effects of Epidermal Growth Factor Receptor Inhibition in Triple-Negative Breast Cancer. *Pharmaceuticals (Basel)* 2021;14. <https://doi.org/10.3390/ph14060589>.
- [593] Jarrold J, Davies CC. PRMTs and Arginine Methylation: Cancer's Best-Kept Secret? *Trends Mol Med* 2019;25:993–1009. <https://doi.org/10.1016/j.molmed.2019.05.007>.
- [594] Yang Y, Bedford MT. Protein arginine methyltransferases and cancer. *Nat Rev Cancer* 2013;13:37–50. <https://doi.org/10.1038/nrc3409>.
- [595] Guccione E, Schwarz M, Di Tullio F, Mzoughi S. Cancer synthetic vulnerabilities to protein arginine methyltransferase inhibitors. *Curr Opin Pharmacol* 2021;59:33–42. <https://doi.org/10.1016/j.coph.2021.04.004>.
- [596] Tang PA, Tsao MS, Moore MJ. A review of erlotinib and its clinical use. *Expert Opin Pharmacother* 2006;7:177–93. <https://doi.org/10.1517/14656566.7.2.177>.
- [597] Minna JD, Dowell J. Erlotinib hydrochloride. *Nat Rev Drug Discov* 2005;Suppl:S14-5. <https://doi.org/10.1038/nrd1612>.
- [598] Collins DM, Conlon NT, Kannan S, Verma CS, Eli LD, Lalani AS, et al. Preclinical Characteristics of the Irreversible Pan-HER Kinase Inhibitor Neratinib

- Compared with Lapatinib: Implications for the Treatment of HER2-Positive and HER2-Mutated Breast Cancer. *Cancers (Basel)* 2019;11. <https://doi.org/10.3390/cancers11060737>.
- [599] Di Veroli GY, Fornari C, Wang D, Mollard S, Bramhall JL, Richards FM, et al. Combenefit: an interactive platform for the analysis and visualization of drug combinations. *Bioinformatics* 2016;32:2866–8. <https://doi.org/10.1093/bioinformatics/btw230>.
- [600] Zhao L, Au JLS, Wientjes MG. Comparison of methods for evaluating drug-drug interaction. *Front Biosci (Elite Ed)* 2010;2:241. <https://doi.org/10.2741/E86>.
- [601] Schneider CA, Rasband WS, Eliceiri KW. NIH Image to ImageJ: 25 years of image analysis. *Nat Methods* 2012;9:671–5. <https://doi.org/10.1038/nmeth.2089>.
- [602] Maire V, Mahmood F, Rigail G, Ye M, Brisson A, Némati F, et al. LRP8 is overexpressed in estrogen-negative breast cancers and a potential target for these tumors. *Cancer Med* 2019;8:325. <https://doi.org/10.1002/CAM4.1923>.
- [603] Lerebours F, Vacher S, Guinebretiere JM, Rondeau S, Caly M, Gentien D, et al. Hemoglobin overexpression and splice signature as new features of inflammatory breast cancer? *J Adv Res* 2021;28:77. <https://doi.org/10.1016/J.JARE.2020.08.009>.
- [604] Tang J, Wennerberg K, Aittokallio T. What is synergy? The Saariselkä agreement revisited. *Front Pharmacol* 2015;6:181. <https://doi.org/10.3389/fphar.2015.00181>.
- [605] Meyer CT, Wooten DJ, Lopez CF, Quaranta V. Charting the Fragmented Landscape of Drug Synergy. *Trends Pharmacol Sci* 2020;41:266–80. <https://doi.org/10.1016/j.tips.2020.01.011>.
- [606] Smith SE, Mellor P, Ward AK, Kendall S, McDonald M, Vizeacoumar FS, et al. Molecular characterization of breast cancer cell lines through multiple omic approaches. *Breast Cancer Research* 2017;19:1–12. <https://doi.org/10.1186/S13058-017-0855-0/FIGURES/5>.
- [607] Fedoriw A, Rajapurkar SR, O'Brien S, Gerhart S V, Mitchell LH, Adams ND, et al. Anti-tumor Activity of the Type I PRMT Inhibitor, GSK3368715, Synergizes with PRMT5 Inhibition through MTAP Loss. *Cancer Cell* 2019;36:100-114.e25. <https://doi.org/10.1016/j.ccell.2019.05.014>.
- [608] Wei X, Yang J, Adair SJ, Ozturk H, Kuscu C, Lee KY, et al. Targeted CRISPR screening identifies PRMT5 as synthetic lethality combinatorial target with gemcitabine in pancreatic cancer cells. *Proc Natl Acad Sci U S A* 2020;117:28068–79. <https://doi.org/10.1073/pnas.2009899117>.
- [609] Wang H, Yang L, Liu M, Luo J. Protein post-translational modifications in the regulation of cancer hallmarks. *Cancer Gene Ther* 2023;30:529–47. <https://doi.org/10.1038/S41417-022-00464-3>.

- [610] Kim H, Ronai ZA. PRMT5 function and targeting in cancer. *Cell Stress* 2020;4:199. <https://doi.org/10.15698/CST2020.08.228>.
- [611] Chen Y, Shao X, Zhao X, Ji Y, Liu X, Li P, et al. Targeting protein arginine methyltransferase 5 in cancers: Roles, inhibitors and mechanisms. *Biomed Pharmacother* 2021;144. <https://doi.org/10.1016/J.BIOPHA.2021.112252>.
- [612] Branon TC, Bosch JA, Sanchez AD, Udeshi ND, Svinkina T, Carr SA, et al. Efficient proximity labeling in living cells and organisms with TurboID. *Nat Biotechnol* 2018;36:880–98. <https://doi.org/10.1038/NBT.4201>.
- [613] Rafiee M, Sigismondo G, Kalxdorf M, Förster L, Brügger B, Béthune J, et al. Protease-resistant streptavidin for interaction proteomics. *Mol Syst Biol* 2020;16. <https://doi.org/10.15252/MSB.20199370>.
- [614] Pouillet P, Carpentier S, Barillot E. myProMS, a web server for management and validation of mass spectrometry-based proteomic data. *Proteomics* 2007;7:2553–6. <https://doi.org/10.1002/PMIC.200600784>.
- [615] Pedersen ME, Østergaard J, Jensen H. Flow-Induced Dispersion Analysis (FIDA) for Protein Quantification and Characterization. *Methods Mol Biol* 2019;1972:109–23. [https://doi.org/10.1007/978-1-4939-9213-3\\_8](https://doi.org/10.1007/978-1-4939-9213-3_8).
- [616] May DG, Scott KL, Campos AR, Roux KJ. Comparative Application of BioID and TurboID for Protein-Proximity Biotinylation. *Cells* 2020;9. <https://doi.org/10.3390/CELLS9051070>.
- [617] Hagemann N, Ackermann N, Christmann J, Brier S, Yu F, Erdmann KS. The serologically defined colon cancer antigen-3 interacts with the protein tyrosine phosphatase PTPN13 and is involved in the regulation of cytokinesis. *Oncogene* 2013;32:4602–13. <https://doi.org/10.1038/ONC.2012.485>.
- [618] Yu F, Sharma S, Skowronek A, Erdmann KS. The serologically defined colon cancer antigen-3 (SDCCAG3) is involved in the regulation of ciliogenesis. *Sci Rep* 2016;6. <https://doi.org/10.1038/SREP35399>.
- [619] McGough IJ, Steinberg F, Gallon M, Yatsu A, Ohbayashi N, Heesom KJ, et al. Identification of molecular heterogeneity in SNX27-retromer-mediated endosome-to-plasma-membrane recycling. *J Cell Sci* 2014;127:4940–53. <https://doi.org/10.1242/JCS.156299>.
- [620] Neznanov N, Neznanova L, Angres B, Gudkov A V. Serologically defined colon cancer antigen 3 is necessary for the presentation of TNF receptor 1 on cell surface. *DNA Cell Biol* 2005;24:777–85. <https://doi.org/10.1089/DNA.2005.24.777>.
- [621] Sharma S, Carmona A, Skowronek A, Yu F, Collins MO, Naik S, et al. Apoptotic signalling targets the post-endocytic sorting machinery of the death receptor Fas/CD95. *Nat Commun* 2019;10. <https://doi.org/10.1038/S41467-019-11025-Y>.

- [622] Maubant S, Tahtouh T, Brisson A, Maire V, Némati F, Tesson B, et al. LRP5 regulates the expression of STK40, a new potential target in triple-negative breast cancers. *Oncotarget* 2018;9:22586. <https://doi.org/10.18632/ONCOTARGET.25187>.
- [623] Maubant S, Tesson B, Maire V, Ye M, Rigai G, Gentien D, et al. Transcriptome Analysis of Wnt3a-Treated Triple-Negative Breast Cancer Cells. *PLoS One* 2015;10. <https://doi.org/10.1371/JOURNAL.PONE.0122333>.
- [624] Close P, East P, Dirac-Svejstrup AB, Hartmann H, Heron M, Maslen S, et al. DBIRD complex integrates alternative mRNA splicing with RNA polymerase II transcript elongation. *Nature* 2012;484:386–9. <https://doi.org/10.1038/NATURE10925>.
- [625] Ligr M, Patwa RR, Daniels G, Pan L, Wu X, Li Y, et al. Expression and function of androgen receptor coactivator p44/Mep50/WDR77 in ovarian cancer. *PLoS One* 2011;6. <https://doi.org/10.1371/JOURNAL.PONE.0026250>.
- [626] Dakroub R, Huard S, Hajj-Younes Y, Suresh S, Badran B, Fayyad-Kazan H, et al. Therapeutic advantage of targeting PRMT5 in combination with chemotherapies or EGFR/HER2 inhibitors in triple-negative breast cancers. *Breast Cancer: Targets and Therapy* 2023;In press.
- [627] Stockhammer A, Benz LS, Freund C, Kuroepka B, Bottanelli F. When less is more - Endogenous tagging with TurboID increases the sensitivity of proximity labelling-based experiments. *BioRxiv* 2021:2021.11.19.469212. <https://doi.org/10.1101/2021.11.19.469212>.
- [628] Hegele A, Kamburov A, Grossmann A, Sourlis C, Wowro S, Weimann M, et al. Dynamic Protein-Protein Interaction Wiring of the Human Spliceosome. *Mol Cell* 2012;45:567–80. <https://doi.org/10.1016/J.MOLCEL.2011.12.034>.
- [629] Jacob A. Proteomic analysis of protein arginine methyltransferases 5 and 7 using BioID method. 2016.
- [630] M Y, F H, H R, Q G, J L. Experimental Study on Sdccag3 Regulating Osteogenesis and Adipogenic Differentiation of Rats Bone Marrow Mesenchymal Stem Cells 2021. <https://doi.org/10.21203/RS.3.RS-1059024/V1>.
- [631] Jin Y, Zhou J, Xu F, Jin B, Cui L, Wang Y, et al. Targeting methyltransferase PRMT5 eliminates leukemia stem cells in chronic myelogenous leukemia. *J Clin Invest* 2016;126:3961–80. <https://doi.org/10.1172/jci85239>.
- [632] Chung J, Karkhanis V, Baiocchi RA, Sif S. Protein arginine methyltransferase 5 (PRMT5) promotes survival of lymphoma cells via activation of WNT/ $\beta$ -catenin and AKT/GSK3 $\beta$  proliferative signaling. *J Biol Chem* 2019;294:7692–710. <https://doi.org/10.1074/JBC.RA119.007640>.
- [633] Zhu K, Peng Y, Hu J, Zhan H, Yang L, Gao Q, et al. Metadherin-PRMT5 complex enhances the metastasis of hepatocellular carcinoma through the WNT- $\beta$ -catenin signaling pathway. *Carcinogenesis* 2020;41:130–8. <https://doi.org/10.1093/CARCIN/BGZ065>.



- [634] Wang N, Yan H, Wu D, Zhao Z, Chen X, Long Q, et al. PRMT5/Wnt4 axis promotes lymph-node metastasis and proliferation of laryngeal carcinoma. *Cell Death & Disease* 2020 11:10 2020;11:1–15. <https://doi.org/10.1038/s41419-020-03064-x>.
- [635] Shailesh H, Siveen KS, Sif S. Protein arginine methyltransferase 5 (PRMT5) activates WNT/ $\beta$ -catenin signalling in breast cancer cells via epigenetic silencing of DKK1 and DKK3. *J Cell Mol Med* 2021;25:1583–600. <https://doi.org/10.1111/JCMM.16260>.
- [636] Addi C, Presle A, Frémont S, Cuvelier F, Rocancourt M, Milin F, et al. The Flemmingsome reveals an ESCRT-to-membrane coupling via ALIX/syntenin/syndecan-4 required for completion of cytokinesis. *Nature Communications* 2020 11:1 2020;11:1–15. <https://doi.org/10.1038/s41467-020-15205-z>.

## **Annexe I**

# **Expression, Localization and Prognosis Association of MEP50 in Breast Cancer**

## Annexe II

# **PRMT1 Regulates EGFR and Wnt Signaling Pathways and Is a Promising Target for Combinatorial Treatment of Breast Cancer**

## Article

# Expression, Localization and Prognosis Association of MEP50 in Breast Cancer

Samyuktha Suresh <sup>1,†</sup> , Mathilde Vinet <sup>1,†</sup>, Rayan Dakroub <sup>1,2</sup>, Laetitia Lesage <sup>3</sup> , Mengliang Ye <sup>1</sup>, Hussein Fayyad-Kazan <sup>2</sup> , André Nicolas <sup>3</sup>, Didier Meseure <sup>3</sup> and Thierry Dubois <sup>1,\*</sup> 

<sup>1</sup> Breast Cancer Biology Group, Translational Research Department, Institut Curie-PSL Research University, 75005 Paris, France

<sup>2</sup> Laboratory of Cancer Biology and Molecular Immunology, Faculty of Sciences-I, Lebanese University, Hadath 1003, Lebanon

<sup>3</sup> Platform of Experimental Pathology, Department of Diagnostic and Theranostic Medicine, Institut Curie-Hospital, 75005 Paris, France

\* Correspondence: thierry.dubois@curie.fr; Tel.: +33-156246250

† These authors contributed equally to this work.

**Simple Summary:** The arginine methyltransferase PRMT5 is an emerging therapeutic target for various cancers including breast cancer. In this study, we examine the expression and subcellular localization of its main cofactor, MEP50, in the different breast cancer subgroups. High levels of MEP50 are found in TNBC and associated with better recurrence-free survival.

**Abstract:** Breast cancer is composed of distinct subgroups, triple-negative breast cancer (TNBC), human epidermal growth factor receptor-2 (HER2), luminal A, and luminal B, which are associated with different prognosis. MEP50 is the main partner of the arginine methyltransferase PRMT5 required for its enzymatic activity. Here, we examined *MEP50* expression in the different breast cancer subgroups from the transcriptomic data obtained on human breast cancer samples and on normal breast tissues in two cohorts (Curie,  $n = 141$ ; The Cancer Genome Atlas—TCGA,  $n = 788$ ). We observed higher levels of *MEP50* mRNA in TNBC (Curie,  $n = 41$ ; TCGA,  $n = 106$ ) compared to the other breast cancer subgroups and normal breast tissues. Using an online KM-plotter database, which allows survival analyses in a larger number of breast cancer patients, we found that high *MEP50* mRNA levels were associated with a more favorable recurrence-free survival (RFS) in TNBC ( $n = 953$ ,  $p = 1.2 \times 10^{-4}$ ) and luminal B ( $n = 1353$ ,  $p = 0.013$ ) tumors, whereas high *PRMT5* mRNA levels were associated with worse RFS in these two subgroups (TNBC:  $n = 442$ ,  $p = 1.0 \times 10^{-4}$ ; luminal B:  $n = 566$ ,  $p = 6.8 \times 10^{-3}$ ). We next determined the expression and the subcellular localization of MEP50 protein by immunohistochemistry (IHC) in our Curie cohort of breast cancer ( $n = 94$ ) and normal tissues ( $n = 7$ ) using a validated MEP50 antibody. MEP50 was more expressed in breast tumors compared to normal breast tissues ( $p = 0.02$ ). MEP50 was more localized to the cytosol in breast cancer cells compared to normal breast tissue ( $p = 4 \times 10^{-4}$ ), and was more found at the plasma membrane in normal tissues compared to breast tumors ( $p = 0.01$ ). We also evaluated PRMT5 activity by IHC in our Curie cohort using a validated antibody (H4R3me2s) detecting histone H4 symmetrically dimethylated on Arg3. High levels of H4R3me2s were found in normal breast tissues, whereas the lowest levels of H4R3me2s were observed in TNBC and HER2 breast cancer subgroups. Altogether, our study reports the expression of the PRMT5 cofactor (MEP50) and substrate (H4R3me2s) in breast cancer and highlights the association of *PRMT5* and *MEP50* mRNA with prognosis in luminal B and TNBC breast cancer subgroups and certain TNBC subtypes.

**Keywords:** triple-negative breast cancer; TNBC; breast cancer; PRMT5; MEP50; H4R3me2s; epigenetics; prognosis; recurrence-free survival



**Citation:** Suresh, S.; Vinet, M.; Dakroub, R.; Lesage, L.; Ye, M.; Fayyad-Kazan, H.; Nicolas, A.; Meseure, D.; Dubois, T. Expression, Localization and Prognosis Association of MEP50 in Breast Cancer. *Cancers* **2022**, *14*, 4766. <https://doi.org/10.3390/cancers14194766>

Academic Editor: David Wong

Received: 2 September 2022

Accepted: 26 September 2022

Published: 29 September 2022

**Publisher's Note:** MDPI stays neutral with regard to jurisdictional claims in published maps and institutional affiliations.



**Copyright:** © 2022 by the authors. Licensee MDPI, Basel, Switzerland. This article is an open access article distributed under the terms and conditions of the Creative Commons Attribution (CC BY) license (<https://creativecommons.org/licenses/by/4.0/>).

## 1. Introduction

Breast cancer is a heterogeneous disease comprising several subgroups associated with different prognosis [1]. Breast tumors are mainly classified depending on the expression of hormone receptors (estrogen and progesterone receptors, ER and PR) and the overexpression of epidermal growth factor receptor 2 (HER2) [1]. Luminal breast cancers express ER and/or PR, and are subclassified into luminal A or luminal B subgroups, the former being less proliferative and associated with a better prognosis. Hormone-negative breast cancers, which are associated with the poorest prognosis, are subdivided into two groups depending on HER2 overexpression: HER2-positive (HER2), characterized by *HER2* amplification, and basal-like (or triple-negative breast cancer, TNBC) [1]. TNBC itself is highly heterogeneous comprising molecularly distinct subtypes: basal-like 1 (BL1), basal-like 2 (BL2), mesenchymal (M), mesenchymal stem-like (MSL), immunomodulatory (IM), and luminal androgen receptor (LAR) [2–4]. This inter-tumor heterogeneity along with a well-established intra-tumor heterogeneity arising from drug-resistant cells pose a major challenge in treating TNBC patients [2–6]. Identifying new therapeutic targets to overcome chemo-resistance and recurrence is a high clinical priority for TNBC patients.

Protein arginine methyltransferases (PRMT1–9) are post-translational modifying enzymes which transfer one or two methyl group(s) to a wide range of cytosolic and nuclear substrates [7–12]. Some PRMTs are emerging as attractive therapeutic targets as they have been shown to be overexpressed in various cancers. We have recently reported that PRMT1 [13] and PRMT5 [14] are promising targets for TNBC. Specific PRMT5 inhibitors are currently under evaluation in clinical trials [8,9,15,16].

PRMT5 regulates gene expression through transcriptional activation and repression, pre-mRNA splicing, translation, growth factor signaling, and DNA damage response, to name a few [16–18]. PRMT5 is the principal enzyme catalyzing symmetric dimethylation of arginine on a myriad of substrates including histones (H2A, H3 and H4), and non-histone proteins. Symmetric dimethylation of arginine 3 on histone H2A (H2AR3me2s) [19] and H4 (H4R3me2s) [20,21] and arginine 8 on histone H3 (H3R8me2s) [21,22] are associated with gene regulation.

The main protein partner of PRMT5 is the methylosome protein 50 (MEP50) [23]. It is also known as WDR77 (WD repeat-containing protein) or as a coactivator of the androgen receptor (p44) [24]. MEP50 forms a hetero-octameric complex with PRMT5 and activates its enzyme activity [25–27]. MEP50 is overexpressed in lung, squamous cell carcinoma, and breast cancer at the RNA level [28–30] and in ovarian [31], lung [32], and squamous cell [33] carcinomas at the protein level. Mutations in the *MEP50* gene that impairs its binding to PRMT5 have been discovered in familial non medullary thyroid cancer [34]. High *MEP50* mRNA levels are associated with poor prognosis in lung [17] and breast [35] cancers. MEP50 localizes both in the cytosol and nucleus of various cancer cells: breast [29,36], ovarian [31], squamous [33], and prostate [37–41] cancers. Cytosolic localization of MEP50 is associated with proliferation while nuclear MEP50 is linked with differentiation in prostate cancer cells [37–42]. Knocking down MEP50 decreases cell proliferation of different cell lines including ovarian cancer [31], squamous cell carcinoma [33], keratinocyte [43], and lung cancer [44] cells. In contrast, its knockdown increases thyroid cancer cell growth [34]. A recent study showed that MEP50 depletion sensitizes prostate cancer cells to radiation [45].

In this study, we examined the expression level of *MEP50* and *PRMT5* mRNA and their association with recurrence-free survival (RFS) in the different breast cancer subgroups and various TNBC subtypes. We determined the expression and the subcellular localization of MEP50 protein by immunohistochemistry (IHC) in our cohort of breast cancer tissues. Lastly, we assessed nuclear PRMT5 activity by analyzing the H4R3me2s methylation mark by IHC in breast tumors and normal tissues.

## 2. Materials and Methods

### 2.1. Human Breast Cancer Cohorts and Transcriptomic Data

Curie cohort: Our cohort has been previously described [14,46–49] and is composed of TNBC (ER-, PR-, HER2-), HER2 (ER-, PR-, HER2+), luminal A (ER+ and/or PR+, HER2-), luminal B (ER+ and/or PR+, HER2+), and normal breast tissues from plastic surgery. Experiments were conducted in accordance with Bioethics Law No. 2004–800 and the Ethics Charter from the French National Institute of Cancer (INCa), and after approval from the ethics committee of our Institution. Transcriptome microarray (U133 Plus 2.0 Affymetrix chips, Thermo Fisher Scientific, Waltham, MA, USA) was performed on TNBC ( $n = 41$ ), HER2 ( $n = 30$ ), luminal A ( $n = 29$ ), luminal B ( $n = 30$ ), and normal human samples ( $n = 11$ ), as previously described [14,46–49] (Table 1).

**Table 1.** Curie Cohort (Transcriptome Analysis): *MEP50* mRNA Expression in Breast Cancer Subgroups and Normal Breast Tissues (Figure 1).

Number of Samples in Breast Cancer Subgroups and in Normal Breast Tissues				
TNBC	HER2	Luminal B	Luminal A	normal breast tissues
41	30	30	29	11

TCGA cohort: the publicly available RNA-SeqV2 Level 3 dataset (January 2015) were downloaded from The Cancer Genome Atlas (TCGA) breast invasive carcinoma cohort (<http://cancergenome.nih.gov/>) [50] and integrated into a platform in knowledge data integration (KDI) at Institut Curie (<https://bioinfo-portal.curie.fr>). We classified the breast cancer subgroups, as we did for the Curie cohort, based on the immunohistochemical status for ER, PR and HER2 which were provided in the dataset. TNBC (ER-, PR-, HER2-;  $n = 106$ ), HER2 (ER-, PR-, HER2+;  $n = 36$ ), luminal A (ER+ and/or PR+, HER2-;  $n = 415$ ), and luminal B (ER+ and/or PR+, HER2+;  $n = 118$ ). The TCGA database includes 113 referenced normal breast tissue samples (Table 2).

**Table 2.** TCGA cohort (transcriptome analysis): *MEP50* mRNA expression in breast cancer subgroups and normal breast tissues (Figure 1).

Number of Samples in Breast Cancer Subgroups and in Normal Breast Tissues				
TNBC	HER2	Luminal B	Luminal A	normal breast tissues
106	36	118	415	113

### 2.2. Survival Analysis

Kaplan–Meier curves for target genes were generated with the online tool Kaplan–Meier Plotter (KM) plotter (<https://www.kmplot.com>, accessed on August 2022) [51]. The best probe sets for *MEP50* (201421\_s\_at) and *PRMT5* (1564520\_s\_at) retrieved the number of patients for survival analyses (Tables 3 and 4 indicate the number of patients analyzed in each breast cancer subgroup and TNBC subtype, respectively). Recurrence-free survival (RFS) of breast cancer patients stratified by high and low expression of *MEP50* or *PRMT5* mRNA (median cutoff setting) was determined from the online tool (<https://www.kmplot.com>).

The survival curves for each breast cancer subgroup were obtained using the PAM50 setting on the website (Basal for TNBC, HER2, luminal B and Luminal A). The table below indicates the number of patients retrieved with the *MEP50* and *PRMT5* probe sets within each breast cancer subgroup (Table 3).

The survival curves for each TNBC subtype were retrieved using the Pietenpol setting classifying the TNBC subtypes as reported by the group of Prof. Pietenpol [2] (basal-like 1, BL1; basal-like 2, BL2; immunomodulatory, IM; mesenchymal, Mes; mesenchymal stem-like, MSL; luminal androgen receptor, LAR). The table below indicates the number

of patients retrieved with the MEP50 and PRMT5 probe sets within each TNBC subtype (Table 4).

**Table 3.** Survival analyses in the breast cancer subgroups (Figure 2).

	Number of Patients Retrieved on <a href="https://www.kmplot.com">https://www.kmplot.com</a> with the MEP50 (201421_s_at) or the PRMT5 (1564520_s_at) Probe Sets			
	TNBC	HER2	Luminal B	Luminal A
MEP50 mRNA	953	695	1353	1809
PRMT5 mRNA	442	358	566	631
PRMT5:MEP50 mRNA	442	358	566	631

**Table 4.** Survival analyses in TNBC subtypes (Figure 3).

	Number of Patients Retrieved on <a href="https://www.kmplot.com">https://www.kmplot.com</a> with the MEP50 (201421_s_at) or the PRMT5 (1564520_s_at) Probe Sets					
	BL1	BL2	IM	Mes	MSL	LAR
MEP50 mRNA	251	101	300	211	81	253
PRMT5 mRNA	126	68	130	112	43	123
PRMT5:MEP50 mRNA	126	68	130	112	43	123

The obtained Hazard Ratio (HR) with 95% confidence interval and log-rank *p*-values were generated automatically from the online tool (<https://www.kmplot.com>) and are shown on the corresponding Figures.

### 2.3. Cell Culture

HCC38, MDA-MB-231 and MDA-MB-453 TNBC cells were purchased from the American Type Culture Collection (ATCC, LGC Promochem, Karnataka, India), authenticated by short tandem repeat profiling in 2021 (not shown). HCC38 cells were cultured in RPMI-1640 (LifeTechnologies, Carlsbad, CA, USA) supplemented with 10% (*vol/vol*) fetal bovine serum (FBS, LifeTechnologies), 1.5 g/L sodium bicarbonate (LifeTechnologies), 10 mmol/L Hepes (LifeTechnologies), 1 mmol/L sodium pyruvate (LifeTechnologies), 100 U/mL penicillin, and 100 µg/mL streptomycin (LifeTechnologies). MDA-MB-453 and MDA-MB-231 cells were cultured in DMEM-F12 (LifeTechnologies) supplemented with 10% FBS, 100 U/mL penicillin, and 100 µg/mL streptomycin.

### 2.4. Validation of the MEP50 Antibodies for Immunohistochemistry (IHC) Staining

HCC38 and MDA-MB-231 cells were transfected with 20 nM of control (Allstars negative control, ref: SI03650318, Qiagen, Hilden, Germany) or MEP50 (ref: SI03152730, Qiagen, target sequence 5'-ATGCTAGATCTGTGCCGTAA-3') siRNA using INTERFERin (Polyplus Transfection, Illkirch-Graffenstaden, France). Forty-eight hours post transfection, protein lysates were extracted from one plate and subjected to Western blot, as previously described [48,52,53], to confirm MEP50 depletion efficiency. The other plates were used to validate the specificity of the MEP50 antibodies for IHC purpose: about 10 million cells per condition (control or MEP50 siRNA treated cells) were pelleted, then fixed with the same fixator (AFA: Alcohol, Formalin, Acetic acid) used to fix the human samples. Fixed cells were then paraffin embedded, and 3 µm-thick sections were cut with a microtome and then stained as the human samples of the Curie cohort.

### 2.5. Validation of the H4R3me2s Antibodies for IHC Staining

MDA-MB-453 cells were incubated for 48 h with vehicle (DMSO) or 1 µM of EPZ015666 (PRMT5 inhibitor, Clinisciences, Nanterre, France). Protein lysates were extracted from one plate, and Western blot analysis was performed using a pan symmetric dimethyl-arginine

(SDMA) antibody to confirm the efficacy of EPZ015666. The other plates were used to validate the specificity of the H4R3me2s antibodies for IHC purpose: about 10 million cells per condition (DMSO or EPZ015666 treated cells) were pelleted, then fixed with the same fixator (AFA) used to fix the human samples. Fixed cells were then paraffin-embedded, and 3 µm-thick sections were cut with a microtome, and stained as the human samples of the Curie cohort.

## 2.6. Immunohistochemistry on Human Samples

IHC was performed on the following number of tumors of our Curie cohort (TNBC:  $n = 26$ ; HER2:  $n = 26$ ; luminal A:  $n = 17$ ; luminal B:  $n = 25$ ) and normal breast tissues ( $n = 7$ ) (Table 5).

**Table 5.** Curie cohort (IHC): MEP50 expression (MEP50 staining, Figures 5 and 6) and PRMT5 activity (H4R3me2s staining, Figure 7) in breast cancer subgroups and normal breast tissues.

Number of Samples in Breast Cancer Subgroups and in Normal Breast Tissues				
TNBC	HER2	Luminal B	Luminal A	normal breast tissues
26	26	25	17	7

AFA-fixed paraffin-embedded tissues, obtained at the time of the initial diagnosis, were retrieved from the archives of the Department of Pathology of Institut Curie Hospital. Three µm-thick sections were cut with a microtome from the paraffin-embedded tissue blocks, and tissue microarrays (TMA) were made. Tissue sections were dewaxed and rehydrated through a series of xylene and ethanol washes before heat-induced epitope retrieval. Antigen retrieval was performed in EDTA buffer pH = 6 (MEP50) or pH = 9 (H4R3me2s). The slides were incubated with primary antibodies against MEP50 (1/1000, 1 h at room temperature) or H4R3me2s (1/1000, 15 min at room temperature). Then, the slides were incubated with secondary antibodies coupled to horseradish peroxidase. A DAB (3,3'-Diaminobenzidine) solution was applied for 5 min for revelation of peroxidase. Slides were counterstained with hematoxylin before mounting with resin. Immunostaining was processed by using a Dako automated machine.

For surface staining quantifications, whole digital slide images were obtained using virtual microscopy (Philips Ultra-Fast Scanner 1.6 RA, Amsterdam, The Netherlands) and analyzed with Digital Image Analysis platform HALO (version 3.0.311.218; Indica Lab, Albuquerque, NM, USA). Tissue classifier was trained to segment the tissue image into tumor (epithelial cells) or stromal compartment. Area Quantification module (v2.1.3, Albuquerque, NM, USA) was used to evaluate the total area of epithelial compartment and the area of tissue positive for MEP50/H4R3me2s staining.

For subcellular localization, MEP50 staining was studied at the nuclear, plasma membrane and cytoplasmic compartments by two pathologists (A.E. and D.M., coauthors of this article) from the Institut Curie Hospital. For each tumor sample, the pathologists assigned IHC scores for MEP50/H4R3me2s staining based on the proportion of positive cells and its corresponding immunostaining intensity for each cellular compartment (only nuclear for H4R3me2s) by the following formula:

$$IHC \text{ score} = \text{percentage of stained cells} \times \text{intensity of immunostaining}$$

Hence, each score ranged between 0 and 3 (0: no staining; 3: strongest staining).

## 2.7. Antibodies

The primary antibodies used for Western blotting were: MEP50 (Cell Signaling Technology, ref. #2018, Danvers, MA, USA), PRMT5 (Merck Millipore, ref. #07-405, Burlington, MA, USA), pan symmetric dimethyl-arginine (SDMA) antibody (Cell Signaling Technology, ref. #13222), β-actin (Sigma-Aldrich, Ref. #A5441, St. Louis, MI, USA), and GAPDH (Cell



Signaling Technology, ref. #2118). The primary antibodies used for IHC were: MEP50 (Cell Signaling Technology, ref. #2018) and H4R3me2s (Abcam, Ref. #ab5823, Cambridge, UK).

### 2.8. Statistical Analysis

R software and GraphPad Prism 9 were used for statistical analyses. Pearson correlation was used to estimate an association between two variables. An ANOVA test was used to calculate the *p*-values when comparing the expression of MEP50/H4R3me2s between two different breast cancer groups.

## 3. Results

### 3.1. TNBC Express Higher Levels of MEP50 mRNA Compared to the Other Breast Cancer Subgroups and Normal Breast Tissues

At the RNA level, *MEP50* has been reported to be overexpressed in breast cancer compared to the normal breast tissue, without accounting for breast cancer heterogeneity [28–30]. Here, we examined *MEP50* mRNA expression in the different breast cancer subgroups. *MEP50* mRNA is heterogeneously expressed within each subgroup, particularly in TNBC, with some tumors expressing low and others high levels of *MEP50* mRNA. Nevertheless, we observed higher levels of *MEP50* mRNA in TNBC compared to the other breast cancer subgroups and normal tissues in both Curie (Table 1) and TCGA (Table 2) cohorts (Figure 1). We observed a positive correlation between *MEP50* and *PRMT5* mRNA levels in our cohort in the whole breast cancer population but not within the different breast cancer subgroups, although a tendency was observed for the luminal B subgroup ( $p = 0.053$ ) (Figure S1).

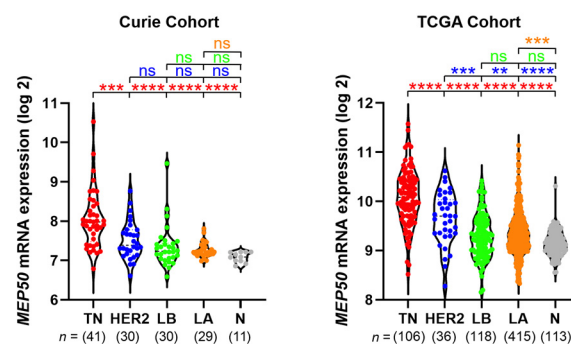


**Figure 1.** TNBC express high levels of *MEP50* mRNA. *MEP50* mRNA expression in the different breast cancer subgroups and in normal breast tissues in Curie (left panel) and TCGA (right panel) cohorts. The breast cancer subgroups are ordered left to right from the most to the least proliferative tumors: TNBC (TN, red), HER2 (blue), luminal B (LB, green), luminal A (LA, orange). Normal breast tissues (N) are in grey. Relative RNA quantifications are logarithmically (log<sub>2</sub>) transformed and illustrated by violin plots with each sample represented by a circle. The statistics in red indicate the comparison vs. TN, in blue vs. HER2, in green vs. LB, and in orange vs. LA: ns (not significant), \*\*  $p < 0.01$ , \*\*\*  $p < 0.001$ , \*\*\*\*  $p < 0.0001$ .

### 3.2. *MEP50* and *PRMT5* mRNA Levels Associate with Recurrence-Free Survival in TNBC and Luminal B Breast Tumors

We examined whether the expression of *MEP50* mRNA was linked to prognosis on the Kaplan–Meier (KM) plotter online database ([www.kmplot.com](http://www.kmplot.com)) [51]. High *MEP50* mRNA levels were associated with a more favorable RFS in TNBC ( $p = 1.2 \times 10^{-4}$ ) and luminal B ( $p = 0.013$ ) tumors (Figure 2A,F). In contrast, high *PRMT5* mRNA levels were associated with worse RFS in these two subgroups (TNBC,  $p = 1.0 \times 10^{-4}$ ; luminal B,  $p = 6.8 \times 10^{-3}$ ; Figure 2B,G). Then, we sought to examine if the tumors with worse RFS were those expressing both high *PRMT5* and low *MEP50* mRNA. For this purpose, we analyzed the prognostic value of *PRMT5* or *MEP50* mRNA in the two subpopulations expressing

high (> median) or low (< median) *MEP50* or *PRMT5* mRNA levels in the different breast cancer subgroups.

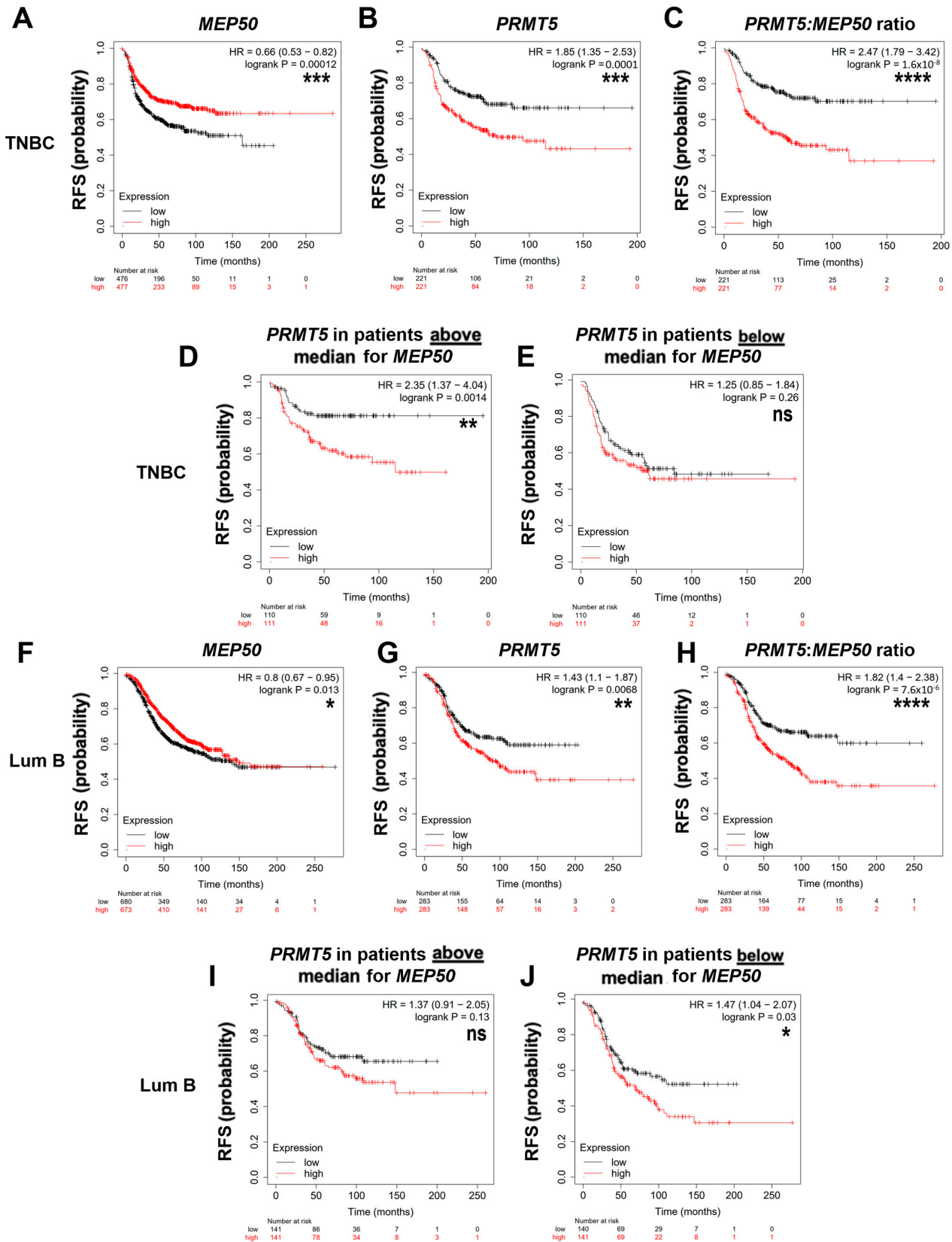


Figure 2. High *MEP50* mRNA expression is associated with a better prognosis in TNBC and luminal B

subgroups. (A–C,F–H). Recurrence-free survival (RFS) based on *MEP50* or *PRMT5* mRNA expression or *PRMT5:MEP50* mRNA ratio were obtained from the Kaplan–Meier (KM) plotter website (<http://kmplot.com>) for TNBC (A–C) and luminal B (Lum B; (F–H)). (D,E,I,J). RFS based on *PRMT5* mRNA expression within patients having either high (above median, (D,I)) or low (below median, (E,J)) *MEP50* mRNA expression (median cutoff). Of note, more patients were retrieved with *MEP50* probe set compared to the *PRMT5* probe set (Table 3). The obtained Hazard Ratio (HR) with 95% confidence interval and log-rank *p*-values are shown. ns (not significant), \* *p* < 0.05, \*\* *p* < 0.01, \*\*\* *p* < 0.001, \*\*\*\* *p* < 0.0001.

In TNBC patients with high *MEP50* (red line with good prognosis, Figure 2A), additionally considering high *PRMT5* expression unveils a population associated with poor prognosis (Figure 2D, *p* = 0.001). However, *PRMT5* expression showed no added prognostic value (Figure 2E, *p* = 0.26) in the TNBC population that expressed low *MEP50* (already associated with a poor prognosis, black line Figure 2A). Conversely, considering low *MEP50* expression within the group of patients with either high (red line Figure 2B) or low (black line Figure 2B) *PRMT5* reveals a population of patients with a worse prognosis (Figure S2A, *p* = 0.012; Figure S2B, *p* =  $7.7 \times 10^{-5}$ ). These observations indicate that considering both *MEP50* and *PRMT5* mRNA levels, instead of each separately, aids in improving patient stratification for RFS. Accordingly, the *PRMT5:MEP50* mRNA ratio is more significantly associated with RFS (*p* =  $1.6 \times 10^{-8}$ ; Figure 2C) than *PRMT5* alone (*p* =  $1.0 \times 10^{-4}$ ; Figure 2B).

In luminal B patients with high (red line in Figure 2F) or low (black line in Figure 2F) *MEP50*, considering high *PRMT5* expression unveils a population associated with poor prognosis (Figure 2I,J). However, *PRMT5* expression added a significant prognostic value only in luminal B expressing low levels of *MEP50* mRNA (although associated with poor prognosis, Figure 2J, *p* = 0.03). As for TNBC, a high *PRMT5:MEP50* mRNA ratio is more significantly associated with a poor prognosis (*p* =  $7.6 \times 10^{-6}$ ; Figure 2H) than high *PRMT5* alone (*p* =  $6.8 \times 10^{-3}$ ; Figure 2G).

In contrast to TNBC and luminal B, *MEP50*, *PRMT5*, and *PRMT5:MEP50* mRNA levels were not associated with RFS in luminal A nor HER2 subgroups (Figure S3).

Together, these observations indicate that *PRMT5* and *MEP50* mRNA levels are inversely associated with prognosis in TNBC and luminal B breast tumors. Taking into account both *PRMT5* and *MEP50* mRNA levels helps to better stratify patients associated with poor prognosis in these two breast cancer subgroups. This suggests that TNBC or luminal B tumors harboring high *PRMT5* and/or low *MEP50* mRNA levels could be at a higher risk of recurrence.

### 3.3. *MEP50* and *PRMT5* mRNA Levels Are Associated with Prognosis in Some TNBC Subtypes

As we observed that *MEP50* mRNA level is significantly associated with RFS in TNBC, we analyzed whether it is the case in the different TNBC subtypes using the KM-plotter database ([www.kmplot.com](http://www.kmplot.com)) [51]. Despite smaller sample sizes (Table 4), high levels of *MEP50* mRNA were associated with better RFS in the mesenchymal (*p* = 0.014) and LAR (*p* = 0.009) subtypes (Figure 3A,B, left panels). A similar trend was observed in BL1 but was not statistically significant (*p* = 0.089; Figure 3C, left panel).

Strikingly, high *PRMT5* mRNA levels were associated with worse RFS only in the mesenchymal (*p* =  $4.1 \times 10^{-4}$ ; Figure 3A, middle panel) and not in the other TNBC subtypes (Figure 3B,C, middle panel, Supplementary Figure S4, middle panels).

The *PRMT5:MEP50* ratio significantly improved the prognostic value in the LAR (*p* = 0.004) and BL1 (*p* =  $1.7 \times 10^{-4}$ ) subtypes (Figure 3B,C, right panels) than *PRMT5* or *MEP50* alone. This was not the case for the mesenchymal subtype (Figure 3A, right panel) in which *PRMT5* alone was already significantly highly associated with a bad prognosis (Figure 3A, middle panel).

*MEP50*, *PRMT5*, and *PRMT5:MEP50* mRNA levels were not associated with RFS in the BL2, IM, and MSL TNBC subtypes (Figure S4).

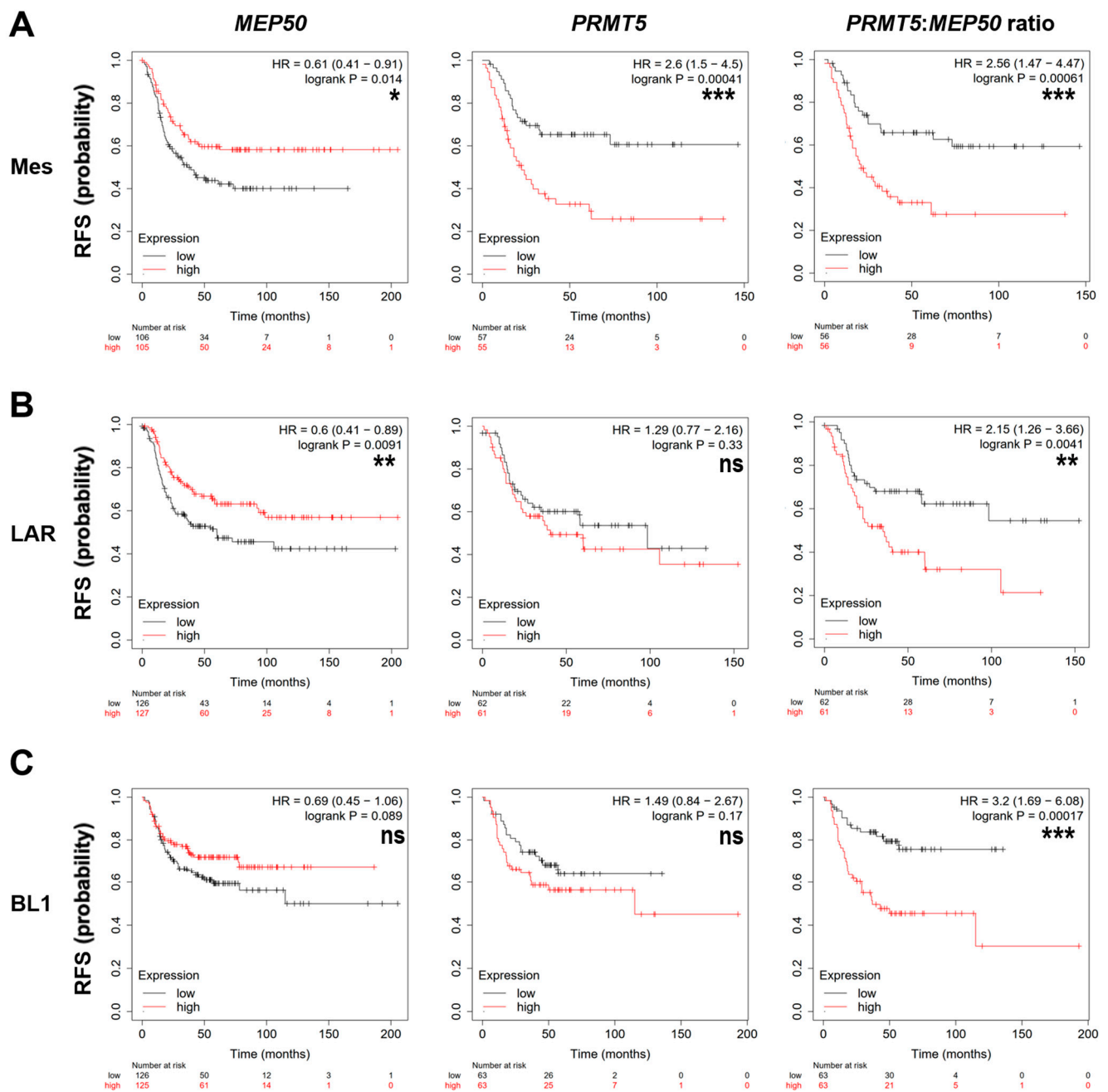


**Figure 3.** High *PRMT5:MEP50* mRNA ratio is associated with worse RFS in mesenchymal, LAR and BL1 TNBC subtypes. (A–C). RFS based on *MEP50* or *PRMT5* mRNA expression or *PRMT5:MEP50* mRNA ratio were obtained from the Kaplan–Meier (KM) plotter website (<http://kmplot.com>) for mesenchymal (Mes; (A)), luminal androgen receptor (LAR; (B)), and basal-like 1 (BL1; (C)) TNBC subtypes. Of note, more patients were retrieved with *MEP50* probe set compared to the *PRMT5* probe set (Table 4). The obtained Hazard Ratio (HR) with 95% confidence interval and log-rank *p*-values are shown. ns (not significant), \* *p* < 0.05, \*\* *p* < 0.01, \*\*\* *p* < 0.001.

### 3.4. *MEP50* Exhibits Differential Subcellular Localization in Breast Cancer Compared to Normal Breast Tissues

Next, we examined *MEP50* expression at the protein level in the different breast cancer subgroups of the Curie cohort. We first validated an anti-*MEP50* antibody for IHC purposes by staining two TNBC cell lines (HCC38 and MDA-MB-231) depleted or not for *MEP50* using *MEP50* siRNA and fixed using the same protocol as the one used for fixing the human tissues (Figure 4). IHC staining revealed that *MEP50* was mainly expressed in the cytosol



in both cell lines but was also detected at the plasma membrane and in the nucleus in some cells (Figure 4, left panels). The IHC staining decreased/disappeared in MEP50-depleted cells, demonstrating the specificity of the antibody (Figure 4, left panels). Western blot analysis confirmed the depletion of MEP50 in cells treated with MEP50 siRNA (Figure 4, right panels).

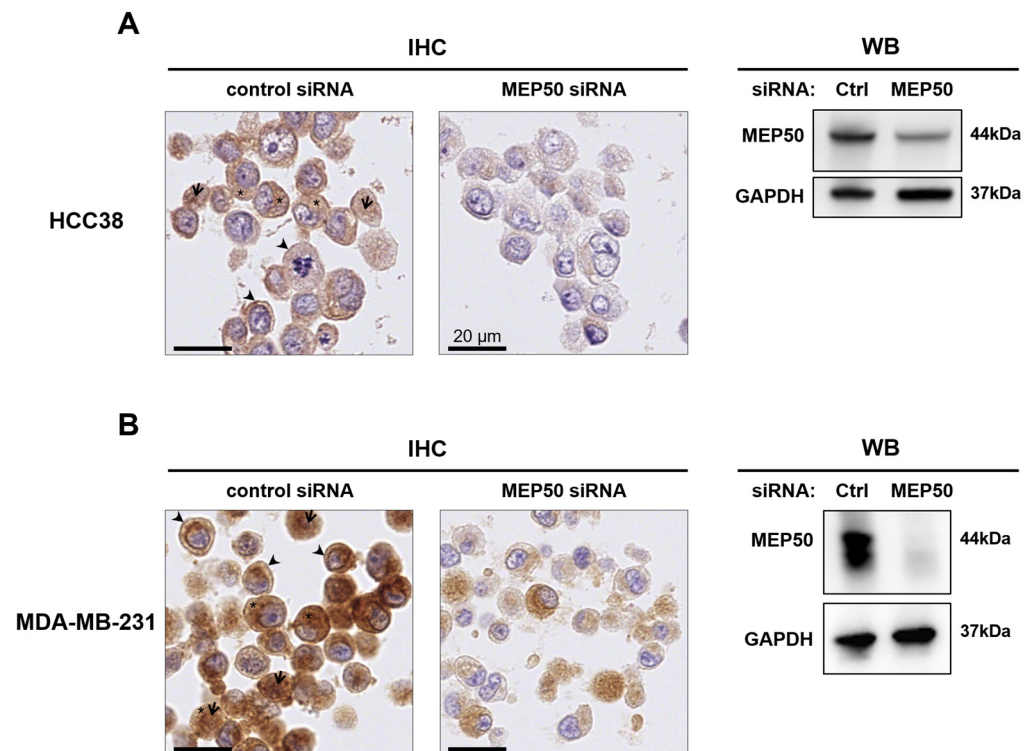


**Figure 4.** Validation of a MEP50 antibody suitable for IHC staining. HCC38 (A) and MDA-MB-231 (B) cells were treated with 20 nM control (Ctrl) siRNA or siRNA targeting MEP50 for 48 h. Cells were pelleted, fixed with AFA, paraffin embedded, and subjected to IHC staining with an anti-MEP50 antibody (scale bars = 20  $\mu$ m) ((A,B), left panels). MEP50 depletion was verified by Western blotting (WB) using an anti-MEP50 antibody ((A,B), right panels). Anti-GAPDH antibodies were used as a loading control. Arrows, arrowheads, and asterisks indicate MEP50 staining in the nucleus, plasma membrane, and cytoplasm, respectively. The uncropped blots are shown in Figure S5.

Using the validated MEP50 antibody for IHC purpose, we next analyzed MEP50 expression in breast cancer samples and normal breast tissues of our Curie cohort (Figure 5). MEP50 was more expressed in breast cancer compared to normal breast tissues ( $p = 0.02$ ) (Figures 5 and 6A). Moreover, TNBC had higher MEP50-expressing tumor cells compared to luminal A and normal breast tissues (Figure 6B). MEP50 was detected in the cytosol (Figure 5, asterisks), in the nucleus (Figure 5, arrow), and also at the plasma membrane of some cells (Figure 5, arrowhead). To quantify the subcellular localization of MEP50, we scored its staining at the plasma membrane (Figure 6C,D), in the cytosol (Figure 6C,E) and in the nucleus (Figure 6C,F) of the different breast cancer subgroups and in normal breast tissues. We observed a high heterogeneity of the MEP50 score, either at the plasma membrane, in the cytosol or in the nucleus, within each analyzed group (Figure 6D–F). Nevertheless, breast tumors had significantly lower levels of MEP50 at the plasma membrane (Figure 6C,D) but higher levels of cytoplasmic MEP50 (Figure 6C,E) compared to normal breast tissues. In the nucleus, there was no significant difference between breast tumors and normal breast tissues (Figure 6C). However, the TNBC subgroup had the lowest MEP50 expression compared to the other groups and normal tissue, but this was only significant with luminal B and HER2 subgroups (Figure 6F).

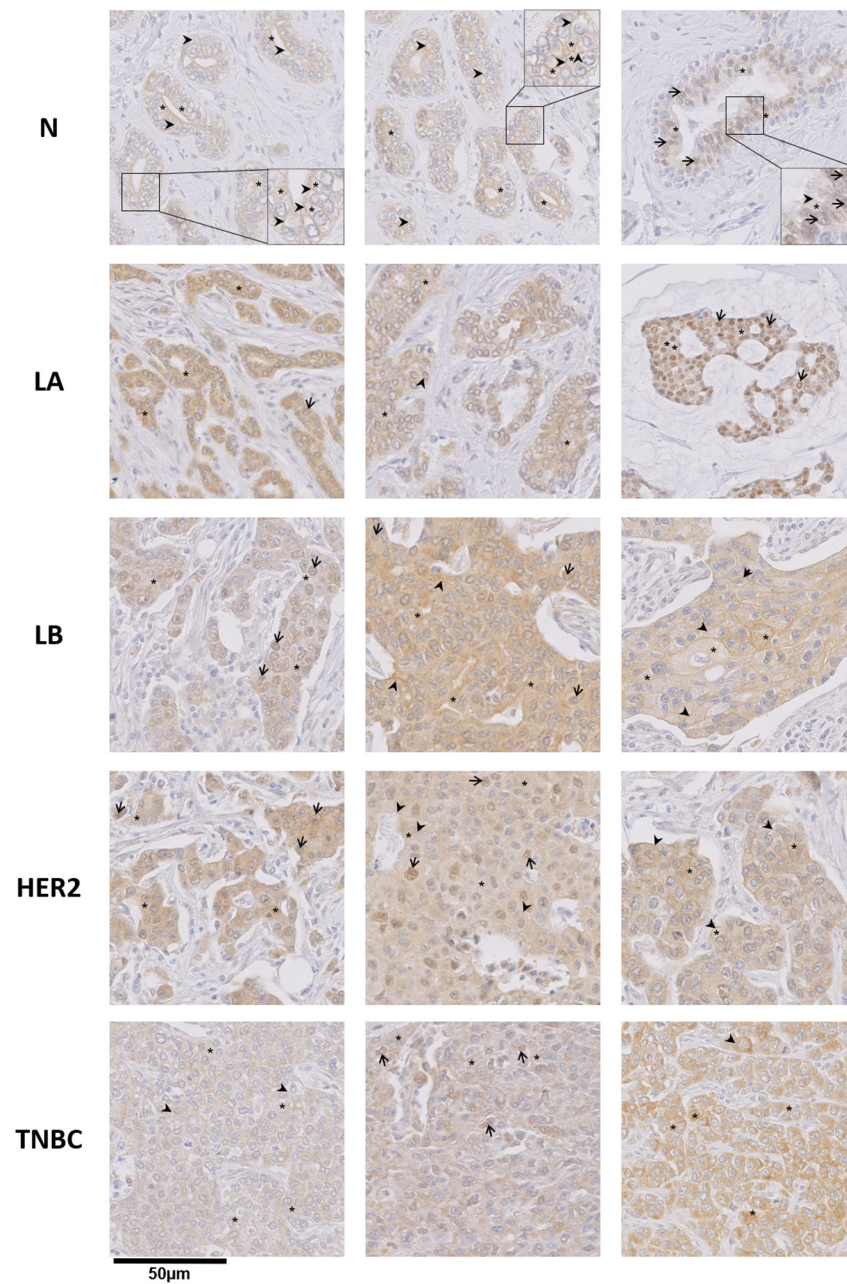


**Figure 5.** MEP50 is more expressed in breast cancer subgroups compared to normal breast tissues. The expression and localization of MEP50 protein were analyzed by IHC in the Curie cohort. Three representative images of MEP50 staining are shown for the different breast cancer subgroups and normal breast tissue to illustrate its heterogeneous expression and distribution (scale bar = 50  $\mu$ m). To better visualize cytoplasmic MEP50 and plasma membrane-associated MEP50 in normal samples, a part of the image is shown with a higher magnification (2 $\times$ ) in the inset. Arrows, arrowheads, and asterisks indicate MEP50 staining in the nucleus, plasma membrane, and cytoplasm, respectively.

Altogether, our study highlights the differential subcellular localization of MEP50 between cancerous and normal breast tissues. Importantly, its subcellular distribution is highly heterogeneous within the cancer tissues as well as normal breast tissues.

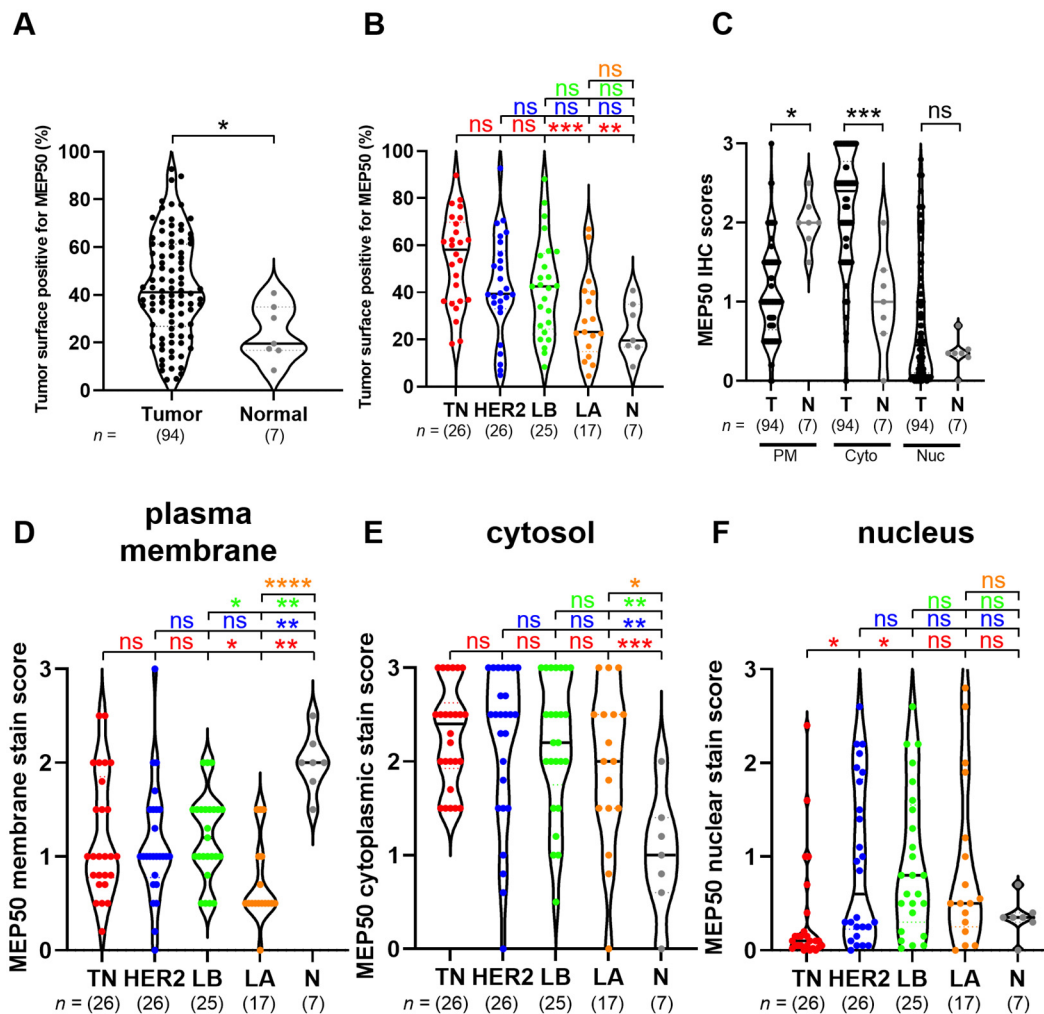


**Figure 6.** Differential subcellular localization of MEP50 among the breast tumor samples and normal breast tissues. Higher percentage of MEP50-expressing tumor cells compared to the normal breast tissues (A). Higher percentage of MEP50-expressing tumor cells in TNBC compared to the other breast cancer subgroups and normal breast tissues (B). Quantification of the tumoral surface positive for MEP50 staining represented as a percentage compared to the total epithelial surface (A,B). MEP50 staining was scored at the plasma membrane (C,D), in the cytosol (C,E) and in the nucleus (C,F) in the samples of the Curie cohort (from Figure 5). The score was obtained by combining the percentage and the intensity of the staining of the epithelial cells (0: no staining, 3: the strongest staining). Tumor (T, black), TNBC (TN, red), HER2 (blue), luminal B (LB, green), luminal A (LA, orange), and normal breast tissues (N, grey). PM: plasma membrane; Cyto: cytosol; Nuc: nucleus. The statistics in red indicate the comparison vs. TN, in blue vs. HER2, in green vs. LB, and in orange vs. LA: ns (not significant); \*  $p < 0.05$ ; \*\*  $p < 0.01$ ; \*\*\*  $p < 0.001$ ; \*\*\*\*  $p < 0.0001$ .

**3.5. The Most Aggressive Breast Cancer Subgroups Display the Lowest Levels of PRMT5-Dependent Symmetric Dimethylation of Histone H4 (H4R3me2s)**

Next, we sought to determine whether the low nuclear expression of MEP50 (this study) and PRMT5 [14] observed in TNBC correlated with low nuclear PRMT5 activity. We measured the level of histone H4 symmetrically dimethylated on Arginine 3 (H4R3me2s) as a marker of PRMT5 nuclear activity. First, we validated an antibody targeting H4R3me2s for IHC purposes in a TNBC cell line (MDA-MB-453) treated with a PRMT5 inhibitor (EPZ015666) and fixed using the same conditions as the human samples of our Curie cohort (Figure 7A). PRMT5 inhibition reduced the methylation of histone H4 (H4R3me2s) as observed by IHC (Figure 7A, left panel), validating this antibody. Western blot anal-



ysis confirmed that EPZ015666 lowered PRMT5 activity, using a pan antibody detecting symmetric dimethylated arginine (SDMA) (Figure 7A, right panel).

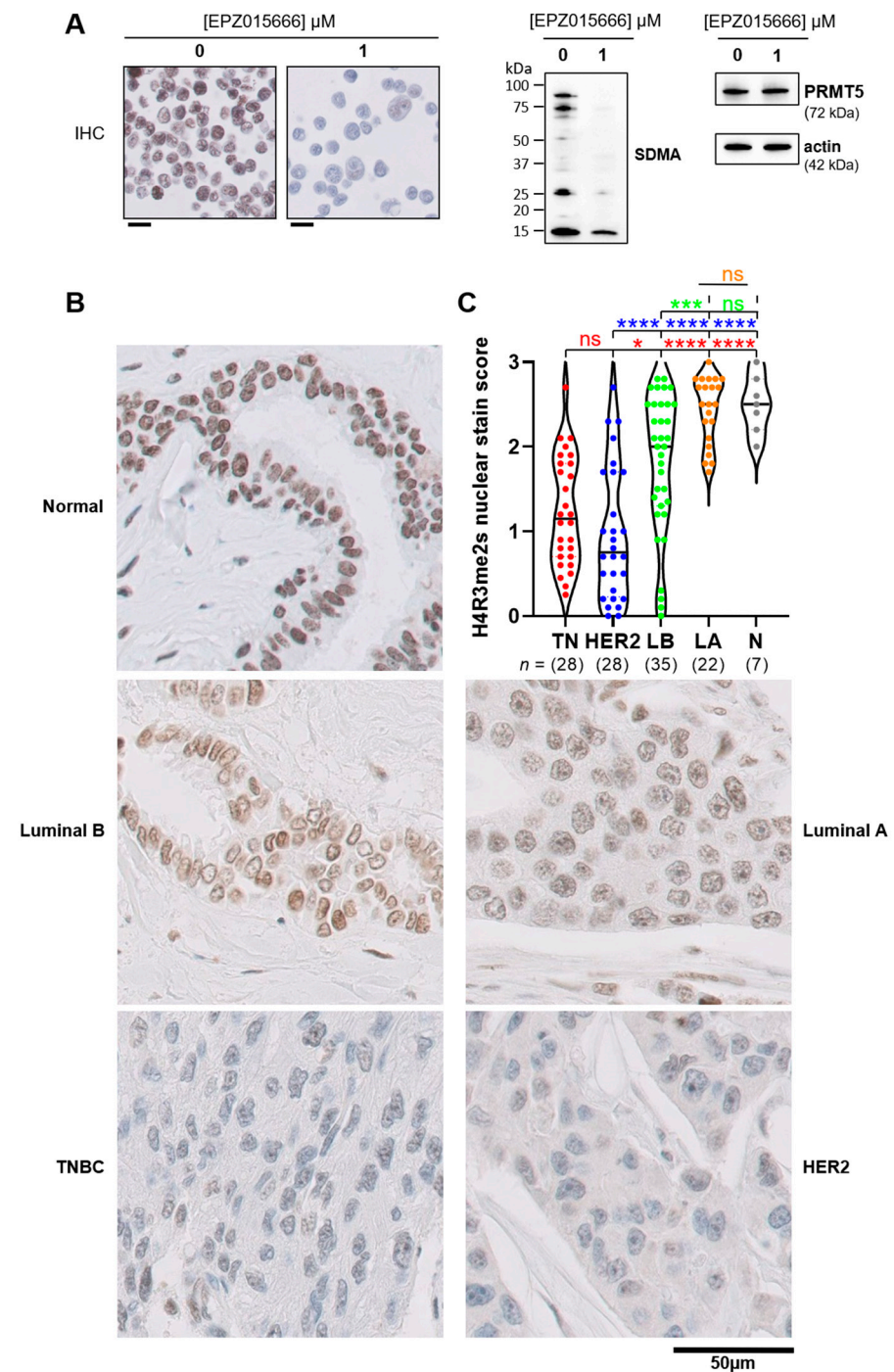


**Figure 7.** The hormone receptor-negative breast tumors express lower levels of symmetrically dimethylated histone H4 on Arginine 3 (H4R3me2s) compared to the other breast cancer subgroups and normal breast tissues. **(A)** Validation of an H4R3me2s antibody suitable for IHC staining. MDA-MB-453 cells were incubated with 1 μM of a PRMT5 inhibitor (EPZ015666) or with DMSO as a control for 48 h. Cells were pelleted, fixed with AFA, paraffin-embedded and subjected to IHC staining with an anti-H4R3me2s antibody (scale bars = 20 μm) (left panel). PRMT5 inhibition was verified by Western blotting using an anti-pan symmetric dimethyl-arginine (SDMA) antibody, and anti-PRMT5 and anti-actin antibodies were used as loading controls (right panel). The uncropped blots are shown in Figure S5. **(B)** Histone H4 is highly symmetrically dimethylated on arginine 3 in normal breast tissues.



The symmetric dimethylation of H4R3 was analyzed by IHC in the Curie cohort. A representative image of H4R3me2s staining is shown for the different breast cancer subgroups and normal breast tissue (scale bar = 50  $\mu$ m). (C). Hormone negative breast tumors (TNBC and HER2) display low levels of H4R3me2s. Nuclear H4R3me2s staining was scored by combining the percentage and the intensity of the staining of the epithelial cells (0: no staining, 3: the strongest staining). TNBC (TN, red), HER2 (blue), luminal B (LB, green), luminal A (LA, orange), and normal breast tissues (N, grey). The statistics in red indicate the comparison vs. TN, in blue vs. HER2, in green vs. LB, and in orange vs. LA: ns, (not significant); \*  $p < 0.05$ , \*\*\*  $p < 0.001$ , \*\*\*\*  $p < 0.0001$ .

Normal breast tissues and luminal A breast cancer displayed the highest scores for H4R3me2s compared to the other breast cancer tissues (Figure 7B,C). The hormone-negative tumors (TNBC and HER2) had similar scores for H4R3me2s staining which was the least compared to the other groups (Figure 7B,C). The highly heterogeneous H4R3me2s staining score is noteworthy within each analyzed group, particularly in TNBC, HER2, and luminal B subgroups (Figure 7C).

Together, our findings indicate that histone H4 is highly symmetrically dimethylated on arginine 3 in normal breast tissue. Low H4R3 dimethylation appears to be associated with the most proliferative breast cancer subgroups (TNBC and HER2).

#### 4. Discussion

*MEP50* mRNA has previously been shown to be overexpressed in breast cancer [28–30], but no study has explored its expression within the different breast cancer subgroups. In this study, we report that the highest expression of *MEP50* mRNA is found in TNBC when compared to luminal A, luminal B, and HER2 breast cancer subgroups, and to normal breast tissues.

Previous studies have shown that high *MEP50* [35] and high *PRMT5* [54] mRNA levels are associated with worse prognosis in the whole breast cancer population. However, as the different breast cancer subgroups are associated with different prognosis, it is crucial to perform survival analyses within each subgroup and not in the entire breast cancer population. Due to too few clinical events, we were not able to analyze the correlation between *MEP50* mRNA expression and survival in our cohort. Nevertheless, using the KM plotter database ([www.kmplot.com](http://www.kmplot.com)) [51], we find that high *MEP50* mRNA is associated with better RFS in TNBC and luminal B patients, with the highest statistical significance in TNBC. Using the same website, Liu and colleagues have reported that high *MEP50* mRNA is associated with a worse prognosis in the entire breast tumor population [35]. In contrast, we observed that high *MEP50* mRNA is associated with better RFS in whole breast cancer patients ( $p$ -value =  $2.9 \times 10^{-4}$ ; 201421\_s\_at probe set; Figure S6). Like *MEP50*, we found that *PRMT5* mRNA is associated with RFS only in TNBC and luminal B patients and not in the other breast cancer subgroups. This is in agreement with previous reports showing that high *PRMT5* mRNA levels are associated with worst overall survival and distant metastasis-free survival in TNBC [14,55,56]. Unexpectedly, *MEP50* and *PRMT5* mRNA levels correlate with RFS in an inverse manner, with high *PRMT5*-expressing patients harboring worse prognosis. This observation suggests that *MEP50* and *PRMT5* could have specific, independent functions, and not always work together within their well-described hetero-octameric protein complex. However, here the prognosis analysis was performed with the mRNA and not protein expression, and thus, it is also possible that *PRMT5* and *MEP50* are differentially regulated at the post-transcriptional level. Interestingly, considering the expression of both *MEP50* and *PRMT5* mRNA further stratifies patients according to their survival outcome. The *PRMT5:MEP50* mRNA ratio could therefore be a valuable prognostic marker to predict RFS in TNBC and luminal B patients.

TNBC itself is highly heterogeneous, with each TNBC subtype being associated with a different prognosis. Among the different TNBC subtypes, the mesenchymal and LAR subtypes have the highest residual cancer burden following neoadjuvant chemother-

apy [57]. Low *MEP50* mRNA is associated with worse RFS only in mesenchymal and LAR, the most chemo-resistant TNBC subtypes, suggesting that mesenchymal and LAR TNBC patients expressing low *MEP50* mRNA, could be more prone to recurrence after chemotherapy. Strikingly, high *PRMT5* mRNA is strongly associated with poor RFS in the mesenchymal subtype, which is enriched in the epithelial-to-mesenchymal transition (EMT) pathway [2–4]. The EMT pathway is implicated in invasion, tumor dissemination and drug resistance [58–61]. As *PRMT5* depletion or inhibition impairs EMT [17,28,62–64], mesenchymal TNBC may represent a niche for *PRMT5* inhibitors. When considering the *PRMT5:MEP50* mRNA expression ratio, a significant correlation is observed with poorer RFS in three subtypes: mesenchymal, LAR, and BL1. The efficacy of *PRMT5* inhibitors, alone or in combination with other drugs, in luminal B and certain TNBC subtypes with high *PRMT5:MEP50* ratio needs to be explored.

Similar to the RNA levels, TNBC express higher protein level of *MEP50* compared to normal breast tissues. *MEP50* protein localizes to the cytosol, nucleus and the plasma membrane with some notable differences between breast tumors and normal breast tissues. Normal breast tissues express higher *MEP50* (in this study) and *PRMT5* [14] compared to breast cancer at the plasma membrane. Therefore, in normal breast tissues, *PRMT5* and *MEP50* may form a complex at the plasma membrane whose physiological relevance is yet to be discovered. Breast cancer tissues express more cytosolic *MEP50* than normal breast tissue. Cytoplasmic *MEP50* is linked to proliferation in prostate cancer cells, whereas nuclear *MEP50* is associated with differentiation [37–42]. However, in our study, cytoplasmic *MEP50* appears to be a marker of breast cancer rather than being linked to proliferation, since luminal A tumors are poorly proliferative but still display high cytosolic *MEP50*. This indicates that cytoplasmic *MEP50* localization is cancer-type specific (between the different breast cancer subgroups and between breast and prostate cancers). TNBC express the least nuclear *MEP50* but it is significant only when compared to luminal tumors.

We have previously shown that TNBC express low levels of nuclear *PRMT5* compared to the other breast cancer subgroups and to normal tissues [14], suggesting a lower nuclear *PRMT5* activity in TNBC. Symmetric dimethylation of H4R3 is one of the readouts for *PRMT5* nuclear activity. We observe the highest H4R3me2s staining in the normal breast tissue and luminal A subgroup and the lowest in the most proliferative breast cancer subgroups (TNBC and HER2). Thus, high H4R3me2s is associated with good prognosis in breast cancer. This *PRMT5*-dependent histone mark is a transcriptional repressor, suggesting that it may repress a subset of genes linked to proliferation and survival of cancer cells. Further exploring the methylation status of cytosolic and other nuclear *PRMT5* substrates may help us to better understand the implication of *PRMT5* in breast cancer.

## 5. Conclusions

This comprehensive study explores the RNA and protein expression of the main *PRMT5* protein partner, *MEP50*, in the different breast cancer subgroups. High *MEP50* is found in TNBC and is associated with a better RFS in the whole TNBC population and in the LAR and mesenchymal TNBC subtypes. Distinct subcellular localization of *MEP50* is a potential marker of breast cancer. The *PRMT5*-mediated methylation of histone H4 (H4R3me2s), which is low in TNBC and HER2, is linked with the good prognosis-associated luminal A tumors.

**Supplementary Materials:** The following are available online at <https://www.mdpi.com/article/10.3390/cancers14194766/s1>, Figure S1: Correlation analyses between *MEP50* and *PRMT5* mRNA expression in the Curie cohort, Figure S2: RFS based on *MEP50* mRNA expression levels within high (above median, left panel) or low (below median, right panel) *PRMT5* mRNA expression (median cutoff) in the different breast cancer subgroups, Figure S3: *MEP50* mRNA expression levels are not associated with RFS in HER2 and luminal A breast cancers, Figure S4: *PRMT5:MEP50* mRNA ratio is not associated with RFS in BL2, IM and MSL TNBC subtypes. Figure S5: Uncropped membranes of Western blots corresponding to Figure 4A (A) and Figure 7A (B). Figure S6: High *MEP50* mRNA expression is associated with a better prognosis in all breast cancers.

**Author Contributions:** Conceptualization, S.S., M.V. and T.D.; data curation, T.D.; formal analysis, S.S., M.V. and M.Y.; funding acquisition T.D.; investigation, S.S., M.V., L.L., D.M., A.N. and T.D.; project administration, T.D.; resources, T.D.; software, M.Y.; supervision, D.M., A.N., H.F.-K. and T.D.; visualization, S.S., M.V., R.D., M.Y. and T.D.; writing—original draft, S.S., M.V. and T.D.; writing—review and editing, S.S., M.V., R.D., M.Y., L.L., D.M., A.N., H.F.-K. and T.D. All authors have read and agreed to the published version of the manuscript.

**Funding:** This work was supported by the Institut Curie and the Institut de Recherches Servier. R.D. was financed by the French Embassy and the Lebanese University (Safar Volet 1). M.V. and S.S. were funded by the European Union’s Horizon 2020 Research and Innovation Programme (Marie Skłodowska-Curie grant agreement No 666003).

**Institutional Review Board Statement:** Animal care and use for this study were performed in accordance with the recommendations of the European Community (2010/63/UE) for the care and use of laboratory animals. Experimental procedures were specifically approved by the ethics committee of the Institut Curie CEEA-IC #118 (Authorization APAFiS# 25870-2020060410487032 v1 given by National Authority) in compliance with the international guidelines.

**Informed Consent Statement:** The cohort used in this study has been previously published [14,46,48,49]. Informed consent was not required. However, women were informed of the research use of their tissues and did not declare any opposition for such research.

**Data Availability Statement:** The data presented in this study are available in this article (and Supplementary Materials).

**Acknowledgments:** We thank Yara Hajj Younes (BCBG lab, Institut Curie) and Renaud Leclere (Platform of Experimental Pathology, Institut Curie) for technical assistance. We thank Solène Huard and Ramon Garcia-Areas (BCBG lab, Institut Curie) for the critical reading of the manuscript. We are also grateful to Amber Anirah for verifying the English language of the manuscript.

**Conflicts of Interest:** The authors declare no conflict of interest.

## References

1. Loibl, S.; Poortmans, P.; Morrow, M.; Denkert, C.; Curigliano, G. Breast cancer. *Lancet* **2021**, *397*, 1750–1769. [[CrossRef](#)]
2. Lehmann, B.D.; Bauer, J.A.; Chen, X.; Sanders, M.E.; Chakravarthy, A.B.; Shyr, Y.; Pietenpol, J.A. Identification of human triple-negative breast cancer subtypes and preclinical models for selection of targeted therapies. *J. Clin. Invest.* **2011**, *121*, 2750–2767. [[CrossRef](#)] [[PubMed](#)]
3. Bou Zerdan, M.; Ghorayeb, T.; Saliba, F.; Allam, S.; Bou Zerdan, M.; Yaghi, M.; Bilani, N.; Jaafar, R.; Nahleh, Z. Triple negative breast cancer: Updates on classification and treatment in 2021. *Cancers* **2022**, *14*, 1253. [[CrossRef](#)] [[PubMed](#)]
4. Newton, E.E.; Mueller, L.E.; Treadwell, S.M.; Morris, C.A.; Machado, H.L. Molecular targets of triple-negative breast cancer: Where do we stand? *Cancers* **2022**, *14*, 482. [[CrossRef](#)] [[PubMed](#)]
5. Lehmann, B.D.; Colaprico, A.; Silva, T.C.; Chen, J.; An, H.; Ban, Y.; Huang, H.; Wang, L.; James, J.L.; Balko, J.M.; et al. Multi-omics analysis identifies therapeutic vulnerabilities in triple-negative breast cancer subtypes. *Nat. Commun.* **2021**, *12*, 6276. [[CrossRef](#)]
6. Bianchini, G.; De Angelis, C.; Licata, L.; Gianni, L. Treatment landscape of triple-negative breast cancer—Expanded options, evolving needs. *Nat. Rev. Clin. Oncol.* **2022**, *19*, 91–113. [[CrossRef](#)]
7. Xu, J.; Richard, S. Cellular pathways influenced by protein arginine methylation: Implications for cancer. *Mol. Cell* **2021**, *81*, 4357–4368. [[CrossRef](#)]
8. Jarrold, J.; Davies, C.C. PRMTs and arginine methylation: Cancer’s best-kept secret? *Trends Mol. Med.* **2019**, *25*, 993–1009. [[CrossRef](#)]
9. Wu, Q.; Schapira, M.; Arrowsmith, C.H.; Barsyte-Lovejoy, D. Protein arginine methylation: From enigmatic functions to therapeutic targeting. *Nat. Rev. Drug Discov.* **2021**, *20*, 509–530. [[CrossRef](#)]
10. Yang, Y.; Bedford, M.T. Protein arginine methyltransferases and cancer. *Nat. Rev. Cancer* **2013**, *13*, 37–50. [[CrossRef](#)]
11. Guccione, E.; Richard, S. The regulation, functions and clinical relevance of arginine methylation. *Nat. Rev. Mol. Cell Biol.* **2019**, *20*, 642–657. [[CrossRef](#)] [[PubMed](#)]
12. Suresh, S.; Huard, S.; Dubois, T. CARM1/PRMT4: Making its mark beyond its function as a transcriptional coactivator. *Trends Cell Biol.* **2021**, *31*, 402–417. [[CrossRef](#)]
13. Suresh, S.; Huard, S.; Brisson, A.; Nemati, F.; Dakroub, R.; Poulard, C.; Ye, M.; Martel, E.; Reyes, C.; Silvestre, D.C.; et al. PRMT1 regulates EGFR and Wnt signaling pathways and is a promising target for combinatorial treatment of breast cancer. *Cancers* **2022**, *14*, 306. [[CrossRef](#)] [[PubMed](#)]

14. Vinet, M.; Suresh, S.; Maire, V.; Monchecourt, C.; Nemati, F.; Lesage, L.; Pierre, F.; Ye, M.; Lescure, A.; Brisson, A.; et al. Protein arginine methyltransferase 5: A novel therapeutic target for triple-negative breast cancers. *Cancer Med.* **2019**, *8*, 2414–2428. [[CrossRef](#)]
15. Kaniskan, H.U.; Jin, J. Recent progress in developing selective inhibitors of protein methyltransferases. *Curr. Opin. Chem. Biol.* **2017**, *39*, 100–108. [[CrossRef](#)] [[PubMed](#)]
16. Motolani, A.; Martin, M.; Sun, M.; Lu, T. The structure and functions of PRMT5 in human diseases. *Life* **2021**, *11*, 1074. [[CrossRef](#)] [[PubMed](#)]
17. Stopa, N.; Krebs, J.E.; Shechter, D. The PRMT5 arginine methyltransferase: Many roles in development, cancer and beyond. *Cell Mol. Life Sci.* **2015**, *72*, 2041–2059. [[CrossRef](#)]
18. Shailesh, H.; Zakaria, Z.Z.; Baiocchi, R.; Sif, S. Protein arginine methyltransferase 5 (PRMT5) dysregulation in cancer. *Oncotarget* **2018**, *9*, 36705–36718. [[CrossRef](#)]
19. Tee, W.W.; Pardo, M.; Theunissen, T.W.; Yu, L.; Choudhary, J.S.; Hajkova, P.; Surani, M.A. Prmt5 is essential for early mouse development and acts in the cytoplasm to maintain ES cell pluripotency. *Genes Dev.* **2010**, *24*, 2772–2777. [[CrossRef](#)]
20. Zhao, Q.; Rank, G.; Tan, Y.T.; Li, H.; Moritz, R.L.; Simpson, R.J.; Cerruti, L.; Curtis, D.J.; Patel, D.J.; Allis, C.D.; et al. PRMT5-mediated methylation of histone H4R3 recruits DNMT3A, coupling histone and DNA methylation in gene silencing. *Nat. Struct. Mol. Biol.* **2009**, *16*, 304–311. [[CrossRef](#)]
21. Majumder, S.; Alinari, L.; Roy, S.; Miller, T.; Datta, J.; Sif, S.; Baiocchi, R.; Jacob, S.T. Methylation of histone H3 and H4 by PRMT5 regulates ribosomal RNA gene transcription. *J. Cell Biochem.* **2010**, *109*, 553–563. [[CrossRef](#)] [[PubMed](#)]
22. Pal, S.; Vishwanath, S.N.; Erdjument-Bromage, H.; Tempst, P.; Sif, S. Human SWI/SNF-associated PRMT5 methylates histone H3 arginine 8 and negatively regulates expression of ST7 and NM23 tumor suppressor genes. *Mol. Cell Biol.* **2004**, *24*, 9630–9645. [[CrossRef](#)]
23. Friesen, W.J.; Wyce, A.; Paushkin, S.; Abel, L.; Rappsilber, J.; Mann, M.; Dreyfuss, G. A novel WD repeat protein component of the methylosome binds Sm proteins. *J. Biol. Chem.* **2002**, *277*, 8243–8247. [[CrossRef](#)] [[PubMed](#)]
24. Hosohata, K.; Li, P.; Hosohata, Y.; Qin, J.; Roeder, R.G.; Wang, Z. Purification and identification of a novel complex which is involved in androgen receptor-dependent transcription. *Mol. Cell Biol.* **2003**, *23*, 7019–7029. [[CrossRef](#)] [[PubMed](#)]
25. Antonysamy, S.; Bonday, Z.; Campbell, R.M.; Doyle, B.; Druzina, Z.; Gheyi, T.; Han, B.; Jungheim, L.N.; Qian, Y.; Rauch, C.; et al. Crystal structure of the human PRMT5:MEP50 complex. *Proc. Natl. Acad. Sci. USA* **2012**, *109*, 17960–17965. [[CrossRef](#)] [[PubMed](#)]
26. Ho, M.C.; Wilczek, C.; Bonanno, J.B.; Xing, L.; Seznec, J.; Matsui, T.; Carter, L.G.; Onikubo, T.; Kumar, P.R.; Chan, M.K.; et al. Structure of the arginine methyltransferase PRMT5-MEP50 reveals a mechanism for substrate specificity. *PLoS ONE* **2013**, *8*, e57008. [[CrossRef](#)]
27. Burgos, E.S.; Wilczek, C.; Onikubo, T.; Bonanno, J.B.; Jansong, J.; Reimer, U.; Shechter, D. Histone H2A and H4 N-terminal tails are positioned by the MEP50 WD repeat protein for efficient methylation by the PRMT5 arginine methyltransferase. *J. Biol. Chem.* **2015**, *290*, 9674–9689. [[CrossRef](#)]
28. Chen, H.; Lorton, B.; Gupta, V.; Shechter, D. A TGFbeta-PRMT5-MEP50 axis regulates cancer cell invasion through histone H3 and H4 arginine methylation coupled transcriptional activation and repression. *Oncogene* **2017**, *36*, 373–386. [[CrossRef](#)]
29. Rengasamy, M.; Zhang, F.; Vashisht, A.; Song, W.M.; Aguilo, F.; Sun, Y.; Li, S.; Zhang, W.; Zhang, B.; Wohlschlegel, J.A.; et al. The PRMT5/WDR77 complex regulates alternative splicing through ZNF326 in breast cancer. *Nucleic Acids Res.* **2017**, *45*, 11106–11120. [[CrossRef](#)]
30. Abe, Y.; Suzuki, Y.; Kawamura, K.; Tanaka, N. MEP50/PRMT5-mediated methylation activates GLI1 in Hedgehog signalling through inhibition of ubiquitination by the ITCH/NUMB complex. *Commun. Biol.* **2019**, *2*, 23. [[CrossRef](#)]
31. Ligr, M.; Patwa, R.R.; Daniels, G.; Pan, L.; Wu, X.; Li, Y.; Tian, L.; Wang, Z.; Xu, R.; Wu, J.; et al. Expression and function of androgen receptor coactivator p44/Mep50/WDR77 in ovarian cancer. *PLoS ONE* **2011**, *6*, e26250. [[CrossRef](#)]
32. Yi, P.; Gao, S.; Gu, Z.; Huang, T.; Wang, Z. P44/WDR77 restricts the sensitivity of proliferating cells to TGFbeta signaling. *Biochem. Biophys. Res. Commun.* **2014**, *450*, 409–415. [[CrossRef](#)] [[PubMed](#)]
33. Saha, K.; Fisher, M.L.; Adhikary, G.; Grun, D.; Eckert, R.L. Sulforaphane suppresses PRMT5/MEP50 function in epidermal squamous cell carcinoma leading to reduced tumor formation. *Carcinogenesis* **2017**, *38*, 827–836. [[CrossRef](#)] [[PubMed](#)]
34. Zhao, Y.; Yu, T.; Sun, J.; Wang, F.; Cheng, C.; He, S.; Chen, L.; Xie, D.; Fu, L.; Guan, X.; et al. Germ-line mutations in WDR77 predispose to familial papillary thyroid cancer. *Proc. Natl. Acad. Sci. USA* **2021**, *118*, e2026327118. [[CrossRef](#)] [[PubMed](#)]
35. Liu, R.; Gao, J.; Yang, Y.; Qiu, R.; Zheng, Y.; Huang, W.; Zeng, Y.; Hou, Y.; Wang, S.; Leng, S.; et al. PHD finger protein 1 (PHF1) is a novel reader for histone H4R3 symmetric dimethylation and coordinates with PRMT5-WDR77/CRL4B complex to promote tumorigenesis. *Nucleic Acids Res.* **2018**, *46*, 6608–6626. [[CrossRef](#)]
36. Peng, Y.; Li, Y.; Gellert, L.L.; Zou, X.; Wang, J.; Singh, B.; Xu, R.; Chiriboga, L.; Daniels, G.; Pan, R.; et al. Androgen receptor coactivator p44/Mep50 in breast cancer growth and invasion. *J. Cell Mol. Med.* **2010**, *14*, 2780–2789. [[CrossRef](#)]
37. Zhou, L.; Hosohata, K.; Gao, S.; Gu, Z.; Wang, Z. cGMP-dependent protein kinase Ibeta interacts with p44/WDR77 to regulate androgen receptor-driven gene expression. *PLoS ONE* **2014**, *8*, e63119. [[CrossRef](#)]
38. Gu, Z.; Zhou, L.; Gao, S.; Wang, Z. Nuclear transport signals control cellular localization and function of androgen receptor cofactor p44/WDR77. *PLoS ONE* **2011**, *6*, e22395. [[CrossRef](#)]



39. Peng, Y.; Chen, F.; Melamed, J.; Chiriboga, L.; Wei, J.; Kong, X.; McLeod, M.; Li, Y.; Li, C.X.; Feng, A.; et al. Distinct nuclear and cytoplasmic functions of androgen receptor cofactor p44 and association with androgen-independent prostate cancer. *Proc. Natl. Acad. Sci. USA* **2008**, *105*, 5236–5241. [[CrossRef](#)]
40. O'Bryant, D.; Wang, Z. The essential role of WD repeat domain 77 in prostate tumor initiation induced by Pten loss. *Oncogene* **2018**, *37*, 4151–4163. [[CrossRef](#)]
41. Zhou, L.; Wu, H.; Lee, P.; Wang, Z. Roles of the androgen receptor cofactor p44 in the growth of prostate epithelial cells. *J. Mol. Endocrinol.* **2006**, *37*, 283–300. [[CrossRef](#)] [[PubMed](#)]
42. Gao, S.; Wang, Z. Subcellular localization of p44/WDR77 determines proliferation and differentiation of prostate epithelial cells. *PLoS ONE* **2012**, *7*, e49173. [[CrossRef](#)] [[PubMed](#)]
43. Saha, K.; Eckert, R.L. Methylosome protein 50 and PKCdelta/p38delta protein signaling control keratinocyte proliferation via opposing effects on p21Cip1 gene expression. *J. Biol. Chem.* **2015**, *290*, 13521–13530. [[CrossRef](#)]
44. Wei, T.Y.; Hsia, J.Y.; Chiu, S.C.; Su, L.J.; Juan, C.C.; Lee, Y.C.; Chen, J.M.; Chou, H.Y.; Huang, J.Y.; Huang, H.M.; et al. Methylosome protein 50 promotes androgen- and estrogen-independent tumorigenesis. *Cell Signal.* **2014**, *26*, 2940–2950. [[CrossRef](#)]
45. Owens, J.L.; Beketova, E.; Liu, S.; Shen, Q.; Pawar, J.S.; Asberry, A.M.; Yang, J.; Deng, X.; Elzey, B.D.; Ratliff, T.L.; et al. Targeting protein arginine methyltransferase 5 suppresses radiation-induced neuroendocrine differentiation and sensitizes prostate cancer cells to radiation. *Mol. Cancer Ther.* **2022**, *21*, 448–459. [[CrossRef](#)] [[PubMed](#)]
46. Maire, V.; Baldeyron, C.; Richardson, M.; Tesson, B.; Vincent-Salomon, A.; Gravier, E.; Marty-Prouvost, B.; De Koning, L.; Rigai, G.; Dumont, A.; et al. TTK/hMPS1 is an attractive therapeutic target for triple-negative breast cancer. *PLoS ONE* **2013**, *8*, e63712. [[CrossRef](#)] [[PubMed](#)]
47. Maire, V.; Mahmood, F.; Rigai, G.; Ye, M.; Brisson, A.; Nemati, F.; Gentien, D.; Tucker, G.C.; Roman-Roman, S.; Dubois, T. LRP8 is overexpressed in estrogen-negative breast cancers and a potential target for these tumors. *Cancer Med.* **2019**, *8*, 325–336. [[CrossRef](#)] [[PubMed](#)]
48. Maire, V.; Nemati, F.; Richardson, M.; Vincent-Salomon, A.; Tesson, B.; Rigai, G.; Gravier, E.; Marty-Prouvost, B.; De Koning, L.; Lang, G.; et al. Polo-like kinase 1: A potential therapeutic option in combination with conventional chemotherapy for the management of patients with triple-negative breast cancer. *Cancer Res.* **2013**, *73*, 813–823. [[CrossRef](#)]
49. Maubant, S.; Tahtouh, T.; Brisson, A.; Maire, V.; Nemati, F.; Tesson, B.; Ye, M.; Rigai, G.; Noizet, M.; Dumont, A.; et al. LRP5 regulates the expression of STK40, a new potential target in triple-negative breast cancers. *Oncotarget* **2018**, *9*, 22586–22604. [[CrossRef](#)]
50. The Cancer Genome Atlas Network. Comprehensive molecular portraits of human breast tumours. *Nature* **2012**, *490*, 61–70. [[CrossRef](#)]
51. Gyorffy, B. Survival analysis across the entire transcriptome identifies biomarkers with the highest prognostic power in breast cancer. *Comput. Struct. Biotechnol. J.* **2021**, *19*, 4101–4109. [[CrossRef](#)] [[PubMed](#)]
52. Baldeyron, C.; Brisson, A.; Tesson, B.; Nemati, F.; Koundrioukoff, S.; Saliba, E.; De Koning, L.; Martel, E.; Ye, M.; Rigai, G.; et al. TIPIN depletion leads to apoptosis in breast cancer cells. *Mol. Oncol.* **2015**, *9*, 1580–1598. [[CrossRef](#)] [[PubMed](#)]
53. Zajac, O.; Leclere, R.; Nicolas, A.; Meseure, D.; Marchio, C.; Vincent-Salomon, A.; Roman-Roman, S.; Schoumacher, M.; Dubois, T. AXL controls directed migration of mesenchymal triple-negative breast cancer cells. *Cells* **2020**, *9*, 247. [[CrossRef](#)] [[PubMed](#)]
54. Lattouf, H.; Poulard, C.; Le Romancer, M. PRMT5 prognostic value in cancer. *Oncotarget* **2019**, *10*, 3151–3153. [[CrossRef](#)] [[PubMed](#)]
55. Zhou, Z.; Feng, Z.; Hu, D.; Yang, P.; Gur, M.; Bahar, I.; Cristofanilli, M.; Gradishar, W.J.; Xie, X.Q.; Wan, Y. A novel small-molecule antagonizes PRMT5-mediated KLF4 methylation for targeted therapy. *EBioMedicine* **2019**, *44*, 98–111. [[CrossRef](#)]
56. Wu, Y.; Wang, Z.; Zhang, J.; Ling, R. Elevated expression of protein arginine methyltransferase 5 predicts the poor prognosis of breast cancer. *Tumor Biol.* **2017**, *39*, 1010428317695917. [[CrossRef](#)]
57. Echavarría, I.; Lopez-Tarruella, S.; Picornell, A.; Garcia-Saenz, J.A.; Jerez, Y.; Hoadley, K.; Gomez, H.L.; Moreno, F.; Monte-Millan, M.D.; Marquez-Rodas, I.; et al. Pathological response in a triple-negative breast cancer cohort treated with neoadjuvant carboplatin and docetaxel according to Lehmann's refined classification. *Clin. Cancer Res.* **2018**, *24*, 1845–1852. [[CrossRef](#)]
58. Gooding, A.J.; Schiemann, W.P. Epithelial-mesenchymal transition programs and cancer stem cell phenotypes: Mediators of breast cancer therapy resistance. *Mol. Cancer Res.* **2020**, *18*, 1257–1270. [[CrossRef](#)]
59. Dudas, J.; Ladanyi, A.; Ingruber, J.; Steinbichler, T.B.; Riechelmann, H. Epithelial to mesenchymal transition: A mechanism that fuels cancer radio/chemoresistance. *Cells* **2020**, *9*, 428. [[CrossRef](#)]
60. Lu, W.; Kang, Y. Epithelial-mesenchymal plasticity in cancer progression and metastasis. *Dev. Cell* **2019**, *49*, 361–374. [[CrossRef](#)]
61. Voon, D.C.; Huang, R.Y.; Jackson, R.A.; Thiery, J.P. The EMT spectrum and therapeutic opportunities. *Mol. Oncol.* **2017**, *11*, 878–891. [[CrossRef](#)] [[PubMed](#)]
62. Gao, J.; Liu, R.; Feng, D.; Huang, W.; Huo, M.; Zhang, J.; Leng, S.; Yang, Y.; Yang, T.; Yin, X.; et al. Snail/PRMT5/NuRD complex contributes to DNA hypermethylation in cervical cancer by TET1 inhibition. *Cell Death Differ.* **2021**, *28*, 2818–2836. [[CrossRef](#)] [[PubMed](#)]
63. Wang, N.; Yan, H.; Wu, D.; Zhao, Z.; Chen, X.; Long, Q.; Zhang, C.; Wang, X.; Deng, W.; Liu, X. PRMT5/Wnt4 axis promotes lymph-node metastasis and proliferation of laryngeal carcinoma. *Cell Death Dis.* **2020**, *11*, 864. [[CrossRef](#)] [[PubMed](#)]
64. Huang, L.; Zhang, X.O.; Rozen, E.J.; Sun, X.; Sallis, B.; Verdejo-Torres, O.; Wigglesworth, K.; Moon, D.; Huang, T.; Cavaretta, J.P.; et al. PRMT5 activates AKT via methylation to promote tumor metastasis. *Nat. Commun.* **2022**, *13*, 3955. [[CrossRef](#)] [[PubMed](#)]

## **Supplementary information for**

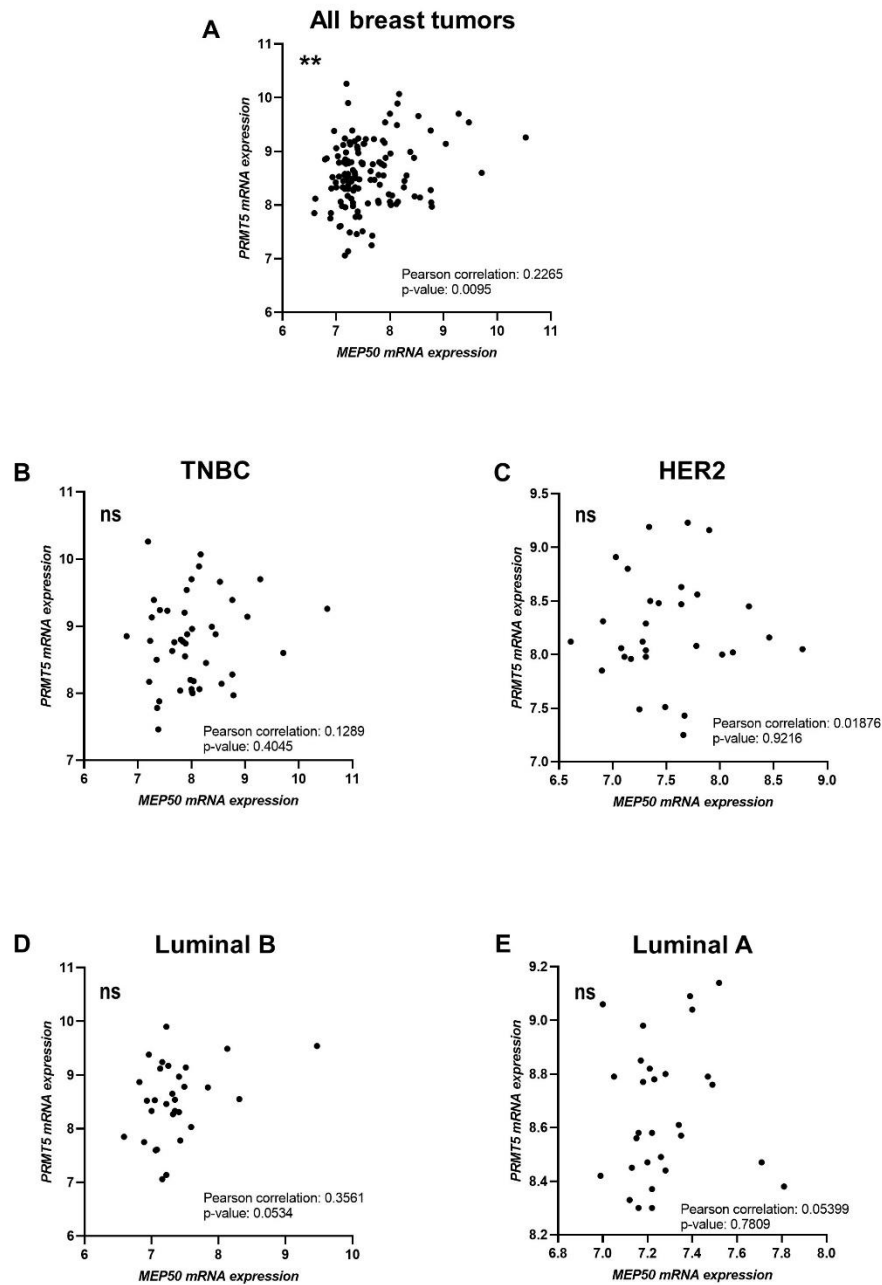
### **Expression, localization and prognosis-association of MEP50 in breast cancer**

Samyuktha Suresh, Mathilde Vinet, Rayan Dakroub, Laetitia Lesage, Mengliang Ye,  
Hussein Fayyad-Kazan, André Nicolas, Didier Meseure, and Thierry Dubois

Correspondence to: [thierry.dubois@curie.fr](mailto:thierry.dubois@curie.fr)

#### **This PDF file includes:**

Supplementary Figures S1 to S6



**Supplementary Figure S1.** Correlation analyses between *MEP50* and *PRMT5* mRNA expression in the Curie cohort. Pearson correlation between the *MEP50* and *PRMT5* mRNA was performed in the curie cohort in the whole breast cancer population (A), TNBC (B), HER2 (C), luminal B (D), and luminal A (E). ns (not significant), \*\*  $p < 0.01$ .

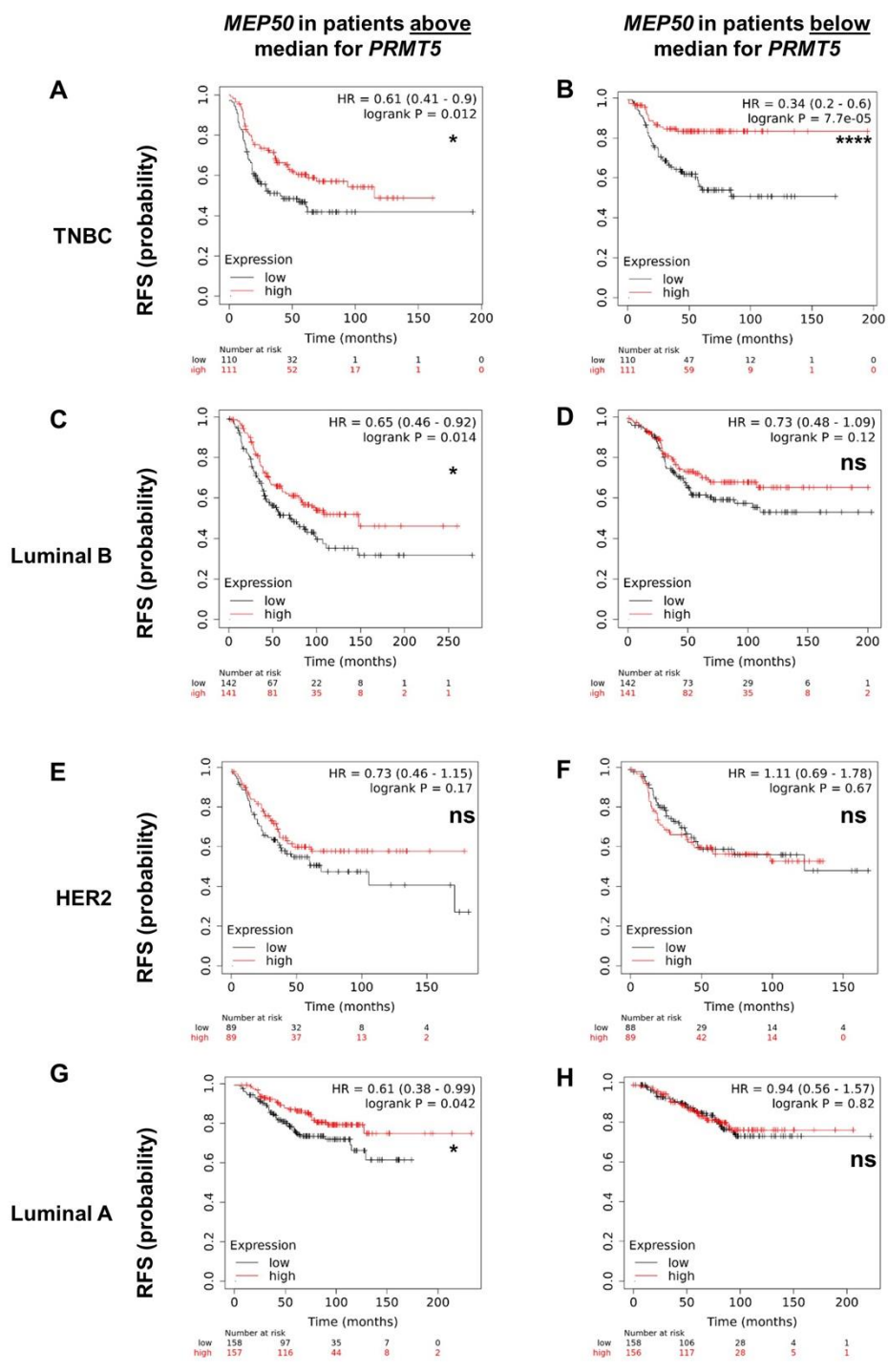


Figure S2



**Supplemental Figure S2.** RFS based on *MEP50* mRNA expression levels within high (above median, left panel) or low (below median, right panel) *PRMT5* mRNA expression (median cutoff) in the different breast cancer subgroups. Data were obtained from the Kaplan-Meier (KM) plotter website (<http://kmplot.com>) for TNBC (A, B), luminal B (C, D), HER2 (E, F), and luminal A (G, H). Luminal B, HER2, luminal A and Basal (for TNBC) breast cancer subgroups were obtained using the PAM50 classification setting. Median cutoff option was used. The obtained Hazard Ratio (HR) with 95% confidence interval and log-rank p-values are shown. ns (not significant), \*p<0.05, \*\*\*\*p<0.0001.

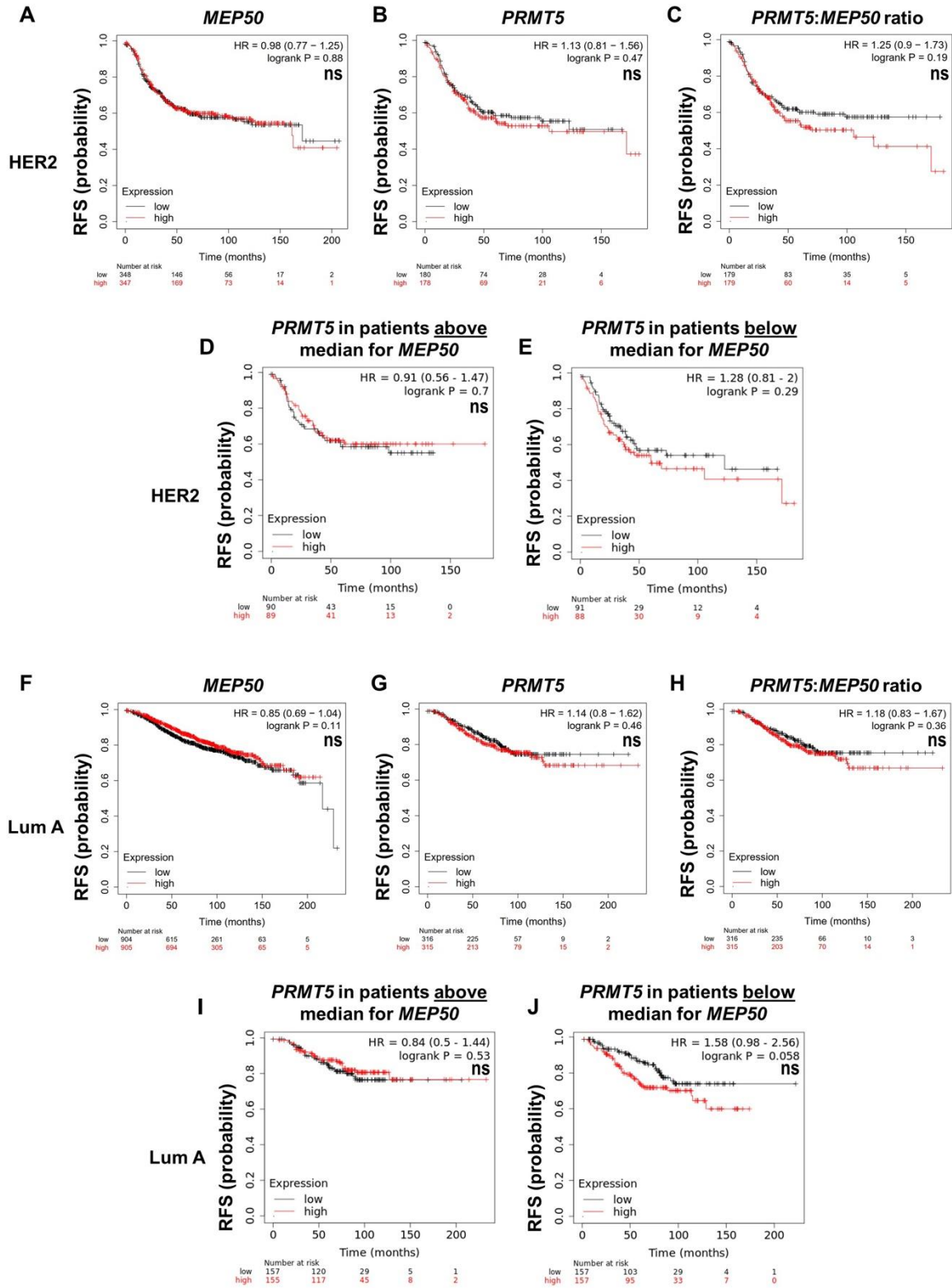
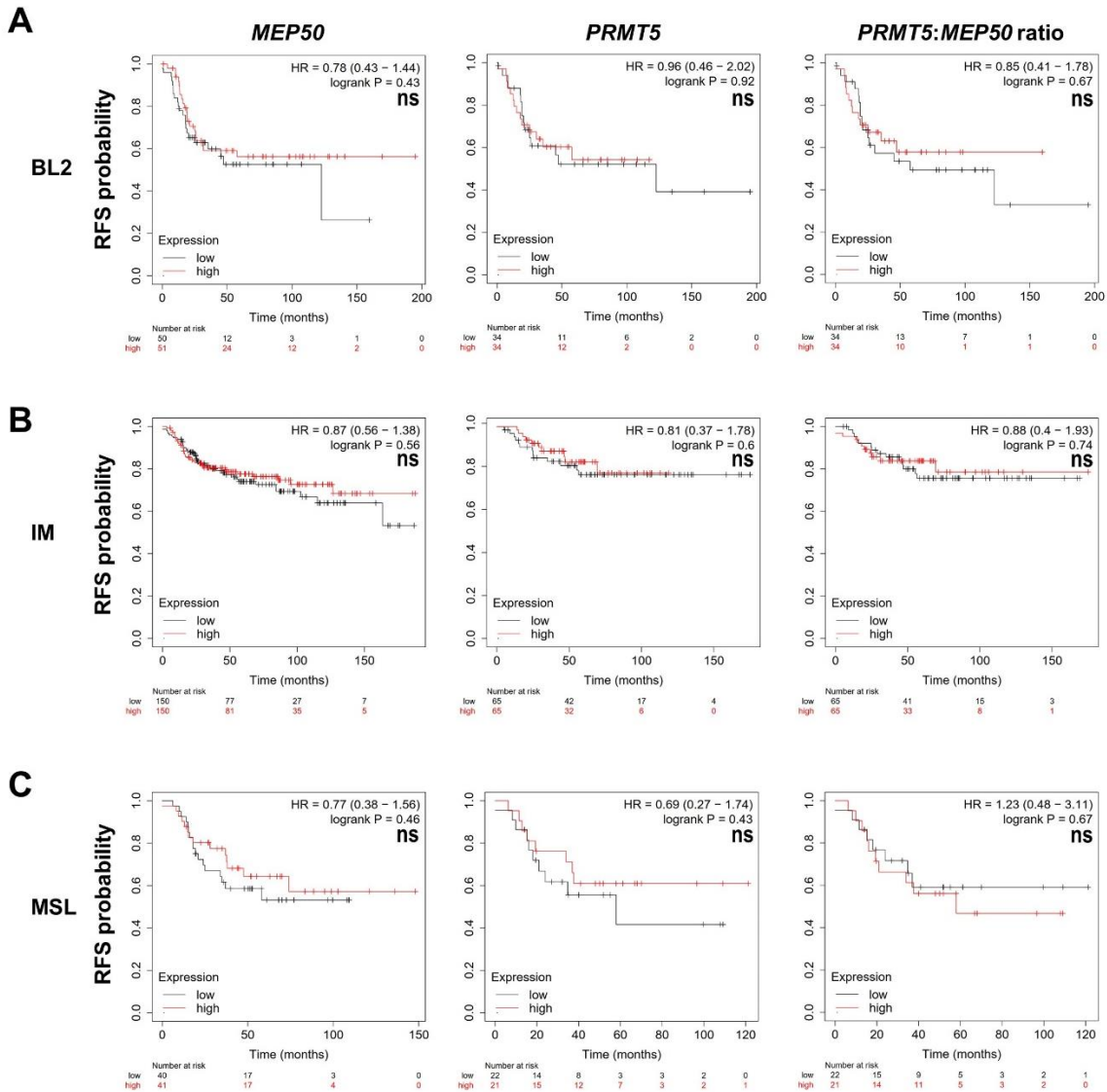
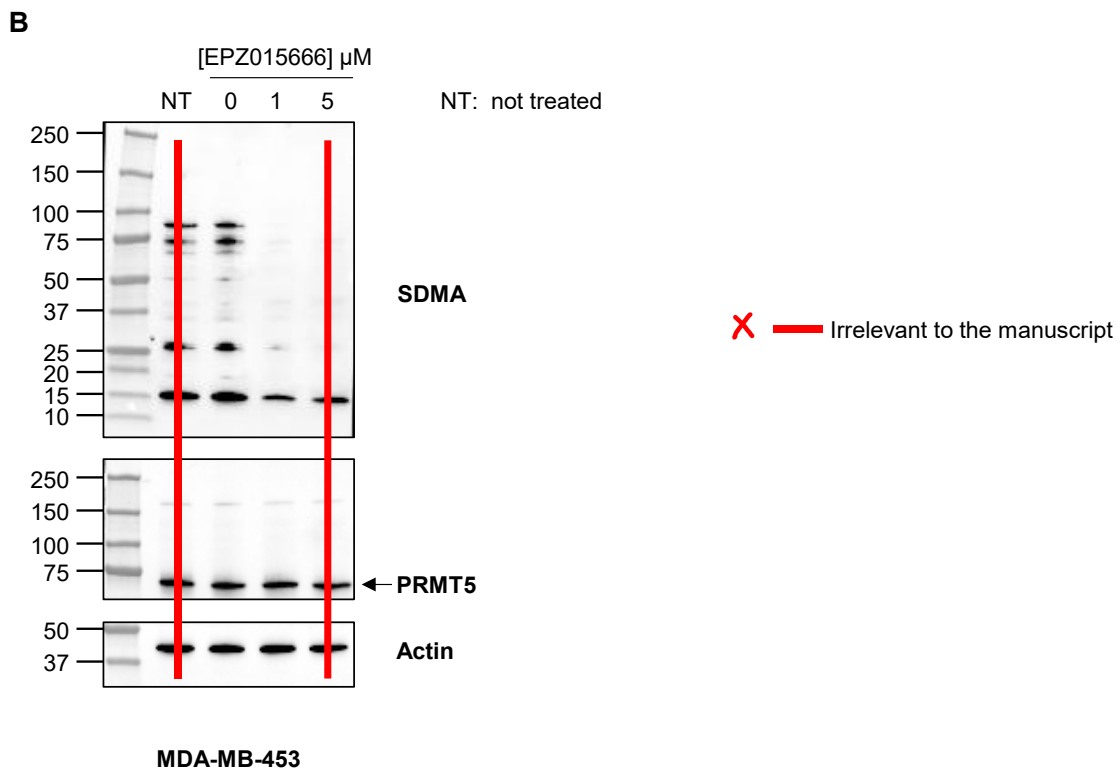
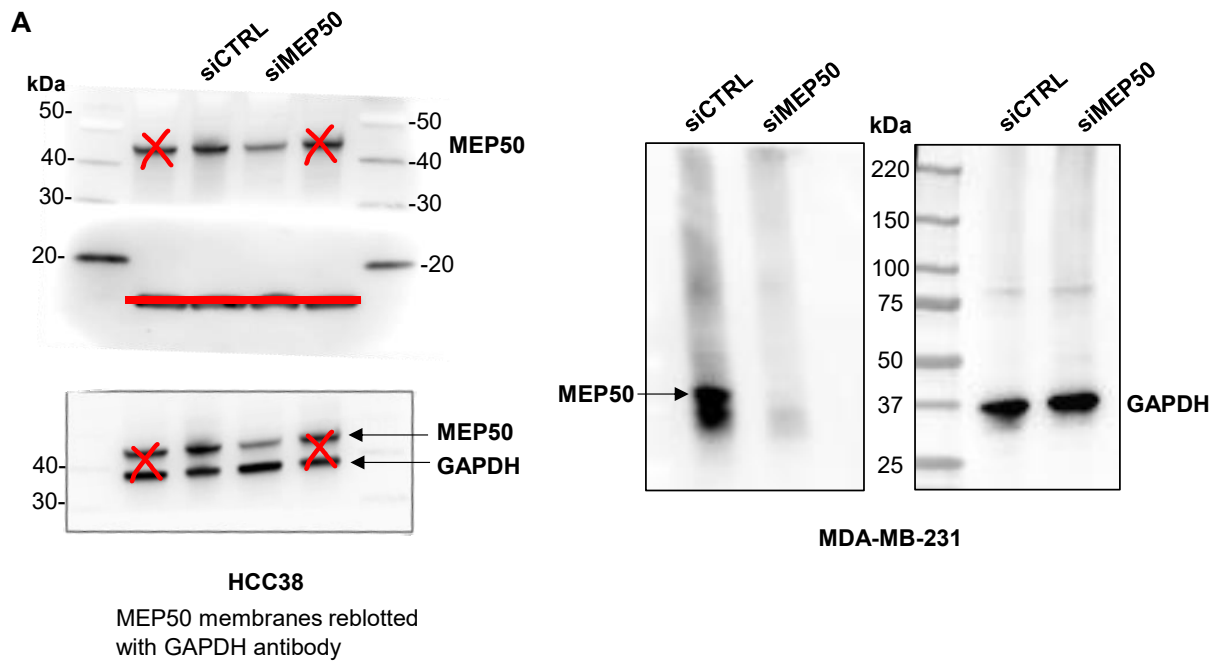


Figure S3

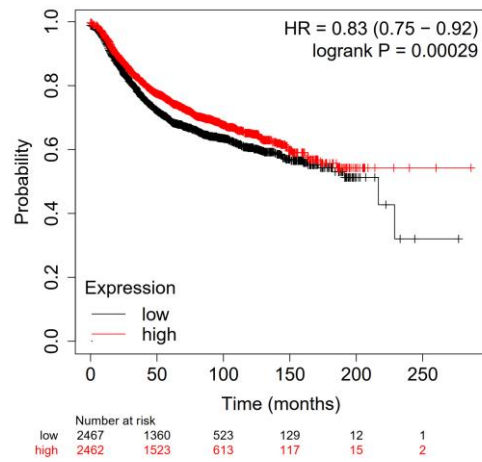
**Supplemental Figure S3.** *MEP50* mRNA expression levels are not associated with RFS in HER2 and luminal A breast cancers. **A-C, F-G.** RFS based on *MEP50* mRNA, *PRMT5* mRNA expression or *PRMT5:MEP50* mRNA ratio were obtained from the Kaplan-Meier (KM) plotter website (<http://kmplot.com>) for HER2 (A, B, C) and luminal A (Lum A; F,G,H). **D,E,I,J.** RFS based on *PRMT5* mRNA expression within patients having either high (above median, left panel) or low (below median, right panel) *MEP50* mRNA expression (median cutoff). Data were obtained from the Kaplan-Meier (KM) plotter website (<http://kmplot.com>) for HER2 (D, E) and luminal A (Lum A; I, J). Of note, more patients were retrieved with *MEP50* probe set compared to the *PRMT5* probe set (see *Materials and Methods* section). The obtained Hazard Ratio (HR) with 95% confidence interval and log-rank p-values are shown. ns (not significant).



**Supplemental Figure S4.** *PRMT5:MEP50* mRNA ratio is not associated with RFS in BL2, IM and MSL TNBC subtypes. **A, B, C.** RFS based on *MEP50* or *PRMT5* mRNA expression or *PRMT5:MEP50* mRNA ratio were obtained from the Kaplan-Meier (KM) plotter website (<http://kmplot.com>) for basal-like 2 (BL2; A), immunomodulatory (IM; B) and mesenchymal stem-like (MSL; C) TNBC subtypes. Of note, more patients were retrieved with *MEP50* probe set compared to the *PRMT5* probe set (see *Materials and Methods* section). The obtained Hazard Ratio (HR) with 95% confidence interval and log-rank p-values are shown. ns (not significant).







**Supplemental Figure S5.** Uncropped membranes of western blots corresponding to Figure 4 (A) and Figure 7A (B). Red crosses and dashes are irrelevant to the manuscript.



**Supplemental Figure S6.** High *MEP50* mRNA expression is associated with a better prognosis in all breast cancers. Recurrence-free survival (RFS) based on *MEP50* mRNA expression was obtained from the Kaplan-Meier (KM) plotter website (<http://kmplot.com>) for breast cancers, including all subgroups of breast cancer. The obtained Hazard Ratio (HR) with 95% confidence interval and log-rank p-values are shown.

## Article

# PRMT1 Regulates EGFR and Wnt Signaling Pathways and Is a Promising Target for Combinatorial Treatment of Breast Cancer

Samyuktha Suresh <sup>1</sup>, Solène Huard <sup>1</sup>, Amélie Brisson <sup>1</sup>, Fariba Némati <sup>2</sup>, Rayan Dakroub <sup>1,3</sup>, Coralie Poulard <sup>4</sup>, Mengliang Ye <sup>1</sup>, Elise Martel <sup>5</sup>, Cécile Reyes <sup>6</sup>, David C. Silvestre <sup>1</sup>, Didier Meseure <sup>5</sup>, André Nicolas <sup>5</sup>, David Gentien <sup>6</sup>, Hussein Fayyad-Kazan <sup>3</sup>, Muriel Le Romancer <sup>4</sup>, Didier Decaudin <sup>2</sup>, Sergio Roman-Roman <sup>7</sup> and Thierry Dubois <sup>1,\*</sup>

- <sup>1</sup> Breast Cancer Biology Group, Translational Research Department, Institut Curie-PSL Research University, 75005 Paris, France; samyuktha.suresh@curie.fr (S.S.); solene.huard@curie.fr (S.H.); brisson.amelie@wanadoo.fr (A.B.); rayan.dakroub@curie.fr (R.D.); mengliang.ye@curie.fr (M.Y.); davidcsilvestre@gmail.com (D.C.S.)
- <sup>2</sup> Pre-Clinical Investigation Laboratory, Translational Research Department, Institut Curie-PSL Research University, 75005 Paris, France; fariba.nemati@curie.fr (F.N.); didier.decaudin@curie.fr (D.D.)
- <sup>3</sup> Laboratory of Cancer Biology and Molecular Immunology, Faculty of Sciences-I, Lebanese University, Hadath, Beirut 1003, Lebanon; hussein.kazan@ul.edu.lb
- <sup>4</sup> Cancer Research Center of Lyon, CNRS UMR5286, Inserm U1052, University of Lyon, 69000 Lyon, France; coralie.poulard@lyon.unicancer.fr (C.P.); muriel.leromancer-cherifi@lyon.unicancer.fr (M.L.R.)
- <sup>5</sup> Platform of Experimental Pathology, Department of Diagnostic and Theranostic Medicine, Institut Curie-Hospital, 75005 Paris, France; elise.martel@curie.fr (E.M.); didier.meseure@curie.fr (D.M.); andre.nicolas@curie.fr (A.N.)
- <sup>6</sup> Genomics Core Facility, Translational Research Department, Institut Curie-PSL Research University, 75005 Paris, France; cecile.reyes@curie.fr (C.R.); david.gentien@curie.fr (D.G.)
- <sup>7</sup> Translational Research Department, Institut Curie-PSL Research University, 75005 Paris, France; sergio.roman-roman@curie.fr
- \* Correspondence: thierry.dubois@curie.fr; Tel.: +33-1-56246250



**Citation:** Suresh, S.; Huard, S.; Brisson, A.; Némati, F.; Dakroub, R.; Poulard, C.; Ye, M.; Martel, E.; Reyes, C.; Silvestre, D.C.; et al. PRMT1 Regulates EGFR and Wnt Signaling Pathways and Is a Promising Target for Combinatorial Treatment of Breast Cancer. *Cancers* **2022**, *14*, 306. <https://doi.org/10.3390/cancers14020306>

Academic Editor: Ana Isabel Fraguas-Sánchez

Received: 13 December 2021

Accepted: 6 January 2022

Published: 8 January 2022

**Publisher's Note:** MDPI stays neutral with regard to jurisdictional claims in published maps and institutional affiliations.



**Copyright:** © 2022 by the authors. Licensee MDPI, Basel, Switzerland. This article is an open access article distributed under the terms and conditions of the Creative Commons Attribution (CC BY) license (<https://creativecommons.org/licenses/by/4.0/>).

**Simple Summary:** Patients with triple-negative breast cancer (TNBC) respond well to chemotherapy initially but are prone to relapse. Searching for new therapeutic targets, we found that PRMT1 is highly expressed in TNBC tumor samples and is essential for breast cancer cell survival. Furthermore, this study proposes that targeting PRMT1 in combination with chemotherapies could improve the survival outcome of TNBC patients.

**Abstract:** Identifying new therapeutic strategies for triple-negative breast cancer (TNBC) patients is a priority as these patients are highly prone to relapse after chemotherapy. Here, we found that protein arginine methyltransferase 1 (PRMT1) is highly expressed in all breast cancer subtypes. PRMT1 depletion decreases cell survival by inducing DNA damage and apoptosis in various breast cancer cell lines. Transcriptomic analysis and chromatin immunoprecipitation revealed that PRMT1 regulates the epidermal growth factor receptor (EGFR) and the Wnt signaling pathways, reported to be activated in TNBC. PRMT1 enzymatic activity is also required to stimulate the canonical Wnt pathway. Type I PRMT inhibitors decrease breast cancer cell proliferation and show anti-tumor activity in a TNBC xenograft model. These inhibitors display synergistic interactions with some chemotherapies used to treat TNBC patients as well as erlotinib, an EGFR inhibitor. Therefore, targeting PRMT1 in combination with these chemotherapies may improve existing treatments for TNBC patients.

**Keywords:** breast cancer; EGFR; PRMT1; drug combinations; Wnt signaling

## 1. Introduction

Breast cancer (BC) is a heterogeneous disease with molecularly distinct subtypes displaying different clinical outcomes and responses to therapies [1]. Patients with “triple-negative” breast cancer (TNBC, lacking the expression of estrogen and progesterone receptors and Her2 overexpression) are mainly treated with conventional chemotherapies [1,2]. However, these patients have the worst prognosis as their treatment is challenging, due to their inter- and intra-tumor heterogeneity, leading to resistance to chemotherapy and relapse [2]. Therefore, more efficacious treatments are needed to improve TNBC patient survival.

EGFR is overexpressed in more than 70% of TNBC patients and is associated with a metastatic phenotype [3]. However, targeting this receptor as a monotherapy has shown only modest to low efficacy in clinical trials for TNBC patients [3]. The Wnt signaling pathway is another pathway activated in TNBC through an overexpression of the transmembrane receptors, Frizzleds and co-receptors low-density lipoprotein receptor-related proteins (LRP6 and LRP5) [4–6]. Wnt ligands (such as Wnt3a), which are secreted upon palmitoylation by the enzyme porcupine [7], activate the Wnt pathway by binding to the transmembrane receptors Frizzleds and co-receptors LRP5/LRP6. This initiates the release of  $\beta$ -catenin from the destruction complex including Dishevelled and Axin. Free  $\beta$ -catenin translocates into the nucleus and binds to the TCF/LEF family of transcription factors to activate the expression of Wnt target genes [4,5,7].

Arginine methylation of histone and non-histone proteins is a post-translational modification catalyzed by Protein Arginine Methyltransferases (PRMTs) [8–13]. Substrate arginine can either be monomethylated or dimethylated (symmetrically or asymmetrically) by PRMTs. Type I PRMTs (PRMT1-4, PRMT6, and PRMT8) are responsible for asymmetric dimethylation and Type II PRMTs (PRMT5 and PRMT9) for symmetric dimethylation [8–14]. PRMTs are ubiquitously expressed, except PRMT8 which is brain-specific [12]. Several PRMTs are overexpressed in various cancer types, including breast cancer, [13,15–17] and are emerging as attractive therapeutic targets [9,10,12,15]. Specific inhibitors targeting PRMT5 are being evaluated in phase I clinical trials (NCT03573310, NCT03854227, NCT02783300) [10]. PRMT1-specific inhibitors are not yet available, nevertheless, two type I PRMT inhibitors (MS023, GSK3368715) have been developed showing more efficacy towards PRMT1, PRMT6 and PRMT8 [18,19]. GSK3368715 is currently in a phase I clinical trial for diffuse large B-cell lymphomas and solid cancers (NCT03666988).

Arginine methylation regulates several cellular processes including transcriptional regulation and signal transduction [8,11,12]. PRMT1 and PRMT5 regulate the EGFR signaling pathway by methylating EGFR (in colorectal and TNBC cells) [20–22], or by methylating histones on the EGFR promoter (in glioblastoma or colorectal cells) [23,24] to regulate its transcription. Furthermore, some PRMTs regulate the canonical Wnt signaling pathway [12]. Indeed, PRMT1 could either activate this pathway by methylating G3BP1 or G3BP2 [25,26], or inhibit it by methylating Axin and Dishevelled [27,28]. Whether PRMT1 regulates the Wnt pathway in breast cancer cells is still unknown.

PRMT1 has been mainly studied in luminal BC due to its well-described function as a transcriptional coactivator of estrogen receptor (ER) [15,29]. However, its implication in the other BC subtypes, specifically in TNBC, remains to be explored. Here, we examined the expression of PRMT1 in the different breast cancer subtypes, evaluated its potential as a therapeutic target, and explored its function in TNBC cells.

## 2. Materials and Methods

### 2.1. Human Samples

Our cohort has been previously described [6,17,30,31] and is composed of 35 luminal A (LA), 40 luminal B (LB), 46 TNBC, 33 Her2+, and 18 normal breast tissues. Experiments were conducted in accordance with Bioethics Law No. 2004–800 and the Ethics Charter from the French National Institute of Cancer (INCa), and after approval from the ethics committee of our Institution. DNA (Affymetrix SNP 6.0, ThermoFisher Scientific, Waltham,



MA, USA) and RNA (Affymetrix U133 plus 2.0, ThermoFisher Scientific) microarrays on this cohort have been previously described [30].

## 2.2. Immunohistochemistry (IHC)

PRMT1 IHC was carried out on tissue microarrays (TMA), containing alcohol, formalin and acetic acid (AFA)-fixed paraffin-embedded tissues, as previously described [30], using a rabbit PRMT1 polyclonal antibody (Table S1). This antibody recognizes residues 298–318 within the C-terminal domain of all isoforms of PRMT1. PRMT1 antibody was validated and optimized for IHC using AFA-fixed pellets from MDA-MB-468 cells treated with PRMT1 siRNAs or control siRNA for 72 h (Figure S1D). For surface staining quantifications, whole digital slide images were obtained using virtual microscopy (Philips Ultra-Fast Scanner 1.6 RA, Amsterdam, Netherlands) and analyzed with Digital Image Analysis platform HALO (version 3.0.311.218; Indica Lab, Albuquerque, NM, USA). Tissue classifier was trained to segment tumor tissue and stroma. Area Quantification module (v2.1.3, Albuquerque, NM, USA) was used to evaluate the area of each tissue class and the area of tissue positive for PRMT1 staining. For subcellular localization of PRMT1 (plasma membrane, nucleus, and cytosol), TMA were read by two pathologists who assigned intensity scores (0–3) for each compartment (0: no staining, 3: strongest staining).

## 2.3. Cell Culture, RNA Interference, Antibodies, Small-Molecule Inhibitors, and Primers

TNBC (MDA-MB-468, HCC38, HCC70, MDA-MB-453), luminal (MCF7, T47D), and Her2+ (SKBr3, HCC1954, BT474) cell lines were purchased from the American Type Culture Collection (ATCC), authenticated in 2021 by short-tandem repeat profiling (data not shown), tested for mycoplasma using MycoAlert Mycoplasma Detection Kit (Lonza Biosciences, Durham, NC, USA), and cultured as previously described [17,32]. The murine cell lines, L-cells and L-Wnt3a were obtained from Institut de Recherches Servier, France. The MDA-MB-231 cell line was a kind gift from Dr. Mina Bissell (University of California, Berkeley, CA, USA). siRNA (20 nM) transfection was performed using Interferin (409-50, Polyplus, New York, NY, USA), according to the manufacturer's instructions. References for antibodies, siRNAs, primers and drugs/small-molecule inhibitors are listed in Table S1.

## 2.4. Cell Proliferation Assay

Cells were seeded in 96-well plates and cell proliferation was determined by MTT (M2128-1G, Sigma-Aldrich, St. Louis, MO, USA), WST-1 (11644807001, Sigma-Aldrich) or CellTiterGlo (G7572, Promega, Madison, WI, USA) assays as previously described [17,30,32].

## 2.5. Apoptosis Assays

Apoptotic activity was determined by the Caspase-Glo 3/7 luminescent assay (G8092, Promega), Annexin-V staining (11988549001, Roche, Basel, Switzerland) or Western blot analysis as previously described [17,30,32].

## 2.6. Colony Formation Assay

Cells transfected with siRNA were seeded in 6-well plates in 2 mL of growth media. Cells were incubated at 37 °C for 6 mitotic cycles (6–14 days), depending on the cell line, until colony formation. Colonies were fixed and stained with 500 µL of coomassie blue solution for 20 min. Colonies were photographed using a LAS-3000 Luminescent Image analyser (Fujifilm, Tokyo, Japan) or Chemidoc MP imager (Bio-rad Laboratories, Hercules, CA, USA) and quantified by ImageJ 1.43u software (NIH, Bethesda, MD, USA).

## 2.7. Soft Agar Assay

A 1 mL bottom layer consisting of 0.5% agar medium (equal volumes of 1% agar and 2 × culture medium) was added to 6-well plates. MDA-MB-468 cells were transfected with RNAi, and 24 h later, they were trypsinized, resuspended in 0.35% agar medium, and plated at 5000 cells/well as a top layer. Cells were incubated 4 weeks at 37 °C and

the colonies were stained with an MTT assay. Plates were photographed with a Fujifilm LAS-3000 Imager, and the clones were quantified using Image J software.

### 2.8. Real-Time—Quantitative PCR Assay (RT-qPCR)

For Wnt target gene expression, MDA-MB-468 cells transfected with siRNA were serum-starved overnight and stimulated with Wnt3a conditioned media at 100 ng/mL for 6 h. RNA was extracted using the RNeasy Mini Kit (74106, Qiagen, Hilden, Germany) following the manufacturer's protocol. Reverse-transcription and RT-qPCR were performed in a one-step reaction using the QuantiTect SYBR Green RT-PCR Kit (204245, Qiagen), according to the manufacturer's protocol. The acquisition was made using a QuantStudio™ 12K Flex Real-Time PCR System (Applied Biosystems, Waltham, MA, USA).

### 2.9. $\beta$ -Catenin-Activated Reporter (BAR) Luciferase Assay

At 24 h post siRNA transfection or 48 h post inhibitor treatment, MDA-MB-468 cells were transfected with the SuperTOPflash (7X Wnt response element containing plasmid) and pRL-TK-Renilla plasmids (both plasmids from Institut de Recherches Servier, Croissy-sur-Seine, France) at a 10:1 ratio using X-tremeGENE™ HP (6366236001, Sigma-Aldrich) as a transfectant. The cells were serum-starved overnight, i.e., 4–5 h post DNA transfection and stimulated with 100 ng/mL of Wnt3a conditioned media for 6 h. Dual-luciferase assay (E1910, Promega) was performed following manufacturer's protocol, and the luminescence signal was measured on the Infinite M200 spectrophotometer (Tecan, Männedorf, Switzerland). The ratio of the signal from firefly (SuperTOPflashCroissy-sur-Seine, France) to renilla (pRL-TK-RenillaCroissy-sur-Seine, France) luciferase was calculated to obtain normalized luciferase activity, representing Wnt/ $\beta$ -catenin activity.

### 2.10. Chromatin Immunoprecipitation (ChIP)

Chromatin was prepared from  $4 \times 10^6$  untreated MDA-MB-468 cells using the simple ChIP plus enzymatic chromatin IP Kit (9004, Cell signaling Technology, Danvers, MA, USA), following the manufacturer's protocol. The chromatin was immunoprecipitated using anti-PRMT1 or anti-IgG antibodies (Table S1) overnight, and the chromatin/antibody complex was pulled down using protein G agarose beads (provided with the kit). Following different washing steps, the chromatin was eluted, and the cross links were reversed using proteinase K. DNA was purified using the spin columns included in the kit, and a qPCR was performed using specific primers designed based on a published ChIP-seq dataset for PRMT1 [33] for the promoter region of each gene (Table S1).

### 2.11. Transcriptomic Analysis of PRMT1-Depleted Cells

The transcriptome of MDA-MB-468 cells depleted for PRMT1 was performed using Affymetrix HTA 2.0 microarray (ThermoFisher Scientific). Differential gene expression between control and PRMT1 siRNA with an adjusted *p*-value cut-off of 0.05 was considered (Table S2). Gene enrichment pathway analysis was performed using the REACTOME database from the GSEA website [34].

### 2.12. GSK3368715 Treatment in Mice

Six-week-old female Swiss-nude mice were purchased from Charles River laboratories (Wilmington, MA, USA) and maintained in specific pathogen-free conditions. Their care and housing were per institutional guidelines as put forth by the French Ethical Committee. GSK3368715 (CS-0100240, ChemScene LLC, South Brunswick, NJ, USA) was formulated in 10% DMSO (Sigma-Aldrich) at 80 mg/mL and subsequently diluted in water. GSK3368715 toxicity studies were performed by administrating 100 mg/kg daily to nude mice.

MDA-MB-468 cells ( $12 \times 10^6$  per mouse) were injected subcutaneously into nude mice until tumors reached 70 mm<sup>3</sup>. The tumor fragments obtained from 2 mice were then grafted into the inter-scapular fat pad of nude mice. Xenografts were randomly assigned to control or treatment groups (*n* = 6/group) when tumors reached a volume comprised

between 60 and 80 mm<sup>3</sup> and treated with vehicle or GSK3368715 at 80 mg/kg once daily orally 5 days/week. During the weekends, the inhibitor was added to the drinking water of mice. The tumor volume was evaluated by measuring two perpendicular tumor diameters with a caliper, twice a week. Mice were euthanized after 8 weeks of treatment. Tumor volumes were calculated as  $V = a \times b^2/2$ ,  $a$  being the largest diameter,  $b$  the smallest. The tumor volumes were then reported to the initial volume as the relative tumor volume (RTV). Means of RTV in the same treatment group were calculated, and growth curves were established as a function of time.

### 2.13. Drug Combinations

MDA-MB-468 cells were seeded 48 h prior to treatment in a 96-well white transparent bottom plate (655098, Greiner Bio-One, Les Ulis, France) and treated with varying concentrations of the drugs/inhibitors. The maximum concentration for each drug/inhibitor was approximately twice the half maximal inhibitory concentration ( $2 \times IC_{50}$ ) (Table S1), and serially diluted two-fold for all drugs except for the type I PRMT inhibitors (three-fold). Cell viability was determined after 7 days of treatment by CellTiterGlo assay (G7572, Promega). The luminescence signal was measured in a Spark spectrophotometer (Tecan). Drug pair interactions using the Loewe model were calculated on the Combenefit software [35]. All drug combinations were performed in triplicate reactions per experiment.

### 2.14. Statistical Analysis

R software and GraphPad Prism 7 were used for statistical analyses. Pearson or Spearman correlation were used to estimate an association between two variables. For cellular assays,  $p$ -values were calculated using the Student  $t$ -test, unless otherwise specified. Independence between tumor subtypes in the TMA was assessed using Fisher's exact test.

All the whole western blot figures can be found in the Supplementary Materials (Figures S9–S21).

## 3. Results

### 3.1. PRMT1 Is Overexpressed in All the Breast Cancer Subtypes Compared to Normal Breast Tissue

With the goal of identifying enzymes overexpressed in BC compared to normal tissue, we have performed gene expression profiling on a cohort of 154 human BC biopsies and healthy breast tissues [6,17,30,31]. We found that *PRMT1* mRNA is overexpressed in all BC subtypes compared to normal tissues and observed the highest expression in TNBC (Figure 1A, left panel). The highest expression of *PRMT1* mRNA in TNBC was confirmed in the publicly available database—the cancer genome atlas (TCGA) cohort (Figure 1A, right panel). We examined whether variations in *PRMT1* expression could be a result of genomic alterations by analyzing DNA microarrays. Indeed, there was a correlation between *PRMT1* mRNA and the gene copy number within the whole cohort (Figure S1A). Interestingly, the *PRMT1* locus showed significantly more gains in TNBC than the luminal BC subtypes and normal tissue (Figure 1B, Table S3). The *PRMT1* mRNA levels also correlated positively with proliferation (*MKI67* mRNA) in our cohort (Figure S1B).

To understand the clinical significance of *PRMT1* mRNA expression, we plotted survival outcomes from the KM-plotter database (Kaplan-Meier Plotter. Available online: <https://kmplot.com/analysis/index.php?p=service&cancer=breast> (accessed on 11 June 2021)) [36]. High *PRMT1* mRNA expression was associated with poor recurrence-free survival (RFS) in all BC ( $p = 1 \times 10^{-8}$ , Figure S1C), as previously reported [37]. However, this analysis did not consider that *PRMT1* is differentially expressed among the BC subtypes (Figure 1A), which are associated with different prognoses. Therefore, we performed this analysis within the different BC subtypes. High *PRMT1* mRNA levels were associated with poor RFS in LA ( $p = 2.5 \times 10^{-6}$ ) and LB ( $p = 0.007$ ) (Figure S1C, top panel). Although this trend was seen in the Her2+ subtype, it was not statistically significant ( $p = 0.13$ )

(Figure S1C, bottom left panel). Conversely, high *PRMT1* mRNA expression showed better RFS ( $p = 0.02$ ) within the TNBC subtype (Figure S1C, bottom right panel).

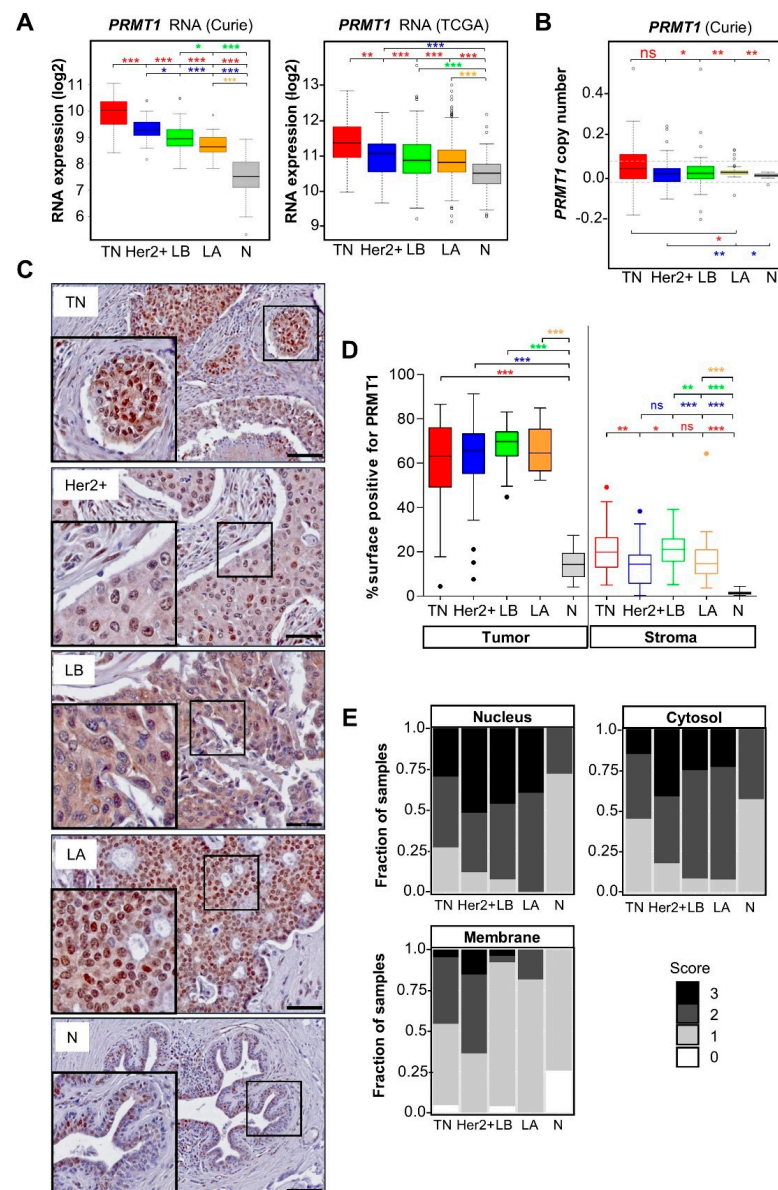


**Figure 1.** *PRMT1* is highly expressed in breast tumors. (A) High levels of *PRMT1* mRNA in breast cancer. *PRMT1* RNA expression in TNBC (TN, red), Her2+ (blue), Luminal B (LB, green), Luminal A (LA, orange), and healthy breast tissues (N, grey) in Curie (left panel) and TCGA (right panel) cohorts is illustrated by box plots (log<sub>2</sub> transformed). (B) High *PRMT1* DNA copy number (CN) in TNBC in the Curie cohort. *PRMT1* DNA CN determined by Affymetrix microarray analysis is presented in boxplots (smoothed segmented CN signal), with dashed lines indicating the thresholds retained to call CN gains and losses (see Table S3 for the number of samples showing loss or gains). (C) High levels of *PRMT1* protein in BC. *PRMT1* protein levels were analyzed by IHC in the Curie cohort. A representative image of *PRMT1* staining is shown for the different BC subtypes (scale bar = 50  $\mu$ M). (D) Quantification of the tumoral (left) or stromal (right) surface positive for *PRMT1* staining represented as a percentage compared to the total surface. Open and closed circles represent outlier tumors within the different populations (A,B,D). (E) Intensity scores of *PRMT1* staining in the different cellular compartments (0: no staining, 3: the strongest staining). \*  $p < 0.05$ ; \*\*  $p < 0.01$ ; \*\*\*  $p < 0.001$ ; ns = not significant, as calculated using the Student *t*-test (A), Fischer exact test (B) or Mann–Whitney test (D).



As mRNA and protein levels do not always coincide, we studied PRMT1 protein expression in breast tumors and normal tissues using a commercial PRMT1 antibody. We first validated this antibody for IHC staining in a TNBC cell line (MDA-MB-468) fixed in the same method as the tissue samples (Figure S1D). IHC analysis confirmed that PRMT1 is highly expressed in all BC subtypes compared to normal tissues (Figure 1C,D). In contrast to mRNA expression, we did not observe any significant difference in PRMT1 protein expression levels between the different BC subtypes (Figure 1C,D). PRMT1 shows both nuclear and cytosolic staining (Figure 1C,E) and was also detected at the plasma membrane, mainly in ER-negative tumors (Figure 1E). Moreover, we observed substantial staining of PRMT1 in the stroma of breast tumors as compared to the normal tissues (Figure 1D). Mononuclear cells, fibroblasts and endothelial cells were positively stained for PRMT1 within the stroma (unpublished data).

Altogether, our results indicate that both PRMT1 mRNA and protein levels are higher in breast tumors compared to normal breast tissues, suggesting that PRMT1 could be targeted in BC.

### *3.2. RNAi-Mediated Depletion of PRMT1 Decreases BC Cell Viability, Clonogenicity and Induces DNA Damage and Apoptosis*

To explore the function of PRMT1 in BC cells, we first depleted PRMT1 using two validated siRNAs (PRMT1#7, PRMT1#8) in MDA-MB-468 TNBC cells (Figure S2A). We observed that cell viability was significantly decreased upon PRMT1 depletion in MDA-MB-468 cells, in a time-dependent manner (Figure 2A). Similar results were found in other BC cell lines (4 TNBC, 1 Her2+, 2 luminal; Figure S2B), suggesting that the effect was independent of BC subtype. PRMT1 depletion decreased colony formation in MDA-MB-468 cells under adherent conditions (Figure 2B) or in an anchorage-independent growth assay in soft agar (Figure 2C), indicating that PRMT1 depletion decreases the tumorigenicity of this TNBC cell line. PRMT1 depletion also decreased colony formation in other BC cells cultured under adherent conditions (Figure S2C). Furthermore, we observed a cleavage of caspases 3, 7, and PARP in MDA-MB-468 cells following PRMT1 depletion (Figure 2D), revealing apoptosis induction. This was confirmed in PRMT1-depleted MDA-MB-468 cells using a caspase 3/7 activity assay (Figure 2E) and by extracellular annexin-V staining (Figure 2F). PRMT1 depletion also significantly increased the phosphorylation of histone H2AX ( $\gamma$ H2AX), a DNA damage marker (Figure 2D). The induction of apoptosis upon PRMT1 knockdown was confirmed in other BC cell lines (HCC70, MDA-MB-231, SKBr3, T47D; Figure S2D). Together, these results demonstrate that PRMT1 is required for BC cell survival.

### *3.3. Type I PRMT Inhibitors Reduce BC Cell Growth*

Next, we sought to explore if the enzymatic activity of PRMT1 was necessary for BC cell survival. For this purpose, we used two recently developed type I PRMT inhibitors: MS023 [18] and GSK3368715 [19]. Under the tested conditions, both inhibitors decreased the PRMT1-specific histone mark H4R3me2a without affecting the methylation of H3R17me2a (by CARM1 and PRMT6) or PABP1 (by CARM1; Figure S3). We tested the effect of both inhibitors on the cell viability in 5 TNBC (MDA-MB-468, MDA-MB-231, HCC38, HCC70, MDA-MB-453), 1 luminal (T47D) and 2 Her2+ (HCC1954, BT474) BC cell lines. HCC1954 cells were the most sensitive cells to type I PRMT inhibition (Figure 3A), followed by MDA-MB-468 and T47D cells (Figure 3A). The other TNBC cell lines were resistant to type I PRMT inhibition ( $IC_{50} > 10 \mu M$ , Figure 3A). We also observed smaller-sized colonies when MDA-MB-468 (Figure 3B) or four other TNBC cell lines (Figure S4) were treated with both inhibitors.

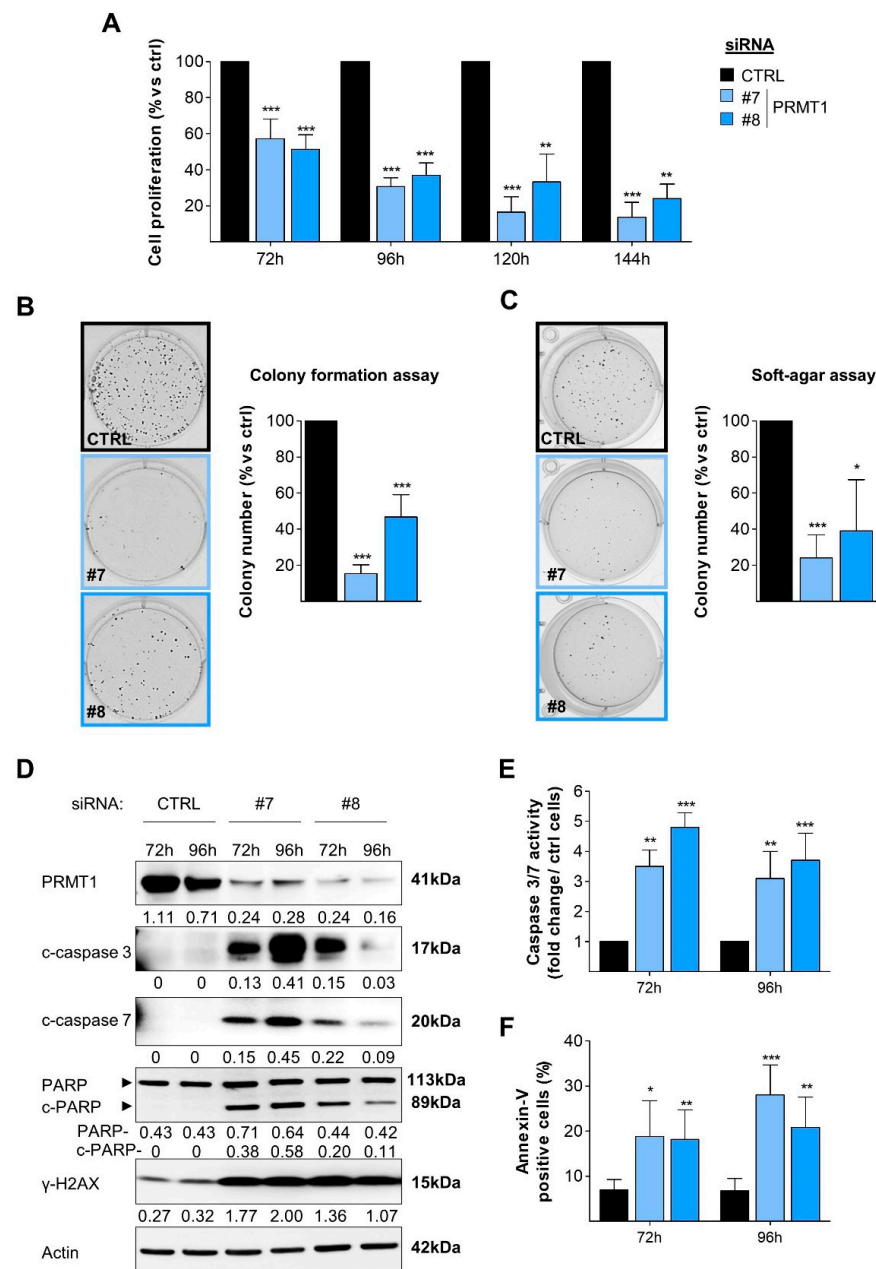


**Figure 2.** PRMT1 depletion decreases cell viability and induces apoptosis of MDA-MB-468 cells. (A) PRMT1 depletion impairs cell viability (MTT assay). Cells were transfected with control (CTRL, black) or two different PRMT1 siRNAs (#7, #8, blue) for 72–144 h. (B,C) PRMT1 depletion impairs colony formation when cells are grown on plastic for 13 days (B) or in soft agar for 4 weeks (C) following siRNA treatment. (D–F) PRMT1 depletion induces apoptosis. Apoptosis was detected by Western blotting using antibodies recognizing the cleaved forms of caspase 7 (c-caspase 7), caspase 3 (c-caspase 3) and PARP (c-PARP) (D), by caspase 3/7 assay (E) or annexin-V staining (F) after 72 h and 96 h following siRNA treatment. DNA damage was detected using an anti- $\gamma$ H2AX antibody (D). PRMT1 depletion was verified using an anti-PRMT1 antibody (D). Anti-actin antibody was used as a loading control and quantification of the bands (normalized to the loading control) are indicated below each blot (D). Results are presented as the percentage (A–C,F) or fold change (E) relative to control cells (CTRL). For the quantifications, the data are expressed as the mean  $\pm$  SD from at least three independent experiments (A–C,E,F). Pictures are from a single experiment, representative of three independent experiments (B–D). *p*-values are calculated from a Student *t*-test and represented as \* *p* < 0.05; \*\* *p* < 0.01; \*\*\* *p* < 0.001 (D).

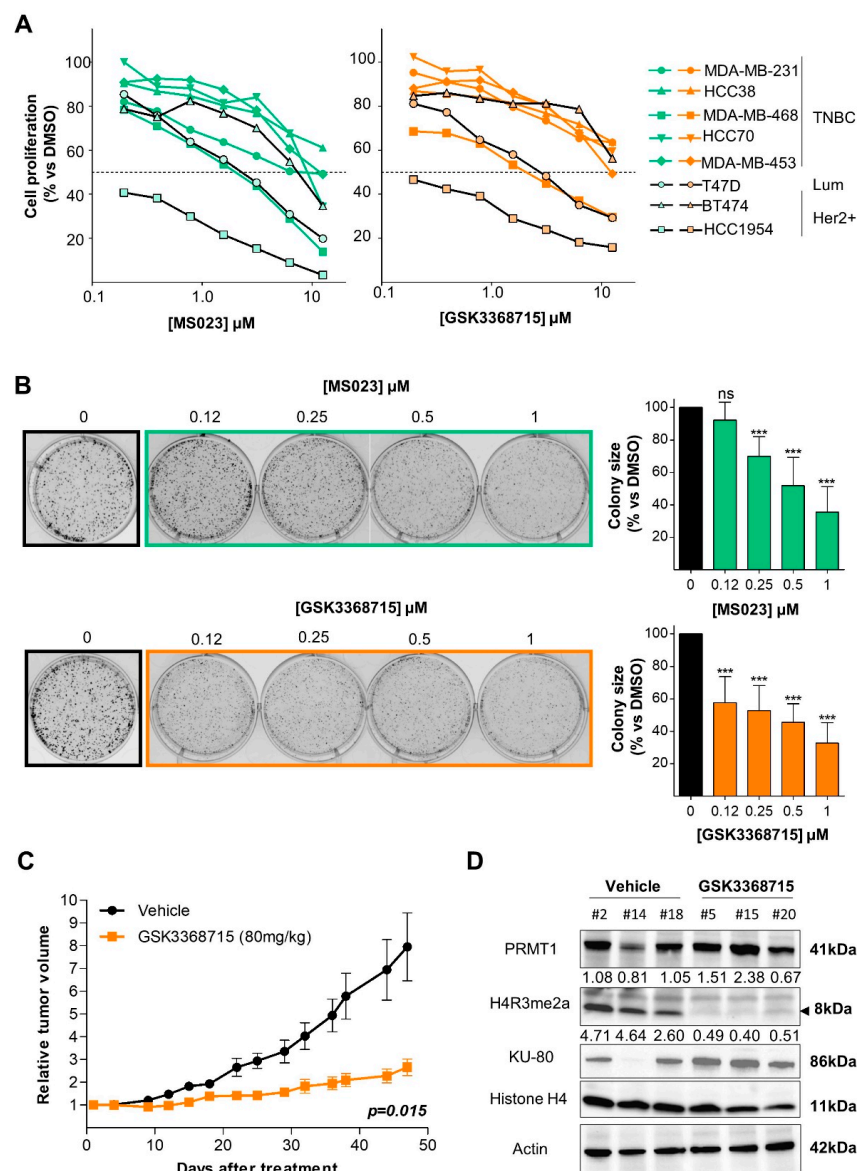


**Figure 3.** Type I PRMT inhibitors reduce cell viability and tumor growth. **(A)** Type I PRMT inhibitors decrease BC cell viability. TNBC, luminal (Lum), and Her2+ cells were treated with MS023 (**left panel**) or GSK3368715 (**right panel**) for 7 days, except MDA-MB-231 (4 days), and proliferation was determined by MTT or WST1 assays. Results are presented as the average percentage of cell growth relative to DMSO-treated cells from three independent experiments. **(B)** Type I PRMT inhibitors reduce the growth of colonies when MDA-MB-468 cells were cultured on plastic for 9 days after MS023 (**top**) or GSK3368715 (**bottom**) treatment. Quantification of colony size is expressed as a percentage relative to DMSO-treated cells, represented as the mean  $\pm$  SD from at least three independent experiments (**right panel**). Pictures are from a single experiment representative of three independent experiments (**left panel**).  $p$ -values are from a Student  $t$ -test and represented as \*\*\*  $p < 0.001$ ; ns = not significant. **C**, GSK3368715 slows tumor growth. Tumors derived from MDA-MB-468 cells were subcutaneously grafted into 12 mice (6 vehicle-treated, black; 6 GSK3368715-treated, orange). Growth curves were obtained by plotting mean relative tumor volume  $\pm$  SEM as a function of time.  $p$ -value was calculated using a Mann–Whitney U test. **(D)** GSK3368715 inhibits PRMT1 activity *in vivo*. PRMT1 expression (anti-PRMT1) and activity (anti-H4R3me2a) were analyzed in the tumors excised from 3 vehicle (#2, #14, #18) or GSK3368715 (#5, #15, #20)-treated mice at the end of the experiment (**C**). Antibodies against histone H4, actin and KU-80 were used as controls and quantification of the bands (normalized to the actin band) are indicated below each blot.

### 3.4. Type I PRMT Inhibition Slows Tumor Growth in a TNBC Xenograft Model

We evaluated the anti-tumor effect of inhibiting PRMT1 using GSK3368715, the only type I PRMT inhibitor currently in a phase I clinical trial for diffuse large B-cell lymphomas and solid tumors (NCT03666988). To better represent clinical conditions, we engrafted tumors derived from MDA-MB-468 cells into Swiss-nude mice (see Materials and Methods). GSK3368715 treatment significantly slowed tumor growth ( $p = 0.015$ ; Figure 3C) with no observed toxicity (Figure S5A). We confirmed that PRMT1 was indeed inhibited in the tumors at the end of the experiment by observing an increase in pan-monomethylation (Figure S5B), as previously reported [38], and a decrease in histone H4R3 methylation (H4R3me2a, Figure 3D).

### 3.5. PRMT1 Regulates the EGFR and Wnt Signaling Pathways at the Transcriptomic Level

PRMT1 plays a crucial role in transcriptional regulation [8,11,12]. Therefore, we performed transcriptomic analysis of PRMT1 depleted MDA-MB-468 cells to gain insight into the molecular mechanisms that mediate the dependency of BC cells on PRMT1.

MDA-MB-468 cells were transfected with two different siRNAs targeting PRMT1 for 24 h and 48 h and the RNA were analyzed using HTA 2.0 microarrays (Affymetrix). We focused on the genes that were commonly deregulated at 24 h and 48 h by both siRNAs (Table S2) to perform a gene enrichment pathway analysis using the REACTOME database [34]. The top ranked pathways (according to adjusted  $p$ -value) revealed that PRMT1 is involved in several cellular processes including signal transduction pathways, immune system response, lipid metabolism and transcriptional regulation (Figure S6). We focused on EGFR ( $p = 6.96 \times 10^{-6}$ ) and Wnt ( $p = 5.07 \times 10^{-6}$ ) signaling pathways, which are known to be activated in TNBC [3–5].

We noticed that *EGFR* mRNA itself was less expressed upon PRMT1 depletion in our microarray analysis (Figure 4A) and confirmed this observation by qPCR (Figure 4B). *EGFR* mRNA was also retrieved in several other deregulated pathways (Figure S6, arrowheads and diamond). PRMT1 was directly recruited to two promoter regions of *EGFR* in MDA-MB-468 cells using an anti-PRMT1 antibody (Figure 4C), previously validated for ChIP experiments [39]. Furthermore, PRMT1 depletion also decreased EGFR protein expression (Figure 4D).

Our microarray analysis revealed two key players of the Wnt signaling pathway, *LRP5* and *PORCN* (Porcupine), to be less expressed following PRMT1 depletion (Figure 4E). *LRP5* and *PORCN* mRNAs were also found in the second-top deregulated pathway (Figure S6, diamond). We validated the decrease in their expression by qPCR (Figure 4F) and identified by ChIP analysis that PRMT1 is enriched on the promoter of *LRP5* and two regions of the *PORCN* promoter (Figure 4G). The expression of *LRP5* was also decreased at the protein level after PRMT1 depletion (Figure 4H). We could not assess porcupine protein expression due to the lack of suitable antibodies for Western blotting.

Overall, these results indicate that PRMT1 regulates the expression of *EGFR*, *LRP5* and *PORCN* by being recruited to their promoter regions.

### 3.6. PRMT1 Activates the Canonical Wnt Signaling Pathway

We hypothesized that PRMT1 could be an activator for the Wnt pathway as both *LRP5* and *PORCN* are required for Wnt activation. We first assessed the Wnt activity by analyzing the expression of the three Wnt target genes (*AXIN2*, *APCDD1*, and *NKD1*) that are the most upregulated in Wnt3a-stimulated MDA-MB-468 cells [40]. We observed that PRMT1 depletion reduced the expression of these three Wnt target genes (Figure 5A). By using the gold standard  $\beta$ -catenin activated reporter (BAR) assay, we confirmed that PRMT1 depletion decreased Wnt signaling activity (Figure 5B). siRNA targeting *LRP6* was used as a positive control in both assays (Figure 5A,B).



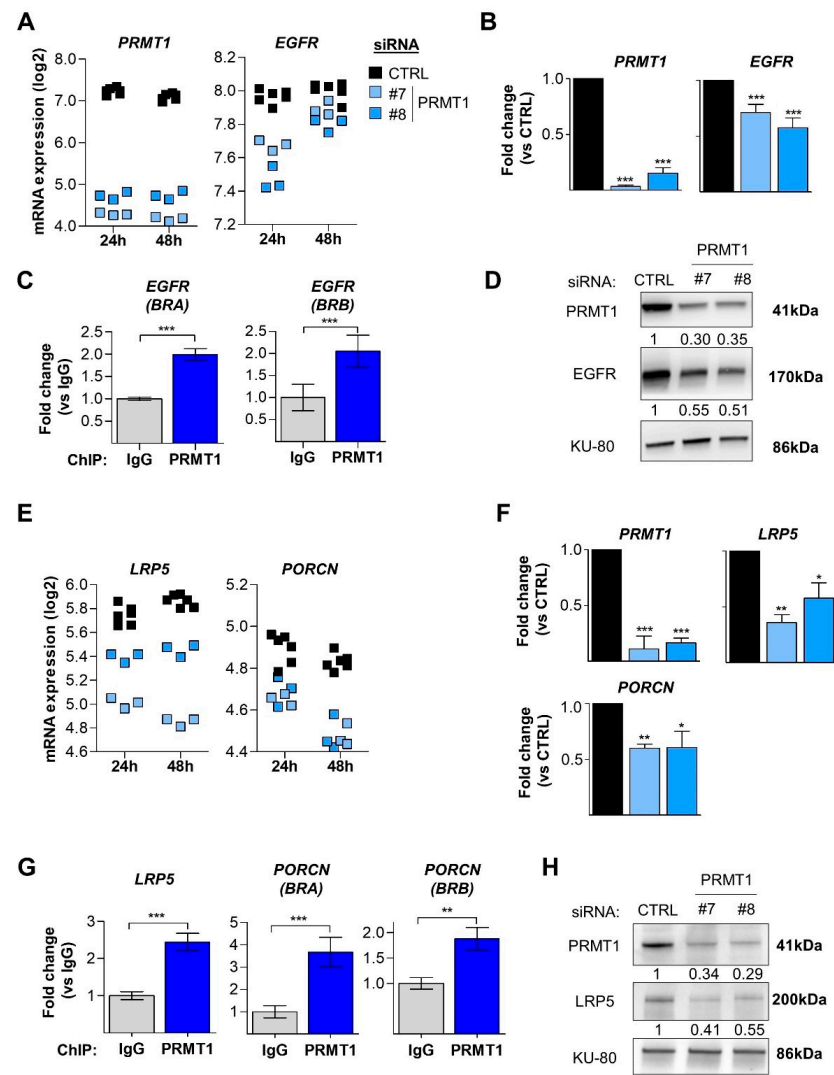


**Figure 4.** PRMT1 is enriched on the promoter of *EGFR*, *LRP5* and *PORCN* and activates their transcription. (A,B) PRMT1 depletion in MDA-MB-468 cells reduces *EGFR* mRNA expression as shown by Affymetrix microarray (A) and verified by qPCR (B). (C) PRMT1 is recruited to two promoter regions (Binding Region A, BRA; BRB) of *EGFR*. (D) PRMT1 depletion reduces *EGFR* protein level as shown by Western blotting. (E,F) PRMT1 depletion reduces *LRP5* and *PORCN* mRNA expression as shown by Affymetrix microarray (E) and validated by qPCR (F). (G) PRMT1 is recruited to the promoter of *LRP5* and two promoter regions (BRA, BRB) of *PORCN*. (H) PRMT1 depletion reduces *LRP5* protein level as shown by Western blotting. MDA-MB-468 cells were transfected with control (black) or two PRMT1 (#7, #8, blue) siRNAs for 24 h (A,B,E) and 48 h (A,D–F,H). mRNA expression was logarithmically transformed (log<sub>2</sub>) and each replicate is represented as a single point on the scatter plot (A,E). ChIP experiments were performed using anti-PRMT1 (blue bars) or anti-IgG (grey bars) antibodies using chromatin isolated from MDA-MB-468 cells (C,G). qPCR was performed using primers targeting the promoter regions of *EGFR* (C), *LRP5* (G) and *PORCN* (G). PRMT1 depletion was verified in the Affymetrix microarray (A), by qPCR (B,F) and by Western blotting (D,H). Antibody against KU-80 was used as a loading control for the Western blots and pictures are representative of at least three independent experiments (D,H). Intensity ratios of the bands, indicated below each blot, represent a fold change relative to control siRNA, after normalization to the loading control (D,H). The quantifications are represented as a fold change relative to the control siRNA (B,F) or control IgG (C,G) and presented as mean ± SD (B,F) or mean ± SEM (C,G) from three independent experiments. *p*-values from Student *t*-test are represented as \* *p* < 0.05; \*\* *p* < 0.01; \*\*\* *p* < 0.001.

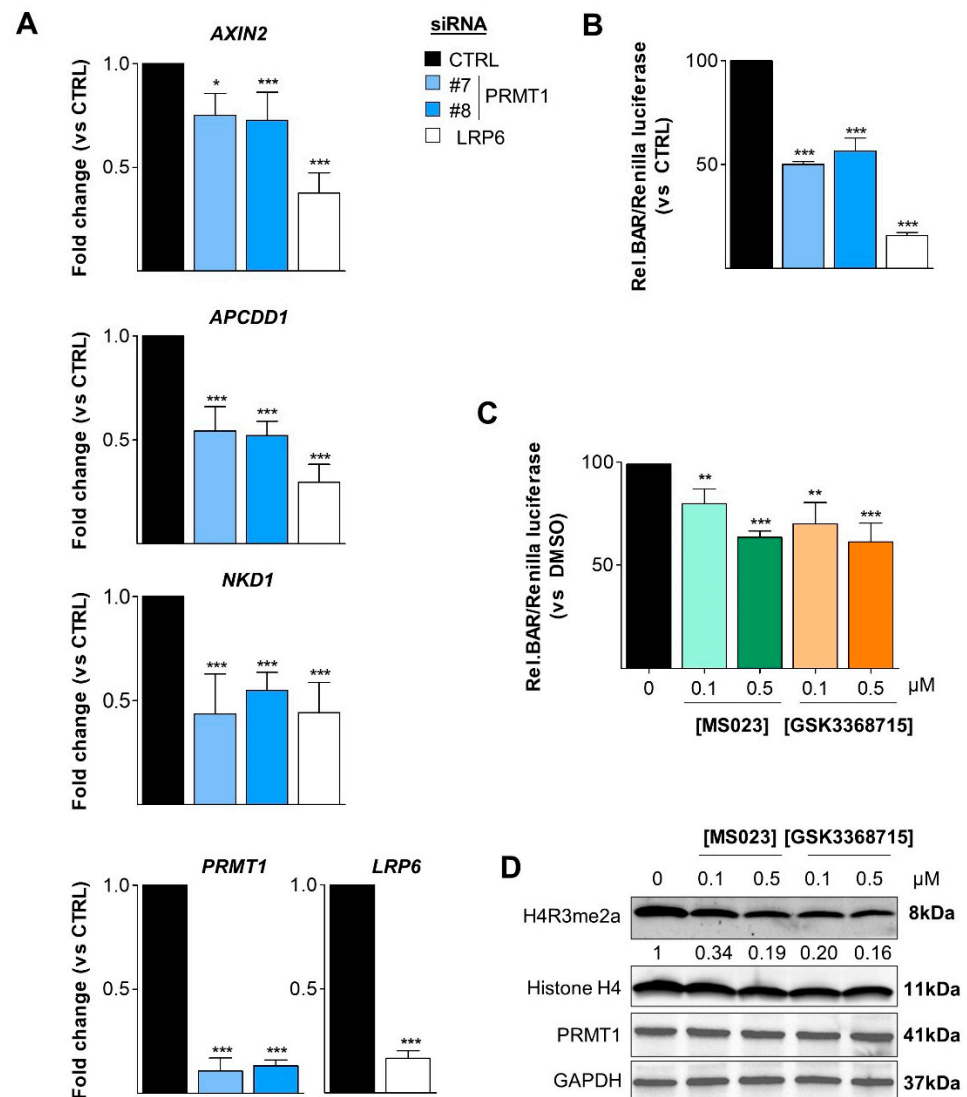


**Figure 5.** PRMT1 activates the canonical Wnt signaling pathway. (A,B) PRMT1 depletion decreases Wnt signaling activity. MDA-MB-468 cells were transfected with control (CTRL, black), two PRMT1 (#7, #8, blue) or LRP6 (white) siRNA for 48 h (A,B), and then co-transfected with plasmids coding for BAR-firefly luciferase and Renilla luciferase for 24 h (B), before Wnt3a stimulation for 6 h (A,B). The expression of *AXIN2*, *APCDD1*, *NKD1* (Wnt target genes), *PRMT1* and *LRP6* were quantified by qPCR (normalized to actin) (A). The relative luciferase signal (firefly luciferase/Renilla luciferase) is represented as a percentage normalized to the control siRNA (CTRL) (B). siRNA targeting LRP6 was used as a positive control (A,B). (C) Type I PRMT inhibitors decrease Wnt signaling activity. MDA-MB-468 cells were treated with 0.1 μM or 0.5 μM of MS023 (green) or GSK3368715 (orange) for 48 h, and then co-transfected with plasmids coding for BAR-firefly luciferase and Renilla luciferase for 24 h, before Wnt3a stimulation for 6 h. The relative luciferase signal (firefly luciferase/Renilla luciferase) is represented as a percentage normalized to the DMSO-treated cells (black). (D) PRMT1 inhibition was verified in this experiment (C) by Western blotting using anti-H4R3me2a antibody. Anti-histone H4, PRMT1, and GAPDH were used as loading controls. Intensity ratio of methylated histone H4 is indicated as a fold change relative to DMSO, after normalization to the loading control (D). All quantifications are represented as a fold change (A) or percentage (B,C) relative to the control. The data are expressed as the mean ± SD from at least three independent experiments (A–C). *p*-values from Student *t*-test are represented as \* *p* < 0.05; \*\* *p* < 0.01; \*\*\* *p* < 0.001.

Next, we checked if PRMT1 enzymatic activity was involved in the regulation of Wnt pathway. MDA-MB-468 cells were treated for 3 days with low doses of MS023 or

GSK3368715 (0.1  $\mu$ M and 0.5  $\mu$ M) and then stimulated for 6 h with Wnt3a, before assessing Wnt activity using the BAR assay (Figure 5C). Both type I PRMT inhibitors decreased the Wnt activity in a dose-dependent manner (Figure 5C). PRMT1 was inhibited under these conditions (Figure 5D).

Collectively, this demonstrates that PRMT1 and its activity are involved in the activation of the canonical Wnt pathway in MDA-MB-468 cells.

### 3.7. Type I PRMT Inhibitors Show Synergistic Interactions with Erlotinib or Chemotherapies

The rationale of drug combinations is to improve the efficacy, limit side-effects and reduce the risk of drug resistance. First, we combined both type I PRMT inhibitors with chemotherapies (cisplatin, camptothecin, cyclophosphamide, taxanes) used in the clinic to treat TNBC patients. MDA-MB-468 cells were treated with varying concentrations of the drugs, starting from about  $2 \times IC_{50}$  (Table S1) for 7 days (equivalent to four mitotic cycles) and cell viability was assessed using CellTiterGlo assay. We applied the Loewe additivity model using the Combenefit software [35] to determine the nature (synergy/additivity/antagonism) of the drug interactions. We used this model as it allows the possibility to analyze two drugs that may act on the same pathway(s) [41]. Both type I PRMT inhibitors synergized with cisplatin (Figures 6A and S7A), camptothecin (Figures 6B and S7B) and cyclophosphamide (Figures 6C and S7C), but not with docetaxel (Figure S8A) or paclitaxel (Figure S8B).

As EGFR is highly expressed in TNBC [3], we also evaluated the potential of combining type I PRMT inhibitors with an EGFR inhibitor (erlotinib) and observed a high synergy in MDA-MB-468 cells (Figures 6D and S7D). These combinations may represent promising alternative therapeutic strategies for TNBC patients.

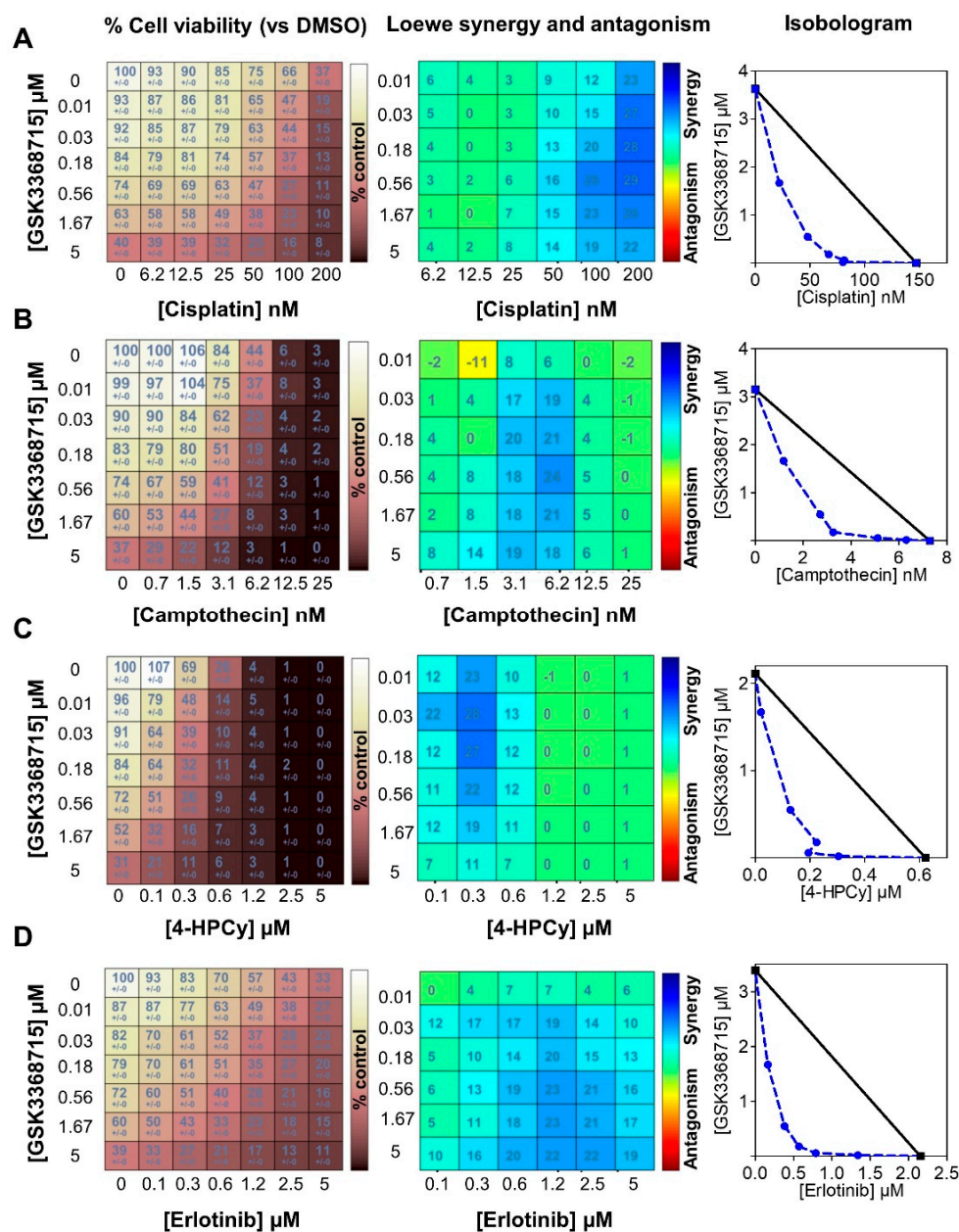


**Figure 6.** Synergistic interactions between GSK3368715 (a type I PRMT inhibitor) and chemotherapies (A–C) or erlotinib (D). MDA-MB-468 cells were seeded in 96-well plates, treated with the indicated drugs for 7 days (equivalent to four doubling times), and cell viability was measured by CellTiterGlo assay. GSK3368715 was serially diluted three-fold and cisplatin (A), camptothecin (B), 4-hydroperoxy cyclophosphamide (4-HPCy; (C)), erlotinib (D) were serially diluted two-fold (concentrations indicated in the figure). The drug interactions were calculated using the Loewe model on the Combenefit software. Cell viability (% compared to DMSO-treated cells, left panel), synergy matrix as calculated using the Loewe excess model (middle panel), and isobolograms (right panel) for each drug pair are indicated. Presented data are representative of three independent experiments.

#### 4. Discussion

The efficacy of breast cancer therapies has considerably improved; however, TNBC still has a poor prognosis compared with other subtypes and is typically correlated with increased recurrence and worse survival. Finding alternative treatments to chemotherapy remains a priority to treat TNBC patients to avoid relapses.

PRMTs are overexpressed in various cancer types and are emerging as attractive therapeutic targets [8–14]. Consequently, several PRMT inhibitors have been developed, and some PRMT5 and type I PRMT inhibitors are being evaluated in clinical trials [10].

At the RNA level, we found that *PRMT1* is more expressed in BC when compared to the normal breast tissue, aligning with previous studies that did not consider BC heterogeneity [42,43]. *PRMT1* mRNA correlates positively with *MKI67* mRNA. Consequently, the highest *PRMT1* mRNA expression was found in TNBC, the most proliferative BC subtype, and this could be a result of DNA copy number gain. High *PRMT1* mRNA expression correlates with poor prognosis in all breast tumors, as reported in [37,44], as well as within LA and LB subtypes. In contrast, TNBC expressing the highest level of *PRMT1* mRNA (most proliferative) display better RFS, possibly because they respond better to chemotherapy, as observed for other targets linked to proliferation [30,31].

At the protein level, PRMT1 is more expressed in BC compared to normal tissues, confirming previous reports [37,44]. Here, we accounted for BC heterogeneity and found that PRMT1 protein is expressed at similar levels in the different BC subtypes. We observed both nuclear and cytosolic staining for PRMT1 which is in apparent contrast to a study showing mainly cytosolic localization [44], using an antibody that also recognizes the C-terminus of PRMT1, thereby detecting all its isoforms [45]. Several PRMT1 splice variants have been described which show cytoplasmic and/or nuclear localization [43]; therefore, it may not be surprising to detect PRMT1 in both compartments. Furthermore, PRMT1 is a well-described regulator of transcription, by methylating histones and transcription factors [14]. PRMT1 interacts with the progesterone receptor in the nucleus of breast cancer cells [39]. In addition, PRMT1 is expressed in both the cytosol and the nucleus in renal [46,47] and pancreatic [48] carcinomas. We also detected PRMT1 at the plasma membrane, preferentially in the ER-negative BC subtypes, possibly since it interacts with some transmembrane receptors such as EGFR [20,21] or IGF-1R [49]. However, we cannot exclude that the PRMT1 antibody we used recognizes the plasma membrane-associated PRMT8, although it is brain-specific, as it shares 80% homology with PRMT1.

Transcriptomic analysis highlighted several pathways regulated by PRMT1. Here, we focused on two pathways that are known to be activated in TNBC [3–5]. PRMT1 has been previously observed to modulate EGFR signaling by two mechanisms: (i) by methylating histone H4 (H4R3me2a) on its promoter in colorectal cancer (CRC) [23] and glioblastoma cells [24] and (ii) by methylating EGFR in CRC and TNBC cells [20,21]. Here, we demonstrate that PRMT1 itself is directly recruited to the promoter of *EGFR*, thus activating its transcription.

The role of PRMT1 on Wnt signaling is ambiguous since PRMT1 can be both an activator and an inhibitor of this pathway. On the one hand, PRMT1 can inhibit Wnt signaling by methylating two antagonists (i) Axin (in HEK293 and L929 cell lines) [27] and (ii) Dishevelled (in HEK293, B2b, and F9 cell lines) [28]. On the other hand, PRMT1 can activate the Wnt signaling pathway by methylating two Dishevelled-binding components: G3BP1 (in F9 cells) [26] and G3BP2 (in F9, HEK293 and SW380 cells) [25]. Therefore, the role of PRMT1 on Wnt signaling may be context dependent. Here, we show that PRMT1 regulates the Wnt signaling pathway at the transcriptomic level. Indeed, we found that PRMT1 activates the transcription of two main components of the Wnt pathway—*LRP5* and *PORCN*—by being recruited to their promoter regions. Furthermore, we demonstrate that PRMT1 activates the canonical Wnt signaling pathway. Additionally, PRMT1 enzymatic activity could be required as type I PRMT inhibitors reduce Wnt signaling pathway. Hence, PRMT1 could activate the pathway by directly methylating Wnt components or methylating histones on their promoters. Together, this implies that PRMT1 may regulate the Wnt signaling pathway by regulating the amounts of LRP5 available at the plasma membrane and by controlling the Porcupine-dependent post-translational modification of Wnt ligands, which is required for their secretion.

As PRMT1 is highly expressed in BC, we evaluated its potential as a therapeutic target. We found that PRMT1 depletion (i) decreased the cell viability, (ii) blocked their



clonogenic potential, and (iii) induced DNA damage and apoptosis in various cell lines of different BC subtypes. This is in accordance with previous reports in TNBC [21,37,50,51] and luminal [39,51,52] BC cell lines as well as cell lines of other cancer types [23,46,53–55]. We next addressed the question whether the enzymatic activity of PRMT1 was required for BC cell survival. To date, there are no PRMT1 specific small-molecule inhibitors, but rather inhibitors that target all type I PRMTs, with some selectivity towards PRMT1, PRMT6, and PRMT8 [18,19]. GSK3368715 targets these three PRMTs at similar  $IC_{50}$  [19], whereas PRMT6 and PRMT8 are more sensitive than PRMT1 to MS023 [18]. We observed differential sensitivity among BC cell lines to both type I PRMT inhibitors, suggesting the need to identify biomarkers of response. This may perhaps help stratify patients who could benefit from treatment with these type I PRMT inhibitors. Together, we found that PRMT1 and its enzymatic activity are required for BC cell survival; however, we cannot rule out the influence of PRMT6 activity when using these inhibitors in our BC cell lines.

When assessing these inhibitors in combination with chemotherapies used in the clinic to treat TNBC patients, we observed synergistic interactions with cisplatin, cyclophosphamide, and camptothecin, but not with docetaxel and paclitaxel in MDA-MB-468 cells. Notably, these synergistic interactions occurred at doses lower than the  $IC_{50}$  of each drug, therefore potentially minimizing their cytotoxic side-effects when used in combination *in vivo*. MS023 treatment was shown to sensitize ovarian cancer cells to cisplatin [56] and CRC cells to SN-38, a camptothecin derivative [57]. In order to generalize our findings, we are currently evaluating these combinations in additional TNBC cell lines.

The highest synergy was observed when we combined both type I PRMT inhibitors with erlotinib in MDA-MB-468 cells, a cell line overexpressing EGFR [17]. It would be valuable to test this combination in other TNBC cell lines to verify whether this synergy is associated with EGFR overexpression. We have previously reported a synergistic interaction between erlotinib and a PRMT5 inhibitor, independently of the EGFR expression status of TNBC cell lines [17]. Although EGFR is overexpressed in TNBC, targeting EGFR on its own has shown only a modest effect in clinical trials in TNBC patients [3]. Considering our results, it may be beneficial to combine EGFR and PRMT inhibitors to treat TNBC. However, this hypothesis must be tested *in vivo* in various TNBC patient-derived xenograft (PDX) models. Additional studies have reported that type I PRMT inhibitors synergize with inhibitors targeting PARP in TNBC [58] and lung cancer [59]; PRMT5 in leukemia, pancreatic, and lung cancer [19,60,61]; FLT3 kinase in leukemia [62,63]; or anti-PD-1/PD-L1 in various cancer types [64,65]. Altogether, this also highlights the potential clinical relevance of combining type I PRMT inhibitors with targeted therapies.

We performed pre-clinical studies to explore the translational relevance of targeting PRMT1 using GSK3368715, which is being evaluated in a phase I clinical trial. We show that this inhibitor significantly reduced tumor growth in an MDA-MB-468-derived xenograft model, aligning with a previous study (supplemental data from [19]). In contrast to Fedoriw et al., who directly injected these cells into the mice [19], we employed a two-step protocol in order to engraft tumors before treating the mice to better represent the clinical setting. In this condition, we observed a similar reduction in tumor growth by using a reduced inhibitor dose (80 mg/kg in our study vs. 150 mg/kg [19]). Type I PRMT inhibitors have also been shown to decrease tumor growth in other cancer types such as lymphoma [19], pancreatic [19,38], hepatocellular carcinoma [66], and colon [64,67] cancers. Therefore, targeting type I PRMTs could represent a new treatment strategy in various cancer types, including BC. Additionally, we have evidence supporting the idea that combining the type I PRMT inhibitors with chemotherapies or targeted therapies could be beneficial for the treatment of TNBC. This must be evaluated in various TNBC PDX models to account for the inter- and intra-tumor heterogeneity observed within TNBC [2]. Intra-tumor heterogeneity poses a major challenge in treating TNBC patients because of a subpopulation of cells resistant to chemotherapies, leading to residual disease and relapse [2]. These chemo-resistant cells are believed to be fueled by developmental pathways such as the Wnt signaling pathway [2,4,5], hence, inhibiting PRMT1 may eradicate

these resistant cells. Therefore, addressing whether the drug combinations identified here (*in vitro*) could overcome relapse in chemo-resistant TNBC PDX models would be clinically valuable.

## 5. Conclusions

The current paucity of targeted therapies for TNBC patients has prompted researchers to find novel treatment strategies. PRMT enzymes have recently emerged as attractive therapeutic targets for several cancer types, including BC. Here, we report that PRMT1, the major type I PRMT, is highly expressed in all BC subtypes, regulates two major signaling pathways activated in TNBC (EGFR and Wnt), and is required for cell survival. In addition, our study suggests that the combinatorial inhibition of type I PRMTs with chemotherapies could be clinically beneficial for TNBC patients.

**Supplementary Materials:** The following are available online at <https://www.mdpi.com/article/10.3390/cancers14020306/s1>, Figure S1: Correlation and survival analyses and validation of PRMT1 antibody for IHC, Figure S2: PRMT1 depletion decreases cell viability, colony forming ability and induces apoptosis in various BC cell lines, Figure S3: Type I PRMT inhibitors decrease PRMT1 but not CARM1 and PRMT6 activity under the tested conditions, Figure S4: Type I PRMT inhibitors decrease colony size in TNBC cells, Figure S5: GSK3368715 treatment shows no toxicity and increases global monomethylation in mice, Figure S6: PRMT1 regulates EGFR and Wnt signaling pathways, Figure S7: Synergistic interactions between MS023 (a type I PRMT inhibitor) and chemotherapies (A–C) or erlotinib (D), Figure S8: Additive interactions between type I PRMT inhibitors and taxanes, Figure S9: Uncropped original blots of Figure 2D, Figure S10: Uncropped original blots of Figure 3D, Figure S11: (A) uncropped original blots of Figure 4D. (B) uncropped original blots of Figure 4H, Figure S12: Uncropped original blots of Figure 5D, Figure S13: Uncropped original blots of Figure S1D, Figure S14: Uncropped original blots of Figure S2A, Figure S15: Uncropped original blots of Figure S2D for HCC70 cell line, Figure S16: Uncropped original blots of Figure S2D for MDA-MB-231 cell line, Figure S17: Uncropped original blots of Figure S2D for SKBr3 cell line, Figure S18: Uncropped original blots of Figure S2D for T47D cell line, Figure S19: Uncropped original blots of Figure S3 (for remaining blots, see Figure S20), Figure S20: Remaining uncropped original blots of Figure S3, Figure S21: Uncropped original blot of Figure S5B, Table S1: Antibodies, primers, siRNAs and drugs, Table S2: Differentially expressed genes in PRMT1-depleted MDA-MB-468 cells, Table S3: PRMT1 DNA copy number gain and loss in the curie cohort.

**Author Contributions:** Conceptualization, S.S. and T.D.; data curation, T.D.; formal analysis, S.S., A.B., F.N. and M.Y.; funding acquisition, S.R.-R. and T.D.; investigation, S.S., S.H., A.B., F.N., R.D., C.P., E.M., C.R., D.C.S., D.M. and A.N.; project administration, T.D.; resources, T.D.; software, M.Y.; supervision, D.M., A.N., D.G., H.F.-K., M.L.R., D.D. and T.D.; validation, S.S., S.H., A.B., R.D. and C.P.; visualization, S.S., S.H., A.B., F.N., R.D., C.P., M.Y. and T.D.; writing—original draft, S.S. and T.D.; writing—review and editing, S.S., S.H., A.B., F.N., R.D., C.P., M.Y., E.M., C.R., D.C.S., D.M., A.N., D.G., H.F.-K., M.L.R., D.D., S.R.-R. and T.D. All authors have read and agreed to the published version of the manuscript.

**Funding:** This work was supported by the Institut Curie, the Institut de Recherches Servier. SS was funded by the European Union’s Horizon 2020 Research and Innovation Programme (Marie Skłodowska-Curie grant agreement No 666003). RD was financed by the French Embassy and the Lebanese University (Safar Volet 1). The laboratory of MLR and CP was funded by “La Ligue contre le Cancer” and “Fondation ARC pour la recherche sur le cancer”.

**Institutional Review Board Statement:** Animal care and use for this study were performed in accordance with the recommendations of the European Community (2010/63/UE) for the care and use of laboratory animals. Experimental procedures were specifically approved by the ethics committee of the Institut Curie CEEA-IC #118 (Authorization APAFiS# 25870-2020060410487032 v1 given by National Authority) in compliance with the international guidelines.

**Informed Consent Statement:** The cohort used in this study has been previously published [6,17,30,31]. Informed consent was not required. However, women were informed of the research use of their tissues and did not declare any opposition for such research.

**Data Availability Statement:** The transcriptomic data generated in this study are available in supplementary data files (Table S2).

**Acknowledgments:** We are grateful to Bérengère Marty-Prouvost for her experimental contribution, particularly for the sample preparation used for the transcriptomic analysis. We thank Virginie Maire for helpful advice, and Faisal Mahmood and Ramon Garcia-Areas for enriching discussion regarding the Wnt signaling pathway. We thank Ausra Surmieliova for performing the PRMT1-ChIP experiments, and Laetitia Lesage for scanning the PRMT1 IHC slides. We are grateful to Amber Anirah for verifying the English language of the manuscript.

**Conflicts of Interest:** The authors declare no conflict of interest.

## References

1. Loibl, S.; Poortmans, P.; Morrow, M.; Denkert, C.; Curigliano, G. Breast cancer. *Lancet* **2021**, *397*, 1750–1769. [[CrossRef](#)]
2. Manjunath, M.; Choudhary, B. Triple-negative breast cancer: A run-through of features, classification and current therapies. *Oncol. Lett.* **2021**, *22*, 512. [[CrossRef](#)]
3. You, K.S.; Yi, Y.W.; Cho, J.; Park, J.S.; Seong, Y.S. Potentiating Therapeutic Effects of Epidermal Growth Factor Receptor Inhibition in Triple-Negative Breast Cancer. *Pharmaceuticals* **2021**, *14*, 589. [[CrossRef](#)]
4. Pohl, S.G.; Brook, N.; Agostino, M.; Arfuso, F.; Kumar, A.P.; Dharmarajan, A. Wnt signaling in triple-negative breast cancer. *Oncogenesis* **2017**, *6*, e310. [[CrossRef](#)]
5. Merikhian, P.; Eisavand, M.R.; Farahmand, L. Triple-negative breast cancer: Understanding Wnt signaling in drug resistance. *Cancer Cell Int.* **2021**, *21*, 419. [[CrossRef](#)]
6. Maubant, S.; Tahtouh, T.; Brisson, A.; Maire, V.; Nemati, F.; Tesson, B.; Ye, M.; Rigaiil, G.; Noizet, M.; Dumont, A.; et al. LRP5 regulates the expression of STK40, a new potential target in triple-negative breast cancers. *Oncotarget* **2018**, *9*, 22586–22604. [[CrossRef](#)] [[PubMed](#)]
7. Torres, V.I.; Godoy, J.A.; Inestrosa, N.C. Modulating Wnt signaling at the root: Porcupine and Wnt acylation. *Pharmacol. Ther.* **2019**, *198*, 34–45. [[CrossRef](#)]
8. Xu, J.; Richard, S. Cellular pathways influenced by protein arginine methylation: Implications for cancer. *Mol. Cell* **2021**, *81*, 4357–4368. [[CrossRef](#)] [[PubMed](#)]
9. Jarrold, J.; Davies, C.C. PRMTs and Arginine Methylation: Cancer’s Best-Kept Secret? *Trends Mol. Med.* **2019**, *25*, 993–1009. [[CrossRef](#)]
10. Wu, Q.; Schapira, M.; Arrowsmith, C.H.; Barsyte-Lovejoy, D. Protein arginine methylation: From enigmatic functions to therapeutic targeting. *Nat. Rev. Drug Discov.* **2021**, *20*, 509–530. [[CrossRef](#)] [[PubMed](#)]
11. Guccione, E.; Richard, S. The regulation, functions and clinical relevance of arginine methylation. *Nat. Rev. Mol. Cell Biol.* **2019**, *20*, 642–657. [[CrossRef](#)] [[PubMed](#)]
12. Yang, Y.; Bedford, M.T. Protein arginine methyltransferases and cancer. *Nat. Rev. Cancer* **2013**, *13*, 37–50. [[CrossRef](#)] [[PubMed](#)]
13. Suresh, S.; Huard, S.; Dubois, T. CARM1/PRMT4: Making Its Mark beyond Its Function as a Transcriptional Coactivator. *Trends Cell Biol.* **2021**, *31*, 402–417. [[CrossRef](#)] [[PubMed](#)]
14. Thiebaut, C.; Eve, L.; Poulard, C.; Le Romancer, M. Structure, Activity, and Function of PRMT1. *Life* **2021**, *11*, 1147. [[CrossRef](#)]
15. Morettin, A.; Baldwin, R.M.; Cote, J. Arginine methyltransferases as novel therapeutic targets for breast cancer. *Mutagenesis* **2015**, *30*, 177–189. [[CrossRef](#)] [[PubMed](#)]
16. Lattouf, H.; Kasseem, L.; Jacquemetton, J.; Choucair, A.; Poulard, C.; Tredan, O.; Corbo, L.; Diab-Assaf, M.; Hussein, N.; Treilleux, I.; et al. LKB1 regulates PRMT5 activity in breast cancer. *Int. J. Cancer* **2019**, *144*, 595–606. [[CrossRef](#)] [[PubMed](#)]
17. Vinet, M.; Suresh, S.; Maire, V.; Monchecourt, C.; Nemati, F.; Lesage, L.; Pierre, F.; Ye, M.; Lescure, A.; Brisson, A.; et al. Protein arginine methyltransferase 5: A novel therapeutic target for triple-negative breast cancers. *Cancer Med.* **2019**, *8*, 2414–2428. [[CrossRef](#)]
18. Eram, M.S.; Shen, Y.; Szewczyk, M.; Wu, H.; Senisterra, G.; Li, F.; Butler, K.V.; Kaniskan, H.U.; Speed, B.A.; Dela Sena, C.; et al. A Potent, Selective, and Cell-Active Inhibitor of Human Type I Protein Arginine Methyltransferases. *ACS Chem. Biol.* **2016**, *11*, 772–781. [[CrossRef](#)]
19. Fedoriw, A.; Rajapurkar, S.R.; O’Brien, S.; Gerhart, S.V.; Mitchell, L.H.; Adams, N.D.; Rioux, N.; Lingaraj, T.; Ribich, S.A.; Pappalardi, M.B.; et al. Anti-tumor Activity of the Type I PRMT Inhibitor, GSK3368715, Synergizes with PRMT5 Inhibition through MTAP Loss. *Cancer Cell* **2019**, *36*, 100–114.e25. [[CrossRef](#)]
20. Liao, H.W.; Hsu, J.M.; Xia, W.; Wang, H.L.; Wang, Y.N.; Chang, W.C.; Arold, S.T.; Chou, C.K.; Tsou, P.H.; Yamaguchi, H.; et al. PRMT1-mediated methylation of the EGF receptor regulates signaling and cetuximab response. *J. Clin. Investig.* **2015**, *125*, 4529–4543. [[CrossRef](#)]
21. Nakai, K.; Xia, W.; Liao, H.W.; Saito, M.; Hung, M.C.; Yamaguchi, H. The role of PRMT1 in EGFR methylation and signaling in MDA-MB-468 triple-negative breast cancer cells. *Breast Cancer* **2018**, *25*, 74–80. [[CrossRef](#)] [[PubMed](#)]
22. Hsu, J.M.; Chen, C.T.; Chou, C.K.; Kuo, H.P.; Li, L.Y.; Lin, C.Y.; Lee, H.J.; Wang, Y.N.; Liu, M.; Liao, H.W.; et al. Crosstalk between Arg 1175 methylation and Tyr 1173 phosphorylation negatively modulates EGFR-mediated ERK activation. *Nat. Cell Biol.* **2011**, *13*, 174–181. [[CrossRef](#)] [[PubMed](#)]



23. Yao, B.; Gui, T.; Zeng, X.; Deng, Y.; Wang, Z.; Wang, Y.; Yang, D.; Li, Q.; Xu, P.; Hu, R.; et al. PRMT1-mediated H4R3me2a recruits SMARCA4 to promote colorectal cancer progression by enhancing EGFR signaling. *Genome Med.* **2021**, *13*, 58. [[CrossRef](#)] [[PubMed](#)]
24. Takai, H.; Masuda, K.; Sato, T.; Sakaguchi, Y.; Suzuki, T.; Suzuki, T.; Koyama-Nasu, R.; Nasu-Nishimura, Y.; Katou, Y.; Ogawa, H.; et al. 5-Hydroxymethylcytosine plays a critical role in glioblastomagenesis by recruiting the CHTOP-methylosome complex. *Cell Rep.* **2014**, *9*, 48–60. [[CrossRef](#)] [[PubMed](#)]
25. Bikkavilli, R.K.; Malbon, C.C. Wnt3a-stimulated LRP6 phosphorylation is dependent upon arginine methylation of G3BP2. *J. Cell Sci.* **2012**, *125*, 2446–2456. [[CrossRef](#)] [[PubMed](#)]
26. Bikkavilli, R.K.; Malbon, C.C. Arginine methylation of G3BP1 in response to Wnt3a regulates beta-catenin mRNA. *J. Cell Sci.* **2011**, *124*, 2310–2320. [[CrossRef](#)]
27. Cha, B.; Kim, W.; Kim, Y.K.; Hwang, B.N.; Park, S.Y.; Yoon, J.W.; Park, W.S.; Cho, J.W.; Bedford, M.T.; Jho, E.H. Methylation by protein arginine methyltransferase 1 increases stability of Axin, a negative regulator of Wnt signaling. *Oncogene* **2011**, *30*, 2379–2389. [[CrossRef](#)]
28. Bikkavilli, R.K.; Avasara, S.; Vanscoyk, M.; Sechler, M.; Kelley, N.; Malbon, C.C.; Winn, R.A. Dishevelled3 is a novel arginine methyl transferase substrate. *Sci. Rep.* **2012**, *2*, 805. [[CrossRef](#)]
29. Poulard, C.; Corbo, L.; Le Romancer, M. Protein arginine methylation/demethylation and cancer. *Oncotarget* **2016**, *7*, 67532–67550. [[CrossRef](#)]
30. Maire, V.; Nemati, F.; Richardson, M.; Vincent-Salomon, A.; Tesson, B.; Rigai, G.; Gravier, E.; Marty-Prouvost, B.; De Koning, L.; Lang, G.; et al. Polo-like kinase 1: A potential therapeutic option in combination with conventional chemotherapy for the management of patients with triple-negative breast cancer. *Cancer Res.* **2013**, *73*, 813–823. [[CrossRef](#)]
31. Maire, V.; Baldeyron, C.; Richardson, M.; Tesson, B.; Vincent-Salomon, A.; Gravier, E.; Marty-Prouvost, B.; De Koning, L.; Rigai, G.; Dumont, A.; et al. TTK/hMPS1 is an attractive therapeutic target for triple-negative breast cancer. *PLoS ONE* **2013**, *8*, e63712. [[CrossRef](#)]
32. Marty, B.; Maire, V.; Gravier, E.; Rigai, G.; Vincent-Salomon, A.; Kappler, M.; Lebigot, I.; Djelti, F.; Tourdes, A.; Gestraud, P.; et al. Frequent PTEN genomic alterations and activated phosphatidylinositol 3-kinase pathway in basal-like breast cancer cells. *Breast Cancer Res.* **2008**, *10*, R101. [[CrossRef](#)]
33. Bao, X.; Siprashvili, Z.; Zarnegar, B.J.; Shenoy, R.M.; Rios, E.J.; Nady, N.; Qu, K.; Mah, A.; Webster, D.E.; Rubin, A.J.; et al. CSNK1a1 Regulates PRMT1 to Maintain the Progenitor State in Self-Renewing Somatic Tissue. *Dev. Cell* **2017**, *43*, 227–239.e5. [[CrossRef](#)]
34. Subramanian, A.; Tamayo, P.; Mootha, V.K.; Mukherjee, S.; Ebert, B.L.; Gillette, M.A.; Paulovich, A.; Pomeroy, S.L.; Golub, T.R.; Lander, E.S.; et al. Gene set enrichment analysis: A knowledge-based approach for interpreting genome-wide expression profiles. *Proc. Natl. Acad. Sci. USA* **2005**, *102*, 15545–15550. [[CrossRef](#)]
35. Di Veroli, G.Y.; Fornari, C.; Wang, D.; Mollard, S.; Bramhall, J.L.; Richards, F.M.; Jodrell, D.I. CombeneFit: An interactive platform for the analysis and visualization of drug combinations. *Bioinformatics* **2016**, *32*, 2866–2868. [[CrossRef](#)]
36. Györfy, B.; Lanczky, A.; Eklund, A.C.; Denkert, C.; Budczies, J.; Li, Q.; Szallasi, Z. An online survival analysis tool to rapidly assess the effect of 22,277 genes on breast cancer prognosis using microarray data of 1809 patients. *Breast Cancer Res. Treat.* **2010**, *123*, 725–731. [[CrossRef](#)]
37. Liu, L.M.; Sun, W.Z.; Fan, X.Z.; Xu, Y.L.; Cheng, M.B.; Zhang, Y. Methylation of C/EBPalpha by PRMT1 Inhibits Its Tumor-Suppressive Function in Breast Cancer. *Cancer Res.* **2019**, *79*, 2865–2877. [[CrossRef](#)]
38. Giuliani, V.; Miller, M.A.; Liu, C.Y.; Hartono, S.R.; Class, C.A.; Bristow, C.A.; Suzuki, E.; Sanz, L.A.; Gao, G.; Gay, J.P.; et al. PRMT1-dependent regulation of RNA metabolism and DNA damage response sustains pancreatic ductal adenocarcinoma. *Nat. Commun.* **2021**, *12*, 4626. [[CrossRef](#)]
39. Malbeteau, L.; Poulard, C.; Languilaire, C.; Mikaelian, I.; Flamant, F.; Le Romancer, M.; Corbo, L. PRMT1 Is Critical for the Transcriptional Activity and the Stability of the Progesterone Receptor. *iScience* **2020**, *23*, 101236. [[CrossRef](#)]
40. Maubant, S.; Tesson, B.; Maire, V.; Ye, M.; Rigai, G.; Gentien, D.; Cruzalegui, F.; Tucker, G.C.; Roman-Roman, S.; Dubois, T. Transcriptome analysis of Wnt3a-treated triple-negative breast cancer cells. *PLoS ONE* **2015**, *10*, e0122333. [[CrossRef](#)]
41. Tang, J.; Wennerberg, K.; Aittokallio, T. What is synergy? The Saariselka agreement revisited. *Front. Pharmacol.* **2015**, *6*, 181. [[CrossRef](#)] [[PubMed](#)]
42. Yoshimatsu, M.; Toyokawa, G.; Hayami, S.; Unoki, M.; Tsunoda, T.; Field, H.I.; Kelly, J.D.; Neal, D.E.; Maehara, Y.; Ponder, B.A.; et al. Dysregulation of PRMT1 and PRMT6, Type I arginine methyltransferases, is involved in various types of human cancers. *Int. J. Cancer* **2011**, *128*, 562–573. [[CrossRef](#)]
43. Goulet, I.; Gauvin, G.; Boisvenue, S.; Cote, J. Alternative splicing yields protein arginine methyltransferase 1 isoforms with distinct activity, substrate specificity, and subcellular localization. *J. Biol. Chem.* **2007**, *282*, 33009–33021. [[CrossRef](#)] [[PubMed](#)]
44. Mathioudaki, K.; Scorilas, A.; Ardavanis, A.; Lymberi, P.; Tsiambas, E.; Devetzi, M.; Apostolaki, A.; Talieri, M. Clinical evaluation of PRMT1 gene expression in breast cancer. *Tumour Biol.* **2011**, *32*, 575–582. [[CrossRef](#)] [[PubMed](#)]
45. Baldwin, R.M.; Moret, A.; Cote, J. Role of PRMTs in cancer: Could minor isoforms be leaving a mark? *World J. Biol. Chem.* **2014**, *5*, 115–129. [[CrossRef](#)]
46. Wang, J.; Wang, C.; Xu, P.; Li, X.; Lu, Y.; Jin, D.; Yin, X.; Jiang, H.; Huang, J.; Xiong, H.; et al. PRMT1 is a novel molecular therapeutic target for clear cell renal cell carcinoma. *Theranostics* **2021**, *11*, 5387–5403. [[CrossRef](#)]

47. Filipovic, J.; Bosic, M.; Cirovic, S.; Zivotic, M.; Dunderovic, D.; Dordevic, D.; Zivkovic-Perisic, S.; Lipkovski, A.; Markovic-Lipkovski, J. PRMT1 expression in renal cell tumors- application in differential diagnosis and prognostic relevance. *Diagn Pathol.* **2019**, *14*, 120. [[CrossRef](#)] [[PubMed](#)]
48. Repenning, A.; Happel, D.; Bouchard, C.; Meixner, M.; Verel-Yilmaz, Y.; Raifer, H.; Holembowski, L.; Krause, E.; Kremmer, E.; Feederle, R.; et al. PRMT1 promotes the tumor suppressor function of p14(ARF) and is indicative for pancreatic cancer prognosis. *EMBO J.* **2021**, *40*, e106777. [[CrossRef](#)]
49. Choucair, A.; Pham, T.H.; Omarjee, S.; Jacquemetton, J.; Kassem, L.; Tredan, O.; Rambaud, J.; Marangoni, E.; Corbo, L.; Treilleux, I.; et al. The arginine methyltransferase PRMT1 regulates IGF-1 signaling in breast cancer. *Oncogene* **2019**, *38*, 4015–4027. [[CrossRef](#)]
50. Gao, Y.; Zhao, Y.; Zhang, J.; Lu, Y.; Liu, X.; Geng, P.; Huang, B.; Zhang, Y.; Lu, J. The dual function of PRMT1 in modulating epithelial-mesenchymal transition and cellular senescence in breast cancer cells through regulation of ZEB1. *Sci. Rep.* **2016**, *6*, 19874. [[CrossRef](#)]
51. Liu, L.M.; Tang, Q.; Hu, X.; Zhao, J.J.; Zhang, Y.; Ying, G.G.; Zhang, F. Arginine Methyltransferase PRMT1 Regulates p53 Activity in Breast Cancer. *Life* **2021**, *11*, 789. [[CrossRef](#)] [[PubMed](#)]
52. Baldwin, R.M.; Moretton, A.; Paris, G.; Goulet, I.; Cote, J. Alternatively spliced protein arginine methyltransferase 1 isoform PRMT1v2 promotes the survival and invasiveness of breast cancer cells. *Cell Cycle* **2012**, *11*, 4597–4612. [[CrossRef](#)]
53. Yin, X.K.; Wang, Y.L.; Wang, F.; Feng, W.X.; Bai, S.M.; Zhao, W.W.; Feng, L.L.; Wei, M.B.; Qin, C.L.; Wang, F.; et al. PRMT1 enhances oncogenic arginine methylation of NONO in colorectal cancer. *Oncogene* **2021**, *40*, 1375–1389. [[CrossRef](#)] [[PubMed](#)]
54. Zhang, X.P.; Jiang, Y.B.; Zhong, C.Q.; Ma, N.; Zhang, E.B.; Zhang, F.; Li, J.J.; Deng, Y.Z.; Wang, K.; Xie, D.; et al. PRMT1 Promoted HCC Growth and Metastasis In Vitro and In Vivo via Activating the STAT3 Signalling Pathway. *Cell Physiol. Biochem.* **2018**, *47*, 1643–1654. [[CrossRef](#)]
55. Chuang, C.Y.; Chang, C.P.; Lee, Y.J.; Lin, W.L.; Chang, W.W.; Wu, J.S.; Cheng, Y.W.; Lee, H.; Li, C. PRMT1 expression is elevated in head and neck cancer and inhibition of protein arginine methylation by adenosine dialdehyde or PRMT1 knockdown downregulates proliferation and migration of oral cancer cells. *Oncol. Rep.* **2017**, *38*, 1115–1123. [[CrossRef](#)]
56. Musiani, D.; Giambruno, R.; Massignani, E.; Ippolito, M.R.; Maniaci, M.; Jammula, S.; Manganaro, D.; Cuomo, A.; Nicosia, L.; Pasini, D.; et al. PRMT1 Is Recruited via DNA-PK to Chromatin Where It Sustains the Senescence-Associated Secretory Phenotype in Response to Cisplatin. *Cell Rep.* **2020**, *30*, 1208–1222.e9. [[CrossRef](#)]
57. Lim, Y.; Lee, J.Y.; Ha, S.J.; Yu, S.; Shin, J.K.; Kim, H.C. Proteome-wide identification of arginine methylation in colorectal cancer tissues from patients. *Proteome Sci.* **2020**, *18*, 6. [[CrossRef](#)]
58. Hsu, W.J.; Chen, C.H.; Chang, Y.C.; Cheng, C.H.; Tsa, I.Y.; Lin, C.W. PRMT1 Confers Resistance to Olaparib via Modulating MYC Signaling in Triple-Negative Breast Cancer. *J. Pers. Med.* **2021**, *11*, 1009. [[CrossRef](#)]
59. Dominici, C.; Sgarioni, N.; Yu, Z.; Sesma-Sanz, L.; Masson, J.Y.; Richard, S.; Raynal, N.J. Synergistic effects of type I PRMT and PARP inhibitors against non-small cell lung cancer cells. *Clin. Epigenetics* **2021**, *13*, 54. [[CrossRef](#)] [[PubMed](#)]
60. Fong, J.Y.; Pignata, L.; Goy, P.A.; Kawabata, K.C.; Lee, S.C.; Koh, C.M.; Musiani, D.; Massignani, E.; Kotini, A.G.; Penson, A.; et al. Therapeutic Targeting of RNA Splicing Catalysis through Inhibition of Protein Arginine Methylation. *Cancer Cell* **2019**, *36*, 194–209.e9. [[CrossRef](#)] [[PubMed](#)]
61. Gao, G.; Zhang, L.; Villarreal, O.D.; He, W.; Su, D.; Bedford, E.; Moh, P.; Shen, J.; Shi, X.; Bedford, M.T.; et al. PRMT1 loss sensitizes cells to PRMT5 inhibition. *Nucleic Acids Res.* **2019**, *47*, 5038–5048. [[CrossRef](#)] [[PubMed](#)]
62. Zhu, Y.; He, X.; Lin, Y.C.; Dong, H.; Zhang, L.; Chen, X.; Wang, Z.; Shen, Y.; Li, M.; Wang, H.; et al. Targeting PRMT1-mediated FLT3 methylation disrupts maintenance of MLL-rearranged acute lymphoblastic leukemia. *Blood* **2019**, *134*, 1257–1268. [[CrossRef](#)]
63. He, X.; Zhu, Y.; Lin, Y.C.; Li, M.; Du, J.; Dong, H.; Sun, J.; Zhu, L.; Wang, H.; Ding, Z.; et al. PRMT1-mediated FLT3 arginine methylation promotes maintenance of FLT3-ITD(+) acute myeloid leukemia. *Blood* **2019**, *134*, 548–560. [[CrossRef](#)]
64. Lu, S.X.; De Neef, E.; Thomas, J.D.; Sabio, E.; Rousseau, B.; Gigoux, M.; Knorr, D.A.; Greenbaum, B.; Elhanati, Y.; Hogg, S.J.; et al. Pharmacologic modulation of RNA splicing enhances anti-tumor immunity. *Cell* **2021**, *184*, 4032–4047.e31. [[CrossRef](#)]
65. Zheng, N.N.; Zhou, M.; Sun, F.; Huai, M.X.; Zhang, Y.; Qu, C.Y.; Shen, F.; Xu, L.M. Combining protein arginine methyltransferase inhibitor and anti-programmed death-ligand-1 inhibits pancreatic cancer progression. *World J. Gastroenterol.* **2020**, *26*, 3737–3749. [[CrossRef](#)]
66. Hu, G.; Yan, C.; Xie, P.; Cao, Y.; Shao, J.; Ge, J. PRMT2 accelerates tumorigenesis of hepatocellular carcinoma by activating Bcl2 via histone H3R8 methylation. *Exp. Cell Res.* **2020**, *394*, 112152. [[CrossRef](#)]
67. Plotnikov, A.; Kozer, N.; Cohen, G.; Carvalho, S.; Duberstein, S.; Almog, O.; Solmesky, L.J.; Shurrush, K.A.; Babaev, I.; Benjamin, S.; et al. PRMT1 inhibition induces differentiation of colon cancer cells. *Sci. Rep.* **2020**, *10*, 20030. [[CrossRef](#)] [[PubMed](#)]

## Supplementary information for

### **PRMT1 regulates EGFR and Wnt signaling pathways and is a promising target for combinatorial treatment of breast cancer**

Samyuktha Suresh, Solène Huard, Amélie Brisson, Fariba Némati, Rayan Dakroub, Coralie Poulard, Mengliang Ye, Elise Martel, Cécile Reyes, David C. Silvestre, Didier Meseure, André Nicolas, David Gentien, Hussein Fayyad-Kazan, Muriel Le Romancer, Didier Decaudin, Sergio Roman-Roman and Thierry Dubois

Correspondence to: [thierry.dubois@curie.fr](mailto:thierry.dubois@curie.fr)

#### **This PDF file includes:**

Supplementary Figures. S1 to S21

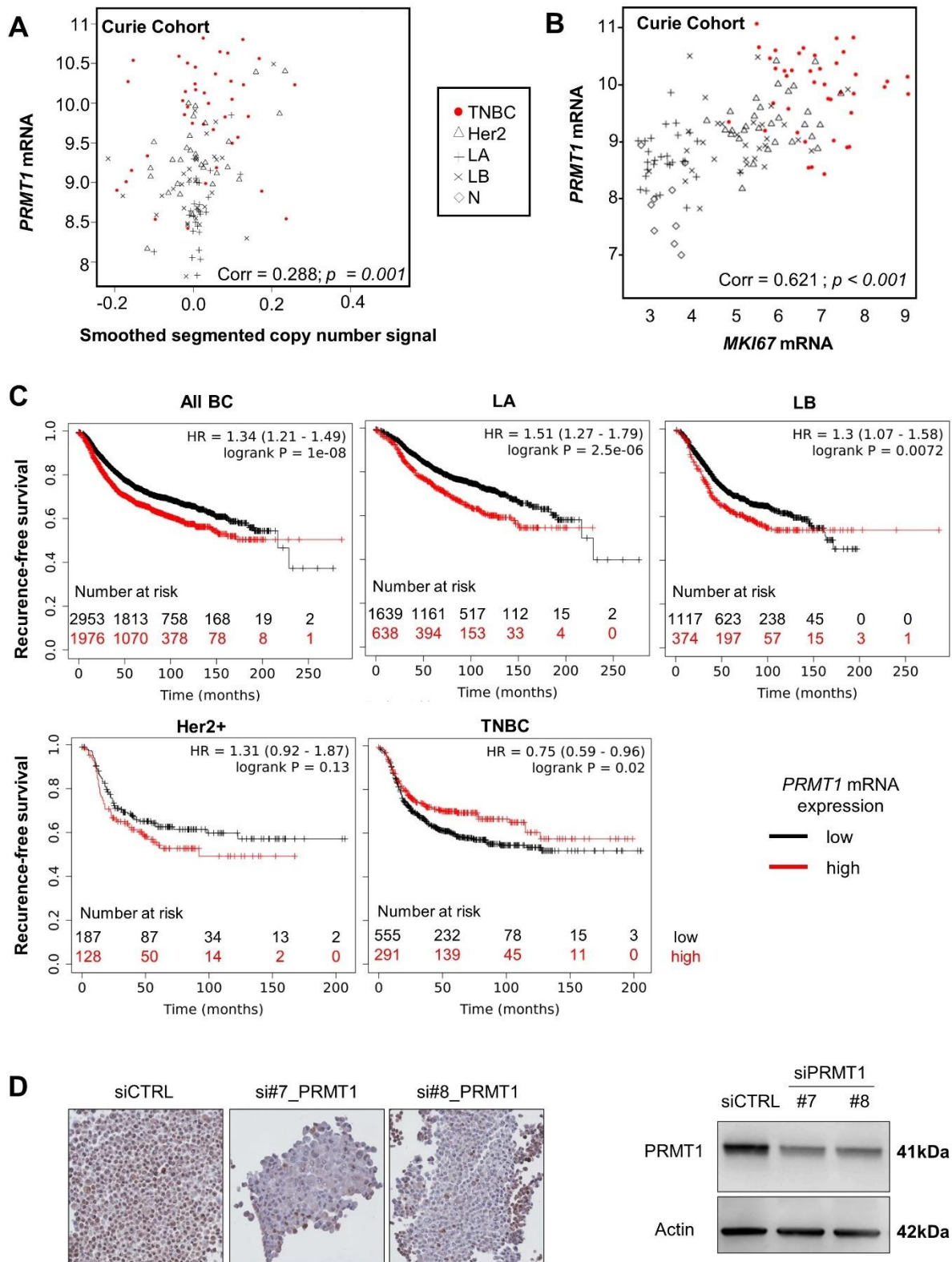
#### **Other Supplementary Materials for this manuscript include the following:**

Table S1 [Antibodies, Primers, siRNAs, and Drugs]

Table S2 [Differentially expressed genes in PRMT1-depleted MDA-MB-468 cells]

Table S3 [PRMT1 DNA copy number gain and loss in the curie cohort]

**Figure S1**



**Figure S1. Correlation and survival analyses and validation of PRMT1 antibody for IHC.** **A**, *PRMT1* mRNA expression correlates with DNA copy number in the whole population of BC in the Curie cohort (Spearman correlation). **B**, *PRMT1* and *MKI67* (proliferative marker) mRNA expression positively correlate in the whole BC population of the Curie cohort (Spearman correlation). **C**, *PRMT1* mRNA expression correlates with prognosis in BC. Recurrence-free survival based on *PRMT1* mRNA expression (Affy probe ID: 206445\_s\_at) was obtained from the Kaplan-Meier (KM) plotter website (<http://kmplot.com>). Best performing cutoff option was used: all BC (n=4929), Luminal B (LB, n=1491), Luminal A (LA, n=2277), Basal for TNBC (TN, n=846), and Her2+ (n=315). Hazard ratio with 95% confidence interval and log-rank p-values were calculated and significance threshold was set at  $p < 0.05$ . Of note, a similar figure plotting *PRMT1* mRNA expression (median cutoff) vs RFS in the whole BC population has been previously published (Liu et al., 2019, "Methylation of C/EBP $\alpha$  by PRMT1 Inhibits Its Tumor-Suppressive Function in Breast Cancer", *Cancer Res.* DOI: 10.1158/0008-5472.CAN-18-3211) but with a lower number of samples (4929 in our study compared to 3951 in their article). **D**, Validation of PRMT1 antibody for IHC staining. Left panel, PRMT1 antibody used for IHC (Fig. 1C) was validated using AFA-fixed cell pellets from MDA-MB-468 cells treated with control siRNA (CTRL) or two siRNAs targeting PRMT1 for 72 h (#7, #8). Right panel, PRMT1 depletion was verified by western blotting using an anti-PRMT1 antibody. Anti-actin antibody was used as a loading control.



**Figure S2**

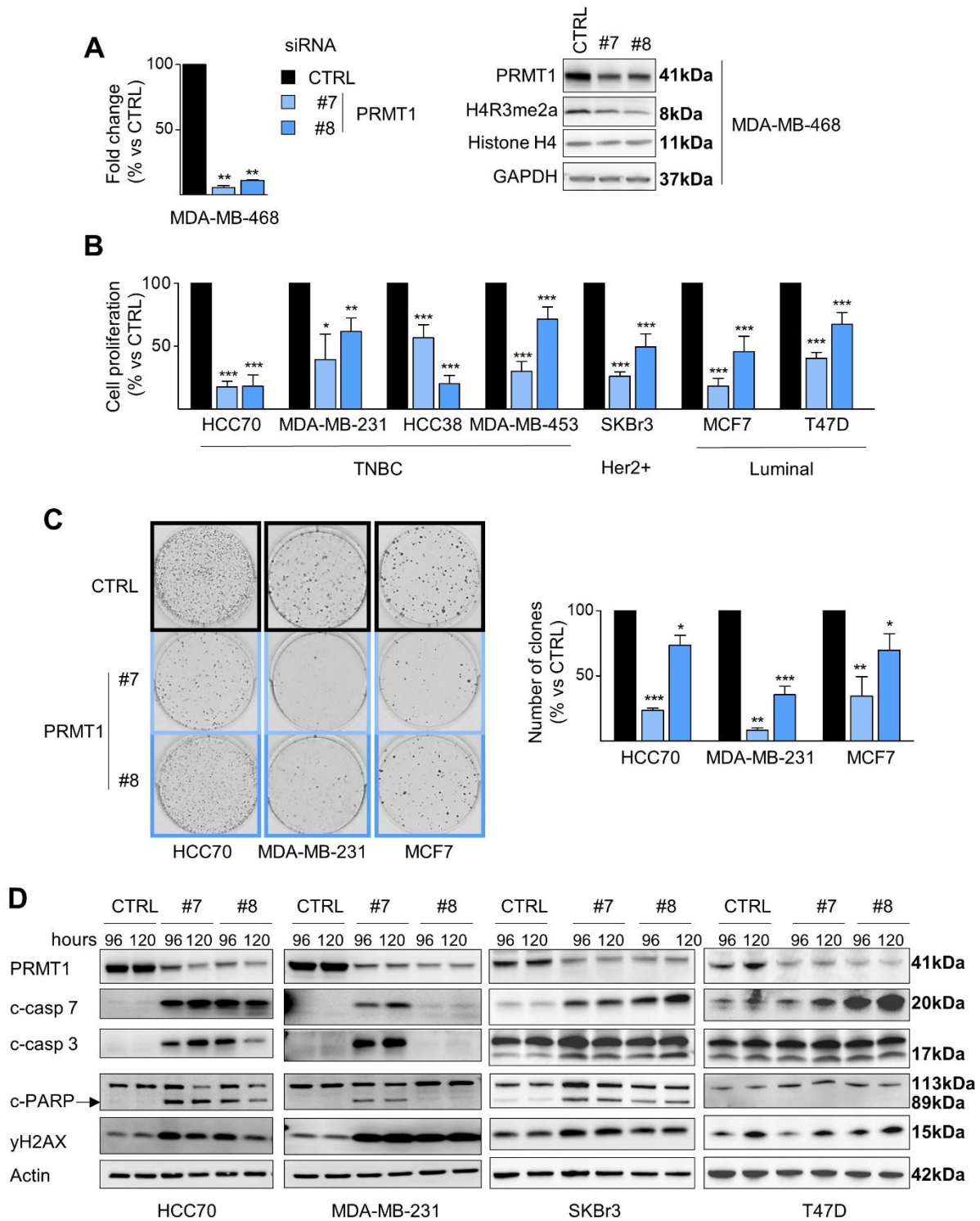


**Figure S2. PRMT1 depletion decreases cell viability, colony forming ability and induces apoptosis in various BC cell lines.**

**A**, Validation of PRMT1 siRNAs. MDA-MB-468 cells were treated with control (CTRL, black) or two PRMT1 (#7, #8, blue) siRNA for 48h. PRMT1 expression was detected at the mRNA (by RTqPCR, normalization by actin; left panel) and protein (by western blotting, right panel) levels. The methylation of histone H4 on Arg 3 (H4R3me2a) was used to measure PRMT1 activity and anti-histone H4 and anti-GAPDH antibodies were used as loading controls. **B**, PRMT1 depletion decreases the viability of BC cells. TNBC, Her2+, and luminal cells were transfected with control (CTRL, black) or two PRMT1 (#7, #8, blue) siRNAs for 144h and cell viability was measured by an MTT or WST1 assay. **C**, PRMT1 depletion decreases colony formation. TNBC and luminal cells were transfected with control (CTRL, black) or two PRMT1 (#7, #8, blue) siRNAs, and then cultured on plastic for 6 mitotic cycles equivalent to 14 (HCC70), 7 (MDA-MB-231) or 12 (MCF7) days. A representative image (left panel) and the quantifications (right panel) are shown. **D**, PRMT1 depletion induces apoptosis in BC cells. TNBC, Her2+ and luminal cells were transfected with control (CTRL) or two PRMT1 (#7, #8) siRNA for 96h or 120h. Apoptosis was detected by western blotting using antibodies recognizing the cleaved forms of caspase 7 (c-casp 7), caspase 3 (c-casp 3) and PARP (c-PARP). DNA damage was detected using an anti- $\gamma$ H2AX antibody. Anti-actin antibody was used as a loading control. The arrow indicates the cleaved form of PARP, while the upper band corresponds to total PARP protein. Results are presented as the percentage (B, C) or percent fold change (A) relative to control cells (CTRL). All data are expressed as the mean  $\pm$  SD from at least three independent experiments (A, B, C). Pictures are from a single experiment, representative of three independent experiments (A, C, D). P-values from a Student t-test are represented as \*p < 0.05; \*\*p < 0.01; \*\*\*p < 0.001.

**Figure S3**

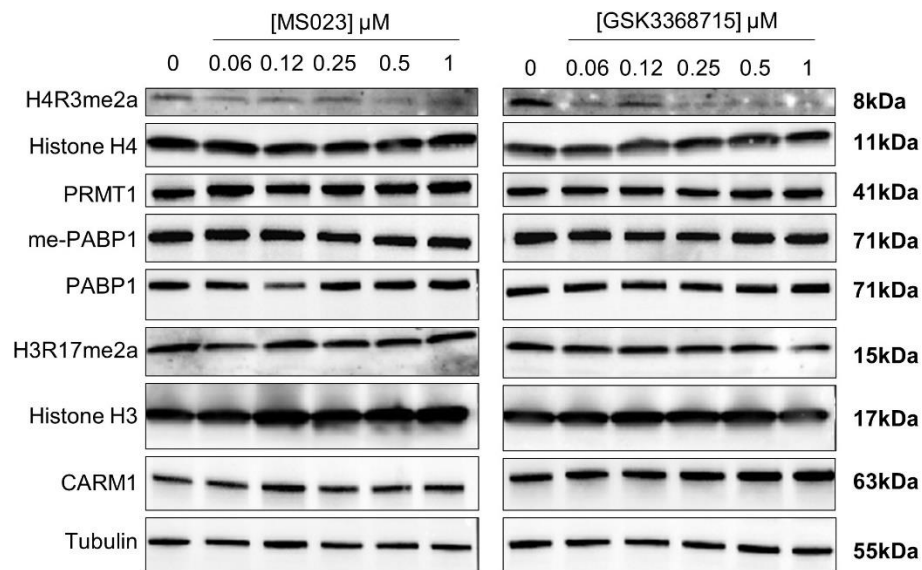


**Figure S3. Type I PRMT inhibitors decrease PRMT1 but not CARM1 and PRMT6 activity under the tested conditions.**

MDA-MB-468 cells were treated with varying concentrations of MS023 or GSK3368715 for 48h. PRMT1 inhibition was assessed by western blotting using anti-H4R3me2a antibody. Methylation of PABP1 (me-PABP1) was used to measure CARM1 activity and histone H3 methylation (H3R17me2a) to assess CARM1 and PRMT6 activities. Anti-PABP1, histone H3, CARM1, and tubulin antibodies were used as loading controls.



Figure S4

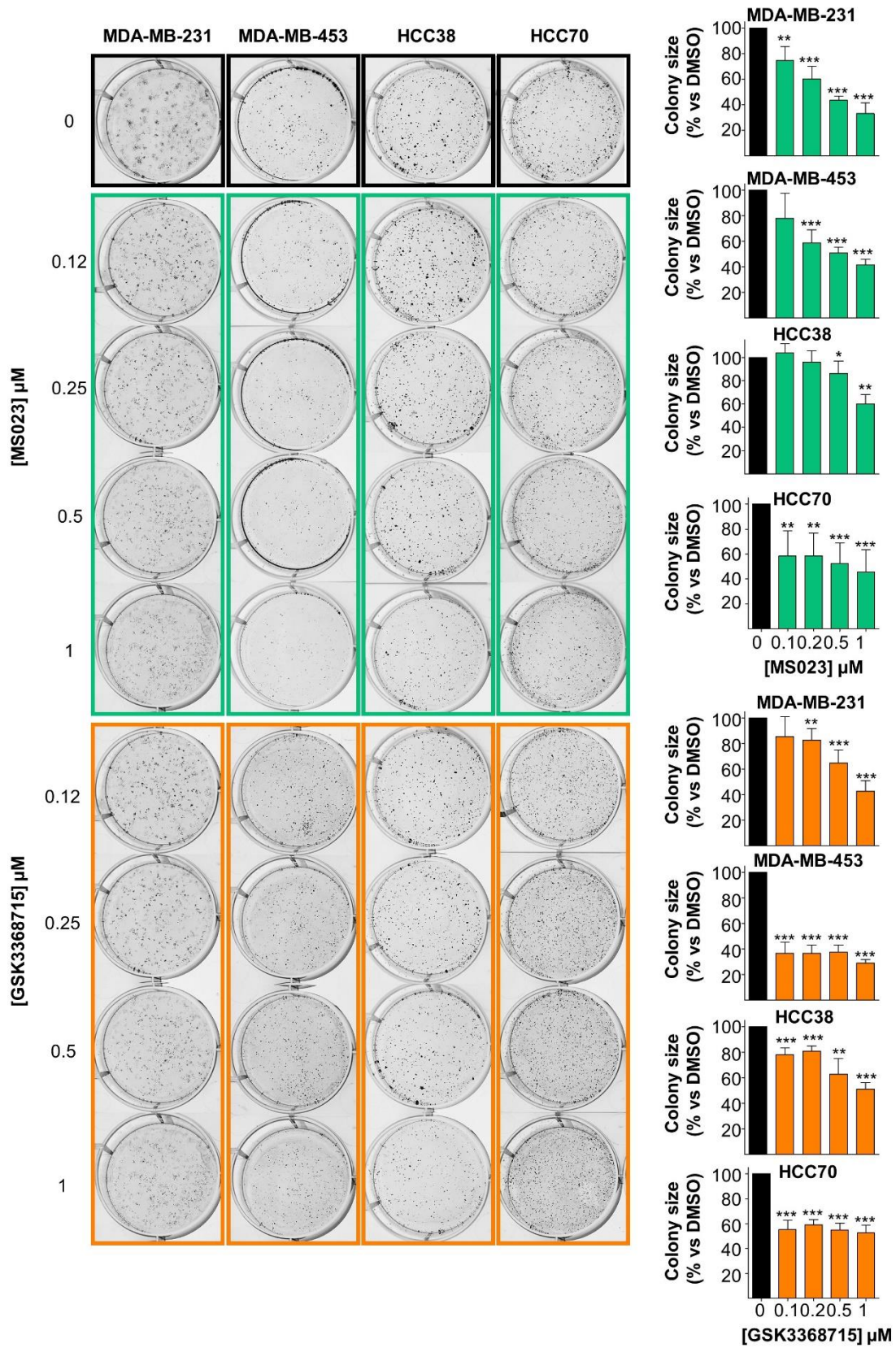


**Figure S4. Type I PRMT inhibitors decrease colony size in TNBC cells.**

MDA-MB-231, MDA-MB-453, HCC38, and HCC70 cells were cultured on plastic for 7 (MDA-MB-231) or 14 (MDA-MB-453, HCC38, and HCC70) days after MS023 (green) or GSK3368715 (orange) treatment. The quantification of colony size is expressed as a percentage relative to DMSO-treated cells (black), represented as the mean  $\pm$  SD from two independent experiments performed in triplicates. P-values are from a Student t-test and represented as \* $p < 0.05$ ; \*\* $p < 0.01$ ; \*\*\* $p < 0.001$ .

Figure S5

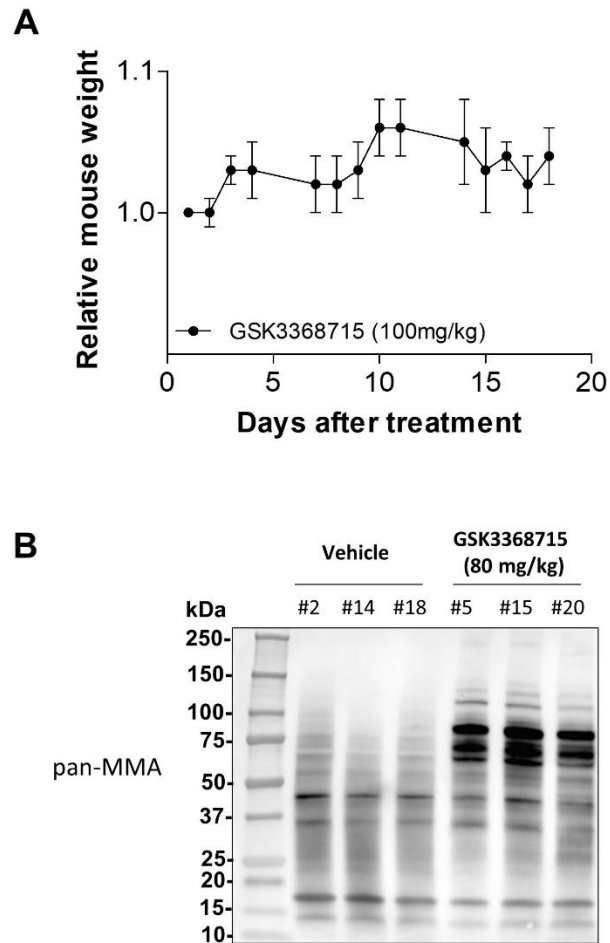


**Figure S5. GSK3368715 treatment shows no toxicity and increases global monomethylation in mice.**

**A**, GSK3368715 treatment is not toxic for mice at the tested dose. GSK3368715 was administered in Swiss-nude mice (n=3) at 100 mg/kg per-os, once daily for 18 days. Treatment was not associated with any mortality or body weight loss during this period.

**B**, GSK3368715 treatment (80 mg/kg) increases global monomethylation, *in vivo*. Total monomethylation was detected by western blotting using anti-pan monomethylated (pan-MMA) antibodies in the tumors excised from 3 vehicle (#2, #14, #18)- or GSK3368715 (#5, #15, #20)-treated mice at the end of the experiment.

Figure S6

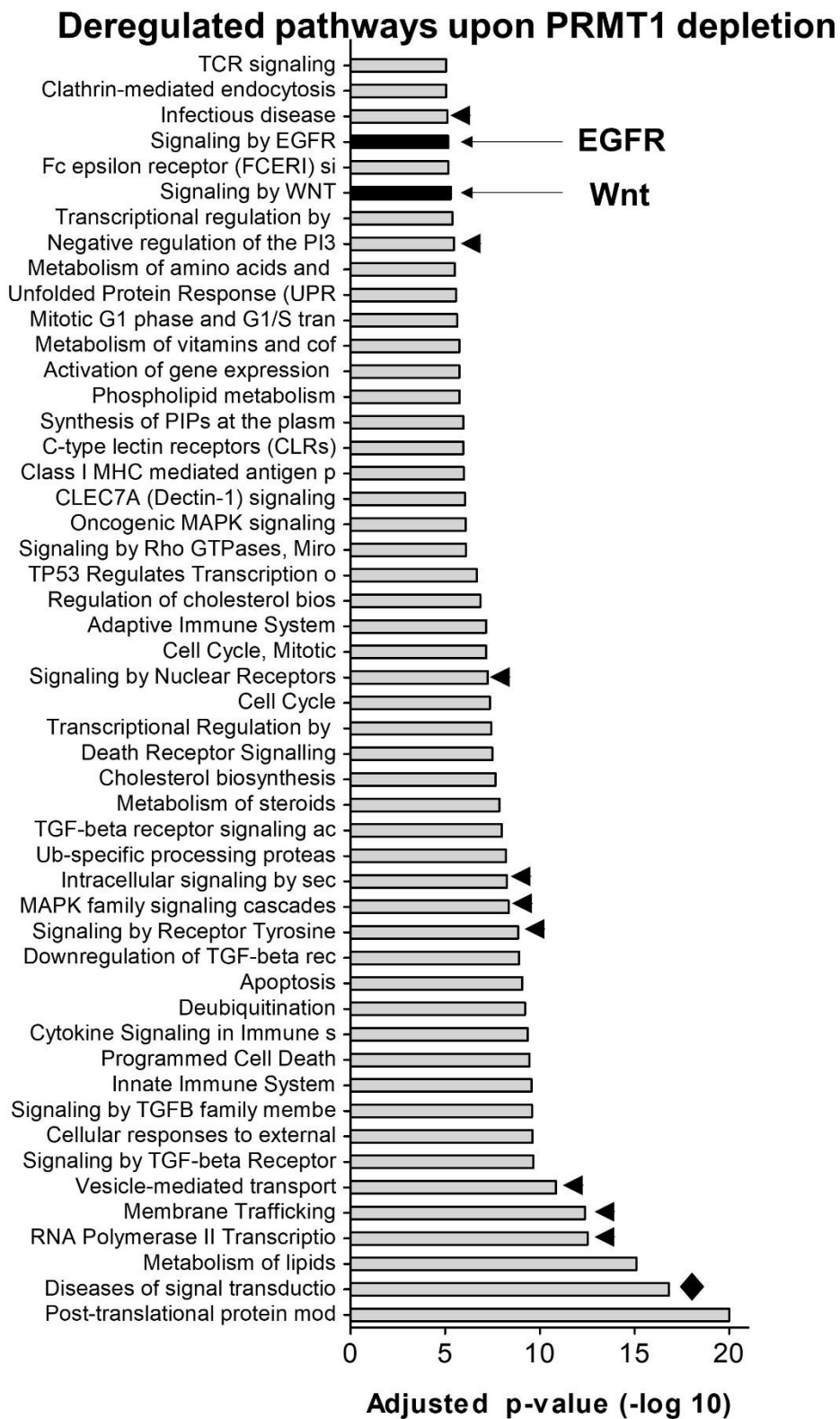


**Figure S6. PRMT1 regulates EGFR and Wnt signaling pathways.**

RNA was extracted from MDA-MB-468 cells transfected with control or PRMT1 (#7, #8) siRNA for 24h and 48h, and analyzed by Affymetrix microarray. Gene enrichment pathway analysis, using the REACTOME database, was performed on the deregulated genes common to both PRMT1 siRNAs. The top 50 deregulated pathways ranked according to their significance (adjusted p-values) is shown. The EGFR and Wnt signalling pathways are highlighted in black. Arrowheads point to pathways including *EGFR*, and diamond points to pathways including *EGFR*, *LRP5* and *PORCN*.

Figure S7

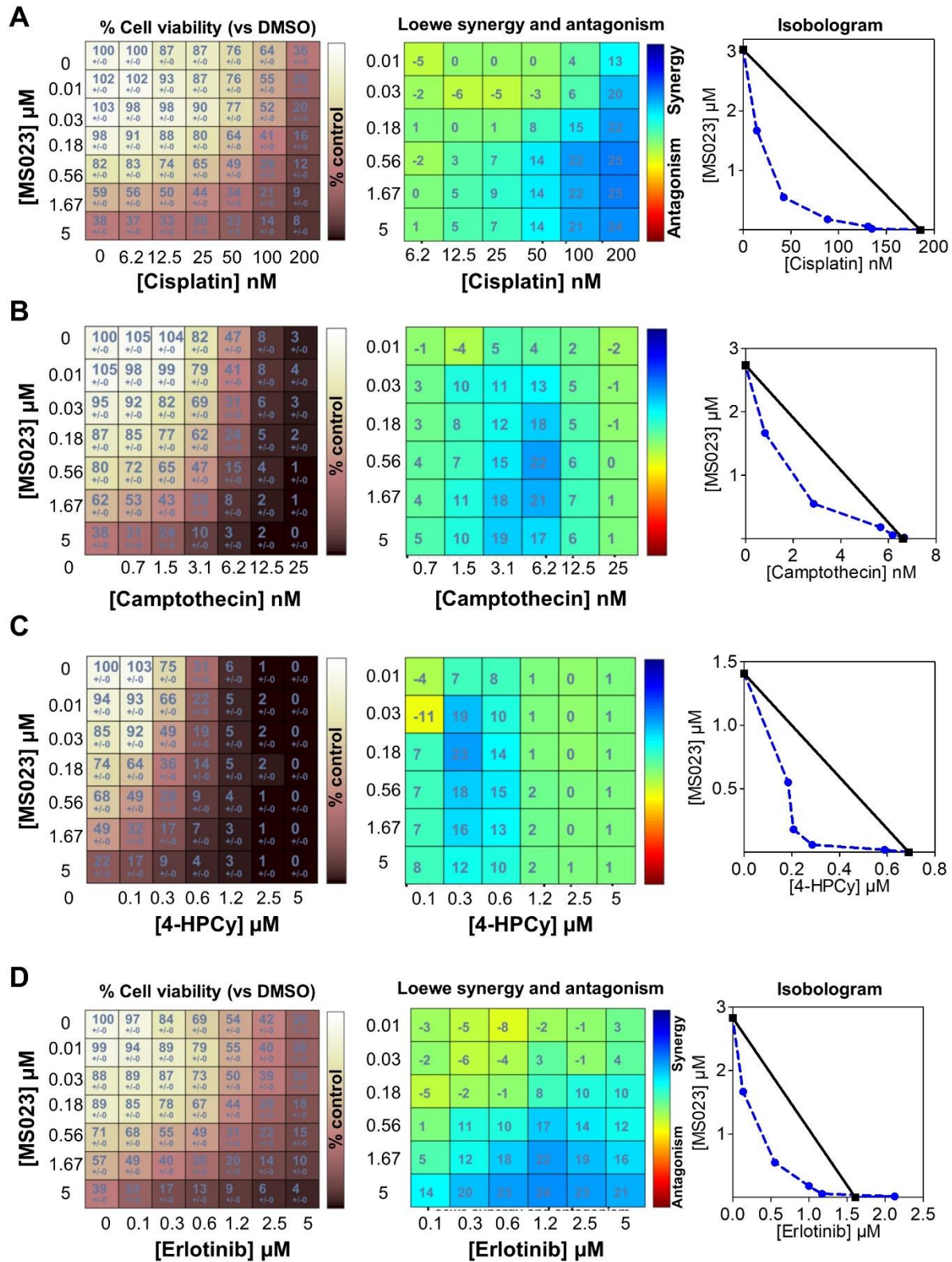


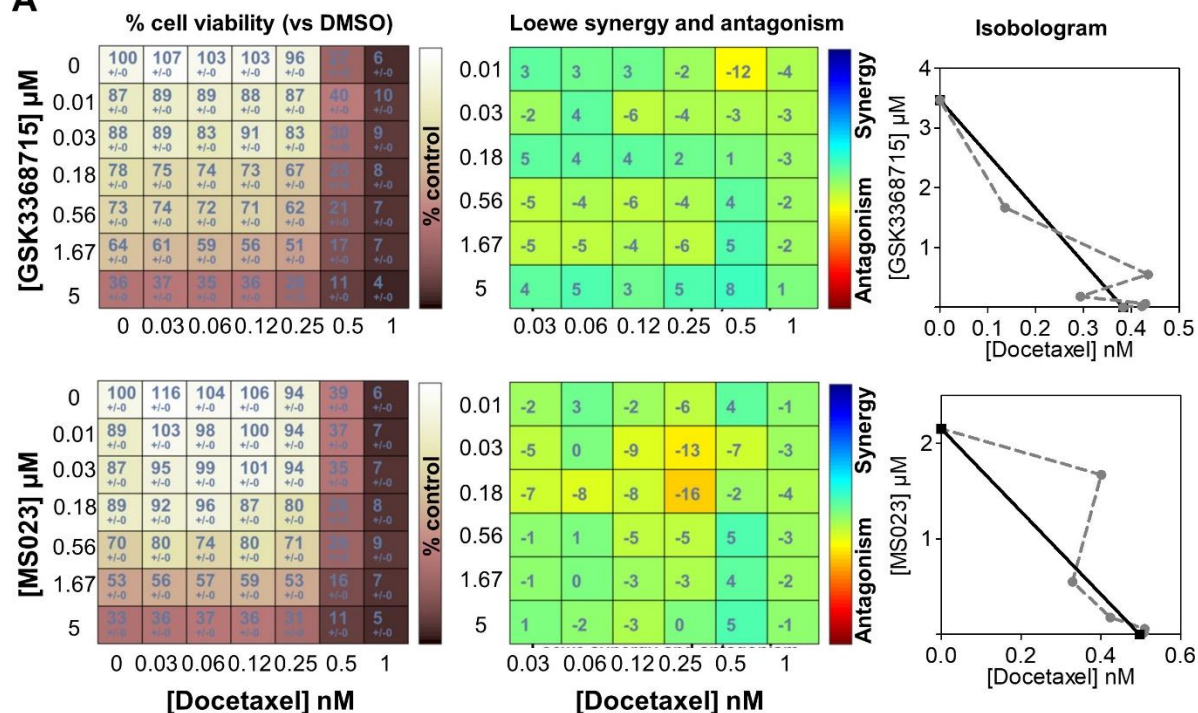
**Figure S7. Synergistic interactions between MS023 (a type I PRMT inhibitor) and chemotherapies (A, B, C) or erlotinib (D).**

MDA-MB-468 cells were seeded in 96-well plates, treated with the indicated drugs for 7 days (equivalent to 4 doubling times), and cell viability was measured by CellTiterGlo assay. MS023 was serially diluted three-fold and cisplatin (A), camptothecin (B), 4-hydroperoxy cyclophosphamide (4-HPCy; C), erlotinib (D) were serially diluted two-fold (concentrations indicated in the Figure). The drug interactions were calculated using the Loewe model on the Combenefit software. Cell viability (% compared to DMSO-treated cells, left panel), synergy matrix as calculated using the Loewe excess model (middle panel), and isobolograms (right panel) for each drug pair are indicated. Presented data are representative of three independent experiments.

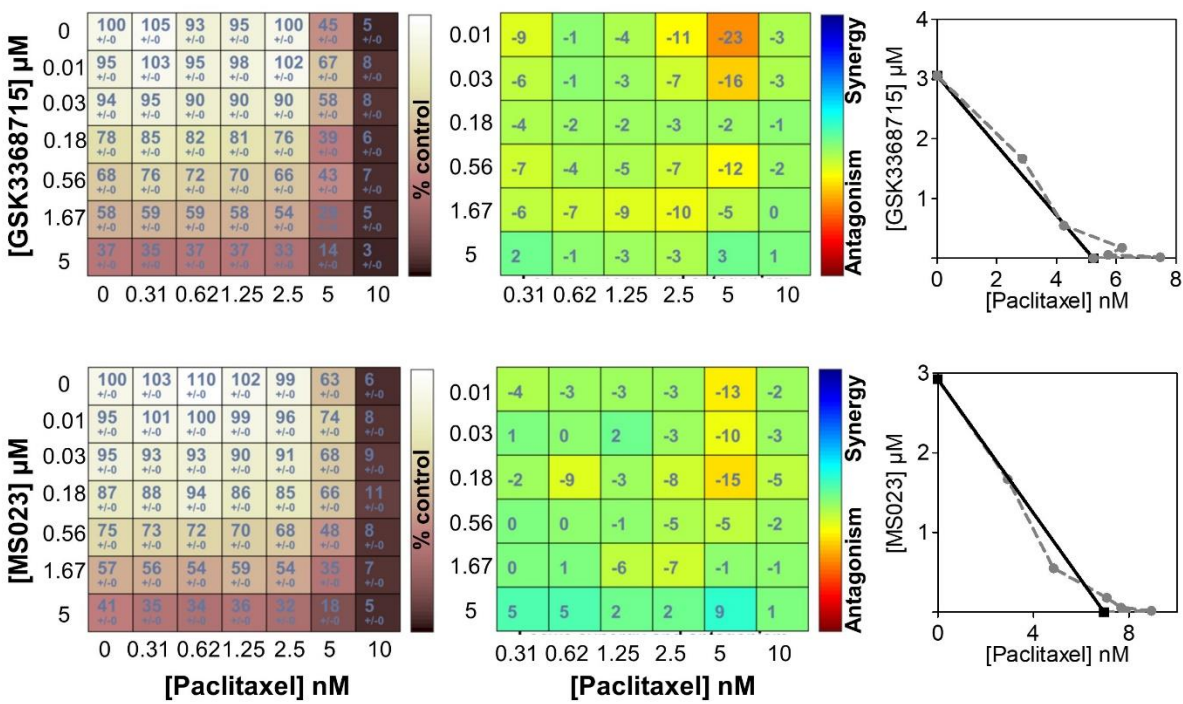


Figure S8

A



B





**Figure S8. Additive interactions between Type I PRMT inhibitors and taxanes.**

**A and B**, MDA-MB-468 cells were seeded in 96-well plates, treated with the indicated drugs for 7 days (equivalent to 4 doubling times) and cell viability was measured by CellTiterglo assay. Type I PRMT inhibitors (MS023, GSK3368715) were serially diluted three-fold and docetaxel (A) or paclitaxel (B) were serially diluted two-fold (concentrations indicated in the figure). The drug interactions were calculated using the Loewe model on the Combenefit software. Cell viability (% compared to DMSO-treated cells, left panel), synergy matrix as calculated using the Loewe excess model (middle panel), and isobolograms (right panel) for each drug pair are indicated. Presented data are representative of three independent experiments.

Figure S9

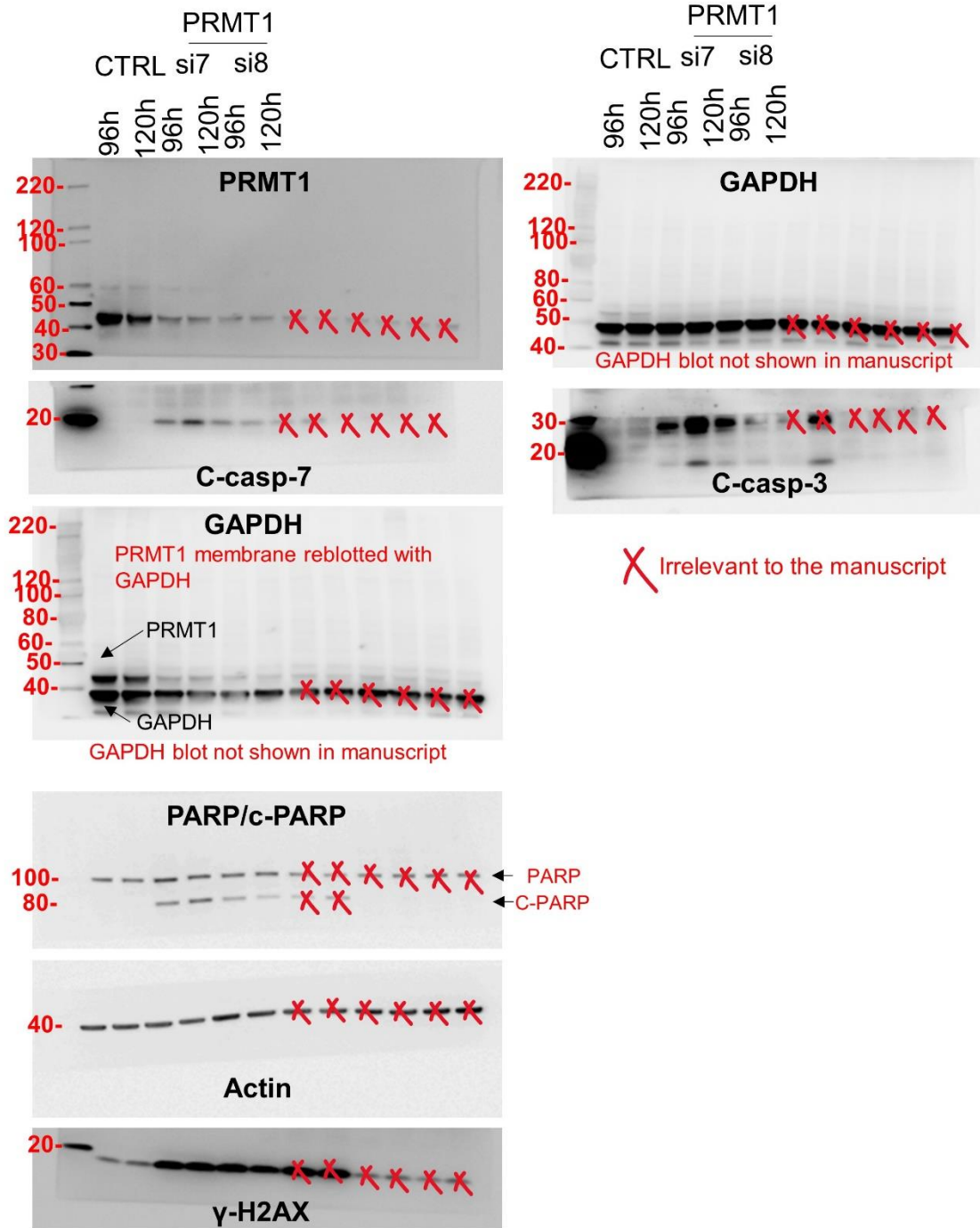
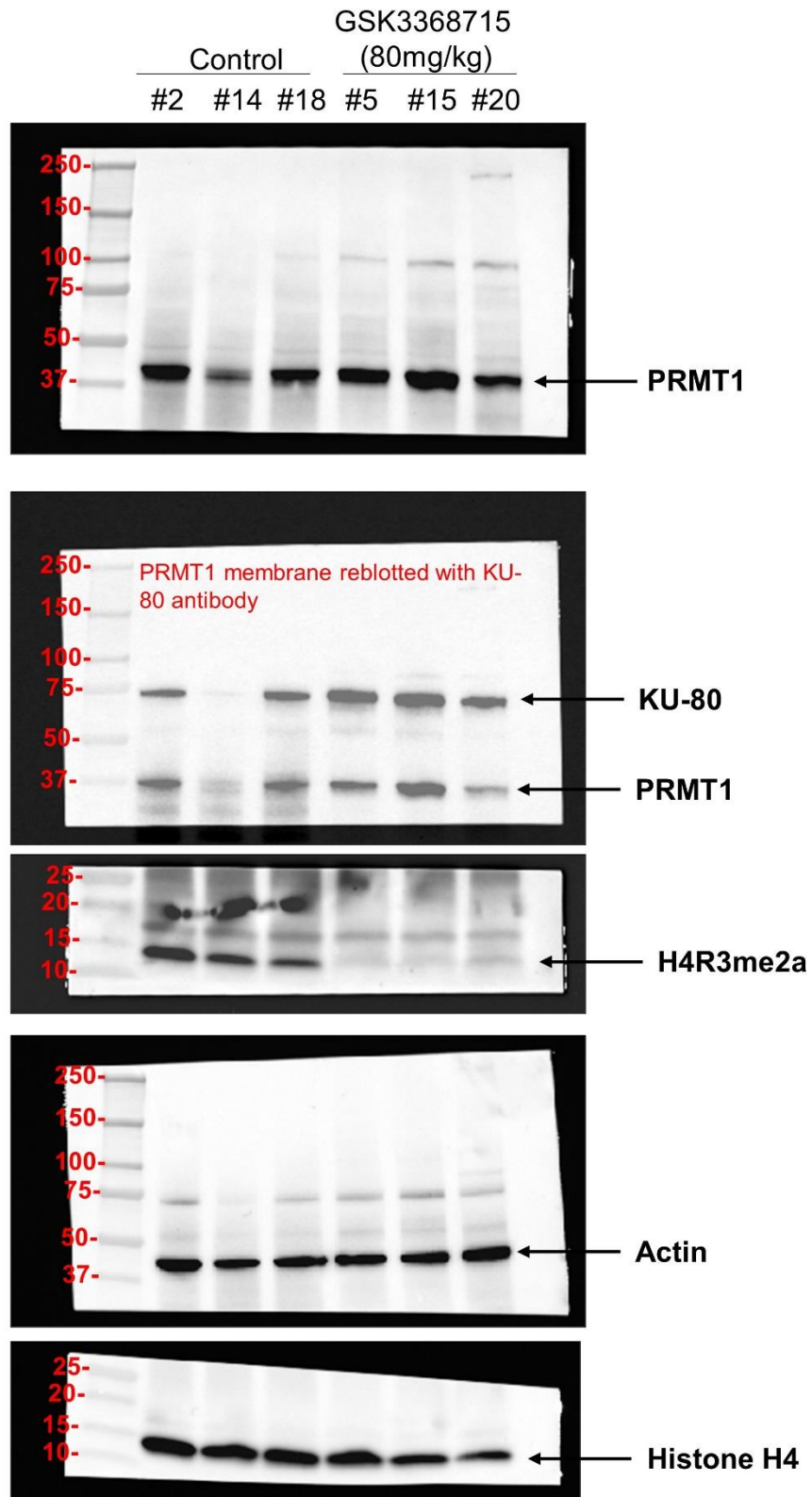


Figure S9. Uncropped original blots of Figure 2D.

**Figure S10**



**Figure S10. Uncropped original blots of Figure 3D.**

Figure S11

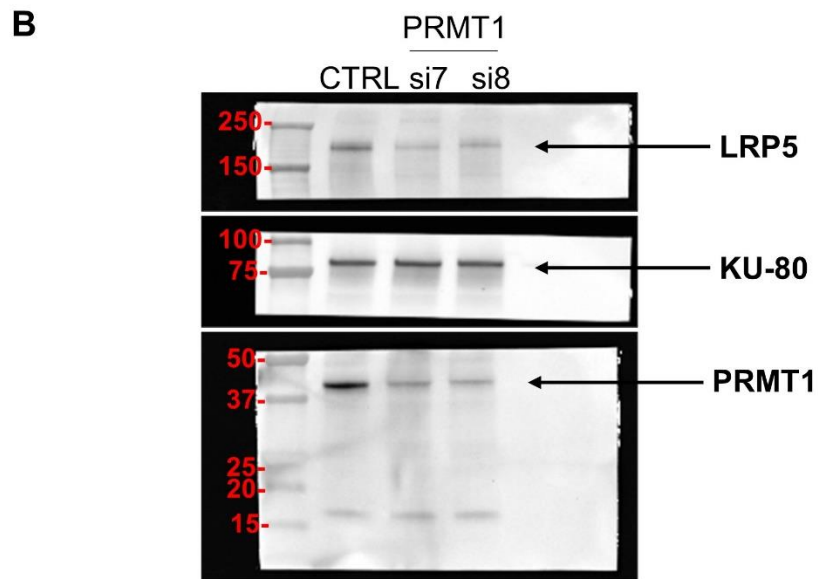
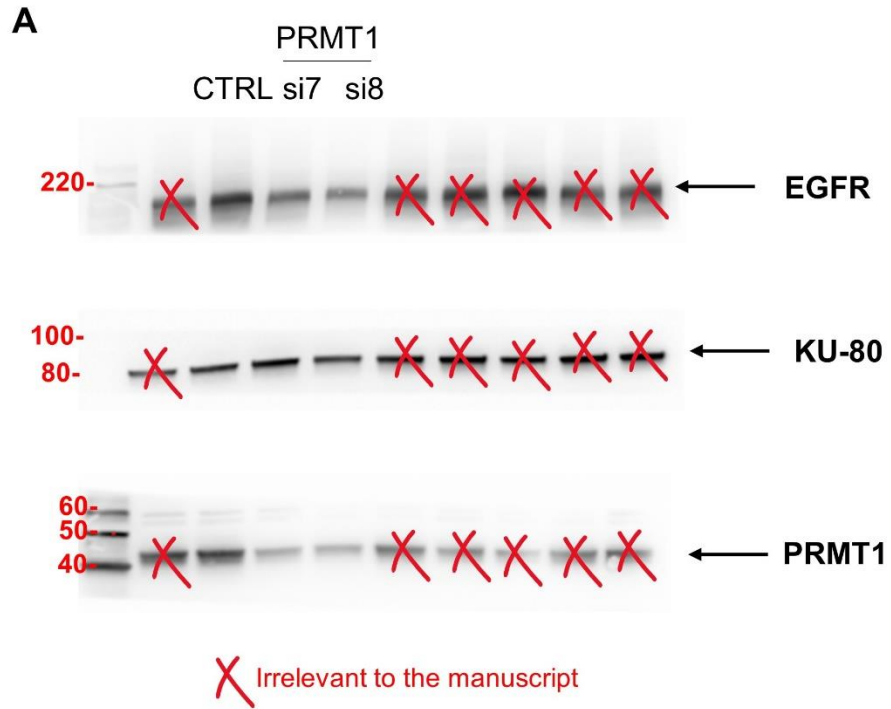


Figure S11. A, uncropped original blots of Figure 4D. B, uncropped original blots of Figure 4H.

Figure S12

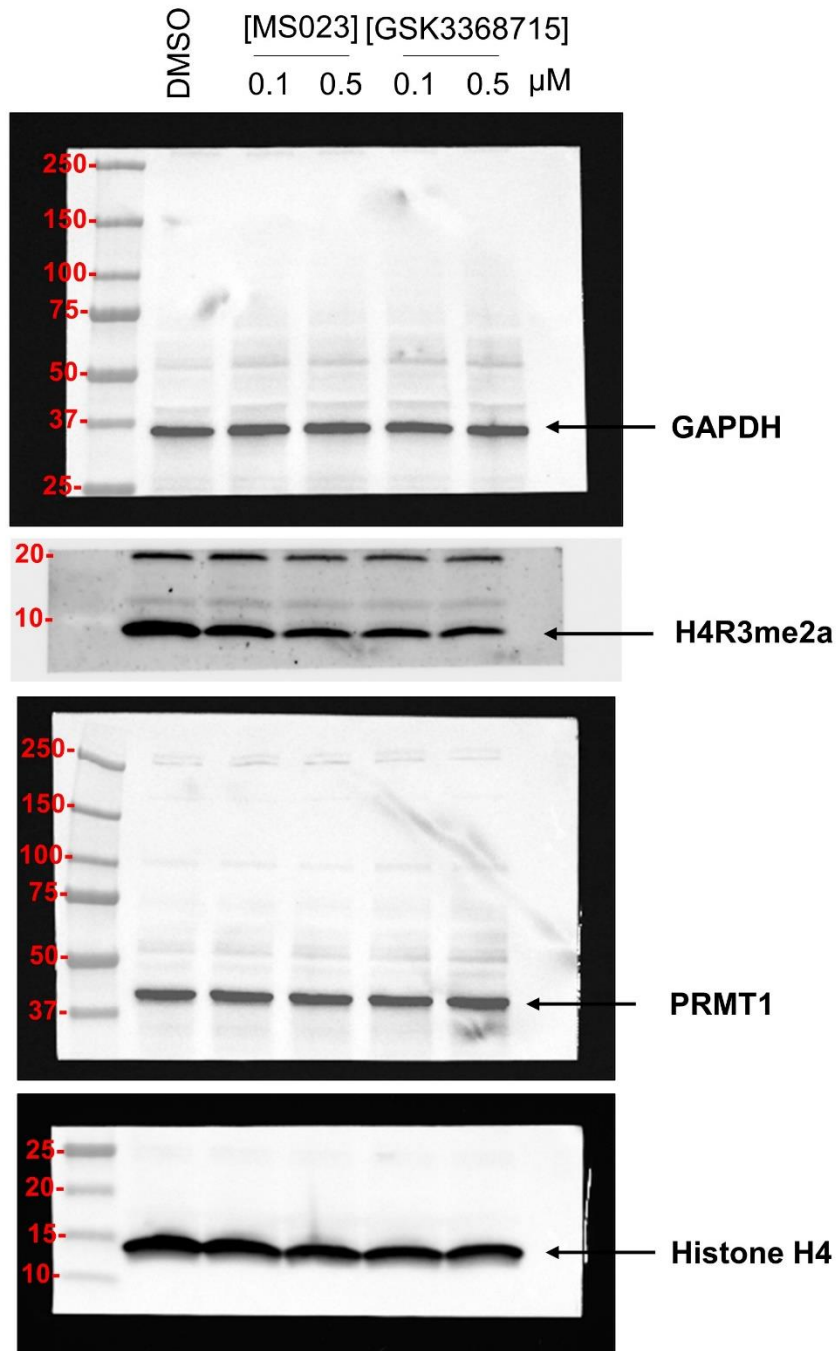


Figure S12. Uncropped original blots of Figure 5D.

Figure S13

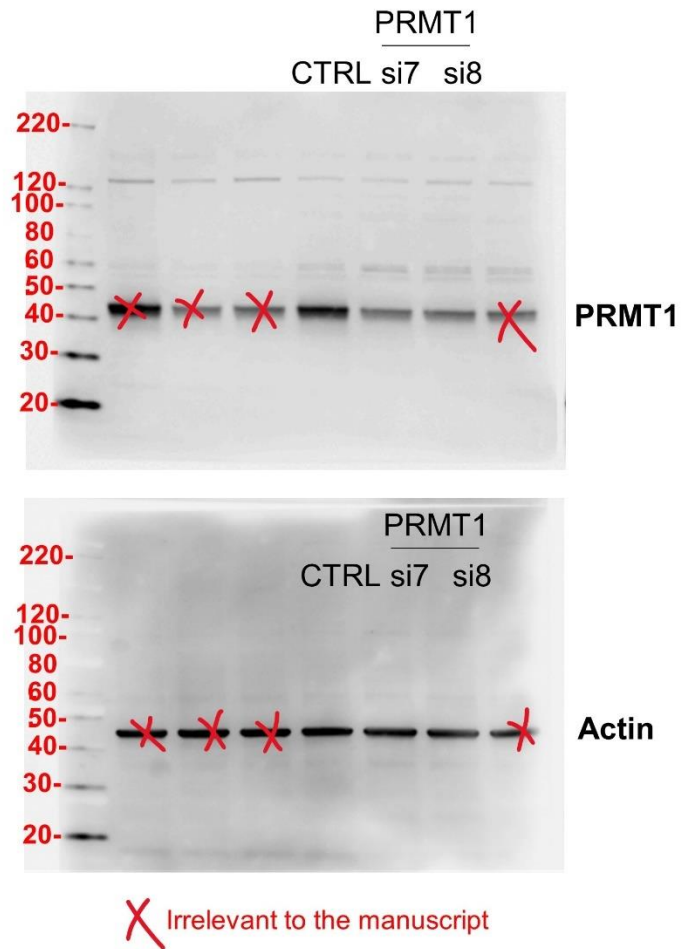


Figure S13. Uncropped original blots of Figure S1D.

Figure S14

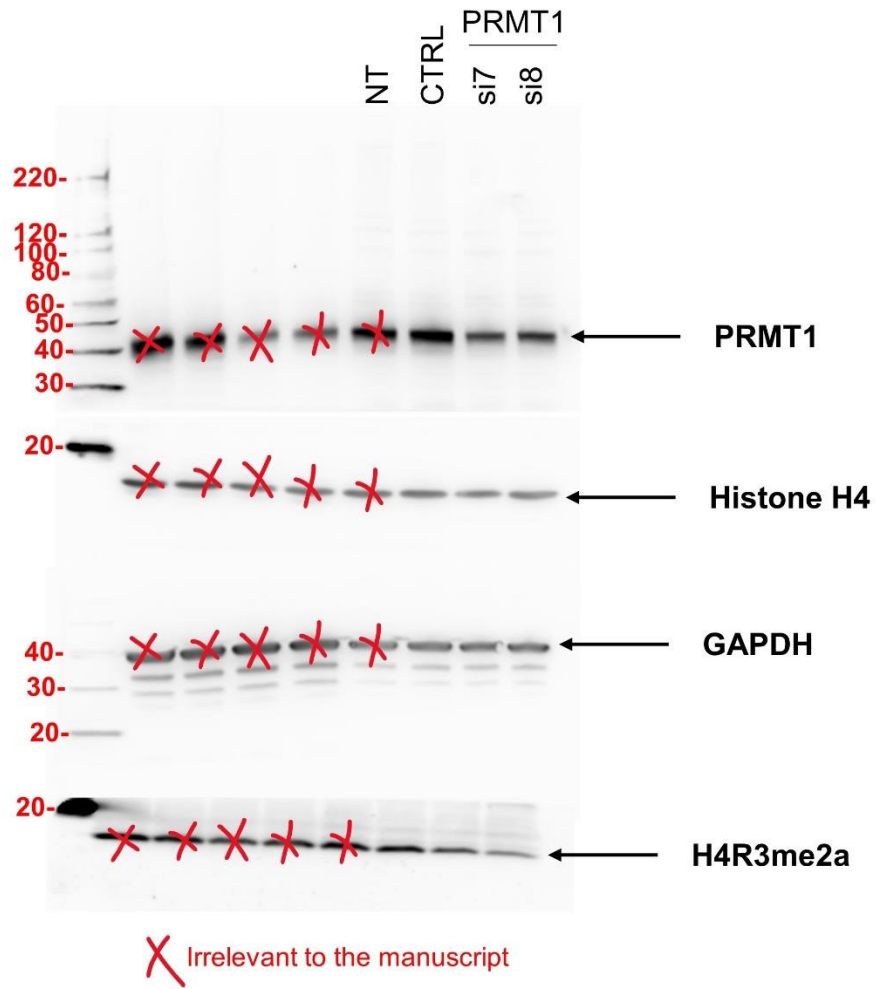


Figure S14. Uncropped original blots of Figure S2A. NT- non treated

Figure S15

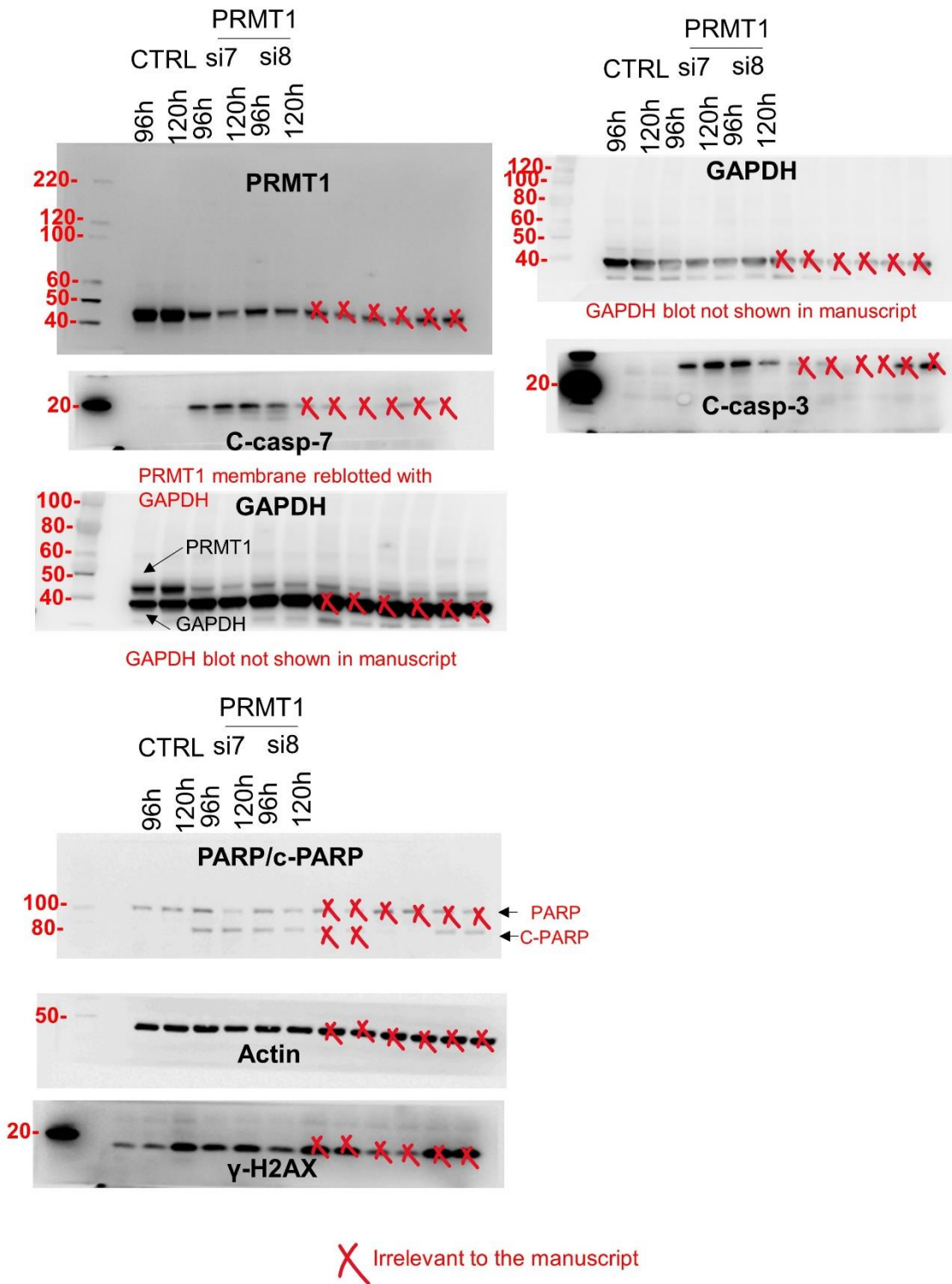
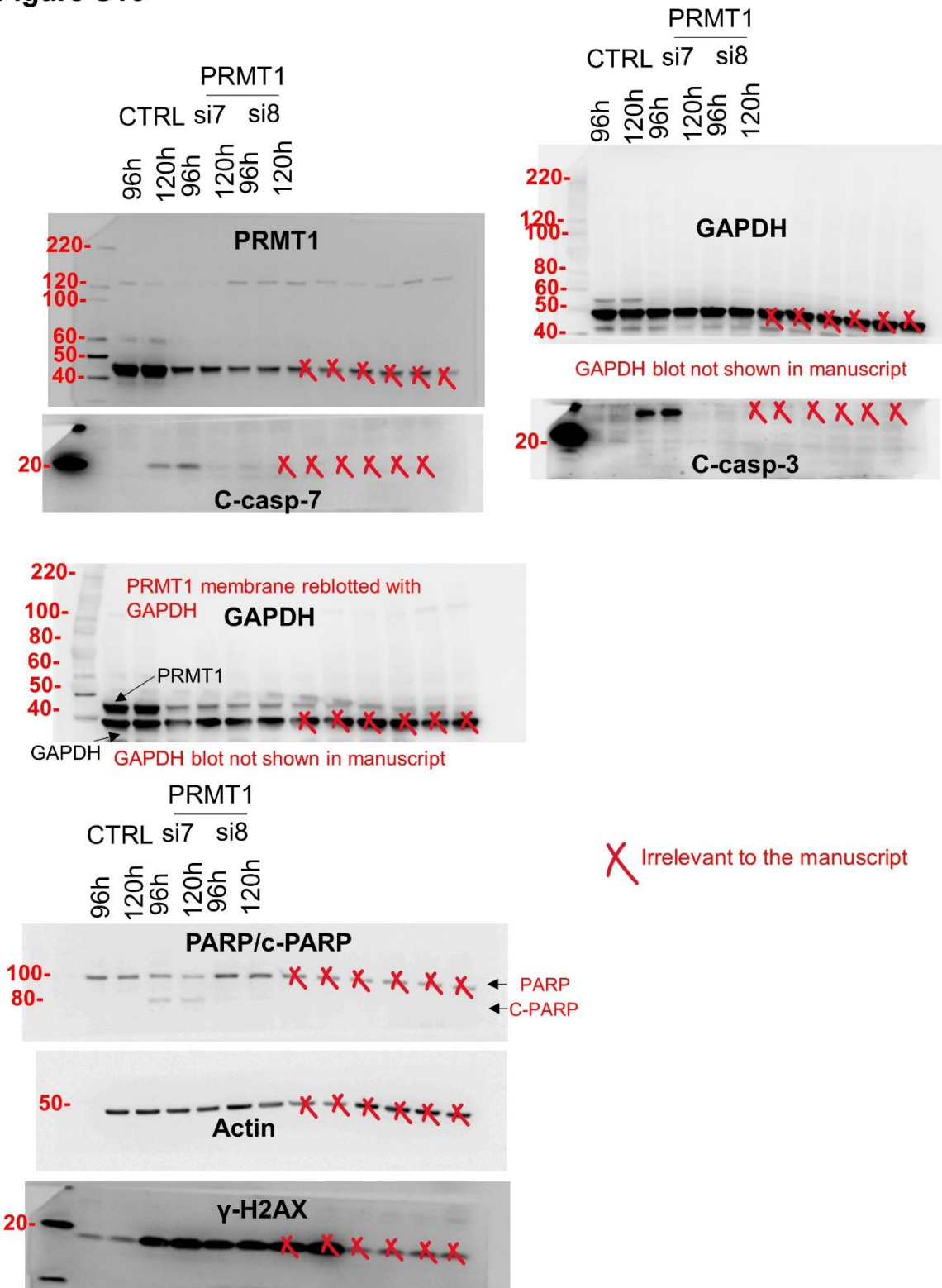


Figure S15. Uncropped original blots of Figure S2D for HCC70 cell line.



**Figure S16**



**Figure S16. Uncropped original blots of Figure S2D for MDA-MB-231 cell line.**

**Figure S17**

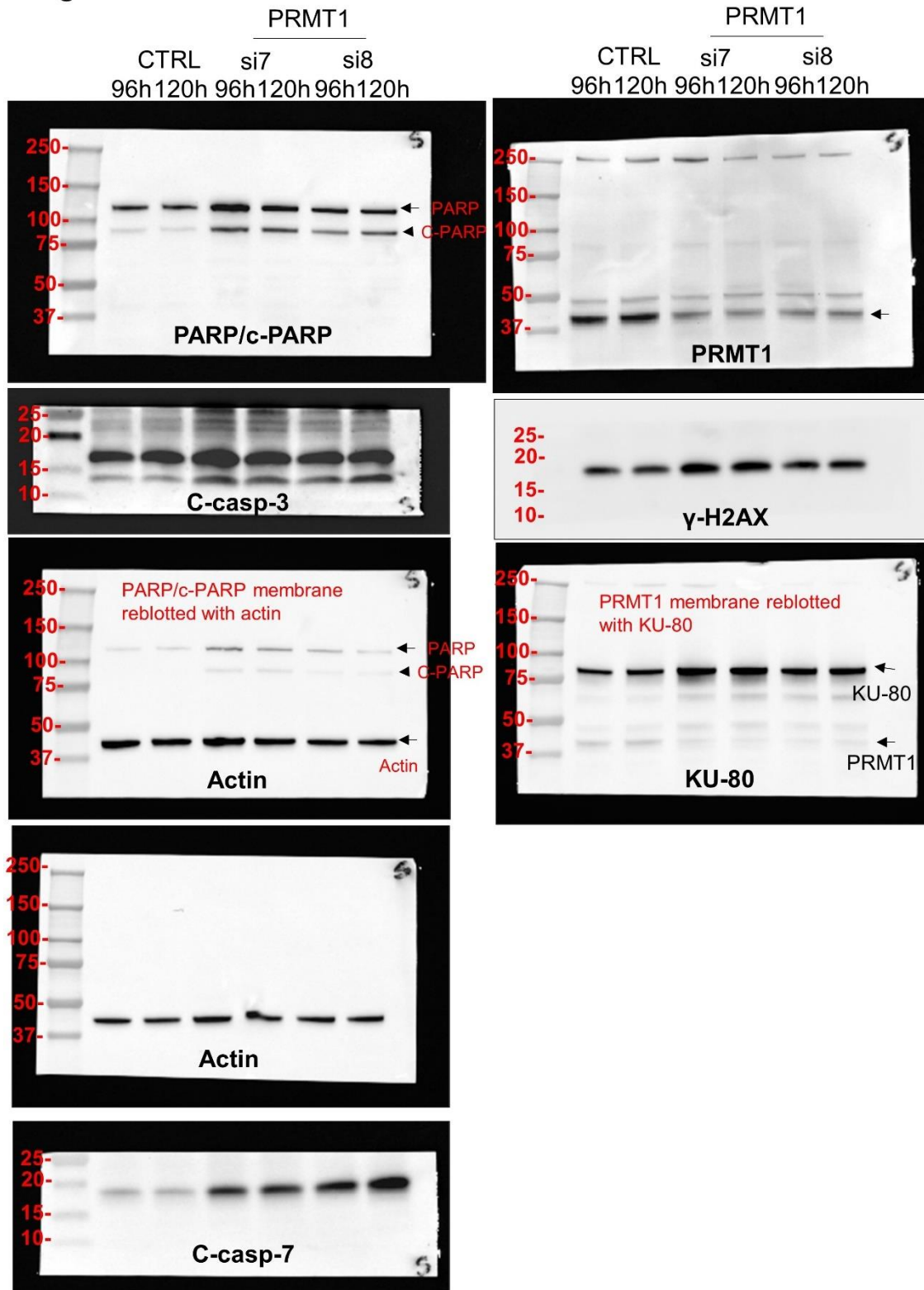


**Figure S17. Uncropped original blots of Figure S2D for SKBr3 cell line.**

**Figure S18**

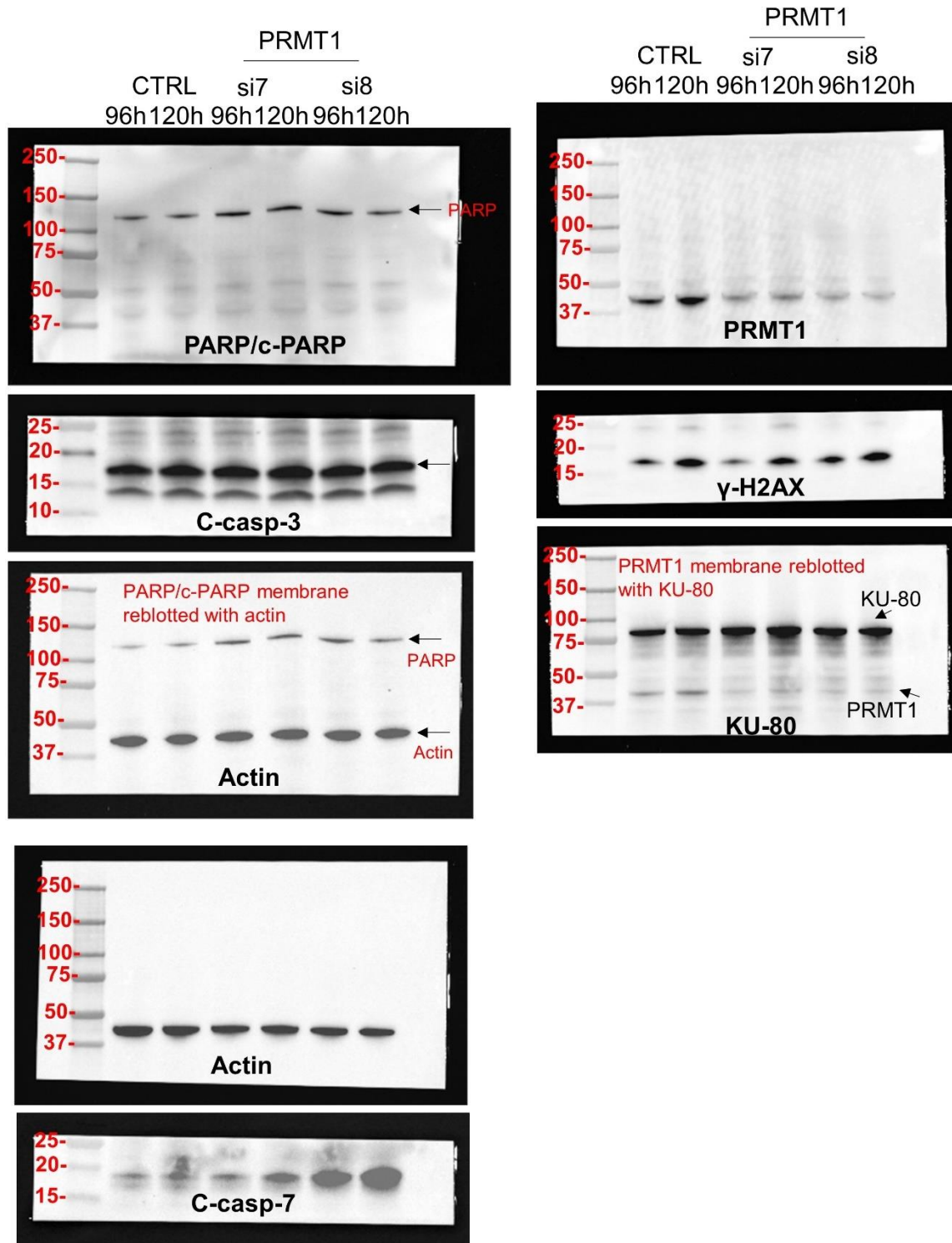


**Figure S18. Uncropped original blots of Figure S2D for T47D cell line.**

Figure S19

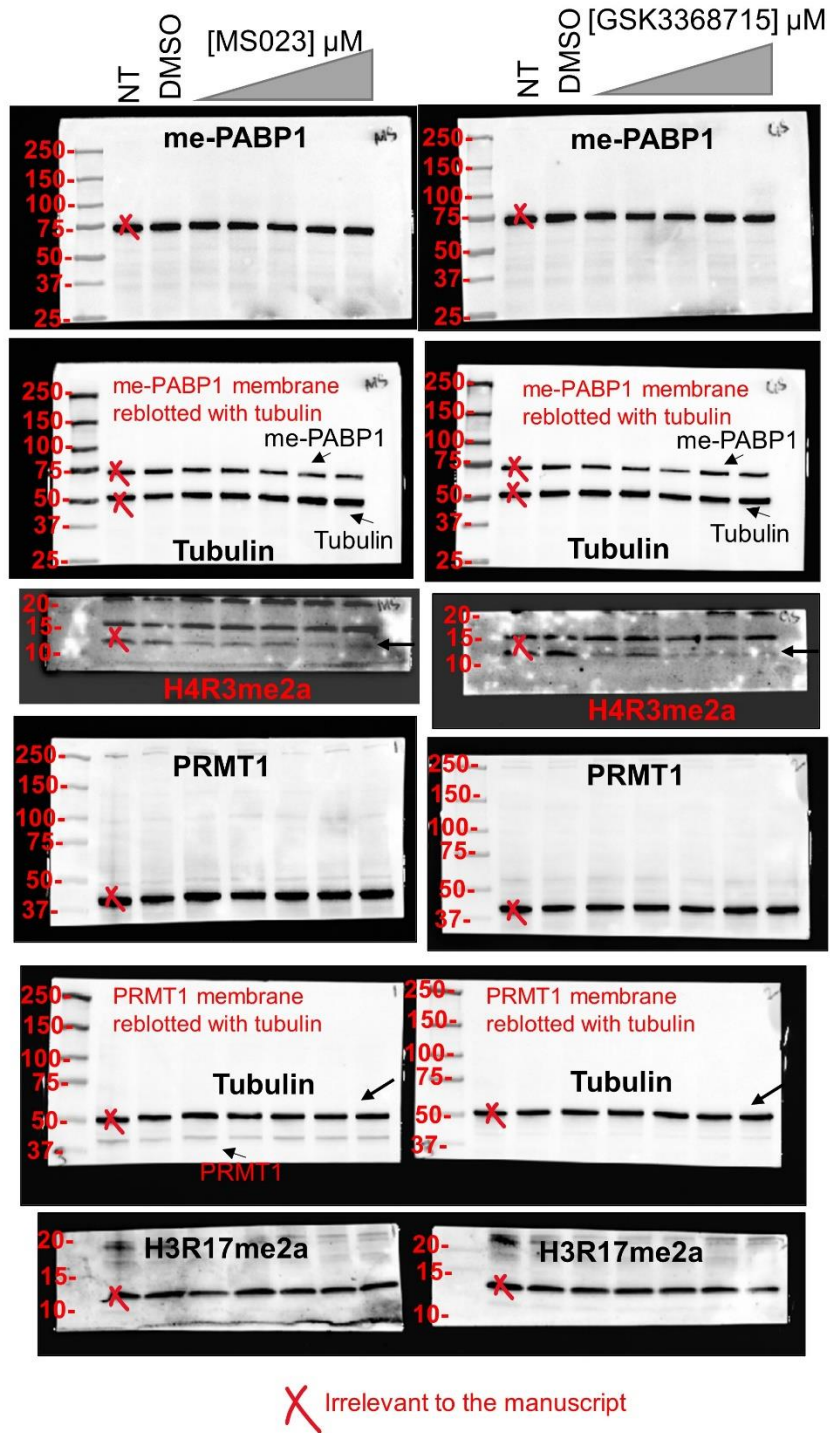


Figure S19. Uncropped original blots of Figure S3 (for remaining blots, see Figure S20). NT- non treated.



Figure S20

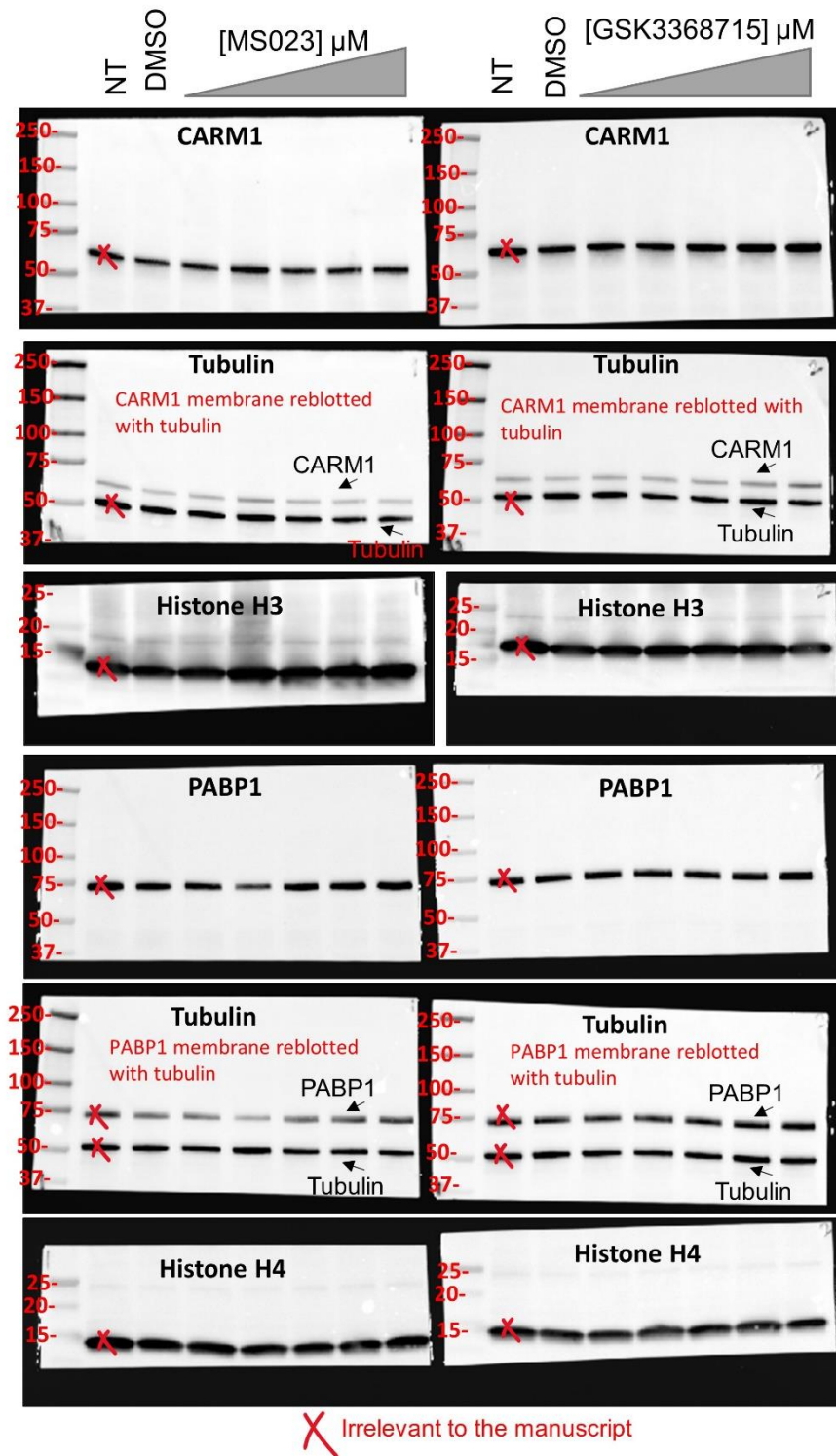
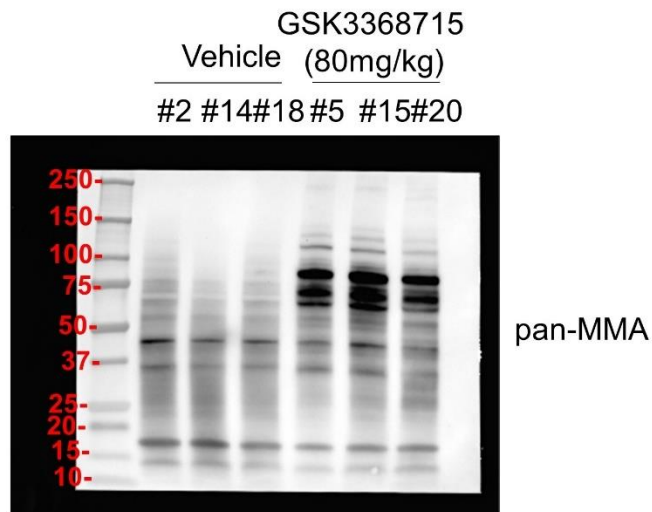


Figure S20. Remaining uncropped original blots of Figure S3. NT- non treated.

## Figure S21



**Figure S21. Uncropped original blot of Figure S5B.**

### **Table S1. (separate file)**

Antibodies, primers, siRNAs and drugs

### **Table S2. (separate file)**

Differentially expressed genes in PRMT1-depleted MDA-MB-468 cells

### **Table S3. (separate file)**

PRMT1 DNA copy number gain and loss in the curie cohort

## RÉSUMÉ

---

Le cancer du sein triple-négatifs (TNBC) est le cancer du sein le plus agressif, caractérisé par une forte hétérogénéité inter- et intra-tumorale, un enrichissement en cellules souches cancéreuses, une résistance au traitement, des taux de rechute élevés et un haut potentiel à former des métastases. La chimiothérapie demeure le traitement standard pour les patientes avec un cancer TNBC. Notre équipe se concentre sur l'exploration de nouvelles approches thérapeutiques pour le cancer TNBC et s'est récemment intéressée aux membres de la famille des protéines arginine méthyltransférases (PRMTs) comme cibles thérapeutiques prometteuses. PRMT5 est la principale enzyme responsable de la diméthylation symétrique. Nous avons précédemment observé que des niveaux élevés d'ARNm de PRMT5 étaient associés à un mauvais pronostic dans les cancers TNBC. De plus, l'inhibition de PRMT5 diminuait la viabilité et les propriétés « stemness » des cellules TNBC, induisait une apoptose et diminuait la croissance tumorale dans un modèle murin TNBC. Dans cette thèse, notre objectif était de valider PRMT5 en tant que cible thérapeutique pour les cancers TNBC et de caractériser ses fonctions. Dans une première étude, nous avons examiné les effets de l'inhibition de PRMT5 en combinaison avec différentes chimiothérapies ou des inhibiteurs ciblant les récepteurs transmembranaires de la famille HER, sur la prolifération de plusieurs lignées cellulaires TNBC. Nous avons démontré un effet synergique entre l'inhibiteur de PRMT5 et le cisplatine, la camptothécine et la doxorubicine pour altérer la prolifération des cellules TNBC. De plus, une synergie a été observée entre l'inhibiteur de PRMT5 et l'erlotinib (inhibiteur de l'EGFR) ou le neratinib (inhibiteur de l'EGFR/HER2/HER4) pour diminuer la viabilité des lignées cellulaires TNBC, en particulier celles exprimant des niveaux élevés d'EGFR. Nous avons aussi observé un effet synergique entre l'inhibiteur de PRMT5 et le neratinib ou le tucatinib (inhibiteur d'HER2) dans une lignée cellulaire TNBC « HER2-low » ainsi que dans une lignée cellulaire HER2+. Des effets synergiques ont pu être observés dans des lignées cellulaires TNBC résistantes à la seule inhibition de PRMT5. Notre seconde étude avait pour but de caractériser l'interactome de PRMT5 pour nous aider à mieux comprendre ses fonctions, en utilisant deux approches différentes. Tout d'abord, nous avons immunoprécipité la protéine PRMT5 endogène ou son cofacteur MEP50, à partir de lysats de cellules TNBC. Cette étude a permis d'identifier FUBP1, un facteur de transcription intervenant aussi dans la régulation de l'épissage alternatif, en tant que partenaire du complexe PRMT5/MEP50. Nous avons ensuite démontré que PRMT5 méthyle FUBP1, facilitant ainsi sa liaison à l'élément FUSE en amont du promoteur du gène MYC. L'approche alternative de « TurboID » permettant un marquage (biotine) in cellulo des protéines à proximité de la protéine d'intérêt, a révélé plusieurs nouveaux partenaires potentiels de PRMT5 dont SDCCAG3. Nous avons confirmé l'interaction entre PRMT5 et SDCCAG3, et initié une étude concernant leur association avec le récepteur Wnt LRP6, ainsi que la régulation de la voie Wnt par SDCCAG3. En résumé, notre étude a permis d'identifier les partenaires du complexe PRMT5/MEP50, de commencer à caractériser leurs fonctions, et a mis en lumière le potentiel thérapeutique d'inhiber PRMT5, en combinaison avec d'autres drogues, pour le traitement du cancer TNBC.

## MOTS CLÉS

---

PRMT5, TNBC, chimiothérapie, thérapie ciblée, méthylation des arginines, interaction protéine-protéine, combinaison de drogues, FUBP1, EGFR, HER2, SDCCAG3, WNT, LRP6, TurboID

## ABSTRACT

---

Triple negative breast cancer (TNBC) is an aggressive tumor characterized by high inter- and intra-tumoral heterogeneity, enrichment in breast cancer stem cells, resistance to treatment, high relapse rates, and a heightened propensity for metastasis. TNBC poses the worst prognosis among breast cancer subtypes, and chemotherapies remain the standard treatment for TNBC patients. The aim of our group is to propose new targeted treatments for TNBC and has recently focused on the family of protein arginine methyltransferases (PRMTs) as potential therapeutic targets for the disease. PRMT5 is the main type II PRMT responsible for symmetric dimethylation. We previously found that high PRMT5 mRNA levels are associated with poor prognosis in TNBC and that inhibiting PRMT5 decreases TNBC cell viability and stemness properties, induces apoptosis, and reduces tumor growth in a TNBC PDX mouse model. In this thesis, we aimed to understand the functions of PRMT5 and validate it as a therapeutic target for TNBC. In a first study, we analyzed the effect of combining a PRMT5 inhibitor with different chemotherapies or tyrosine kinase inhibitors targeting the HER family members on the proliferation of various TNBC cell lines. We found that PRMT5 inhibition synergized with the chemotherapies cisplatin, camptothecin, and doxorubicin to impair TNBC cell proliferation. Moreover, PRMT5 inhibition demonstrated synergism with erlotinib (EGFR inhibitor) and neratinib (EGFR/HER2/HER4 inhibitor) to impair the viability of TNBC cell lines, particularly in those expressing high levels of EGFR. Additionally, we observed a synergistic effect between the PRMT5 inhibitor and neratinib or tucatinib (HER2 inhibitor) in both a HER2-low TNBC cell line as well as in a HER2-positive breast cancer cell line. Importantly, the synergistic effects could be achieved in TNBC cell lines that had previously demonstrated resistance to PRMT5 inhibition when used alone. In a second study, we aimed to decipher the interactome of PRMT5 using two different approaches. First, we immunoprecipitated endogenous PRMT5 or its co-factor MEP50 from TNBC cell lysates. This led to the identification of FUBP1, a transcription and pre-mRNA splicing factor, as a partner of the PRMT5/MEP50 complex. We subsequently demonstrated that PRMT5 methylates FUBP1, facilitating its binding to the FUSE element upstream of the MYC promoter. Second, we used a proximity labelling assay (TurboID) which revealed several potential novel partners of PRMT5, including SDCCAG3. We confirmed the interaction between PRMT5 and SDCCAG3, and initiated investigations into their association with the Wnt receptor LRP6, as well as the influence of SDCCAG3 on the Wnt pathway. To summarize, these findings enhance our understanding of the function of PRMT5 in the context of TNBC and highlight its potential as a promising target for combinatorial therapies in the treatment of TNBC.



## KEYWORDS

---

PRMT5, TNBC, chemotherapies, targeted therapies, arginine methylation, protein-protein interaction, drug combinations, FUBP1, EGFR, HER2, SDCCAG3, WNT, LRP6, TurboID